GEOLOGICAL SURVEY OF CANADA
PAPER 89-13

STUDIES OF LATERALLY HETEROGENEOUS STRUCTURES USING SEISMIC REFRACTION AND REFLECTION DATA

Edited by A.G. Green

1990

Energy, Mines and Resources Canada
Énergie, Mines et Ressources Canada

Canada

THE ENERGY OF OUR RESOURCES

THE POWER OF OUR IDEAS

GEOLOGICAL SURVEY OF CANADA
PAPER 89-13

STUDIES OF LATERALLY HETEROGENEOUS STRUCTURES USING SEISMIC REFRACTION AND REFLECTION DATA

Edited by A.G. Green

1990

Available in Canada through authorized

bookstore agents and other bookstores

or by mail from

Canadian Government Publishing Centre
Supply and Services Canada
Ottawa, Canada K1A 0S9

and from

Geological Survey of Canada offices:

601 Booth Street
Ottawa, Canada K1A 0E8

3303-33rd Street N.W.
Calgary, Alberta T2L 2A7

100 West Pender Street,
Vancouver, B.C. V6B 1R8

A deposit copy of this publication is also available
for reference in public libraries across Canada

Cat. No. 0-660-13611-2
ISBN M44-89/13E

Price subject to change without notice

Cover description

Artistic cartoon of the Vancouver Island
subduction zone by R.P. Riddihough (1978)

Original manuscript received: 26-06-89
Final version approved for publication: 02-04-90

CONTENTS

STUDIES OF LATERALLY HETEROGENEOUS STRUCTURES USING SEISMIC REFRACTION AND REFLECTION DATA

INTRODUCTION

In August 1987, the International Association of Seismology and Physics of the Earth's Interior (IASPEI) Commission on Controlled Source Seismology held its 7th workshop at Whistler Village in the Coast Mountains of British Columbia. As for previous workshops, the primary objective was to compare and assess the various processing and interpretation methods that can be applied to crustal seismic data. The choice of topics for this workshop was influenced by the growing number of groups employing the powerful seismic reflection techniques, and in particular by the increased application of these techniques in combination with seismic refraction methods to resolve the structure of the crust and uppermost mantle. At Whistler, special emphasis was given to the combined interpretation of coincident multichannel seismic reflection and seismic refraction data recorded in an onshore-offshore environment, the processing of both land and marine multichannel seismic reflection data, and the interpretation of a synthetic seismic reflection section.

The observed data given to the workshop participants were collected between 1981 and 1985 by Canadian university and government geoscientists during COCRUST and LITHOPROBE studies along the continental margin of British Columbia. In this region, the Juan de Fuca oceanic plate is being subducted beneath the collage of exotic terranes that constitute Vancouver Island and the western North American mainland. The synthetic data set was designed and generated by Roy Johnson (University of Arizona), Scott Smithson (University of Wyoming) and Walter Mooney (United States Geological Survey).

Forty-six scientists from thirteen different countries attended the workshop and several others submitted contribu-tions. Each participant was invited to work on one or more of the following topics :

I A combined interpretation of multichannel seismic reflection and seismic refraction/wide-angle reflection data collected across Vancouver Island and the adjacent continental margin.

II Enhanced processing of stacked data from a land multichannel seismic reflection profile collected on Vancouver Island.

III Processing of unstacked data from a land multichannel seismic reflection profile collected on Vancouver Island.

INTRODUCTION

En août 1987, la Commission sur la sismologie à source contrôlée (CSSC) de l'Association Internationale de Séismologie et de Physique de l'Intérieur de la Terre (AISPIT) a tenu son septième atelier à Whistler dans la chaîne côtière de la Colombie-Britannique. Comme pour les ateliers précédents, le principal objectif était de comparer et d'évaluer les diverses méthodes de traitement et d'interprétation pouvant être appliquées à des données sismiques de la croûte terrestre. Le choix des sujets pour cet atelier a été marqué par le nombre croissant de groupes utilisant les techniques puissantes de la sismique réflexion, et en particulier par l'application accrue de ces techniques combinées à des méthodes de sismique réfraction pour définir la structure de la croûte et du manteau supérieur. À Whistler, l'accent a été mis sur l'interprétation combinée de données coïncidentes de sismique réflexion multicanale et de sismique réfraction enregistrées dans un milieu tant marin que terrestre sur le traitement de données de sismique réflexion multicanale terrestre et marine, et sur l'interprétation d'un profil synthétique de sismique réflexion.

Les données réelles, fournies aux participants de l'atelier, ont été recueillies entre 1981 et 1985 par des scientifiques des universités et du gouvernement du Canada au cours de travaux réalisés dans le cadre des programmes COCRUST et LITHOPROBE le long de la marge continentale de la Colombie-Britannique. Dans cette région, la plaque océanique de Juan de Fuca plonge sous le collage de blocs exotiques qui constituent l'île de Vancouver et la partie occidentale du continent nord-américain. Les données synthétiques ont été conçues et réalisées par MM. Roy Johnson (Université de l'Arizona), Scott Smithson (Université du Wyoming) et Walter Mooney (United States Geological Survey).

Quarante-six scientifiques venant de 13 pays différents ont participé à l'atelier et plusieurs autres y ont contribué. Chacun des participants a été invité à travailler sur au moins un des jeux de données suivants :

I Interprétation combinée de données de sismique réflexion multicanale et sismique réfraction/réflexion grand angle provenant de l'île de Vancouver et de la marge continentale adjacente.

II Traitement amélioré de données sommées provenant d'un profil terrestre de sismique réflexion multicanale effectué sur l'île de Vancouver.

III Traitement de données individuelles provenant d'un profil terrestre de sismique réflexion multicanale effectué sur l'île de Vancouver.

IV Processing of unstacked data from a marine multichannel seismic reflection profile collected off the west coast of Vancouver Island.

V Interpretation of a synthetic multichannel seismic reflection section.

A total of thirty-three papers was presented. Data set I proved to be the most popular amongst the participants with fourteen presentations. Reprocessing the three seismic reflection data sets (II-IV) was the focus of fifteen talks and four attempts were made at unravel-ling the mystery of synthetic data set V. Sixteen of the papers presented are included in this volume. Each of the submitted papers received an editorial review and a minimum of two external evaluations. Papers were evaluated by Isa Asudeh, Ron Clowes, Fred Cook, Bob Ellis, Dave Forsyth, Alan Green, Roy Johnson, Carmen Lowe, Bernd Milkereit, Patrick Morel-à-l'Huissier, George Spence and Carl Spencer.

The organizing committee appreciates the support of H. Shimamura and N. Pavlenkova, Chairman and Vice-Chairman respectively of the Commission on Controlled Source Seismology, and thanks all of the participants who contributed so much of their time to the workshop. Special thanks are extended to those who put in the extra effort to submit a paper for this publication. IASPEI provided financial support towards the travel costs of some participants. The able assistance of Mrs. Gwen Mason in the preparation of the workshop topics and the formating of the manuscripts is greatly appreciated.

A.G. Green, B. Milkereit, P. Morel-à-l'Huissier and C. Spencer
Continental Geoscience Division,
Geological Survey of Canada, Ottawa, Ontario
Canada, K1A 0Y3

R.M. Ellis, R.M. Clowes
Department of Geophysics and Astronomy,
University of British Columbia
Vancouver, BC Canada, V6T 1W5

J. Ansorge
Institute of Geophysics
ETH-Hoenggerberg, Zurich, Switzerland, CH-8093

IV Traitement de données individuelles provenant d'un profil marin de sismique réflexion multicanale établi au large de la côte ouest de l'île de Vancouver.

V Interprétation d'un profil synthétique de sismique réflexion multicanale.

On a présenté au total 33 communications. Avec 14 exposés, le jeu de données I a été le plus populaire chez les participants. Le retraitement des trois jeux de données de sismique réflexion (II-IV) a été le sujet de 15 exposés ; enfin, quatre présentations ont porté sur le décryptage du jeu de données synthétiques V. Le présent rapport renferme 16 des communications présentées. Chacune des communications présentées a été révisée, et a été évaluée au moins deux fois à l'extérieur, notamment par Isa Asudeh, Ron Clowes, Fred Cook, Bob Ellis, Dave Forsyth, Alan Green, Roy Johnson, Carmen Lowe, Bernd Milkereit, Patrick Morel-à-l'Huissier, George Spence et Carl Spencer.

Le comité organisateur tient à remercier monsieur H. Shimamura et madame N. Pavlenkova, respectivement président et vice-présidente de la Commission sur la sismologie à source contrôlée pour leur appui, ainsi que tous les participants qui ont consacré beaucoup de leur temps à cet atelier. Il remercie particulièrement ceux qui ont fourni un effort spécial pour présenter une communication dans la présente publication. L'AISPIT a remboursé les frais de déplacement de certains participants. L'aide et la compétence de Mme Gwen Mason lors de la préparation des sujets de l'atelier et lors de la mise en forme des manuscrits ont été grandement appréciées.

A.G. Green, B. Milkereit, P. Morel-à-l'Huissier et C. Spencer
Division de la géologie du continent,
Commission géologique du Canada, Ottawa, Ontario
Canada, K1A 0Y3

R.M. Ellis, R.M. Clowes
Departement de géophysique et d'astronomie,
Université de la Colombie-Britannique
Vancouver, C.-B. Canada, V6T 1W5

J. Ansorge
Institut de géophysique
ETH-Hoenggerberg, Zurich, Suisse, CH-8093

Crustal studies across Vancouver Island and adjacent offshore margin

A.G. Green[1], R.M. Clowes[2] and R.M. Ellis[2]

Green, A.G., Clowes, R.M., and Ellis, R.M., Crustal Studies across Vancouver Island and adjacent offshore margin; in Studies of Laterally Heterogeneous Structures Using Seismic Refraction and Reflection Data, ed. A.G. Green; Geological Survey of Canada, Paper 89-13, p. 3-25, 1990.

Abstract

In an attempt to delineate structures associated with ancient terrane accretion and active plate convergence along the west coast of North America, a number of geophysical and geological surveys have been conducted across Vancouver Island and the adjacent offshore continental margin. Early models based on gravity data and other information have been tested and refined by COCRUST using refraction methods, and by LITHOPROBE using multichannel seismic reflection, magnetotelluric, heat flow, seismicity, aeromagnetic and a range of geological/geochemical techniques. A large block of underplated oceanic lithosphere, characterized by anomalously high densities and velocities have been mapped at crustal depths beneath Vancouver Island. The subducting Juan de Fuca oceanic plate lies below the underplated block, with northeasterly dip increasing from about 3° under the offshore accretionary wedge to 10-15° under the northern part of the island.

Résumé

Un certain nombre de levés géophysiques et géologiques ont été effectués dans l'île de Vancouver et sur la marge continentale océanique adjacente en vue de délimiter les structures associées à l'accrétion ancienne de terrains et à la convergence active de plaques le long de la côte ouest de l'Amérique du Nord. Les premiers modèles fondés sur des données gravimétriques et d'autres renseignements ont été vérifiés, puis perfectionnés par COCRUST au moyen de la méthode de sismique réfraction et par LITHOPROBE au moyen de la sismique réflexion multicanale, de la magnétotellurie, du flux thermique, de la sismicité, de l'aéromagnétisme ainsi que diverses techniques géologiques et géochimiques. Un grand bloc de lithosphère océanique, caractérisé par des densités et des vitesses anormalement élevées, a été cartographié sous la croûte sous l'île de Vancouver. La plaque océanique de Juan de Fuca en subduction active gît sous ce bloc, et son pendage nord-est passe d'environ 3° sous le prisme d'accrétion sous-marin à 10-15° sous la partie nord de l'île.

[1] Continental Geoscience Division, Geological Survey of Canada, Ottawa, Ontario, K1A 0Y3
[2] University of British Columbia, Vancouver, B.C., V6T 2B4

TECTONIC AND GEOLOGICAL SETTING

Much of the North American Cordillera is a collage of accreted blocks or terranes that have been carried thousands of kilometres from their sites of origin. Among the best recognized terranes is the dispersed Wrangellia block, pieces of which are now found in southeast Alaska, the Queen Charlotte Islands, Vancouver Island, and eastern Oregon (Jones et al., 1977). Most of Vancouver Island to the north of the San Juan and Survey Mountain faults belongs to Wrangellia (Fig. 1 and 2). This region consists of a mixture of Paleozoic metavolcanic and metasedimentary rocks of probable island arc origin, an overlying thick plateau of late Triassic submarine to subaerial tholeiitic flood basalts, and a younger island arc igneous complex of Jurassic age (Muller, 1977a, b; Monger and Price, 1979). Paleomagnetic and paleontological data have

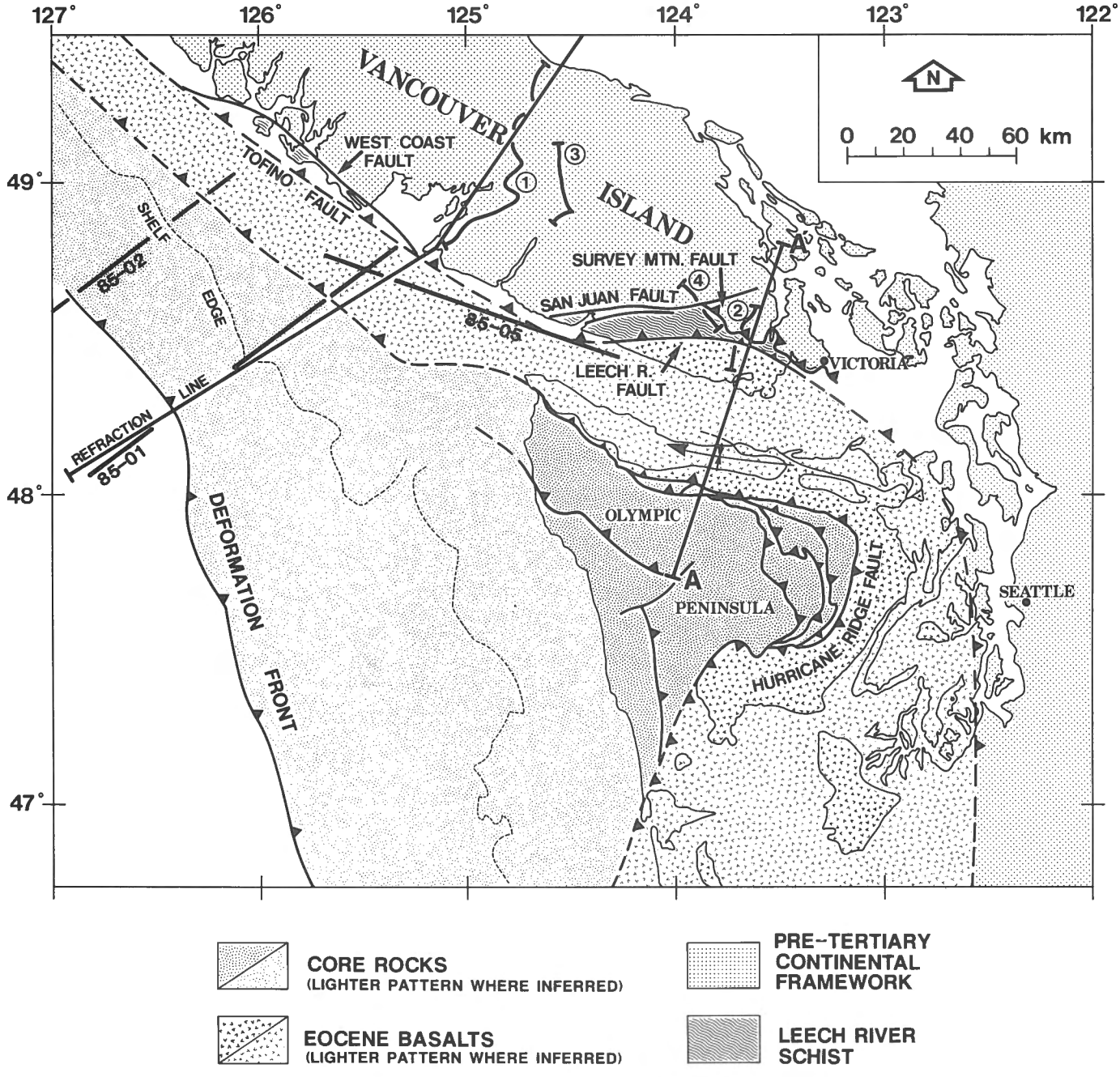

Figure 1. Geological location map of southern Vancouver Island and the Olympic Peninsula of northwest Washington (modified from Clowes et al., 1987a). The circled numbers identify LITHOPROBE seismic reflection profiles 1 to 4 on Vancouver Island, and 85-01, 85-02 and 85-05 are marine seismic reflection profiles. LITHOPROBE land profile 1 and marine profile 85-01 (from Clowes et al., 1987b) were distributed to CCSS workshop participants. Cross-section A-A' is discussed in Clowes et al., 1987a.

demonstrated that in late Triassic times Wrangellia was situated a significant distance to the south of its present position relative to the rest of North America (Yole and Irving, 1980). It has been proposed that Wrangellia was accreted to North America sometime prior to the Tertiary and since then has been fragmented by thrusting and translation along strike-slip faults (Coney et al., 1980). Along northeast Vancouver Island and within the Strait of Georgia, Nanaimo basin sediments of late Cretaceous age overlie the crystalline rocks of Wrangellia (Muller, 1977a, b).

Southeast of Wrangellia, rocks of the Leech River complex are wedged between the San Juan-Survey Mountain fault system and the Leech River fault. The Leech River complex is mostly a mélange of turbidite and minor volcanic rocks of probable late Cretaceous age that were metamorphosed and penetratively deformed during a late Eocene deformational event. Rock units similar to the Leech River complex are observed at a number of locations along the west coast of North America, including the Pacific Rim region of west Vancouver Island (Fig. 1;

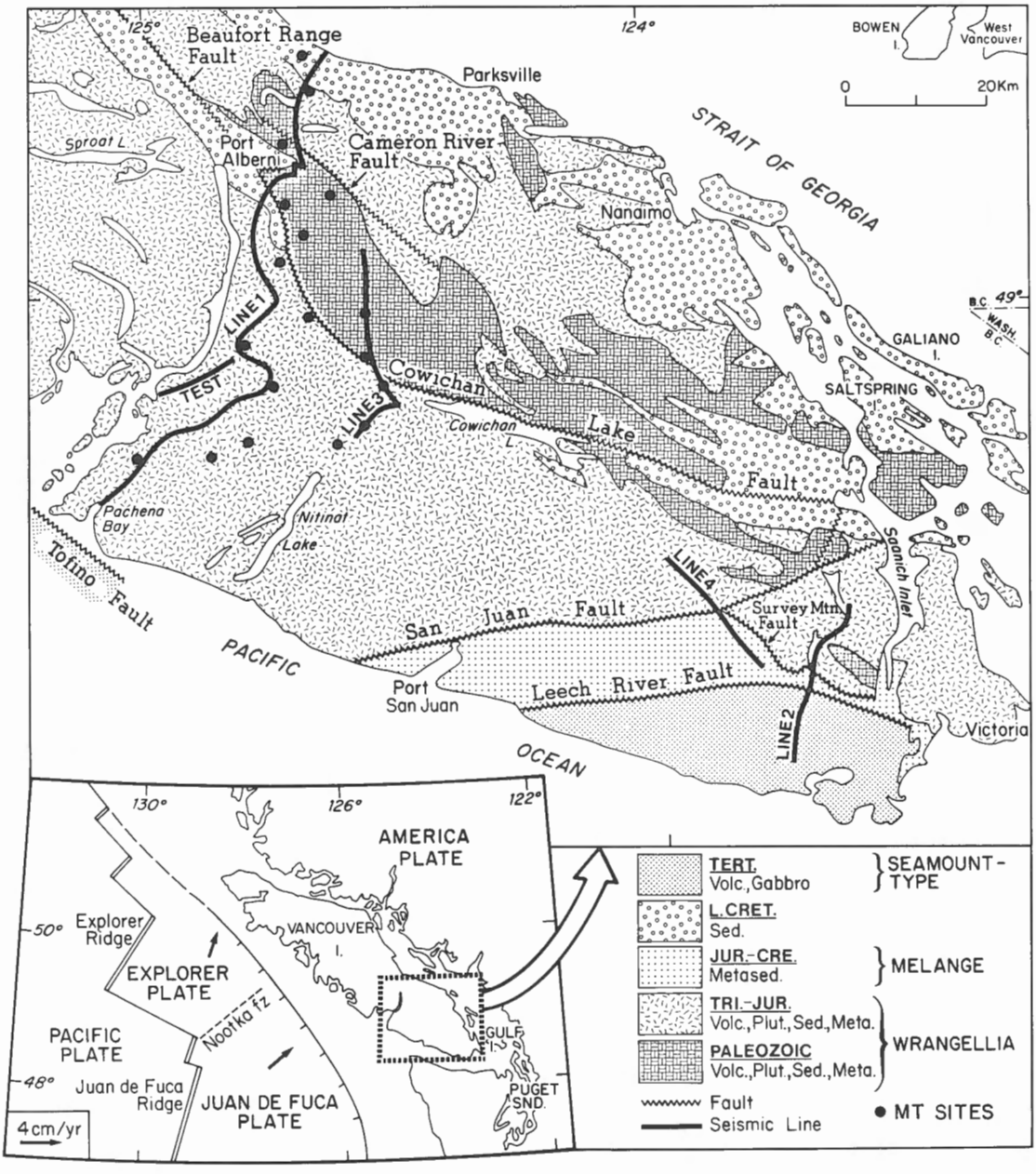

Figure 2. Simplified geological map of southeast Vancouver Island from Green et al. (1986a) showing the locations of the four LITHOPROBE seismic reflection profiles, lines 1 to 4, the short seismic reflection profile, TEST, of Clowes et al., 1983 and the locations of the eighteen magnetotelluric sites from Kurtz et al. (1986). Geology is simplified from Muller et al. (1977b).

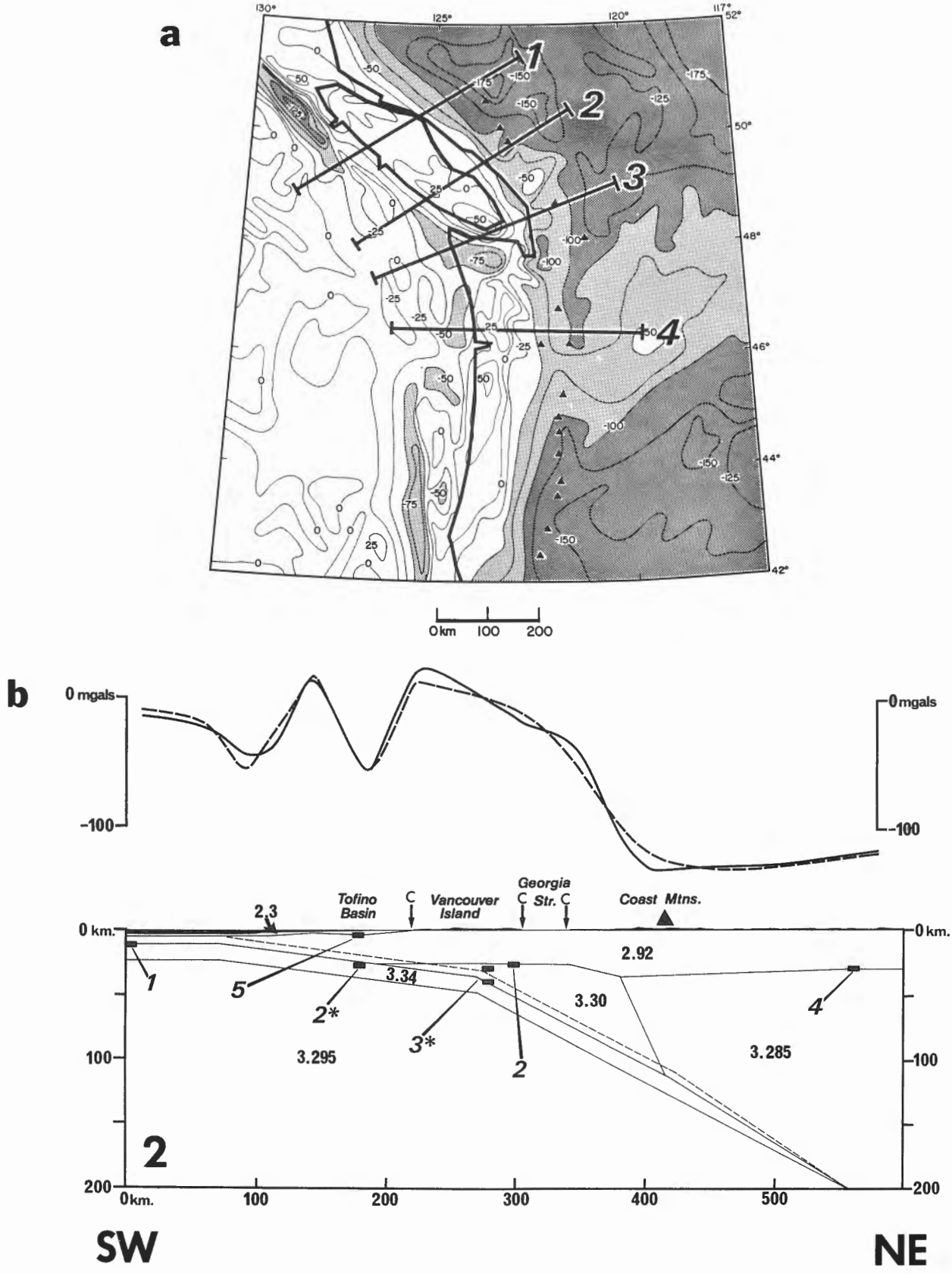

Figure 3. (a) Regional gravity field across Vancouver Island (from Riddihough, 1979). Gravity values are Free Air over the sea and Bouguer over land. (b) Data and model for profile 2 of (a). Solid line shows the observed data and the dashed line shows the model values. Bars are seismic control points from earlier seismic surveys.

Rusmore and Cowan, 1985; Clowes et al., 1987a). The tectonic setting in which rocks of the Leech River complex were deposited has not been firmly established, although Fairchild and Cowan (1982) inferred that they were probably deposited somewhere near to an active island arc, or near to a continental margin with an adjacent transform fault or spreading ridge.

Along the southeast tip of Vancouver Island, Metchosin basalts and associated intrusive rocks are equivalent to the more extensive Crescent formation on the adjacent Olympic Peninsula in the state of Washington (Tabor and Cady, 1978; Muller, 1980; Clowes et al., 1987a). This combined igneous unit has been interpreted as either an island chain (seamount) complex that was accreted to the continental margin in late Eocene times (Duncan, 1982), or a pile of rift material created along an oblique spreading axis in a forearc basin (Clowes et al., 1987a). It is juxtaposed against the Leech River complex along the Leech River fault, and similar Metchosin-type basalts extend into the offshore area west of Vancouver Island (Fig. 1), where they are observed at the base of exploratory wells that penetrate Tertiary sediments of the Tofino basin (Shouldice, 1971; Macleod et al., 1977).

Since the last major phase of terrane amalgamation, tectonism in the Pacific northwest has been dominated by subduction of the Juan de Fuca oceanic plate. Onset of this phase of subduction was marked by the initiation of Cascade arc volcanism (Armstrong, 1979; Robinson et al., 1984), formation of the extensive Tofino-Fuca forearc basin and development of the Core accretionary complex west of the Metchosin-Crescent basalts (Fig. 1; Tabor and Cady, 1978; Clowes et al., 1987a). The inset map of Figure 2 shows the current plate boundaries in this region, together with Riddihough's (1977, 1984) estimates of the convergence vectors. That subduction is still occurring along this margin is demonstrated by the existence of a deep sediment-filled trench (*see* papers in the supplementary reference list: Offshore Reflection Profiling), intense compressional deformation of the continental slope (Silver, 1981; Barr, 1974), continued activity of the inland andesitic volcanoes (Dickinson, 1976), paired (low/high) heat flow and gravity anomalies (Riddihough, 1979; Lewis et al., 1988), active onshore deformation (Savage et al., 1981; Riddihough, 1982; Adams, 1984), onshore crustal earthquakes with compressional axes parallel to the direction of plate convergence (Weaver and Smith, 1983), sinistral strike-slip earthquakes along the Nootka fault (Fig. 2; Rogers, 1979) and a well-defined Benioff-Wadati zone (Rogers, 1981; Crosson, 1981; Kulm et al., 1984; Taber and Smith, 1985; G. Rogers in Clowes, 1987).

One of the first deep structural models for Vancouver Island was produced by Riddihough in 1979 (Fig. 3). His density model was constructed to satisfy the geophysical information that was available to him at that time, as well as the essential features of an active subduction zone. The geophysical information consisted of the gravity data and a range of early seismic results from deep ocean refraction experiments, industry multichannel seismic surveys and

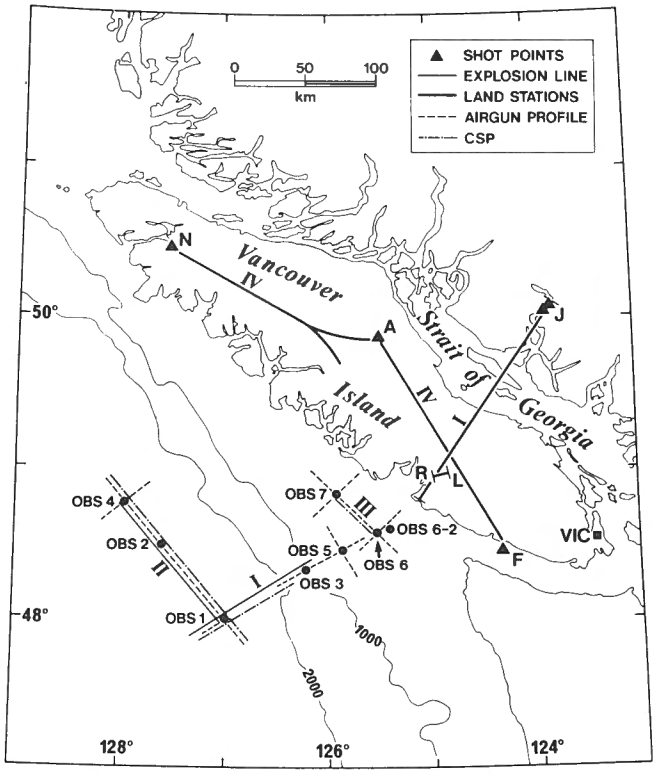

Figure 4. Location map of the four VISP seismic refraction profiles I to IV and related seismic lines.

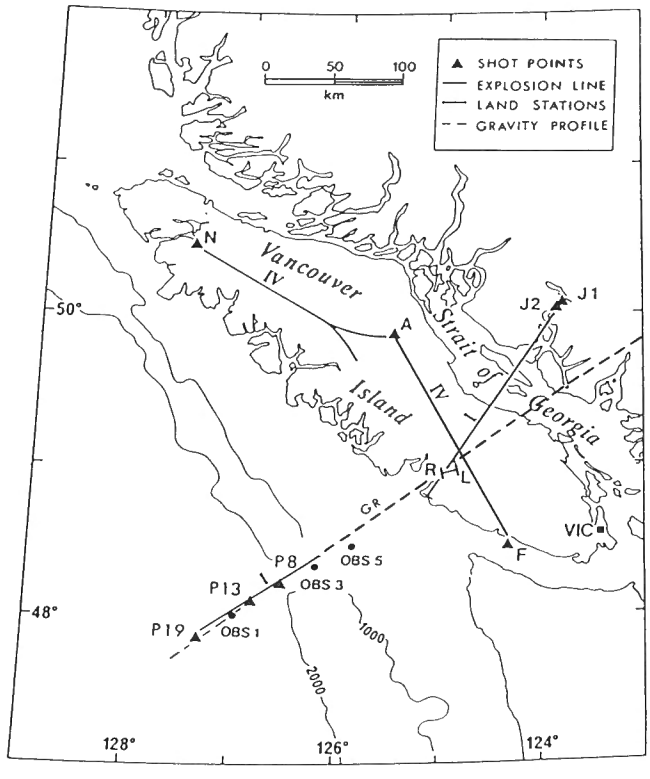

Figure 5. Map showing the location of the two VISP seismic refraction profiles, including appropriate shot point (J1, P8, etc.) and OBS locations, used for the CCSS workshop.

boreholes on the continental shelf, surface wave analyses between onshore seismic stations, and previous land-based refraction experiments. In addition, it was assumed that the deepest earthquake hypocentres at 50-70 km depths would have to lie within the downgoing plate. The features of a subduction zone that were used as constraints comprised a mantle divided into a lithosphere and asthenosphere, a descending oceanic plate that bends downward near the base of the continental slope, and a depth of roughly 100 km to the top of the descending plate adopted in order to be consistent with other active margins and the petrology of lavas associated with the volcanic chain. An important component of Riddihough's model (Fig. 3 ; 1979) is the shallow wedge of high density material beneath Vancouver Island and the Strait of Georgia, which is required to explain the high amplitude positive gravity anomaly across that region.

VANCOUVER ISLAND SEISMIC PROJECT (VISP)

In 1980, COCRUST conducted the Vancouver Island Seismic Project (VISP), a series of large-scale seismic refraction and reflection surveys that utilized both land-based and ocean bottom seismographs (OBSs) with explosive and airgun sources (Fig. 4). Complete details of the 1980 refraction and reflection programs can be found in Ellis and Clowes (1981), Clowes et al. (1983, 1986), Ellis et al. (1983), and Spence et al. (1985). One of the major objectives of VISP was to test and refine the structural model of Riddihough (1979). A brief summary of the most important aspects of the VISP seismic refraction program is outlined below. Results of the short seismic reflection surveys of 1980 (Clowes et al., 1983) have largely been superceded by the results of the 1984 LITHOPROBE program and will not be discussed further here.

The refraction program consisted of the four profiles shown in Figure 4, and the two profiles relevant to the workshop are highlighted in Figure 5. The principal refraction profile, I, extended across Vancouver Island from near the volcanic arc to the deep ocean, and profile IV was shot along the length of Vancouver Island approximately parallel to the continental margin. For profile I, up to 32 land seismographs were deployed along a 160 km recording line on Vancouver Island, on islands in the Strait of Georgia, and on the British Columbia mainland. In addition, four OBSs were deployed in the offshore region, although only data from the three OBSs shown in Figure 5 are of concern here. Two 825 kg shots (J1 and J2), separated by approximately 7 km, were detonated at the eastern end of the profile, and 17 shots with charges ranging from 200 to 825 kg, designated the P series, were fired over the continental slope and ocean basin into the land and marine detectors. The section recorded from shot point J1 and the three sections from western shot points P8, P13 and P19 were distributed for the workshop. These

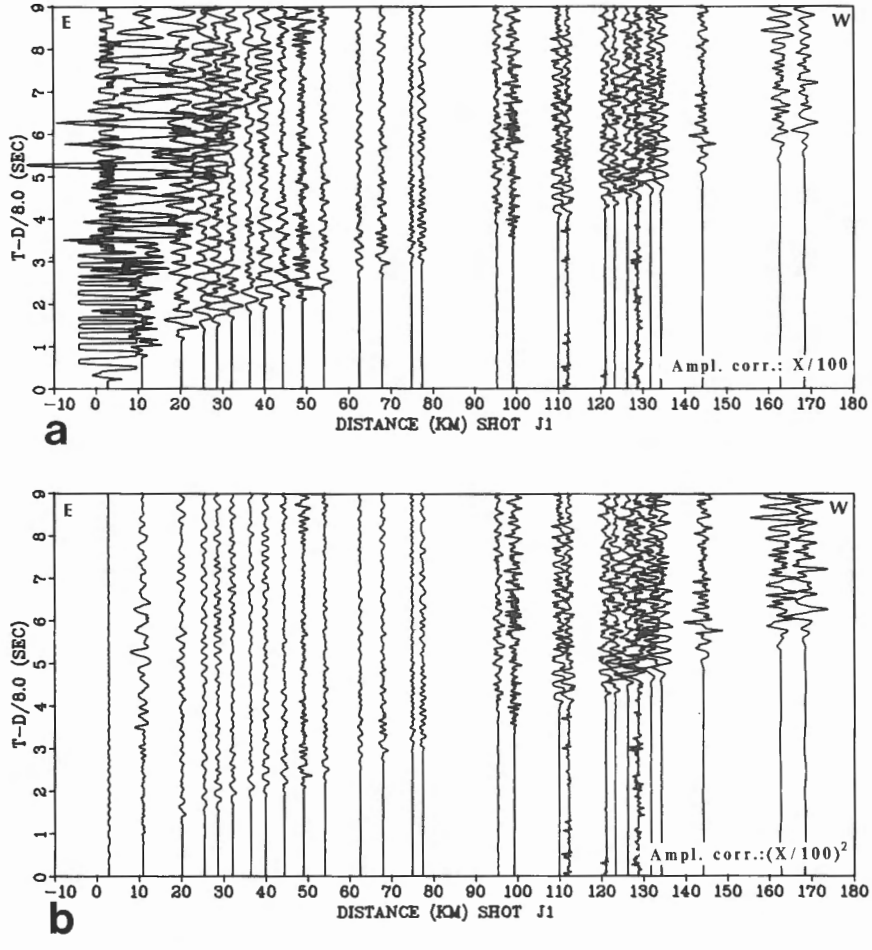

Figure 6. Seismic refraction section recorded across Vancouver Island and adjacent regions from shot point J1. (a) is scaled true amplitude times distance and (b) is scaled true amplitude times distance squared. The two displays have been scaled to have the same amplitude at 100 km distance. These sections at approximately three times the scale shown here were distributed to CCSS workshop participants.

sections, which contain most of the information used to constrain the velocity model of Spence et al. (Fig. 13 ; 1985), are shown plotted with two amplitude scaling factors (true amplitude times distance, and true amplitude times distance squared) in Figures 6 to 9.

Eighteen additional 50 kg charges were detonated for recordings on the OBSs alone. Information on OBS 1, shown in Figure 10 (scaling factor of true amplitude times distance squared), was recorded from shots to the northeast, and on OBS 3 (Fig. 11) and OBS 5 (Fig. 12) information from shots to the southwest was recorded ; shots were detonated between and along the extensions of the line defined by P8 to P19 in Figure 5. Finally, a continuous seismic profile (CSP) using a 5-litre airgun was recorded along the marine portion of profile I (published in Ellis et al., 1983), and a 32-litre airgun was fired along profiles over each OBS, to determine sedimentary structure, basement depths and upper crustal structure (an example of a 32-litre airgun section is given in Ellis et al., 1983).

Previous interpretations of various parts of the refraction data set, mostly based on two-dimensional ray tracing and synthetic seismogram analyses, are included in Ellis et al. (1983), McMechan and Spence (1983), Spence (1984), Waldron (1982), Spence et al. (1985) and Clowes et al. (1986). A velocity structure model that summarizes the important results of studies of profile I is shown in Figure 13a, and a stylized tectonic model that accounts for the seismic refraction information and various geological and other geophysical data is shown in Figure 13b (Monger et al., 1985). An important control for the interpretation of the cross-island profile I was obtained from the two-dimensional interpretation of the along-island profile IV

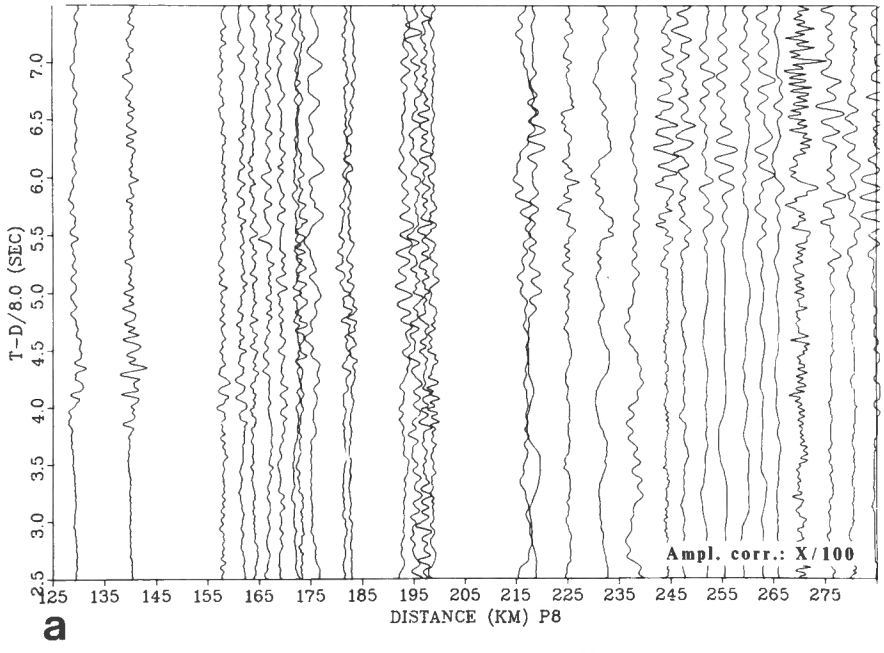

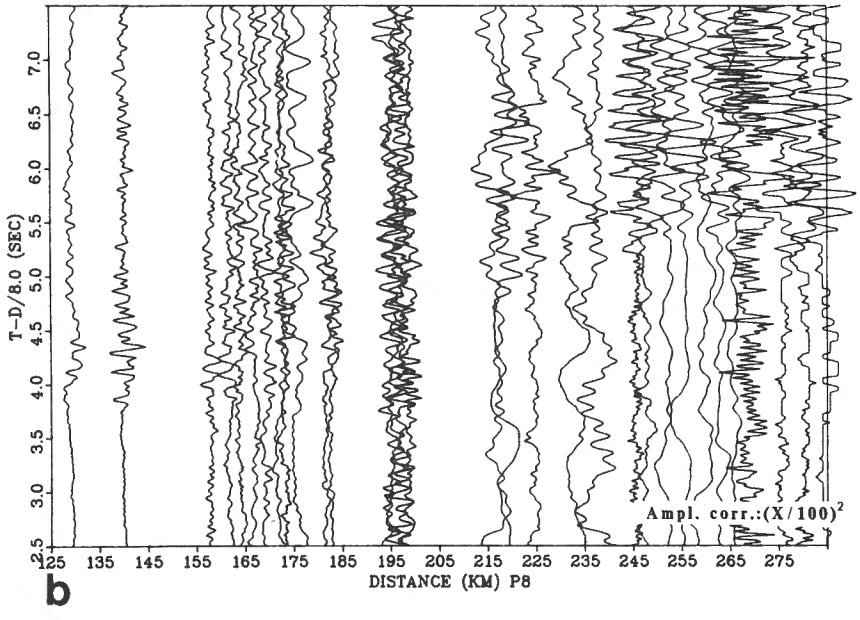

Figure 7. Seismic refraction section recorded across Vancouver Island and adjacent regions from shot point P8. (a) is scaled true amplitude times distance and (b) is scaled true amplitude times distance squared. These sections at approximately three times the scale shown here were distributed to CCSS workshop participants.

by McMechan and Spence (1983). This provided a crustal velocity model for the region near the intersection of the two profiles. To a depth of roughly 20 km the McMechan and Spence (1983) model is relatively well-constrained, but lower crustal structure is not resolved. McMechan and Spence's preferred model contained a low velocity zone throughout the lower crust and an upper mantle velocity of 7.5 km/s at 37 km depth.

In broad agreement with Riddihough's model (Fig. 3 ; 1979), Figure 13 shows the Juan de Fuca oceanic plate dipping eastwards at shallow angles (about 3° to roughly 15°). According to Spence et al. (1985) the depth and attitude of the subducting plate are only weakly constrained by the onshore-offshore seismic refraction data. Wrangellia and terranes to the east are represented by a mixture of material with velocities between 5.4 and 6.95 km/s. An anomalous feature of this particular model is a segment of high velocity material (7.7 km/s) above the downgoing plate in the depth range 20 to 25 km. McMechan and Spence (1983) concluded that a similar block of high velocity material was required at about 20 km depth beneath parts of profile IV. These regions of high velocity material in the middle crust are in the same general depth range as the block of anomalously high density material required by Riddihough's model (Fig. 3 ; 1979), and indeed Spence et al. (1985) have shown that with minor modifications the structural model of Figure 13 is consistent with the regional gravity data. Spence et al. (1985) have speculated that the high velocity-high density material may represent the remnants of a subducted slab, perhaps detached when the

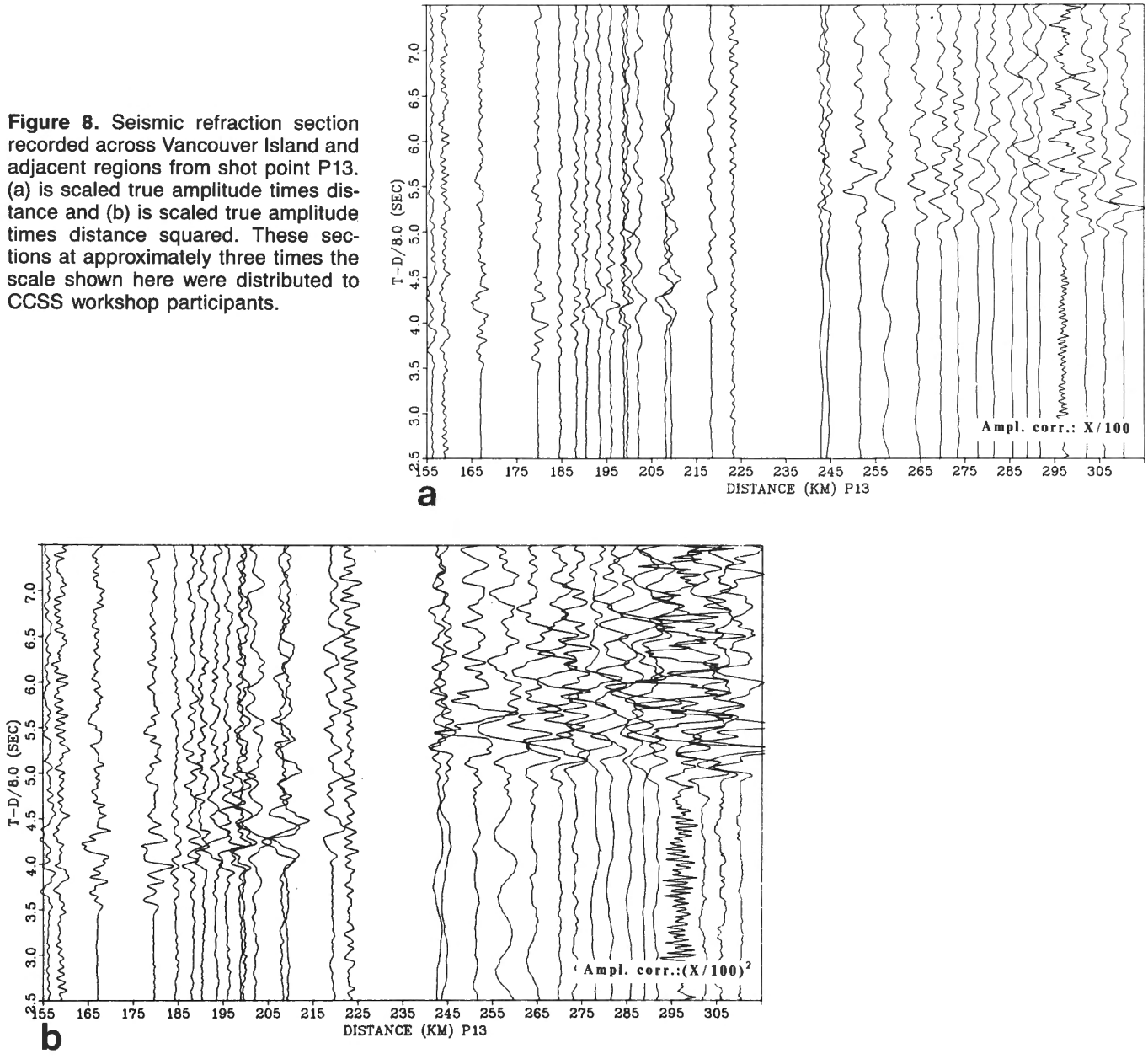

Figure 8. Seismic refraction section recorded across Vancouver Island and adjacent regions from shot point P13. (a) is scaled true amplitude times distance and (b) is scaled true amplitude times distance squared. These sections at approximately three times the scale shown here were distributed to CCSS workshop participants.

subduction zone moved westwards to its present position (*see* also Clowes et al., 1984, 1987a, and Green et al., 1986a, b). Included in the tectonic model of Figure 13b is the speculative concept that assemblages corresponding to older terranes are vertically stacked and are underlain by the descending Juan de Fuca plate.

LITHOPROBE

Seismic work continued on Vancouver Island in 1984 under the auspices of LITHOPROBE. A total of 205 km of deep seismic reflection data were recorded along the four profiles shown in Figure 2. Recording and processing parameters used to produce the Veritas stacked section of Figure 14 are reproduced from Green et al. (1985) in Tables 1 and 2. An F-K migrated version of Figure 14 is shown in Figure 15. Interpretations of various aspects of these data are included in Yorath et al. (1985a, b), Clowes et al. (1984, 1986, 1987a), and Green et al. (1986a, b, 1987).

Profile 1 crosses the width of the island and is almost coincident with the gravity profile of Figure 3 (Riddihough, 1979) and the onshore-offshore seismic refraction profile I of Figures 4 to 13. The primary objectives of this profile were to image the anomalous block of high velocity-high density material inferred from the seismic refraction and gravity studies, and to map the subducting Juan de Fuca plate as it descended beneath Vancouver Island. Some three-dimensional control on the interpretation of profile 1

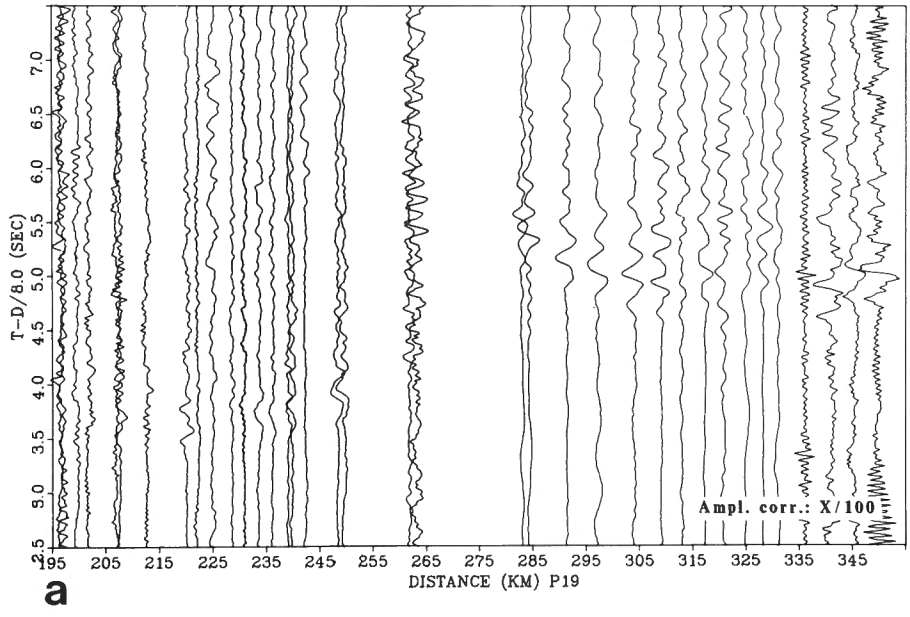

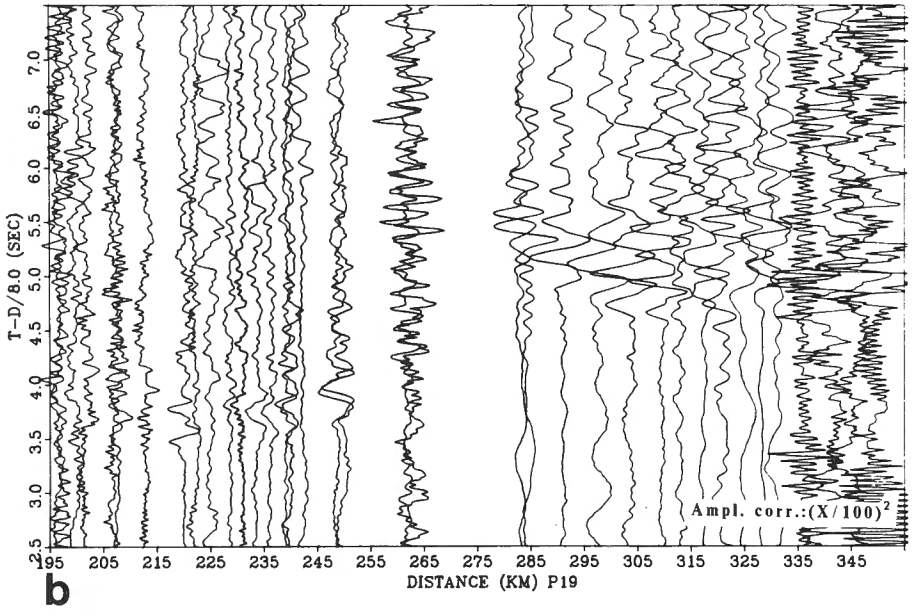

Figure 9. Seismic refraction section recorded across Vancouver Island and adjacent regions from shot point P19. (a) is scaled true amplitude times distance and (b) is scaled true amplitude times distance squared. These sections at approximately three times the scale shown here were distributed to CCSS workshop participants.

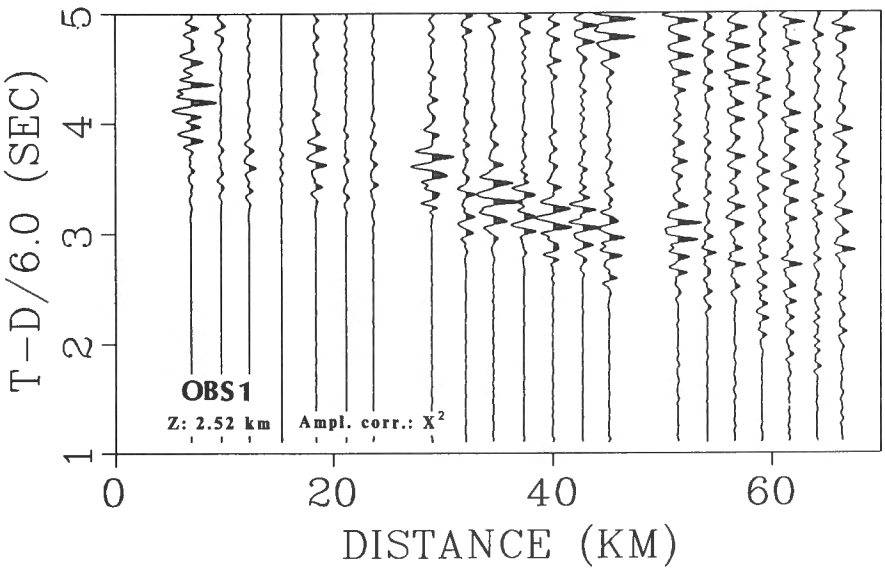

Figure 10. Seismic refraction section recorded at OBS 1. Shot points lie northeast of the instrument. Scaled true amplitude times distance squared. This section at approximately three times the scale shown here was distributed to CCSS workshop participants.

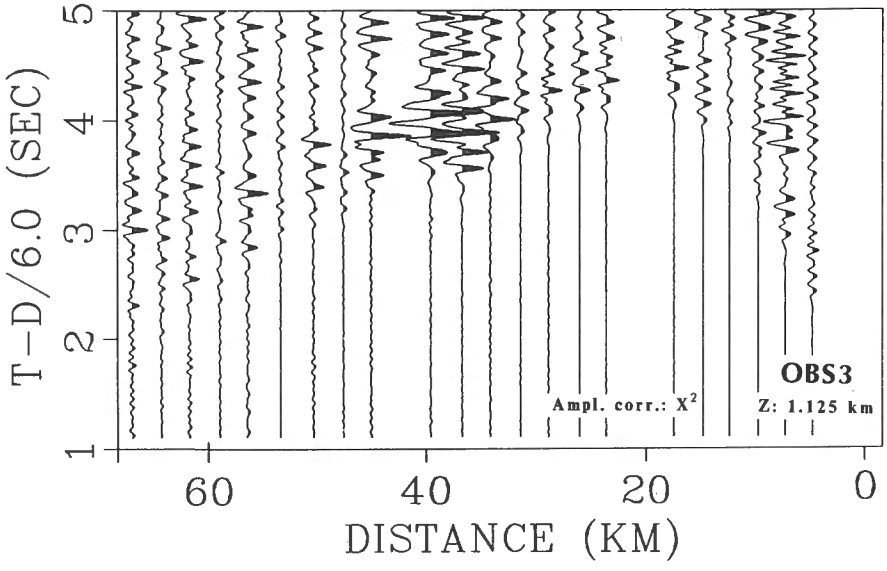

Figure 11. Seismic refraction section recorded at OBS 3. Shot points lie southwest of the instrument. Scale true amplitude times distance squared. This section at approximately three times the scale shown here was distributed to CCSS workshop participants.

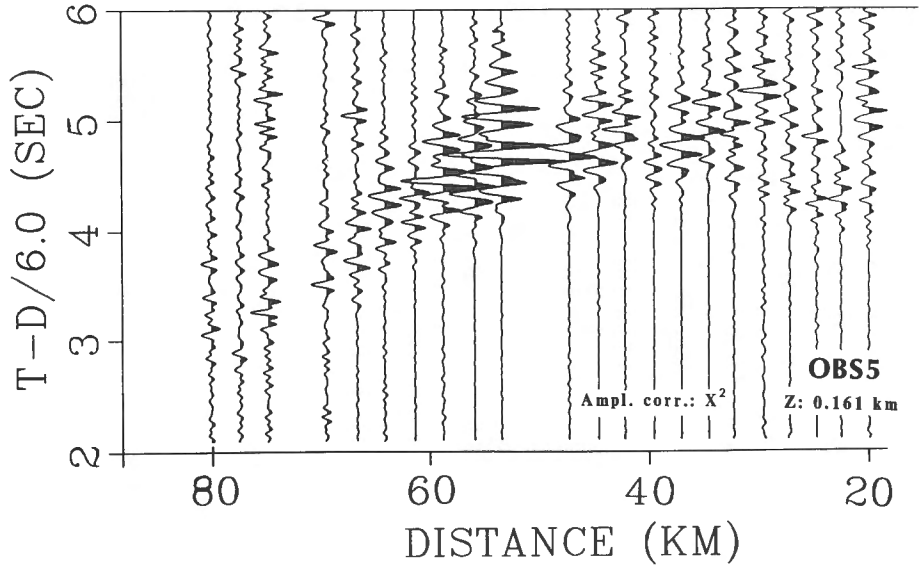

Figure 12. Seismic refraction section recorded at OBS 5. Shot points lie southwest of the instrument. Scaled true amplitude times distance squared. This section at approximately three times the scale shown here was distributed to CCSS workshop participants.

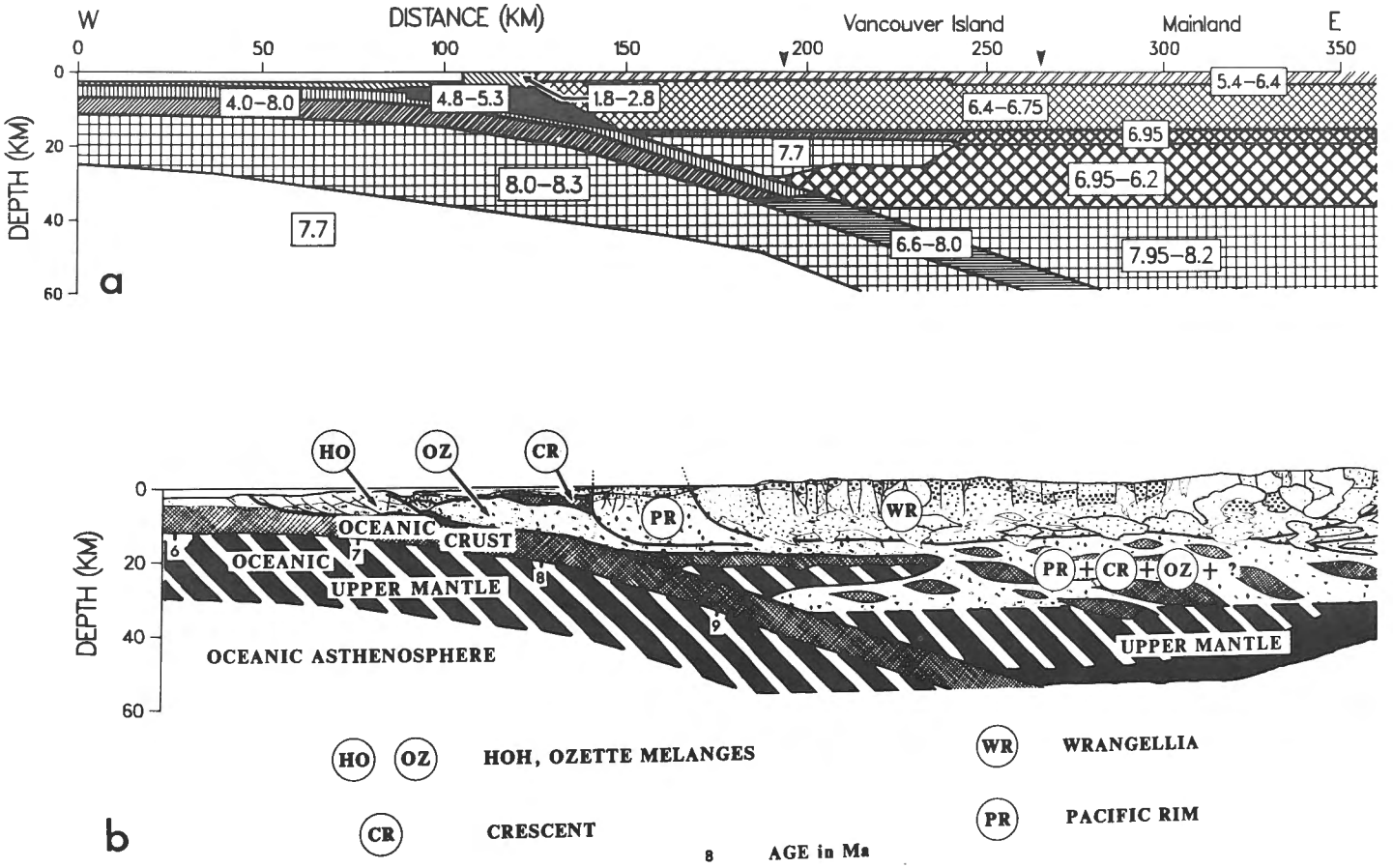

Figure 13. (a) Generalized seismic velocity model for VISP refraction line I; details of all the blocks included in the modeling are not shown here (*see* Spence et al., 1985 for this information). Numbers are velocities (km/s) at the top and bottom of blocks distinguished by shading. Vancouver Island lies between the arrow heads. (b) Stylized tectonic cross-section modified from the Continent-Ocean Transect B2 (Monger et al., 1985). These cross-sections predate the acquisition of the LITHOPROBE seismic reflection data and its interpretation. No vertical exaggeration.

Table 1. Field parameters for the land seismic reflection survey

Receiver information	
Geophone group interval	— 90 m
Geophone configuration	— 18 at 5.3 m
Geophone type	— Mark products L15, 8 Hz
Recording instrument	— DFS *V*, 120 channels with auxiliary stacker, correlator and noise reject systems
Field filter	— 0-64 Hz (notch out)
Gain mode	— independent floating point
Sample interval	— 4 ms
Record length (after correlation)	— 16 s
Source information	
Source interval	— 180 m
Source layout	— 4 vibrators at 40 m
Source type	— Mertz model 18 vibrators (peak force 20,000 kg per vibrator) with Pelton electronics
Sweep frequency	— 8-40 Hz (linear)
Sweep fength	— 16 s
Coverage	— 3000 %
	1 30 x 31 120
Spread layout	2880 — 270 270 — 8280 m

Roll-on and roll-off at each end of line (on some lines the roll-on and/or roll-off was achieved more rapidly by vibrating at a 90 m interval instead of the regular 180 m interval).

Table 2. Processing parameters for the land seismic reflection survey

DEMULTIPLEX (sample rate 4 ms)
AMPLITUDE RECOVERY AND ADJUSTMENT (apply exponential gain)
CROOKED LINE GEOMETRY
AUTOMATIC GAIN CONTROL (200 ms window)
INDIVIDUAL TRACE EDIT
COMMON REFLECTION POINT TRACE GATHER
FIRST BREAK MUTES x = 1620, 3780, 5670, 10,800 m
t = 500, 1200, 1900, 3,000 ms
VELOCITY ANALYSIS
NORMAL MOVEOUT CORRECTIONS
ELEVATION STATIC CORRECTIONS (datum — sea level, replacement velocity 5000 m/s)
TRIM STATICS (correlation window 1000-12000 ms)
COMMON REFLECTION POINT STACK
DIGITAL FILTER (bandpass (5/8 — 40/45 Hz))
TRACE-TO-TRACE AMPLITUDE EQUALISATION (4000-8000 ms window)
PLOT (36 traces/", 1.875 "/s)

was available from reflection profile 3 located 15 to 20 km to the east and from the short reflection test line collected during the 1980 VISP program (TEST in Fig. 2 ; Clowes et al., 1983). The two southeast profiles were designed to determine the depth extents and attitudes of the terrane-bounding San Juan, Survey Mountain and Leech River faults.

Line drawings based on the four LITHOPROBE seismic reflection profiles are shown in Figure 16. The very prominent reflection zones, C and E in Figures 15 and 16, are observed on all seismic reflection sections. They underlie most of southeastern Vancouver Island including the youngest allochthonous terranes along the southeast tip of the island. Both reflection zones dip northeast, parallel to the direction of convergence between the Juan de Fuca and North American plates. Other important features on the seismic section include the reflections from the Leech River, Survey Mountain and Tofino faults. Detailed discussions of these aspects of the seismic sections can be found in Green et al. (1986a, b, 1987), Clowes et al. (1987a), Milkereit (1987a, b), and Mayrand et al. (1987).

At its shallowest location, beneath the south end of profile 1, the top of reflection zone C is at a depth of about 11 km (based on migrated travel times and velocities determined from the refraction data) and its deepest location, beneath the north end of profile 3, it is at a depth of approximately 20 km. Reflection zone C is therefore coincident with the top of the high velocity-high density block of material in the Spence et al. (1985) structural model (Fig. 13). In accord with the suggestion of Spence et al. (1985), reflection zone C and the region immediately below it have been interpreted as tectonically underplated and somewhat deformed oceanic lithosphere (Yorath et al., 1985b ; Clowes et al., 1986, 1987a ; Green et al., 1986a, b, 1987).

Reflection zone E lies at a depth of roughly 23 km beneath the south end of profile 1 and is deepest at approximately 34 km beneath the north-central region of the island. Its overall dip in the vicinity of profile 1 is northeast at an angle of 9-13°. Figure 16 shows that the depth to zone E is somewhat less than the depth to the active subduction zone of the Spence et al. (1985) seismic refraction model, but its depth and attitude match well Riddihough's (1979) estimates for the top of the subduction zone. Toward the north end of profile 1 there is some evidence for an increase in the dip of reflection zone E. It is near this location that the subducting plate in Riddihough's density model (Fig. 3 ; Riddihough, 1979) begins to plunge more steeply into the mantle. Such a feature is quite common in other subduction zones and is consistent with the steeply dipping slab of high velocity material required to explain the pattern of travel time anomalies to the northeast of Puget Sound (McKenzie and Julian, 1971).

A comprehensive discussion of the possible nature of reflection zones C and E will not be given here. Instead, the reader is referred to Yorath et al. (1985b), Clowes et al. (1987a), Green et al. (1986b, 1987), Clowes (1987) and Hyndman (1988). However, there is a variety of other geophysical data that should be considered in any assessment of the results of CCSS data set I. Information from seismic networks in British Columbia and Washington has been used to delineate an undulating Benioff-Wadati zone that is best defined beneath Puget Sound, the Olympic Peninsula and the Gulf Islands (Fig. 17 ; Rogers, 1981 ; Crosson, 1981 ; Taber and Smith, 1985), but which can also be traced beneath south-central Vancouver Island (G. Rogers in Clowes, 1987). In the Puget Sound region the

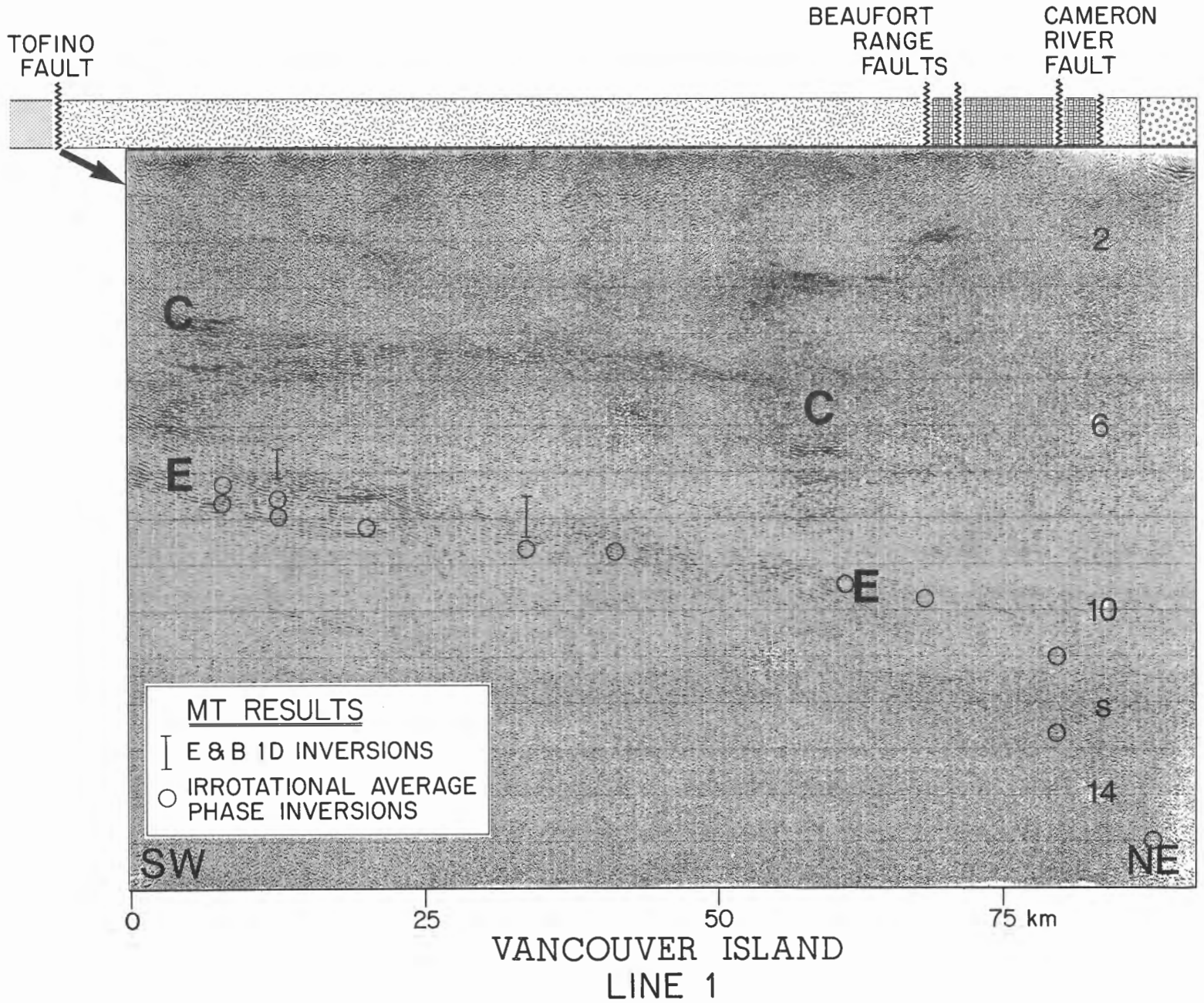

Figure 15. Migrated seismic reflection section and one-dimensional inversions of magnetotelluric data recorded along LITHOPROBE profile 1 (from Green et al., 1987). Patterns at the top of the section show the surface geology crossed ; an explanation of the various patterns is given in the legend of the location map of Figure 2.

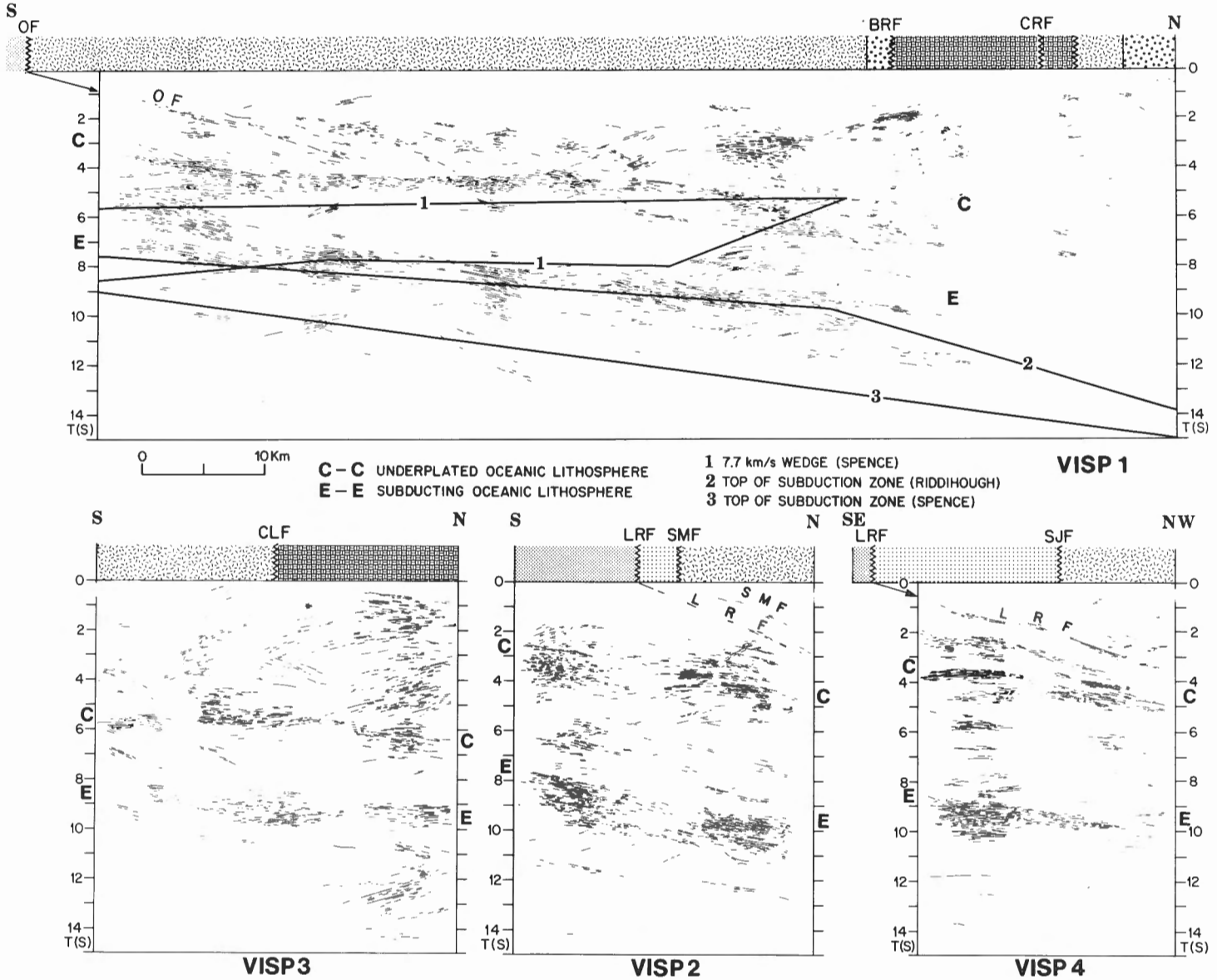

Figure 16. Line diagrams showing the unmigrated reflections recorded on the four LITHOPROBE seismic reflection profiles. Vertical scale is two-way travel time in seconds (from Green et al., 1986a). Patterns at the top of the section show the surface geology crossed ; an explanation of the various patterns is given in the legend of the location map of Figure 2. On the profile 1 section the -1- border delineates the high velocity-high density block identified by Spence et al. (1985), and the -2- and -3- boundaries show, respectively, the Riddihough (1979) and Spence et al. (1985) estimates for the top of the subducting Juan de Fuca plate. BRF — Beaufort Range fault, CRF — Cameron River fault, CLF — Cowichan Lake Fault, LRF — Leech River fault, OF — Tofino fault, SMF — Survey Mountain fault, SJF — San Juan fault (locations of these faults are shown in Fig. 2).

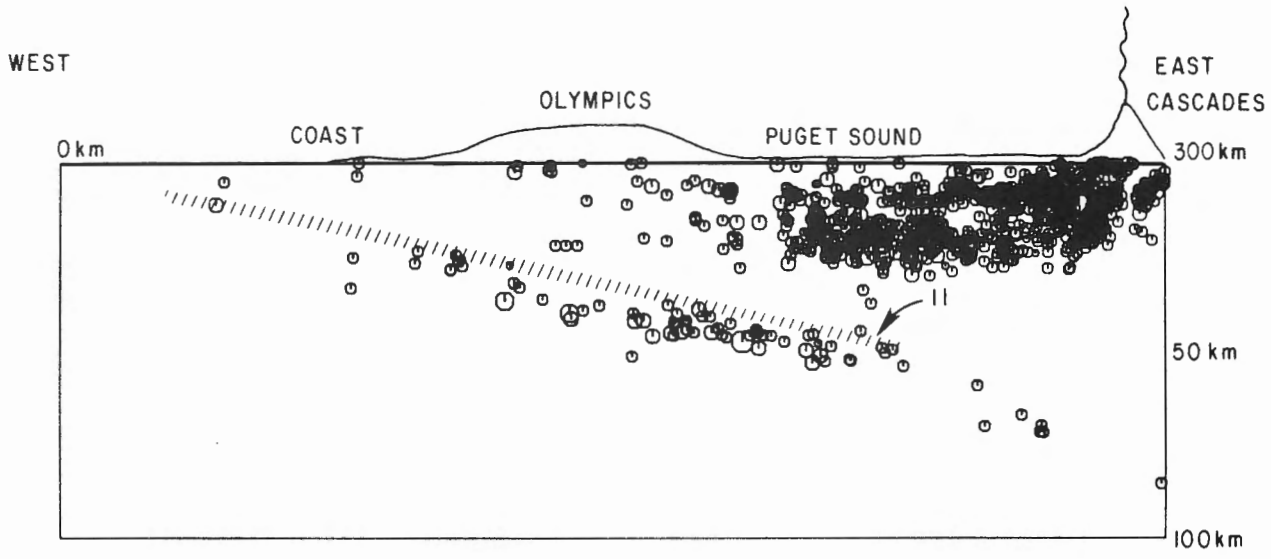

Figure 17. Cross-section of seismicity observed beneath the state of Washington from Taber and Smith (1985).

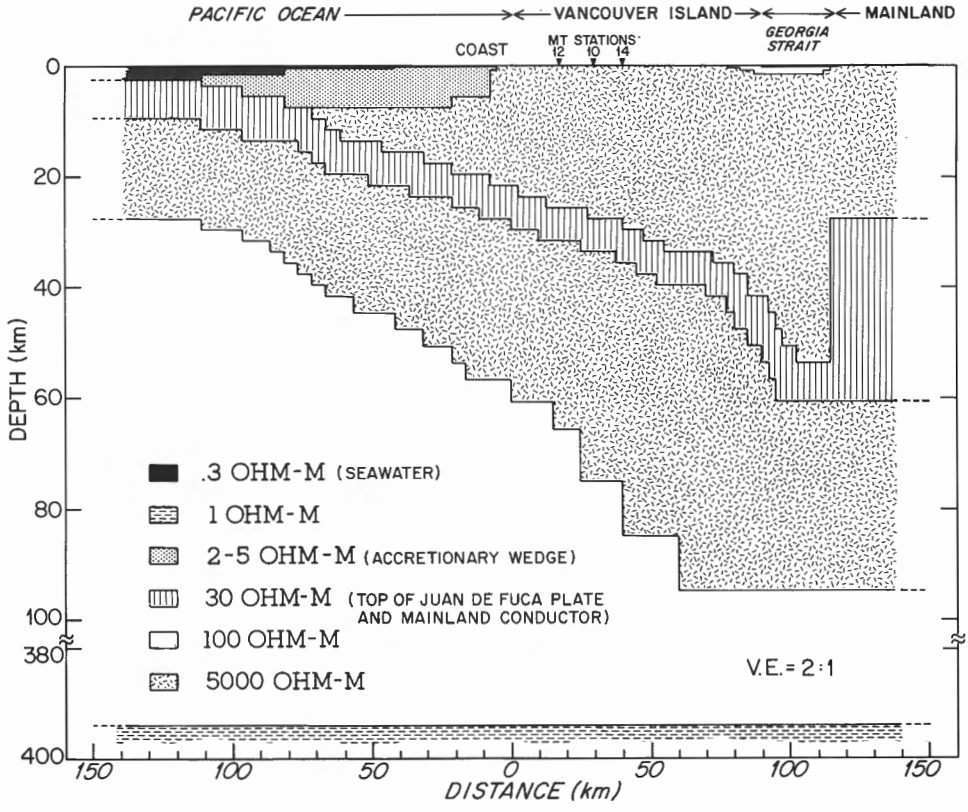

Figure 18. Two-dimensional electrical resistivity model representing the subducting Juan de Fuca plate (from Kurtz et al., 1986). The conductor that is closely associated with the E reflection (30 ohm.m) is near the top of the plate. The bold horizontal bars beneath sites 10, 12 and 14 indicate the depths to the E reflection horizon. Location of the recording profile is given in Figure 2.

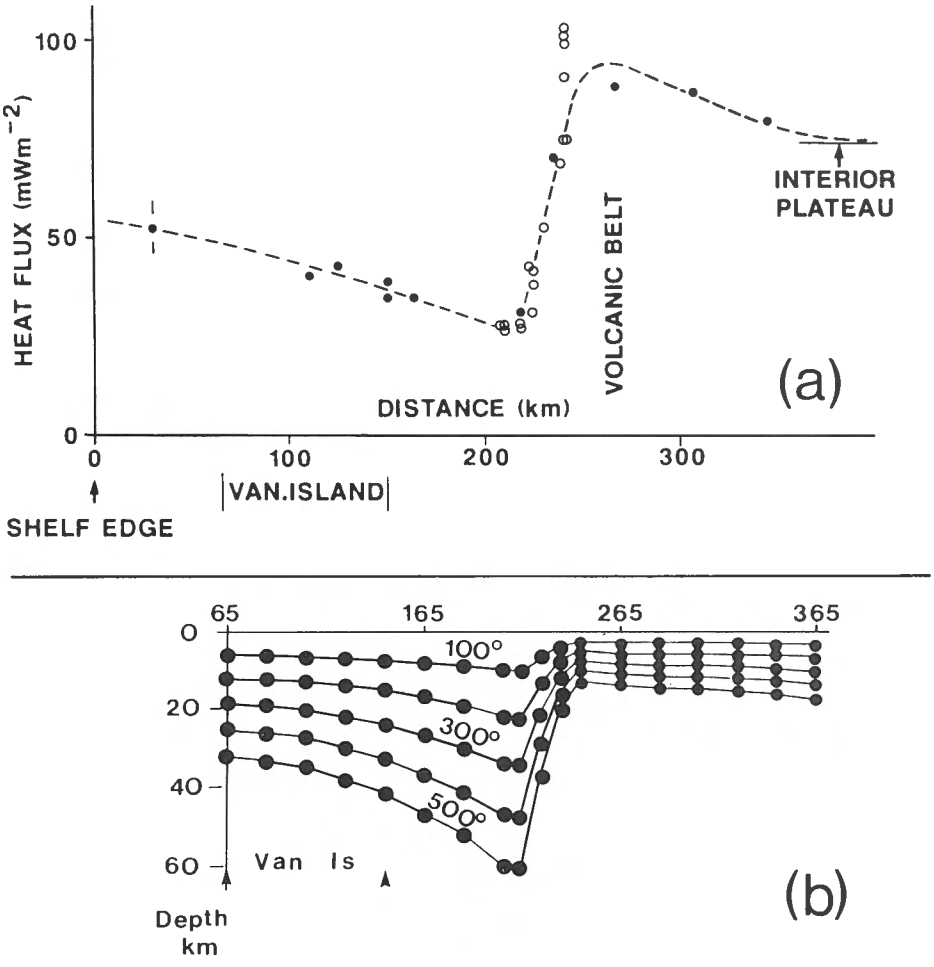

Figure 19. (a) Heat flow extending from the continental shelf, approximately coincident with the VISP onshore-offshore seismic refraction profile I, to the interior plateau (Lewis et al., 1988). A very large increase in heat flow occurs about 30 km west of the volcanic belt. It coincides roughly with a high electrical conductivity block required by the magnetotelluric data (Fig. 18). (b) Isotherms computed from the heat flow data.

Table 3. Field parameters for the marine seismic reflection survey

Receiver information	
Hydrophone group interval	— 25 m
Hydrophone configuration	— 15 at 1.66 m
Hydrophone type	— T.I. acceleration cancelling
Cable length/average depth	— 3017 m/16 m
Recording instrument	— DFS V
Field filter	— 3-64 Hz
Gain mode	— independent floating point
Sample interval	— 4 ms
Record length	— 16 s
Source information	
Source interval	— 50 m
Source type	— tuned airgun array (4 elements), 6110 cu"/2000 P.S.I.
	— 50 guns/51.2 ms delay
Average source depth	— 12 m
Coverage	— 3000 %
Spread layout	X 1 120 m 290 3307 m

Table 4. Processing parameters for the marine reflection survey

DEMULTIPLEX
RESAMPLE (4 ms to 8 ms)
TRUE AMPLITUDE RECOVERY
PRE-DECONVOLUTION MUTE (first breaks)
VELOCITY FILTER IN SHOT DOMAIN (-4 to 12 ms/traces)
DESIGNATURE IN SHOT DOMAIN
TRACE EQUALIZATION
DEMULTIPLE (Shots 101-926) — water bottom and pegleg multiple attenuation
DECONVOLUTION (Shots 927-2877) — 1 x 400 ms operator, Gap — ZW, Datum = water bottom
VELOCITY ANALYSIS
NORMAL MOVEOUT CORRECTIONS
TRACE MUTE
COMMON REFLECTION POINT STACK
DECONVOLUTION — 1 x ZW2 operator, Gap = ZW
Autocorr start/end = 50/16000 ms
Datum = water bottom
DIPFILT (-5 to 5 ms/trace)
MIGRATION (Kirchoff — 30°)
TIME/SPACE VARIANT FILTER (3/7 — 28/23 at OS)
TIME/SPACE VARIANT DISPLAY GAIN
EVERY THIRD TRACE DISPLAYED (48 traces/", 1,875 "/s)

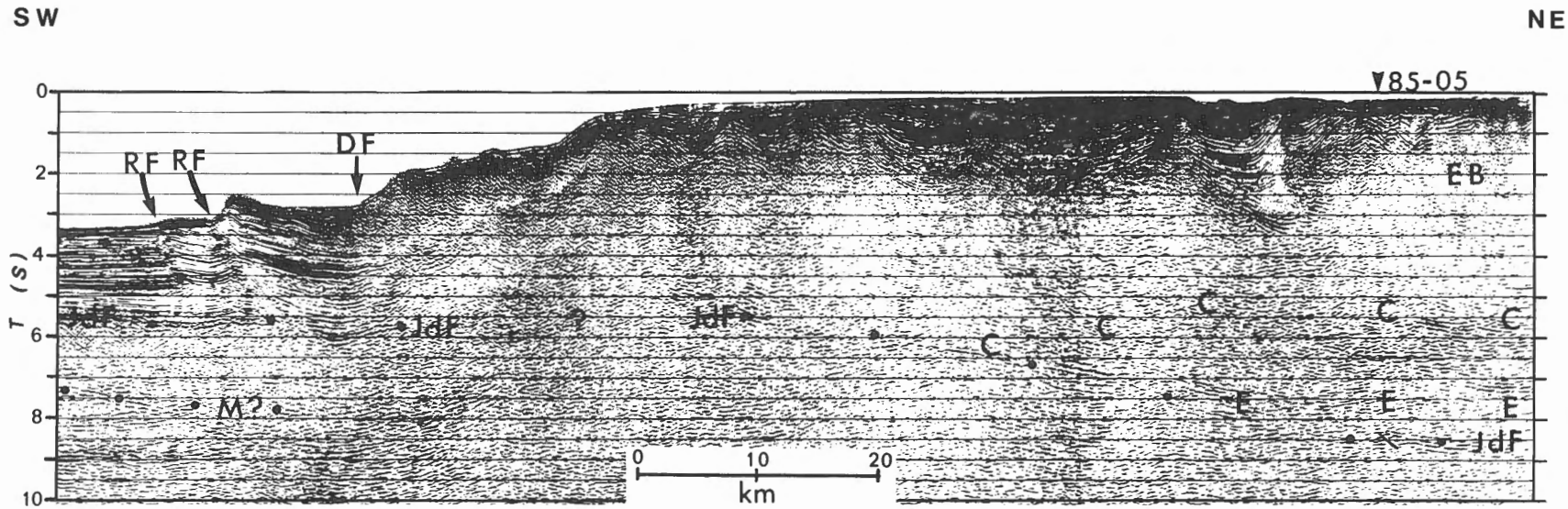

Figure 20. Stacked and migrated seismic reflection section recorded along the offshore seismic reflection profile 85-01. Location of the profile is shown in Figure 1 and details of the acquisition and processing parameters are given in Tables 4 and 5. Vertical scale is two-way travel time in seconds. This section was distributed at four times the scale shown here to CCSS workshop participants.

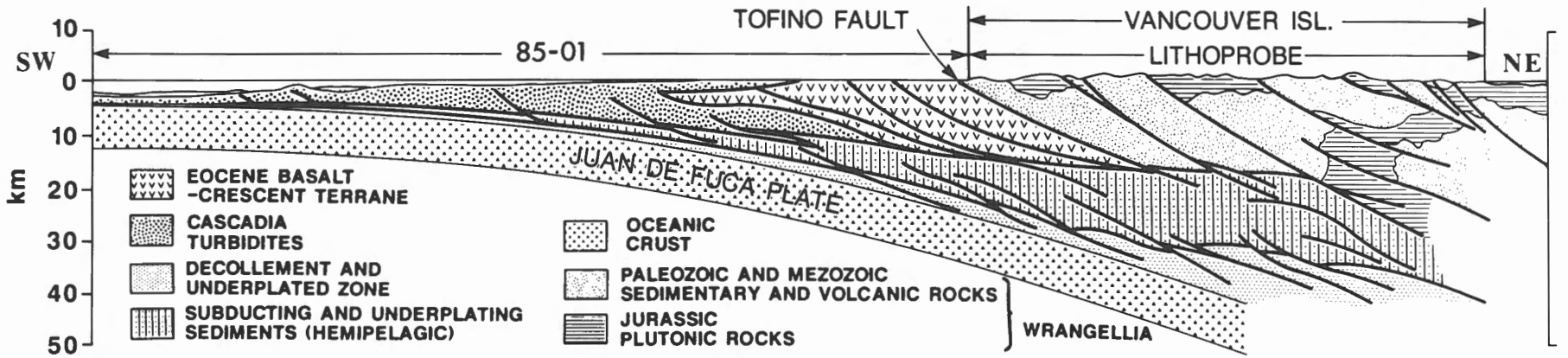

Figure 21. Part of Figure 20 showing the interpretation of Clowes et al. (1987b). RF — ramp fault, DF — deformation front, JdF with dots — top of Juan de Fuca plate, M? with dots — possible oceanic Moho, EB — Eocene basalts, C — upper boundary of high reflectivity band, E -lower boundary of high reflectivity.

zone of seismicity dips eastward at roughly 11°, whereas beneath Vancouver Island it appears to lie 5 to 10 km below the E reflection zone and have a steeper dip of approximately 15°. It should be emphasized that the earthquakes detected in this general region are not thrust events between the subducting and overriding plates, but are events that occur within the descending plate.

Kurtz et al. (1986) have collected wideband magnetotelluric (MT) and geomagnetic depth sounding data (GDS) at 18 sites along LITHOPROBE seismic reflection profiles 1 and 3 (Fig. 2). Figure 15 shows the one-dimensional MT inversion results superimposed on the profile 1 seismic reflection section (taken from Green et al., 1987). The bars and circles delineate the top of a major electrical conductivity anomaly (conductance of about 200 S). At two of the sites along profile 1 and one along profile 3, the MT data were nearly isotropic, thus allowing one-dimensional inversions of the **combined** apparent resistivity and phase information. These results are shown by bars in Figure 15. Circles show depth estimates to the conductivity anomaly obtained by constraining the resistivity of the mid-crust to 8000 ohm.m (estimates from the isotropic stations ranged from 5000 to 15000 ohm.m) and inverting the rotationally invariant averages of the phases from **all** stations. Two-dimensional modeling by Kurtz et al. (1986) has confirmed the essential results obtained from the simple one-dimensional approaches. Their model (Fig. 18) explains the important phase information recorded on all stations across the island as well as all geomagnetic transfer functions for periods greater than 0.1 s. It is clear from Figures 15 and 18 that the E reflection zone is closely associated with a region of enhanced electrical conductivity. Kurtz et al. (1986) have suggested that the electrical conductivity estimates near the E reflection zone are compatible with the presence of trapped fluids in a rock matrix with porosity of 1.6 to 3.6 %.

Finally, heat flow measurements compiled by Lewis et al. (1988) reveal a classic low-high heat flow anomaly centred northeast of the Strait of Georgia (Fig. 19). Subsurface temperatures inferred from the heat flow data suggest that under Vancouver Island the 450°C isotherm lies approximately parallel to and between the E reflection zone and Benioff-Wadati zone.

OFFSHORE REFLECTION PROFILES

In 1985, to extend offshore the results of the LITHOPROBE work on Vancouver Island, 520 km of marine seismic reflection data were recorded along five profiles across the western Canada convergent margin (Clowes et al., 1987b). Only one of the profiles, 85-01, was distributed to workshop participants. The location of this profile, which begins 15 km seaward of LITHOPROBE profile 1, is shown in Figure 1 and the migrated seismic section is shown in Figures 20 and 21 (Fig. 20 is contained in the pocket at the back of this volume.) Recording and processing parameters used to produce the GSI stacked and migrated sections of Figures 20 and 21 are given in Tables 4 and 5. The primary navigation control system, based on Loran C and supplemented by transit satellite, initiated the shots at 50 m intervals.

A preliminary interpretation of marine profile 85-01 is shown in Figure 22 from Clowes et al. (1987b). These authors interpret the reflection marked JdF in Figure 21 as the top of the Juan de Fuca plate beneath the oceanic basin and the lower slope. Although this reflection is lost beneath much of the slope, it seems to reappear below the innermost slope and can then be followed for about 70 km beneath the shelf. Similar events are observed on the two other seismic reflection profiles recorded in this region, 85-02 and 85-05 (Fig. 1). On line 85-05, which ties with 85-01, the event can be followed along its entire 95 km length. Clowes et al. (1987b) suggest that these reflections may correlate with a weak deep reflection at the western end of LITHOPROBE profile 1 and with similar reflections on profiles 2 and 4, which had tentatively been identified previously as the oceanic Moho of the downgoing plate (Clowes et al., 1987a). These new marine data suggest, instead, that the deeper events on the LITHOPROBE profiles may be reflections from the top of the descending slab.

Another prominent feature of the marine data is a band of high reflectivity (C-E on Fig. 21) that starts about 60 km landward of the deformation front and thickens rapidly inland to 2 s, eventually reaching a thickness of 3 s. The C-E band corresponds well with the converging C and E reflection zones observed at the southeast end of LITHOPROBE profile 1 (Fig. 14-16). The new data show clearly that only one thick band of high reflectivity is delineated offshore and that it may be separated from the top of the plate by a narrow zone of lesser reflectivity. Clowes et al. (1987b) outlined briefly some of the implications of these correlations, as well as describing the shallow structure imaged in the offshore data.

CONCLUSIONS

The convergent margin of western Canada, where the Juan de Fuca plate is being subducted beneath the North American plate, is one of the most thoroughly studied subduction zones in the world. As shown by the extensive reference list, the data base includes the results of a wide spectrum of geophysical and geological studies. A recent addition is Sea Mark acoustic imagery of the deformation front at the westward extent of the accretionary prism (Davis and Hyndman, 1989).

As evidenced by the papers in this volume, which deal almost exclusively with seismic data, the tectonic interpretation of this region is not expected to remain static. As an example, Hyndman (1988), following earlier ideas by Jones (1987) and others, has suggested an alternative interpretation of the deep E seismic reflection zone, one based on a non-structural cause — fluids trapped below an impermeable layer formed by precipitates at a metamorphic front!

ACKNOWLEDGMENTS

The onshore-offshore seismic refraction field program was conducted by COCRUST (Consortium for Crustal Reconnaissance Using Seismic Techniques) with participants from the Geological Survey of Canada and the Universities of

Alberta, British Columbia, Manitoba, Saskatchewan, and Western Ontario. Financial support was provided mainly by the Department of Energy, Mines and Resources (EMR) and the Natural Sciences and Engineering Research Council (NSERC). Seismic reflection data were recorded on Vancouver Island as part of LITHOPROBE Phase I, for which funding was received from EMR and an NSERC Collaborative Special Projects grant. Veritas Geophysical and Veritas Seismic of Calgary, Alberta, acquired and processed respectively the Vancouver Island reflection data. The offshore seismic reflection data were acquired as part of the Geological Survey of Canada's Frontier Geoscience Project. Geophysical Services Incorporated (GSI) of Calgary, Alberta, acquired and processed the offshore reflection data. LITHOPROBE publication number 41.

REFERENCES

Adams, J.
1984 : Active deformation of the Pacific northwest continental margin ; Tectonics, v. 3, p. 449-472.

Armstrong, R.L.
1979 : Cenozoic igneous history of the U.S. Cordillera from latitude 42 to 49° north ; *in* Cenozoic Tectonics and Regional Geophysics of the Western Cordillera ; Geophysical Society of America, Memoir, 152, p. 265-282.

Barr, S.
1974 : Structure and tectonics of the continental slope west of southern Vancouver Island ; Canadian Journal of Earth Sciences, v. 11, p. 1187-1199.

Clowes, R.M.
1987 : LITHOPROBE : Exploring the subduction zone of western Canada ; Leading Edge, v. 6, p. 12-19.

Clowes, R.M., Brandon, M.T, Green, A.G., Yorath, C.J., Sutherland Brown, A., Kanasewich, E.R., and Spencer, C.
1987a : LITHOPROBE — southern Vancouver Island : Cenozoic subduction complex imaged by deep seismic reflections ; Canadian Journal of Earth Sciences, v. 24, p. 31-51.

Clowes, R.M., Ellis, R.M., Hajnal, Z., and Jones, I.F.
1983 : Seismic reflections from subducting lithosphere ? ; Nature, v. 303, p. 105-123.

Clowes, R.M., Green, A.G., Yorath, C.J., Kanasewich, E.R., West, G.F., and Garland, G.D.
1984 : LITHOPROBE — a national program for studying the third dimension of geology ; Journal of the Canadian Society of Exploration Geophysicists, v. 20, p. 23-39.

Clowes, R.M., Spence, G.D., Ellis, R.M., and Waldron, D.A.
1986 : Structure of the lithosphere in a young subduction zone : results from reflection and refraction studies ; *in* Reflection Seismology : The Continental Crust ; American Geophysical Union, Geodynamic Series, v. 14, p. 313-312.

Clowes, R.M, Yorath, C.J., and Hyndman, R.D.
1987b : Reflection mapping across the convergent margin of western Canada ; Royal Astronomical Society, Geophysical Journal, v. 89, p. 79-84.

Coney, P.J., Jones, D.L., and Monger, J.W.H.
1980 : Cordilleran suspect terranes ; Nature, v. 288, p. 329-333.

Crosson, R.S
1981 : Review of seismicity in the Puget sound region from 1970 through 1978 ; United States Geological Survey, Proceedings of Workshop XIV, Earthquake Hazards of the Puget Sound Region, Washington, p. 6-18.

Davis, E.E. and Hyndman, R.D.
1990 : Recent deformation and accretion of sediments above the northern Cascadia subduction zone off Vancouver Island ; Tectonics.

Dickinson, W.R.
1976 : Sedimentary basins developed during evolution of Mesozoic-Cenozoic arc-trench systems in western North America ; Canadian Journal of Earth Sciences, v. 13, p. 1268-1287.

Duncan, R.A.
1982 : A captured island chain in the Coast Range of Oregon and Washington ; Journal of Geophysical Research, v. 87, p. 10827-10837.

Ellis, R.M. and Clowes, R.M.
1981 : Acquisition of crustal reflection and refraction profiles across Vancouver Island ; Earth Physics Branch, Open File Report, 81-11, 72 p.

Ellis, R.M., Spence, G.D., Clowes, R.M., Waldron, D.A., Jones, I.F., Green, A.G., Forsyth, D.A., Mair, J.A., Berry, M.J., Mereu, R.F., Kanasewich, E.R., Cumming, G.L., Hajnal, Z., Hyndman, R.D., McMechan, G.A., and Loncarevic, B.D.
1983 The Vancouver Island Seismic Project : a COCRUST onshore-offshore study of a convergent margin ; Canadian Journal of Earth Sciences, v. 20, p. 719-741.

Fairchild, L.H. and Cowan, D.S.
1982 : Structure, petrology, and tectonic history of the Leech River complex northwest of Victoria, Vancouver Island ; Canadian Journal of Earth Sciences, v. 19, p. 1817-1835.

Green, A.G., Berry, M.J., Spencer, C.P., Kanasewich, E.R., Chiu, S., Clowes, R.M., Yorath, C.J., Stewart, D.B., Unger, J.D., and Poole, W.H.
1986a : Recent seismic reflection studies in Canada ; *in* Reflection Seismology : A Global Perspective ; American Geophysical Union, Geodynamic Series, v. 13, p. 85-98.

Green, A.G., Clowes, R.M., and Yorath, C.J.
1985 : LITHOPROBE seismic reflection profiles from southeastern Vancouver Island ; Geological Survey of Canada, Open File, 1180.

Green, A.G., Clowes, R.M., Yorath, C.J., Spencer, C., Kanasewich, E.R., Brandon, M.T., and Sutherland Brown, A.
1986b : Seismic reflection imaging of the subducting Juan de Fuca plate ; Nature, v. 319, p. 210-213.

Green, A.G., Milkereit, B., Mayrand, L., Spencer, C., Kurtz, R.D., and Clowes, R.M.
1987 : Lithoprobe seismic reflection profiling across Vancouver Island ; Royal Astronomical Society, Geophysical Journal, v. 89, p. 85-90.

Hyndman, R.D.
1988 : Dipping reflectors, electrically conductive zones and free water beneath a subduction zone ; Journal of Geophysical Research, v. 93, p. 13391-13405.

Jones, D.L., Silberling, N.J., and Hillhouse, J.
1977 : Wrangellia — a displaced terrane in northwestern North America ; Canadian Journal of Earth Sciences, v. 14, p. 2565-2577.

Kulm, L.D. et al.
1984 : Western North American Continental Margin and Adjacent Ocean Floor off Oregon and Washington ; Marine Science International, Regional Atlas Series, Atlas 1, Ocean Margin Drilling Program.

Kurtz, R.D., DeLaurier, J.M., and Gupta, J.C.
1986 : A magnetotelluric sounding across Vancouver Island detects the subducting Juan de Fuca plate ; Nature, v. 321, p. 596-599.

Lewis, T.J., Bentkowski, W.H., Davis, E.E., Hyndman, R.D., Souther, J.G., and Wright, J.A.
1988 : Subduction of the Juan de Fuca plate : thermal consequences ; Journal of Geophysical Research, v. 93, p. 15207-15225.

Macleod, N.S., Tiffin, D.L., Snavely, P.D., and Currie, R.G.
1977 : Geological interpretation of magnetic and gravity anomalies in the Strait of Juan de Fuca, U.S.-Canada ; Canadian Journal of Earth Sciences, v. 14, p. 223-238.

Mayrand, L., Green, A., and Milkereit, B.
1987 : A quantitative approach to bedrock velocity resolution and precision — the LITHOPROBE Vancouver Island experiment ; Journal of Geophysical Research, v. 92, p. 4837-4845.

McKenzie, D.P. and Julian, B.
1971 : Puget Sound, Washington, earthquake and the mantle structure beneath the northwestern United States ; Geological Society of America, Bulletin, v. 82, p. 3519-3524.

McMechan, G.A. and Spence, G.D.
1983 : P-wave velocity structure of the Earth's crust beneath Vancouver Island ; Canadian Journal of Earth Sciences, v. 20, p. 742-752.

Milkereit, B.
1987a : Migration of noisy crustal seismic data ; Journal of Geophysical Research, v. 92, p. 7916-7930.
1987b : Decomposition and inversion of seismic data — an instantaneous slowness approach ; Geophysical Prospecting, v. 35, p. 875-894.

Monger, J.W.H., Clowes, R.M., Price, R.A., Simony, P.S., Riddihough, R.P., and Woodsworth, G.J.
1985 : Continent-Ocean Transect B2 : Juan de Fuca plate to Alberta plains ; Geological Society of America, Centennial Continent/Ocean Transect No. 7.

Monger, J.W.H. and Price, R.A.
1979 : Geodynamic evolution of the Canadian Cordillera — progress and problems ; Canadian Journal of Earth Sciences, v. 16, p. 770-791.

Muller, J.E.
1977a : Evolution of the Pacific margin, Vancouver Island, and adjacent regions ; Canadian Journal of Earth Sciences, v. 14, p. 2062-2085.
1977b : Geology of Vancouver Island ; Geological Survey of Canada, Open File, 463, (3 sheets).
1980 : Chemistry and origin of the Eocene Metchosin volcanics, Vancouver Island, British Columbia ; Canadian Journal of Earth Sciences, v. 17, p. 199-209.

Riddihough, R.P.
1977 : A model for recent plate interactions off Canada's west coast ; Canadian Journal of Earth Sciences, v. 14, p. 384-396.
1979 : Gravity and structure of an active margin — British Columbia and Washington ; Canadian Journal of Earth Sciences, v. 16, p. 350-363.
1982 : Contemporary movements and tectonics on Canada's west coast ; a discussion ; Tectonophysics, v. 86, p. 319-341.
1984 : Recent movements of the Juan de Fuca plate system ; Journal of Geophysical Research, v. 89, p. 6980-6994.

Robinson, P.T., Brem, G.F., and McKee, E.H.
1984 : John Day formation of Oregon : a distal record of early cascade volcanism ; Geology, v. 12, p. 229-232.

Rogers, G.C.
1979 : Earthquake fault plane solutions near Vancouver Island ; Canadian Journal of Earth Sciences, v. 16, p. 523-531.
1981 : Some comments on the seismicity of the northern Puget Sound — southern Vancouver Island region ; United States Geological Survey, Proceedings of Workshop XIV, Earthquake Hazards of the Puget Sound Region, Washington, p. 6-18.

Rusmore, M.E. and Cowan, D.S.
1985 : Jurassic-Cretaceous rock units along the southern edge of the Wrangellia terrane on Vancouver Island ; Canadian Journal of Earth Sciences, v. 22, p. 1223-1235.

Savage, J.C., Lisowski, M., and Prescott, W.H.
1981 : Geodetic strain measurements in Washington ; Journal of Geophysical Research, v. 86, p. 4929-4940.

Shouldice, D.H.
1971 : Geology of the western Canadian continental shelf ; Bulletin of Canadian Petroleum Geologists, v. 19, p. 405-436.

Silver, E.
1972 : Pleistocene tectonic accretion of the continental slope off Washington ; Marine Geology, v. 13, p. 239-249.

Spence, G.D.
1984 : Seismic structure across the active subduction zone of western Canada ; unpublished PhD thesis, University of British Columbia, Vancouver, 191 p.

Spence, G.D., Clowes, R.M., and Ellis, R.M.
1985 : Seismic structure across the active subduction zone of western Canada ; Journal of Geophysical Research, v. 90, p. 6754-6772.

Taber, J.J. and Smith, S.W.
1985 : Seismicity and focal mechanisms associated with the subduction of the Juan de Fuca plate beneath the Olympic Peninsula, Washington ; Seismological Society of America, Bulletin, v. 75, p. 237-249.

Tabor, R.W. and Cady, R.W.
1978 : The structure of the Olympic mountains, Washington — analysis of a subduction zone ; United States Geological Survey Professional Paper, 1033, 38 p.

Waldron, D.A.
1982 : Structural characteristics of a subducting ocean plate ; unpublished MSc thesis, University of British Columbia, Vancouver, 121 p.

Weaver, C.S. and Smith, S.W.
1983 : Regional tectonic and earthquake hazard implications of a crustal fault zone in southwestern Washington ; Journal of Geophysical Research, v. 88, p. 10371-10383.

Yole, R.W. and Irving, E.
1980 : Displacement of Vancouver Island : Paleomagnetic evidence from the Karmutsen Formation ; Canadian Journal of Earth Sciences, v. 17, p. 1210-1228.

Yorath, C.J., Clowes, R.M., Green, A.G., Sutherland Brown, A., Brandon, M.T., Massey, N.W.D., Spencer, C., Kanasewich, E.R., and Hyndman, R.D.
1985a : LITHOPROBE — Phase I : Southern Vancouver Island : Preliminary analyses of reflection seismic profiles and surface geological studies ; *in* Current Research, Part A, Geological Survey of Canada, Paper 85-1A, p. 543-554.

Yorath, C.J., Green, A.G., Clowes, R.M., Sutherland Brown, A., Brandon, M.T., Kanasewich, E.R., Hyndman, R.D., and Spencer, C.
1985b : LITHOPROBE, southern Vancouver Island : seismic reflection sees through Wrangellia to the Juan de Fuca plate ; Geology, v. 13, p. 759-762.

SUPPLEMENTARY REFERENCES

Refraction and Reflection Studies

Au, D. and Clowes, R.M.
1982 : Crustal Structure from an OBS survey of the Nootka fault zone off western Canada ; Royal Astronomical Society, Geophysical Journal, v. 68, p. 27-47.
1984 : Shear-wave velocity structure of the oceanic lithosphere from ocean bottom seismometer studies ; Royal Astronomical Society, Geophysical Journal, v. 77, p. 105-123.

Berg, J.W., Trembly, L., Emilia, D.A., Hutt, J.R., King, J.M., Long, T.L., McKnight, W.R., Sarmah, S.K., Souders, R., Thiruvathukal, J.V., and Vossler, D.A.
1966 : Crustal Refraction profile, Oregon Coast Range ; Seismological Society of America, Bulletin, v. 56, p. 1357-1362.

Berry, M.J. and Forsyth, D.A.
1975 : Structure of the Canadian Cordillera from seismic refraction and other data ; Canadian Journal of Earth Sciences, v. 12, p. 182-208.

Cheung, H.P.Y. and Clowes, R.M.
1981 : Crustal structure from P-and S-wave analyses : ocean bottom seismometer results in the north-east Pacific ; Royal Astronomical Society, Geophysical Journal, v. 65, p. 47-73.

Clowes, R.M and Knize, S.
1979 : Crustal structure from a marine seismic survey off the west coast of Canada ; Canadian Journal of Earth Sciences, v. 16, p. 1265-1280.

Crosson, R.S.
1976 : Crustal structure modeling of earthquake data 2. Velocity structure of the Puget Sound region, Washington ; Journal of Geophysical Research, v. 81, p. 3047-3054.

Dehler, S.A. and Clowes, R.M.
1989 : The Queen Charlotte Islands refraction project : Part I — the Queen Charlotte fault zone ; Canadian Journal of Earth Sciences, v. 25, p. 1857-1870.

Forsyth, D.A., Berry, M.J., and Ellis, R.M.
1974 : A refraction survey across the Canadian Cordillera at 54°N ; Canadian Journal of Earth Sciences, v. 11, p. 533-548.

Horn, J.R., Clowes, R.M., Ellis, R.M., and Bird, D.N.
1984 : The seismic structure across an active oceanic-continental transform fault zone ; Journal of Geophysical Research, v. 89, p. 3107-3120.

Johnson, S.M. and Couch, R.W.
1970 : Crustal structure in the north Cascades Mountains of Washington and British Columbia from seismic refraction measurements ; Seismological Society of America, Bulletin, v. 60, p. 1259-1269.

Johnson, S.H., Couch,R.W., Gemperle, M., and Banks, E.R.
1972 : Seismic refraction measurements in southeast Alaska and western British Columbia ; Canadian Journal of Earth Sciences, v. 9, p. 1756-1765.

Keach, R.W., Potter, C.J., Oliver, J.E., Brown, L.D., and Kaufman, S.
1989 : Cenozoic active margin and shallow Cascades structure : COCORP results from western Oregon ; Geological Society of America, Bulletin, v. 101, p. 783-794.

Langston, C.A.
1981 : Evidence for the subducting lithosphere under southern Vancouver Island and western Oregon from teleseismic P-wave conversions ; Journal of Geophysical Research, v. 86, p. 3857-3866.
Langston, C.A. and Blum, D.E.
1977 : The April 29, 1965, Puget Sound earthquake and the crustal and upper mantle structure of western Washington ; Seismological Society of America, Bulletin, v. 67, p. 693-711.
Leaver, D.S., Mooney, W.D., and Kohler, W.M.
1984 : A seismic refraction study of the Oregon Cascades ; Journal of Geophysical Research, v. 89, p. 3121-3134
Mackie, D.A., Clowes, R.M., Dehler, S.A., Ellis, R.M., and Morel-à-l'Huissier, P.
1989 : The Queen Charlotte Islands refraction project : Part II — structural model for transition from Pacific plate to America plate ; Canadian Journal of Earth Sciences, v. 26, p. 1713-1725..
Shor, G.G., Dehlinger, P., Kirk, H.K., and French, W.S.
1968 : Seismic refraction studies off Oregon and northern California ; Journal of Geophysical Research, v. 73, p. 2175-219.
Taber, J.J. and Lewis, B.T.R.
1986 : Crustal structure of the Washington continental margin from refraction data ; Seismological Society of America, Bulletin, v. 76, p. 1011-1024.
Tatel, H.E. and Tuve, M.A.
1955 : Seismic exploration of a continental crust ; Geological Society of America, Special Paper 62, p. 35-50.
White, D.J. and Clowes, R.M.
1984 : Seismic investigation of the Coast Plutonic Complex — Insular Belt boundary beneath the strait of Georgia ; Canadian Journal of Earth Sciences, v. 21, p. 1033-1049.
White, W.R.H., Bone, M.N., and Milne, W.G.
1968 : Seismic refraction surveys in British Columbia, 1964-1966 : A preliminary interpretation ; *in* The Crust and Upper Mantle of the Pacific Area ; American Geophysical Union, Geophysical Monograph, 12, p. 81-93.
White, W.R.H. and Savage, J.C.
1965 : A seismic refraction and gravity study of the Earth's crust in British Columbia ; Seismological Society of America, Bulletin, v. 55, p. 463-486.
Wickens, A.J.
1977 : The upper mantle of southern British Columbia ; Canadian Journal of Earth Sciences, v. 14, p. 1100-1115.

Potential Field and Induction Studies

Brown, R.D. and Hanna, W.F.
1971 : Aeromagnetic evidence and geologic structure, northern Olympic Peninsula and Strait of Juan de Fuca, Washington ; American Association of Petroleum Geologists, Bulletin, v. 55, p. 1939-1953.
Coles, R.L. and Currie, R.G.
1977 : Magnetic anomalies and rock magnetizations in the southern Coast Mountains, British Columbia : possible relation to subduction ; Canadian Journal of Earth Sciences, v. 14, p. 1753-1770.
DeLaurier, J.M., Auld, D.R., and Law, L.K.
1983 : The geomagnetic response across the continental margin off Vancouver Island : Comparison of results from numerical modelling and field data ; Journal of Geomagnetism and Geoelectricity, v. 35, p. 517-528.
Raff, A.D. and Mason, R.G.
1961 : Magnetic survey off the west coast of North America, 40°N to 52°N ; Geological Society of America, Bulletin, v. 72, p. 1267-1270.
Stacey, R.A.
1973 : Gravity anomalies, crustal structure and plate tectonics in the Canadian Cordillera ; Canadian Journal of Earth Sciences, v. 10, p. 615-628.
Stacey, R.A. and Stephens, L.E.
1969 : An interpretation of gravity measurements on the west coast of Canada ; Canadian Journal of Earth Sciences, v. 6, p. 463-474.
Srivastava, S.P.
1973 : Interpretation of gravity and magnetic measurements across the continental margin of British Columbia ; Canadian Journal of Earth Sciences, v. 10, p. 1664-1677.
Vine, F.J.
1966 : Spreading of the ocean floor, new evidence ; Science, v. 154, p. 1405-1415.
Vine, F.J. and Wilson, J.T.
1965 : Magnetic anomalies over a young oceanic ridge off Vancouver Island ; Science, v. 150, p. 485-489.
Wilson, J.T.
1965 : Transform faults, oceanic ridges and magnetic anomalies southwest of Vancouver Island ; Science, v. 150, p. 482-485.

Offshore reflection profiling

Barnard, W.D.
1978 : The Washington continental slope : Quaternary tectonics and sedimentation ; Marine Geology, v. 27, p. 79-114.
Barr, S.M. and Chase, R.L.
1974 : Geology of the northern end of Juan de Fuca Ridge and sea-floor spreading ; Canadian Journal of Earth Sciences, v. 11, p. 1138-1406.
Carson, B.
1973 : Acoustic stratigraphy, structure and history of Quaternary deposition in Cascadia Basin ; Deep-Sea Research, v. 20, p. 387-396.
Carson, B.
1977 : Tectonically induced deformation of deep-sea sediments off Washington and northern Oregon : Mechanical consolidation ; Marine Geology, v. 24, p. 289-307.
Carson, B., Yuan, J., Myers, P.B., and Barnard, W.D.
1974 : Initial deep-sea sediment deformation at the base of the Washington continental slope : a response to subduction ; Geology, v. 2, p. 561-564.
Chase, R.M., Tiffin, D.L., and Murray, J.W.
1975 : The Western Canadian continental margin ; *in* Canada's Continental Margins and Offshore Petroleum Exploration ; Canadian Society of Petroleum Geologists, Memoir 4, p. 701-721.
Davis, E.E.
1982 : Evidence for extensive basalt flows on the sea floor ; Geological Society of America, Bulletin, v. 93, p. 1023-1029.
Davis, E.E. and Clowes, R.M.
1986 : Unusual seismic properties of Pleistocene turbidites off western Canada ; Royal Astronomical Society, Geophysical Journal, v. 84, p. 381-400.
Davis, E.E. and Lister, C.R.B.
1977 : Tectonic structures on the Juan de Fuca Ridge ; Geological Society of America, Bulletin, v. 88, p. 346-363.
Davis, E.E. and Seemann, D.A.
1981 : A compilation of seismic reflection profiles across the continental margin of western Canada, Geological Survey of Canada, Open File 751.
Kulm, L.D. and Fowler, G.A.
1974 : Oregon continental margin structure and stratigraphy : a test of the imbricate thrust model ; *in* The Geology of Continental Margins, ed. C.A. Burk and C.L. Drake ; Springer Verlag, New York, p. 261-283.
McManus, D.A., Holmes, M.L., Carson, B., and Barr, S.M.
1972 : Late Quaternary tectonics, northern end of Juan de Fuca Ridge (northeast Pacific) ; Marine Geology, v. 12, p. 141-164.
Murray, J.W. and Tiffin, D.L.
1974 : Patterns of deformation, sedimentation and tectonism, southwestern Canadian continental margin ; Annales de la Société Géologique de Belgique, v. 97, p. 169-183.
Rohr, K.M.M., Milkereit, B., and Yorath, C.J.
1988 : Asymmetric deep crustal structure across the Juan de Fuca ridge ; Geology, v. 16, p. 533-537.
Seely, D.R., Vail, P.P., and Walton, G.G.
1974 : Trench slope model ; *in* The Geology of Continental Margins, ed. C.A. Burk and C.L. Drake ; Springer Verlag, New York, p. 249-260.
Snavely, P.D. and Wagner, H.C.
1981 : Geological cross-section across the continental margin off Cape Flattery, Washington, and Vancouver Island, British Columbia ; United States Geological Survey, Open File Report, 81-978.

Snavely, P.D., Wagner, H.C., and Lander, D.L.
1980 : Interpretation of the Cenozoic geological history, central Oregon continental margin : cross-section summary ; Geological Society of America, Bulletin, v. 91, p. 143-146.
Tiffin, D.L., Cameron, B.E.B., and Murray, J.W.
1972 : Tectonics and depositional history of the continental margin off Vancouver Island, British Columbia ; Canadian Journal of Earth Sciences, v. 9, p. 280-296.
Yorath, C.J.
1980 : The Apollo structure in Tofino Basin, Canadian Pacific continental margin ; Canadian Journal of Earth Sciences, v. 17, p. 758-775.

Related Geophysical Reviews

Berry, M.J., Jacoby, W.R., Niblett, E.R., and Stacey, A.A.
1971 : A review of geophysical studies in the Canadian Cordillera ; Canadian Journal of Earth Sciences, v. 8, p. 788-801.
Keen, C.E. and Hyndman, R.D.
1979 : Geophysical review of the continental margins of eastern and western Canada ; Canadian Journal of Earth Sciences, v. 16, p. 712-747.
Riddihough, R.P.
1985 : A symposium on the deep structure of southern Vancouver Island : results of LITHOPROBE phase I ; Geoscience Canada, v. 12, p. 112-114.
Riddihough, R.P., Beck, M.E., Chase, R.L., Davis, E.E., Hyndman,R.D., Johnson, S.H., and Rogers, G.C.
1983 : Geodynamics of the Juan de Fuca plate ; *in* Geodynamics of the Eastern Pacific Region, Caribbean and Scotia Arcs, American Geophysical Union, Geodynamics Series, v. 9, p. 5-21.
Riddihough, R.P. and Hyndman, R.D.
1976 : Canada's active western margin — the case for subduction ; Geoscience Canada, v. 3, p. 269-279.

Paleomagnetism

Irving, E.
1979 : Paleopoles and paleolatitudes of North America and speculations about displaced terranes ; Canadian Journal of Earth Sciences, v. 16, p. 669-694.
1985 : Whence British Columbia ; Nature, v. 314, p. 673-674.
Irving, E. and Yole, R.W.
1972 : Paleomagnetism and the kinematic history of mafic and ultramafic rocks in fold mountain belts ; Publication of the Earth Physics Branch, v. 42, p. 87-97.
Panuska, B.C.
1985 : Paleomagnetic evidence for a post Cretaceous accretion of Wrangellia ; Geology, v. 13, p. 880-883.
Schwarz, E.J., Muller, J.E., and Clark, K.R.
1980 : Paleomagnetism of the Karmutsen basalts from southeast Vancouver Island ; Canadian Journal of Earth Sciences, v. 17, p. 389-399.
Stone, D.B.
1977 : Plate tectonics, paleomagnetism and the tectonic history of the N.E. Pacific ; Geophysical Surveys, v. 3, p. 3-37.
Symons, D.T.A.
1971 : Paleomagnetism of the Jurassic island intrusions of Vancouver Island, British Columbia ; Geological Survey of Canada, Paper 70-63.
1971 : Paleomagnetism notes on some minor Tertiary igneous bodies and on the Karmutsen basalts, Vancouver Island, British Columbia ; Geological Survey of Canada, Paper 71-24.

Onshore Geology

Brandon, M.T.
1986 : Comments on the growth of accretionary wedges ; Geology, v. 14, p. 986.
Cowan, D.S.
1982 : Geological evidence for post-40 my B.P. large-scale northwestward displacement of part of southwestern Alaska ; Geology v. 10, p. 309-313.
Dickinson, W.R. and Seeley, D.R.
1979 : Structure and stratigraphy of forearc regions ; American Association of Petroleum Geologists, Bulletin, v. 63, p. 2-31.
Hughes, J.M., Stoiber, R.E., and Carr, M.J.
1980 : Segmentation of the Cascade volcanic chain ; Geology, v. 8, p. 15-17.
Johnson, S.Y.
1984 : Evidence for a margin-truncating transcurrent fault (pre-late Eocene) in western Washington ; Geology v. 12, p. 538-541.
Johnson, S.Y., Zimmermann, R.A., Naeser, C.W., and Whetten, J.T.
1986 : Fission track dating of the tectonic development of the San Juan Islands, Washington ; Canadian Journal of Earth Sciences, v. 23, p. 1318-1330.
McWilliams, R.G.
1978 : Early Tertiary rifting in western Oregon-Washington ; American Association of Petroleum Geologists, Bulletin, v. 62, p. 1193-1197.
Massey, N.W.A.
1986 : Metchosin igneous complex, southern Vancouver Island : Ophiolite stratigraphy developed in an emergent island setting ; Geology, v. 14, p. 602-605.
Rogers, G.C.
1985 : Variation in Cascade volcanism with margin orientation ; Geology, v. 13, p. 495-498.
Rogers, J.J.W. and Noitsky-Evans, J.M.
1977 : Evolution from oceanic to continental crust in northwestern U.S.A. ; Geophysical Research Letters, v. 4, p. 347-350.
Tabor, R.W. and Cady, W.M.
1978 : Geological map of the Olympic Peninsula, Washington ; United States Geological Survey, Miscellanous Investigation Series, Map I-994.

Plate tectonic aspects

Atwater, T.
1970 : Implications of plate tectonics for the Cenozoic tectonic evolution of western North America ; Geological Society of America, Bulletin, v. 81, p. 3513-3536.
Cowan, D.S., Botros, M., and Johnson, H.P.
1986 : Bookshelf tectonics : Rotated crustal blocks within the Sovanco fracture zone ; Geological Research Letters, v. 13, p. 995-998.
Engebretson, D.C.
1986 : Relative motions between oceanic and continental plates in the Pacific basin ; Geological Society of America, Special Paper, 206, 59 p.
Engebretson, D.C., Cox, A., and Gordon, R.G.
1984 : Relative plate motions between oceanic plates of the Pacific basin ; Journal of Geophysical Research, v. 89, p. 10291-10310.
Farrar, E. and Dixon, J.M.
1980 : Miocene ridge impingement and the spawning of secondary ridges of Oregon, Washington and British Columbia ; Tectonophysics, v. 69, p. 321-348.
McKenzie, D.P. and Parker, R.L.
1967 : The north Pacific : an example of tectonics on a sphere ; Nature, v. 216, p. 1276-1280.
Moore, J.C., Byrne, T., Plumley, P.W., Reid, M., Gibbons, H., and Coe, R.S.
1983 : Paleogene evolution of the Kodiak Islands, Alaska : consequences of ridge-trench interaction in a more southerly latitude ; Tectonics, v. 2, p. 265-293.
Nishimura, C., Wilson, D.S., and Hey, R.N.
1984 : Pole of rotation analysis of present-day Juan de Fuca plate motion ; Journal of Geophysical Research, v. 89, p. 10283-10290.
Rea, D.K. and Duncan, R.A.
1986 : North Pacific plate convergence : a quantitative record of the past 140 m.y. ; Geology, v. 14, p. 373-376.
Riddihough, R.P.
1980 : Gorda plate motions from magnetic anomaly analysis ; Earth and Planetary Science Letters, v. 15, p. 163-170.
1982 : One hundred million years of plate tectonics in western Canada ; Geoscience Canada, v. 9, p. 28-34.
Silver, E.A.
1971 : Small plate tectonics in the northeastern Pacific, Geological Society of America, Bulletin, v. 82, p. 3491-3496.

Wells, R.E., Engebretson, D.C., Snavely, P.D., and Coe, R.S.
1984 : Cenozoic plate motions and the volcano-tectonic evolution of western Oregon and Washington ; Tectonics, v. 3, p. 275-294.

Seismicity, neotectonics and seismic risk

Crosson, R.S.
1986 : Comment on 'Geodetic strain measurements in Washington' by J.C. Savage, M. Lisowski and W.H. Prescott ; Journal of Geophysical Research, v. 91, p. 7555-7561.
Heaton, T.H. and Hartzell, S.H.
1986 : Source characteristics of hypothetical subduction earthquakes in the northwestern United States ; Seismological Society of America, Bulletin, v. 76, p. 675-708.
Heaton, T.H. and Kanamori, H.
1984 : Seismic potential associated with subduction in the northwestern United States ; Seismological Society of America, Bulletin, v. 74, p. 933-941.
Hyndman, R.D. and Ellis, R.M.
1981 : Queen Charlotte fault zone : Microearthquakes from a temporary array of land stations and ocean bottom seismographs ; Canadian Journal of Earth Sciences, v. 18, p. 776-788.
Hyndman, R.D. and Rogers, G.C.
1981 : Seismicity surveys with ocean bottom seismographs off western Canada ; Journal of Geophysical Research, v. 86, p. 3867-3880.
Hyndman, R.D. and Weichert, D.H.
1983 : Seismicity and rates of relative motion on the plate boundaries ; Royal Astronomical Society, Geophysical Journal, v. 72, p. 59-82.
Ihnen, S.M. and Hadley, D.M.
1986 : Prediction of strong ground motion in the Puget Sound region : the 1965 Seattle earthquake ; Seismological Society of America, Bulletin, v. 76, p. 905-922.
Milne, W.G., Rogers, G.C., Riddihough, R.P., McMechan, G.A., and Hyndman, R.D.
1978 : Seismicity of western Canada ; Canadian Journal of Earth Sciences, v. 15, p. 1170-1193.
Rogers, G.C. and Hasegawa, H.S.
1978 : A second look at the British Columbia earthquake of June 23, 1946 ; Seismological Society of America, Bulletin, v. 68, p. 653-675.
Sbar, M.L.
1983 : An explanation for contradictory geodetic strain and fault plane solution data in western North America ; Geophysical Research Letters, v. 10, p. 177-180.
Tabor, R.W.
1986 : Changing concepts of geological structure and the problems of siting nuclear reactors : Examples from Washington state ; Geology, v. 14, p. 738-742.
Tobin, P.G. and Sykes, L.R.
1968 : Seismicity and tectonics of the northeast Pacific Ocean ; Journal of Geophysical Research, v. 72, p. 3821-3846.
Weaver, C.S. and Smith, S.W.
1983 : Regional tectonic and earthquake hazard implications of a crustal fault zone in southwestern Washington ; Journal of Geophysical Research, v. 88, p. 10371-10383.
Weichert, D.H. and Hyndman, R.D.
1981 : A comparison of the rate of seismic activity and several estimates of deformation in the Puget Sound area ; United States Geological Survey, Proceedings of Workshop XIV, Earthquake Hazards of the Puget Sound Region, Washington, p. 105-122.

Offshore structures-Queen Charlotte Islands and related features

Clowes, R.M. and Gens-Lenartowicz.
1985 : Upper crustal structure of southern Queen Charlotte basin from sonobuoy refraction studies ; Canadian Journal of Earth Sciences, v. 22, p. 1696-1710.
Davis, E.E. and Riddihough, R.P.
1982 : The Winona basin : structure and tectonics ; Canadian Journal of Earth Sciences, v. 19, p. 767-788.
Hyndman, R.D., Lewis, T.J., Wright, J.A., Burgess, M., Chapman, D.S., and Yamano, M.
1982 : Queen Charlotte fault zone : heat flow measurements ; Canadian Journal of Earth Sciences, v. 198, p. 1657-1669.
Hyndman, R.D., Riddihough, R.P., and Herzer, R.
1979 : The Nootka fault zone — a new plate boundary off western Canada ; Royal Astronomical Society, Geophysical Journal, v. 58, p. 667-683.
Hyndman, R.D., Rogers, G.C., Bone, M.N., Lister, C.R.B., Wade, U.S., Barrett, D.L., Davis, E.E., Lewis, T., Lynch, S., and Seeman, D.
1978 : Geophysical measurements in the region of the Explorer ridge off western Canada ; Canadian Journal of Earth Sciences, v. 15, p. 1508-1525.
Riddihough, R.P., Currie, R.G., and Hyndman, R.D.
1980 : The Dellwood Knolls and their role in triple junction tectonics off northern Vancouver Island ; Canadian Journal of Earth Sciences, v. 17, p. 577-593.
Sutherland Brown, A.
1968 : Geology of the Queen Charlotte Islands, British Columbia ; British Columbia Department of Mines and Petroleum Resources, Bulletin 54, 226 p.
Yorath, C.J. and Chase, R.L.
1981 : Tectonic history of the Queen Charlotte Islands and adjacent areas — a model ; Canadian Journal of Earth Sciences, v. 18, p. 1717-1729.
Yorath, C.J. and Hyndman, R.D.
1983 : Subsidence and thermal history of Queen Charlotte basin ; Canadian Journal of Earth Sciences, v. 20, p. 135-159.

Guidelines for workshop topics I to IV

A.G. Green[1], C. Spencer[1], B. Milkereit[1], R.M. Clowes[2] and R.M. Ellis[2]

Green, A.G., Spencer, C., Milkereit, B., Clowes, R.M., and Ellis, R.M., Guidelines for workshop topics I to IV; in Studies of Laterally Heterogeneous Structures Using Seismic Refraction and Reflection Data, ed. A.G. Green; Geological Survey of Canada, Paper 89-13, p. 27-30, 1990.

Abstract

Four of the five topics for the Commission on Controlled Source Seismology (CCSS) workshop at Whistler, British Columbia, involved seismic data collected from Vancouver Island and the adjacent offshore continental margin. Workshop topic I concerned the combined interpretation of onshore-offshore seismic refraction and multichannel seismic reflection data, topic II the post-stack processing of an entire line of multichannel seismic reflection data, and topics III and IV were aimed at pre- and post-stack processing of short segments of land and marine multichannel seismic reflection data.

Résumé

Quatre des cinq jeux de données sélectionnés pour l'atelier de la Commission sur la sismologie à source contrôlée (CSSC) qui s'est tenu à Whistler, en Colombie-Britannique, incluaient des données sismiques provenant de l'île de Vancouver et de la marge continentale océanique adjacente. Le jeu I traitait de l'interprétation combinée des données de sismique réfraction et de sismique réflexion multicanale recueillies sur terre et en mer, le jeu II concernait le traitement après sommation d'une ligne complète de données de sismique réflexion multicanale, et les jeux III et IV portaient sur le traitement avant et après sommation de courts segments de données de sismique réflexion multicanale, recueillies sur terre et en mer.

[1] Continental Geoscience Division, Geological Survey of Canada, Ottawa, Ontario, K1A 0Y3
[2] University of British Columbia, Vancouver, B.C., V6T 2B4

GENERAL INFORMATION

Each active participant in the workshop was sent the following package of information :

- one comprehensive list of references (included in Green et al., 1990) ;
- one 1 : 1 000 000 map showing the locations of the onshore and offshore seismic reflection profiles ;
- one full-size copy of the non-migrated (stacked) multichannel seismic reflection section recorded along LITHOPROBE onshore line 1 (*see* Fig. 14 and 15 of Green et al., 1990) ;
- one preprint of the paper by Clowes et al. (1987a).

WORKSHOP TOPIC I

The aim of topic I was to produce a combined interpretation of coincident seismic refraction and multichannel (3000 % data recorded at 90 or 100 m spacing) seismic reflection data collected across Vancouver Island and the adjacent continental margin. In this region, the Juan de Fuca oceanic plate is being subducted beneath Vancouver Island and the North American mainland. Previous interpretations of the onshore-offshore seismic refraction data are included in Ellis et al. (1983), Waldron (1982), Spence (1984), Spence et al. (1985) and Clowes et al. (1986) and previous interpretations of the onshore seismic reflection data (LITHOPROBE line 1) are included in Yorath et al. (1985a, b), Clowes et al. (1984, 1986, 1987a), and Green et al. (1986a, b, 1987). A preliminary interpretation of the offshore seismic reflection data (line 85-01) is included in Clowes et al. (1987b). The interpretation of the along island seismic refraction profile IV (shot points N, A and F in Figures 4 and 5 of Green et al., 1990) is presented in McMechan and Spence (1983) ; the data from profile IV were not distributed to workshop participants. Information critical to understanding this topic is included in the above mentioned papers and papers referenced in Green et al. (1990).

In addition to the general package of information sent to all active participants in topics I to IV, the following was specifically included for topic I :

- Figure 4 of Green et al. (1990) showing the locations of shot points J1, P8, P13 and P19 and the onshore recording line ;
- Figure 5 of Green et al. (1990) showing the approximate locations of the ocean bottom seismometers (OBSs) ;
- Figures 6 to 9 of Green et al., (1990) showing the seismic refraction sections recorded on Vancouver Island and adjacent regions from shots J1, P8, P13 and P19 plotted with two different amplitude scaling factors ;
- Figures 10 to 12 of Green et al., (1990) showing the seismic sections recorded at OBS1, OBS3 and OBS5 ;
- one full-size copy of the migrated multichannel seismic reflection section recorded along offshore line 85-01 (*see* Fig. 20 and 21 of Green et al., 1990) ;
- one preprint of the paper by Clowes et al. (1987b).

WORKSHOP TOPIC II

The objective of this exercise was to produce an improved image of the subsurface beneath Vancouver Island along LITHOPROBE profile 1 using various **post-stack** processing techniques such as migration, deconvolution, coherency filtering, colour plots, inversions, etc. In addition to the general package sent to all participants in topics I to IV, the following was included specifically for topic II :

- one SEGY format computer tape containing the information and data necessary to apply various post-stack processes to give an improved image of the onshore LITHOPROBE line 1 ;
- one set of notes (Appendix "A") describing the information on the SEGY tape.

WORKSHOP TOPIC III

The objective of this exercise was to produce an enhanced image of a portion of the onshore LITHOPROBE seismic reflection line 1 collected across Vancouver Island using various **pre- and post-stack** processing techniques. In addition to the general package sent to all participants in topics I to IV, the following was included specifically for topic III :

- two SEGY format computer tapes containing the information and data necessary to apply various pre- and post-stack processes to give an improved image of the southwest portion of onshore LITHOPROBE seismic reflection line 1 ;
- one set of notes (Appendix "B") describing the information on the SEGY tapes ;
- one set of 1 : 50 000 maps showing the line location.

WORKSHOP TOPIC IV

The objective of this exercise was to produce an improved image of the subsurface beneath the continental margin off the west coast of Vancouver Island using various **pre- and post-stack** processing techniques. In addition to the general packages sent to all participants in topics I and IV, the following was included specifically for topic IV :

- seven SEGY format computer tapes containing the information and data necessary to apply various pre- and post-stack processes to give an improved image of the northeast portion of the offshore seismic reflection line 85-01 ;
- one set of notes (Appendix "C") describing the information on the SEGY tapes ;
- one full-size copy of the migrated multichannel seismic reflection section recorded along offshore line 85-01 (*see* Fig. 20 and 21 of Green et al., 1990) ;
- one preprint of the paper by Clowes et al. (1987b).

REFERENCES

Clowes, R.M., Brandon, M.T, Green, A.G., Yorath, C.J., Sutherland Brown, A., Kanasewich, E.R., and Spencer, C.
1987a : LITHOPROBE — southern Vancouver Island : Cenozoic subduction complex imaged by deep seismic reflections ; Canadian Journal of Earth Sciences, v. 24, p. 31-51.

Clowes, R.M., Green, A.G., Yorath, C.J., Kanasewich, E.R., West, G.F., and Garland, G.D.
1984 : LITHOPROBE — a national program for studying the third dimension of geology ; Journal of the Canadian Society of Exploration Geophysicists, v. 20, p. 23-39.

Clowes, A.G., Spence, G.D., Ellis, R.M., and Waldron, D.A.
1986 : Structure of the lithosphere in a young subduction zone : results from reflection and refraction studies ; *in* Reflection Seismology : The Continental Crust ; American Geophysical Union, Geodynamic Series, v. 14, p. 313-322.

Clowes, R.M., Yorath, C.J., and Hyndman, R.D.
1987b : Reflection mapping across the con-vergent margin of western Canada ; Royal Astronomical Society, Geophysical Journal, v. 89, p. 79-84.

Ellis, R.M., Spence, G.D., Clowes, R.M., Waldron, D.A, Jones, I.F., Green, A.G., Forsyth, D.A., Mair, J.A., Berry, M.J., Mereu, R.F., Kanasewich, E.R, Cumming, G.L., Hajnal, Z., Hyndman, R.D., McMechan, G.A., and Loncarevic, B.D.
1983 : The Vancouver Island Seismic Project : A COCRUST onshore-offshore study of a convergent margin ; Canadian Journal of Earth Sciences, v. 20, p. 719-741.

Green, A.G., Clowes, R.M., and Ellis, R.M.
1990 : Crustal studies across Vancouver Island and adjacent offshore margin ; *in* Studies of Laterally Heterogeneous Structures Using Seismic Refraction and Reflection Data, ed. A.G. Green ; Geological Survey of Canada, Paper 89-13, p. 3-25..

Green, A.G., Berry, M.J., Spencer, C.P., Kanasewich, E.R., Chiu, S., Clowes, R.M., Yorath, C.J., Stewart, D.B., Unger, J.D., and Poole, W.H.
1986a : Recent seismic reflection studies in Canada ; *in* Reflection Seismology : A Global Perspective ; American Geophysical Union, Geodynamic Series, v. 13, p. 85-98.

Green, A.G., Clowes, R.M., Yorath, C.J., Spencer, C., Kanasewich, E.R., Brandon, M.T., and Sutherland Brown, A.
1986b : Seismic reflection imaging of the subducting Juan de Fuca plate ; Nature, v. 319, p. 210-213.

Green, A.G., Milkereit, B., Mayrand, L., Spencer, C., Kurtz, R.D., and Clowes, R.M.
1987 : Lithoprobe seismic reflection profiling across Vancouver Island ; Royal Astronomical Society, Geophysical Journal, v. 89, p. 85-90.

McMechan, G.A. and Spence, G.D.
1983 : P-wave velocity structure of the Earth's crust beneath Vancouver Island ; Canadian Journal of Earth Sciences, v. 20, p. 742-752.

Spence, G.D.
1984 : Seismic structure across the active subduction zone of western Canada ; unpublished Ph,D, thesis, University of British Columbia, Vancouver, 191 p.

Spence, G.D., Clowes, R.M., and Ellis, R.M.
1985 : Seismic structure across the active subduction zone of western Canada ; Journal of Geophysical Research, v. 90, p. 6754-6772.

Waldron, D.A.
1982 : Structural characteristics of a subducting ocean plate ; unpublished MSc thesis, University of British Columbia, Vancouver, 121 p.

Yorath, C.J., Clowes, R.M., Green, A.G., Sutherland Brown, A., Brandon, M.T., Massey, N.W.D., Spencer, C., Kanasewich, E.R., and Hyndman, R.D.
1985a : LITHOPROBE — Phase I : Southern Vancouver Island : Preliminary analyses of reflection seismic profiles and surface geological studies ; *in* Current Research, Part A, Geological Survey of Canada, Paper 85-1A, p. 543-554.

Yorath, C.J., Green, A.G., Clowes, R.M., Sutherland Brown, A., Brandon, M.T., Kanasewich, E.R., Hyndman, R.D., and Spencer, C.
1985b : LITHOPROBE, southern Vancouver Island : seismic reflection sees through Wrangellia to the Juan de Fuca plate ; Geology, v. 13, p. 759-762.

APPENDIX A

Workshop topic II — technical description of stacked section

Tape Format

The tapes are 9 track at 6250 B.P.I. The data are in SEGY (Geophysics, v. 40, p. 334-352) demultiplexed format with samples stored as 4 byte floating point words (Data sample format code = 1).

Header Information

The following header items are set:

a) line header: line number, number of traces per record, samples per trace, data format.

b) trace header: trace sequence number within line, trace sequence number within reel, original field record number, energy source point number, trace identification code, number of samples, sample interval.

Data Description

The stacked seismic data are 16 s, 1976 traces within the line. Common midpoint spacing is 45 m (crooked line!), with trace number 1 located at the southwest end of the line. Vibroseis sweeps were conducted with frequencies from 8-40 Hz. The original processing of this data set was completed by contract. A description of the original processing sequence is given in Green et al. (1990).

APPENDIX B

Workshop topic III — technical description of land shot gathers

Tape Format

The tapes are 9 track at 6250 B.P.I. The data are in SEGY (Geophysics, v. 40, p. 334-352) demultiplexed format with samples stored as 4 byte floating point words (Data sample format code = 1).

Header Information

The following header items are set:

a) line header: reel number, number of traces per record, samples per trace, measurement system, data format.

b) trace header: trace sequence number within line, trace sequence number within reel, original field record number, energy source point number, trace identification code, shot elevation, receiver elevation, source co-ordinate X, source co-ordinate Y, receiver co-ordinate X, receiver co-ordinate Y, co-ordinate units, number of samples, sample interval.

Data Description

The data are 16 s, 120 channel records collected with a 4 ms sample rate. There are 138 shots, 69 on each tape. Geophone spacing is 90 m with numbers running down from 1466 at the start of the line. When in routine mode Vibroseis sweeps were conducted every other geophone point with sweep frequencies from 8-40 Hz. However, for the first 32 shots the crew were "rolling in" and shooting every geophone location. At the start of the line, the end 120 geophone points were active. As the crew moved into the line the cable configuration became 90 channels active behind the shot (higher geophone point numbers) and 30 ahead. When in this shooting pattern a 3 geophone gap was left between the shot and first active traces. All this information may be gleaned from the SEGY headers. The data are "raw" as no distance or time dependent scaling factors have been applied.

APPENDIX C

Workshop topic IV — technical description of marine shot gathers

Tape Format

The tapes are 9 track at 6250 B.P.I. The data are in SEGY (Geophysics, 40, 334-352) demultiplexed format with samples stored as 4 byte floating point words (Data sample format code = 1).

Data Description

The data are 16 s, 120 channel records recorded with a 4 ms sample rate, 4001 samples per trace. The data cover about 25 km at the northeast end of line 85-01 with shotpoints 2308 to 2727 being included. Shotpoints are 50 m apart with hydrophone spacing of 25 m. There is a 287 m gap between the source and closest hydrophone (channel 120). Full details may be found in the side panel of the migrated section and on the tape itself.

Interpretation of a combined refraction and reflection profile across the western Canadian active margin

Joanna Morgan [1] and Mike Warner [2]

Morgan, J. and Warner, M., Interpretation of a combined refraction and reflection profile across the western Canadian active margin; in Studies of Laterally Heterogeneous Structures Using Seismic Refraction and Reflection Data, ed. A.G. Green; Geological Survey of Canada, Paper 89-13, p. 31-41, 1990.

Abstract

The Spence et al. refraction model was refined by including information from coincident reflection profiles and modeling using Maslov ray theory. The refraction and reflection data did not uniquely constrain the deep structure of the margin. At the mainland receivers, a contrast between early low-amplitude, high-frequency arrivals and late high-amplitude, low-frequency arrivals proved difficult to model. Tunnelling rays, summation of more than one phase, wide angle reflections from gradient zones, interference between reflections from layered sequences, and diffractions were all considered as possible solutions to this problem. Diffractions best explained the low amplitude early arrivals. A low velocity zone in the lower crust below the mainland, perhaps related to high fluid content, was proposed to explain the 1 s delay in travel time between arrivals at Vancouver Island and the mainland.

Résumé

Le modèle de réfraction de Spence et coll. a été perfectionné en incluant les données des profils de réflexion coïncidents et les résultats de la modélisation selon la théorie des rayons de Maslov. Les données de réfraction et de réflexion n'ont pas permis de déterminer la structure profonde de la marge de manière unique. Aux récepteurs disposés sur le continent, il a été difficile de modéliser un contraste entre les premières arrivées de faible amplitude et de haute fréquence et les arrivées secondaires d'amplitude élevée et de basse fréquence. L'effet de canalisation des rayons, la sommation de plusieurs phases, les réflexions grand-angle de zones à fort gradient, l'interférence entre des réflexions de séquences stratifiées et les diffractions sont des solutions qui ont été considérées pour résoudre ce problème. Ce sont les diffractions qui ont le mieux expliqué les premières arrivées de faible amplitude. La présence d'une zone de faible vitesse dans la croûte inférieure sous le continent, due peut-être à une teneur élevée en fluides, a été proposée pour expliquer le retard d'une seconde entre les arrivées observées dans l'île de Vancouver et sur le continent.

[1] Bullard Laboratories, Madingley Road, Cambridge, CB3 0EZ, England.
[2] Department of Geology, Imperial College, Prince Consort Road, London, SW7 2BP, England.

INTRODUCTION

CCSS data set 1 included the VISP refraction line 1, the onshore LITHOPROBE reflection line and the offshore reflection line 85-01 described by Green et al. (1990). In the present paper, the OBS3 and OBS5 data sets are not considered as they constrain only a shallow part of the model.

It is immediately apparent from the refraction and reflection data sets that the deep structure of the margin is not well constrained by the data. The OBS1 and J1 data have maximum ranges of 70 and 165 km, so that first arrivals penetrate only about the top 12 and 20 km respectively. The reflection data sets show reflectors down to 8 s (13 km) in the oceanic basin and 11 s (30 km) beneath Vancouver Island. The P-shot ray paths pass through both shallow and deep, oceanic and continental structure. Therefore, only the following parts of the model are constrained by more than one data set:

1. the top 12 km of the oceanic basin (including the water);
2. the top 30 km below Vancouver Island;
3. the top 20 km beneath the mainland.

The Spence et al. (1985) model was taken as a starting point, adjusted to obtain a better fit with the reflection data set, and modified further by forward modeling the two shallow refraction data sets OBS1 and J1. The deep structure was modelled using the P shots keeping the shallow structure constant.

MODELING

The ray diagrams and synthetic seismograms are calculated using a program written by David Lyness based on Maslov ray theory (Chapman and Drummond, 1982). Maslov ray theory combines asymptotic ray theory with the WKBJ transform. Since the two solutions break down at different points, they can be combined to produce a uniform solution. Unlike asymptotic ray theory, Maslov ray theory can produce accurate seismograms at caustics and critical points. The present implementation of the program is fast since the model is represented by triangles with linear gradients, and seismograms are interpolated at receivers, thereby removing the need for time-consuming two-point ray tracing. Ray diagrams and seismograms for the entire model can be produced in under four minutes on a VAX 11/750.

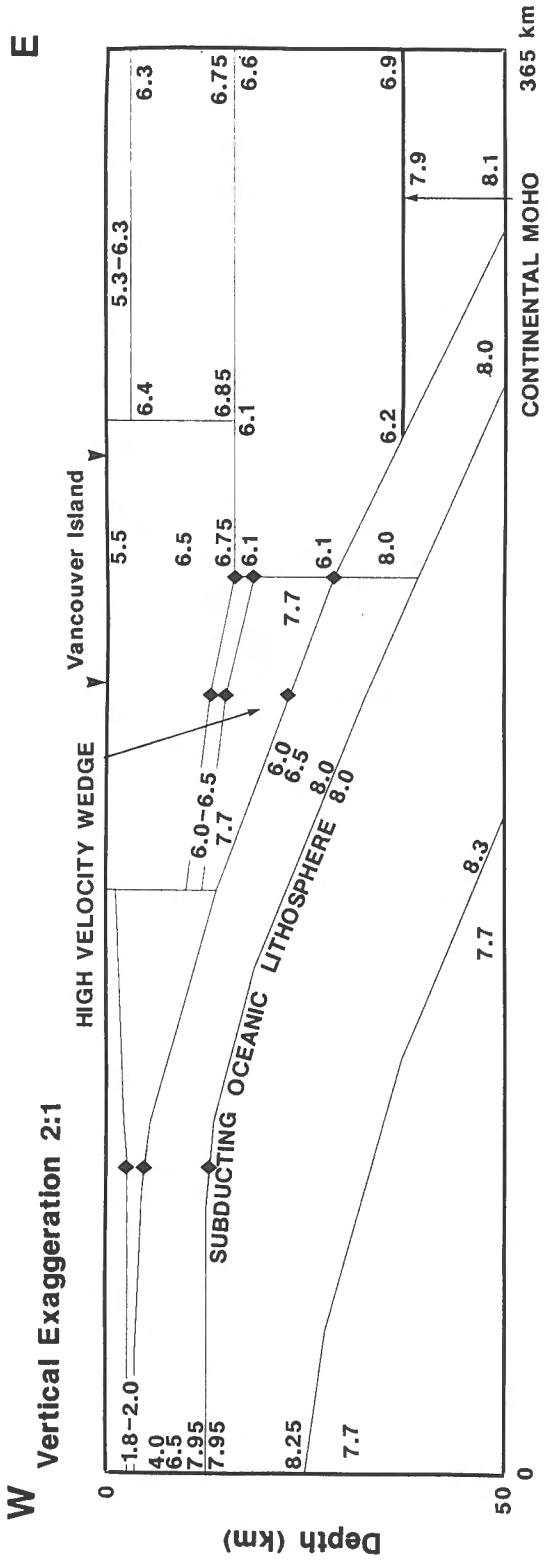

Figure 1. Final velocity depth model. The diamonds mark picks from the reflection data. The velocity varies uniformly between the top and bottom of each layer.

RESULTS

Reflection Data

The reflectors labelled Jdf and M? in Figure 22 of Green et al. (1990) are interpreted as the top and bottom of the Juan de Fuca plate, and C and E in Figure 15 of Green et al. (1990) are interpreted as the top and bottom of the high velocity wedge. Depths to these interfaces were calculated using a combination of the Spence et al. (1985) refraction velocities and interval velocities from the final stack. The Spence et al. (1985) model was then adjusted to agree better with the reflection data. In the final model of Figure 1, the diamonds mark the picks from the reflection data sets.

OBS 1

In forward modeling the OBS 1 data, a few minor changes to the original model were found to be necessary. Figures 2a, b and c show respectively the ray diagram, synthetic and observed seismograms for OBS 1. Synthetic arrivals marked with solid lines are geometric. All other arrivals are non-geometric events that are not predicted by asymptotic ray theory. Non-geometric arrivals are described by Thompson and Chapman (1986); they may represent end point effects or real signals, such as head waves or shadow zone arrivals. Picks from the observed data are plotted as dots on the synthetic section. No velocity discontinuity has been included at the base of the crust; a change in velocity gradient produces a Moho reflection of low amplitude. The high amplitudes between 28 and 45 km, seen in the observed data, are successfully modeled by turning rays through the oceanic crust. The non-geometric secondary arrivals add some reverberation to the synthetic seismograms, although the data do not show clearly any equivalent coherent phases.

Shot J1

Figures 3a, b and c show respectively the ray diagram, synthetic and observed seismograms for shot J1. Diving rays through the crust produce the observed amplitude highs between 20-40 and 110-130 km range.

P Shots — First Arrivals

There are two striking features in the observed P-shot seismograms (Fig. 4c, 5c and 6c). First, there is an approximate 1 s delay in first arrival travel time between the Vancouver Island and mainland receivers. Second, there is a marked change in amplitude and frequency between the first and second arrivals at the mainland. As discussed above, the shallow structure was kept constant during forward modeling of the P shots. The deep structure was modeled by varying three parameters: the dip of the subducting plate, the velocity gradient in the lower oceanic lithosphere and velocities in the lower continental crust. The dip of the plate was varied between 9° and 17°, a range that includes dips of 11° and 15° estimated from seismicity by Taber and Smith (1985) and Rogers (1979). The velocity gradient in the lower oceanic lithosphere was varied between 0.005 and 0.015 s^{-1}, considered to be reasonable values for young oceanic lithosphere (Steinmetz et al., 1977). Velocities in the lower continental crust were varied between 6.0 and 6.8 km/s; McMechan and Spence (1983) found anomalously low lower crustal velocities under Vancouver Island.

A series of solutions were obtained by varying these parameters between the stated limits. The model that best fits the data is shown in Figure 1. It has a plate dip of 11°, a velocity gradient of 0.01 s^{-1}, and lower continental velocities of 6.1 km/s trending eastwards into higher values more typical of lower continental crust. Figures 4 to 6 show the ray diagrams, synthetic and observed seismograms for shots P8, P13 and P19 respectively.

The 1 s delay in travel time between Vancouver Island and the mainland was judged not to be due to a shallow feature as no similar delay was observed on the seismograms for shot J1. In the original Spence et al. (1985) interpretation, this jump was modeled by a combination of two features: the high velocity wedge was shaped so that rays were totally internally reflected from its bottom edge, and deeper rays were deflected under a fortuitously positioned continental Moho. The exact shape of the wedge and position of the Moho are critical in this interpretation. The LITHOPROBE onshore reflection line (Green et al., 1990) does not support the shape of the wedge and no other data constrain the position of the continental Moho.

In the present interpretation, the travel time jump is also modeled by truncating the Vancouver Island phase and delaying deeper diving rays. However, the mechanism is quite different from that of Spence et al. (1985) and probably more realistic. Figures 4a, 5a and 6a show that rays travelling subhorizontally *through* the high velocity wedge are totally internally reflected from the underside of a boundary at 16 km depth above which the velocity increases. There is evidence from the VISP refraction line IV (McMechan and Spence, 1983) that there is an appropriate velocity inversion at about this depth. The eastern boundary of the high velocity wedge coincides with a marked change in reflection character on LITHOPROBE reflection line. This change in reflection character marks the bottom of an easterly dipping deformation front, presumably related to under-thrusting of the subducting plate. Rays diving *below* the high velocity wedge turn and hit the 16 km boundary at steep angles, allowing transmission up to the mainland receivers. These deeper rays arrive late at the mainland because of the proposed low velocities in the lower continental crust.

P Shots — Second Arrivals

P shot second arrivals at the mainland receivers have five times the amplitude and a quarter of the frequency (2-3 Hz) of the first arrivals (~ 8 Hz). Five possible ways of explaining these differences are discussed below.

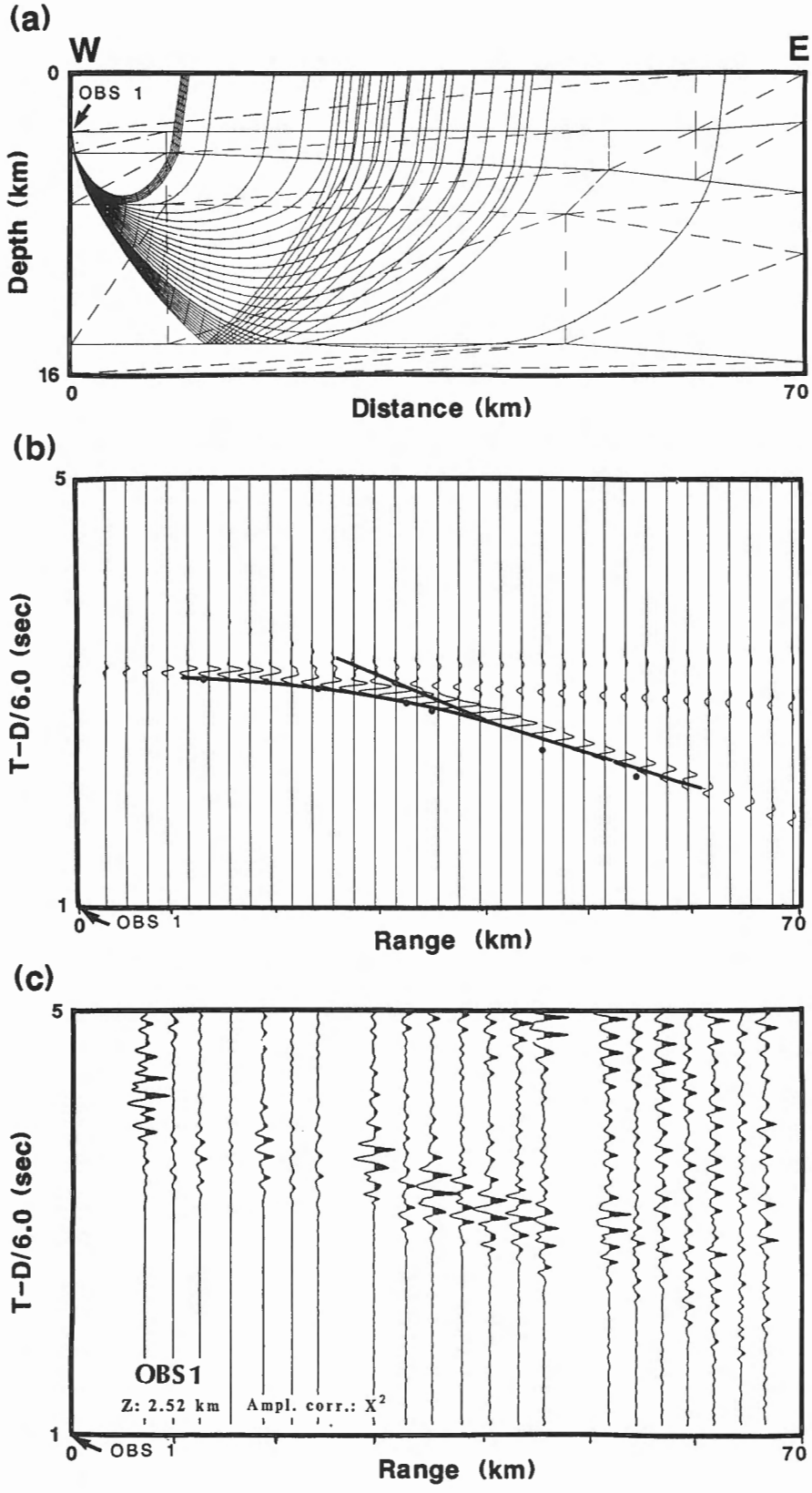

Figure 2. a) Ray diagram, b) synthetic seismograms and c) observed seismograms for OBS1. Solid lines on the synthetic seismograms mark geometric arrivals, dots represent travel time picks from the observed seismograms. Both observed and synthetic seismograms have an amplitude correction of range $^2/100$ and are reduced at 6 km/s.

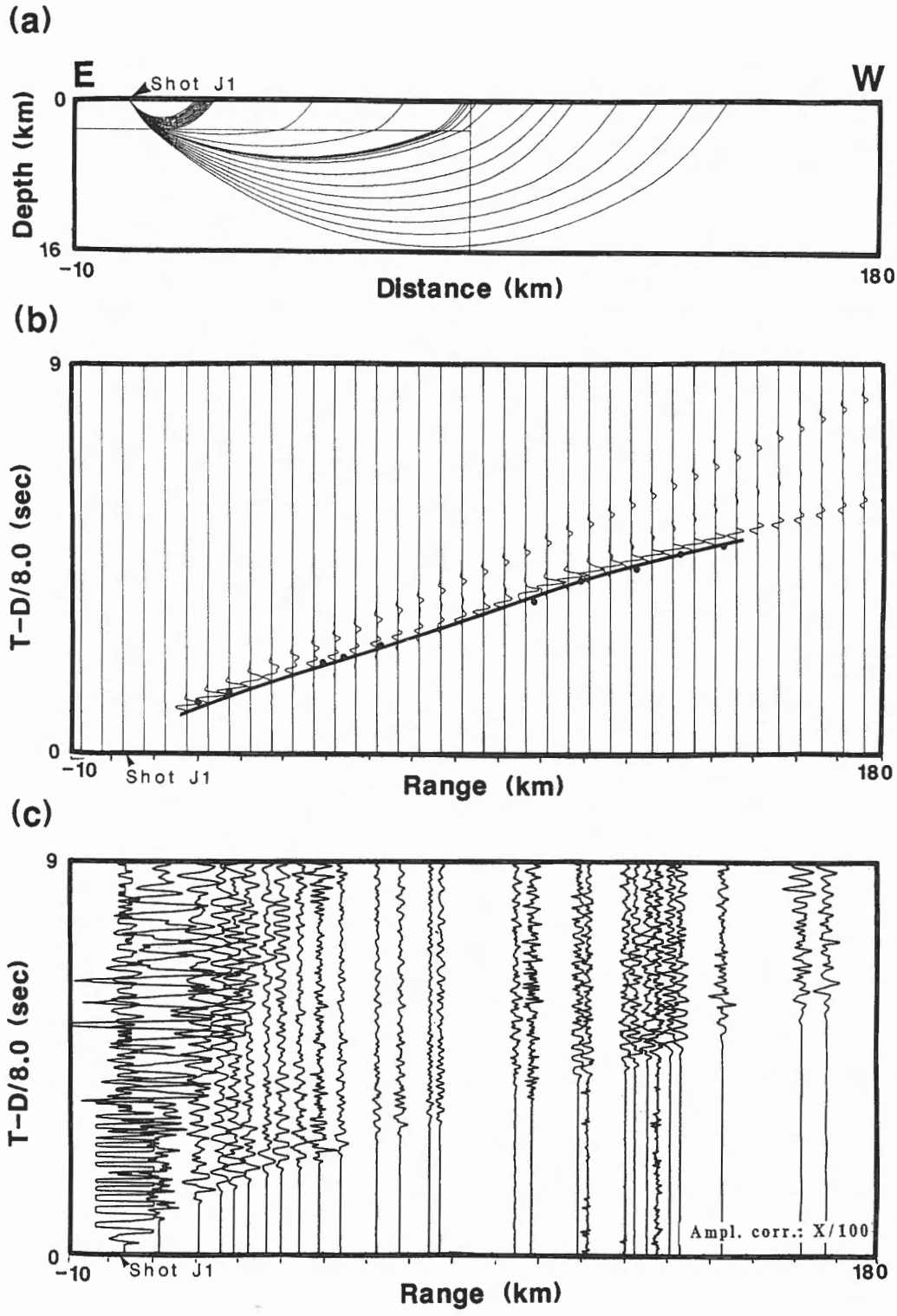

Figure 3. a) Ray diagram, b) synthetic seismograms and c) observed seismograms for shot J1. Amplitude correction is range/100, reduction velocity is 8 km/s.

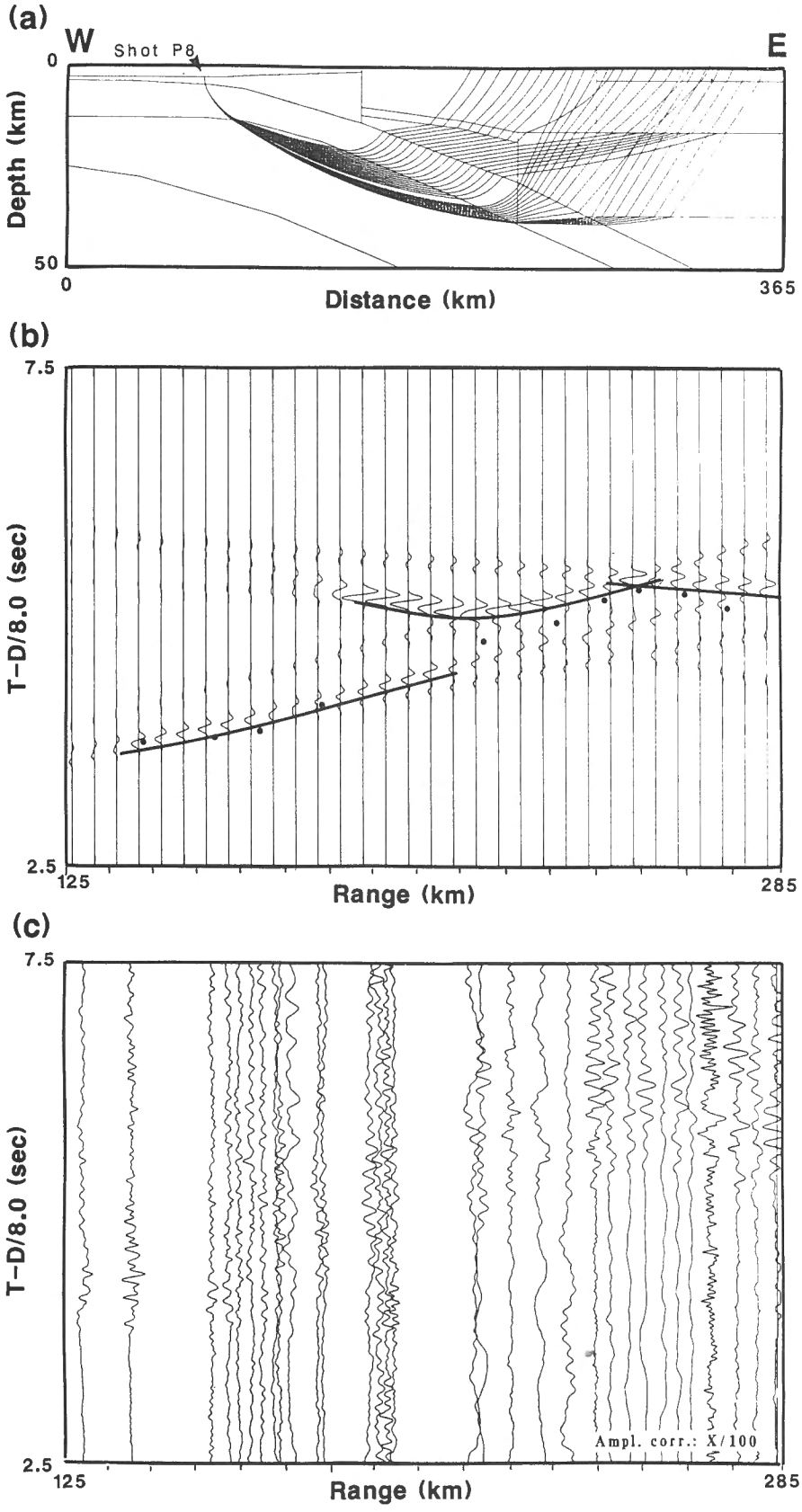

Figure 4. a) Ray diagram, b) synthetic seismograms and c) observed seismograms for shot P8. Amplitude correction is range/100, reduction velocity is 8 km/s. Rays that stop at the 16 km deep boundary between 300 and 365 km are totally internally reflected.

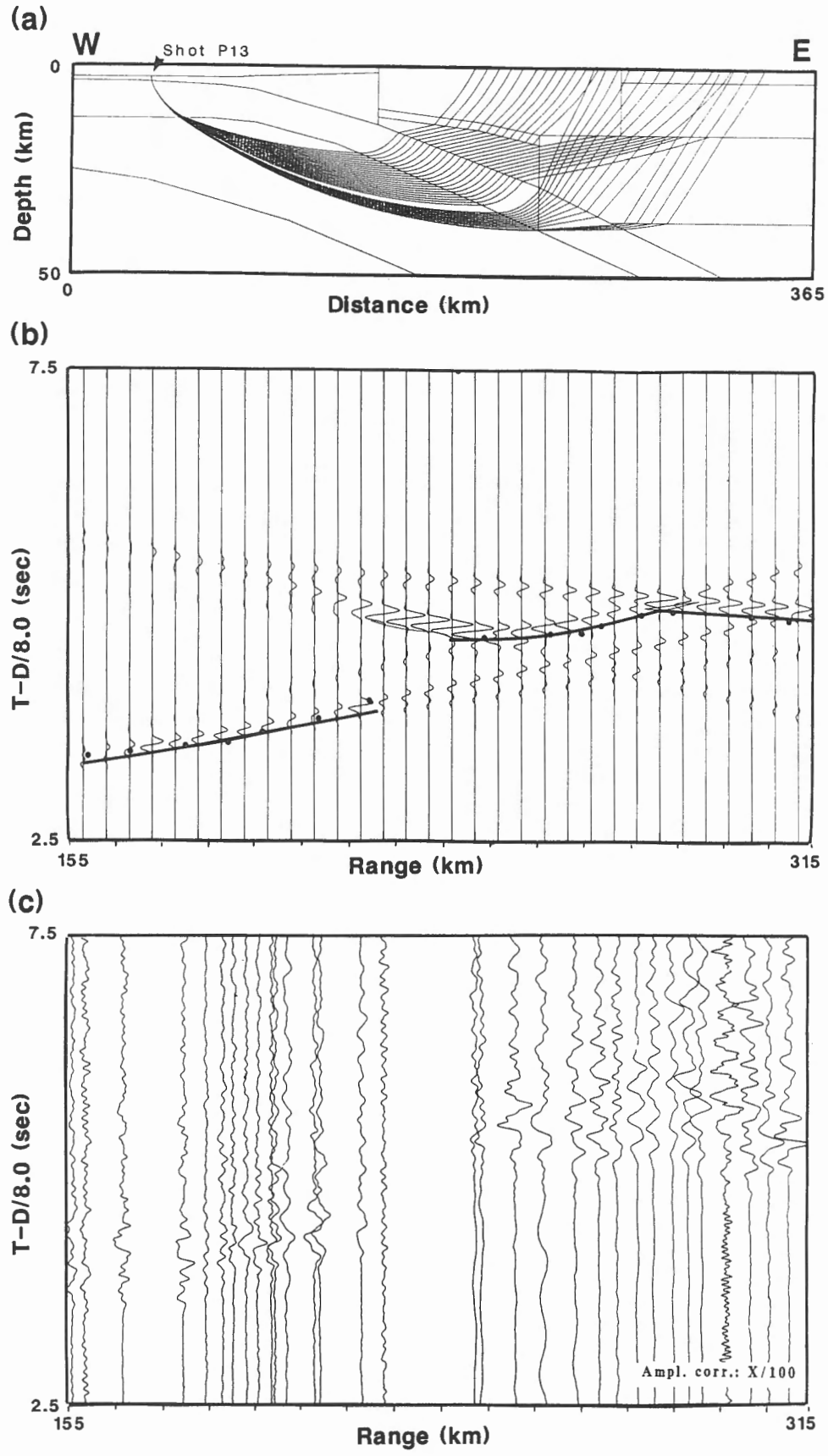

Figure 5. a) Ray diagram, b) synthetic seismograms and c) observed seismograms for shot P13. Amplitude correction is range/100, reduction velocity is 8 km/s.

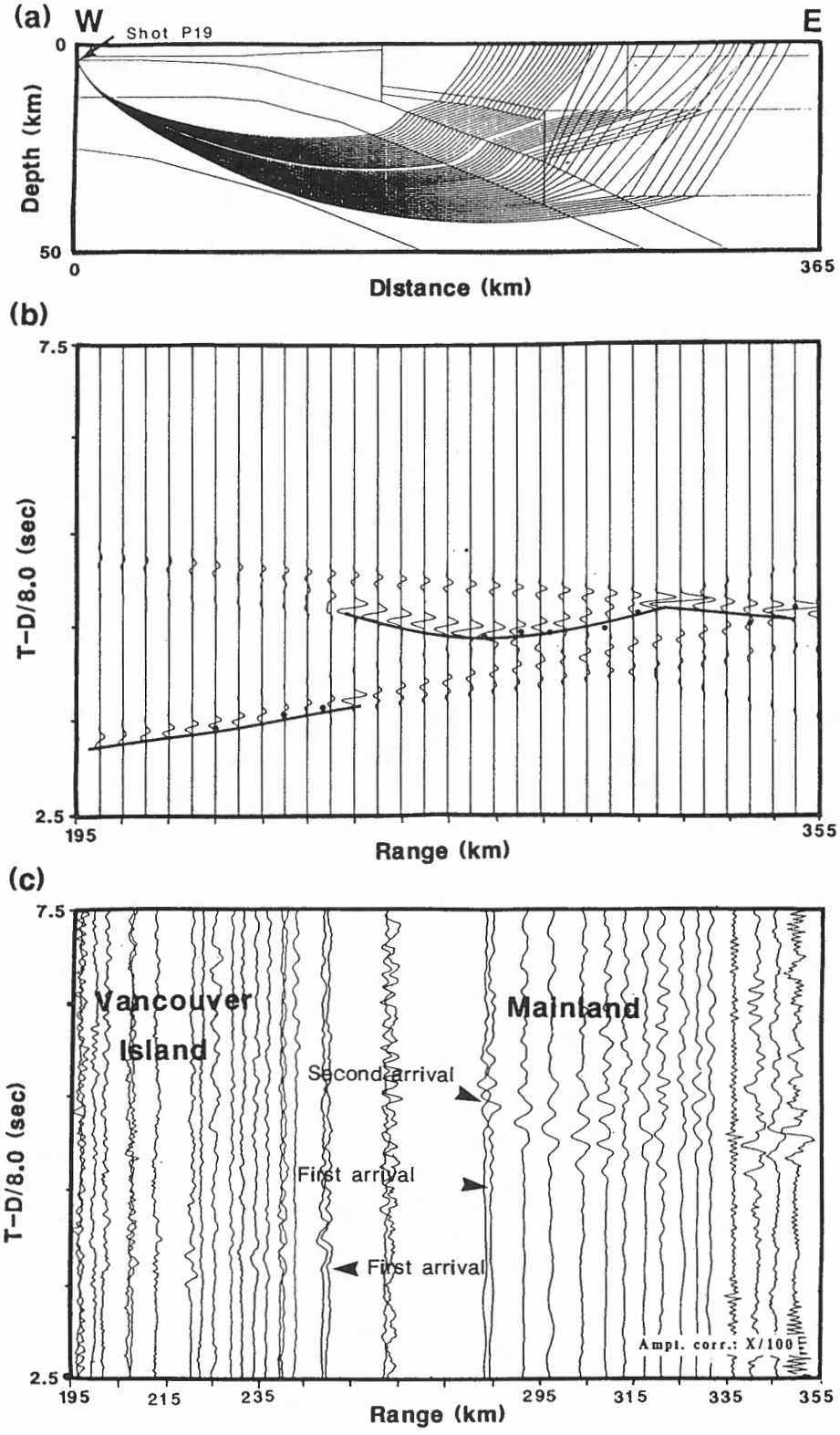

Figure 6. a) Ray diagram, b) synthetic seismograms and c) observed seismograms for shot P19. Amplitude correction is range/100, reduction velocity is 8 km/s.

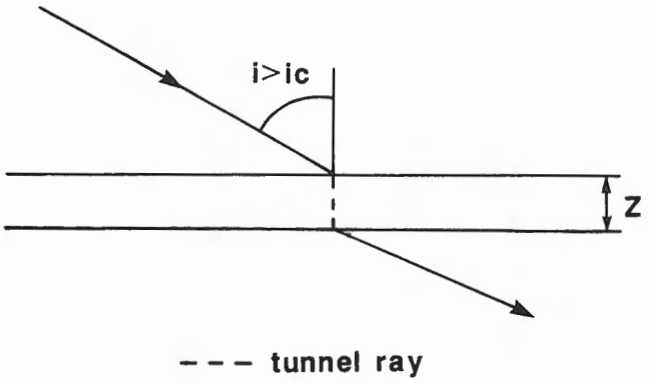

Figure 7. Tunnelling through a thin high velocity layer. Postcritical body waves leak through a high velocity layer and convert back to body waves at the lower boundary. The amplitude of the emerging ray will be of the same order as the incident ray if z is less than a quarter-wavelength.

Tunnelling through high velocity layers

In solving the wave equation, the complex solution is usually ignored. Complex or tunnelling rays decay exponentially but, in some cases, they can produce large amplitude arrivals. Figure 7 shows body waves super-critically reflected from a thin high velocity layer. Tunnelling rays leaking through the layer are converted back to body waves at its lower interface. The decay in amplitude of these tunnelling rays is described by :

$$A \sim \exp\,[-wz\,(1-c^2/V^2)^{1/2}\,/c]$$

where w is the angular frequency, c is the phase velocity, V is the velocity in the layer of thickness z. Fuchs and Schulz (1976) showed that a thin high velocity layer could transmit high amplitude tunnelling rays as long as z is smaller than a quarter wavelength. Tunnelled rays have a substantially lower frequency content because their amplitudes decay exponentially with frequency. Such a thin high

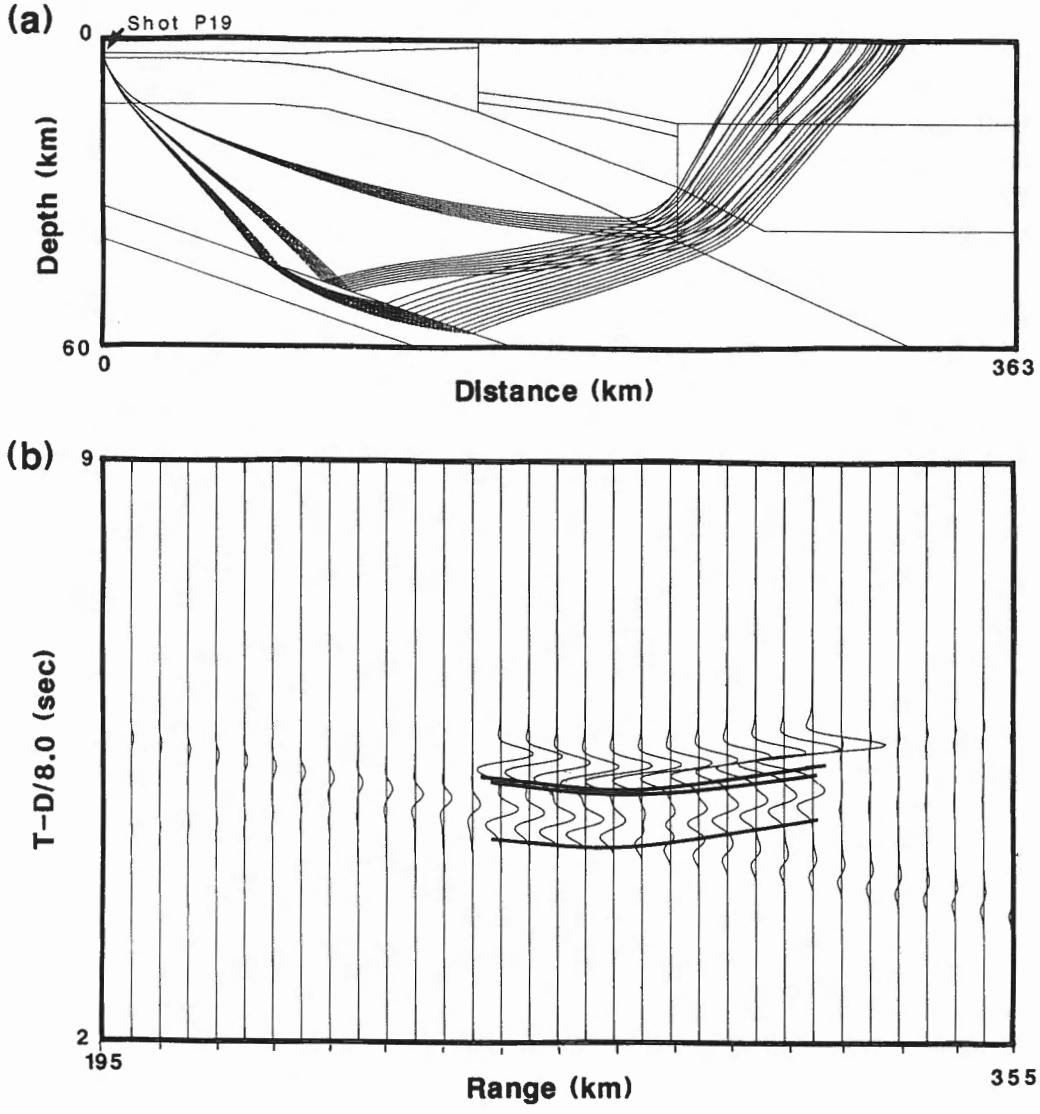

Figure 8. a) Ray diagram and b) synthetic seismograms for shot P19. The seismograms of a deep reflection and turning ray interfere at the mainland receivers. The resulting observed arrival has a higher amplitude and lower frequency than either of the two phases alone.

velocity layer in the lower oceanic lithosphere could produce the required low frequencies of the second mainland arrivals, but they would not explain their high amplitudes relative to other arrivals on the observed seismograms.

Interference of two or more phases

Figure 8 shows the results of constructively interfering a reflection and a turning ray from a deep transition zone. In this example, two high amplitude arrivals have been added to yield a slight increase in amplitude and an apparent decrease in frequency. Obtaining a consistent constructive interference pattern proved difficult with a strongly two-dimensional structure. Therefore, it is unlikely that this approach could produce the change in amplitude and frequency required to model the observed difference between first and second arrivals.

Reflections from a gradient zone

A gradient zone reflects low frequencies and transmits high frequencies at sub-critical angles. The relationship between reflection coefficient, dominant wavelength and zone thickness is shown in Figure 9 (Jones, 1986) for the normal incidence case. The first arrivals on the record sections for P13 and P19 have a frequency of about 8 Hz. If the gradient zone had an average velocity of 8 km/s and was 1 km wide, it would have a relative reflection coefficient of 0.15. Lower frequencies in the incident signal, say 2 Hz, would have a relative reflection coefficient of 0.85. A gradient zone thus can preferentially reflect low frequencies, but again their amplitudes would not be large compared to other arrivals on the seismograms.

Interference between reflections from laminae

Interference between reflections from alternating high and low velocity layers has been proposed by many authors to explain high amplitude deep reflections. Fuchs (1969) modeled reflections from laminae and showed that amplitudes increased with increasing impedance contrast and number of layers. The increase in amplitude depends greatly on fine tuning of the laminae and it is difficult to obtain a five times increase in amplitude by this method.

Diffractions

The 1 s jump in travel time between the Vancouver Island and mainland arrivals was explained by most authors at the CCSS workshop as being due to a structure that truncates the Vancouver Island phase. The modeled structures were placed at or near the deformation front seen at about shotpoint 1450 in Figure 1 of Green et al. (1990). Such a structure could produce diffractions. In the synthetic seismograms for the P shots (Fig. 4b, 5b and 6b), the non-geometric early arrivals at the mainland receivers are produced by a truncation of the Vancouver Island phase. Because of the limitations of the ray method, these arrivals have incorrectly large amplitudes and their arrival times

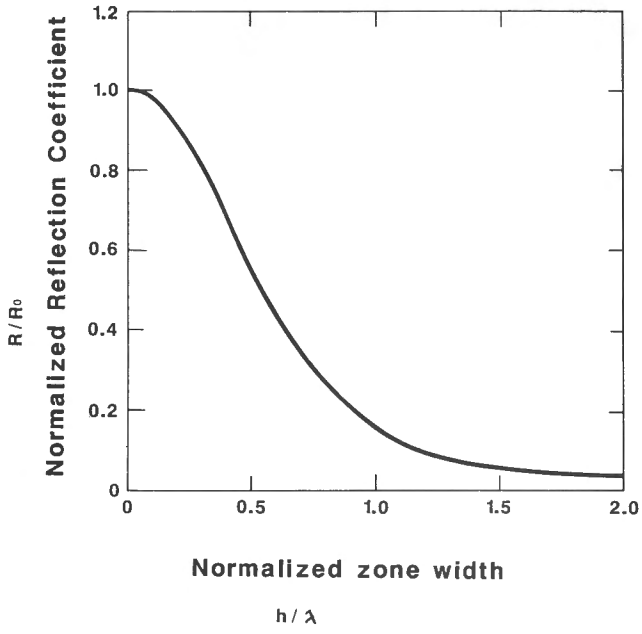

Figure 9. The variation of reflection coefficient with frequency for a gradient zone at normal incidence. R/R_0 is plotted against h/λ where R is the reflection coefficient, R_0 is the reflection coefficient for a perfectly sharp interface, h is the thickness of the gradient zone, and λ is the dominant wavelength of the incident wavelet.

are calculated assuming lateral homogeneity. Correctly calculated arrivals would have smaller amplitudes and arrival times depending on lateral structural changes. The first arrivals between 280 and 305 km (Fig. 6c) could thus be diffracted shadow zone arrivals ; they would have the required low amplitudes and high frequencies. Deeper turning or reflected rays that dive below the deformation front could produce the second mainland arrivals ; they would have higher amplitudes than the diffracted rays, and could also have a lower frequency content if the high frequencies were attenuated due to the longer ray paths.

CONCLUSIONS

If the first and second arrivals are deep turning and reflected rays respectively, it is extremely difficult to explain the difference in their amplitude and frequency content. Therefore, it is proposed that the small amplitude first arrivals are in fact diffractions and that the second arrivals are deeper diving or reflected rays. The main differences between the Spence et al. (1985) model and the model proposed here are summarized in Table 1. The most significant improvements are :

(i) the new model is consistent with the reflection data,

(ii) the model is not dependent on exact boundary shapes,

(iii) the final model is one of a series of solutions, and

(iv) amplitudes and frequencies, as well as travel times, have been considered.

Table 1.

Spence et al. Model	New Model
The intersection between the continental Moho and subducting plate produces the one-second delay.	Low velocity zone in the lower continental crust gives the delay.
Dip of high velocity wedge = 0°	Dip of high velocity wedge = 6°
Dip of subducting plate = 14°	Dip of subducting plate = 11°
First and second mainland arrivals are modeled with turning and reflected rays respectively.	First mainland arrivals are interpreted to be diffractions and the second arrivals deeper turning rays.

The proposed low velocity zone in the lower crust below the mainland could be explained by rock with high fluid content. The deformation front is likely to be highly fractured and permeable, compared with the high velocity (presumably mafic) material to its west and, therefore, may be used as a conduit for water escaping from the downgoing plate. In a magnetotelluric model over the margin, Kurtz et al. (1986) found a conductive block coincident with the low velocity zone proposed here, supporting the hypothesis that this zone may have a high fluid content.

In conclusion, the importance of acquiring a multitude of data sets is demonstrated here. The refraction data alone do not resolve the deep structure of the margin ; further constraints from seismicity, magnetotelluric and reflection profiling data are invaluable. To further investigate the deep structure of the margin, deep refraction and reflection profiles on the mainland may help resolve the lower continental velocities and Moho depth.

ACKNOWLEDGMENTS

Forward modeling was computed on the Bullard Laboratories' VAX 11/750. Thanks to George Spence for ideas and discussion, and Dave Lyness and Chris Chapman for the Maslov forward modeling program.

Cambridge Earth Science contribution Number ES 1081.

REFERENCES

Chapman, C.H. and Drummond, R.
1982 : Body wave seismograms in inhomogeneous media using Maslov asymptotic theory ; Seismological Society of America, Bulletin, v. 72, p. 5277-5317.

Fuchs, K.
1969 : On the properties of deep crustal reflectors ; Journal of Geophysics, v. 35, p. 133-149.

Fuchs, K. and Schulz, K.
1976 : Tunnelling of low-frequency waves through the sub-crustal lithosphere ; Journal of Geophysics, v. 42, p. 175-190.

Green, A.G., Clowes, R.M., and Ellis, R.M.
1990 : Crustal studies across Vancouver Island and adjacent offshore margin ; Studies of Laterally Heterogeneous Structures Using Seismic Refraction and Reflection Data, ed. A.G. Green ; Geological Survey of Canada, Paper 89-13, p. 3-25.

Jones, R.H.
1986 : Seismic reflections from major faults ; unpublished Ph.D. thesis, University of Cambridge, UK.

Kurtz, R.D., De Laurier, J.M., and Gupta, J.C.
1986 : A magnetotelluric sounding across Vancouver Island detects the subducting Juan de Fuca plate ; Nature, v. 321, p. 569-599.

McMechan, G.A. and Spence, G.D.
1983 : P-wave velocity structure of the Earth's crust beneath Vancouver Island ; Canadian Journal of Earth Sciences, v. 20, p. 742-752.

Rogers, G.C.
1979 : Earthquake fault plane solutions near Vancouver Island ; Canadian Journal of Earth Sciences, v. 16, p. 523-531.

Spence, G.D., Clowes, R.M., and Ellis, R.M.
1985 : Seismic structure across the active subduction zone of western Canada ; Journal of Geophysical Research, v. 90, p. 6754-6772.

Steinmetz, L., Whitmarsh, R.B., and Moreira, V.S.
1977 : Upper mantle structure beneath the Mid-Atlantic Ridge, north of the Azores based on observations of compressional waves ; Royal Astronomical Society, Geophysical Journal, v. 50, p. 353-380.

Taber, J.J. and Smith, S.W.
1985 : Seismicity and focal mechanisms associated with the subduction of the Juan de Fuca plate beneath the Olympic Peninsula, Washington ; Seismological Society of America, Bulletin, v. 75, p. 237-249.

Thompson, C.J. and Chapman, C.H.
1986 : End point contributions to synthetic seismograms ; Royal Astronomical Society, Geophysical Journal, v. 87, p. 285-294.

Application of the Gaussian beam method to refraction data from the subduction zone beneath Vancouver Island and the North American mainland

M.H. Weber [1]

Weber, M.H., Application of the Gaussian beam method to refraction data from the subduction zone beneath Vancouver Island and the North American mainland; in Studies of Laterally Heterogeneous Structures Using Seismic Refraction and Reflection Data, ed. A.G. Green; Geological Survey of Canada, 89-13, p. 43-52, 1990.

Abstract

The seismic refraction sections J1, P8, P13 and P19 recorded across Vancouver Island and adjacent areas were modeled by the Gaussian beam method. Starting from the Spence et al. model, a velocity structure was determined using travel time information only. The inclusion of attenuation with Q-values of either 375 or 750 changed the amplitudes markedly, especially for large source-receiver offsets. Unfortunately the data quality was not good enough for a final choice of Q structure. Nevertheless, there are indications that this range of Q-values leads to an agreement between synthetics and the data which is as good as, or better than a medium without attenuation.

Résumé

Les profils de sismique réfraction J1, P8, P13 et P19 enregistrés sur l'île de Vancouver et les environs ont été modélisés au moyen de la méthode du faisceau gaussien. Partant du modèle de Spence et coll., on a déterminé une structure de vitesse en n'utilisant que des renseignements sur le temps de parcours. La prise considération de l'atténuation avec des valeurs Q de 375 ou de 750 a changé énormément les amplitudes, particulièrement pour les grandes distances source-récepteur. Malheureusement, la qualité des données n'était pas suffisante pour arrêter le choix d'une structure de Q. Certaines indications montrent néanmoins que l'utilisation de ces valeurs de Q se traduit par un accord entre les données synthétiques et les données observées qui est aussi bon sinon meilleur que pour un milieu sans atténuation.

[1] Seismologisches Zentralobservatorium GRF, Krankenhausstr. 1, D-8520 Erlanger, F.R.G.

GAUSSIAN BEAM METHOD

The Gaussian beam method (GBM) is a high-frequency approximation that combines the advantages of ray methods (RM) with elements of wave theory. The GBM is applicable in complicated 2- and 3- dimensional media with absorption. Whereas the RM breaks down at caustics, critical distances and in shadow zones, the GBM produces relatively accurate seismograms in these areas.

Following Červený and Pšenčík (1984) the principal component of a Gaussian beam in the frequency domain in 2-D media can be expressed as:

$$u(s,n,w) = A(s)\cdot e^{[-iwT]}\cdot a(s) \qquad (1)$$

where

$$A(s) = \left[\frac{v(0)\sigma(0)q(0)}{v(s)\sigma(s)q(s)}\right]^{1/2},$$

$$T = \{\gamma(s) + 0.5\cdot M(s)\cdot n^2\},$$

$$a(s) = \begin{matrix} t \text{ for P Gaussian beams} \\ n \text{ for SV Gaussian beams} \\ b \text{ for SH Gaussian beams,} \end{matrix}$$

and A(s) is the complex valued amplitude term, t is the tangent vector to the central ray in the (x,z) plane, n lies in the (x,z) plane and t, n, b form a right-handed system of unit vectors. In equation (1), s and n are the ray-centred co-ordinates along the central ray, where s is the distance along the central ray from the source and n perpendicular to it, and v and σ are velocity and density, respectively. $\gamma(s)$ is the travel time along the central ray and $M(s) = p(s)/q(s)$ is given by the functions:

$$p(s) = \epsilon p_1(s) + p_2(s)$$
$$q(s) = \epsilon q_1(s) + q_2(s)$$
$$\epsilon = \epsilon_1 + \epsilon_2, \qquad \epsilon_2 \geq 0$$

where ϵ is the Gaussian beam parameter and p_i, q_i, $i = 1, 2$ are the two real, independent solutions of the dynamic ray-tracing system:

$$(p_i)_s = \frac{(-v)_{nn}}{v^2}\cdot q_i \; ; \; (q_i)_s = v\cdot p_i \qquad (2)$$

Here the subscripts s and nn denote single and double differentiation with respect to the appropriate ray-centred co-ordinates. The initial conditions at $s = 0$ are chosen as:

$$p_1(0) = 0, \; p_2(0) = 1 \; [skm^{-1}]$$

$$q_1(0) = 1, \; q_2(0) = 0 \; [km].$$

Summing all beams for all frequencies at a receiver and transforming the result into the time domain yields the Gaussian beam seismogram.

At caustics, RM become invalid because of problems with divergent amplitudes, which are produced when the cross-sectional area of the ray tube, a term equivalent to q(s) in equation (1), becomes zero. This problem does not arise for Gaussian beams because q(s) is non-zero for all s.

A computational advantage of the GBM as compared to RM is that time-consuming two-point ray-tracing is not necessary. There is no need to find the ray(s) which exactly hits the receiver as in RM, because the imaginary part of $[0.5.M(s).n^2]$ in equation (1) distributes the energy of the beam in a Gaussian bell-shaped amplitude profile, so that all beams in the neighbourhood of a receiver location contribute to the seismogram. For details and a comparison of the GBM with other synthetic seismogram methods see Weber (1988a).

APPLICATION OF THE GBM

The seismic sections J1, P8, P13 and P19 (Fig. 6 to 9 of Green et al., 1990) were modeled by GBM. Results are presented here for sections J1 and P13. The aim of this study was to deduce the velocity structure under these profiles and gain information on the Q structure.

PROCEDURE EMPLOYED

Parameterization

A starting velocity model was created using Figure 13 of Green et al. (1990). In the GBM program the model is parameterized by triangles with arbitrary linear density and velocity gradients:

$$v_p^t(x,z) = a^t x + b^t z + c^t$$

$$v_s^t(x,z) = d^t x + e^t z + f^t$$

$$\sigma^t(x,z) = g^t x + h^t z + j^t$$

where v_p^t, v_s^t and ^{t} are P-velocity, S-velocity and density in each triangle t and a^t through j^t are real numbers. Modeling media with wedge-shaped discontinuities is relatively straight-forward using triangles, whereas using spines for such a structure would be cumbersome. For a media with linear velocity increases the dynamic and the kinematic ray-tracing is very fast because analytical solutions exist for the differential equations. In general, the model adopted here is a smoothed version of the starting model thus avoiding the creation of artificial interfaces, like the vertical interfaces separating blocks with different velocities and gradients of Figure 13 of Green et al. (1990).

Model adjustments using travel times

The velocity model was improved by finding, via educated trial and error, modifications to the original model to produce a better fit of the travel time curves to the onset of phases in the data. This was achieved by moving the knots of the triangle net (*see* Fig. 1) and/or by changing the velocity at these knots. The procedure employed was to start with the high quality section J1 and proceed to successively lower quality data sets, i.e., in the order P13, P19 and P8. The model was modified until the travel times in all sections were matched adequately. Only minor modifications to the initial model were necessary. Figure 2 shows the P-velocity isoline plot of the final model and Figure 3 shows the discontinuities of first order and selected P-phases used in the modeling.

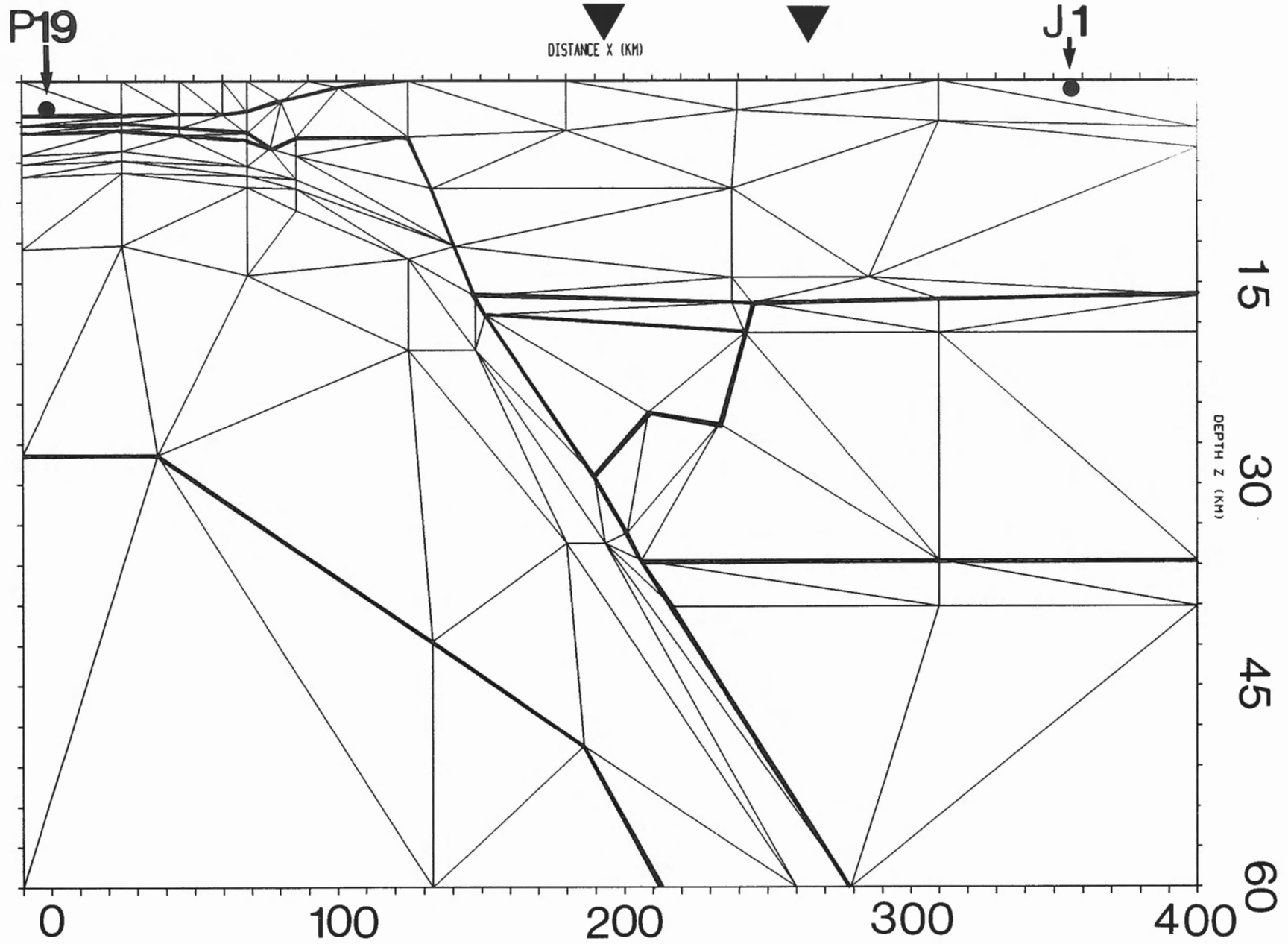

Figure 1. Triangles used to model the crustal structure under Vancouver Island and adjacent areas. Profile from shots P19 to J1. The bold lines are the discontinuities of first order. The arrowheads indicate the west and east coasts of Vancouver Island. To show the finer details of the model, the vertical exaggeration is 4.6.

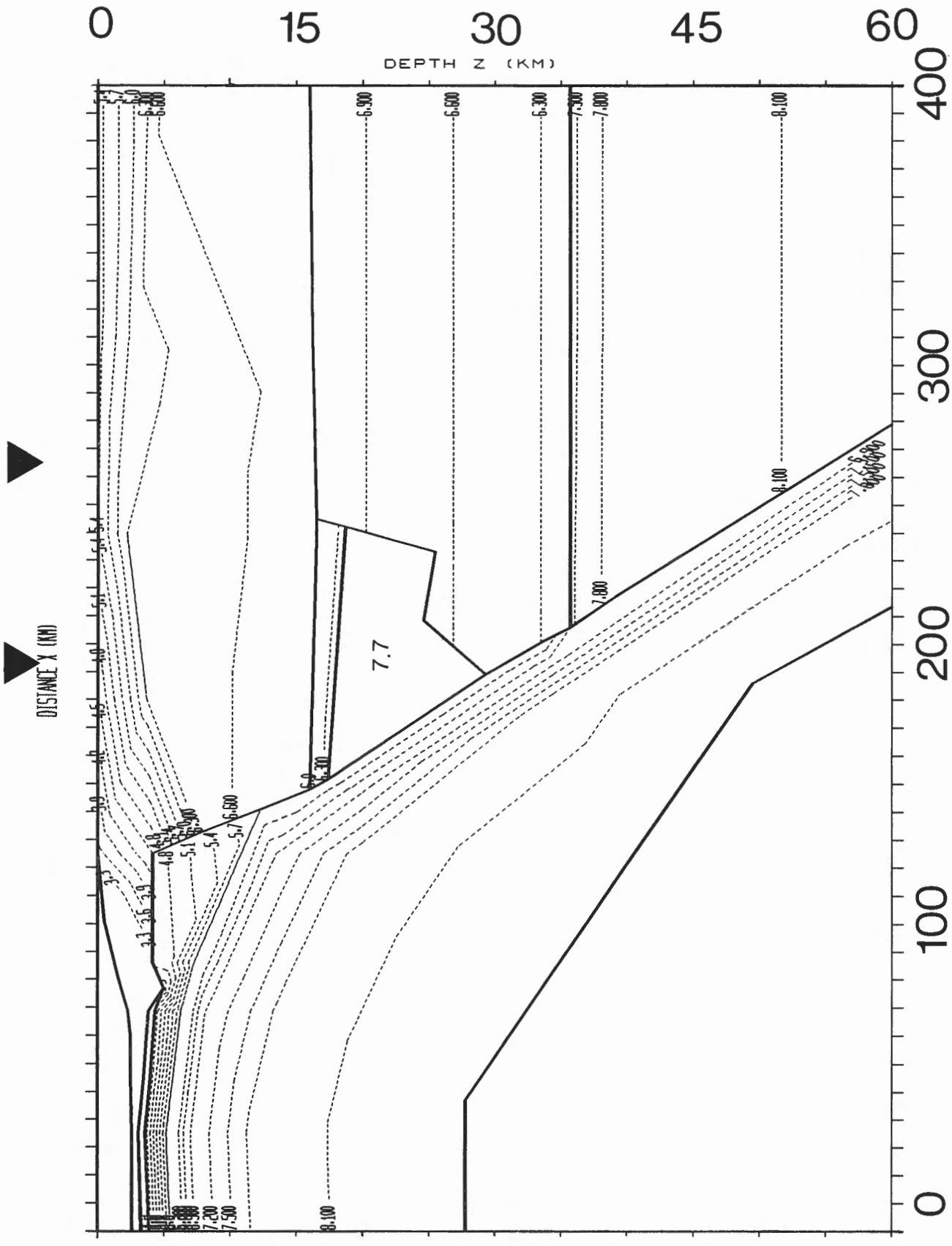

Figure 2. Final model, P velocity isolines larger than 3.0 km/s in 0.3 km/s steps. The vertical exaggeration is 4.6.

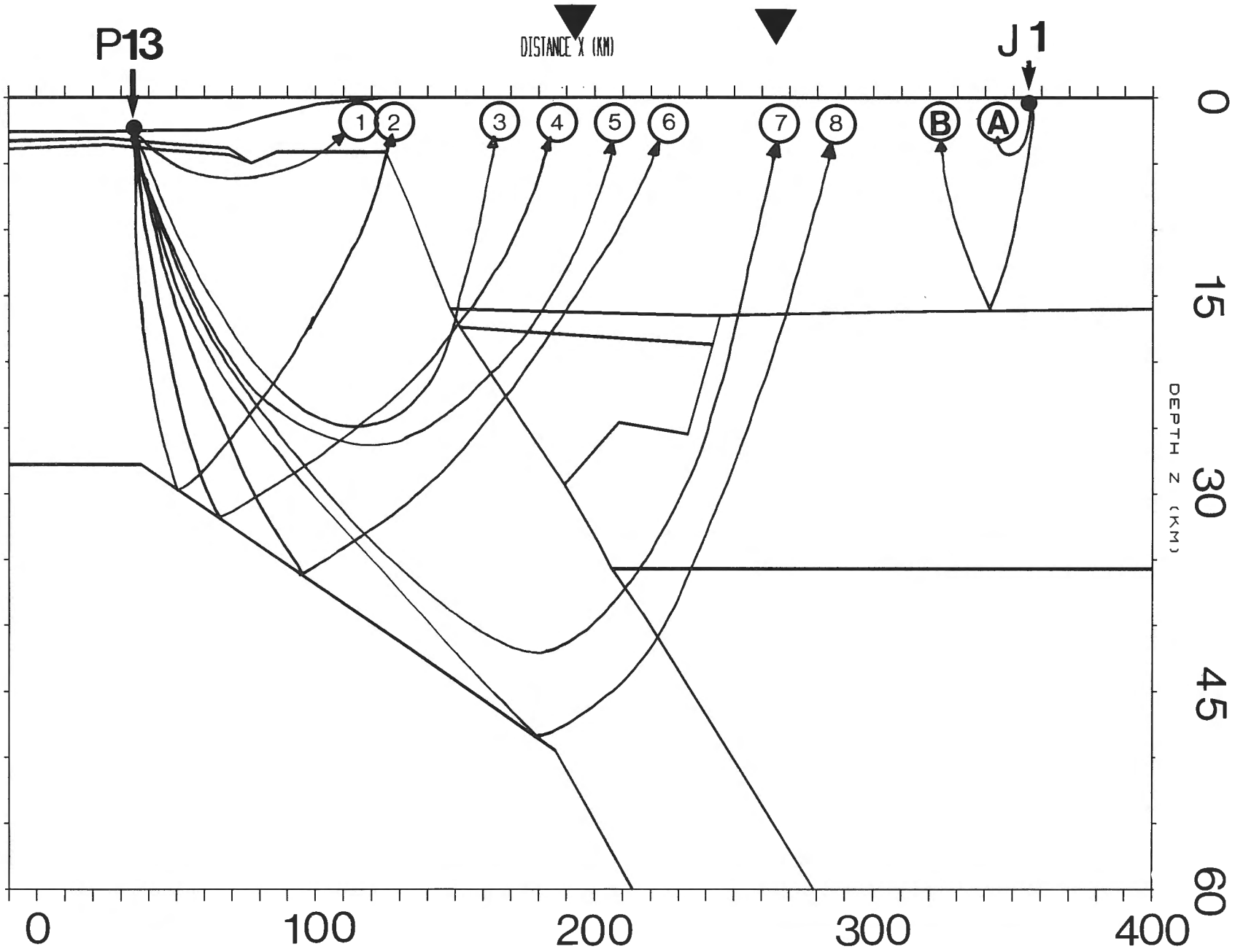

Figure 3. Sketch of primary P-reflections and diving waves in the final model as represented by the first order discontinuities. The vertical exaggeration is 4.6.

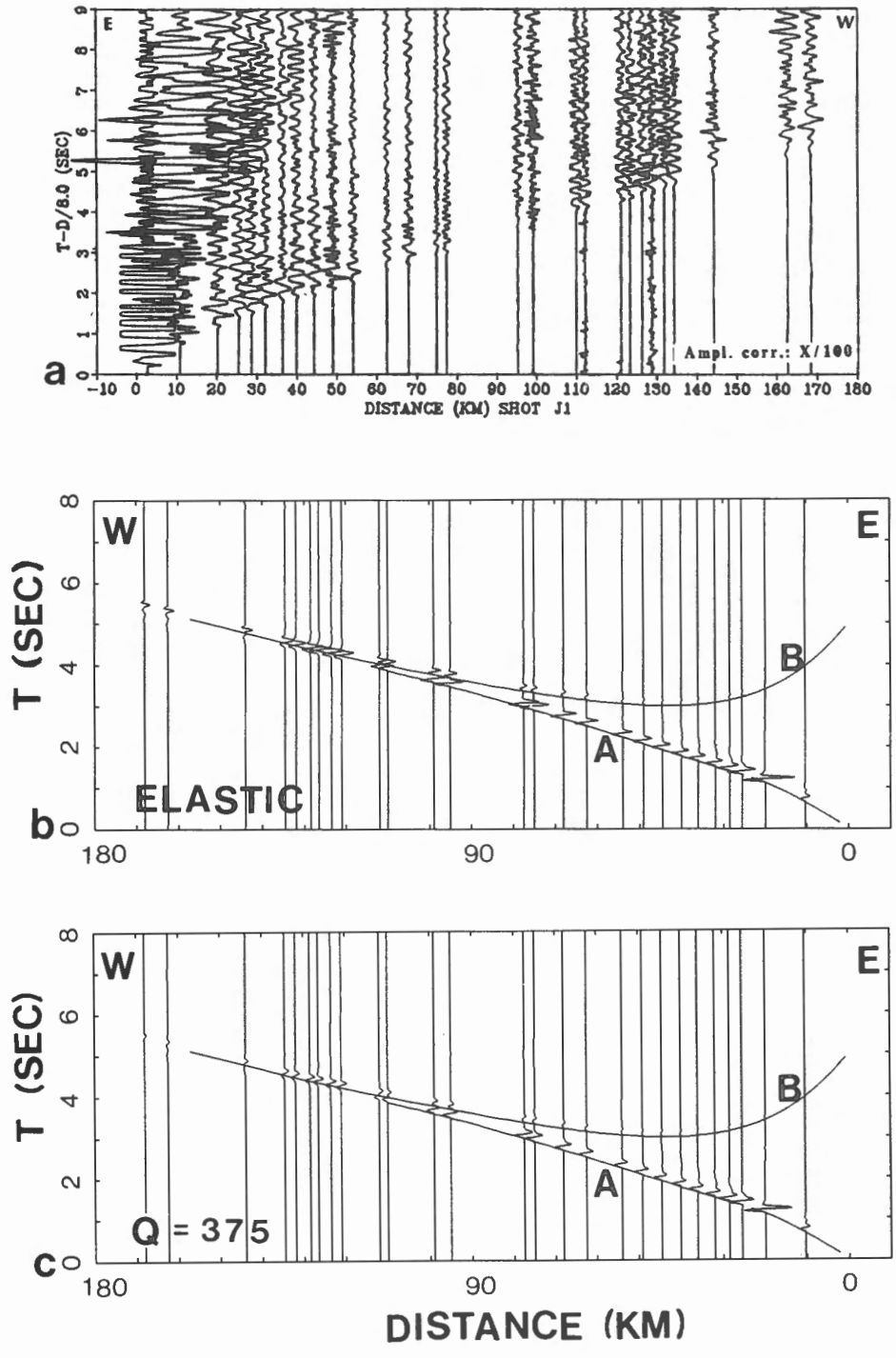

Figure 4. (a) Seismic refraction section recorded across Vancouver Island and adjacent regions from shot point J1. (b) Section of vertical-component seismograms computed with the GBM for the profile of shot J1. The reduction velocity is 8.0 km/s. Phase A is the diving wave, and phase B is the reflection from the discontinuity at 16 km depth (*see* Fig. 3). All amplitudes are multiplied by a factor proportional to the source-receiver distance. The medium is assumed to be elastic. Note that this synthetic section is reversed relative to (a). (c) As for (b), but the quality factor Q is 375 throughout the model.

Amplitude information

In the following, only seismic sections J1 and P13 are shown because their data have the best quality. The other two sections, P8 and P19, were also used but are not shown here.

The velocity structure was determined via the travel times, and then the amplitudes of signals were used to gain information on the attenuation structure. This procedure was chosen because travel time depends only on the velocity and attenuation has almost no influence on travel time. In contrast, amplitudes are influenced heavily by attenuation so cannot be used as independent parameters to gain velocity information.

Before presenting the seismograms it is worth pointing out that it is very difficult with these kind of data to compute estimates of the Q structure. Amplitude-distance curves (i.e., the relative amplitudes of adjacent traces) cannot be used to gain information on Q because of the variable coupling of the seismometers to the ground, multiples produced by layered structures (e.g., sediments), and diffractions from small local inhomogeneities. Because the size of these effects is at least of the same order as the effects of attenuation along the path of propagation it is doubtful that even trends in relative amplitudes of adjacent traces can be used to draw firm conclusions on the Q structure. Therefore, only the amplitude ratios of the different phases within the same trace are useful for studies of Q. Unfortunately, due to the reasons mentioned above and the generally noisy character of the data, the identification of additional later phases in the Vancouver Island traces is at best speculative. Nevertheless, we model different Q values to show their effect on amplitudes. Weber (1988b) showed an example of where amplitudes were used to infer information on the Q structure in a complicated crust.

DISCUSSION OF DATA SETS J1 AND P13

Figure 4b shows the synthetic section computed for the velocity model of Figures 1 to 3 for the elastic case, and Figure 4c shows the synthetic section for a Q value of 375 throughout the model. This rather low crustal Q value was chosen on the basis of studies of absorption in western North America, which indicate a remarkably low Q value compared to that of eastern North America (Singh and Herrmann, 1983). The travel time fit is generally very good, so the velocity model describes the crustal structure well. Nevertheless, it should be mentioned that this is not the only possible model, because of the non-uniqueness of the modeling process. Note that the GBM gives realistic amplitudes in shadow zones (phase A at 26 km and phase B from 160 to 170 km), whereas RM would give no contributions in these regions. To suppress cut-off phases produced by computing only beams leaving the source within a limited range of takeoff angles, a tapering function has been applied. The tapering function reduces the amplitude of phase A at the first receiver.

Comparing the synthetic seismograms for the elastic case with the synthetic seismograms for the model with Q factor equal to 375, the most obvious effect is the change in relative amplitudes of phases A and B at receivers with source-receiver offsets larger than 120 km. Amplitudes of phase B for Q = 375 are reduced to about 50 % of the elastic model amplitudes ; beams of phase B travel longer in the absorbing crust than beams of phase A and are therefore more attenuated. This amplitude reduction can also be seen by comparing phase A from the elastic case (Fig. 4b) with phase A in the case of absorption (Fig. 4c) for distances larger than 50 km.

Comparison of the synthetics (Fig. 4b and 4c) with the observed section (Fig. 4a) seems, not surprisingly, to favour the model with attenuation. The effect of attenuation is most obvious at the two receivers between 160 and 170 km distance, where the onset of seismic energy at 5.5 s is very weak in the data. Because of the problems with amplitude-distance curves mentioned above, this only hints at the true nature of the crust, and is not conclusive. A Q-value of 750, which is about the upper limit for regions west of the Rocky Mountains according to Singh and Herrmann (1983), gives very similar results.

Figure 5 shows ray paths for P-phases from shot P13, and Figure 6 shows the observed data recorded from shot P13 and the appropriate GBM synthetic sections for the elastic case and for the same velocity model with Q factor of 375. The travel time fit to the data is satisfactory, so the velocity model seems to be appropriate. The advantage of the GBM compared to the RM is visible in the areas where gaps in the travel time curves occur (e.g. phase 5 at 200 km).

Comparing the synthetic seismograms (Fig. 6b and 6c), the reduction in amplitude of about 50 % for distances larger than 235 km is the most prominent effect of Q. Phases 8 and 9 penetrate much deeper than phases 3, 5 and 6 (*see* Fig. 3 and Fig. 5), so they travel longer in the attenuating media and are therefore damped more severely. Q also produces a low-pass filtering effect that lengthens the signal ; the superposition of phases 7 and 8 results in an "apparent" phase change of the seismic signal for distances larger than 235 km.

As before, the smaller amplitudes in the synthetic section computed with attenuation (Fig. 6c) seem to fit the data better than the results for the elastic model (Fig. 6b), but the data are not good enough for a definitive conclusion on the Q structure.

CONCLUSIONS

1. The velocity model derived is appropriate ; it yields a travel time fit consistent with the data. Due to the non-uniqueness of modeling, other models may also explain the observed data.

2. The data were not good enough (i.e., no clear later arrivals could be identified in the traces) to decide whether the tested Q structure is appropriate for this area of the crust and uppermost mantle. Nevertheless, there are indications that models with Q-values of 375 to 750 lead to synthetic seismograms that agree with the data at least as well as, or better than synthetic seismograms from a model without attenuation.

Figure 5. Ray paths of the P-phases traced through the model from shot P13. The arrowheads indicate the west and east coasts of Vancouver Island. The bold lines are the first order discontinuities. Vertical exaggeration is set to 4.6.

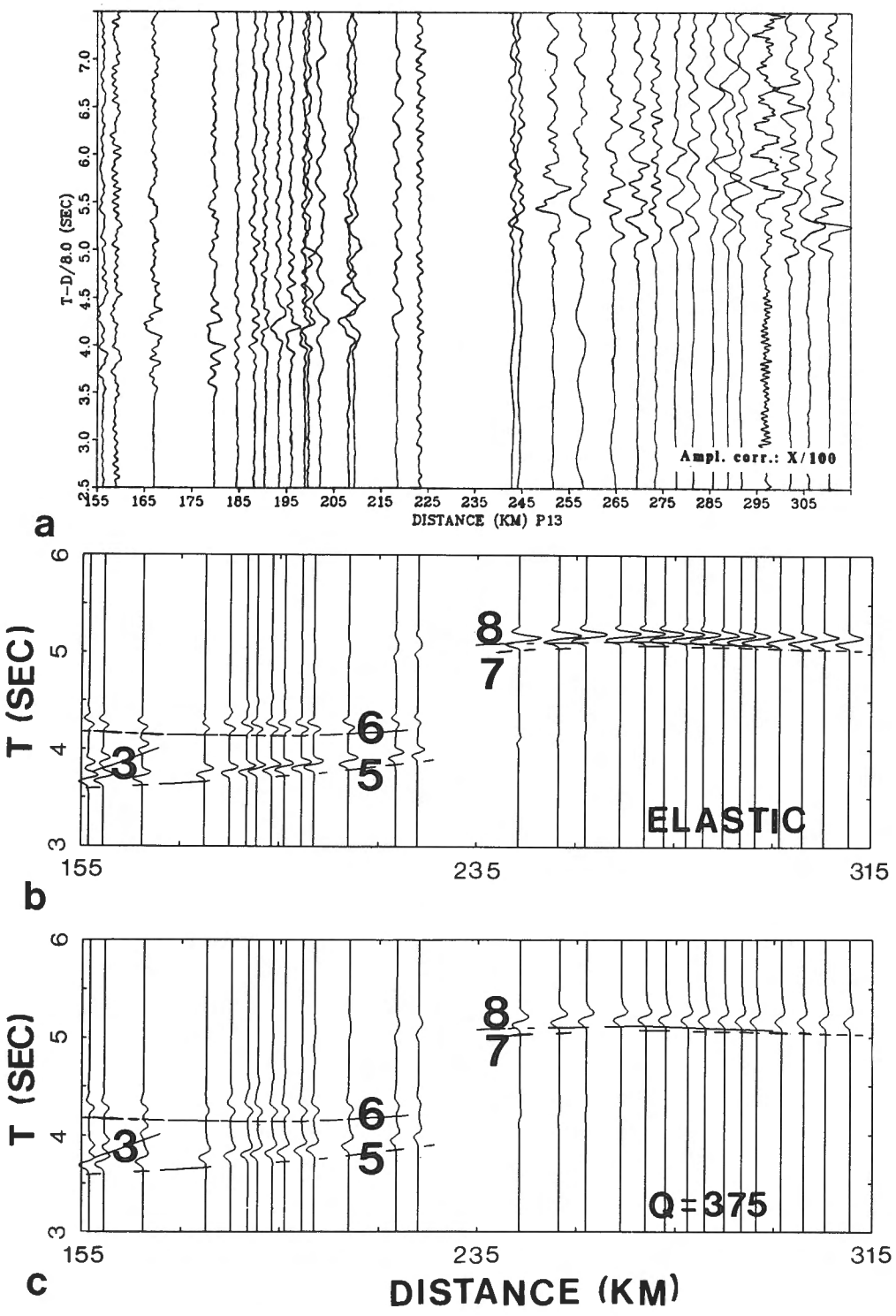

Figure 6. (a) Seismic refraction section recorded across Vancouver Island and adjacent regions from shot point P13. (b) Section of vertical-component seismograms computed with the GBM for the profile of shot P13. The reduction velocity is 8.0 km/s. For the code of the P-phases see Figure 3. All amplitudes are multiplied by a factor proportional to the source-receiver distance. The medium is assumed to be elastic. (c) As for (b), but the quality factor Q is 375 throughout the model.

ACKNOWLEDGMENTS

I would like to thank Alan Green and two anonymous reviewers for numerous comments to the initial version of this paper.

REFERENCES

Červený, V. and Pšencík, I.
1984 : Gaussian beams in two-dimensional laterally varying layered structures ; Royal Astronomical Society, Geophysical Journal, v. 78, p. 65-91.

Green, A.G., Clowes, R.M., and Ellis, R.M.
1990 : Crustal studies across Vancouver Island and adjacent offshore margin ; *in* Studies of Laterally Heterogeneous Structures Using Seismic Refraction and Reflection Data, ed. A.G. Green ; Geological Survey of Canada, Paper 89-13, p. 3-25.

Singh, S. and Herrmann, R.B.
1983 : Regionalisation of crustal coda Q in the continental United States ; Journal of Geophysical Research, v. 88, p. 527-538.

Spence, G.D., Clowes, R.M., and Ellis, R.M.
1985 : Seismic structure across the active subduction zone of western Canada ; Journal of Geophysical Research, v. 90, p. 6754-6772.

Weber, M.H.
1988a : Computation of body-wave seismograms in absorbing 2-D media using the Gaussian beam method : comparison with exact methods ; Royal Astronomical Society Geophysical Journal, v. 92, p. 9-24.
1988b : Application of the Gaussian beam method in refraction seismology — Urach revisited ; Royal Astronomical Society Geophysical Journal, v. 92, p. 25-31.

An interpretation of CCSS data set I using the triangular block model method

R.F. Mereu [1]

Mereu, R.F., An interpretation of CCSS data set I using the triangular block model method ; in Studies of Laterally Heterogeneous Structures Using Seismic Refraction and Reflection Data, ed. A.G. Green ; Geological Survey of Canada, Paper 89-13, p. 53-63, 1990.

Abstract

The combined seismic refraction-reflection CCSS data set I from across Vancouver Island and the adjacent continental margin was interpreted with an iterative 2-D ray-tracing program. In this program, lateral and vertical heterogeneities were incorporated in the solution by dividing the earth model into a set of triangular blocks each with its own linear velocity function. The final model consisted of 3 fundamental regions : the oceanic crust, the transition zone and the continental crust. Major changes in travel time can be attributed to rapid increases in crustal thickness between the ocean and continent. The overall tectonic picture suggests that as the Juan de Fuca plate is subducted under Vancouver Island, the oceanic sediments are being skimmed off the top and piled up against the continental crust to create a rather complex laterally and vertically varying geological structure.

Résumé

Les données combinées de sismique réfraction et de sismique réflexion du jeu I de la CSSC provenant de l'île de Vancouver et de la marge continentale adjacente ont été interprétées à l'aide d'un programme itératif de tracé bidimensionnel des rayons. Dans ce programme, on a incorporé des hétérogénéités latérales et verticales dans la solution en divisant le modèle en un ensemble de blocs triangulaires auxquels sont associés des fonctions de vitesse linéaire propres. Le modèle final comprenait trois régions fondamentales : la croûte océanique, la zone de transition et la croûte continentale. Les changements importants dans le temps de parcours peuvent être attribués à des augmentations rapides de l'épaisseur de la croûte entre l'océan et le continent. La situation tectonique générale laisse penser que, à mesure que la plaque de Juan de Fuca s'enfonce sous l'île de Vancouver, les sédiments océaniques sont arrachés du dessus et empilés contre la croûte continentale pour créer une structure géologique plutôt complexe, qui varie latéralement et verticalement.

[1] Department of Geophysics, University of Western Ontario, London, Ontario, N6A 5B7.

INTRODUCTION

The combined seismic refraction-reflection data set I from across Vancouver Island and adjacent continental margin was interpreted with an iterative 2-D ray-tracing program using the following steps :

(i) A simple starting model was first determined by combining the results of a least squares analysis of first arrival refraction data (*see* Fig. 6 to 12 of Green et al., 1990) with information from the reflection record sections (onshore LITHOPROBE line 1 and offshore line 85-01 in Fig. 14 and 20 respectively of Green et al., 1990 ; these figures are contained in the pocket at the back of this volume) and known geology of the region.

(ii) In order to handle both vertically and laterally varying structures, the simple model was divided into a set of triangular blocks, each with its own two-dimensional linear velocity function of the form :

$$V(x,z) = ax + bz + c$$

where :

— V(x,z) is the seismic velocity at any point (x,z) in the model ;

— a, b and c are constants that are determined from the given values of velocity at each vertex of each triangle.

The three constants are different for each triangle. The velocity gradient in each triangle is constant and is given by the gradient vector :

$$\text{Grad } V = a\,i + b\,k$$

where i and k are unit vectors in the x and z directions respectively. The linear form of the velocity function and hence constant form of the gradient ensures that all ray paths within each triangle are arcs of circles, thus enabling one to trace rays through the model very quickly. The ray tracing is achieved by solving ray arc equations with triangular boundary line equations and applying Snell's law at each intersection point. High speed is obtained if the ray paths are not plotted, as then the whole problem can be handled by working with only the intersection points. The technique of dividing the model into triangular blocks enables one to work with a relatively small number of parameters. When the structure is simple the triangles may be large, whereas when the structure is complex, such as in the folded sedimentary section of our model, small triangles are required. The presence of sloping boundaries and faults presents no inherent difficulty provided the sides of the triangles are chosen to lie along the geological boundaries. The manner in which the model is divided into triangles is not unique. However, numerous tests have shown that in general the travel time and amplitudes are not very sensitive to this non-unique problem.

Synthetic seismograms are generated from transfer functions that are computed from the time delays, free surface effects, geometric spreading effects as well as all of the complex transmission and reflection coefficients associated with the boundaries that the ray encounters along its path. The computer program automatically searches the model for all major travel time branches, numerically codes the branches, determines their end points and then ray traces through the model with appropriate angle ranges for computing arrival times and synthetic seismograms. Details of this program were first presented at the 1983 CCSS workshop held in Einsiedeln, Switzerland (Mereu, 1983). Further examples were given at the 1985 CCSS workshop in Shizuoka, Japan (Mereu, 1987). The ray tracing method described here is similar to many of the other techniques described in this volume. The main differences are associated with the parameterization of the velocity model.

(iii) For a given modeling iteration, rays were traced from the source location in the model to the free surface and a comparison was made between the computed and observed travel times. Small adjustments were made to the velocity gradients and boundary positions until a good fit was obtained between all theoretical and observed travel time and amplitude data. These adjustments were made by varying the position of the vertices as well as the seismic velocity at each vertex. The program was written such that adjustments could be made very quickly in an interactive manner to whole sets of triangles at once. The procedure of iterating to a good model started at the top, fitting the near source observations and working gradually to greater depths in the model with the more distant observations.

RESULTS

The final triangular block model and corresponding velocity model are presented in Figures 1 and 2 respectively. The number of triangles used to outline the model's lateral and vertical heterogeneities is 140. Many of these triangles were required to model the complex fault system in the folded sedimentary section (region F of Fig. 2). Figure 2 is a velocity model that shows major discontinuities and regions such as H, J,and M where the velocity gradients are high. Since gradient lines are not constrained to lie along the edges of triangles, the lines drawn in Figure 2 may not always coincide with lines in Figure 1. Figures 3 to 9 show the results of the ray tracing, travel time and amplitude analyses for the OBS1, OBS3 and OBS5 sites and the J1, P-8, P-13, and P-19 shot points. These diagrams show that most of the major variations in travel time and amplitude are explained by the proposed model.

DISCUSSION

Figure 2 summarizes the main results of our analysis and incorporates the information derived from refraction analysis as well as the added information inferred from the reflection lines (LITHOPROBE line 1 and offshore line 85-01). The structure may be divided into 3 major zones as follows :

The oceanic crust (0-70 km)

Sediments appear undisturbed on a crust that thickens eastward from 10.5 to 14.5 km. Seismic velocities vary from 2 km/s in the sediments on the ocean bottom to 7 km/s just above the Moho. The changes in velocity occur through

a series of gently dipping discontinuities. The complex character of signals on the OBS1, OBS3 and OBS5 sections results mainly from the flat thin layered geometry in region B (Fig. 2), the disturbed area of the deformation front of region D and the western part of region F. It was difficult to model this oceanic region to give synthetics that agreed with the observed amplitudes precisely. Part of the problem may be due to small changes in the physical properties of the ocean bottom, which can have significant effects on the transmitted signal amplitude. Very significant variations in amplitude over a fraction of a kilometre were observed recently in refraction profiles of the 1986 GLIMPCE (Great Lakes International Multidisciplinary Program for Crustal Evolution) experiment (Mereu et al. 1989). Deep apparent reflectors in the mantle below the sediments observed on the 85-01 reflection section were interpreted as a series of multiples of the crustal reflection series and were thus ignored.

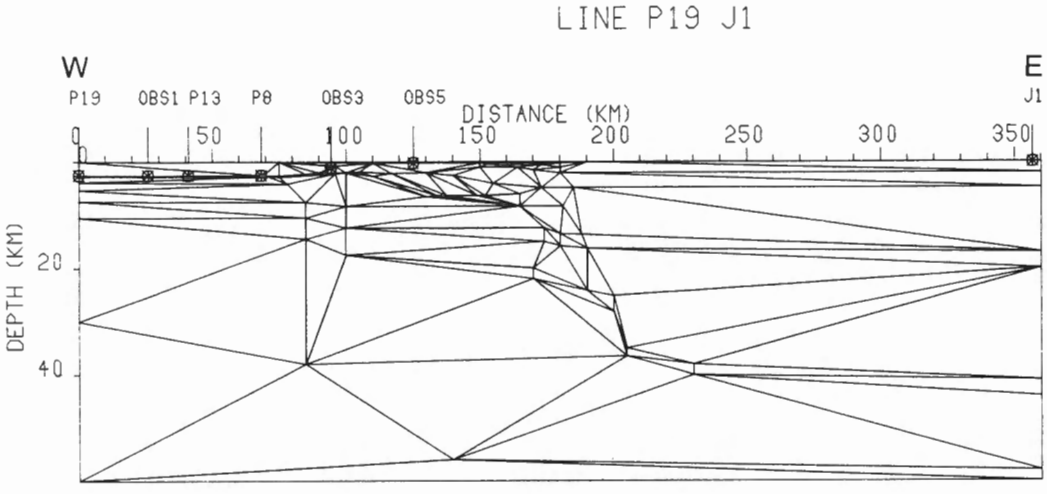

Figure 1. Triangular block model for line P19-J1. Each triangle is represented by a linear velocity function. The total number of triangles used to model the vertical and horizontal structures is 140.

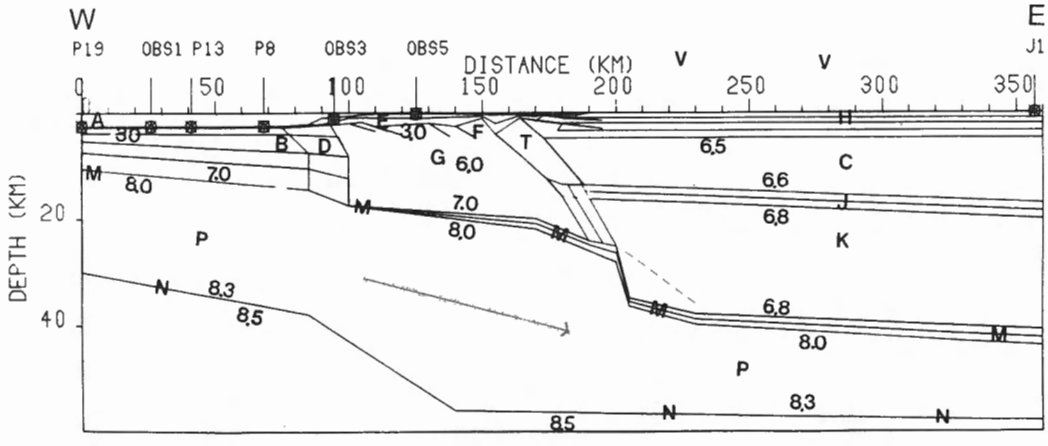

Figure 2. Velocity model for line P19-J1 showing major tectonic features as follows:

A. — Pacific Ocean
B. — Oceanic sediments and crust
C. — Intermediate continental crust
D. — Deformation front
E. — Young low velocity sediments
F. — Folded/faulted sediments
G. — Basement rocks
H. — Upper continental crust
J. — Intermediate discontinuity
K. — Lower crust with zero gradient
M. — Moho
P. — Juan de Fuca plate
V. — Vancouver Island.
T. — Tofino fault
N. — see text

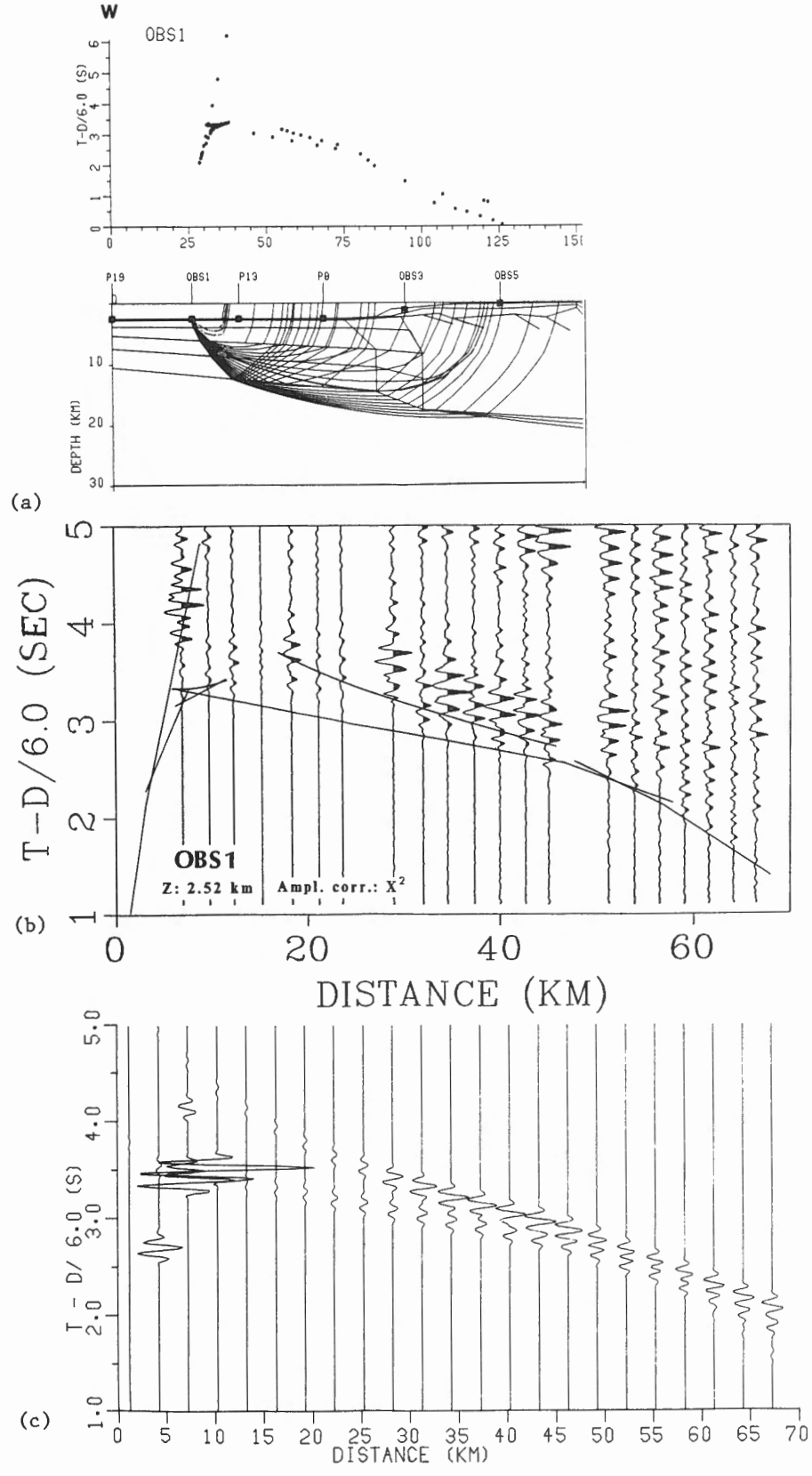

Figure 3. (a) OBS1 rays and travel times, (b) OBS1 observed data and theoretical travel time curves, (c) OBS1 synthetics.

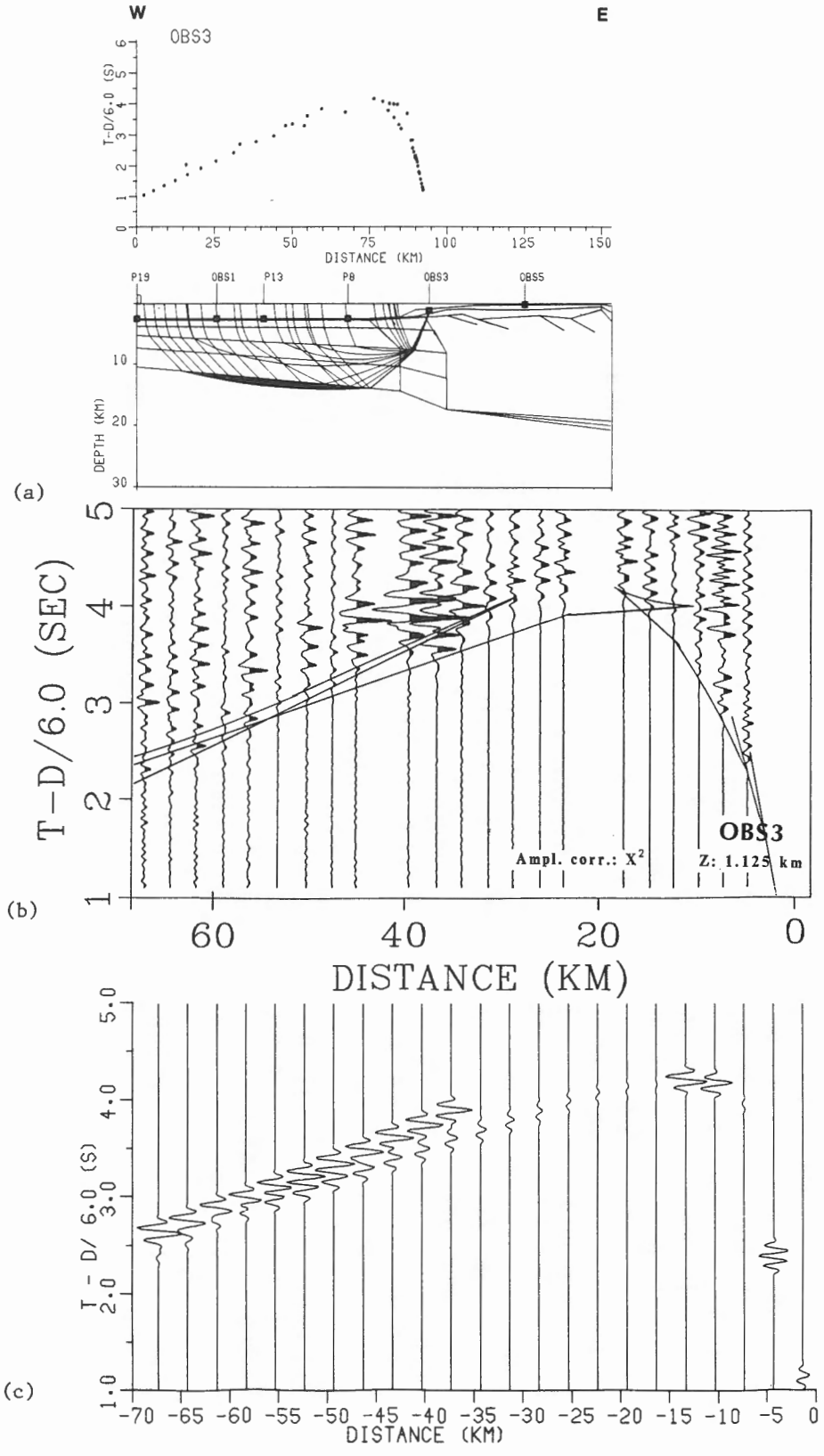

Figure 4. (a) OBS3 rays and travel times, (b) OBS3 observed data and theoretical travel time curves, (c) OBS3 synthetics.

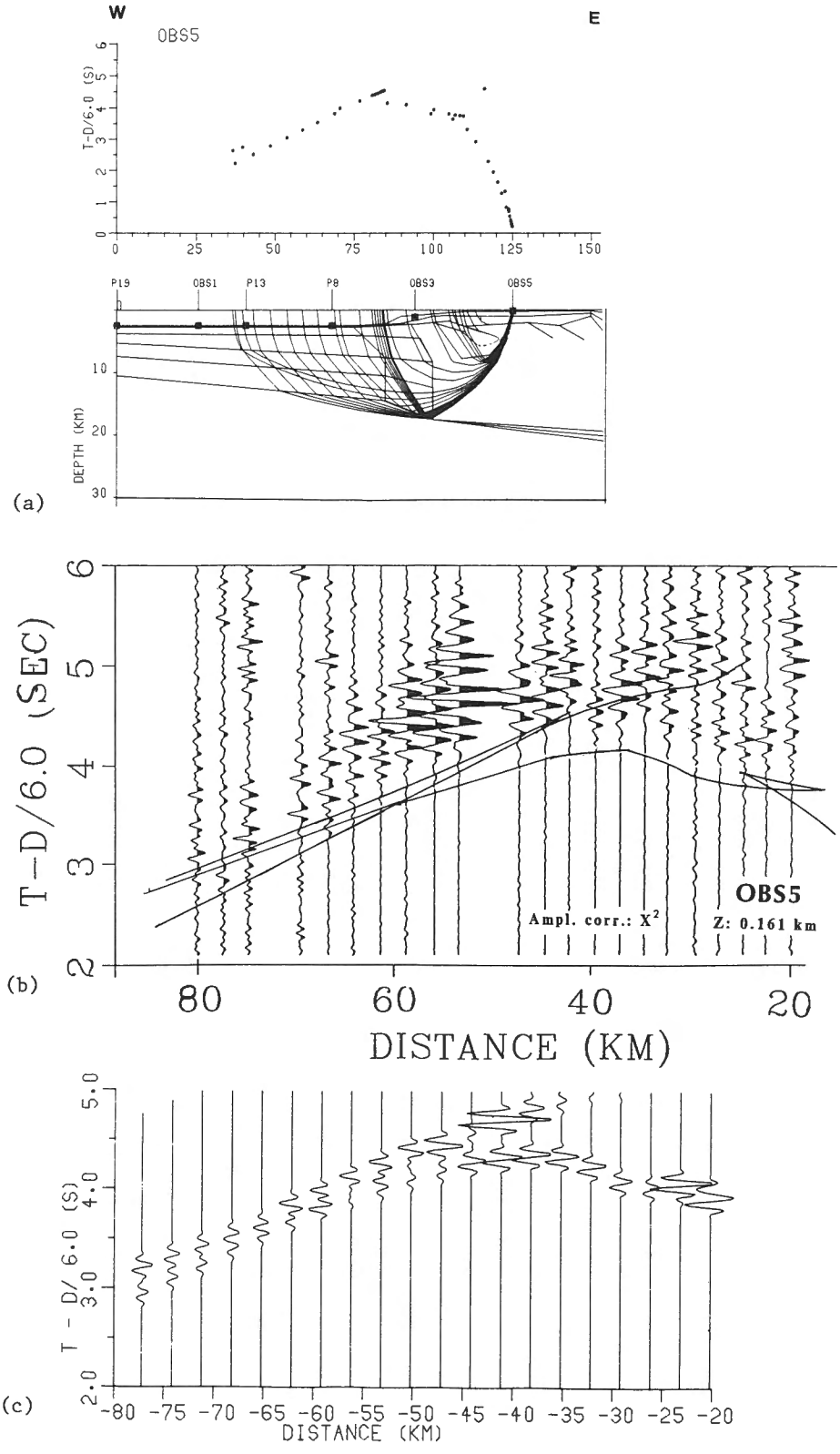

Figure 5. (a) OBS5 rays and travel times, (b) OBS5 observed data and theoretical travel time curves, (c) OBS5 synthetics.

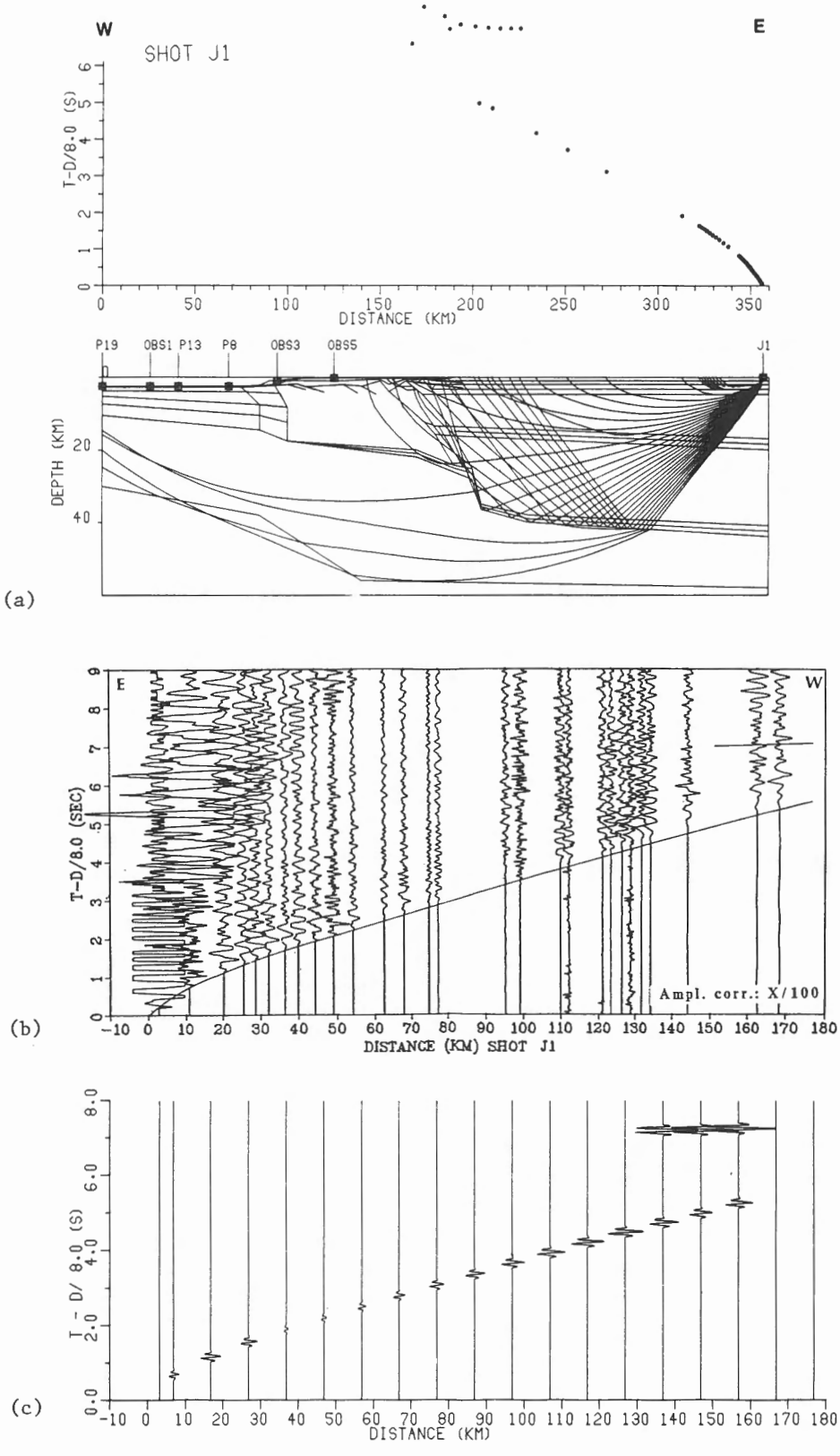

Figure 6. (a) J1 rays and travel times, (b) J1 observed data and theoretical travel time curves, (c) J1 synthetics.

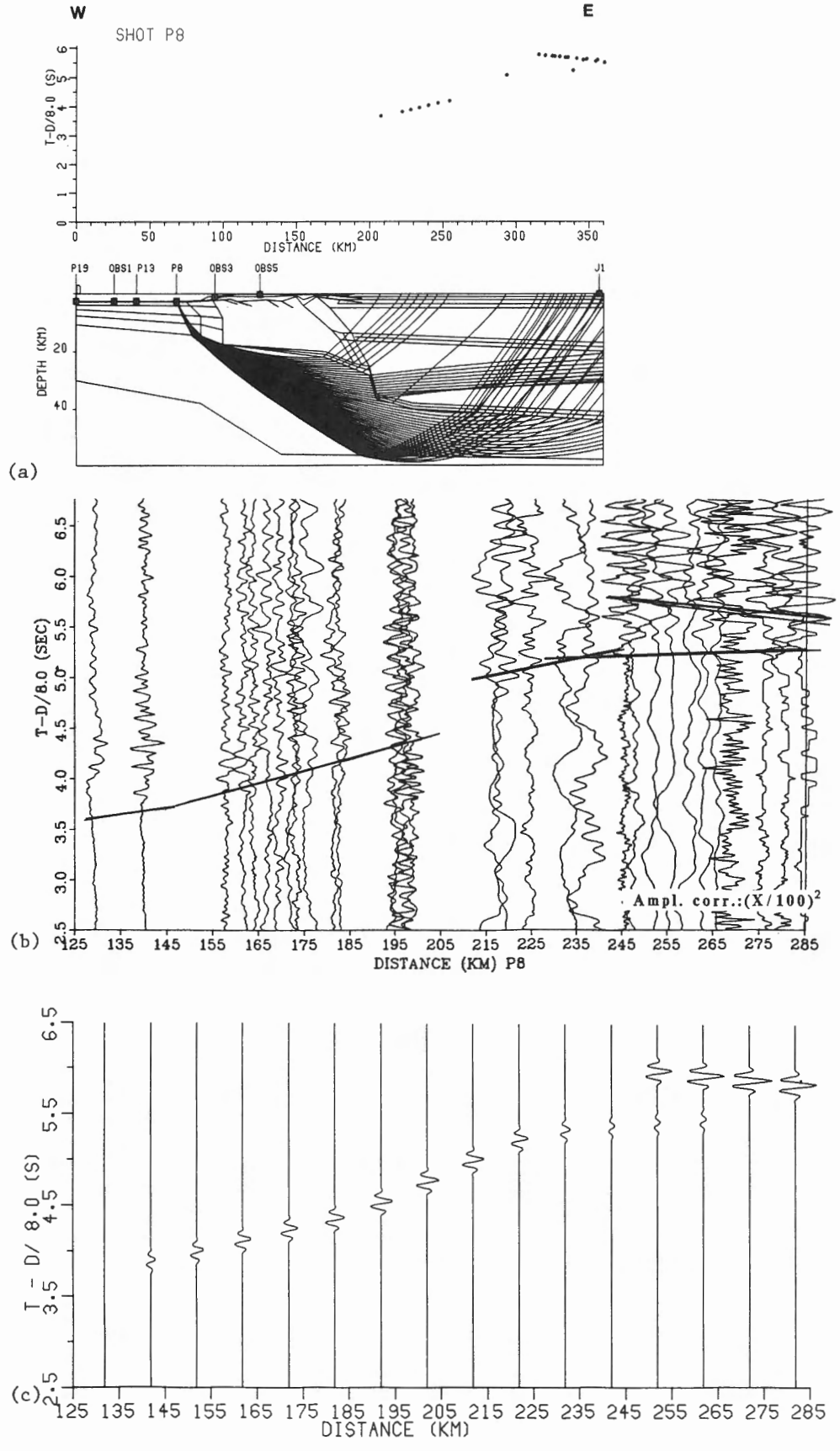

Figure 7. (a) P-8 rays and travel times, (b) P-8 observed data and theoretical travel time curves, (c) P-8 synthetics.

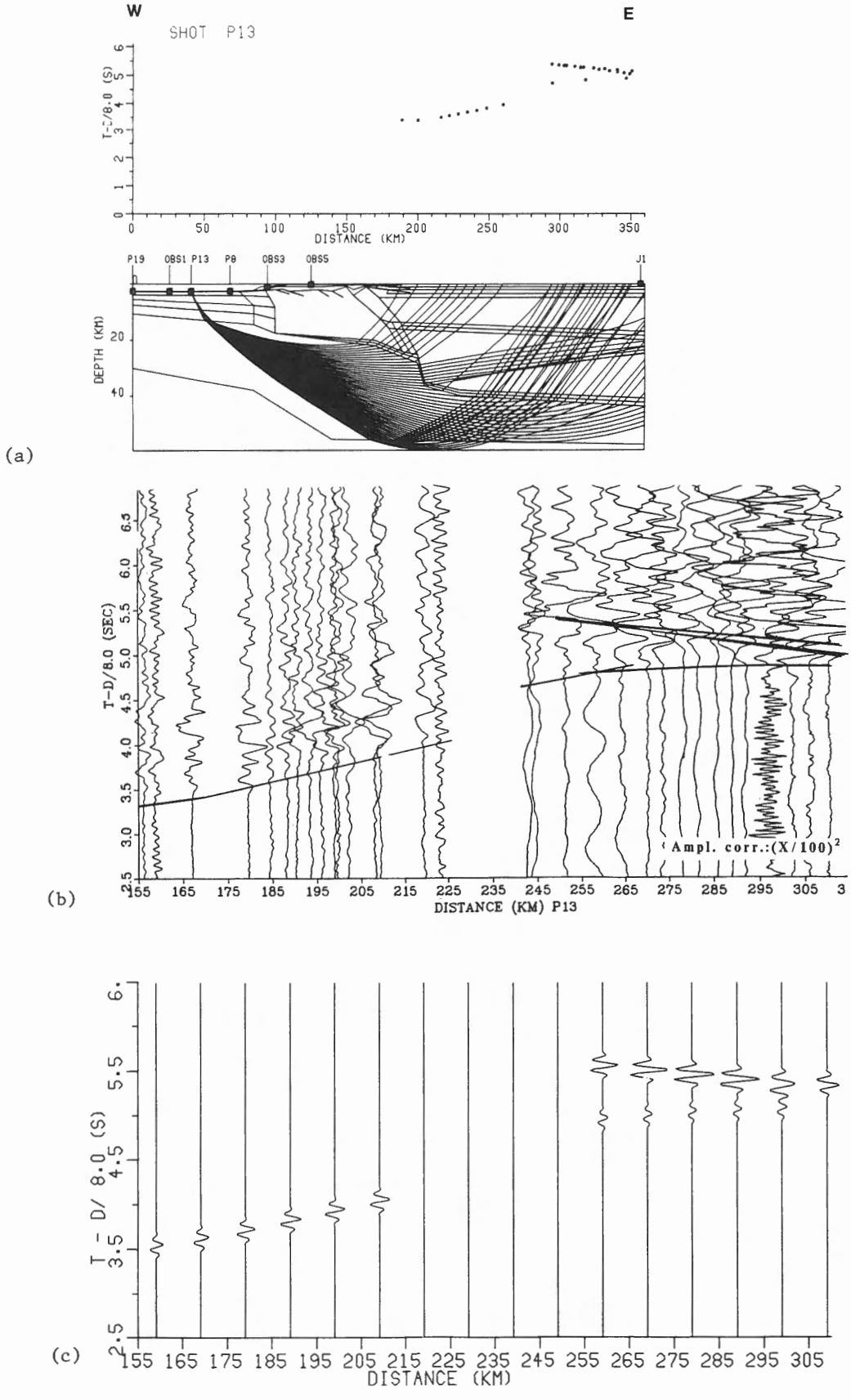

Figure 8. (a) P-13 rays and travel times, (b) P-13 observed data and theoretical travel time curves, (c) P-13 synthetics.

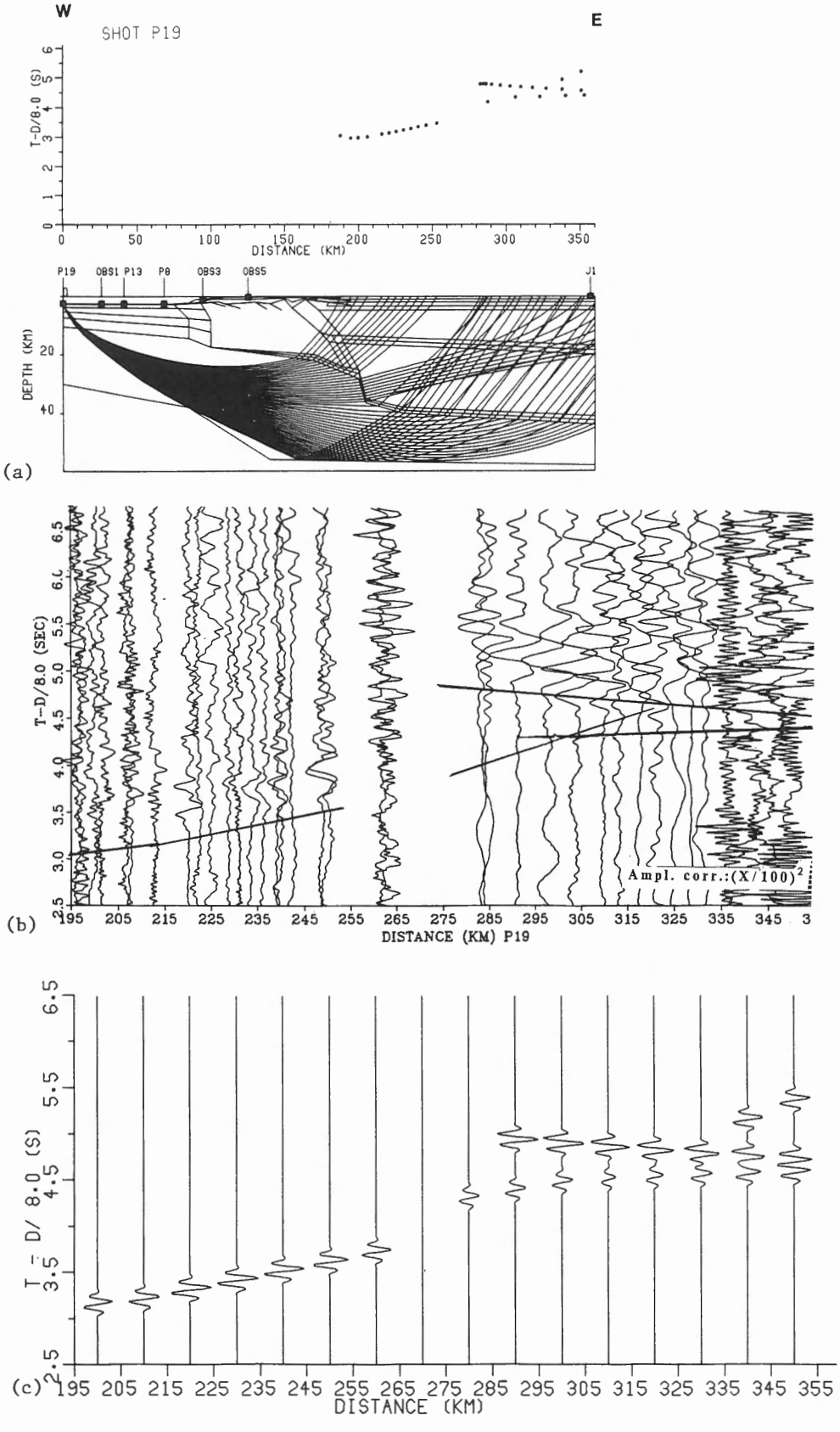

Figure 9. (a) P-19 rays and travel times, (b) P-19 observed data and theoretical travel time curves, (c) P-19 synthetics.

The transition zone (70-200 km)

Sediments in the transition zone are greatly thickened, faulted and folded as is seen on the reflection section 85-01. Pockets of low velocity sediments appear to fill valleys created by the faulted block structures. A deformation front, located near 100 km separates the disturbed and undisturbed regions. A large deep fault (Tofino fault ; T in Fig. 2) separates the disturbed region from the continental crust to the east. This fault may be associated with a deep sediment-filled valley near the 150 km point close to the surface. Evidence for connecting this structure to a major offset on the Moho is suggested by some patterns on the reflection sections.

The Continental Crust (200-360 km)

Observations for shot J1 were relatively simple and explained with upper crustal velocities varying rapidly from 5.0 km/s at the surface to 6.45 km/s at a depth of 5 km and then more slowly to 6.6 km/s at a depth of 14-18 km. Evidence for a discontinuity at this depth comes from both the reflection section and from the McMechan and Spence (1983) model of the refraction profile along the length of the island. The offsets in the P-8, P-13, and P-19 shot data were explained entirely in my model by a step associated with the downward extension of the Tofino fault. These data also provided strong evidence that the velocity gradient in region K above the Moho is either zero or negative. In an alternative interpretation to that presented here, a low velocity layer could easily be placed in this region (Spence et al.,1985).

The dashed line marked across the lower part of region K outlines the position of a major reflector seen on LITHOPROBE seismic section 1 (*see* E on Fig. 15 of Green et al., 1990). It is quite possible that this event is a reflection from the Moho. An alternative hypothesis attributes this reflector to an imbricated sedimentary layer that was scraped off the top of the subducting Juan de Fuca plate (Clowes et al., 1987) The discrepancy in location between the reflection and refraction observations could be explained easily by the fact that the reflection and refraction lines are not in exactly the same place. The record sections observed from shot points P-13 and P-19 also show a strong hyperbolic reflection-type arrival (Fig. 8 and 9). These are explained by a sub-Moho discontinuity in the upper mantle at a depth of about 55 km (N in Fig. 2). Although its western geometry is not constrained by the data, it is highly likely that this boundary is associated with the geometry of the dipping slab, which is inferred to be present from other evidence (Green et al.,1990).

SUMMARY

The overall tectonic picture suggests that as the Juan de Fuca plate is subducted under Vancouver Island, the oceanic sediments are being skimmed off the top of the oceanic plate and piled up against the continent to create a rather complex laterally and vertically varying geological structure.

The interpretation presented here is in good agreement with most of the other interpretations presented in this workshop volume. The main areas of disagreement occur in parts of the model where there are few seismic ray passages and hence fewer controls to provide a well-constrained picture.

ACKNOWLEDGMENTS

I would like to thank the organizers, A. Green, R. Ellis, B. Milkereit, R. Clowes and C. Spencer and their colleagues for the work they did in preparing the data sets and selecting a beautiful site for the CCSS workshop. This research was supported by the Canadian Natural Sciences and Energy research Grant (NSERC) number A1793.

REFERENCES

Clowes, R.M., Brandon, M.T., Green, A.G., Yorath, C.J., Sutherland Brown, A., Kanasewich, E.R., and Spencer, C.
1987 : LITHOPROBE-southern Vancouver Island : Cenozoic subduction complex imaged by deep seismic reflections ; Canadian Journal of Earth Sciences, v. 24, p. 31-51.

Green, A.,G., Clowes, R.M., and Ellis, R.M.
1990 : Crustal studies across Vancouver Island and adjacent offshore margin ; *in* Studies of Laterally Heterogeneous Structures Using Seismic Refraction and Reflection Data, ed. A.G. Green ; Geological Survey of Canada, Paper 89-13, p. 3-25..

McMechan, G.A. and Spence G.D.
1983 : P-wave velocity structure of the Earth's crust beneath Vancouver Island ; Canadian Journal of Earth Sciences, v. 20, p. 742-752.

Mereu, R.F.
1983 : The generation of synthetic seismograms in laterally heterogeneous media ; Conference Proceedings of the Commision on Controlled Source Seismology Workshop on the Interpretation of Seismic Wave Propagation in Laterally Heterogeneous Structures, Einsiedeln, Switzerland, August, 1983.
1987 : An interpretation of the seismic refraction data recorded along profile SJ-6 : Morro Bay-Sierra Nevada, California ; United States Geological Survey, Open-file Report 87-73, p. 30-37.

Mereu, R.F., Epili, D., and Green, A.G.
1990 : Pg shingles : Preliminary results from the onshore GLIMPCE refraction experiment ; Tectonophysics, v. 173, p. 617-626.

Spence, G.D., Clowes, R.M., and Ellis, R.M.
1985 : Seismic structure across the active subduction zone of western Canada ; Journal of Geophysical Research, v. 90, p. 6754-6772.

Interpretation of coincident seismic reflection and refraction profiles across the active subduction zone of western Canada

Hans Thybo[1]

Thybo, H., Interpretation of coincident seismic reflection and refraction profiles across the active subduction zone of western Canada ; in Studies of Laterally Heterogeneous Structures Using Seismic Refraction and reflection Data, ed. A.G. Green ; Geological Survey of Canada, Paper 89-13, p. 65-77, 1990.

Abstract

The two-dimensional seismic P-wave velocity structure across the active subduction zone of western Canada has been investigated via an integrated interpretation of the coincident reflection and refraction profiles of CCSS data set I. The model consists of three parts : (1) A well resolved oceanic part to the southwest, where the base of the crust at 12 km depth dips gently northeast. (2) The shelf area in the middle of the profile, where the northeast dip of the Moho increases and crustal thickness increases from 14 to 28 km. Crustal velocity information is generally sparse and there is non-reversed control of mantle velocities. A strongly dipping intra-mantle reflector was identified at depths between 35 and 45 km, but some uncertainty remains concerning its detailed geometry and the velocity beneath it. (3) The onshore northeast part of the profile, where the subducting slab dips steeply northeast and forms a transition zone into the continental environment. The velocity structures of the mainland crust and the crust beneath Vancouver Island are different, and the depth to the continental Moho is 38 km.

Résumé

La structure bidimensionnelle de vitesse des ondes sismiques P pour la zone de subduction active de l'Ouest canadien a été étudiée au moyen d'une interprétation intégrée des profils coïncidents de sismique réflexion et de sismique réfraction du jeu de données I de la CSSC. Le modèle se décompose trois parties. 1) Une partie océanique bien définie, située au sud-ouest, dans laquelle la base de la croûte, à 12 km de profondeur, présente un léger pendage vers le nord-est. 2) Le secteur de la plate-forme continentale, situé au milieu du profil, où le pendage nord-est du Moho augmente et l'épaisseur de la croûte passe de 14 à 28 km. Les renseignements concernant la vitesse dans la croûte sont généralement rares, et il n'existe aucun contrôle inverse des vitesses dans le manteau. Un réflecteur à fort pendage, situé à l'intérieur du manteau, a été identifié à des profondeurs situées entre 35 et 45 km, mais une incertitude demeure en ce qui concerne la géométrie précise de ce réflecteur et la vitesse en-dessous de ce dernier. 3) La partie terrestre située au nord-est du profil, dans laquelle la dalle de subduction a un fort pendage vers le nord-est et constitue une zone de transition avec le milieu continental. Les structures de vitesse dans la croûte au-dessous du continent et dans la croûte se trouvant au-dessous de l'île de Vancouver sont différentes ; la profondeur du Moho sous le continent est de 38 km.

[1] Institut for almen Geologi, Copenhagen University, Øster Voldgade 10, DK-1350 Copenhagen K, Denmark.

INTRODUCTION

CCSS data set I (Green et al., 1990a, b) forms almost exclusively the basis for the seismic model that I have derived for the Juan de Fuca subduction zone of western Canada. That the Juan de Fuca plate is being subducted beneath the North American continent was the starting hypothesis for the interpretation. In addition to the data set itself, the velocity structure for the deeper continental parts of the model was extracted from the literature.

The interpreted seismic P-wave velocity model is shown in Figure 1 together with information on the available data coverage. Data density and quality vary greatly along the profile. The southwest part of the model is relatively well constrained, whereas the middle, which is on the continental shelf, is "defined" by assuming continuity of the oceanic crust and by the marine reflection line. The onshore reflection line to the northeast shows excellent reflections to around 10 s, and farther to the northeast the velocity model is only partly determined by the data set because the refraction profiles are essentially non-reversed. The interpretation proceeded by :

a) Extracting structural information from the reflection lines. This information, which was continuously updated during the interpretation, formed a basis for steps b) and c).

b) Building velocity-depth models (i) from the refraction profiles by one-dimensional (1D) ray tracing and (ii) from the velocity analyses of the offshore reflection data.

c) Utilizing the ray tracing program of McMechan and Mooney (1980) to trial and error model the inferred two-dimensional (2D) velocity structure to produce a best fit with the available data.

Throughout the interpretation procedure the model was kept as simple as possible. The data were acquired along different lines all oriented mainly northeast. Hence, the offshore reflection line and its northeast continuation was chosen as the base line. The origin was set at shot point P19 and all information was projected on to this line.

REFLECTION INTERPRETATION

The land reflection section (Fig. 14 and 15 of Green et al., 1990b ; Fig. 14 is in the pocket at the back of this volume) shows strong reflective zones down to more than 10 s. The quality of the data is so good that an immediate understanding of the geological structures along the line is obtainable. The major reflections have been drawn as straight lines in Figure 2a. Only the uppermost reflection of any reflection zone is drawn. The profile is crooked,

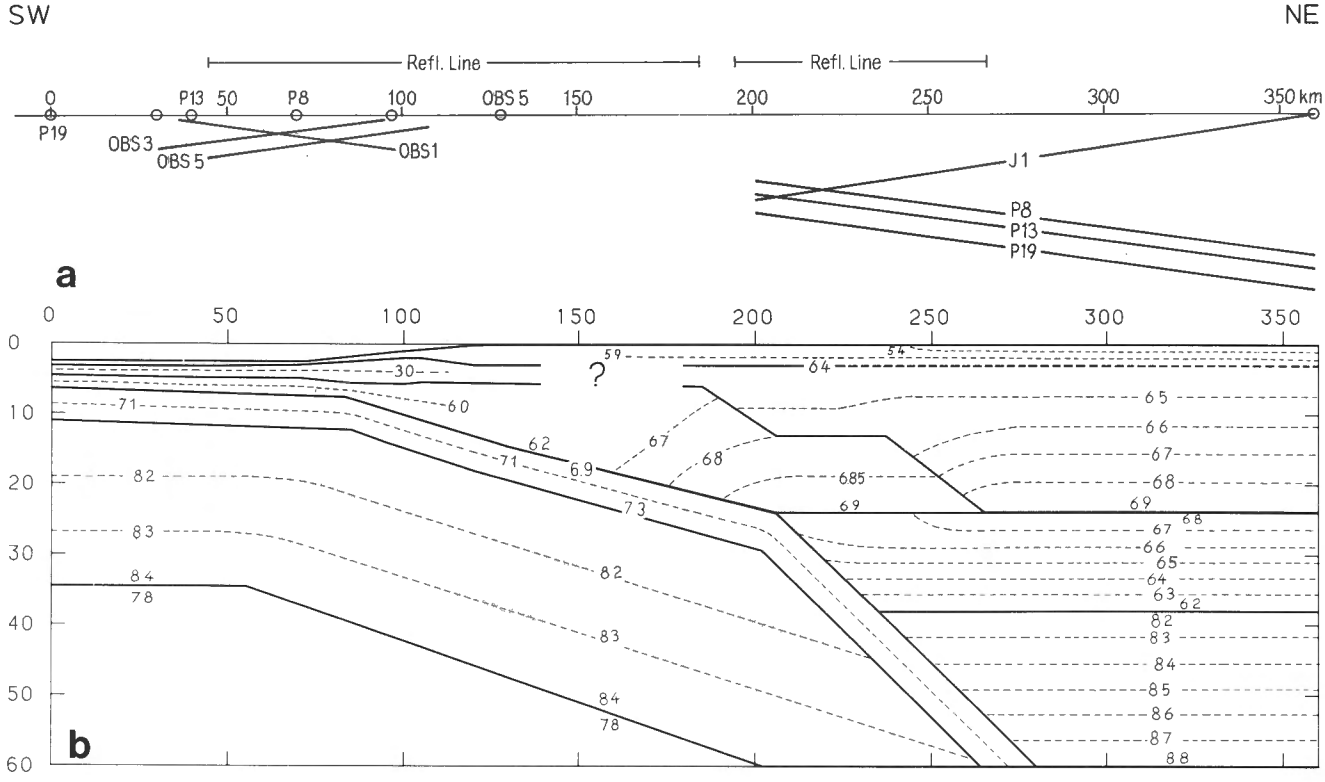

Figure 1. (a) Locations of marine and land seismic reflection lines and various refraction recording lines (OBS1, OBS3, OBS5, J1, P8, P13, and P19). (b) Interpreted model showing first order discontinuities by heavy lines and isovelocities by dashed lines. Note the large variation in data coverage along the profile.

and the horizontal reflections are generally found where the direction of the profile is at a steep angle to the base line. This indicates that the structural strike in the vicinity of the profile is essentially perpendicular to the base line (i.e. there is a dominant northwesterly strike). Figure 2b shows the result of projecting the reflections on to the base line. As expected, many of the flat reflections are shortened or nearly removed by this process.

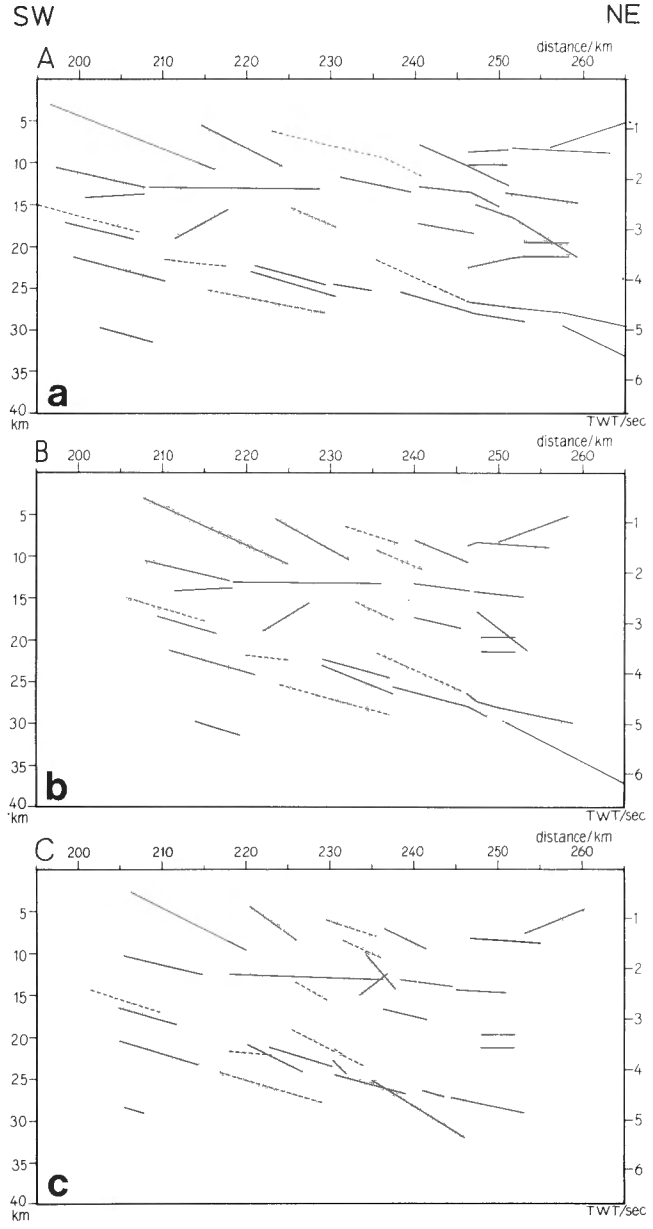

Figure 2. (a) Reflection seismic interpretation of the land profile. Reflections are drawn as straight lines and only the uppermost reflection of the main reflection zones are included. A velocity of 6 km/s was employed for depth conversion. (b) The interpretation in (a) projected on the base line. (c) Migrated version of the reflections in (b).

On the basis of data from refraction shot J1, a constant velocity of 6 km/s was used for depth converting the reflections. Due to their relatively high dip angles, the interpreted reflections were also migrated by hand (Fig. 2c). The upper 11 km of the crust is strongly (thrust) faulted. At 20-30 km depth there is a northeast dipping transition zone to an interval that could represent the subducting plate. In the southwest part of the line diagram, a strong short reflection is shown at a depth of 30 km. This may originate from the base of the subducting slab.

The offshore seismic reflection section (Fig. 20 to 22 of Green et al., 1990b; Fig. 20 is in the pocket at the back of this volume) resolves the sedimentary structure and part of the basement. In the southwest oceanic part where some crustal reflections can be identified, structures are relatively flat layered. At 4.5 km depth the thick line in Figure 3a shows the interpreted top of the oceanic crust after depth conversion. The main part of the marine reflection section across the continental shelf shows strong folding, and deep reflections are largely hidden by multiples. Between shotpoints 100-400 the reflection at 7.5 s (Fig. 20 of Green et al., 1990b) has been interpreted as a primary reflection, probably from the oceanic Moho. This reflection is coincident in Figure 3a with the thin line identifying an increase in velocity from 7.3 to 8.0 km/s at 12 km depth. Velocity analyses of the reflection data provided some additional structural information. The three dashed lines in Figure 3a show the depths where velocities of 3.0, 5.8, and 8.0 km/s are reached. The lower dashed line may follow the geometry of the subducting oceanic plate; the middle one may follow the top of the crystalline crust, which apparently becomes shallow under the northeast part of the line; and the upper dashed line may follow a sedimentary boundary. Note, that the middle line follows closely the 3.2 to 5.9 km/s interface in the southwest part of the profile, whereas it goes much deeper at distances between 90 and 150 km. This observation could be of importance for future processing of the reflection seismic profile.

ONE-DIMENSIONAL VELOCITY INTERPRETATION

Iterative modeling assuming flat-layers with linear velocity gradients was applied to obtain estimates of the variation of velocity versus depth near the receivers. First arrivals and, where they could be distinguished, later reflection phases were used for this process. Only the P-shots gave estimates of mantle velocities, which were around 8 km/s.

Only first arrivals can be correlated for the J1 record section (Fig. 6 of Green et al., 1990b). Later phases are seen faintly but cannot be clearly identified. The preferred model varies from 5.6 km/s at the surface to 6.4 km/s at 3 km and 6.75 km/s at 12 km depth. No information was extracted for greater depths.

The OBS recordings provide fair correlation of first arrivals, but the mantle phases are weak (Fig. 10 to 12 of Green et al., 1990b). The reflections from the M-discontinuity (P_MP) are very clear and there are other possible reflections. Using the reciprocity theorem the recordings were interpreted as if the shot was at the OBS location and the receivers at the shot positions. Arrival times were corrected for water depth before modeling (i.e. a static correction was applied to each shot with the aim of simulating flat layering and constant water depths for the upper parts of the models). The sea bottom was deeper at OBS1 than at the shot positions, so sediment was replaced by water for the correction of OBS1 arrival times. Water depth was shallower at OBS3 and OBS5 than at the shot positions and for these stations water was replaced by sediments. The correction velocity was 3 km/s, which is the velocity of the first phase seen in the records. The correction was up to 0.4 s on the farthest traces. During modeling, the principal seismic reflections were used as constraints on two-way travel times to the interfaces. The sea bottom sediments were, for simplicity, represented by a layer with low velocity and high gradient. The resulting velocity versus depth models are shown in Figure 3a by thin lines. A good fit between observed data and modeled arrival times was obtained by varying only the depths to the interfaces, working with the same velocities within the individual layers for all OBSs. This may indicate that the layering is fairly continuous between OBS1 and OBS5.

TWO-DIMENSIONAL MODELING

The resulting velocity model for the entire profile was determined by 2D trial and error modeling with the reflection interpretation and the 1D results forming the basis for the initial model. The velocity control in the deeper continental part of the model was rather poor, so the preferred velocity model of McMechan and Spence (1983) was used for this region.

The Oceanic Reversed Spread

The profile between OBS1 and OBS3 is the best constrained part of the model with reverse coverage and additional control from OBS5. The final 2D velocity model is shown in Figure 3b. It does not differ significantly from the initial model, but the modeling process has imposed narrower limits on the depth to the sedimentary base, on the dip and

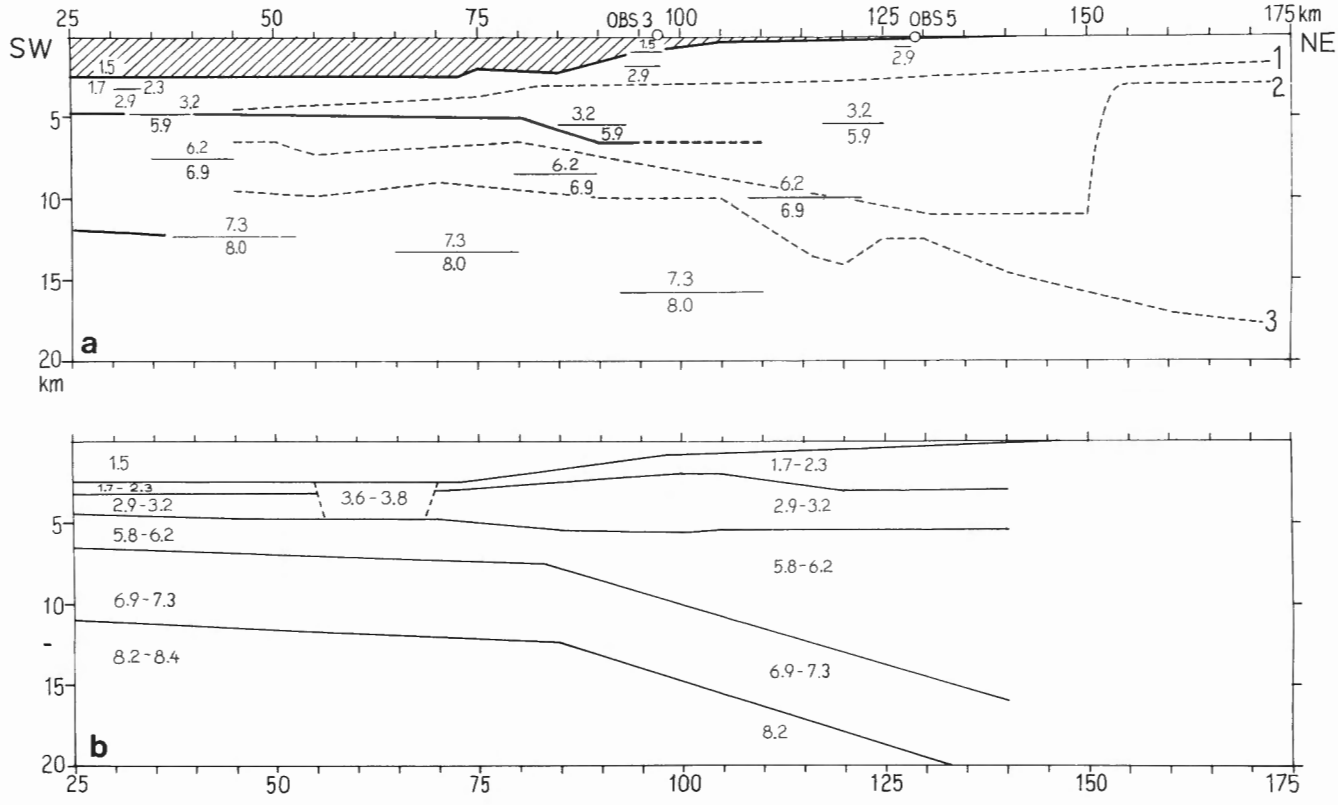

Figure 3. (a) Interpretation of the marine reflection line (thick lines) and velocities from one-dimensional modeling of the OBS recordings. Dashed lines 1, 2 and 3 identify velocity contours of 3.0, 5.8 and 8.0 km/s inferred from stacking velocity analyses of the marine reflection data. (b) Interpreted model showing first order discontinuities and velocities within the individual layers.

thickness of the subducting slab, and on the mantle velocity. In the southwest part of the model, crustal thickness is 12-14 km and the Moho dips gently northeast beneath relatively flat-layered structures. Between OBS3 and OBS5 the subducting slab steepens without affecting the flat layering above.

The results of the ray trace modeling are shown in Figures 4 to 6. In each figure (a) shows the observed data with the synthetic travel times of refractions and super-critical reflections superimposed, (b) shows the synthetic seismograms calculated by asymptotic ray theory (scaled by $x^{1.7}$ instead of x^2 in order to simulate absorption losses), and (c) shows the ray paths for the considered arrivals.

The synthetic travel times follow closely the observed arrivals, though it is difficult to make a clear correlation of individual phases. Although the sea bottom is not resolved by the refraction data, it can be extracted from the reflection section. The OBS data contain information primarily about the crust, which has been interpreted in terms of two layers. It is difficult to make a clear distinction between upper and lower crustal arrivals, but an intracrustal reflection was recorded on the OBS5 section. The P_MP critical point is strong on all record sections, whereas the mantle refracted wave is weak and difficult to correlate.

The synthetic seismograms resemble fairly well the observed data, showing strong amplitudes in the appropriate regions. The synthetic P_MP reflection amplitudes are too strong at large offsets, especially for the OBS1 and OBS3 sections. This may indicate that the model is too simple and smooth, and that the effects of the strong folding and faulting on the slope and shelf ought to be taken into account. However, the amplitude increase at the P_MP critical point is too small in the synthetic seismograms for OBS1 and OBS3. The fit is better for OBS5, which was shot "up-dip". Therefore, the amplitude discrepancies might be resolved by increasing the velocity gradient in the lower crust. This would limit the distance range of refractions from the lower crust and probably increase the amplitudes of the super-critical P_MP reflections.

The Continental Part

The seismic refraction data for the continental part of the profile are relatively sparse. Shot J1 gives non-reversed information on the upper continental velocity structure, whereas the P shots yield information on velocities and structures in the deeper parts of the model. Figure 1a shows that there are no refraction data between OBS5 and the west coast of Vancouver Island. Hence, the velocity structure in this part of the model cannot be determined from existing refraction data and is constrained mainly by the assumption that the subducting slab is continuous between different parts of the model. Such continuity of structures is supported by the marine seismic reflection data. Crustal thickness increases from 14 to 28 km under the shelf. A strongly northeast dipping intra-mantle reflection is interpreted from the P series of shots at depths between 35 and 45 km, but uncertainty remains concerning its detailed geometry and the underlying velocity.

No deep reflections can be correlated in the northeast part of the marine section due to low signal to noise conditions, but weak near-vertical reflections can be identified at arrival times predicted from the velocity model. The weak reflections originating from the top of the lower crust and the oceanic Moho can be traced across most of the section. The reflection from the oceanic Moho can be extended to the lowermost strong reflection seen in the southwest part of the land reflection line. This reflection is, therefore, interpreted to originate from the base of the slab, and its continuation beneath the continent can then be determined from the P series of shots.

The 1D model determined from J1 is adopted for the upper northeast parts of the 2D model. Velocities under the land reflection line and in the deeper northeast parts of the model are taken from the preferred model of McMechan and Spence (1983), who included a layer with negative gradient in the lower part of the continental crust. Northeast of the coast of Vancouver Island, the slab is steeply dipping (26°). The velocity structures of the mainland crust and the crust beneath Vancouver Island are different, and the continental crust is 38 km thick.

The results from modeling the J1-data are shown in Figure 7. Waves travelling through the upper crust explain satisfactorily the first arrivals. The figure also includes later arrivals although no correlations with the observed data are generally possible. The short reflection phase from the edge of the wedge, interpreted from the reflection data, matches strong arrivals in the record section. The reflection from the top of the lower crust is too weak to be detected (*see* velocity contours in Fig. 1). The P_MP reflection is too strong in the synthetic section, so the Moho is probably too sharp in the model. Making the Moho smoother, (e.g. with a gradient zone) would call for a less negative or a positive gradient in the lower crust. This would probably still be in agreement with CCSS data set I, but it would conflict with the preferred model of McMechan and Spence (1983).

Data recorded from the P series of shots look similar, with a pronounced 1 s offset in arrival time between Vancouver Island and the mainland at about 275 km distance from P19 (Fig. 7 to 9 of Green et al., 1990b). The offset is probably caused by structure in the deeper parts of the crust and upper mantle since the J1 data do not show a similar feature. Early arrivals on Vancouver Island are interpreted as refractions through the mantle beneath the subducting slab, and the delayed arrivals on the mainland are probably refractions through the continental mantle. Strong secondary arrivals at both the near and far receivers are interpreted as intra-mantle reflections. They show similar pronounced time offsets. The refraction and reflection phases constrain the dip of the deeper parts of the subducting slab. Modeling results for the P series of shots are shown in Figures 8, 9 and 10. The synthetic travel times are in fair agreement with phases in the observed record sections although the mantle reflections tend to be too late on the near traces for shots P8 and P13. The synthetic seismograms (amplitudes were scaled by $x^{1.8}$ instead of x^2 to correct for absorption losses) show the same qualitative amplitude behaviour as the observed

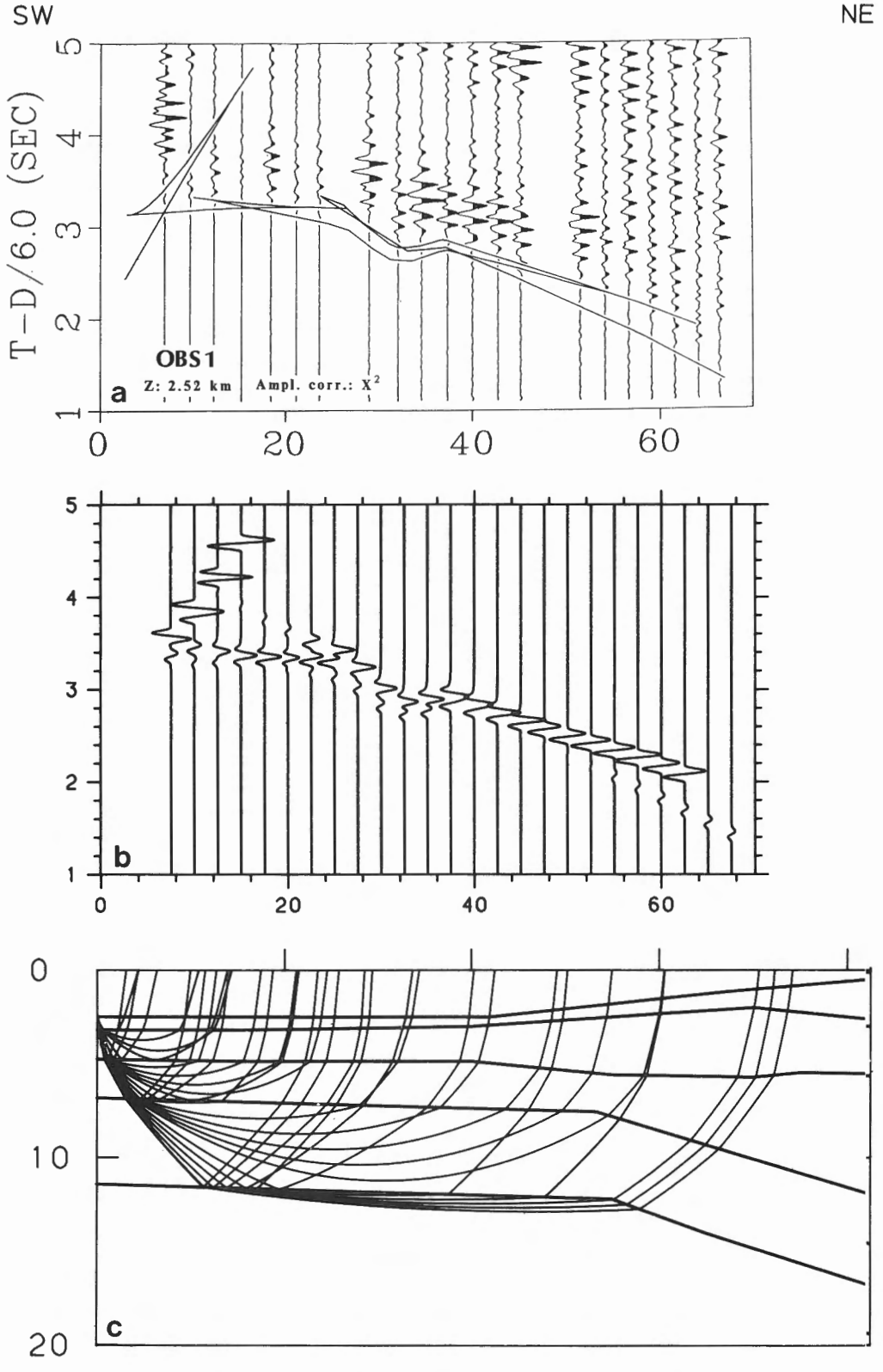

Figure 4. Results from ray-tracing modeling of the OBS1 data. (a) Synthetic travel times of refractions and reflections are superimposed on the observed data. Only super-critical reflections are shown for interfaces with positive velocity contrasts. (b) The synthetic seismogram calculated by asymptotic ray theory. (c) Diagram showing rays of the considered arrivals.

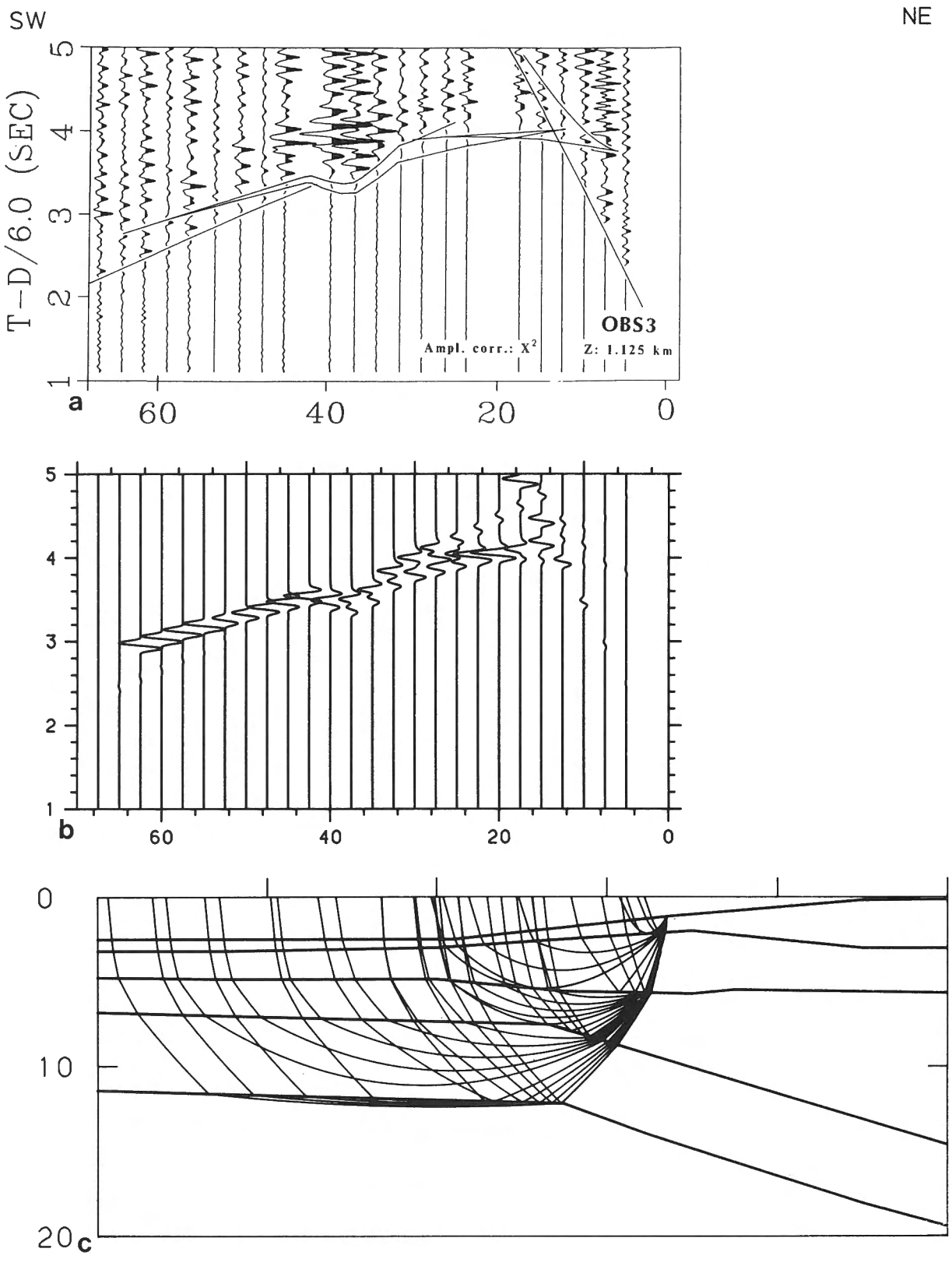

Figure 5. Results from ray-tracing modeling of the OBS3 data. See caption for Figure 4.

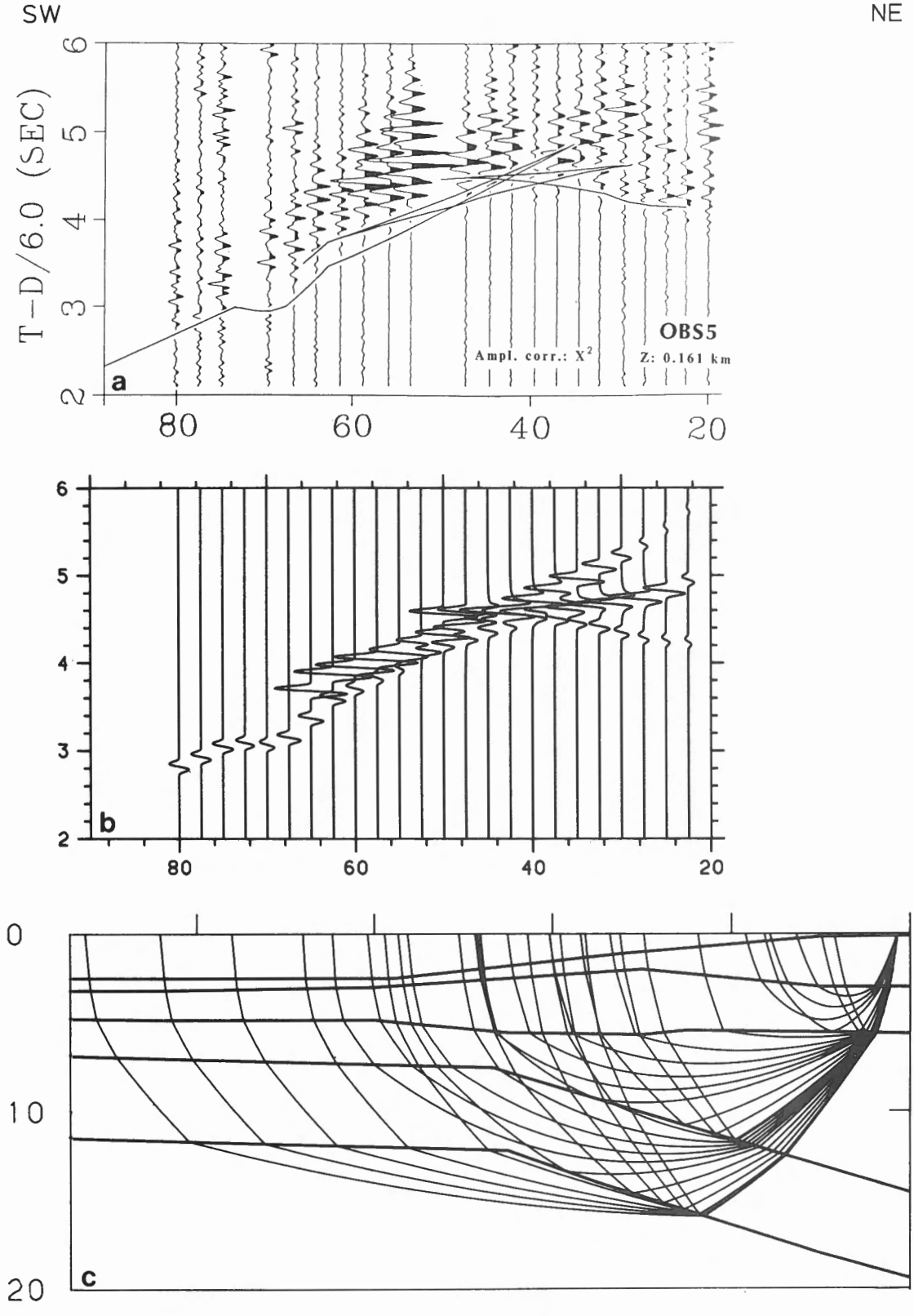

Figure 6. Results from ray-tracing modeling of the OBS5 data. See caption for Figure 4.

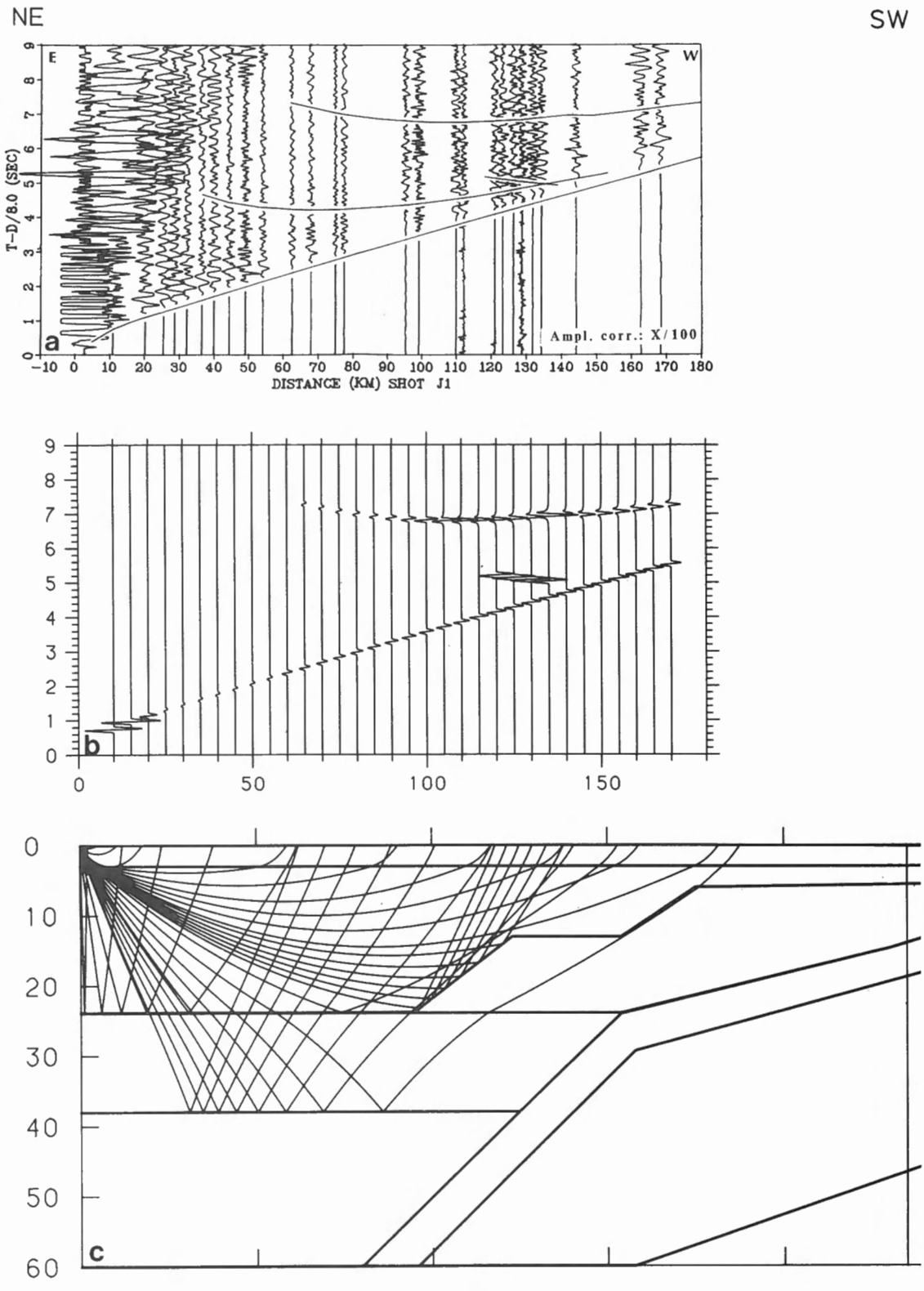

Figure 7. Results from ray-tracing modeling of the J1 data. See caption for Figure 4.

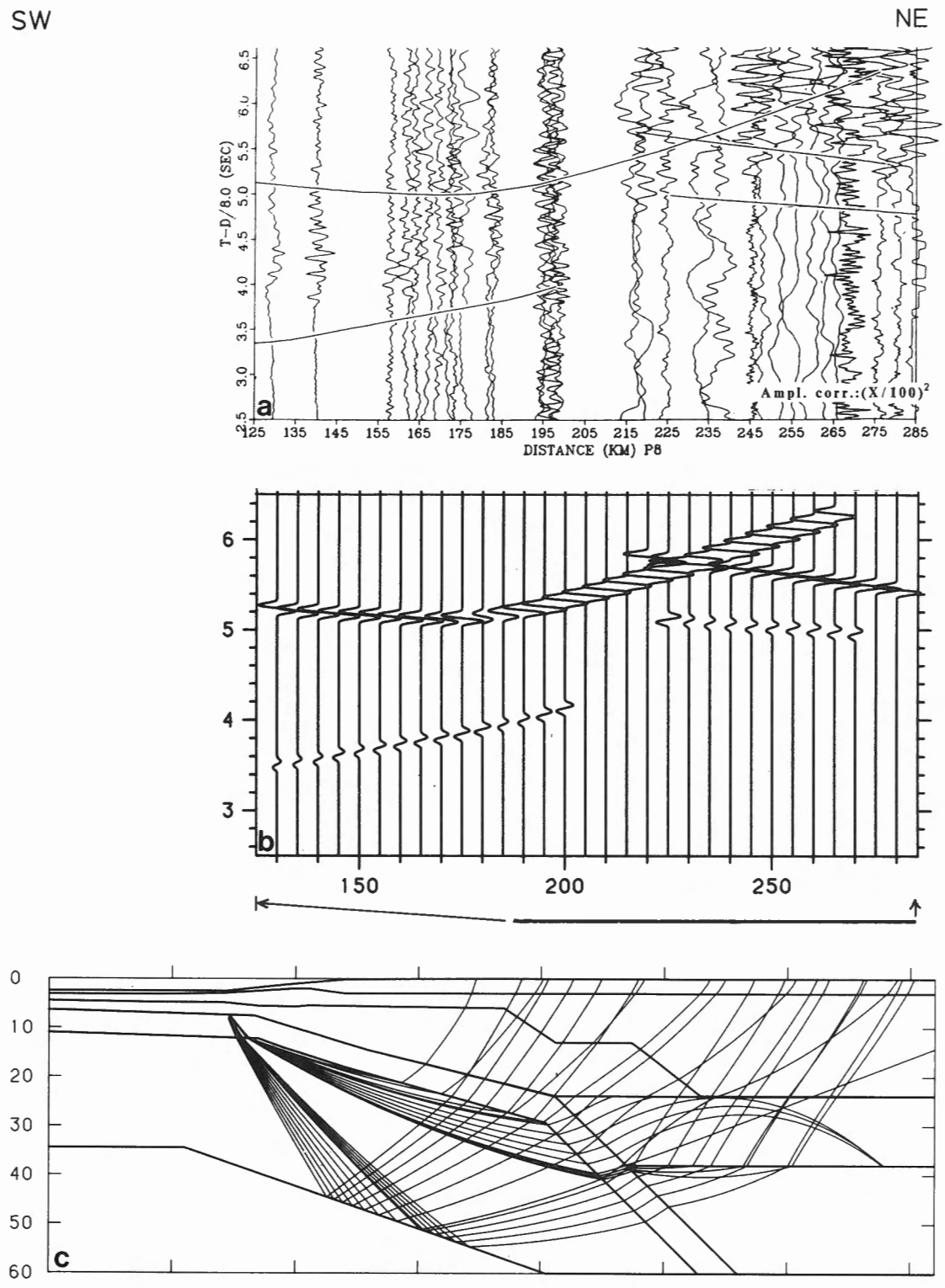

Figure 8. Results from ray-tracing modeling of the P8 data. See caption for Figure 4.

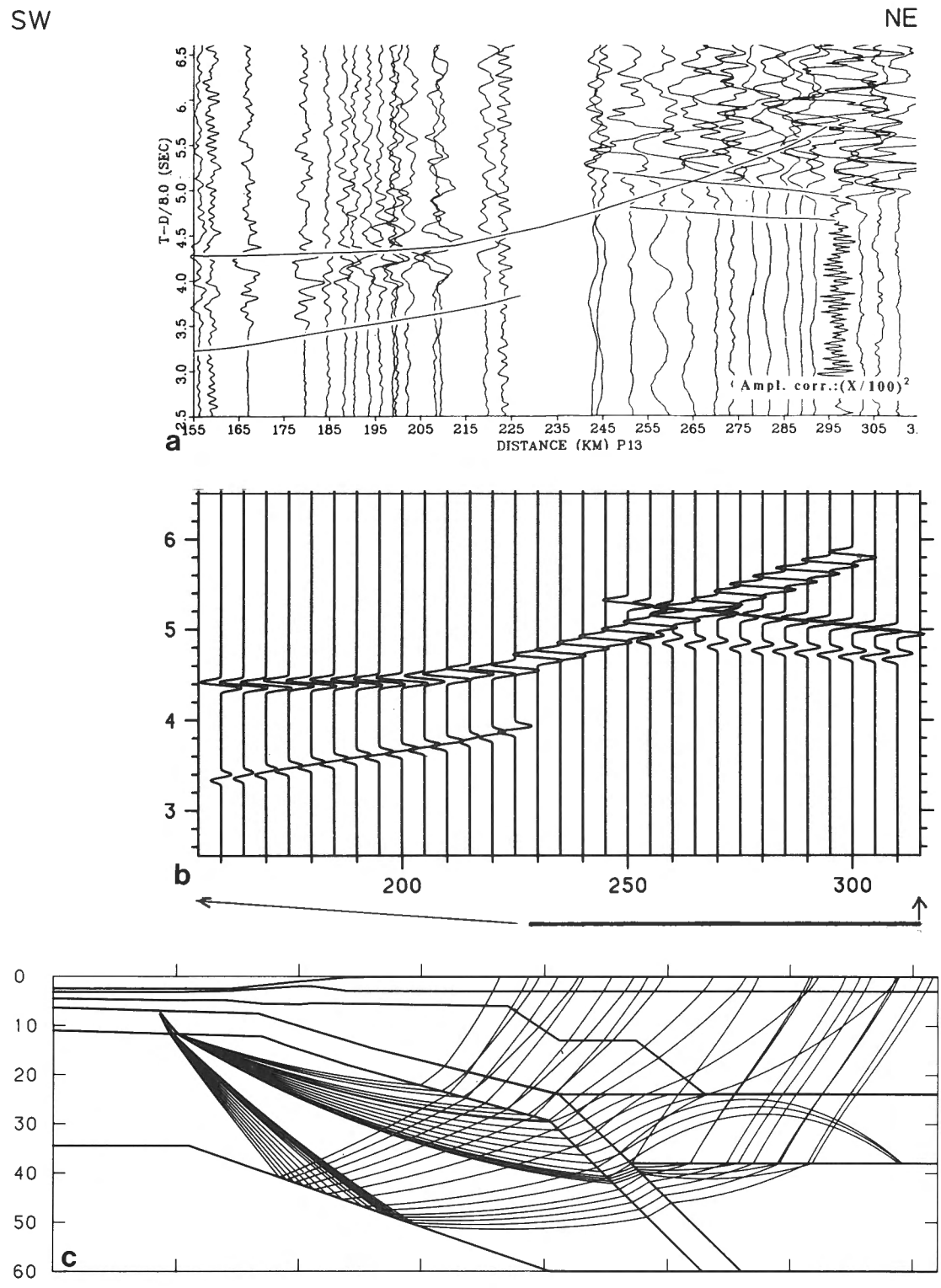

Figure 9. Results from ray-tracing modeling of the P13 data. See caption for Figure 4.

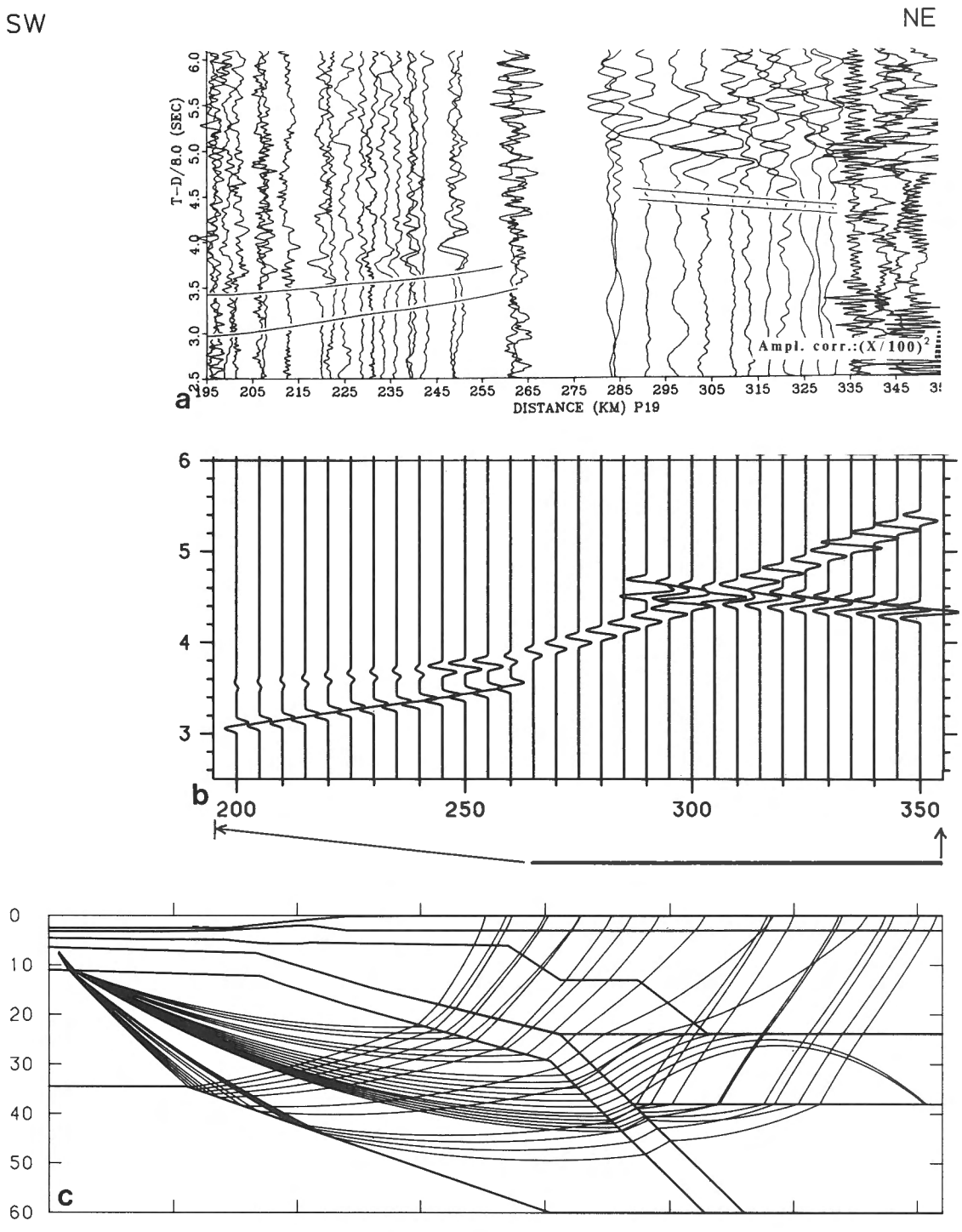

Figure 10. Results from ray-tracing modeling of the P19 data. See caption for Figure 4.

sections, although the reflection phase from P8 tends to be too strong on the synthetic seismograms near the source. The major exception is a numerical effect on the P19 synthetic section, where the edge of the intra-mantle reflector causes amplitudes to become too small on the near traces.

The choice of 7.8 km/s for the lower mantle layer is rather arbitrary. Spence et al. (1985) argued that there is a negative velocity contrast across their mantle reflector. This conclusion was based on a model where no reflections reached the far continental receivers, which is not the case for my model. Hence, the observed arrivals could equally well be explained by super-critical reflections from an intra-mantle reflector with a positive velocity contrast. The small amplitudes of the secondary arrivals on the observed seismograms nearest to shot P8 would then be explained by pre-critical reflections from this boundary.

The model presented here is similar in many respects to that of Spence et al. (1985), although the dip of the subducting slab differs; Spence et al., (1985) found a northeast dip of 18° whereas in Figure 1 the dip is 26°, which is in agreement with earlier interpretations of gravity data (Riddihough, 1979) and MT data (Kurtz et al., 1986). As a consequence, my model does not require the pronounced high-velocity sliver with velocity of 7.7 km/s in the lower crust. Also, the shallow structure differs. Here, the base of the thrust faults is interpreted to represent a boundary with only slightly higher velocity than the surrounding layers.

CONCLUSIONS

The two-dimensional P-wave velocity model for the Juan de Fuca subduction zone of western Canada, shown in Figure 1b, was derived almost exclusively by a combined seismic refraction and seismic reflection interpretation of the CCSS data set I. The model does not contradict the data set, but data density and data coverage vary greatly along the profile (note the details of the seismic lines in Fig. 1a). Hence, it is a plausible model with varying degrees of control along the profile.

The velocities of the oceanic crust and uppermost mantle in the southwest part of the profile are well resolved due to good reflection data and the reversed refraction data coverage between OBS1 and OBS5. Crustal thickness is about 12 km in this part of the model, and the Moho dips gently northeast. No refraction data were acquired on the shelf between OBS5 and the coast, so the shallow part of the velocity model can only be inferred from the seismic reflection data. Moho is in the depth range 14 to 28 km and the northeast dip has increased relative to earlier interpretations. Velocities in the oceanic mantle were interpreted from the P series of shots, employing structural constraints imposed by the seismic reflection lines. The dipping strong intra-mantle reflector, in the depth range 35 to 45 km, was identified confidently from reflections seen in the refraction data, but some uncertainty remains concerning its detailed geometry and the underlying velocity.

Excellent reflection data provided structural information on the crust beneath Vancouver Island. Upper crustal velocities were interpreted from the non-reversed J1 data, and velocities in the deeper onshore parts of the model were extracted from the literature. My interpretation does not include a high-velocity sliver in the continental crust. However, the velocity structure of the crust beneath Vancouver Island is different from the velocity structure of the mainland continental crust, which is 38 km thick. The depth to the base of the subducting slab near the southwest coast of Vancouver Island was determined from the reflection seismic sections. With this as a constraint it was possible to interpret the dip of the slab beneath the continental part of the model from the P series of shots. The interpreted dip was found to be in agreement with previous results from gravity and MT studies in the area.

The interpretation of CCSS data set I clearly illustrates the advantages of integrated modeling of seismic refraction and reflection data. The refraction data provide reliable velocity values when the reflection data are employed for structural control, and the derived velocity values facilitate depth conversion of the seismic reflections.

ACKNOWLEDGMENTS

Valuable suggestions and comments from A.G. Green and the anonymous reviewers are gratefully acknowledged. Financial support was provided from the Danish Natural Science Research Council, J.No. 11-6376.

REFERENCES

Green, A.G., Spencer, C., Milkereit, B., Clowes, R.M., and Ellis, R.M.
1990a : Guidelines for CCSS workshop topics I to IV ; *in* Studies of Laterally Heterogeneous Structures Using Seismic Refraction and Reflection Data, ed. A.G. Green ; Geological Survey of Canada, Paper 89-13, p. 27-30.

Green, A.G., Clowes, R.M., and Ellis, R.M.
1990b : Crustal studies across Vancouver Island and adjacent offshore margin ; *in* Studies of Laterally Heterogeneous Structures Using Seismic Refraction and Reflection Data, ed. A.G. Green ; Geological Survey of Canada, Paper 89-13, p. 3-25.

Kurtz, R.D., DeLaurier, J.M., and Gupta, J.C.
1986 : A magnetotelluric sounding across Vancouver Island detects the subducting Juan de Fuca plate ; Nature, v. 321, p. 596-599.

McMechan, G.A. and Mooney, W.D.
1980 : Asymptotic ray theory and synthetic seismograms for laterally varying structures : Theory and application to the Imperial Valley, California ; Seismological Society of America, Bulletin, v. 70, p. 2021-2035.

McMechan, G.A. and Spence, G.D.
1983 : P-wave velocity structure of the Earth's crust beneath Vancouver Island ; Canadian Journal of Earth Sciences, v. 20, p. 742-752.

Riddihough, R.P.
1979 : Gravity and structure of an active margin — British Columbia and Washington ; Canadian Journal of Earth Sciences, v. 16, p. 350-363.

Spence, G.D., Clowes, R.M., and Ellis, R.M.
1985 : Seismic structure across the active subduction zone of Western Canada ; Journal of Geophysical Research, v. 90, p. 6754-6772.

Analysis of CCSS data set I: reflection-refraction data from the Vancouver Island continental margin of western Canada

C.M.R. Fowler[1] and B.I. Pandit[1]

Fowler, C.M.R. and Pandit, B.I., Analysis of CCSS data set I: reflection-refraction data from the Vancouver Island continental margin of western Canada; in Studies of Laterally Heterogeneous Structures Using Seismic Refraction and Reflection Data, ed. A.G. Green; Geological survey of Canada, Paper 89-13, p. 79-90, 1990.

Abstract

The P19, P13 and P8 refraction data from the Vancouver Island continental margin have been reinterpreted. Ray tracing and synthetic seismogram computations were performed using the two-dimensional ray tracing program SEIS81. One of the original interpretations of these data had a high velocity wedge above the subducting Juan de Fuca plate. Models without a high velocity wedge were studied in order to determine whether such a wedge is an essential part of any velocity model.

Résumé

On a réinterprété les données de sismique réfraction P19, P13 et P8 provenant de la marge continentale de l'île de Vancouver. Le traçage des rayons et le calcul des sismogrammes synthétiques ont été effectués au moyen du programme bidimensionnel de traçage des rayons SEIS81. Une des premières interprétations de ces données avait montré l'existence d'un prisme à vitesse élevée situé au-dessus de la plaque de subduction de Juan de Fuca. Des modèles sans prisme à vitesse élevée ont été testés afin de déterminer si ce type de prisme est un élément essentiel de tout modèle de vitesse.

[1] Department of Geological Sciences, University of Saskatchewan, Saskatoon, Saskatchewan S7N 0W0.

INTRODUCTION

The Juan de Fuca plate is being subducted beneath the North American plate along the west coast of Canada. A series of reflection and refraction lines have been shot across this plate boundary in an attempt to determine the crustal and upper mantle structure (Spence et al., 1985 ; Green et al., 1987). Participants at the 1987 CCSS workshop were supplied with some of these reflection and refraction data in order to investigate the uniqueness of the seismic models.

The main feature of the P19, P13 and P8 refraction record sections is the difference in arrival time of the first mantle phase between the Vancouver Island and mainland recording stations (Fig. 2a and 3a). The arrival is delayed at the mainland stations. In addition, the second arrival at the mainland stations is of much larger amplitude than the first arrival (Fig. 2a, 3a). One of the principal features of the Vancouver Island reflection lines (e.g. line 1 in Fig. 15 of Green et al., 1990) is the large amplitude reflection zone C. This reflection zone has been associated with a thin wedge of high velocity (7.7 km/s) material immediately above the subducting Juan de Fuca plate (*see* Fig. 13a of Green et al., 1990). This proposed high velocity region has also been used to account for the difference in arrival time between mantle phases on Vancouver Island and mantle phases on the mainland. It is, geologically, a very important part of the velocity model, as it has considerable implications for the history of the subduction zone.

REINTERPRETATION

The Juan de Fuca subduction zone is unusual in a number of ways : there is no bathymetric expression of any trench, there is a prominent accretionary wedge, the background level of seismicity is fairly low and the dip of the downgoing slab is shallow. In all these respects it is similar to the Makran subduction zone where the Arabian plate is being subducted beneath the Eurasian plate (White and Louden, 1982). Numerous seismic velocity determinations obtained from wide-angle reflection-refraction experiments made on transects crossing the Makran accretionary prism indicate that considerable sediment compaction and dewatering is occurring there (Fowler et al., 1985). This is demonstrated by the seismic velocity increase from approximately 2.5 km/s at 1 km depth to 5 km/s at 4 km depth (Fowler et al., 1985). The velocity analysis for the Vancouver Island offshore reflection line 85-01 (supplied as part of CCSS data set I) is very similar to that determined for the Makran prism. Such high sedimentary velocities as appear to be indicated both by the velocity analysis and by comparison with the Makran region, would mean that the top of the subducting Juan de Fuca plate should be deeper than it is shown in the published models (e.g. Fig. 13a of Green et al., 1990).

The refraction record sections for shots P19 and P13 (Fig. 2a and 3a) appear to show a low amplitude arrival some 0.3-0.5 s ahead of the main large amplitude arrival at the mainland stations. Previous interpretations have not separated these two arrivals. In this paper the first arrival at the Vancouver Island stations (model distance 195-250 km ; reduced travel time 3.5-3.9 s) and the low amplitude first arrival at the mainland stations (model distance 285-350 km ; reduced travel time 4.3-4.7 s) are interpreted as a wave refracted through the Juan de Fuca mantle. The large amplitude second arrival at the mainland stations (model distance 285-350 km ; reduced travel time 5.3-4.6 s) is interpreted as a wide-angle reflection from the base of the Juan de Fuca lithosphere.

MODELLING OF REFRACTION DATA

An idealized two-dimensional velocity model was set up and rays traced through it using the synthetic seismogram ray tracing program SEIS81 of Červený and Pšencík (1981). In order to avoid having to specify the shallow structure in unnecessary detail, shots P19, P13 and P8 were placed at the base of the oceanic crust on the Juan de Fuca plate and a constant time correction applied for the shallow structure. This procedure does mean that long range arrivals are plotted too early compared with the shorter range arrivals ; however, the maximum introduced error is no more than 0.1 s, which is better than the accuracy with which the mainland first arrivals can be picked.

As an intellectual exercise the seismic velocity models shown in this paper have been constructed in an attempt to explain the prominent features of the data without having to include a high velocity region above the Juan de Fuca plate. These models are thus in some sense a test of the uniqueness of the published structure (e.g. Spence et al., 1985) — not a test of the uniqueness of the fine detail of the model, but a test of what is geologically and tectonically an exceedingly important part of the proposed model.

The parameters which were varied in an attempt to fit the travel times were : (1) velocity of the continental lower crust and the depth of the continental Moho ; (2) velocity of the thin horizontal layer below 16 km depth on the continental side of the subduction zone ; (3) dip of the subducting Juan de Fuca plate ; and (4) velocity of the Juan de Fuca lithosphere.

The results of varying these parameters were as follows :

(1) Models with a deeper continental Moho than shown in Figure 13a of Green et al., (1990) were unsatisfactory, as it was not then geometrically possible to propagate energy into the continental mantle and up to the mainland recording stations. In order for the arrivals at the mainland stations to have a mantle-type phase velocity, it was necessary for energy to propagate into the continental upper mantle. The continental structure used was therefore a simplified version of that determined from the JI section (Fig. 13a of Green et al., 1990).

(2) Reducing the velocity of the thin layer below 16 km depth from 6.95 km/s to 6.0 km/s, or lower, in the region adjacent to the subducting plate had the effect of delaying the first arrival from the mantle at 230 and 240 km by about 0.1 s. This gives a higher phase velocity for the first arrivals between 230 and 250 km in agreement with observations.

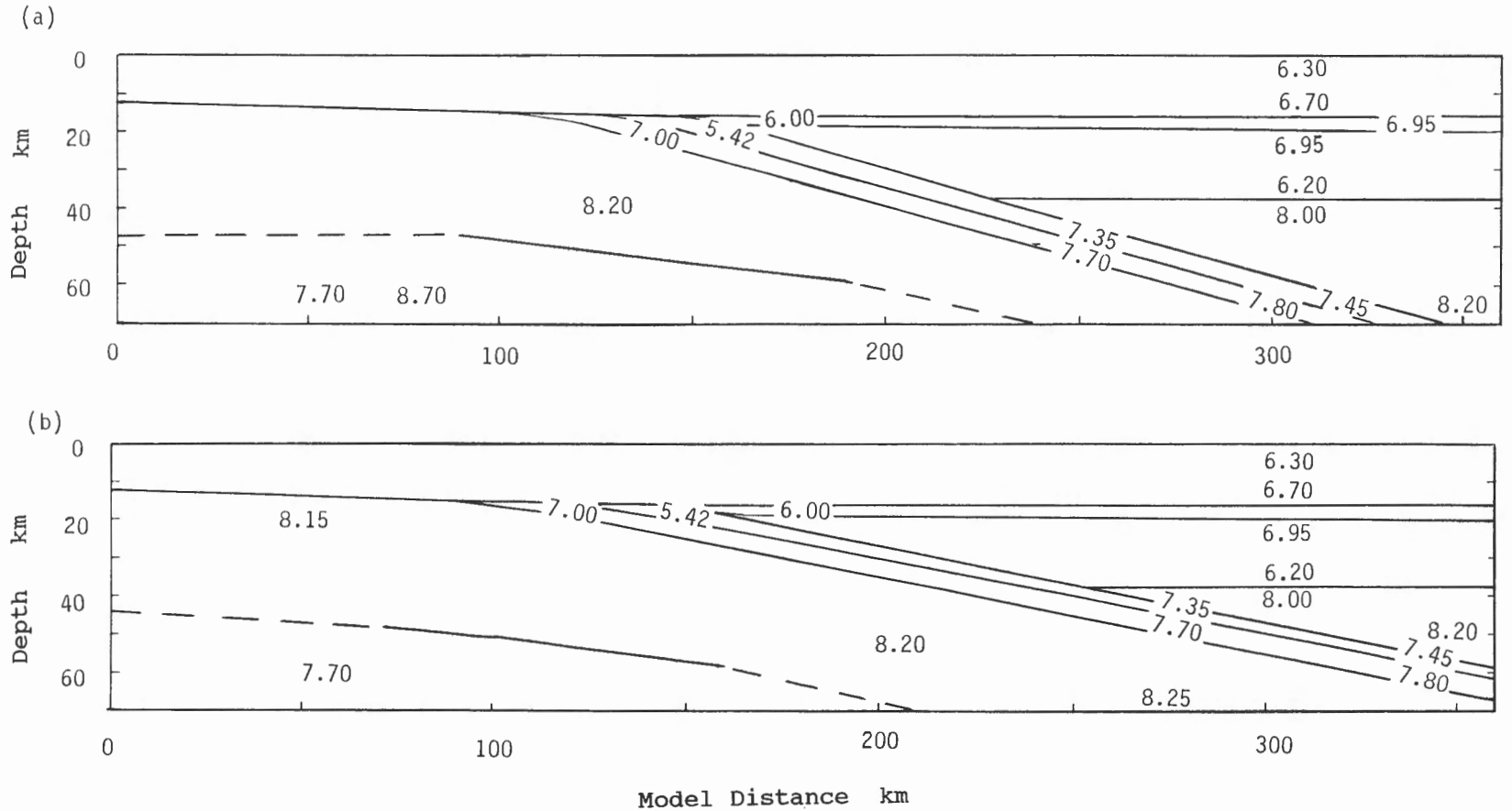

Figure 1. Two possible models of the P-wave velocity structure in the vicinity of Vancouver Island. No vertical exaggeration. (a) Slab dips at 14° and the velocity of the Juan de Fuca mantle is 8.2 km/s. (b) Slab dips at 11° and the velocity of the Juan de Fuca mantle is 8.15-8.25 km/s.

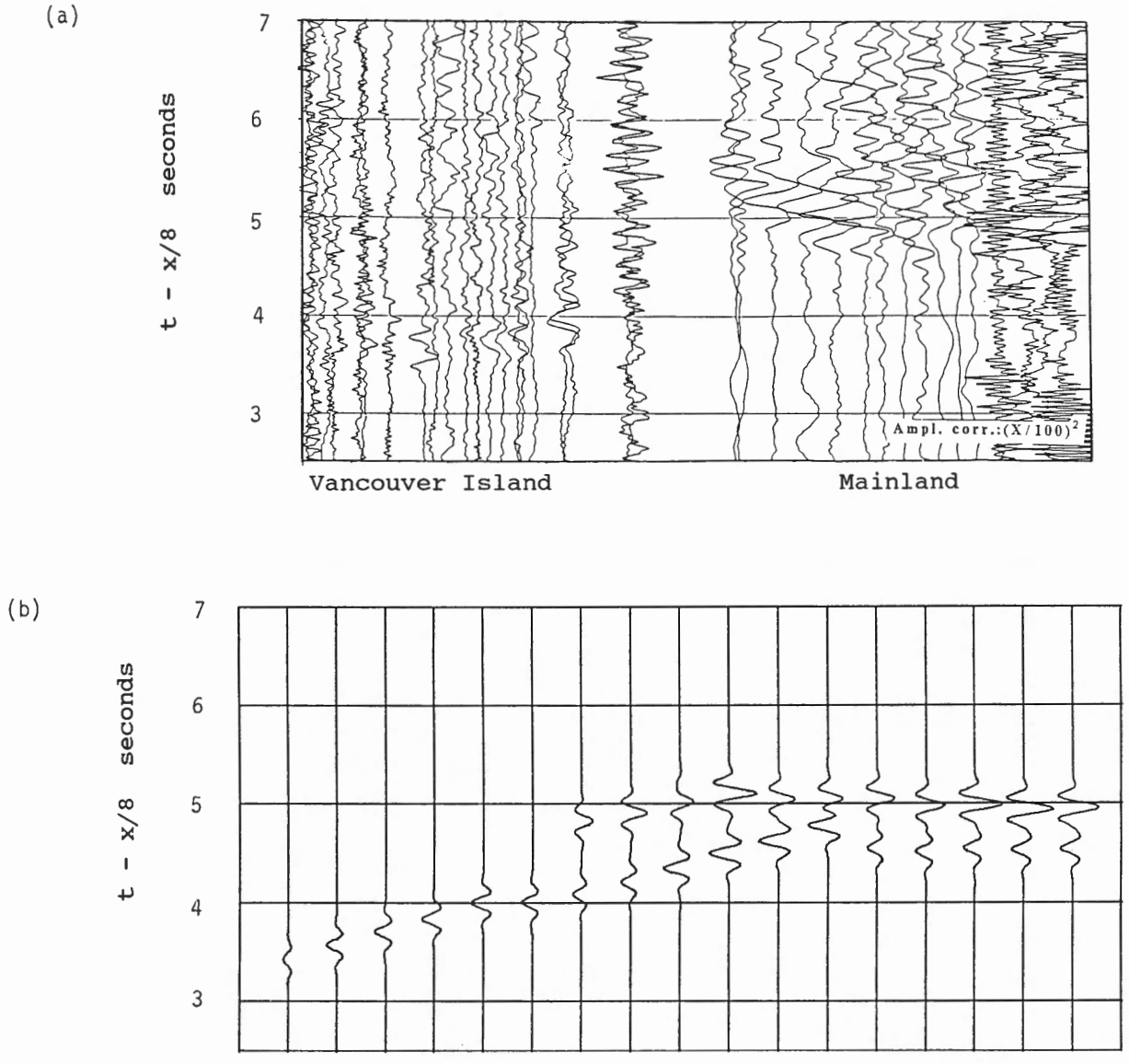

Figure 2. (a) Record section for shot P19 reduced to 8 km/s. (b) Synthetic seismograms for model shown in Figure 1a. Velocity of lowermost layer is 7.7 km/s. (c) Synthetic seismograms for model shown in Figure 1a. Velocity of lowermost layer is 8.7 km/s. (d) Ray paths for P19 shot and model shown in Figure 1a. Synthetic seismograms are plotted with amplitude scaling $(x/100)^2$ and normalized to the maximum amplitude in the record section.

(c)

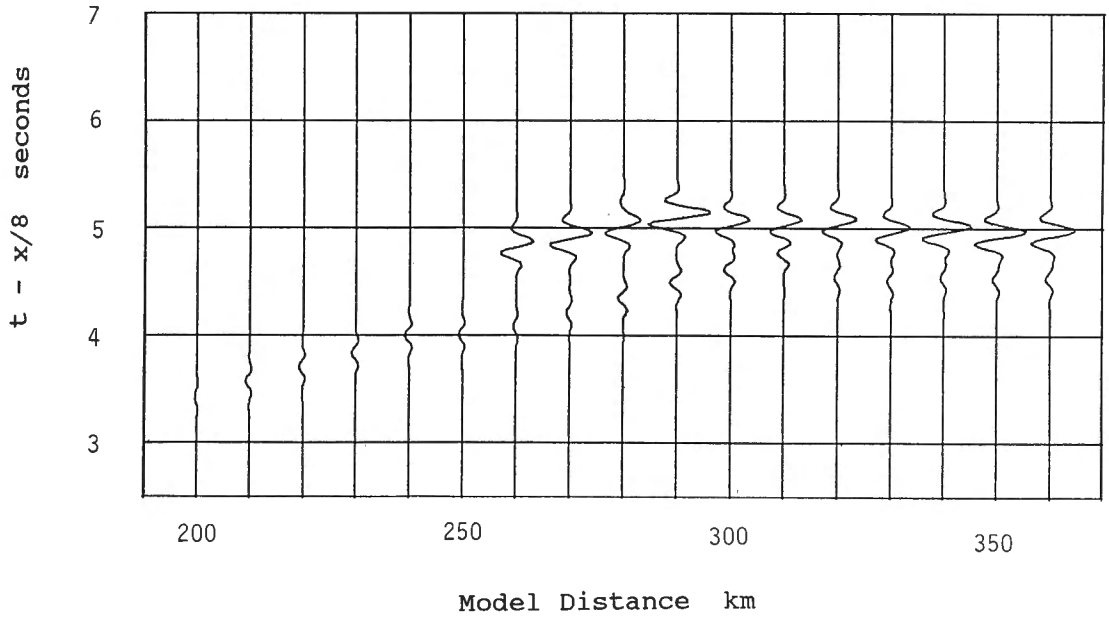
7
6
5
4
3
t - x/8 seconds
200
250
300
350
Model Distance km

(d)

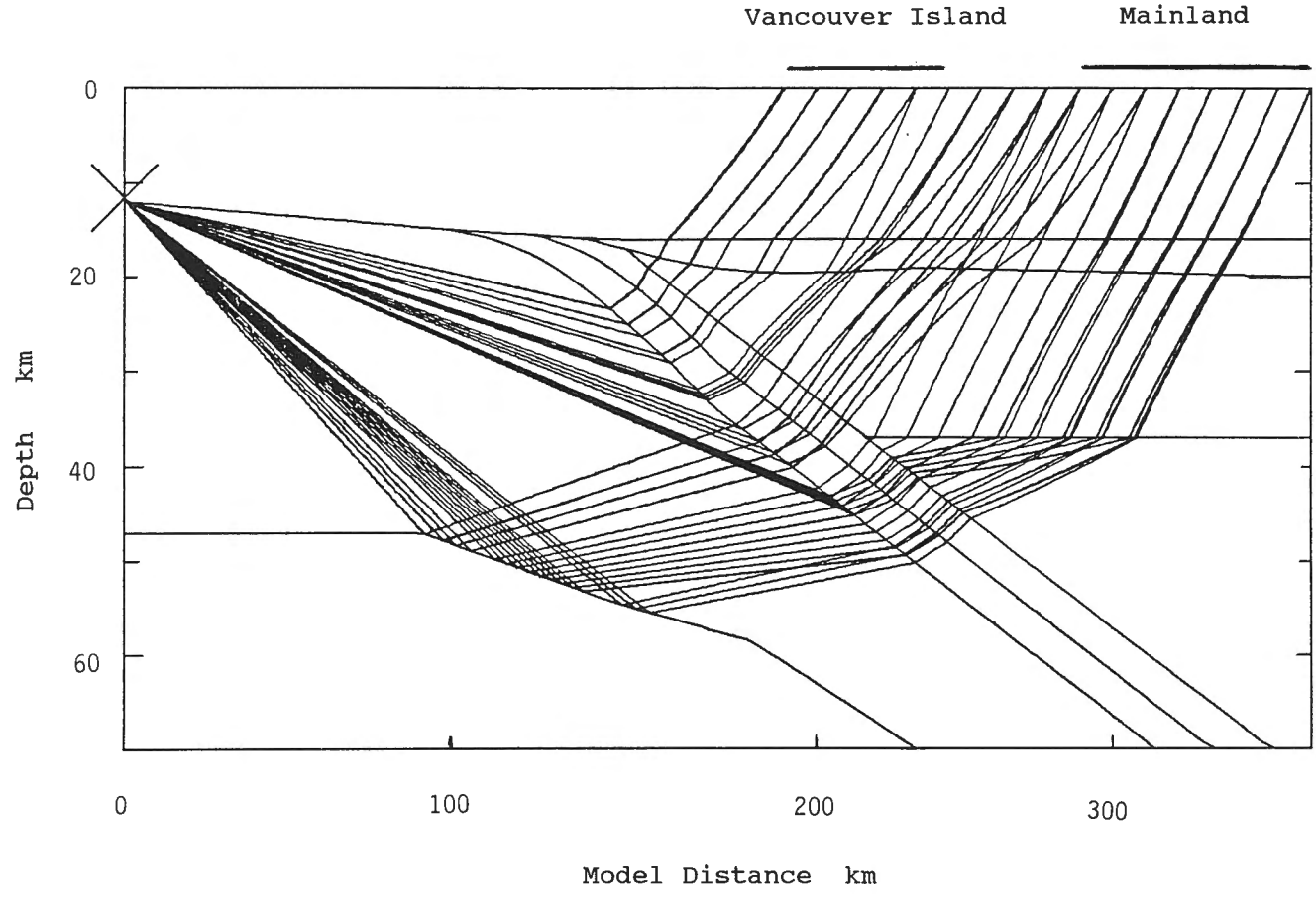
Vancouver Island
Mainland
0
20
40
60
Depth km
0
100
200
300
Model Distance km

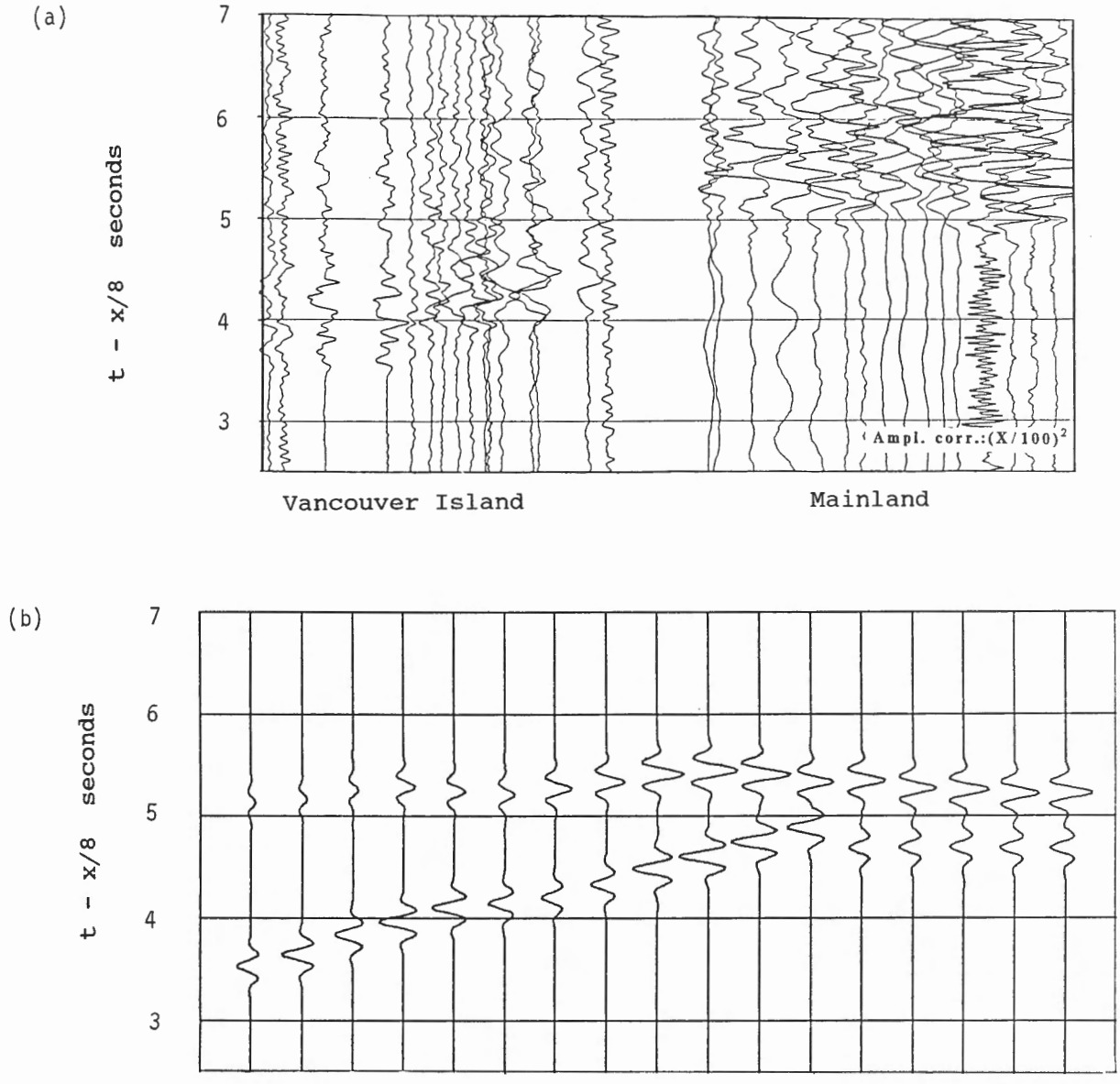

Figure 3. (a) Record section for shot P13 reduced to 8 km/s. (b) Synthetic seismograms for model shown in Figure 1a. Velocity of lowermost layer is 7.7 km/s. (c) Synthetic seismograms for model shown in Figure 1a. Velocity of lowermost layer is 8.7 km/s. (d) Ray paths for P13 shot and model shown in Figure 1a. Synthetic seismograms are plotted with amplitude scaling $(x/100)^2$ and normalized to the maximum amplitude in the record section.

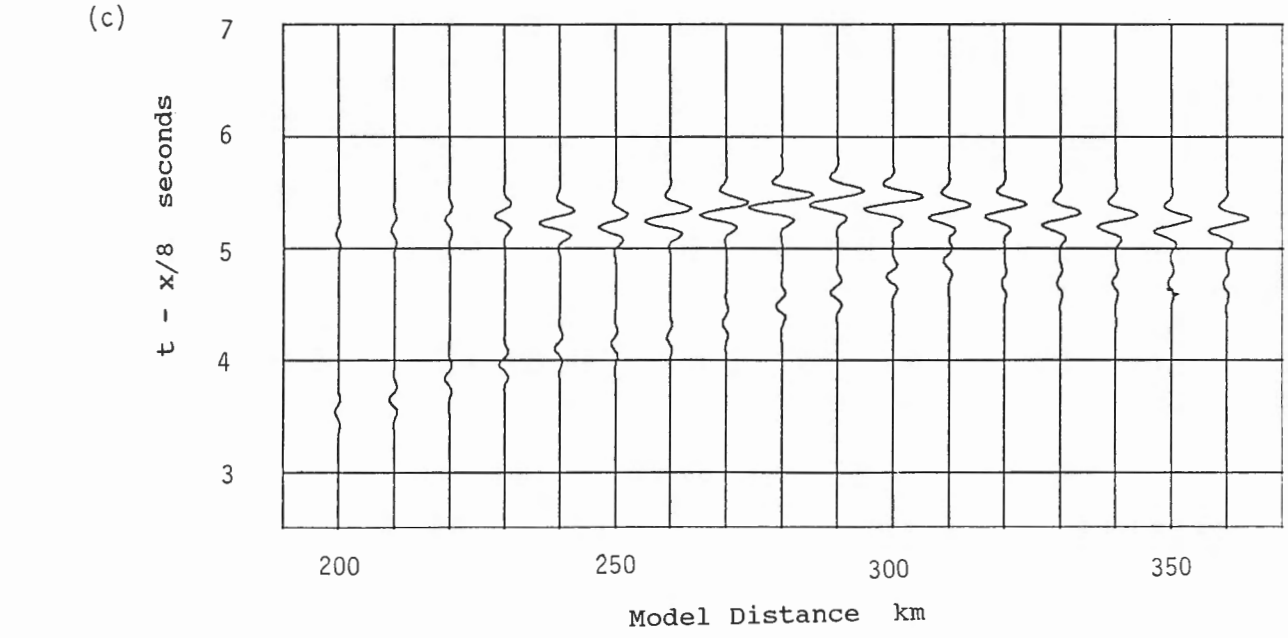
(c)
7
6
5
4
3
t - x/8 seconds
200
250
300
350
Model Distance km

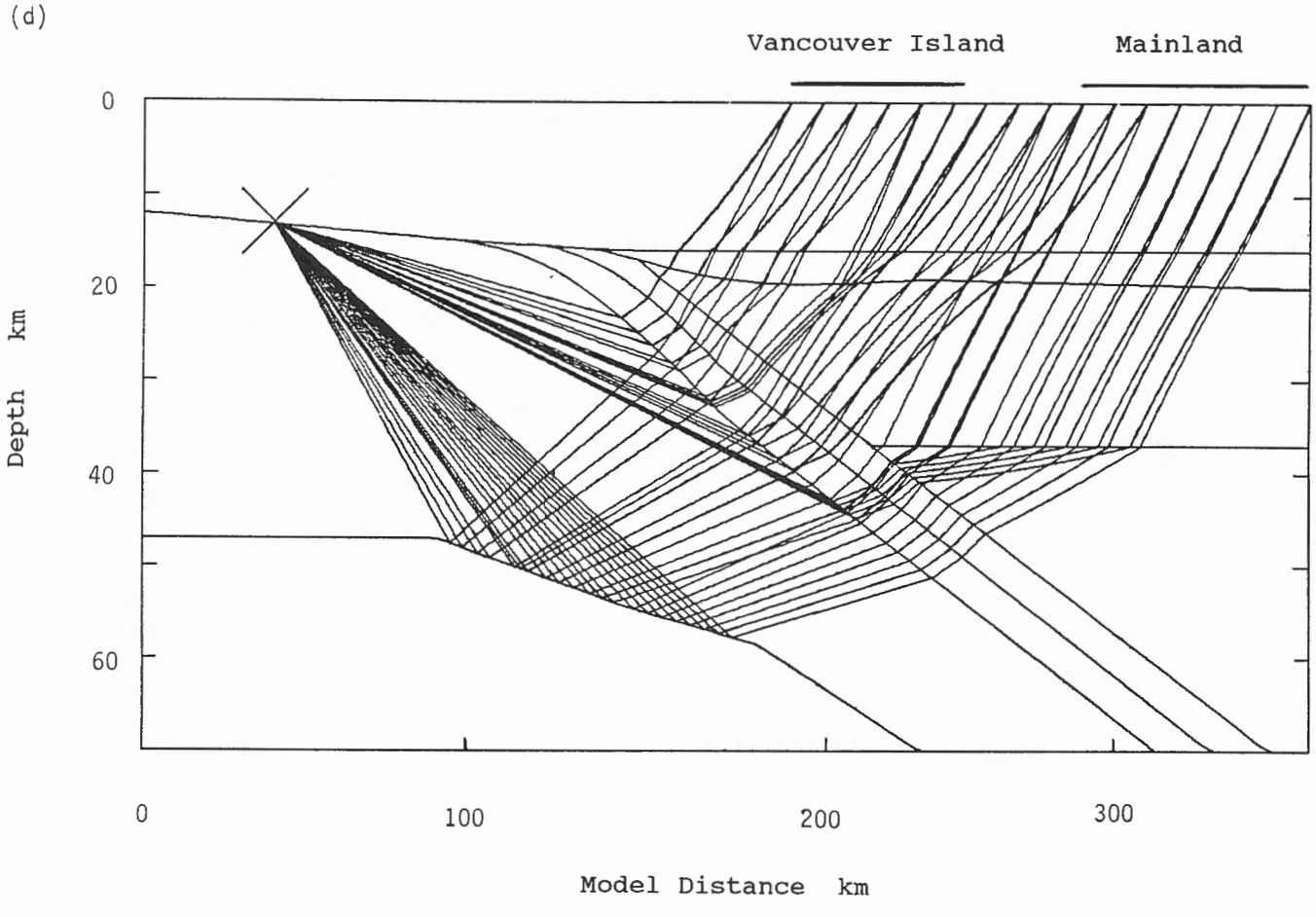
(d)
Vancouver Island
Mainland
0
20
40
60
Depth km
0
100
200
300
Model Distance km

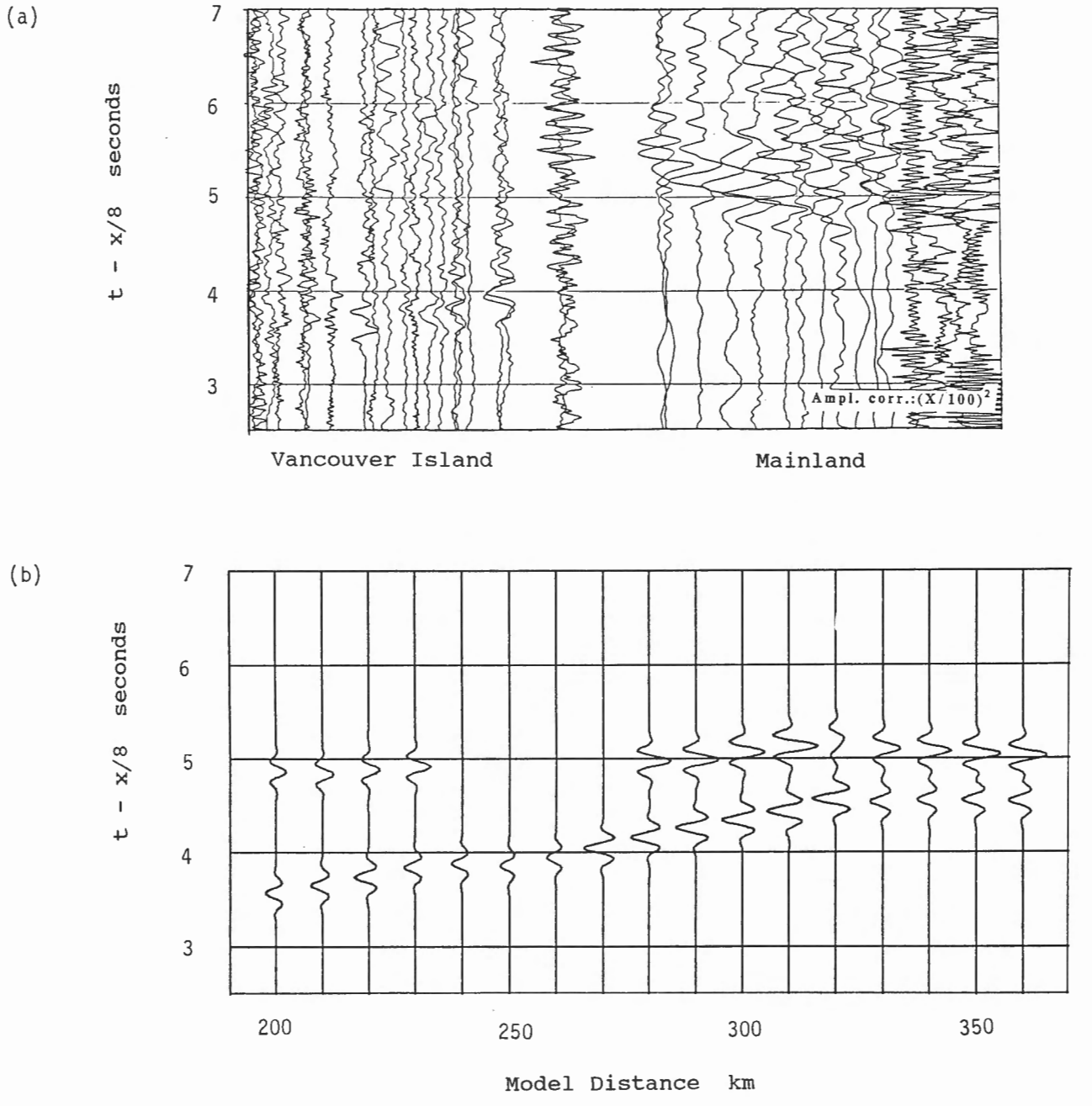

Figure 4. (a) Record section for shot P19 reduced to 8 km/s. (b) Synthetic seismograms for model shown in Figure 1b. (c) Ray paths for P19 shot and model shown in Figure 1b. Synthetic seismograms are plotted with amplitude scaling $(x/100)^2$ and normalized to the maximum amplitude in the record section.

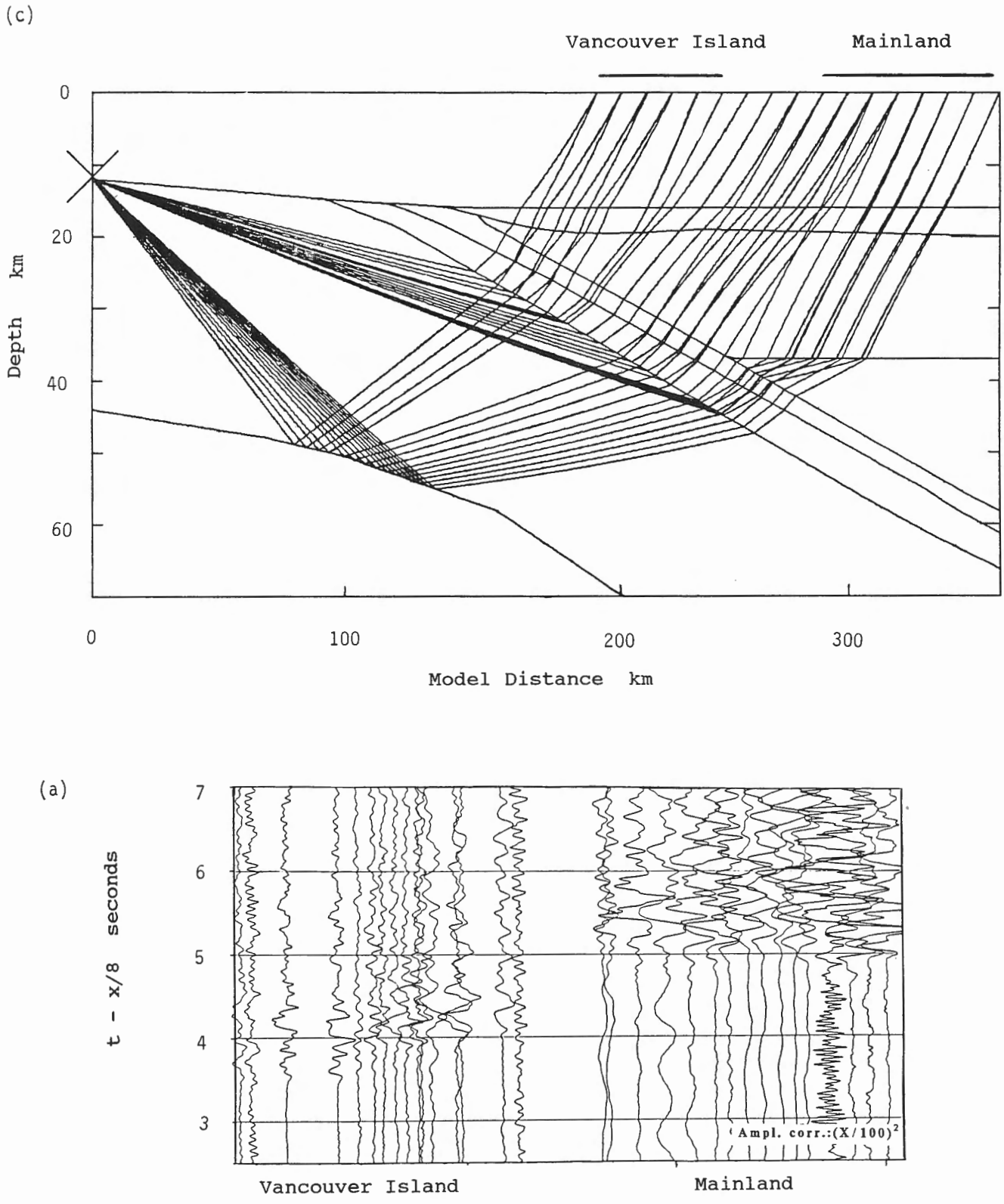

Figure 5. (a) Record section for shot P13 reduced in 8 km/s. (b) Synthetic seismograms for model shown in Figure 1b. (c) Ray paths for P13 shot and model shown in Figure 1b. Synthetic seismograms are plotted with amplitude scaling $(x/100)^2$ and normalized to the maximum amplitude in the record section.

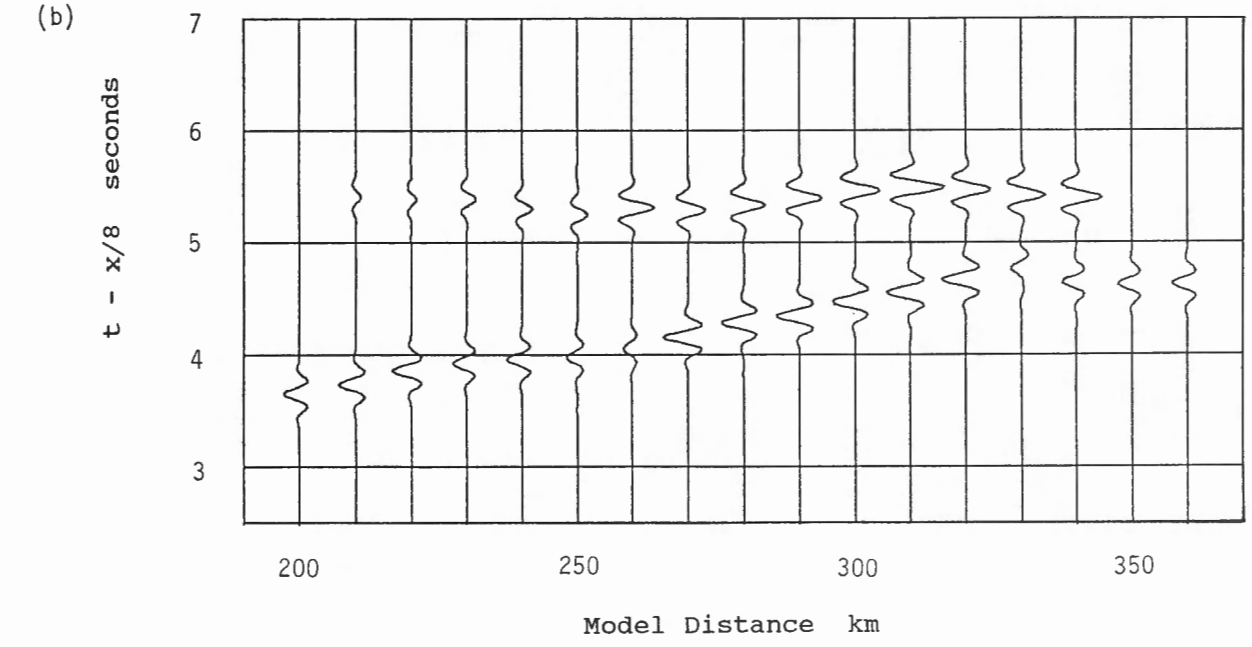
(b)
7
6
5
4
3
t - x/8 seconds
200
250
300
350
Model Distance km

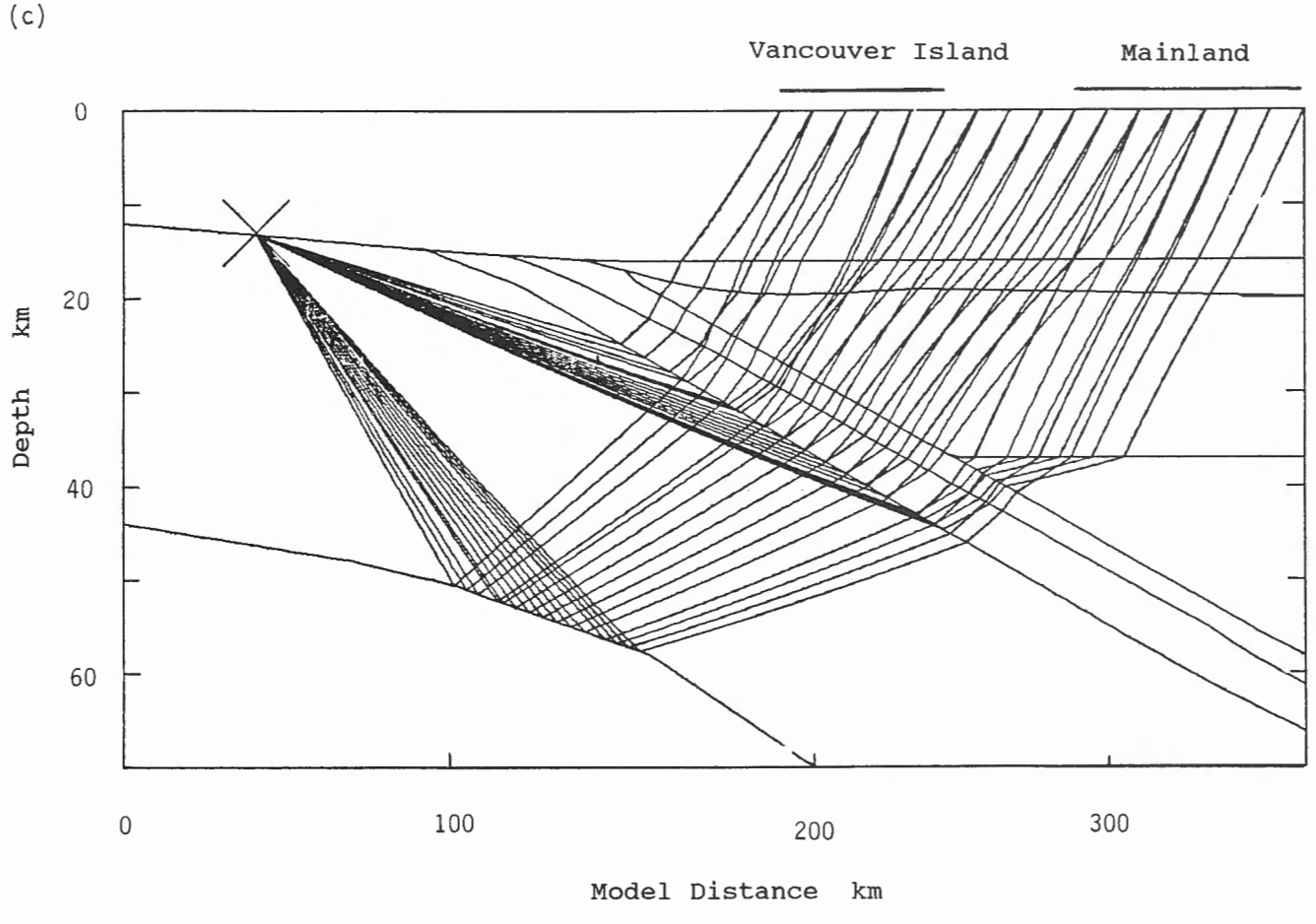
(c)
Vancouver Island
Mainland
0
20
40
60
Depth km
0
100
200
300
Model Distance km

(3) and (4) By changing the dip and velocity of the mantle of the Juan de Fuca plate it was possible to find combinations that fitted the main features of the mantle travel times reasonably well. The mantle velocity was assumed to be pressure (i.e., depth) dependent and not age dependent. Thus lateral variations in mantle velocity were not considered. As the travel times were sensitive to the velocity gradient chosen, were lateral gradients allowed, a better fit to the times could presumably be achieved. The velocity of the oceanic crust was assumed to increase with depth as increasing pressure closes cracks and then as gabbro transforms to eclogite. However, this is not an important feature of the model ; the travel times were not particularly sensitive to the velocity structure of the oceanic crust.

Two seismic velocity models are shown in Figure 1. The synthetic seismograms for the models are shown in Figures 2b, 2c, 3b, 3c, 4b and 5b. The velocity models are not perfect but they do serve to illustrate the fact that the refraction data are not of sufficiently good quality, nor the lines long enough, to permit an unambiguous interpretation. The model shown in Figure 1a is better than that shown in Figure 1b. Synthetic seismograms for the model shown in Figure 1a are shown for two possible velocities of the lowermost layer (the region beneath the Juan de Fuca lithosphere), 8.7 and 7.7 km/s (Fig. 2b, 2c, 3b and 3c). Changing the P-wave velocity of this layer only affects the amplitude of the reflection from its upper surface, which is the second arrival at the mainland stations. The amplitude of this reflection is larger and in better agreement with observations when the velocity of the lowermost layer is 8.7 km/s. The low velocity of the layer at 16 km depth beneath Vancouver Island should be sufficient to produce a large amplitude normal incidence reflection C.

In conclusion, we suggest that the previous interpretations of these data are not unique and that other structures, which do not have the high velocity ''underplated'' C zone, should also be studied. This zone is particularly important because its presence, or absence, and structure are critically important to subsequent geological and tectonic models of the subduction zone.

REFERENCES

Červený V. and Pšencík, I.
1981 : 2-D Seismic Ray Package ; Research Report, Institute of Geophysics, Charles University, Prague.

Fowler, S.R., White, R.S., and Louden, K.E.
1985 : Sediment dewatering in the Makran accretionary prism ; Earth and Planetary Science Letters, v. 75, p. 427-438.

Green, A.G., Clowes, R.M., and Ellis, R.M.
1990 : Crustal studies across Vancouver Island and adjacent offshore margin ; *in* Studies of Laterally Heterogeneous Structures Using Seismic Refraction and Reflection Data, ed. A.G. Green ; Geological Survey of Canada, Paper 89-13, p. 3-25.

Green, A.G., Milkereit, B., Mayrand, L., Spencer, C., Kurtz, R., and Clowes, R.M.
1987 : Lithoprobe seismic reflection profiling across Vancouver Island : results from reprocessing ; Royal Astronomical Society, Geophysical Journal, v. 89, p. 85-90.

Spence, G.D., Clowes, R.M., and Ellis, R.M.
1985 : Seismic structure across the active subduction zone of western Canada ; Journal of Geophysical Research, v. 90, p. 6754-6772.

White, R.S. and Louden, K.E.
1982 : The Makran continental margin : structure of a thickly sedimented convergent plate boundary ; *in* Studies in Continental Margin Geology, ed. J.S. Watkins and C.L. Drake ; American Association of Petroleum Geologists, Memoir 34, p. 499-518.

Velocity structure model determined from onshore-offshore seismic profiling across Vancouver Island and adjacent continental margin

Takaya Iwasaki[1] **and Hideki Shimamura**[1]

Iwasaki, T. and Shimamura, H., Velocity structure model determined from onshore-offshore seismic profiling across Vancouver Island and adjacent continental margin ; in Studies of Laterally Heterogeneous Structures Using Seismic Refraction and Reflection Data, ed. A.G. Green ; Geological Survey of Canada, Paper 89-13, p. 91-103, 1990.

Abstract

We have constructed a velocity structure model of the subduction zone in the vicinity of Vancouver Island from the onshore-offshore seismic data collected under the auspices of the Vancouver Island Seismic Project (VISP). We employed our usual methods of marine refraction analysis. The derived model is a rather simple one because the supplied data have insufficient resolving power to elucidate detailed structure in the subduction zone. In the oceanic part of the model, the velocity structure was determined mainly from recordings of refraction data on ocean bottom seismometers (OBSs). The subducting Moho boundary is defined by P_mP and P_n signals in the observed record sections. Crustal thickness is about 10 km beneath the oceanic basin, increasing to 15-17 km under the continental slope. We found no evidence for velocity discontinuities in the oceanic crust. A P velocity of 8.0 km/s was determined, which is normal for the oceanic upper mantle. In the continental part of the profile, we constructed a crustal model composed of flat layers. The depth of the continental Moho was determined to be about 35 km using refraction data from the marine shots. The dip angle of the subducting oceanic lithosphere increases steeply from 2-6° to more than 20° beneath Vancouver Island.

Résumé

Un modèle de la structure de vitesse pour la zone de subduction située dans la région de l'île de Vancouver a été établi à partir des données de profils sismiques terrestres et océaniques, recueillies sous les auspices du Projet sismique de l'île de Vancouver (PSIV). Les méthodes habituelles d'analyse de sismique réfraction marine ont été utilisées. Le modèle obtenu est plutôt simple, car les données fournies ont un pouvoir de résolution insuffisant pour élucider la structure précise de la zone de subduction. Dans la partie océanique de ce modèle, la structure de vitesse a été déterminée principalement à partir d'enregistrements de données de sismique réfraction provenant de sismomètres placés au fond de l'océan (OBS). La limite de subduction du Moho est définie par les ondes P_mP et P_n des coupes sismiques observées. L'épaisseur de la croûte sous le bassin océanique est d'environ 10 km, atteignant 15 à 17 km sous le talus continental. Aucune discontinuité de vitesse n'a été observée dans la croûte océanique. On a déterminé la vitesse des ondes P_n à 8 km/s, c'est-à-dire une vitesse normale pour le manteau supérieur océanique. Dans la partie continentale du profil, le modèle crustal se compose de couches horizontales. La profondeur du Moho continental est évaluée à environ 35 km, sur la base des données de sismique réfraction provenant de tirs en mer. Le pendage de la lithosphère océanique s'enfonçant augmente rapidement de 2 à 6° à plus de 20° sous l'île de Vancouver.

[1] Laboratory for Ocean Bottom Seismology, Faculty of Science, Hokkaido University, Sapporo 060, Japan.

ANALYSIS PROCEDURES

The data set we used consisted of seismic refraction and multichannel seismic reflection data recorded across Vancouver Island and the adjacent continental margin. The location map of the survey is presented in Figures 4 and 5 of Green et al. (1990).

The analysis method we applied was similar to that used previously in our interpretation of marine data (Iwasaki et al., 1989). As a first step, we computed one-dimensional velocity structures for each shot or receiver (ocean bottom seismometer — OBS) using apparent velocities and intercept times. Next, we obtained a two-dimensional velocity model by ray tracing. This model explained simultaneously all of the observed travel time data. The starting model for this procedure was constructed by simple interpolation of the one-dimensional models. The reflection data were used to constrain the configuration of some model interfaces.

Our ray tracing program can treat two-dimensional laterally heterogeneous velocity structures with curved interfaces, some of which may partially coincide (Iwasaki, 1988). We obtain ray diagrams and travel time curves with rather short computation times because the ray equation is solved as an initial value problem. For a desired type of ray, our program automatically finds the corresponding range of incident angles. This is especially useful for the computation of diving waves in which a very narrow beam from the source spreads over a wide offset range.

Finally, we computed synthetic seismograms based on asymptotic ray theory, and modified our model to satisfy both the travel time and amplitude data. The computer program we used was a modified version of SEIS 83 (Červený and Pšencík, 1983). The original SEIS83 program, however, was designed for shots fired at depth and receivers on the surface. It was clear that the original program was not suitable for modeling the Vancouver Island offshore data, because simple reciprocity between shots and receivers at different levels within the earth does not apply in the computation of amplitudes. In order to model marine refraction data collected on OBSs, the synthetic seismogram program has been modified to treat the case in which the receiver is on the seabed and the shots are fired at the surface (Hirata and Shinjo, 1986).

INTERPRETATION OF MARINE DATA

The velocity structure along the marine profile (marine line I) was determined from refraction data recorded at OBSs 1, 3 and 5 (*see* Fig. 4 of Green et al., 1990). These data could not resolve detailed shallow structure due to insufficient distribution of explosions and OBSs. For this reason, we depended on the sediment and basement structures described by Spence et al. (1985), in which seismic profiling, multichannel reflection and airgun data had been taken into account.

Figure 1 shows the velocity structure obtained for the marine profile. Synthetic seismograms computed from our model are compared with observed record sections in Figures 2 to 4. Amplitude balancing for the synthetics is the same as for the observed data. The theoretical travel time curves are superimposed on each observed record section. It is seen that the travel time and amplitude data are explained fairly well by our model, the features of which are described below.

The structure in the oceanic basin was determined mainly from the refraction data recorded at OBSs 1 and 3 (*see* Fig. 2 and 3). In this part of the model the structure is quite simple, with crustal thickness determined to be 10 km. The P-wave velocity increases from 4.0 to 7.7 km/s in the oceanic crust, but we found no evidence for velocity discontinuities. The three "interfaces" in the crust (Fig. 1) were introduced to adjust velocity gradients.

The Moho boundary was determined from P_n and P_mP phases, which were clearly recognized in the observed sections. The P-wave velocity just above the Moho boundary is about 7.7 km/s and may not be lower than this value. For example, if we adopt a value of 7.5 km/s, the P_mP phase should have been recorded over a wider distance range than was observed. We found a normal oceanic upper mantle velocity of 8.0 km/s. The velocity gradient in the mantle was estimated to be 0.015 s^{-1} from the amplitude data of the P phase.

The structure beneath the continental slope is complex compared to that of the oceanic crust. Between OBSs 3 and 5, the crustal thickness increases landward from 15 to 17-20 km. The subducting Moho boundary is traced in the refraction data at OBS 5 to within about 80 km of the western edge of the profile. The P-wave velocity beneath the continental slope sediments is 4.6-5.0 km/s, which is greater than that in the oceanic crust. Our estimate of the velocity gradient in the uppermost crust is 0.15 s^{-1} beneath OBS 5, which is less than the 0.2 s^{-1} of the Spence et al. (1985) model. For a model with velocity gradient greater than ours, the computed amplitudes of first arrivals become much larger than observed.

The detailed velocity structure of the transition from oceanic basin to continental slope was not constrained by the CCSS data. In order to decrease the ambiguity in modeling and to obtain finer structure, we would need denser record sections than those supplied.

INTERPRETATION OF LAND DATA

Data from Shot J1

We have determined the crust and upper mantle structure beneath Vancouver Island from the onshore seismic profiles. The upper crustal structure was determined mainly from the refraction data generated by shot J1. We assumed a one-dimensional structure (i.e. a flat-layered model) for

the upper crust because ray paths from shot J1 were not reversed. Figure 5 shows our results. The synthetic seismograms are presented with the observed record section in Figure 6. Amplitude balancing for the synthetics is the same as for the observed data.

The P-wave velocity increases from 5.4 to 6.5 km/s in the depth range 0 to 12.5 km. Amplitudes of the first arrival decrease beyond approximately 150 km. The second arrivals, on the other hand, have strong amplitudes in this distance range. In order to explain such features, we introduced a boundary at a depth of 12.5 km, beneath which the velocity was estimated to be 6.7 km/s. The "boundary" at 20 km depth was required to adjust the velocity gradient in the 6.7 km/s layer. Our synthetic seismograms explain well the gross features of the observed wave field (Fig. 6).

Spence et al. (1985) introduced lateral heterogeneity of the P-wave velocity in the shallower part of the crust. However, strong evidence for such lateral velocity variation was not found in the observed section of shot J1.

Data from Shots P8, P13 and P19

We used the data from marine shots P8, P13 and P19 to determine the structure of the lower crust and upper mantle at the collision front in the Vancouver Island region. In constructing a model extending from offshore to onshore, we incorporated the structure of the upper crust based on our interpretations of the marine profile and the onshore profile from shot J1. Then we matched the arrival time and amplitude data from shots P8, P13 and P19 by adjusting the deeper structure.

Figure 7 shows our entire model. In the continental part, the P-wave velocities of the lower crust and uppermost mantle are 6.7-6.85 km/s and 7.95 km/s respectively. The Moho boundary is at a depth of about 35 km. It is seen that the dip of the oceanic lithosphere increases steeply to about 22° beneath Vancouver Island.

Synthetic seismograms generated from this model are presented with the corresponding observed record sections in Figures 8 to 10. Amplitude balancing for the synthetic seismograms is the same as for the observed data. In the observed sections, we see two remarkable phases at reduced times of 3.5 to 5.0 s and 4.5 to 5.0 s appearing in distance ranges of 200-250 and 285-325 km measured from Shot P19. We interpreted these phases by two groups of rays that have turning points in the oceanic upper mantle, but different paths in the continental crust and upper mantle. For example, the arrivals between 285 and 325 km correspond to rays transmitted through the continental upper mantle. The behaviour of these rays is sensitive to the continental Moho depth. If we take the Moho depth to be

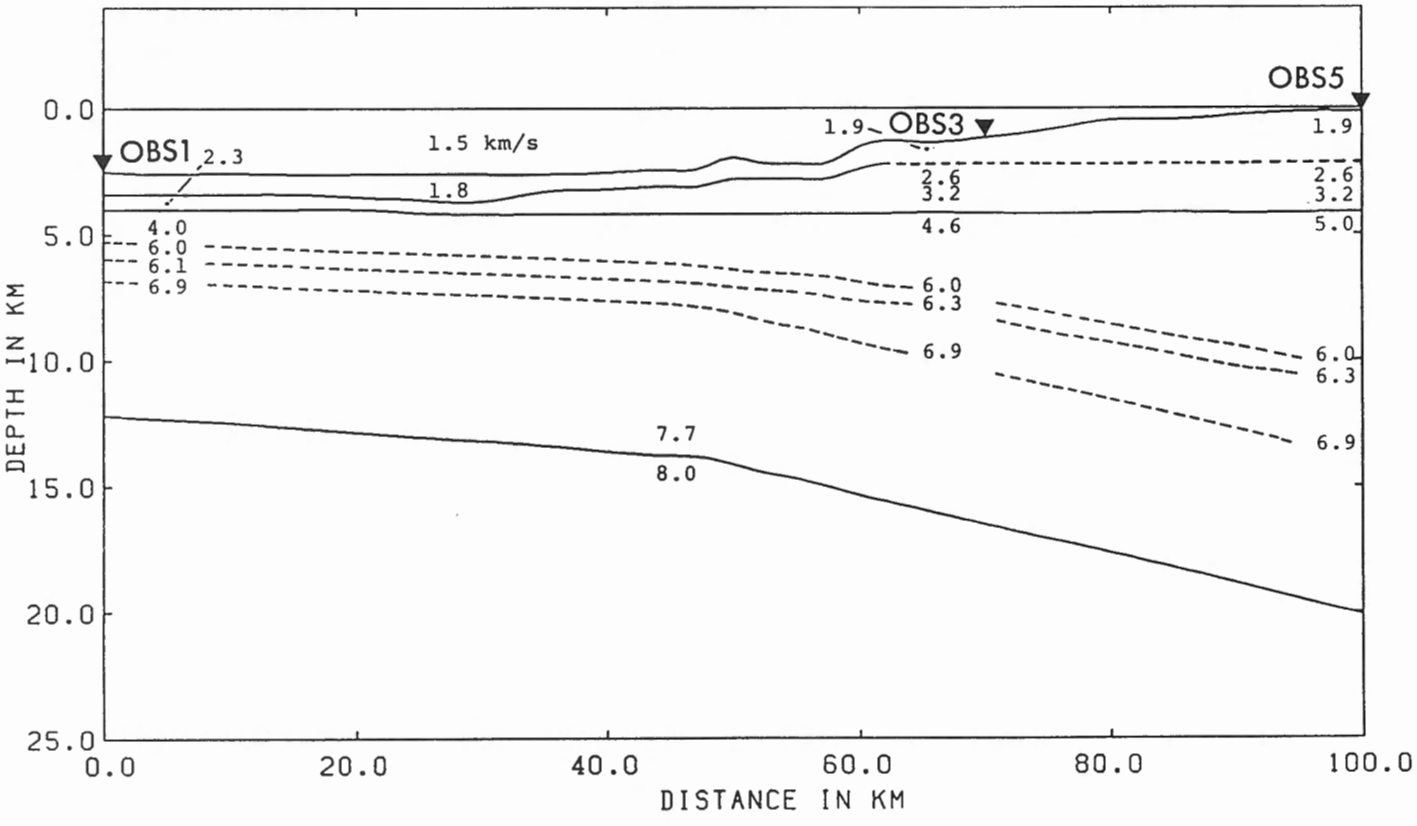

Figure 1. Velocity model for the marine portion of the CCSS profile. Solid and broken lines denote zero and first order interfaces respectively. We found no evidence for velocity discontinuities within the oceanic crust.

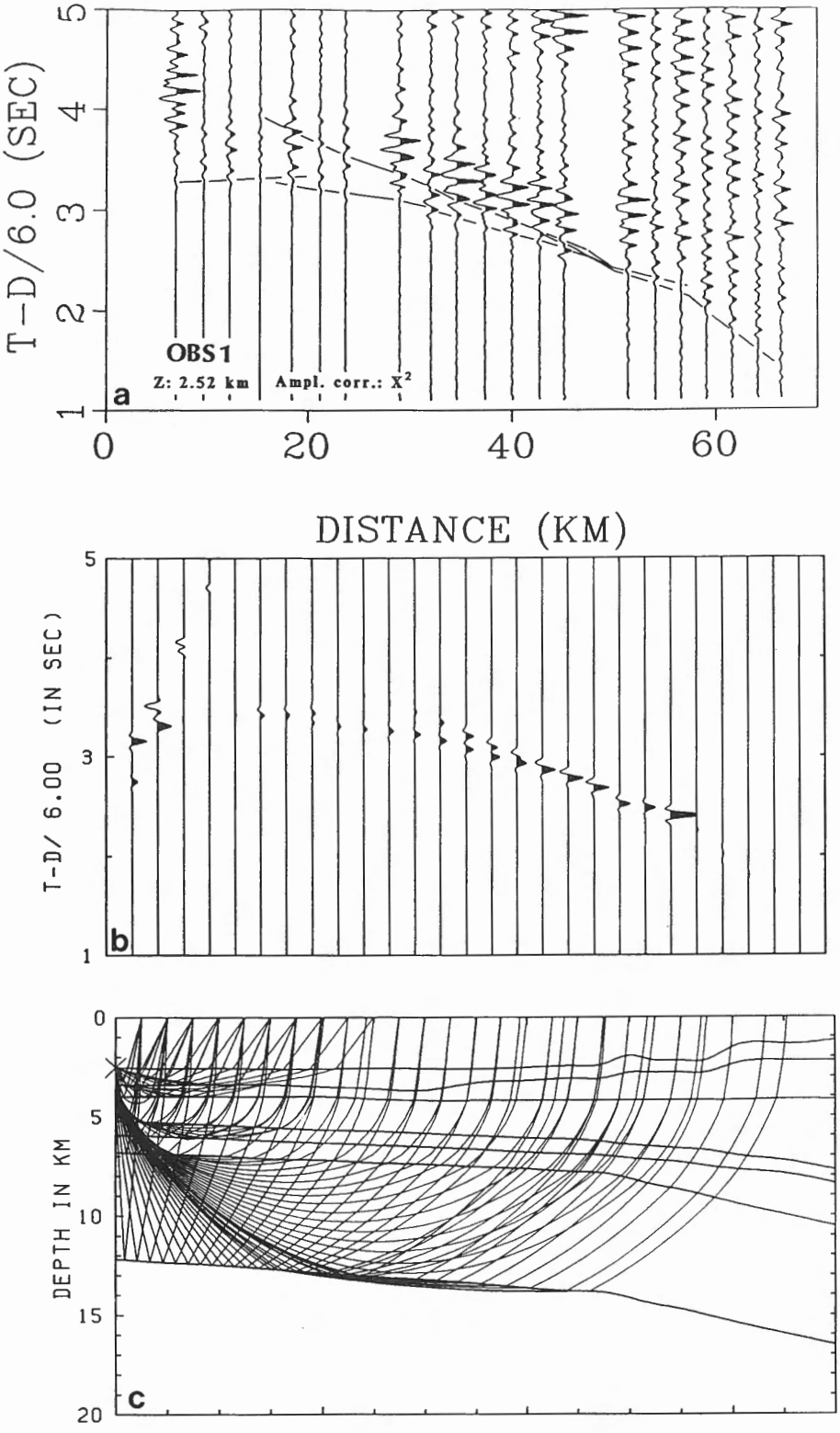

Figure 2. Observed and synthetic seismograms for OBS1. (a) Observed seismograms. (b) Synthetic seismograms. (c) Ray diagram. Note how the large amplitudes of the later arrivals in the 30-45 km range are well explained by the synthetic seismograms.

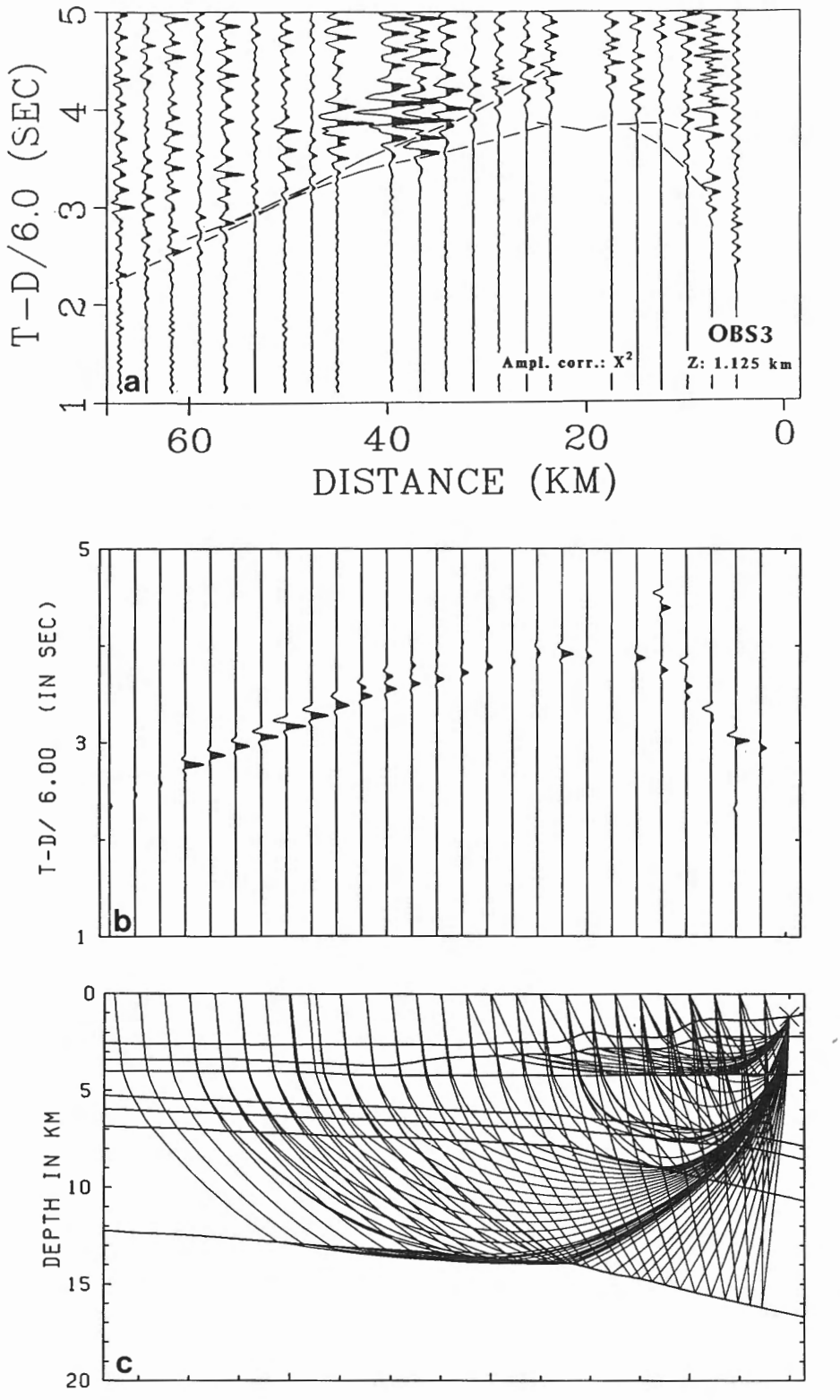

Figure 3. Observed and synthetic seismograms for OBS3. (a) Observed seismograms. (b) Synthetic seismograms. (c) Ray diagram. Later arrivals in the 30-40 km range are explained as P_mP phases.

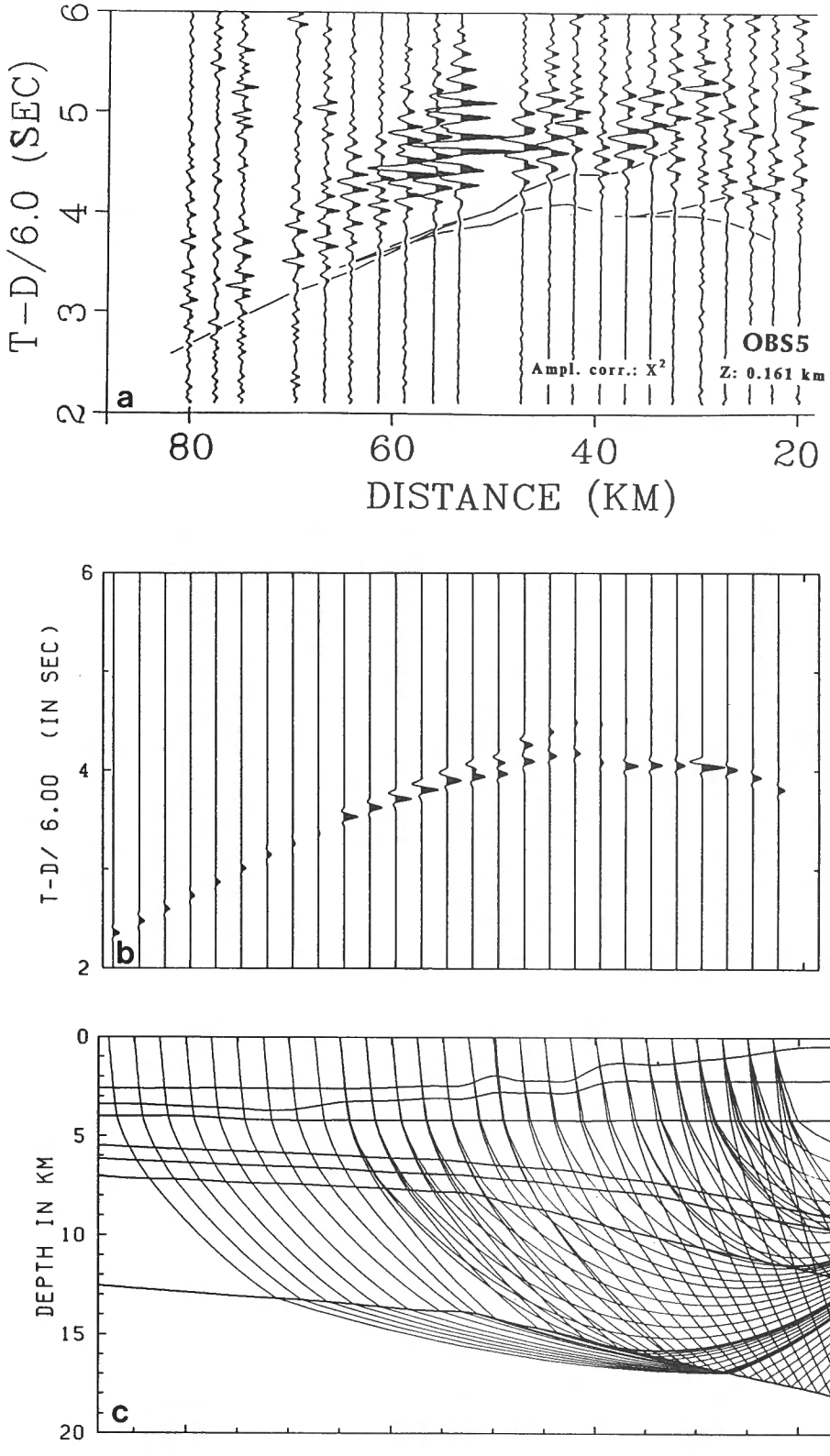

Figure 4. Observed and synthetic seismograms for OBS5. (a) Observed seismograms. (b) Synthetic seismograms. (c) Ray diagram. Later arrivals in the 40-60 km range are explained as P_mP phases.

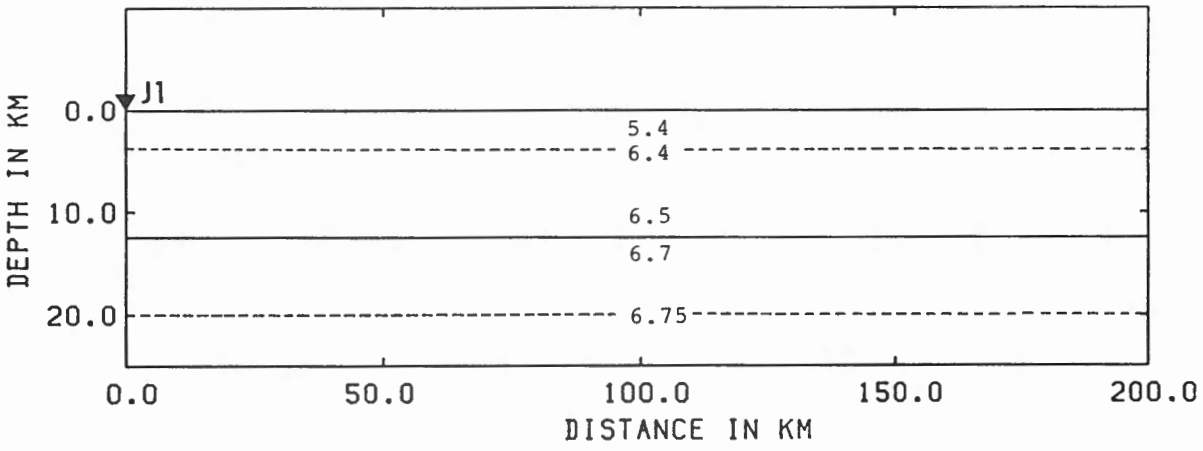

Figure 5. Velocity structure model for the unreversed land profile (shot J1).

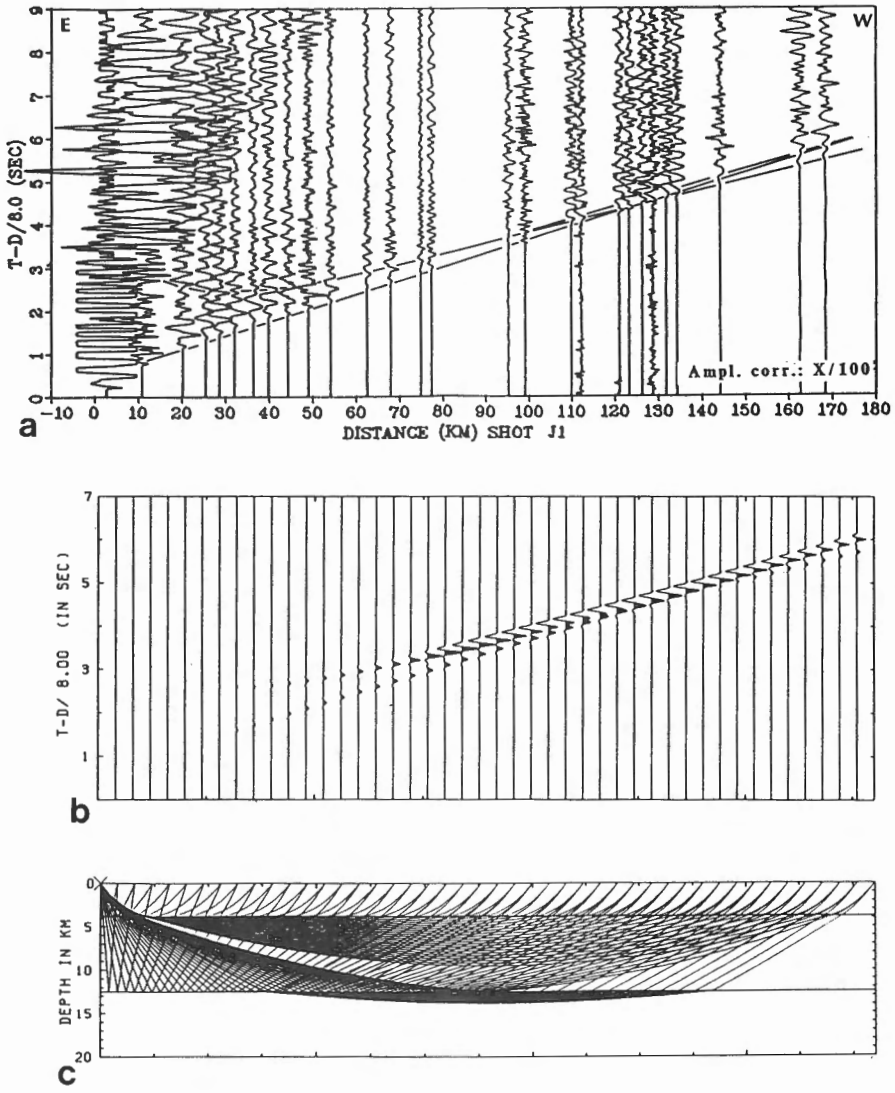

Figure 6. Observed and synthetic seismograms for shot J1. (a) Observed seismograms. (b) Synthetic seismograms. (c) Ray diagram. The gross features of the observed section are well-explained by the model.

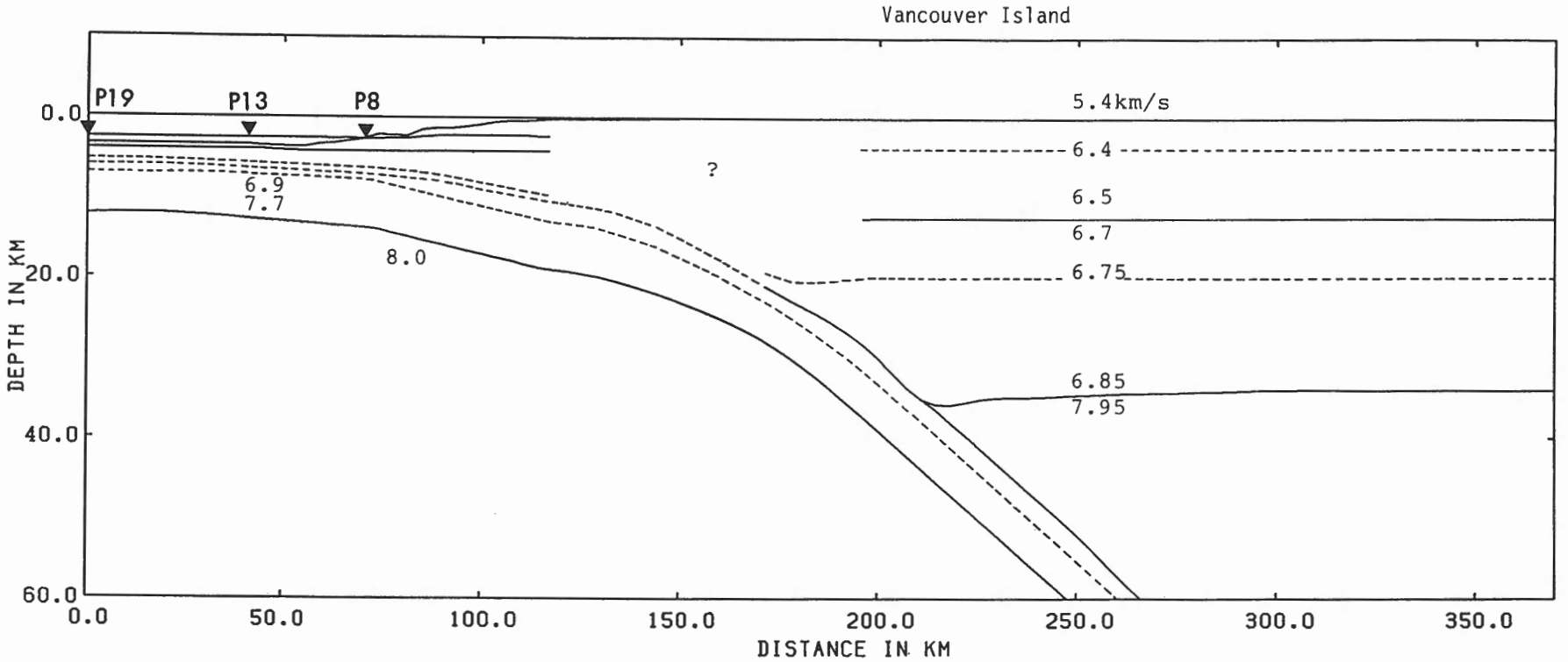

Figure 7. Velocity model for the onshore-offshore portion of the CCSS profile. Unfortunately, a critical part of the subduction zone cannot be resolved by the supplied data.

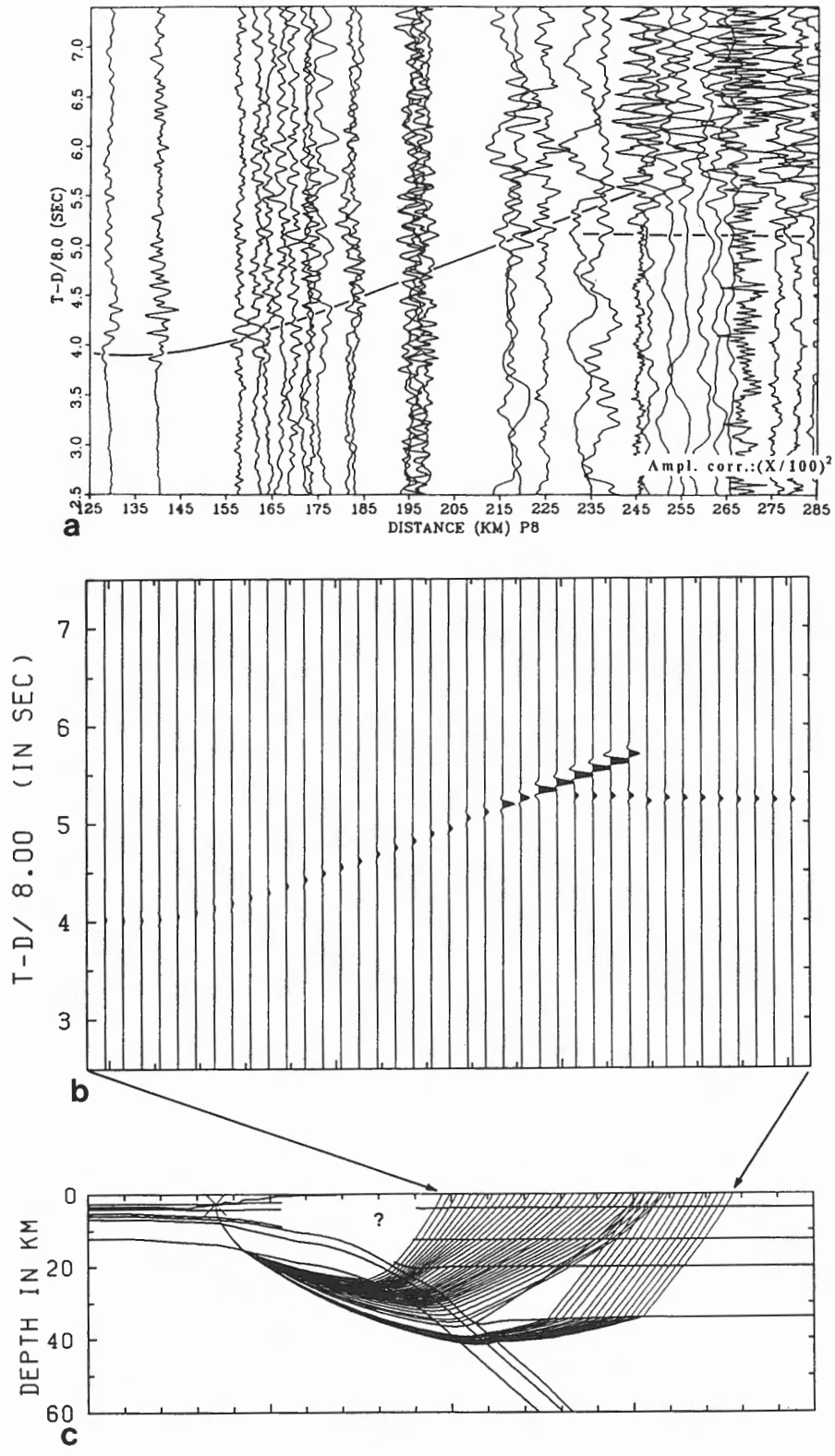

Figure 8. Observed and synthetic seismograms for shot P8. (a) Observed seismograms. (b) Synthetic seismograms. (c) Ray diagram.

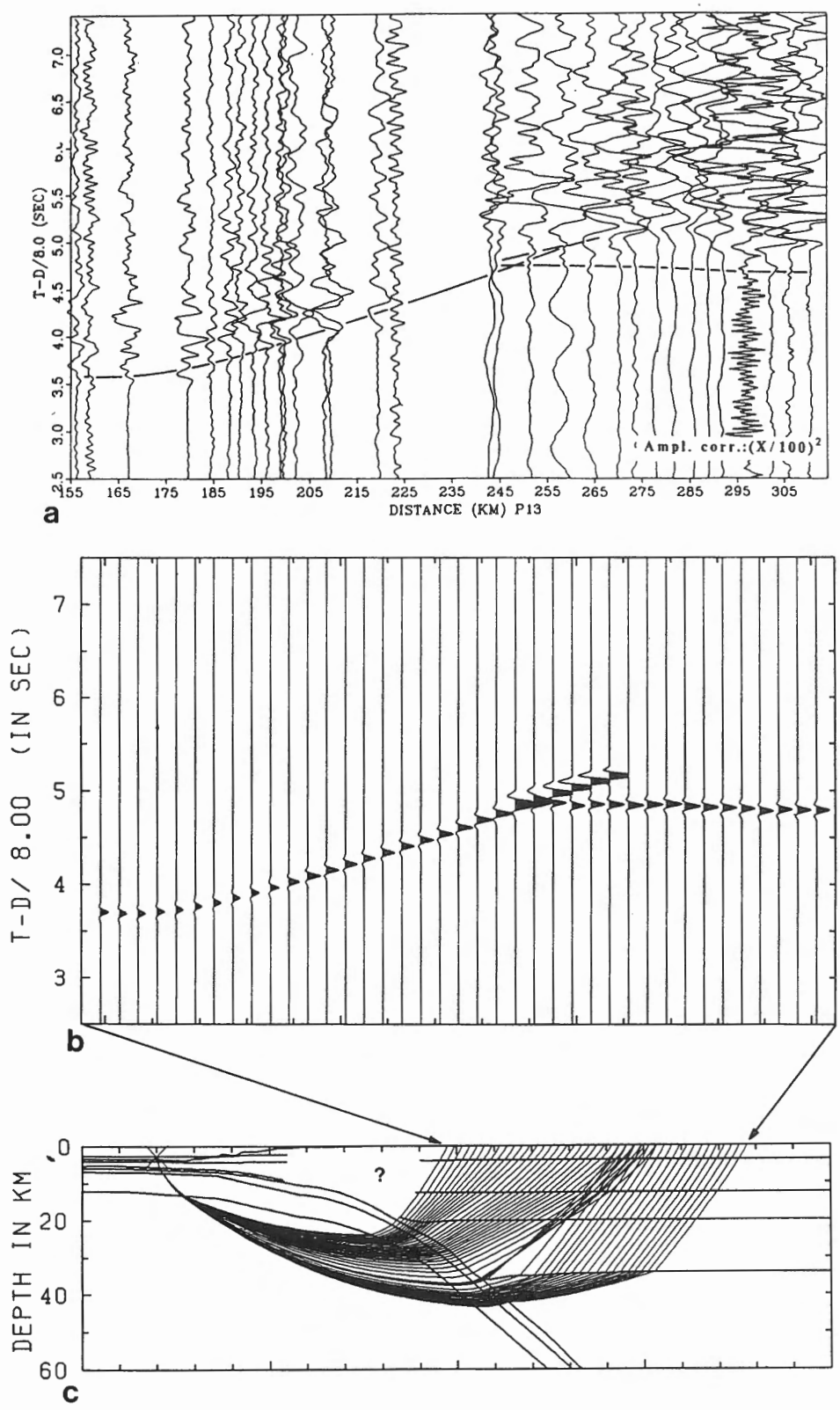

Figure 9. Observed and synthetic seismograms for shot P13. (a) Observed seismograms. (b) Synthetic seismograms. (c) Ray diagram.

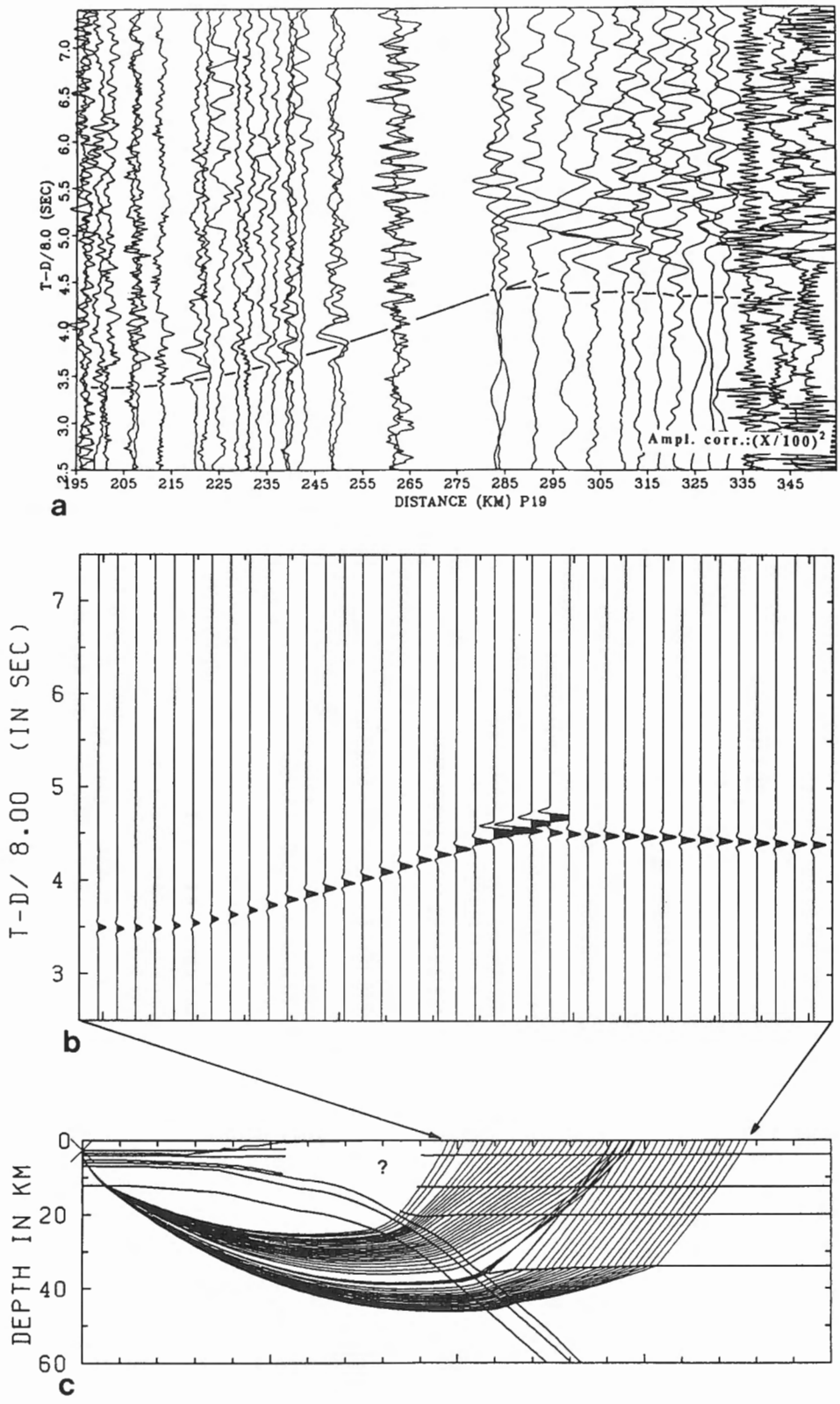

Figure 10. Observed and synthetic seismograms for shot P19. (a) Observed seismograms. (b) Synthetic seismograms. (c) Ray diagram. Our model does not explain the large amplitude later arrivals in the range 285-310 km.

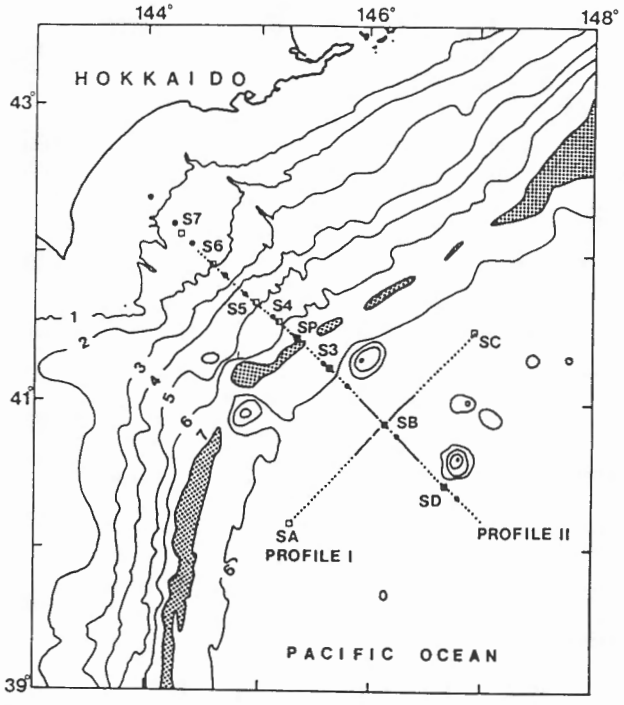

a

Figure 11. Velocity structure in the Kuril Trench. (a) Location map of the two seismic profiles. (b) Velocity structure under seismic profile II. We obtained (Iwasaki et al., 1989) a detailed image of the smooth subduction of the oceanic second layer without forming a wedge. The subducting oceanic second layer forms a low-velocity layer in the continental part of the trench.

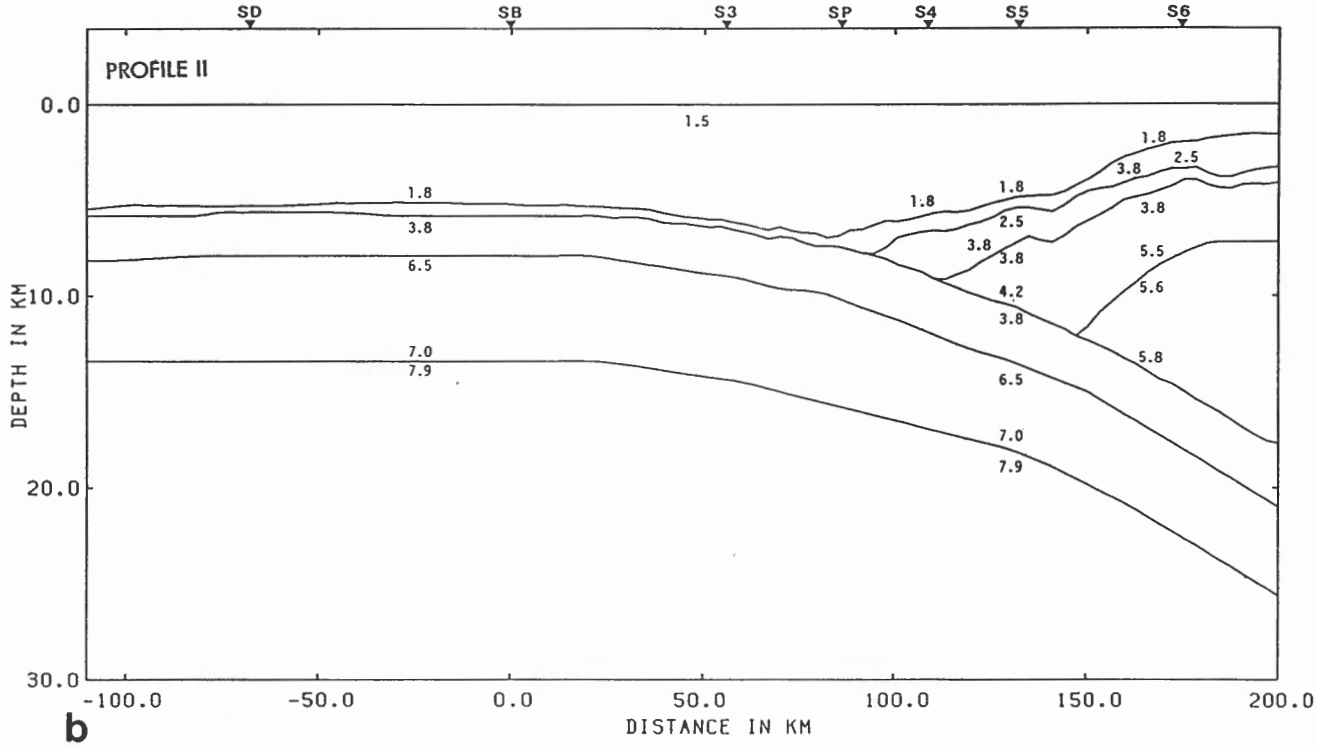

b

greater than 38 km, the rays only appear beyond 300 km, and the distance range 285-300 km becomes a shadow zone. For a Moho depth shallower than 30 km, the discrepancy between observed and calculated travel times becomes large.

Travel times of the first arrivals are explained fairly well by our model. However, our model does not explain the strong later arrivals from shot P19 appearing beyond 285 km (Fig. 10). In the synthetic seismograms for P8, quite large amplitudes are yielded in the range of 285-315 km (Fig. 8b). Such a strong phase is also found in the seismograms for P13 and P19 (Fig. 9b and 10b). This phase corresponds to rays transmitted near junctions of velocity interfaces, where the definition of the velocity field is quite subjective (*see* ray diagrams presented in Figures 8c, 9c and 10c). We suggest that the strong amplitudes are artificial, resulting from simplified and inadequate modeling of the junction between oceanic and continental crustal sections.

We see no evidence for low velocity layers in the continental crust. We suggest that it is difficult to determine such structure from the supplied data. In order to improve our model, more constraints are needed.

DISCUSSIONS AND CONCLUSIONS

The P-wave velocity structure model in the Vancouver Island region was constructed from onshore-offshore seismic data consisting of seismic refraction and multichannel reflection measurements. The structure in the marine portion of the profile was determined mainly from refraction data recorded on the three OBSs (OBSs 1, 3 and 5). The P-wave velocity increased from 4.0-5.0 to 7.7 km/s in the oceanic crust, without significant velocity discontinuities.

The Moho of the subducting oceanic plate was traced to 16 km depth by using P_mP and P_n phases, which are clearly recognized in the OBS data. The dip of the Moho boundary was 2-6° under the continental slope. We found a normal oceanic upper mantle beneath the Moho with P velocity of 8.0 km/s.

The velocity structure in the continental crust was determined from the onshore, unreversed refraction profile recorded from shot J1. The data were explained by a model consisting of three layers with P-wave velocities of 5.4-6.4, 6.4-6.5 and 6.7 km/s. The thickness of the upper two layers was determined to be 3.8 and 8.7 km, respectively.

We determined the deeper structure beneath the continental margin by modeling refraction profiles recorded from marine shots P8, P13 and P19. The P-wave velocities of the lower crust (deeper than 20 km) and the upper mantle were found to be 6.75-6.85 and 7.95 km/s, respectively. The Moho depth was estimated to be 35 km. The dip of the subducting oceanic lithosphere was about 22° beneath Vancouver Island, which is much steeper than that beneath the marine portion of the profile. However, these estimates have considerable uncertainty due to the poor resolving power of the data.

It is interesting to compare the result obtained from Vancouver Island with the velocity structure in another subduction zone. In Figure 11 we present the crustal and upper mantle structure in the Kuril trench area (northwest Pacific ; Iwasaki, 1988), determined from an OBS experiment conducted in 1983. We fired 179 explosive shots as well as airgun shots along two profiles (Fig. 11a). Because of the dense receiver and shot spacing, we were able to derive the detailed picture of the subduction zone shown in Figure 11b.

The thickness of the oceanic crust in the Kuril Trench area was determined to be 8 km, which is comparable to that off Vancouver Island. Except for the sedimentary layers, we found no high impedence interfaces within the oceanic crust. The P-wave velocity in the uppermost mantle was determined to be 7.9-8.0 km/s. Beneath the profile, the oceanic lithosphere, including layer 2, subducts beneath the continental slope at an angle of about 5°. The structure in the Kuril Trench is in marked contrast to our results for the Ryukyu Trench (southwest Japan), where a huge accretionary wedge with maximum thickness of about 12 km is formed beneath the continental slope.

ACKNOWLEDGMENTS

We wish to express sincere thanks to Alan Green and colleagues for kindly supplying their data to the CCSS workshop. The data set was quite suitable, generating interest amongst the CCSS members. It was the first occasion for the CCSS workshop to tackle marine data, which must have helped give important intuitions to those who have not treated such data before. Also, we thank Jorge Ansorge and Robert M. Ellis who were active in preparing and organizing the successful workshop in a very comfortable environment.

REFERENCES

Červený, V. and Pšencík, I.
1983 : 2-D Seismic Ray Package ; SEIS83, Prague.
Green, A.G., Clowes, R.M., and Ellis, R.M.
1990 : Crustal studies of Vancouver Island and adjacent continental margin ; *in* Studies of Laterally Heterogeneous Structures Using Seismic Refraction and Reflection Data, ed. A.G. Green ; Geological Survey of Canada, Paper 89-13, p. 3-25.
Hirata, N. and Shinjo, N.
1986 : SEISOBS : Modified version of SEIS83 for ocean bottom seismograms ; Zisin, v. 39, p. 317-321.
Iwasaki, T.
1988 : Ray-tracing program for study of velocity structure by ocean bottom seismographic profiling ; Zisin, v. 41, p. 263-266.
Iwasaki, T., Shiobara, H., Nishizawa, A., Kanazawa, T., Suyehiro, K., Hirata, N., Urabe, T., and Shimamura, H.
1989 : A detailed subduction structure in the Kuril Trench deduced from ocean bottom seismographic refraction studies ; Tectonophysics.
Spence, G.D., Clowes, R.M., and Ellis, R.M.
1985 : Seismic structure across the active subduction zone of western Canada ; Journal of Geophysical Research, v. 90, p. 6754-6772.

Seismic structure of a subducting oceanic plate off western Canada

D.A. Waldron[1,2], R.M. Clowes[2], and D.J. White[1,3]

Waldron, D.A., Clowes, R.M. and White, D.J., Seismic structure of a subducting plate off western Canada; in Studies of Laterally Heterogeneous Structures Using Seismic Refraction and Reflection Data, ed. A.G. Green; Geological Survey of Canada, Paper 89-13, p. 105-113, 1990.

Abstract

A two-dimensional seismic model for the Juan de Fuca plate, extending from the deep ocean to 60 km landward of the trench, is derived from seismic refraction data recorded on three ocean bottom seismographs and other information. The interpretation is based on travel time and amplitude comparisons between the observed data and synthetic sections calculated using asymptotic ray theory. Within the sediments, velocities increase landward, probably due to greater compaction. Below the slope at depths from 4 to 10 km, a large block with velocity characteristics (higher initial value, lower gradient) different from those at similar depths farther seaward probably represents a major part of the accretionary wedge formed by offscraping and imbrication of marine sediments. The velocity structure of the Juan de Fuca plate is similar to that for other oceanic plates; layers 2A, 2B, 3A and 3B can be distinguished on the basis of velocity. The crust-mantle boundary is represented by a step increase in velocity from 7.3 to 8.0 km/s and the oceanic upper mantle has a low velocity gradient of 0.01 km/s/km. As the plate subducts beneath the outer continental margin at a dip of about 8°, its structural integrity is maintained.

Résumé

Un modèle sismique bidimensionnel de la plaque de Juan de Fuca, qui s'étend des profondeurs océaniques jusqu'à 60 km sur le côté continental de la fosse de subduction, a été élaboré à partir de données de sismique réfraction enregistrées par trois sismographes de fond océanique et à partir d'autres renseignements. L'interprétation se fonde sur des comparaisons des temps de parcours et des amplitudes entre les données observées et les profils synthétiques calculés selon la théorie des rayons asymptomatiques. Au sein des sédiments, les vitesses augmentent vers le continent, en raison probablement d'une augmentation de la compaction. Sous le talus, à des profondeurs de 4 à 10 km, un gros bloc caractérisé par des vitesses (valeur initiale plus élevée, gradient plus faible) différentes de celles observées à des profondeurs similaires vers le large constitue probablement une partie importante du prisme d'accrétion formé par le décapage et l'imbrication de sédiments marins. La structure des vitesses dans la plaque de Juan de Fuca est semblable à celle d'autres plaques océaniques; les couches 2A, 2B, 3A et 3B peuvent être différenciées en fonction de la vitesse. La limite croûte-manteau est présentée par une augmentation graduelle de vitesse de 7,3 à 8,0 km/s et le manteau supérieur océanique donne un gradient de vitesse faible de 0,01 km/s/km. Lors de la subduction de la plaque sous la marge continentale extérieure suivant un angle d'environ 8°, son intégrité structurale est conservée.

[1] University of British Columbia, 2219 Main Mall, Vancouver, B.C. V6T 1W5
[2] Present Address : Rural Delivery 6, Raetihi, New Zeland
[3] Present Address : Geological Survey of Canada, 1 Observatory Crescent, Ottawa, Ontario, K1A 0Y3.

INTRODUCTION

The Vancouver Island Seismic Project (VISP) was carried out in 1980 by the Canadian Consortium for Crustal Reconnaissance Using Seismic Techniques (COCRUST) with the major objective of deriving a seismic structural model to upper mantle depths from the deep ocean of the Juan de Fuca plate across the convergent margin to the inland volcanic arc of the American plate. A series of onshore-offshore seismic refraction and seismic reflection experiments were conducted ; details of the program are included in Ellis et al. (1983). Spence et al. (1985) presented a structural model for the complete 350 km onshore-offshore line. The portion of their model below the deep ocean and continental slope was based on Waldron's (1982) interpretation of the offshore component of the line. Parts of the latter interpretation were included in models presented by Clowes et al. (1986).

Using the Waldron (1982) study as a basis, this paper provides a revised structural model for the Juan de Fuca plate extending from the deep ocean to 60 km landward of the trench axis, as derived from seismic refraction data recorded on three ocean bottom seismographs (OBSs) and other information. The latter includes (i) a coincident single channel seismic reflection profile (CSP ; Ellis et al., 1983) ; (ii) velocity analyses from an industry multichannel reflection profile that crossed the refraction line near the base of the continental slope ; (iii) sonic log and geological data from an industry drill hole (Shouldice, 1971) on the outer continental shelf about 18 km southeast of the refraction profile ; (iv) a United States Geological Survey multichannel reflection line running parallel and 15 km southeast of the refraction line (Clowes et al., 1986) ; and (v) an interpretation of the gravity data (Waldron, 1982). The new model constitutes the offshore part of the re-interpreted structural model developed by Drew and Clowes (1990) for the entire onshore-offshore line. Figures 4 and 5 of Green et al. (1990) show the locations of the OBSs and the seismic refraction lines along which explosive and airgun sources were fired. Figures 10 to 12 of Green et al. (1990) display respectively the seismic sections recorded at OBSs 1, 3 and 5 from the explosions.

The three OBSs were deployed along a 100 km line extending from the deep ocean (OBS1) across the continental slope (OBS3) to the outer shelf (OBS5). Due to environmental restrictions, explosions could only be detonated west of the mid-slope, so a full reversal over the offshore line was not possible. Interpretation was initiated using travel time-distance data corrected to a datum equal to each OBS depth and, for OBS1 only, corrected for variations in the sediment-basement interface (Waldron, 1982). The corrected data were transformed into the tau-p domain and a linear programming technique was used to determine one-dimensional (1-d) models for each OBS site. Both airgun and explosion data were considered at this stage. A two-dimensional (2-d) starting model was then determined from a juxtaposition of the 1-d models. The 2-d model was adjusted iteratively until the travel time data for each OBS (without the corrections used in the 1-d analyses) were matched by the synthetic times calculated using the ray tracer of Whittall and Clowes (1979). The final interpretation was based on subjective comparisons of observed travel times and amplitudes with those computed using the asymptotic ray approach of Spence et al. (1984).

AIRGUN DATA SET

For the CCSS workshop, only the explosion data recorded on the three OBSs were distributed. However, to provide some control on the uppermost crustal structure, travel time and limited amplitude information from the airgun data have been used in the interpretation presented here.

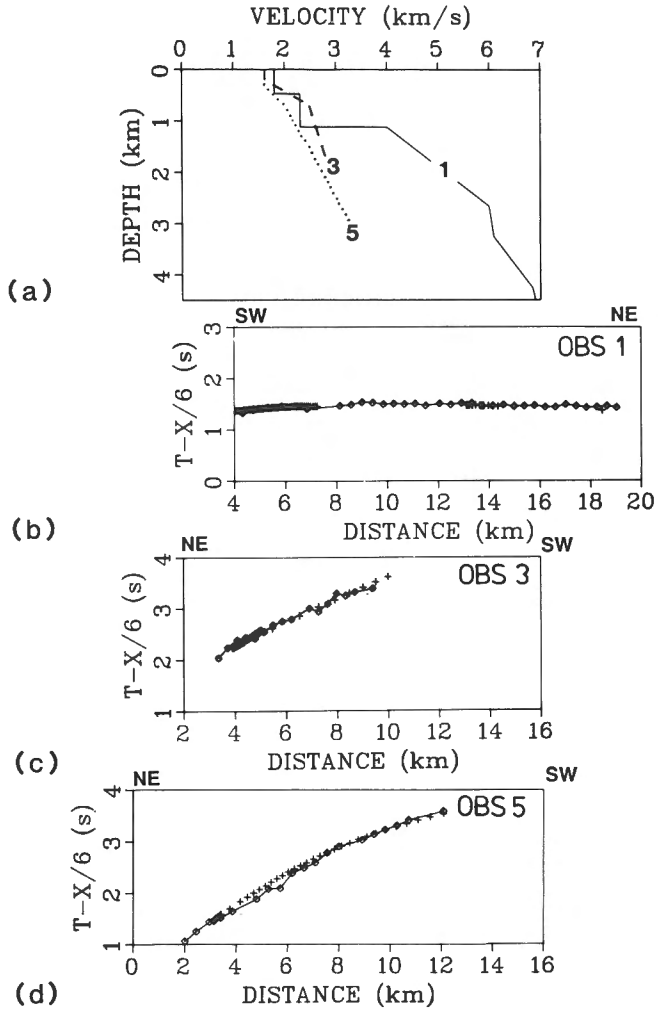

Figure 1. (a) One-dimensional velocity-depth profiles 1, 3 and 5 derived from the airgun data recorded on OBSs 1, 3 and 5 respectively. Zero depth corresponds to the sea bottom ; the water columns of 2.52 km for OBS1, 1.12 km for OBS3 and 0.16 km for OBS5 are not included in the profiles. (b) OBS1 travel time-distance plots for the airgun data (closed symbols joined with a line) and for the corresponding velocity-depth profile 1 (crosses). (c) same as (b) for OBS3 and velocity-depth profile (3). (d) same as (b) for OBS5 and velocity-depth profile (5).

On the OBS1 airgun records, first arrivals can be picked to about 20 km source-receiver distance ; the apparent velocity along the section is close to 6.0 km/s (Fig. 1b). After the corrections noted previously, one-dimensional travel time inversion by linear programming gave a preliminary velocity model (Fig. 1a). Sediment velocities were also constrained by CSP data, pre-existing multichannel data including velocity analyses, and the need to match the time of the first OBS1 refraction arrival. The airgun data reveal a region of rapid velocity increase (1.4 km/s/km) below the sediment-basement interface. At a depth of 5.1 km (including 2.52 km of water), a velocity of 6.0 km/s is attained and there is a decrease in velocity gradient. Between 5.8 and 6.8 km depth, the velocity increases relatively rapidly (0.75 km/s/km) to a value of 6.85 km/s. This structure, which is constrained by the airgun data to a depth of about 7 km, is very similar to that found by Au and Clowes (1982) on the Juan de Fuca plate approximately 100 km to the northwest.

On OBS3, first arrivals on the airgun data are only visible to about 10 km offset (Fig. 1c). The absence of appreciable energy beyond this distance is probably due to : (1) the use of a 16 litre airgun instead of the 32 litre airgun used at OBS1, and (2) the highly attenuating nature of the underlying continental slope material. The data do not constrain directly the velocity of the upper few hundred metres of sediment, but in order to explain the travel times the velocity must be low, close to 1.6 km/s. For about 0.5 km, the velocity increases rapidly to approximately 2.5 km/s, below which the gradient decreases. The OBS data constrain the velocity structure only to a depth of about 2.9 km (including 1.12 km of water).

On OBS5, first arrivals are only visible to about 12 km offset (Fig. 1d), probably for the same reasons as suggested for OBS3. Below the inferred 1.6 km/s material in the upper few hundred metres, the velocity increases fairly rapidly, reaching 3.2 km/s at a depth of approximately 3.2 km (including the 0.16 km water column). As shown by Waldron (1982), this velocity structure (Fig. 1a) is consistent with sonic log information from the Shell-Anglo Cygnet drillhole, situated ~ 18 km southeast of the OBS site.

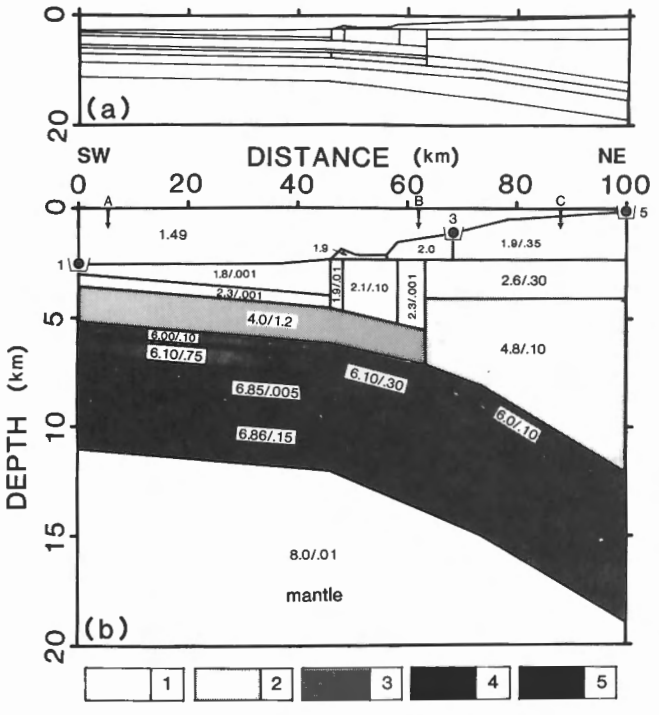

Figure 2. (a) Two-dimensional velocity structural model at 1 : 1 scale. (b) Details of velocity structural model derived in this study. The first number in each block is the velocity (km/s) along the top boundary, and the second number, when present, is the linear velocity gradient (km/s/km). Symbols marked 1, 3 and 5 identify the locations of the three OBSs. Arrows at A, B and C identify the positions of the velocity-depth profiles shown in Figure 6. Shading identifies principal parts of the model : 1 — sediments ; 2 — accretionary wedge ; 3 — upper oceanic crust ; 4 — middle oceanic crust ; 5 — lower oceanic crust.

EXPLOSION DATA SET

Final derivation of the crustal velocity model (Fig. 2) followed an interactive trial-and-error modeling procedure involving the three OBS explosion record sections. The model was adjusted through more than a hundred iterations until an acceptable fit to the observed travel times and amplitudes was achieved. Nevertheless, a high degree of non-uniqueness is associated with the procedure. One a priori assumption was that all boundaries below and including the sediment-basement interface are parallel ; in the deep water this is established on CSP and multichannel reflection data.

An important characteristic of the three record sections is that the source-receiver distance of the principal amplitude group moves to greater offsets from OBS1, where it is around 35 km, to OBS5 where it is nearer 55 km. This implies that the lower crustal structure from which the strong energy returns is deeper to the east. Similarly, apparent velocities at large offsets increase from 8 km/s at OBS1 to 10 km/s at OBS5, indicating either an eastward increase in Moho dip or, much less likely, a significant eastward increase in mantle velocity.

The ~1° eastward dip of the sedimentary material and the sediment-basement interface was derived from the CSP record (Ellis et al., 1983) and pre-existing multichannel seismic reflection data. Based on the reflection data (Clowes et al., 1986), the edge of the continental rise is approximated by a vertical boundary. The lateral increase in sediment velocity to the east, presumably due to compaction and deformation, is represented by additional (and artificial) vertical boundaries. The observed data, synthetic sections and ray diagrams for the three OBSs are presented in Figures 3 to 5 ; note the two distance scales in the figures : model distances correspond to the distances of Figure 2 and are measured eastward from the southwest end of the line, and source-receiver distances are measured from the respective OBSs.

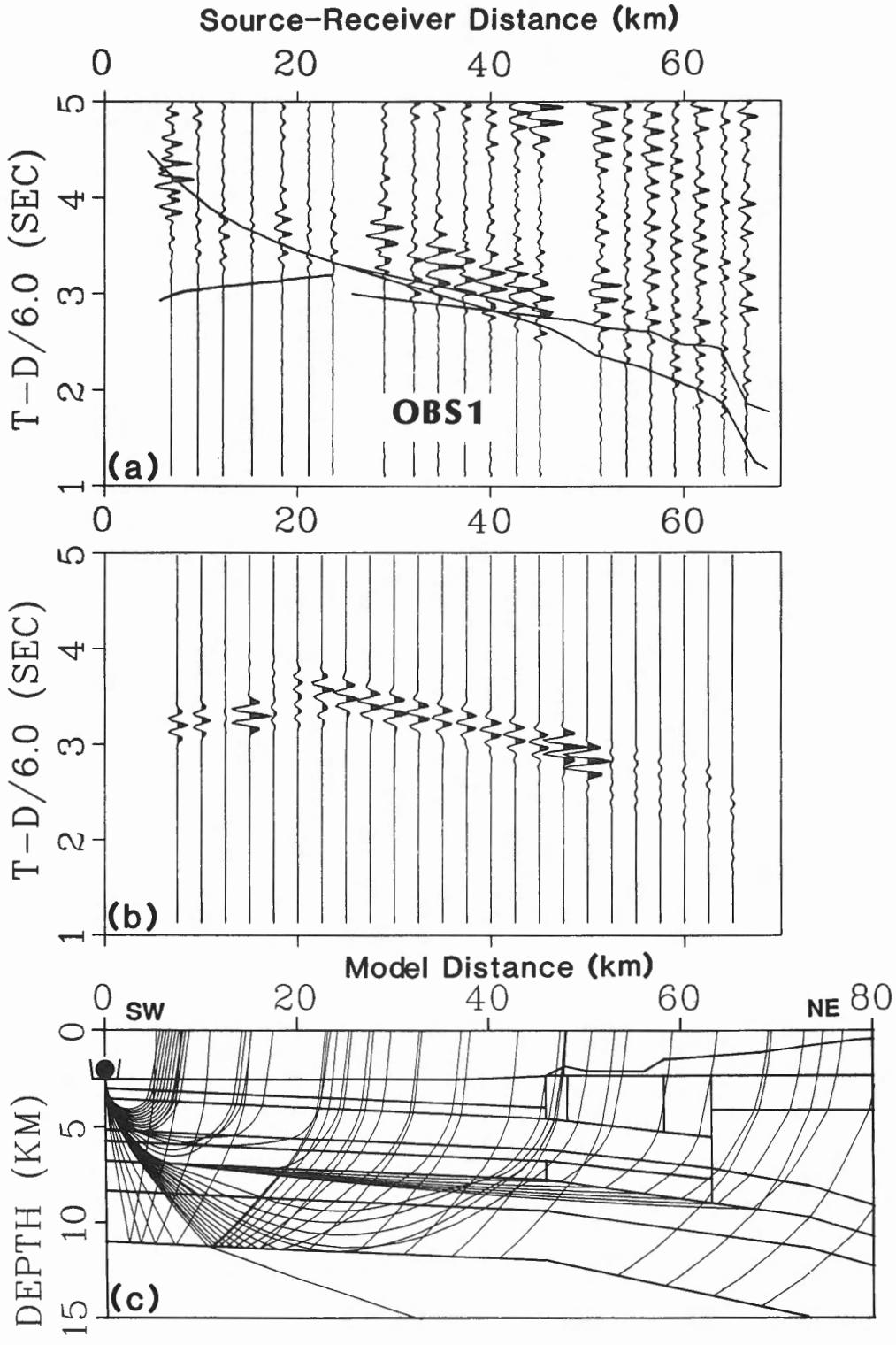

Figure 3. (a) Data from OBS1. The section is true relative amplitude with a distance enhancement factor of X^2 to show more clearly the arrivals at larger offsets. Theoretical travel time curves for the velocity structure model of Figure 2 are superimposed. (b) Synthetic record section calculated for the model of Figure 2. The presentation is identical to that used for the observed data. Model distance is measured eastward from OBS1 and corresponds to the distances of Figure 2. (c) Ray diagram for OBS1. For clarity only a limited number of rays for the different phases are displayed.

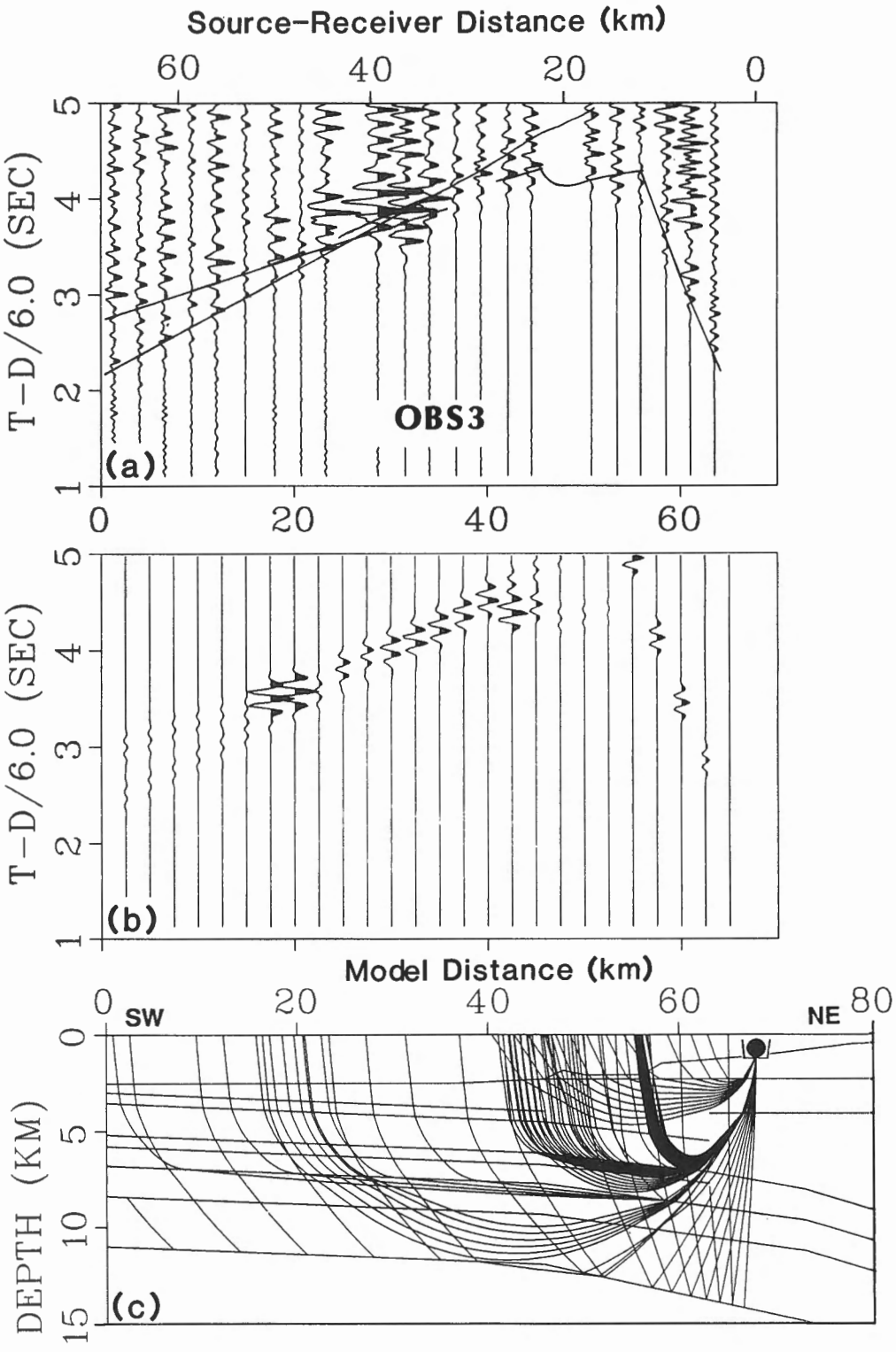

Figure 4. (a) Data from OBS3. (b) Synthetic record section for the model of Figure 2. (c) Ray trace diagram. See Figure 3 caption for details.

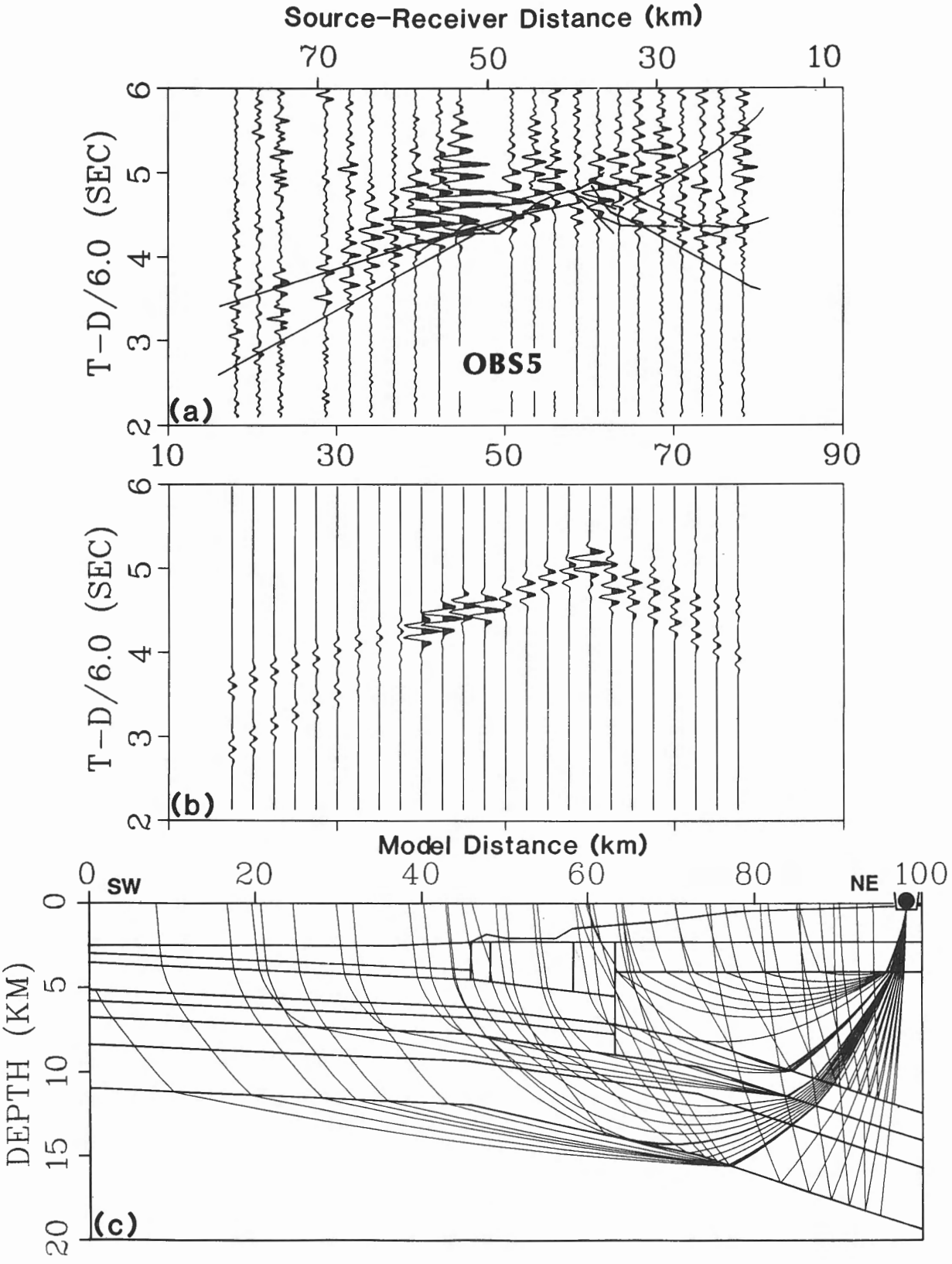

Figure 5. (a) Data from OBS5. (b) Synthetic record section for the model of Figure 2. (c) Ray trace diagram. See Figure 3 caption for details.

OBS1

On OBS1, first arrivals can be picked to offsets of 70 km. The corresponding apparent velocities range from 5.7 to 8.0 km/s (Fig. 3a). The main amplitude group occurs between 28 and 52 km source-receiver distance. At greater distances the amplitudes are significantly less. The large amplitude arrival at about 4 s on the first trace is a water wave phase and is not considered here.

Figure 3b shows the synthetic record section calculated from the model of Figure 2. On average, amplitudes to 20 km source-receiver distance are too large on the theoretical traces. This is due to the high gradients required to match travel times and apparent velocities. The main amplitude group and the weak events with two possible phases at the longer source-receiver offsets are matched well. The extended range of the larger amplitudes is due to superposition of turning rays in the lower crust and rays reflected from the oceanic Moho (Fig. 3c). The abrupt travel time advance at 65 km is associated with rays that penetrate the 4.8 km/s block (Fig. 2), which has a higher velocity at shallow depths than the adjacent sediments (Fig. 3c). As discussed below, this higher velocity block was required to satisfy data from OBS5.

OBS3

On the OBS3 record section, first arrivals can be picked reliably to about 70 km source-receiver distance (Fig. 4a). Apparent velocities of the first arrivals increase from 2.8 to 8.2 km/s along the profile. The only well-defined large amplitude group lies between about 32 and 46 km. At source-receiver offsets greater than 50 km, two weak phases with different apparent velocities are inferred, although the existence of the second phase is equivocal.

Figure 4b shows the theoretical record section ; corresponding travel times are superimposed on the data in Figure 4a. The match between the amplitudes on the synthetic and observed sections is not particularly good. The large amplitude group of arrivals between 32 and 46 km source-receiver distance is represented on the synthetic section by a moderate amplitude phase spread over a greater distance range. The amplitude high at 20 km model distance is not represented in the data ; it is caused by a strong focusing of rays in the lower crust of the model.

The lack of good agreement between model and recorded amplitudes illustrates the difficulty of obtaining a single velocity model that is consistent with multiple data sets. Of particular importance in this region are complex, rapidly varying lateral heterogeneities, which cannot be represented adequately on low-resolution refraction data. As one example, the early high amplitude arrival near source-receiver distance 35 km (Fig. 4a) probably is due to a localized bathymetric or sub-bottom feature. The multichannel seismic reflection data (Fig. 20 in Green et al., 1990 ; the seismic section is contained in the pocket at the back of this volume) below the slope are of poor quality, presumably in part the result of complex deformation processes associated with the accretionary wedge. Many features resulting from such processes cannot be modeled in any meaningful way, although collectively they must have a strong effect on the seismic waves.

OBS5

On OBS5, first arrival energy is observed to 80 km source-receiver distance (Fig. 5a). Apparent velocities increase from about 4.5 km/s at near offsets to about 10 km/s at offsets greater than 60 km. Amplitudes are generally moderate to high with the main large amplitude group between 40 and 60 km. Like the OBS3 section, there is weak evidence for a secondary phase with a lower apparent velocity extending from 60 to 80 km.

Figure 5b shows the synthetic record section, and the corresponding theoretical travel times are superimposed on the observed section of Figure 5a. In this case the agreement between the two sections is good. Amplitudes on the theoretical section are generally moderate to high with the largest ones being generated on traces between 60 and 40 km model distance. Below the low sediment velocities identified on the airgun data, significantly higher velocities than determined at similar depths farther seaward are required by the arrivals on the first 5 traces (source-receiver distances 20 to 30 km). These events are explained by a large block of 4.8 km/s material (velocity gradient of 0.1 km/s/km). Refraction arrivals through this block and reflected arrivals from its base generate travel times and amplitudes that provide a good fit with the recorded data, including an extended wave coda. Although a number of phases contribute to the large amplitudes between 60 and 40 km model distance, the effect of the turning rays through the lower crust of the subducting plate dominate. As shown in Figure 5c, refracted rays through the oceanic mantle below the dipping structure generate the high-velocity first arrivals. The low-velocity secondary arrivals travel through the middle oceanic crustal layer (6.85 km/s with a low gradient of 0.005 s-1, Fig. 2).

DISCUSSION AND SUMMARY

A two-dimensional velocity model that is compatible with the travel time and amplitude information contained in three refraction record sections has been derived (Fig. 2). It was also constrained by information from a CSP, a few pre-1985 multichannel seismic reflection sections and well-log data. Such a structure should also be consistent with the gravity field. Riddihough (1979) showed that the principal gravity anomaly, a low-high couple that is a common feature of subduction zones, was readily replicated with a density model based on subduction of the Juan de Fuca plate beneath the continental margin and Vancouver Island. By converting his velocity model to a density model, Waldron (1982) demonstrated that his interpretation, similar in its main features to that of Figure 2, agreed with the gravity data. This was supported by Spence et al. (1985) who tested their long onshore-offshore seismic model by converting it to a density model and comparing the calculated and observed gravity fields ; Figure 18 of Spence et al.(1985) demonstrates the excellent agreement between the observed and calculated gravity fields in the offshore region.

Sediment velocities were determined from CSP travel times, normal moveout velocity determinations and travel times from pre-1985 multichannel reflection sections, sonic logs from a nearby well, and interpretation of VISP 80

airgun refraction data. These velocities increase eastward in the continental rise region; a concomitant increase in density is also required. Such increases are probably due to greater compression and compaction of material at the margin. Compressive structures (asymmetric folds and northeastward dipping imbricated thrusts, as indicated on the seismic reflection sections) result from the relative northeastward underthrusting of the Juan de Fuca plate beneath the North American plate.

To illustrate similarities and differences in velocity structure along the model, three velocity-depth profiles corresponding to the positions marked with arrows in Figure 2b are shown in Figure 6. Below the sediments, oceanic layer 2A, distinguished by its high velocity gradient of 1.2 km/s/km, is identified from the deep ocean to about the mid-slope region. Farther east, data from OBS5 required much higher velocities at shallower depths and a significantly lower velocity gradient leading to a relatively low average velocity for the entire block (Fig. 6). As shown in Figure 6c, this anomalous block may extend to the top of layer 2B. There is no evidence for a sharp transition associated with the lateral change in velocity structure.

The anomalous block probably represents a major part of the accretionary wedge formed by offscraping and imbrication of marine sediments and also possibly by underplating (Clowes et al., 1987). In the latter reference, it was suggested that subduction thrust faulting might on occasion extend into the oceanic crust itself. In the deep part of the accretionary wedge, intercalation of sediments with upper oceanic crustal rocks could cause the generally lower seismic velocities and therefore mask the existence of layer 2A. Complete detachment of layer 2A from the descending plate (as indicated in Fig. 2) is not probable; 2 km of such material would produce a mass 400 km^2 in cross-section in about 1 Ma. Perhaps the lower part of the "accretionary wedge" is the result of resistance to subduction, the upper oceanic crustal layer being compressed and deformed whilst still remaining attached to the Juan de Fuca plate; note the average velocity for the lower 2 km of the wedge is about the same as that for layer 2A. Existing data and their interpretations are inadequate to clarify what tectonic processes are taking, or have taken, place.

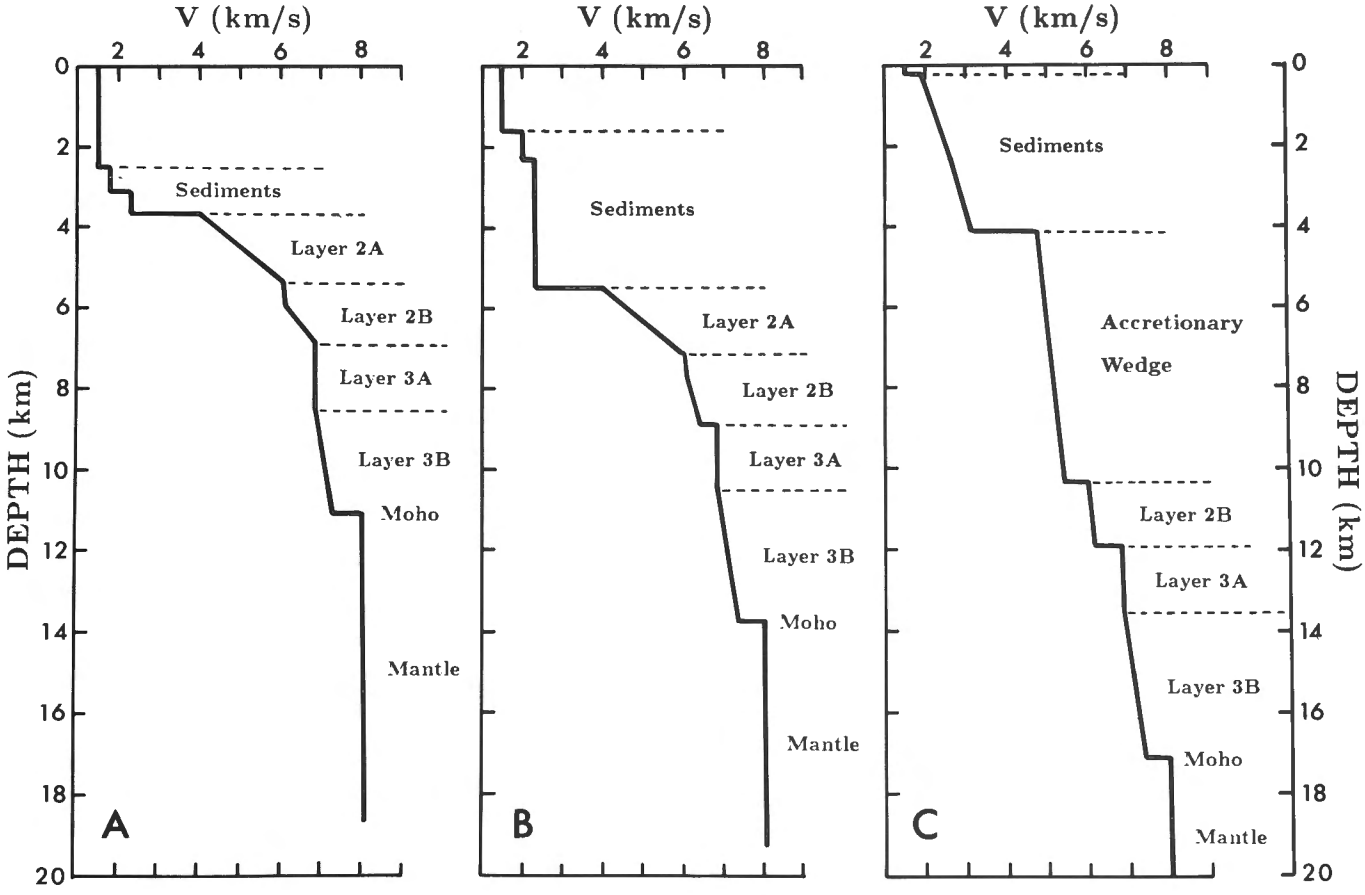

Figure 6. Velocity-depth profiles from locations A, B and C marked on Figure 2. A generic interpretation of the velocity profiles is indicated.

The interpretation illustrated in Figures 2 and 6 indicates that below layer 2A the main part of the Juan de Fuca plate extends as a single structure at a shallow angle of dip below the continental slope. At the base of the slope, the dip increases from ~1° below the deep ocean to ~2° and then increases again below the mid-slope to ~8°. The thicknesses of layers 2B and 3A remain constant over the extent of the model, although the velocity structure of layer 2B changes slightly. The reduced velocity gradient landward (0.75 to 0.10 km/s/km) could be due to the increased lithostatic pressure as the plate subducts deeper. Layer 3B is shown to increase in thickness from ~2.5 km at the ocean end to ~3.5 km at the shelf end. Moho is represented by a step increase in velocity from 7.3 km/s to 8.0 km/s. The oceanic upper mantle has a low velocity gradient of 0.01 s-1.

The overall velocity structure derived in this study shows that the Juan de Fuca plate is similar in its structure to other oceanic plates and that its integrity is maintained, with the possible exception of layer 2A, as the plate subducts beneath the continental margin. In terms of the velocity structure, the present study has not incorporated the additional information now available from the 1985 multichannel seismic reflection section 85-01 ; most of our study was completed prior to the final processing of the 1985 data. It is interesting to note that the depth to the top of the plate in our model, after conversion to two-way travel time, is almost identical with that shown on line 85-01 (*see* Fig. 20 of Green et al., 1990). Additional information from the reflection data includes the velocities in the upper part of the section and the general geometry of structures. Poor reflection data quality below the continental slope hinders any major contribution to a revision of the refraction velocity model. Nevertheless, an ''ultimate'' final model should include an attempt to incorporate the new seismic reflection data.

ACKNOWLEDGMENTS

The field program in which the data herein were acquired was conducted by COCRUST (Consortium for Crustal Reconnaissance Using Seismic Techniques) with participation by the Earth Physics Branch (Ottawa) and Pacific Geoscience Centre (both now incorporated in the Geological Survey of Canada), Atlantic Geoscience Centre, and the Universities of Alberta, British Columbia, Manitoba, Saskatchewan, and Western Ontario. Financial support for the study was provided by NSERC Canada operating grant A7707 and strategic grant G0738, and by EMR Research Agreements in 1981 and 1982. D.A.W. acknowledges financial support from a Canadian Commonwealth Scholarship ; D.J.W. received financial support from a Ph.D. Trainee Program within the Geological Survey of Canada. LITHOPROBE Publication no. 43.

REFERECNES

Au, D. and Clowes, R.M.
1982 : Crustal structure from an OBS survey of the Nootka fault zone off western Canada ; Royal Astronomical Society, Geophysical Journal, v. 68, p. 27-47.

Clowes, R.M., Spence, G.D., Ellis, R.M., and Waldron, D.A.
1986 : Structure of the lithosphere in a young subduction zone : results from reflection and refraction studies ; *in* Reflection Seismology : The Continental Crust, Geodynamics Series, v. 14, p. 313-321.

Clowes, R.M., Brandon, M.T., Green, A.G., Yorath, C.J., Sutherland Brown, A., Kanasewich, E.R., and Spencer, C.P.
1987 : LITHOPROBE — southern Vancouver Island : Cenozoic subduction complex imaged by deep seismic reflections ; Canadian Journal of Earth Sciences, v. 24, p. 31-51.

Drew, J.J. and Clowes, R.M.
1990 : A re-interpretation of the seismic structure across the active subduction zone of western Canada ; *in* Studies of Laterally Heterogeneous Structures Using Seismic Refraction and Reflection Data, ed. A.G. Green ; Geological Survey of Canada, Paper 89-13, p. 115-132.

Ellis, R.M. , Spence, G.D., Clowes, R.M., Waldron, D.A., Jones, I.F., Green, A.G., Forsyth, D.A., Mair, J.A., Berry, M.J., Mereu, R.F., Kanasewich, E.R., Cumming, G.L., Hajnal, Z., Hyndman, R.D., McMechan, G.A., and Loncarevic, B.D.
1983 : The Vancouver Island Seismic Project : a COCRUST onshore-offshore study of a convergent margin ; Canadian Journal of Earth Sciences, v. 20, p. 719-741.

Green, A.G., Clowes, R.M., and Ellis, R.M.
1990 : Crustal studies across Vancouver Island and adjacent offshore margin ; *in* Studies of Laterally Heterogeneous Structures Using Seismic Refraction and Reflection Data, ed. A.G. Green ; Geological Survey of Canada, Paper 89-13, p. 3-25.

Riddihough, R.P.
1979 : Gravity and structure of an active margin — British Columbia and Washington ; Canadian Journal of Earth Sciences, v. 16, p. 350-363.

Shouldice, D.H.
1971 : Geology of the western Canadian continental shelf ; Bulletin of Canadian Petroleum Geology, v. 19, p. 405-436.

Spence, G.D., Whittall K.P., and Clowes, R.M.
1984 : Practical synthetic seismograms for laterally varying media calculated by asymptotic ray theory ; Seismological Society of America, Bulletin, v. 74, p. 1209-1223.

Spence, G.D., Clowes, R.M., and Ellis, R.M.
1985 : Seismic structure across the active subduction zone of western Canada ; Journal of Geophysical Research, v. 90, p. 6754-6772.

Waldron, D.A.
1982 : Structural characteristics of a subducting oceanic plate ; unpublished M,Sc, thesis, University of British Columbia, 121 p.

Whittall, K.P. and Clowes, R.M.
1979 : A simple, efficient method for the calculation of travel times and ray paths in laterally in homogeneous media ; Journal of the Canadian Society of Exploration Geophysicists, v. 15, p. 21-29.

A re-interpretation of the seismic structure across the active subduction zone of western Canada

Jeff J. Drew[1] and Ron M. Clowes[2]

Drew, J.J. and Clowes, R.M., A re-interpretation of the seismic structure across the active subduction zone of western Canada; in Studies of Laterally Heterogeneous Structures Using Seismic Refraction and Reflection Data, ed. A.G. Green; Geological Survey of Canada, Paper 89-13, p. 115-132, 1990.

Abstract

Since publication of the original interpretations of the VISP onshore-offshore refraction line from the deep ocean across Vancouver Island to the mainland and the VISP line along Vancouver Island, new multichannel seismic reflection data have been acquired in the region. The vertical travel times to prominent reflectors observed in these data are used as constraints in constructing revised velocity models that are consistent with both the refraction and reflection data. For the onshore-offshore profile, the primary difference lies within the structure below Vancouver Island: between depths of 15 and 30 km, the revised model shows a four-layer structure with two thin low velocity layers (6.35 km/s) alternating with two thick high velocity layers (about 7.2 km/s). The location of the top of the subducting Juan de Fuca plate in the model is consistent with a clear reflection; the plate has an average dip of 14 to 16°. For the along Vancouver Island profile, the revised model was determined iteratively with the onshore-offshore one so all aspects of the two models are consistent with each other as well as the geometry indicated by the reflection data. The major change from the previous interpretation is the inclusion of the four-layer structure, with variations in layer thicknesses along profile in the depth range from 10 to 35 km. This structure overlies the top of the subducting plate.

Résumé

Depuis la publication des premières interprétations du profil VISP de sismique réfraction terrestre-océanique allant du domaine océanique jusqu'au continent en passant par l'île de Vancouver, et du profil VISP longeant l'île de Vancouver, de nouvelles données de sismique réflexion multicanale ont été acquises dans la région. Les temps de parcours verticaux jusqu'aux réflecteurs principaux, tels que recueillies dans ces données, servent de contraintes dans l'élaboration de modèles de vitesse révisés satisfaisant les données de réfraction et de réflexion. Pour le profil terrestre-océanique, la principale différence réside dans la structure sous-jacente de l'île de Vancouver: entre les profondeurs de 15 à 30 km, le modèle révisé montre une structure à quatre couches composée de deux couches minces à vitesse faible (6,35 km/s) alternant avec deux couches épaisses à vitesse élevée (environ 7,2 km/s). L'emplacement du sommet de la plaque de Juan de Fuca en subduction dans le modèle correspond à une réflexion marquée; la plaque plonge à un angle moyen de 14 à 16°. En ce qui concerne le profil longeant l'île de Vancouver, le modèle révisé a été établi de façon itérative avec le profil terrestre-océanique de sorte que tous les aspects des deux modèles sont cohérents tout comme l'est la géométrie indiquée par les données de réflexion. La principale différence par rapport à l'interprétation précédente est l'inclusion de la structure à quatre couches caractérisée par des couches de différentes épaisseurs le long du profil dans l'intervalle de profondeur variant de 10 à 35 km. Cette structure repose sur le sommet de la plaque en subduction.

[1] 114 E. Sunset Drive, Redlands, CA, 92373 U.S.A.; also at LITHOPROBE, University of British Columbia, Vancouver, B.C. V6T 1W5.

[2] Department of Geophysics and Astronomy, 2219 Main Mall, University of British Colombia, Vancouver, B.C. V6T 1W5.

INTRODUCTION

The 1980 Vancouver Island Seismic Project (VISP) was conducted to investigate lithospheric structure associated with the underthrusting oceanic Juan de Fuca plate and the overriding continental North America plate (Ellis and Clowes, 1981 ; Ellis et al., 1983). The principal components of the survey were : (1) an onshore-offshore refraction line, which was approximately perpendicular to the continental margin (line I in Fig. 4 and 5 of Green et al., 1990), and (2) a refraction line that ran along the length of Vancouver Island approximately parallel to the continental margin (line IV). VISP lines I and IV were originally interpreted by Spence et al., (1985) and McMechan and Spence (1983), respectively. Since the original interpretations of these lines, deep multichannel seismic reflection data have been obtained on southern Vancouver Island as part of the 1984 LITHOPROBE Phase I project (Yorath et al., 1985 ; Green et al., 1986 ; Clowes et al., 1987a) and off the west coast of the island during a 1985 Frontier Geoscience Program (FGP) marine survey (Clowes et al., 1987b). Figures 1, 2, 4 and 5 of Green et al., (1990) show the locations of the relevant refraction and reflection profiles.

This study was undertaken to resolve differences between the subsurface structures proposed in the original interpretations of lines I and IV and those suggested by the deep reflection data. The vertical travel times to prominent reflectors, observed in the onshore and offshore deep reflection data, were used as constraints in constructing velocity models consistent with both the reflection and refraction data. The travel times and amplitudes observed in the VISP refraction data were modeled using the Spence et al., (1984) two-dimensional ray tracing/synthetic seismogram routine. Our final velocity models were derived from simultaneous modeling of **complete** data sets for lines I and IV. Thus they are based on more data than were available to CCSS workshop participants. Results presented here will concentrate on line I, but some examples and the model for line IV will be included for completeness. Throughout the paper, distances are quoted as model distances, zero being located at shot P19 for VISP line 1.

THE DATA SET

Onshore-offshore profile

Seven refraction sections from line I were interpreted in detail to develop a two-dimensional onshore-offshore model, although many other sections had been recorded and were also considered. This was possible since many of these sections exhibited the same characteristics as those used in the modeling process. Three of the sections examined (P8, P13 and P19) were from workshop topic I. The four other interpreted sections were common receiver gathers, two from receivers X6 and X22 located on Vancouver Island and two from receivers X35 and X45 located on the mainland ; these represent recordings at each receiver of the 17 P-series shots fired off the west coast of the island (Ellis et al., 1983 ; Spence et al., 1985).

Record sections P8, P13 and P19 are shown in Figures 7, 8 and 9 of Green et al., (1990) ; those reproduced in Figures 3b, 4b and 5b have been filtered with a 2.5-9 Hz bandpass filter. All three sections have a data gap coresponding to the location of Georgia Strait. The sections show a jump in the first break travel times of approximately 0.75 s across this gap. The apparent velocity of the first arrivals across Vancouver Island is between 7.5 and 7.7 km/s, whereas across the mainland the apparent velocity of the first arrivals is closer to 8 km/s. Amplitudes are slightly larger for receivers located on the mainland than for receivers located on Vancouver Island, and there are significant fluctuations in amplitude from trace to trace. A set of secondary arrivals 0.25 s after the first arrivals may be present on the Vancouver Island stations in section P13. Such arrivals are less clear on section P19 and may or may not exist on P8. The signal-to-noise ratio is considerably lower on section P8 than on P13 or P19, probably due to its smaller charge (200 kg versus 825 kg).

On the four common receiver sections, X6, X22 (Fig. 6b), X35 and X45 (Fig. 7b), a clear first arrival is generally present, but on X35 and X45 it is not easy to follow for distances greater than 150 and 80 km respectively. The apparent velocity of the first arrival across the common receiver sections is ~ 8.5 km/s. Possible secondary arrivals are identified on sections X22 and X6, although they appear to die out at the traces generated by the shots closer to the coast than P8. The apparent velocity of the secondary arrivals is about 9.2 km/s. Like the common shot sections, the amplitudes of the first and secondary arrivals vary significantly from trace to trace across the four sections.

Along-island profile

Six refraction sections were recorded along line IV and all were used in modeling. With reference to Figures 4 and 5 of Green et al., (1990), sections N-North and A-North will refer to a shot at N and A, respectively, recorded along the segment A-N ; sections A-South and F-South will refer to a shot at A and F, respectively, recorded along the segment A-F. Section F(S-N) refers to a shot at F recorded on all receivers to the north and N(N-S) refers to a shot at N recorded on receivers to the south. Note that the bend in line IV at A represents an approximate 30° change in profile direction. Consequently a different subsurface region is sampled by sections F-North and N-South than by the shorter in-line reversed sections. This situation necessitated the derivation of two slightly different cross-sectional models, one from N through A to F and one corresponding approximately from N directly to F.

Data on the shorter in-line reversed sections are of good quality and show clear first breaks with apparent velocities ranging from about 5.5 km/s at the shortest offsets to 7 km/s at the langest offsets of 190 km. Prominent secondary arrivals are observed on section A-South (Fig. 8b), but equivalent arrivals on the three other sections are not clear. On sections F(S-N) (Fig. 9b) and N(N-S), the data quality at the far-offset receivers is poor. Careful filtering (*see* Drew, 1987) helped clarify arrivals on these sections relative to the earlier study of McMechan and Spence (1983).

1984 LITHOPROBE reflection data

On Vancouver Island, 205 km of crustal reflection data were acquired along four lines during the 1984 LITHOPROBE Phase 1 program. Figures 1 and 2 of Green et al., (1990) show the locations of these profiles. Line 1 is the most relevant since it coincides approximately with VISP refraction line I and intersects VISP line IV. Reflection profile 3 is also important since it provides some three-dimensional control southeast of line 1 and approaches refraction line IV. Reflection lines 2 and 4 provide insight into the possible structures near the southern end of VISP line IV.

Figures 14 and 15 of Green et al., (1990; Fig. 14 is contained in the pocket at the back of this volume) show unmigrated reflection sections for line 1. Two prominent reflective zones, C and E, are observed across most of the section. The travel times to the top and bottom of these distinct bands of reflectivity were used in constructing the velocity model. On the basis of the offshore profile, the short reflection F? below the E reflective zone is interpreted as the top of the subducting Juan de Fuca plate, thereby providing a vertical travel time constraint for this boundary.

The three other reflection sections show deep reflecting zones that correlate with those on line 1 as depicted on the line drawings displayed in Figure 16 of Green et al., (1990); see also Green et al., (1986). Thus, the structures generating the reflective zones, which are characterized by substantial lateral variations, appear to be ubiquitous beneath southern Vancouver Island.

1985 Marine reflection survey

The 1985 marine crustal reflection survey consisted of five lines, for which the locations of three are shown in Figure 1 of Green et al., (1990). Line 85-01 is most relevant to this study since it coincides approximately with the offshore portion of VISP refraction line I. Lines 85-02 and 85-05 are also important since they provide some 3-d control for 85-01 and corroborate important features interpreted from it.

Figures 20 and 21 of Green et al., (1990; Fig. 20 is contained in the pocket at the back of this volume) show the migrated reflection section for line 85-01. Many shallow reflectors can be followed for considerable distances. The reflection of greatest interest, labelled JdF, starts at about 5.5 s on the western edge of the section. This reflector, although faint in some areas, can be followed discontinuously from the western edge of the section, where it can be unequivocally identified as the top of the oceanic Juan de Fuca plate, to the eastern edge. It probably correlates with the deepest reflection segment (F?) on LITHOPROBE line 1. Reflecting zones C and E on line 1 (Fig. 15 of Green et al., 1990) merge into a thicker zone at the western edge of Vancouver Island and correspond to the zone of reflectivity between C and E on section 85-01 (Fig. 21 of Green et al., (1990). The principal deep reflections mentioned for 85-01 are observed also on lines 85-05 and 85-02. In particular, reflection JdF can be followed along the entire 100 km extent of 85-05, which parallels the southwest coast of Vancouver Island (Green et al., 1990; *see* also Clowes et al., 1987b).

INTERPRETATION OF THE ONSHORE-OFFSHORE PROFILE

Characteristics of the final model

The final velocity structure model is shown in Figure 1 and a series of velocity-depth profiles are shown in Figure 2. The heavier lines beneath Vancouver Island and the continental shelf correspond to boundaries that have been constrained by the deep reflection data. The two shots fired at shotpoint J (Fig. 5 of Green et al., 1990) and recorded on the mainland and Vancouver Island were modeled by Spence et al., (1985). Since no new data are available for that portion of the onshore-offshore profile, it remains unchanged and was not remodeled. The portion of the model shown in Figure 1c was derived from an interpretation of the OBS data by Waldron et al., (1990); only minor changes were made during the course of this reinterpretation. The increased dip of the subducting plate at a depth of ~40 km (Fig. 1) has been drawn to be consistent with the depth to the subducting slab under the Cascade volcanoes as suggested by Dickinson (1970) on the basis of the geochemistry of the lavas, and with the average worldwide slab depth to active volcanism of about 100 km (e.g. Isacks and Barazangi, 1977). The 7.1 km/s velocity between reflective zones C and E in the revised onshore-offshore model (Figure 1) is constrained by the new interpretation of VISP line IV (Fig. 11). Both reflectors have been extended as far east as the observed data permit. Figure 15 of Green et al., (1990) shows the two reflecting zones dying out about three-quarters of the way across the section toward the east. The reason they do not extend to the eastern edge of the section is unknown, but they die-out where a major structural change in the velocity model was required to replicate a travel time delay seen in the refraction data recorded on the mainland (e.g. sections P8, P13, and P19).

Interpretation of P-series sections

Section P19

Shot P19 was fired at the western end of onshore-offshore line I. The first arrivals (Fig. 3b) are relatively easy to follow across the mainland stations, but are very difficult to see on the Vancouver Island stations. Because precise time picks could only be made on a few of the traces, the trend and approximate start of first arrival energy was all that could be modeled. Turning rays through the oceanic upper mantle generate first arrivals at model distances corresponding to Vancouver Island and the mainland (Fig. 3a). The oceanic upper mantle velocity ranges from 8.10 km/s to approximately 8.16 km/s at the base of the westernmost block of the model, and from 8.17 km/s to approximately 8.33 km/s at the base of the easternmost block. The division of the upper mantle into a series of blocks that gradually increase in velocity from west to east was required to satisfactorily match travel times.

The most conspicuous feature of the observed data, and one that is evident on all P-series sections, is the 0.75 s offset in travel time across Georgia Strait (Fig. 3b). In the model this offset is explained by differences in the

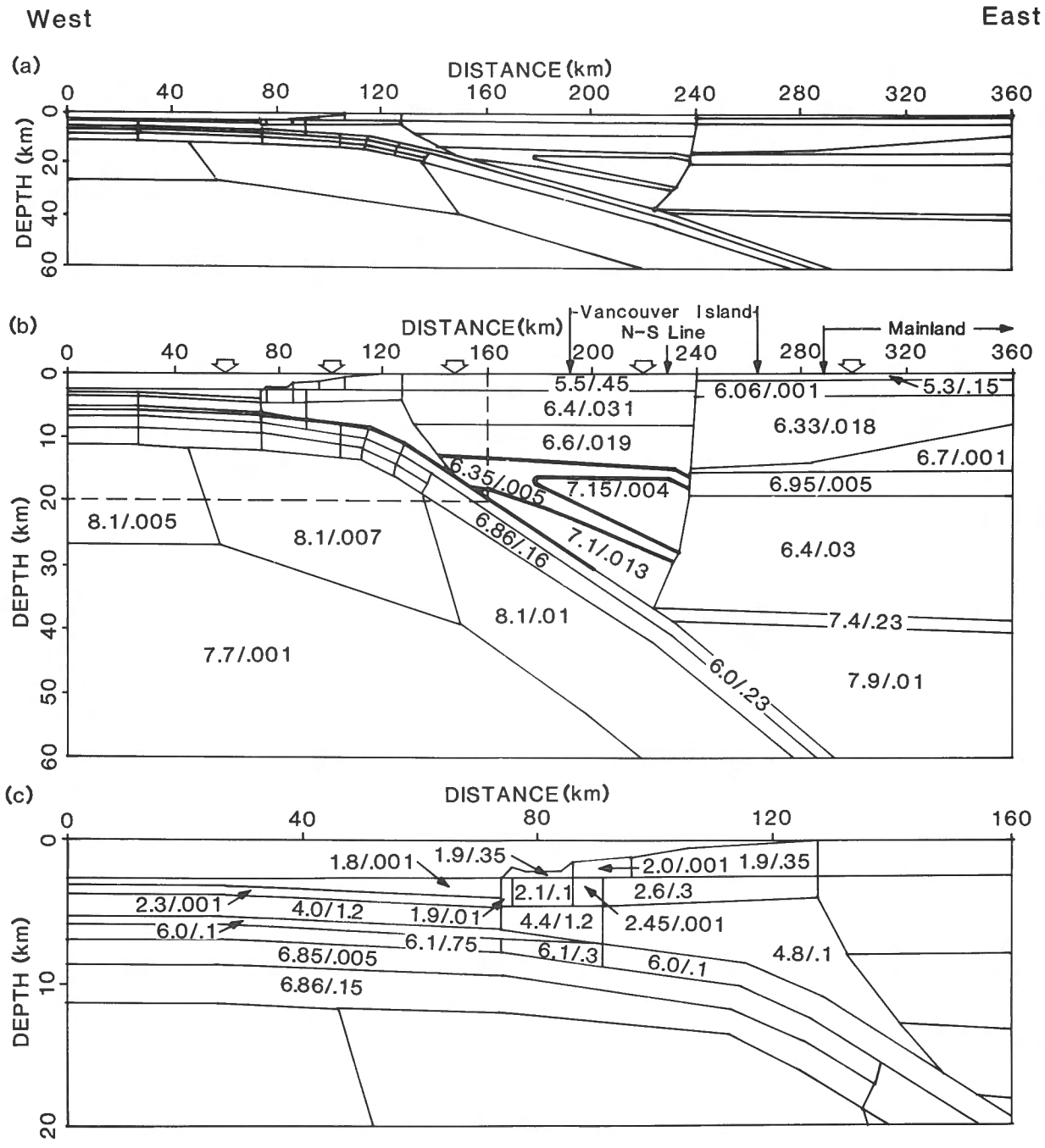

Figure 1. Velocity model corresponding to refraction line I, extending from the deep ocean off the west coast of Vancouver Island, across the island, and onto the mainland of British Columbia. (a) 1 : 1 representation of the velocity model. (b) Velocity model with velocity and gradient assigned to each block. (c) Enlarged version of the area outlined by the dashed lines in the upper left-hand corner of the model in (b). Velocities (km/s) are given for the top of each block, followed by the velocity gradient (km/s/km). Heavy lines in (b) indicate the boundaries constrained by the deep reflection data collected along LITHOPROBE line 1 and FGP line 85-01. The hollow triangles indicate the location of the five velocity-depth profiles in Figure 2.

raypaths taken to Vancouver Island compared to those taken to the mainland (Fig. 3a). The rays arriving on Vancouver Island travel through material beneath the island that has a higher average velocity than material at the same depth beneath Georgia Strait and the mainland. The velocity-depth profiles corresponding to the onshore-offshore model (Fig. 2) illustrate the differences in velocity structure used to model this travel time offset.

The synthetic seismogram section is shown in Figure 3c. In the observed data, the first arrivals at the Vancouver Island stations have, in general, lower amplitudes than the first arrivals at the mainland stations. This feature was not reproduced in the synthetics where the first arrivals across Vancouver Island have the higher amplitudes.

The upper mantle boundary that intersects the western edge of the model at 27 km depth is modeled with a velocity of 7.7 km/s (Fig. 1). However, the velocity at this boundary is poorly constrained since the observed data do not require refracted rays traveling through material below it. Reflections from this boundary generate secondary arrivals on Vancouver Island only 0.2 to 0.1 s later than the refraction arrival; on the synthetic section the two arrivals merge and appear as a single event. Similarly, on the observed P19 data on Vancouver Island there is little evidence for two arrivals.

In contrast, the section recorded on the mainland (280 km) shows reasonably strong and coherent secondary arrivals with high apparent velocities (arrow on Fig. 3b). These arivals cannot be due to the reflections described above, because of differing travel time characteristics. We have not modeled these arrivals; they probably originate from a reflector within the oceanic asthenosphere as suggested by a number of papers in this volume.

Section P13

Of the three P-series shots used in modeling, the seismic section recorded from shot P13 has the best quality data. First arrivals (Fig. 4b) are relatively easy to follow across the entire section, although the precise start of the first breaks is not easy to pick; both filtered and unfiltered sections were examined to determine the start of first arrival energy.

Calculated and observed travel times of first arrivals at both the Vancouver Island and mainland stations match (Fig. 4b). A possible secondary phase, modeled as a reflection from the boundary within the upper mantle, is seen on the Vancouver Island stations approximately 0.3 s after the first arrivals; calculated travel times agree saitfactorily with the data.

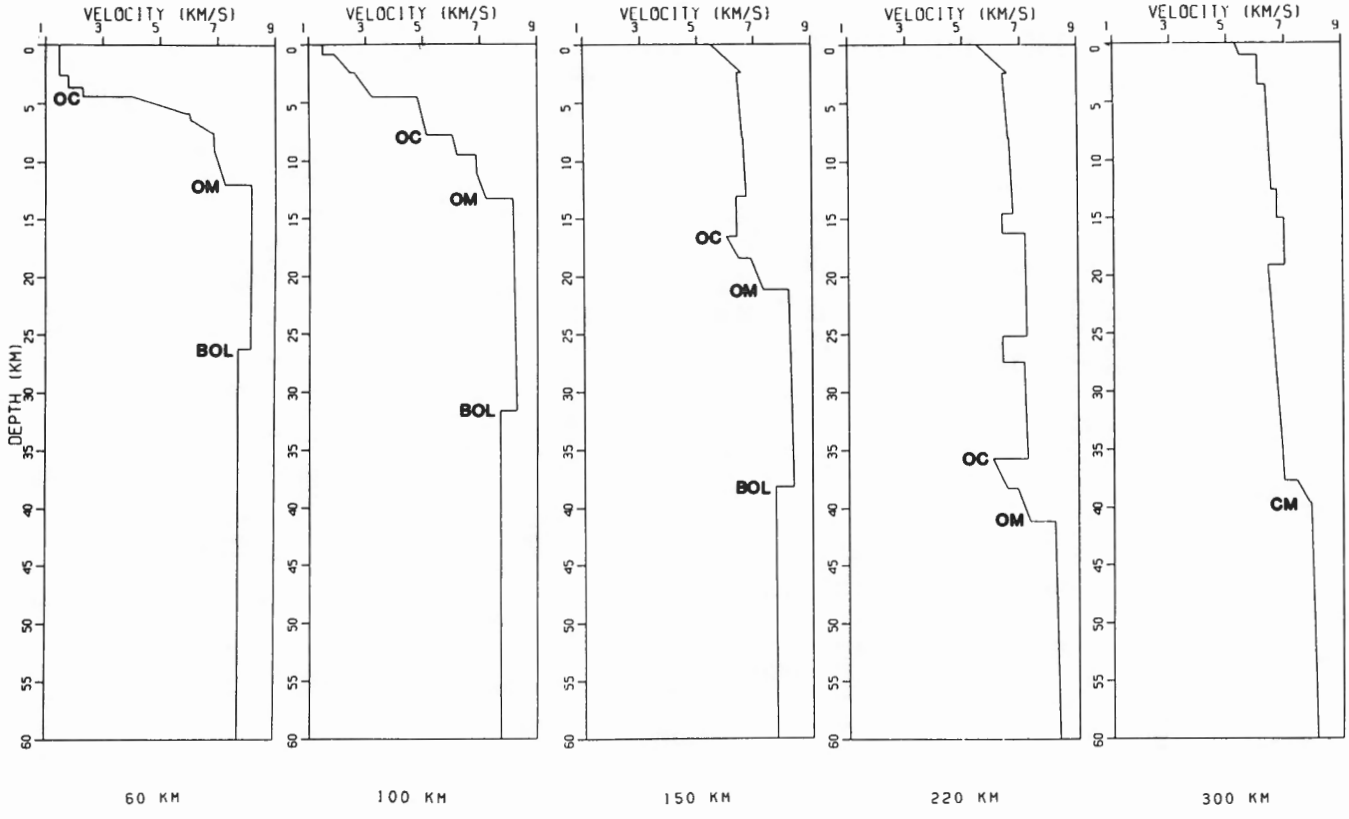

Figure 2. Velocity-depth profiles at the five locations marked in Figure 1. The distances at the bottom of each profile correspond to the location of the profile with respect to shot P19 at the western edge of Figure 1.

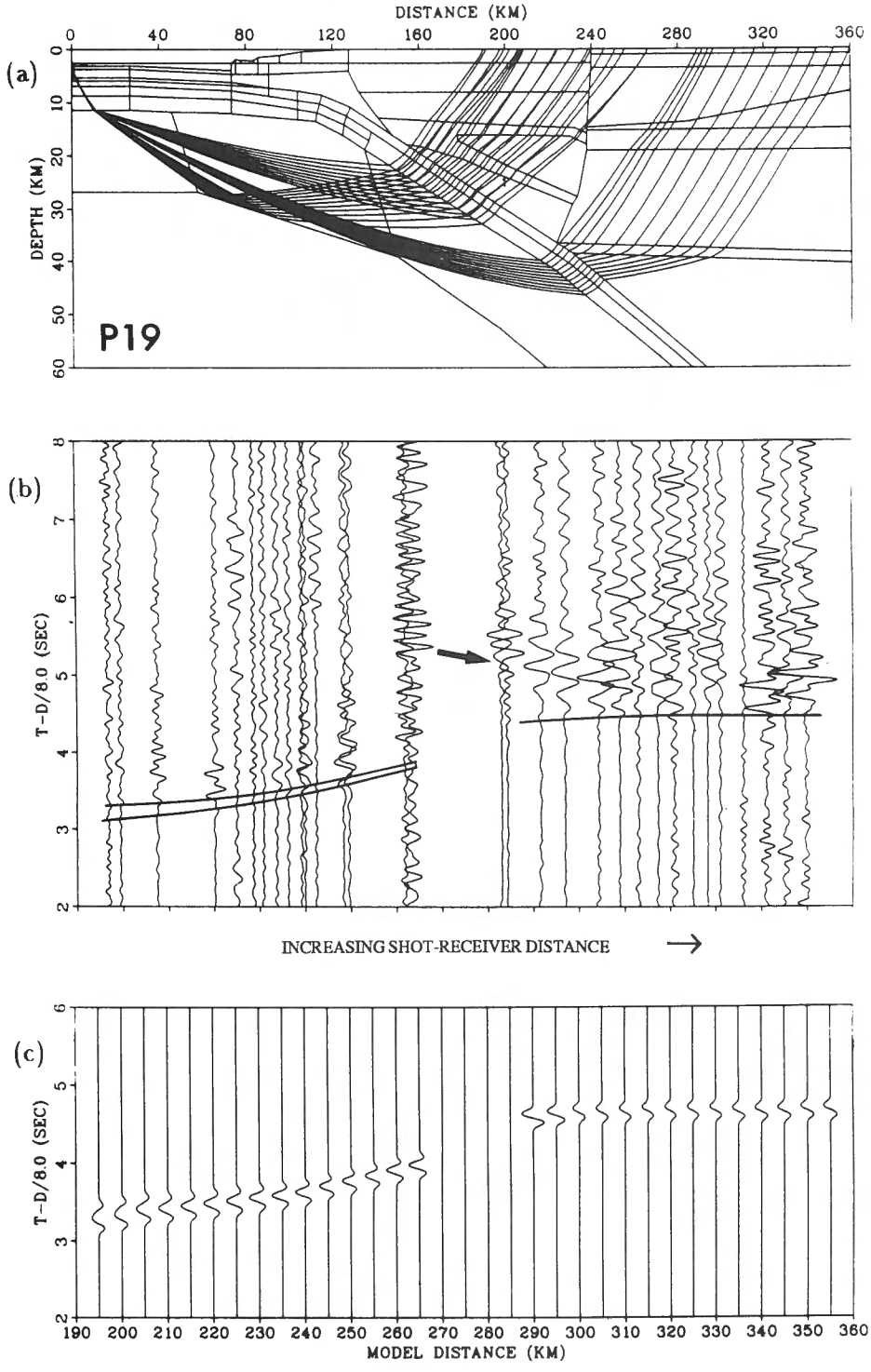

Figure 3. (a) Raytracing diagram for shotpoint P19. (b) Theoretical travel time curve superimposed on section P19 (filtered 2.5-9 Hz). The arrow identifies a secondary arrival (not modeled), which could be a wide-angle reflection from within the oceanic asthenosphere. (c) Synthetic section corresponding to the raytracing diagram in (a). Wavelet used in (c) was chosen to represent the average waveform of the first arrival in (b).

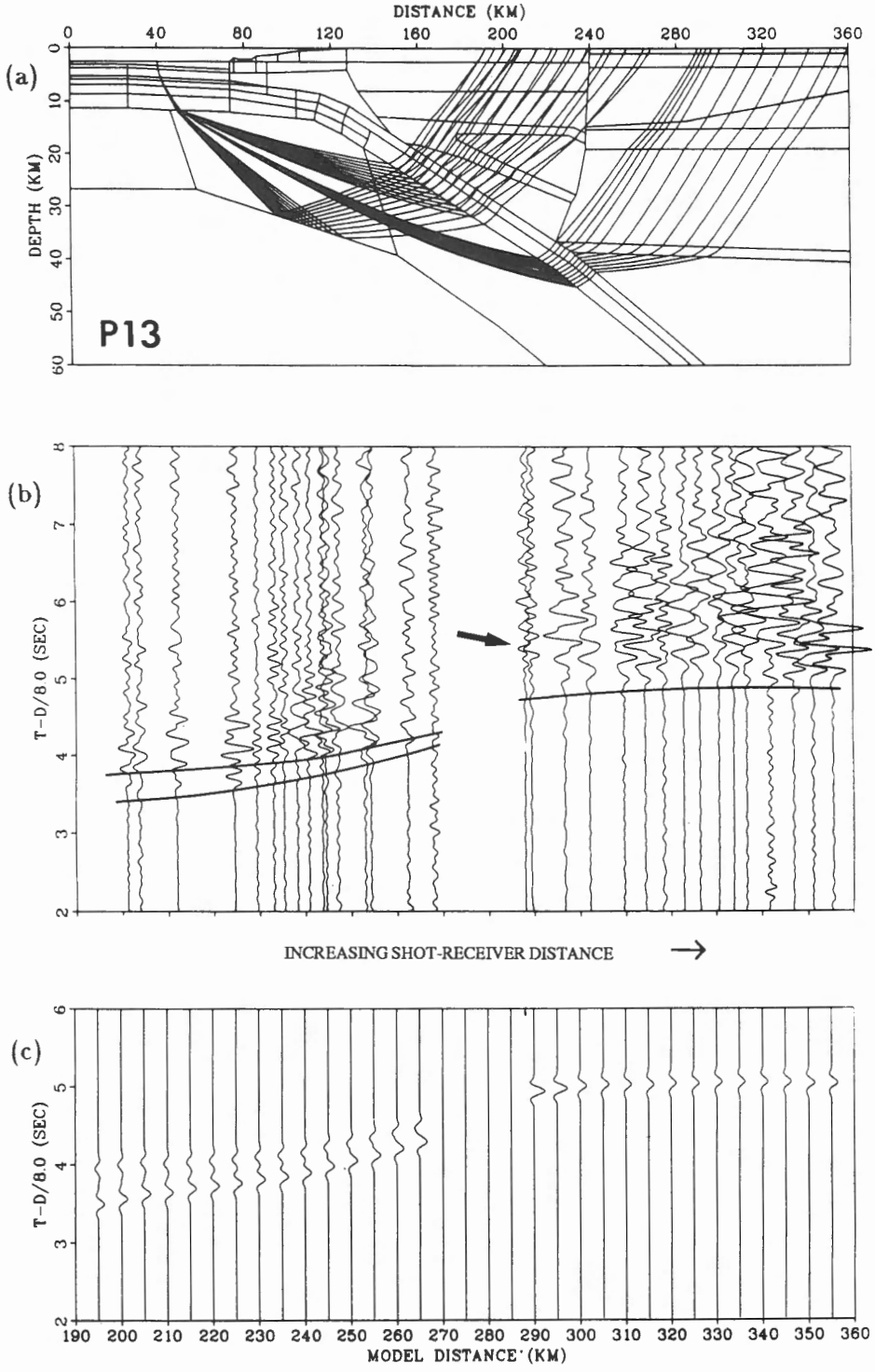

Figure 4. (a) Raytracing diagram for shotpoint P13. (b) Theoretical travel time curve superimposed on section P13 (filtered 2.5-9 Hz). The arrow identifies a secondary arrival (not modeled) ; see Figure 3 caption. (c) Synthetic section corresponding to the raytracing diagram in (a). Wavelet used in (c) was chosen to represent the average waveform of the first arrival in (b).

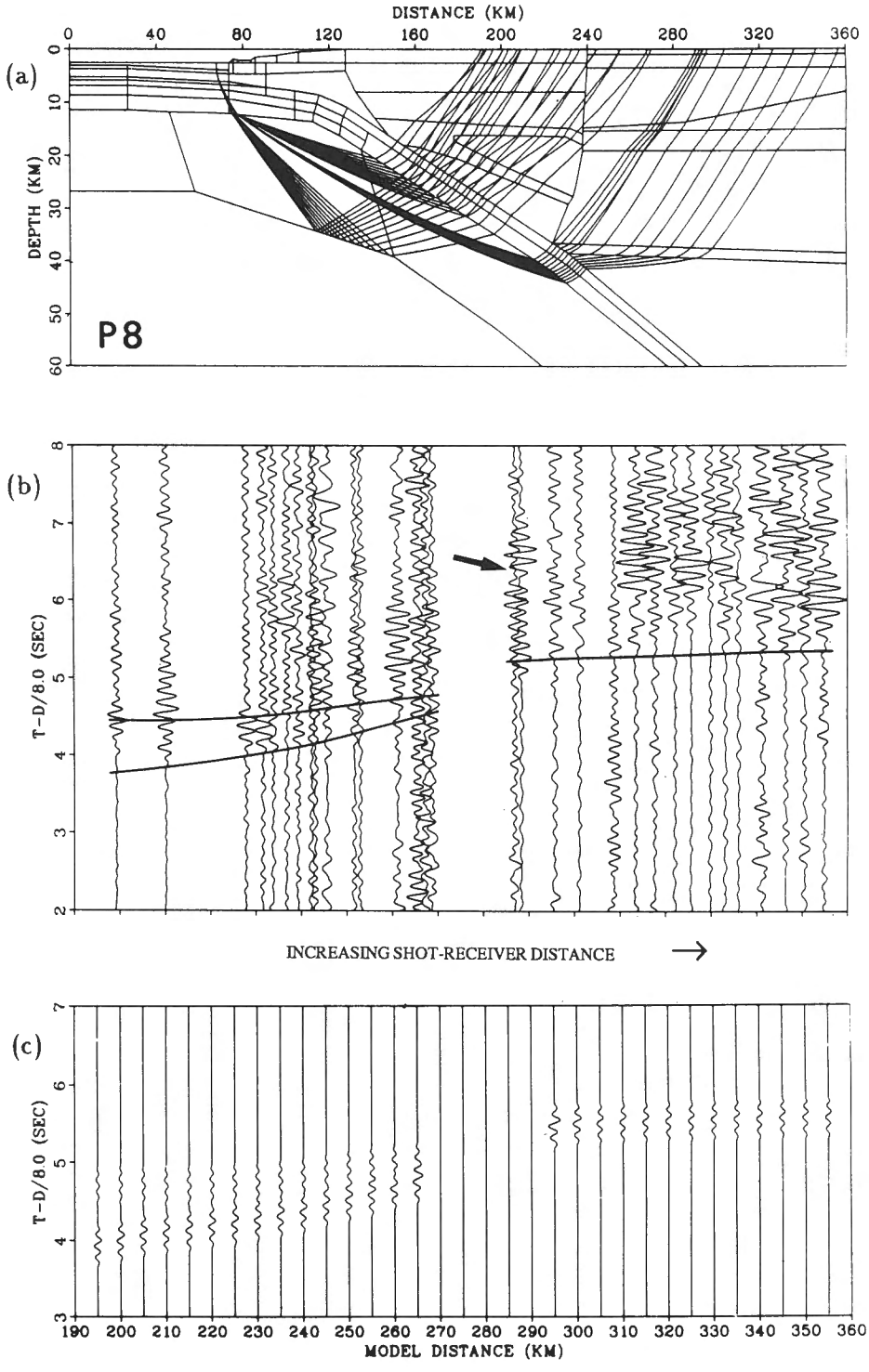

Figure 5. (a) Raytracing diagram for shotpoint P8. (b) Theoretical travel time curve superimposed on section P8 (filtered 2.5-9 Hz). The arrow identifies a secondary arrival (not modeled); see Figure 3 caption. (c) Synthetic section corresponding to the raytracing diagram in (a). Wavelet used in (c) was chosen to represent the average waveform of the first arrival in (b).

The average amplitude of the observed first arrivals is reproduced in the synthetic section (Fig. 4c), although the average amplitude of synthetic secondary arrivals on Vancouver Island is a little lower than seen in the data. The amplitude of these wide-angle reflections is sensitive to the magnitude of velocity contrast at the reflecting boundary. After testing a range of velocities from 7.5 to 8.6 km/s for the material below this upper mantle reflector, it was found that a velocity of 7.7 km/s provided the best overall fit to the data collected along line I. However, a velocity of 8.6 km/s provided a better fit to the secondary arrivals recorded on Vancouver Island from shot P13. As discussed for shot P19, there are secondary arrivals with high apparent velocities on the mainland stations (arrow on Fig. 4b) that were not modeled in this study.

Section P8

The P8 section, which was generated with a 200 kg charge fired over the ocean basin near the base of the continental slope, is the most difficult of the three sections to interpret because of its low signal-to-noise ratio. Nevertheless, a clear band of first arrival energy can be followed across much of the section. The calculated travel times agree reasonably with the estimated location of the observed first breaks (Fig. 5b). Synthetic reflected arrivals generated for the Vancouver Island stations are not observed in the data. Although less clear than on sections P19 and P13, there is an indication of a secondary phase with high apparent velocity on the mainland stations (arrow on Fig. 5b).

Interpretation of X-series sections

The common receiver sections (X-series) allow an independent check of the velocity structure modeled from the common shot sections (P-series). Including information from the X-series data resulted in only minor changes to the velocity model.

Sections X6 and X22

The sections recorded at receivers X6, near the west coast of Vancouver Island, and X22, near the east coast of the island, were modeled by tracing rays from the receiver to the approximate location of the line of offshore shots. The first arrival energy observed on both sections (e.g. Fig. 6) is easy to follow, with apparent velocities of approximately 8.6 km/s to 8.7 km/s. Turning rays through the lower oceanic lithosphere are used to model these events (Fig. 6a). Although the calculated first arrival times generally match the observed data quite well (Fig. 6b), they are up to 0.22 s too late for traces at short offsets (e.g. model distances $>$ 80 km for section X22). The short offset traces were generated from shots fired over the continental slope (shots P1 — P6); the time corrections required to put these shots at the 2600 m datum were much larger and less constrained than those for shots over the deep ocean.

The offset in arrival time observed on the P-series sections is not present on X6 and X22 since all the rays traveling from these receivers to the offshore shots pass through the higher velocity material beneath Vancouver Island. Calculated travel times of reflections from the upper mantle reflector match the observed travel times of possible secondary arrivals (Fig. 6b).

For the X6 and X22 synthetic seismograms (Fig. 6c) no attempt was made to reproduce the trace-to-trace fluctuations in amplitude observed in the data, but the synthetic seismograms do reproduce the overall trend in amplitudes. In general, the synthetic secondary arrivals have slightly lower amplitudes than the observed events.

Sections X35 and X45

First arrivals on X35 and X45 (Fig. 7), both located on the mainland, are relatively clear, with apparent velocities ranging from approximately 8.0 km/s to 8.9 km/s. Turning rays through the lower oceanic lithosphere were used to model these events. It is difficult to assess the travel time fit for traces at distances greater than 70 km on section X45, since these traces have low signal-to-noise ratios.

The synthetic first arrivals generated for section X45 (Fig. 7c) agree relatively well with the data, although the amplitudes of the synthetic sections generated at model distances less than 50 km are lower than corresponding arrivals in the data.

INTERPRETATION OF THE ALONG-ISLAND PROFILE

With the additional constraints provided by the 1984 LITHOPROBE reflection survey, two slightly different velocity models (one for the hinged line N-A-F, one for N-F; *see* Fig. 4 of Green et al., 1990) were developed for the refraction data along VISP line IV. Workshop topic I did not include these data, so only a brief presentation of results will be given here. The revised models for lines I and IV were developed simultaneously. This is in contrast to the interpretations presented in McMechan and Spence (1983) and Spence et al., (1985), in which line IV was interpreted first (McMechan and Spence, 1983) and at the point of intersection with line I its velocities were considered fixed (Spence et al., 1985). Significant changes from the McMechan and Spence (1983) model have resulted from this re-interpretation. Although all 6 refraction record sections from line IV and the LITHOPROBE reflection data were used in the model development, we show only two refraction records.

Section A-South

The first arrivals are easy to follow across section A-South (Fig. 8b) and are explained by successive families of refractions through the upper 20 km (first 4 layers) of the velocity model (Fig. 8a). Deeper penetrating refracted rays emerge at locations off the end of the line and are not considered. Layers 3 and 5 are low velocity layers that correspond to the "C" and "E" reflective zones of the LITHOPROBE seismic reflection data.

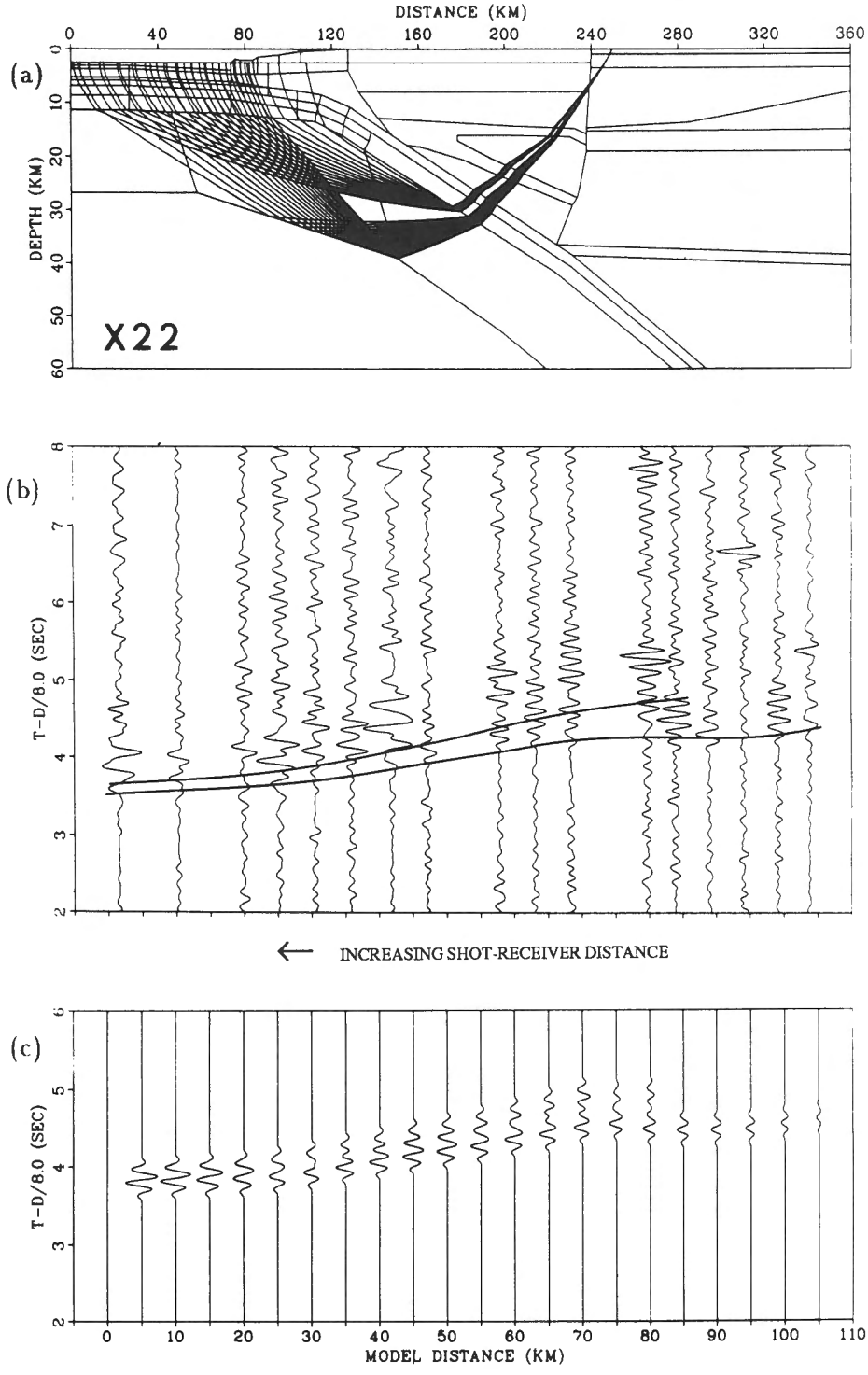

Figure 6. (a) Raytracing diagram for receiver section X22. (b) Theoretical travel time curve superimposed on section X22 (filtered 2.5-9 Hz). (c) Synthetic section corresponding to the raytracing diagram in (a). Wavelet used in (c) was chosen to represent the average waveform of the first arrival in (b).

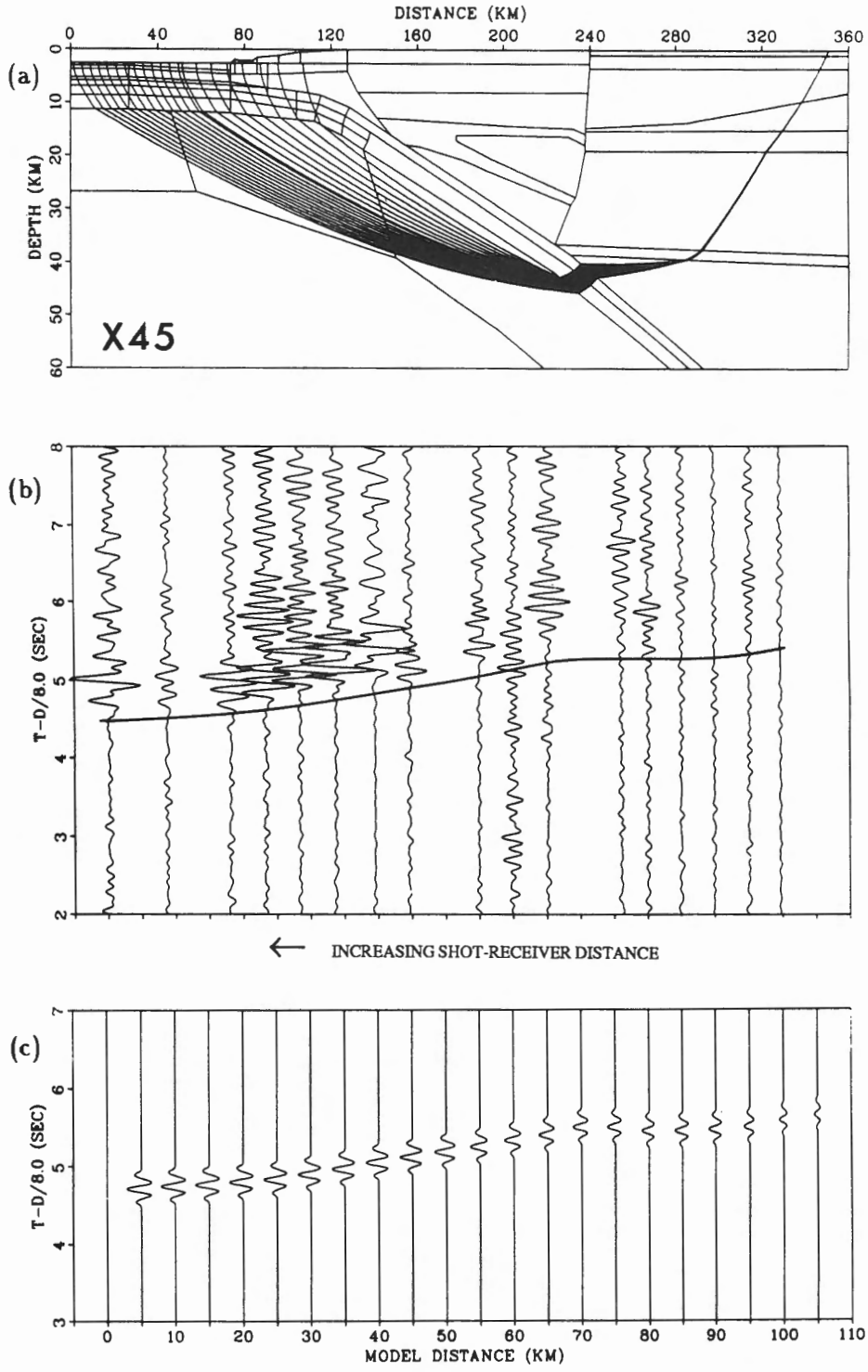

Figure 7. (a) Raytracing diagram for receiver section X45. (b) Theoretical travel time curve superimposed on section X45 (filtered 2.5-9 Hz). (c) Synthetic section corresponding to the raytracing diagram in (a). Wavelet used in (c) was chosen to represent the average waveform of the first arrival in (b).

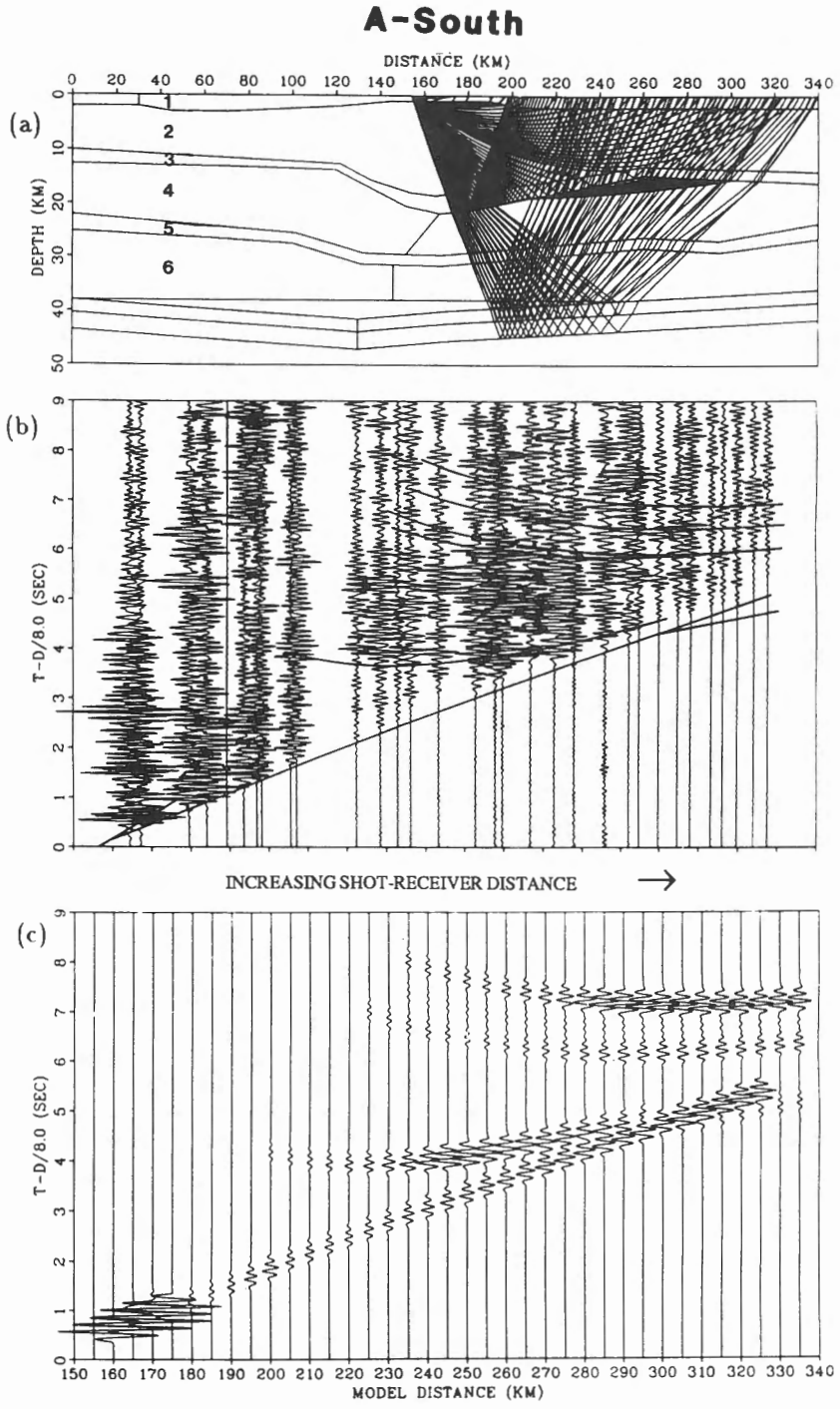

Figure 8. (a) Raytracing diagram shotpoint A. (b) Theoretical travel time curve superimposed on section A-South (filtered 6-13 Hz). (c) Synthetic section corresponding to the raytracing diagram in (a). Wavelet used in (c) was chosen to represent the average waveform of the first arrival in (b).

As shown in Figures 8b and 8c, there is good correspondence between the observed and calculated first arrival times. There is a reasonable matching of amplitudes, although the synthetic waveforms for layer 2 are too large, particularly at model distances greater than 290 km.

Synthetic wide-angle reflections from the top of the fourth layer (base of "C" reflective zone) and layers below 35 km were generated. The reflected phase from the fourth layer (4 s travel time) explains an event on A-South ; the agreement between this arrival and features on section F-South is not so good (southern half of Fig. 9). Reflections from the top and bottom of low velocity layer 5 would add phases between those at 4 and 6 s, contributing to the reverberatory nature of the observed data where no coherent phases can be discerned. Similarly, reflections from layers below 35 km cause the calculated phases between 6 and 8 s, but no corresponding coherent phases are observed even though considerable energy is evident. Thus, the lower layers are not required by the along-island data ; they are included in the model to maintain consistency between it and the onshore-offshore model at their position of intersection.

Section F(S-N)

Section F(S-N) of Figure 9 comprises all seismograms recorded along line IV from shot F (Fig. 4 of Green et al., 1990). The two most interesting features in F(S-N) and N(N-S) are the first arrivals, which can be followed more than halfway across both sections, and the secondary seismic energy at reduced times later than 5.5s. The first arrivals from 330 to 180 km distance are modeled as refractions in the upper two layers (Fig. 9a). A reflection from the base of the "C" low velocity layer generates a secondary arrival between 280 and 215 km distance. First arrivals observed on traces at distances less than 180 km (note that these traces correspond to the longer source receiver distances) become increasingly more difficult to follow, even when the amplitudes are enhanced (Drew, 1987). The calculated travel time curves agree with the first arrival travel times to within 50 km of the far-offset ends of both F(S-N) and N(N-S). Amplitudes of first arrivals on the observed and synthetic sections are extremely weak. Refracted arrivals penetrating deeper than layer 4 are not included because they arrive off the end of the recording line.

Secondary seismic energy later than 6s is modeled by reflections from the three boundaries below 30 km (Fig. 9a). Of the three corresponding layers below the discontinuities, the upper two are modeled as layers of the subducting oceanic crust and the lower one is modeled as the oceanic upper mantle. These deep reflectors correspond to similar features in the N-A-F model on Figure 8a, although in the model of Figure 9a they occur at slightly shallower depths, and no boundary corresponding to the continental Moho is present. The difference in structure between the N-A-F and N-F models is an indication that layers associated with the subducting slab are shallow to the west of line IV.

DISCUSSIONS AND CONCLUSIONS

The Onshore-Offshore Profile

The first objective of this study was to resolve differences between the onshore-offshore velocity model proposed by Spence et al., (1985) and the deep reflection data recorded along approximately the same line during the 1984 LITHOPROBE and 1985 FGP surveys. Geometries of major reflections, determined via depth conversions of travel times using inital refraction velocities, were incorporated in the revised model (note that the depth conversion is not very sensitive to details of the refraction model). The result is a velocity model that is consistent with both the refraction data and the deep reflection data recorded along line I.

Figure 10a is a simplified version of the detailed onshore-offshore velocity model in Figure 1. For comparison, Figure 10b shows a similar representation for the velocity model proposed by Spence et al., (1985). The velocity model in Figure 10a is a composite model derived from interpretations of several associated seismic data sets. The velocity structure of the oceanic crust at the western end of the model was determined originally by Waldron (1982) using marine refraction data from OBSs 1, 3, and 5 (Fig. 4 of Green et al., 1990). Waldron et al., 1990) re-interpreted these data and made some minor modifications to the original model. Spence et al., (1985) used the results from the study of Waldron (1982). The upper 18 km at the eastern end of the onshore-offshore velocity model (beyond 240 km) was modeled by Spence et al., (1985) and since no new data were available for this portion of the model, its velocity structure has not changed. The upper 10 km of the Vancouver Island velocity structure was taken from McMechan and Spence's (1983) model for line IV. However, deep reflection results from southern Vancouver Island and a more detailed re-interpretation of the refraction data collected along line IV (Drew, 1987), have shown that much of the McMechan and Spence (1985) model below 10 km, particularly for the southern half of the island, is inconsistent with features in both the reflection and refraction data. The re-interpretation of line IV was integrated with that of line I.

The primary differences between the onshore-offshore model proposed by Spence et al., (1985 ; Fig. 10b) and that determined in this study (Fig. 10a) occur beneath Vancouver Island (140 to 240 km distance) and the mainland (240 to 360 km distance). Of these, the revised structure for below 10 km in the Vancouver Island region is the best constrained. The original model for line I (Spence, 1984 ; Spence et al., 1985) required a block of 7.7 km/s material beneath Vancouver Island underlain by lower velocity material (Fig. 10b). The same region in the revised model (Fig. 10a) has a four-layer structure with two low velocity layers (6.35 km/s) alternating with two high velocity layers (7.15 km/s and 7.1 — 7.18 km/s). The velocity in the uppermost high velocity layer was determined from refracted arrivals recorded along line IV. The other three layers also appear in the model developed for line IV, but since there were only reflected phases from

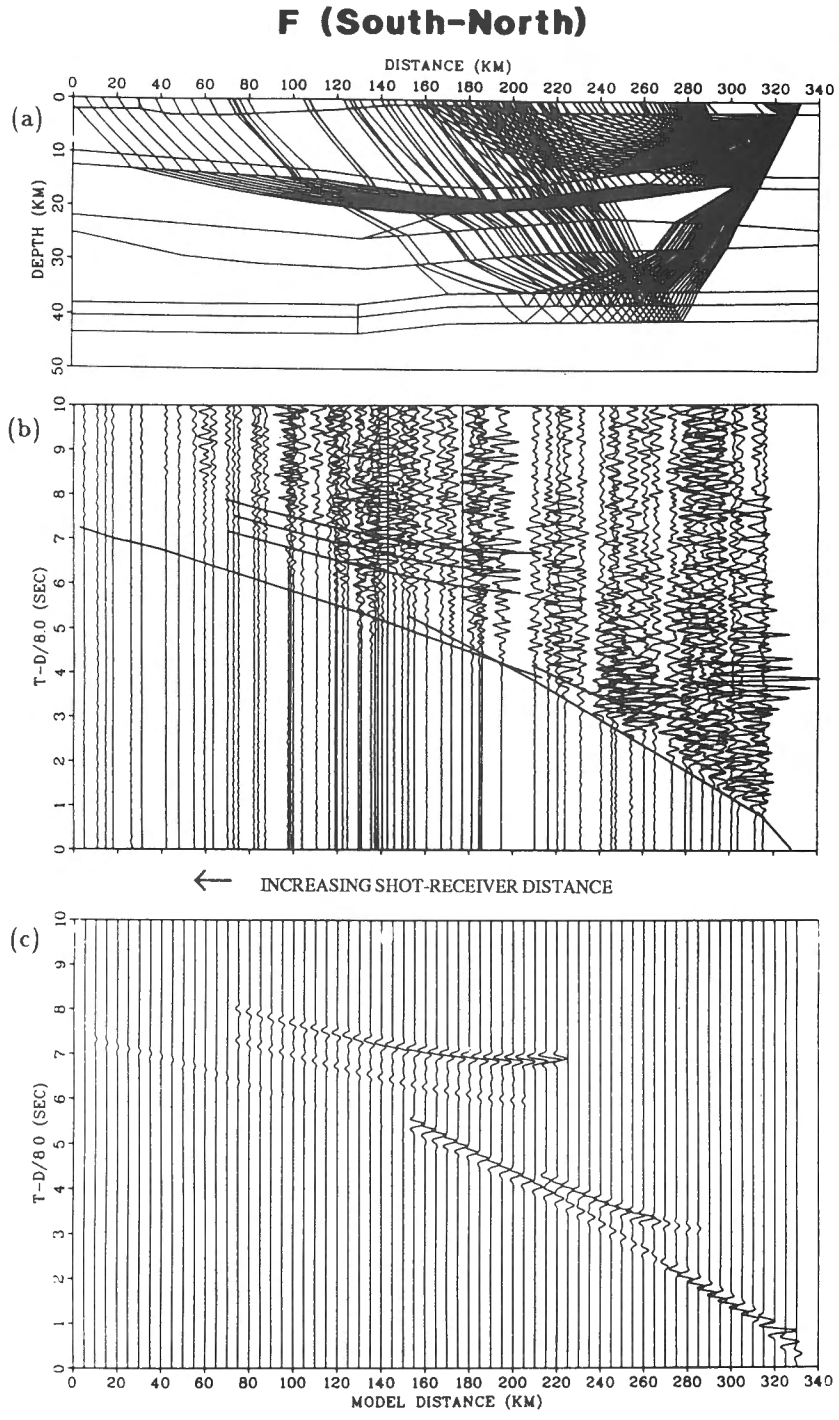

Figure 9. (a) Raytracing diagram for a shot at shotpoint F. (b) Theoretical travel time curve superimposed on section F(S-N) (filtered 1-10 Hz). (c) Synthetic section corresponding to the raytracing diagram in (a). Wavelet used in (c) was chosen to represent the average waveform of the first arrival in (b).

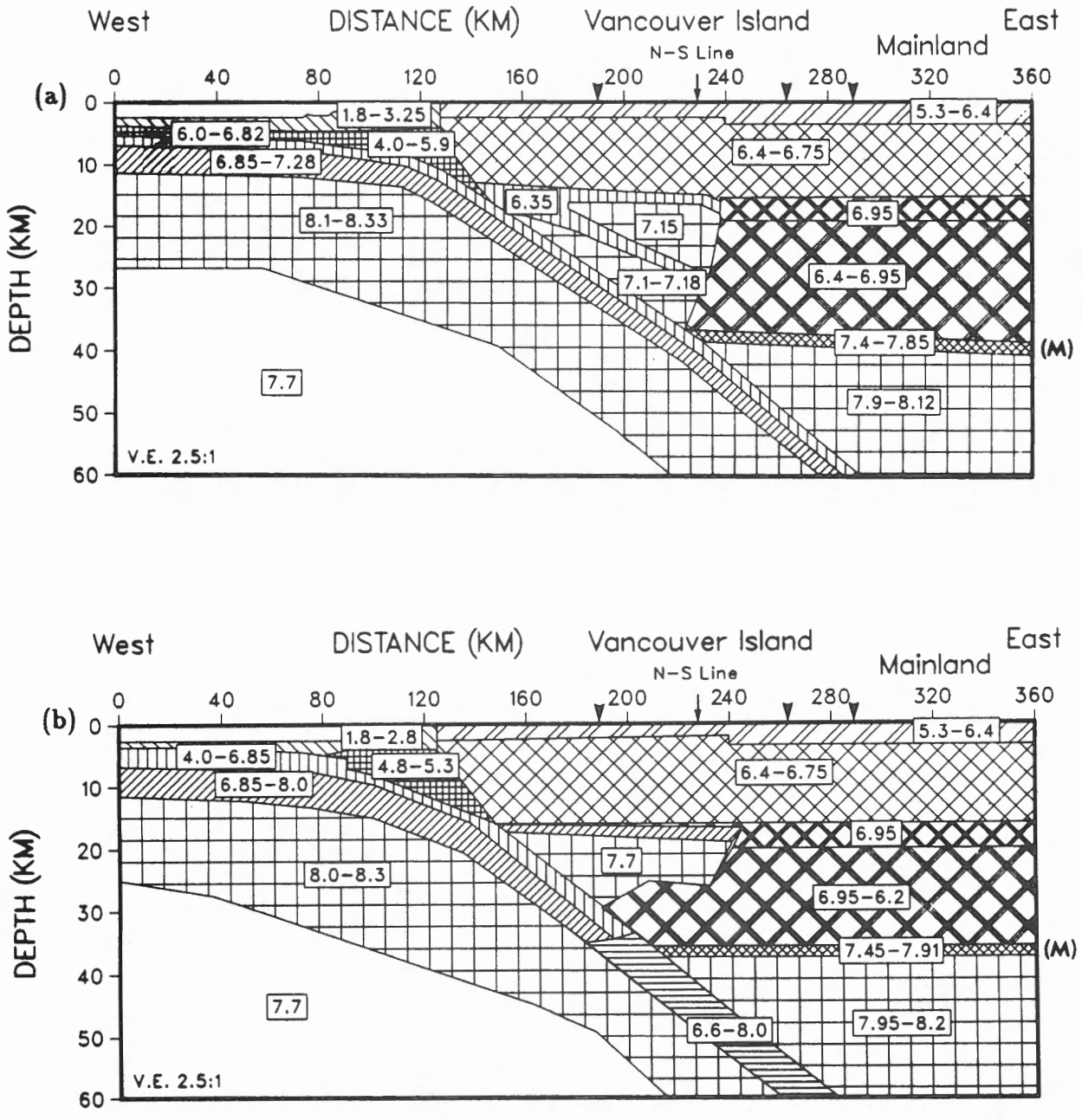

Figure 10. (a) Generalized velocity model interpreted from the onshore-offshore refraction and reflection data along line I. (b) Generalized velocity model proposed by Spence et al., (1985) based on the refraction data along line I. Numbers assigned to each block indicate the range of velocities (km/s) at the shallowest and deepest points within that block. The larger arrowheads represent the boundaries of Vancouver Island and the mainland. (M) indicates the location of the continental Moho.

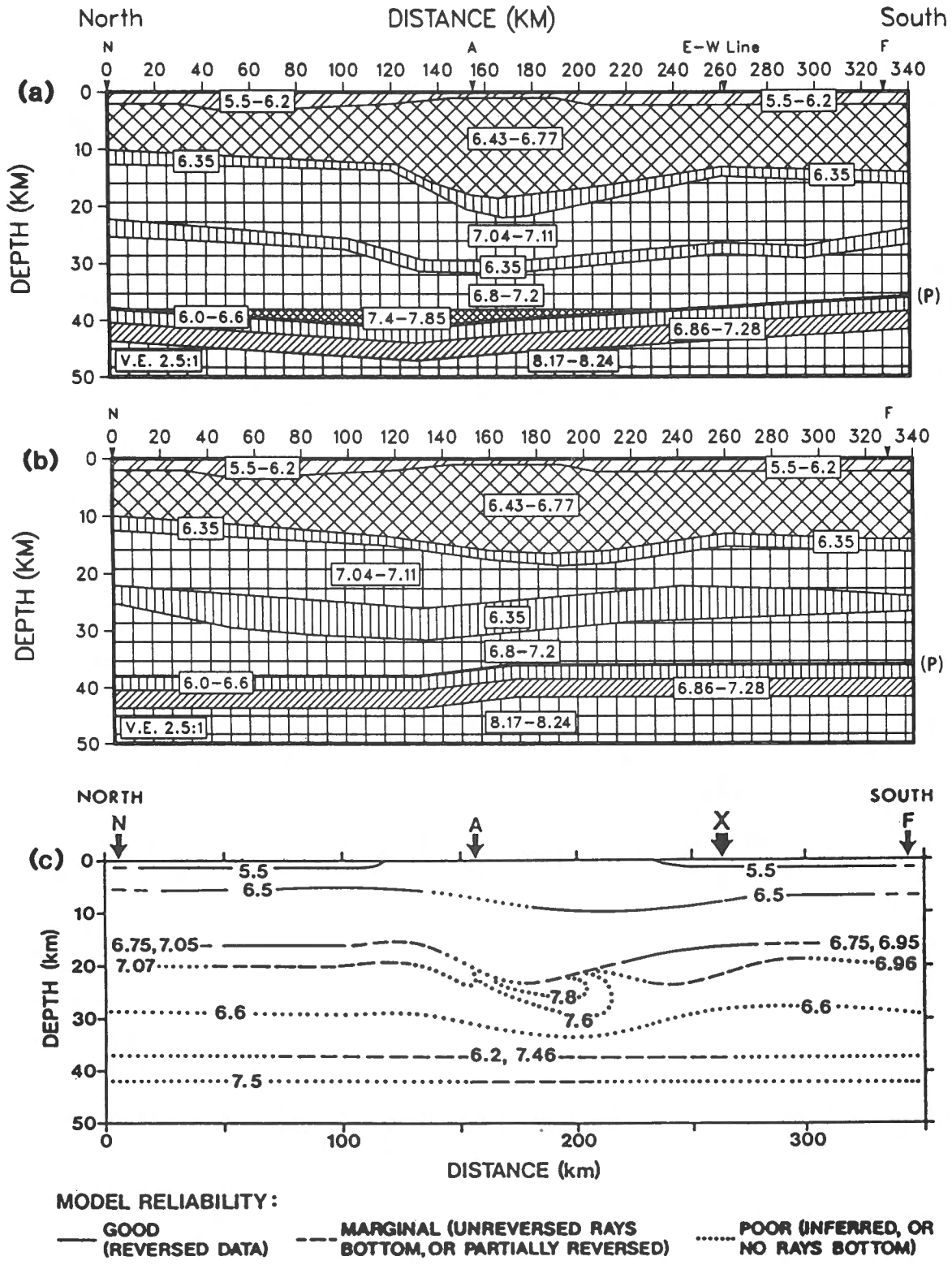

Figure 11. Generalized velocity models interpreted from the refraction data along line IV and for (a) and (b) the reflection data obtained in the LITHOPROBE experiment. N, A and F are shotpoint locations. (a) The hinged model, based on data recorded along the two shorter reversed segments of line IV (N-A and A-F). (b) The offline model, based on data from the full length of line IV. Numbers assigned to each block indicate the range of velocities (km/s) within that block. (P) indicates the location of the top of the subducting plate. (c) Velocity model interpreted by McMechan and Spence (1983) based on data along line IV. X is the intersection point with line I. Velocities (km/s) are shown at boundaries; where two values are provided, these represent the velocities directly above and below the boundary. Reliability of the subsurface structure is indicated by the line type (after McMechan and Spence, 1983).

these (ie. no turning rays), the velocities were poorly constrained. Thus the velocities within the lower three crustal layers were determined from travel time and amplitude constraints in the refraction data recorded along both lines I and IV. Changes in the crustal structure beneath Vancouver Island required minor changes in the velocity structure of the upper mantle to fit the refraction travel time data recorded on the island. However, the velocity structure in the upper mantle is poorly constrained in comparison with structures at shallower depths.

After changing the upper mantle velocity it was necessary to alter the velocity structure at depths greater than 18 km below the mainland in order to match travel time data from the P-series shots. The positive velocity gradient in the low velocity zone below 18 km in the revised model proved helpful in turning rays up toward the surface. Nevertheless, the velocity structure below 18 km at the mainland stations is probably the most poorly constrained part of the model since there are no reflection data on the mainland and the existing refraction data do not include rays turning in this area of the model.

The location of the subducting plate in the revised model is consistent with vertical travel times to a reflector considered to be the top of the subducting Juan de Fuca plate in the onshore-offshore deep reflection data. The plate was found to have an average dip of 14 to 16°, which is approximately the same as that proposed by Spence et al., (1985).

The Along-Island Profile

The second objective of our study, though not part of workshop topic I, was to remodel the refraction data collected along VISP line IV. In order to model these data satisfactorily, while maintaining consistency with the deep reflection data, two velocity models were required to explain the azimuthally distributed data. Generalized versions of the two velocity models are presented in Figures 11a and 11b, and Figure 11c shows the original model determined by McMechan and Spence (1983).

The structure along the southern half of line IV is relatively well constrained since it is based on the refraction data and structures delineated by the deep reflection data. These structures have been extended to the northern half of the model, although no deep reflection data are available there. The velocity structure in the northern region is constrained by the refraction data to a depth of approximately 20 km. Below 20 km the velocity structure is based primarily on a continuation of the structure beneath the southern portion of line IV as well as the offline data N(N-S) and F(S-N).

The Explorer plate subducts beneath the northern region of Vancouver Island (segment N-A of line IV), whereas the Juan de Fuca plate subducts beneath the southern region. Gravity data indicate differences in structure beneath north and south Vancouver Island (Riddihough, 1979). The major difference between the velocity structure derived for the southern part of Vancouver Island and that derived for the northern part is the depth to the top of the subducting plate. Based on an analysis of all the data along line IV, the top of the subducting plate to the north is modeled as being, on average, 2-3 km deeper than to the south.

The two upper layers in the N-S models (Fig. 11), as well as the corresponding layers in the onshore-offshore model (Fig. 10a), are equivalent to Wrangellia, indicating that this terrane (*see* Green et al., 1990), varies in thickness between 10 and 18 km. Such a relatively shallow extent suggests that either the terrane had less than normal lithospheric thickness when it was accreted, or a substantial volume of its lithosphere has been removed through subduction erosion and/or uplift and erosion. The four underlying layers (Fig. 11) are part of the Cenozoic subduction complex (Clowes et al., 1987a), whereas layers below 35 km are associated with the currently subducting oceanic lithosphere.

Additional geophysical data are required to resolve areas of uncertainty in the models. The primary area of uncertainty in the onshore-offshore model is the structure beneath the mainland and Georgia Strait. An additional deep reflection profile extending from the eastern end of LITHOPROBE line 1 on the east coast of Vancouver Island to shot-point J (Fig. 4 of Green et al., 1990) on the mainland might help constrain the subsurface structure beneath this region. Logistically, this represents a difficult but not insurmountable problem. Similarly, additional deep reflection profiles recorded on northern Vancouver Island would help constrain the subsurface structure there.

ACKNOWLEDGMENTS

Financial support for this research was received from the LITHOPROBE Phase I Collaborative Special Project grant and from operating grant A7707, both from NSERC. Land-based reflection data were acquired as part of LITHOPROBE Phase I; the offshore data were acquired under the Frontier Geoscience Program of the Geological Survey of Canada. LITHOPROBE Publication no. 42.

REFERENCES

Clowes, R.M., Spence, G.D., Ellis, R.M., and Waldron, D.A.
1986 : Structure of the lithosphere in a young subduction zone : results from reflection and refraction studies ; *in* Reflection Seismology : The Continental Crust, ed. M. Barazangi and L. Brown ; American Geophysical Union, Geodynamic Series, v. 14, p. 313-321.

Clowes, R.M., Brandon, M.T., Green, A.G., Yorath, C.J., Sutherland Brown, A., Kanasewich, E.R., and Spencer, C.P.
1987a : LITHOPROBE — Southern Vancouver Island : Cenozoic subduction complex imaged by deep seismic reflections ; Canadian Journal of Earth Sciences, v. 24, p. 31-51.

Clowes, R.M., Yorath, C.J., and Hyndman, R.D.
1987b : Reflection mapping across the convergent margin of western Canada ; Royal Astronomical Society, Geophysical Journal, v. 89, p. 79-84.

Dickinson, W.R.
1970 : Relations of andesites, granites, and derivative sandstones to arc-trench tectonics ; Reviews of Geophysics and Space Physics, v. 8, p. 813-860.

Drew, J.J.
1987 : A re-evaluation of the seismic structure across the active subduction zone of western Canada ; unpublished MSc, thesis. University of British Columbia, 144 p.
Ellis, R.M. and Clowes, R.M.
1981 : Acquisition of crustal reflection/ refraction data across Vancouver Island ; Earth Physics Branch Open File Report 81-11, 72 p.
Ellis, R.M., Spence, G.D., Clowes, R.M., Waldron, D.A., Jones, I.F., Green, A.G., Forsyth, D.A., Mair, J.A., Berry, M.J., Mereu, R.F., Kanasewich, E.R., Cumming, G.L., Hajnal, Z., Hyndman, R.D., McMechan, G.A., and Loncarevic, B.D.
1983 : The Vancouver Island Seismic Project : A COCRUST onshore-offshore study at a convergent margin ; Canadian Journal of Earth Sciences, v. 20, p. 719-741.
Green, A.G., Clowes, R.M., Yorath, C.J., Spencer, C.P., Kanasewich, E.R., Brandon, M.T., and Sutherland Brown, A.
1986 : Seismic reflection imaging of the subducting Juan de Fuca plate ; Nature, v. 319, p. 210-213.
Green, A.G., Clowes, R.M., and Ellis, R.M.
1990 : Crustal studies across Vancouver Island and adjacent offshore margin ; *in* Studies of Laterally Heterogeneous Structures Using Seismic Refraction and Reflection Data, ed. A.G. Green ; Geological Survey of Canada, Paper 89-13, p. 3-25.
Isacks, B. and Barazangi, M.
1977 : Geometry of Benioff zones : lateral segmentation and downward bending of the subducting lithosphere in island arcs ; *in* Deep Sea Trenches and Back-Arc Basins, ed. M. Talwani and W.C. Pitman. American Geophysical Union, Maurice Ewing Series, v. 1, p. 243-258.
McMechan, G.A. and Spence, G.D.
1983 : P-wave velocity structure of the Earth's crust beneath Vancouver Island ; Canadian Journal of Earth Sciences, v. 20, p. 742-752.
Riddihough, R.P.
1979 : Gravity and structure of an active margin — British Columbia and Washington ; Canadian Journal of Earth Sciences, v. 16, p. 350-363.
Spence, G.D.
1984 : Seismic structure across the active subduction zone of western Canada : unpublished PhD thesis. University of British Columbia, Vancouver, 191 p.
Spence, G.D., Whittall, K.P., and Clowes, R.M.
1984 : Practical synthetic seismograms for laterally varying media calculated by asymptotic ray theory ; Seismological Society of America, Bulletin, v. 74, p. 1209-1223.
Spence, G.D., Clowes, R.M., and Ellis, R.M.
1985 : Seismic structure across the active subduction zone of western Canada ; Journal of Geophysical Research, v. 90, p. 6754-6772.
Waldron, D.A.
1982 : Structural characteristics of a subducting oceanic plate : unpublished MSc thesis. University of British Columbia, 121 p.
Waldron, D.A., Clowes, R.M., and White, D.J.
1990 : Seismic structure of a subducting oceanic plate off western Canada ; *in* Studies of Laterally Heterogeneous Structures Using Seismic Refraction and Reflection Data, ed. A.G. Green ; Geological Survey of Canada, Paper 89-13, p. 105-113.
Yorath, C.J., Green, A.G., Clowes, R.M., Sutherland Brown, A., Brandon, M.T., Kanasewich, E.R., Hyndman, R.D., and Spencer, C.P.
1985 : LITHOPROBE, Southern Vancouver Island : Seismic reflection sees through Wrangellia to the Juan de Fuca Plate ; Geology, v. 13, p. 759-762.

Interpretation of seismic refraction data-CCSS data set I: Vancouver Island - continental margin

A. Egger[1] and J. Ansorge[1]

Egger, A. and Ansorge, J., Interpretation of seismic refraction data-CCSS data set I: Vancouver Island — continental margin; in Studies of Laterally Heterogeneous Structures Using Seismic Refraction and Reflection Data, ed. A.G. Green; Geological Survey of Canada, Paper 89-13, p. 133-150, 1990.

Abstract

This paper summarizes a contribution to the IASPEI Commission on Controlled Source Seismology workshop in Whistler, British Columbia, 1987. A set of combined refraction and reflection seismic data recorded from the continental margin off Vancouver Island to the mainland are interpreted by two-dimensional ray-tracing. The main results are: (a) there is a thickening of the lower crust between the pure oceanic area near OBS 1 and the collision zone with the continent; (b) more structural details than contained in previous models were derived for the middle crust in the collision zone between OBS 3 and OBS 5 preserving the thickness of the subducted oceanic crust; (c) the depth of the Moho under the continent is weakly constrained; (d) the transition from the lower lithosphere to the asthenosphere is more complicated than previously proposed; (e) below the subducted oceanic Moho the velocity increases only slightly over a depth range of about 15 km, followed by a 15 km thick layered transition zone with alternating high and low velocities.

Résumé

Cet article résume une contribution à la réunion de travail organisée par la Commission sur la sismologie à source contrôlée qui s'est tenue en 1987 à Whistler, Colombie-Britannique. Un jeu de données coïncidentes de sismique réfraction et de sismique réflexion recueillies sur la marge continentale au large de l'île de Vancouver et sur le continent est interprété au moyen de la méthode de traçage bidimensionnel des rayons. Les résultats principaux sont: a) on a noté un épaississement de la croûte inférieure entre la région purement marine près de la station OBS1 et la zone de collision avec le continent; b) les structures de la croûte intermédiaire dans la zone de collision entre les stations OBS3 et OBS5 ont pû être décrites avec plus de détails que dans les modèles antérieurs, tout en conservant l'épaisseur de la plaque océanique de subduction; c) la profondeur du Moho sous le continent est faiblement définie; d) la transition entre la lithosphère inférieure et l'asthénosphère est plus complexe que dans les modèles précédents; e) sous le Moho océanique, dans la région de la subduction, l'accroissement de vitesse est minime sur une profondeur d'environ 15 km. Cette zone est suivie par une région de transition d'environ 15 km d'épaisseur, caractérisée par une alternance de couches à haute et faible vitesses.

[1] Institute of Geophysics, ETH Hoenggerberg, CH-8093 Zürich, Switzerland.

INTRODUCTION

This contribution to the IASPEI Controlled Source Seismology workshop in Whistler, British Columbia, 1987, summarizes the interpretation and results derived from the combined refraction and reflection seismic data set I. The data set included seismic sections from three OBS stations that recorded a series of offshore explosions across the continental margin, and four record sections obtained from stations on Vancouver Island, on islands in the Strait of Georgia, and on the mainland (shotpoints J1, P8, P13 and P19 ; *see* Fig. 5 of Green et al., 1990).

The interpretation was carried out by means of the program package RAY87, which was originally developed by Luetgert (Hill et al., 1985) based on the ray theoretical technique of Červený et al. (1977) and modified recently by Sierro (1988). The program allows interactive two-dimensional ray tracing and computes synthetic seismograms for the same structure. The velocity model is defined by layers of variable depth, thickness and lateral extent. The velocity can vary vertically and laterally at given vertical grid lines along the boundaries of the layers and is interpolated linearly within the layers.

The lithospheric cross-section along the profile was determined by first interpreting the OBS data in the southwest, then the continental part in the northeast, and finally combining the two sections for the central transition zone. All models shown were constrained only by the travel times. The synthetic sections were calculated subsequently without modifying the structure since the fit with observed amplitudes seemed to be satisfactory. The synthetic and observed amplitudes are plotted with the same distance-dependent scaling factor.

OBS DATA

The true amplitude record sections are characterized by rather low amplitude first arrivals (Fig. 1 to 4). The travel times of these weak, but obvious, first arrivals were determined by correlating the next phase, which arrives with a relatively constant time delay and larger amplitude. The starting model was set up with reference to the structural model derived by Waldron (1982) from the same data, and the marine seismic reflection section. This model was then modified iteratively to match calculated and observed travel times. The ray-tracing and travel time plots in Figures 1 to 3 contain only refracted rays. Reflections are excluded from these plots in order to maintain clarity, but they are included in the plotted synthetic sections. The observed large amplitudes that appear as secondary arrivals are interpreted as over-critical reflections from the Moho. The signal length of about 0.8 s must be a source function effect. Extraordinary large amplitudes at 40 km and 55 km distance on the OBS 3 and OBS 5 data, respectively (Fig. 2 and 3), can probably be attributed to local structural features. Figure 4 shows the derived velocity-depth section for the marine part of the profile ; no pronounced low velocity zone was found in this section. The main differences between the model in Figure 4 and that of Waldron (1982) are :

— There is a thickening of the lower oceanic crust 20 to 50 km from OBS 1 (Fig. 1 and 4), included to explain the slightly shorter travel times observed there. This reduction of travel time is observed on all three OBS record sections.

— The continental and oceanic crust between OBS 3 and OBS 5 (Fig. 3 and 4) contains more detail relative to the "mélange unit" derived by Waldron (1982). This approximately preserves the thickness of the subducted oceanic crust and explains the apparent velocity of about 6 km/s from 25 to 40 km distance (Fig. 4).

LAND DATA

The upper part of the continental crust at the northeast end of the profile was determined from recordings of shot J1 (Fig. 5). Unfortunately, the crustal structure derived for this section, especially the Moho depth, is the most uncertain of the entire model. No reverse observations were available for this section and the data (Fig. 5) show few structural details. This fact is also expressed in the poor fit of calculated and observed amplitudes.

The marine and continental sections were fixed during modeling of the deep structure in the transition zone (Fig. 6 to 8 and 10 to 12). The LITHOPROBE land reflection data were used mainly to constrain the shape of the intermediate block in the upper crust and the upper boundary of the subducting oceanic crust (Fig. 6 to 9). Major differences between this model, A, and that of Spence et al. (1985) are :

— Our model does not require a low-velocity zone in the lower continental crust. Although the data set available to us can be explained without such a feature, additional data may lead to a low-velocity zone as shown by Spence et al. (1985). The depth to the Moho is only weakly constrained.

— In contrast to the interpretation of Spence et al. (1985), the strong phases observed on Vancouver Island and the mainland (Fig. 7 and 8) are interpreted as reflections from two different interfaces. The early weak but continuous first arrivals are modeled as "Pn" phases from below the oceanic Moho.

In model A the strong reflections at 200 to 260 km on Vancouver Island (Fig. 7 and 8) originate from an interface in the lower lithosphere where the velocity increases slightly over a short depth range and then decreases by about 0.3 km/s over a depth interval of 12 km. The subsequent abrupt velocity increase and the slightly different slope at the deeper interface causes the second strong reflection starting at 280 km on the mainland (Fig. 7 and 8). The inadequate determination of crustal thickness under the continental section from shotpoint J1 (Fig. 5) leaves some flexibility with respect to depth of Moho and Pn velocity for the interpretation of record sections from shots P8, P13 and P19. We did not use the record section from shot P8 (Fig. 6) in our modeling.

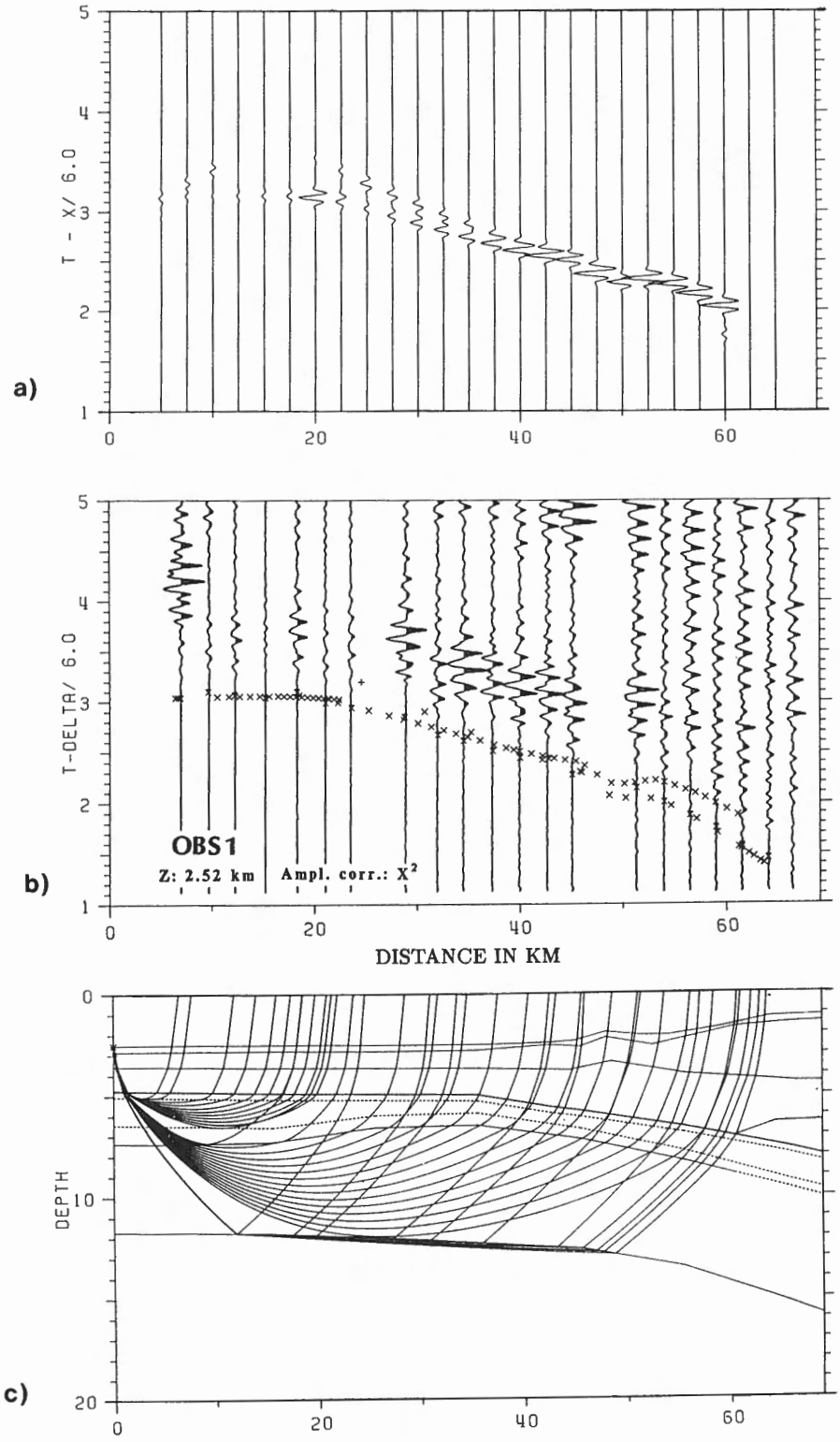

Figure 1. Record section (b) for OBS1 with true amplitude multiplied by distance squared. (+) and (x) indicate calculated travel times of reflections and refractions, respectively, for rays traced in the structural model (c). (x) on the recorded traces denotes correlated first arrivals. Upper section shows the synthetic seismograms (a) plotted with the same amplitude scaling as the data.

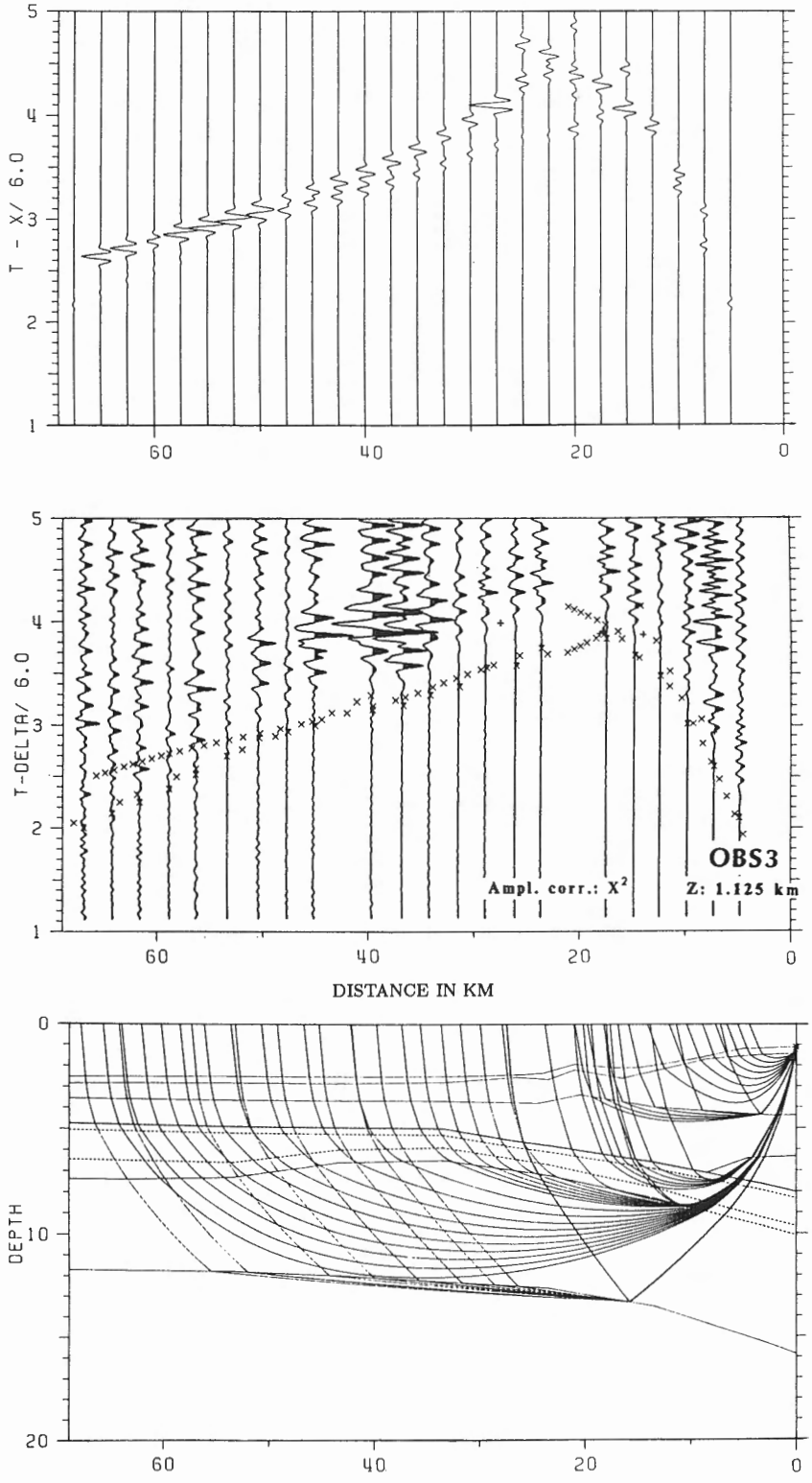

Figure 2. Record section, ray-tracing model, and synthetic seismograms for OBS3.

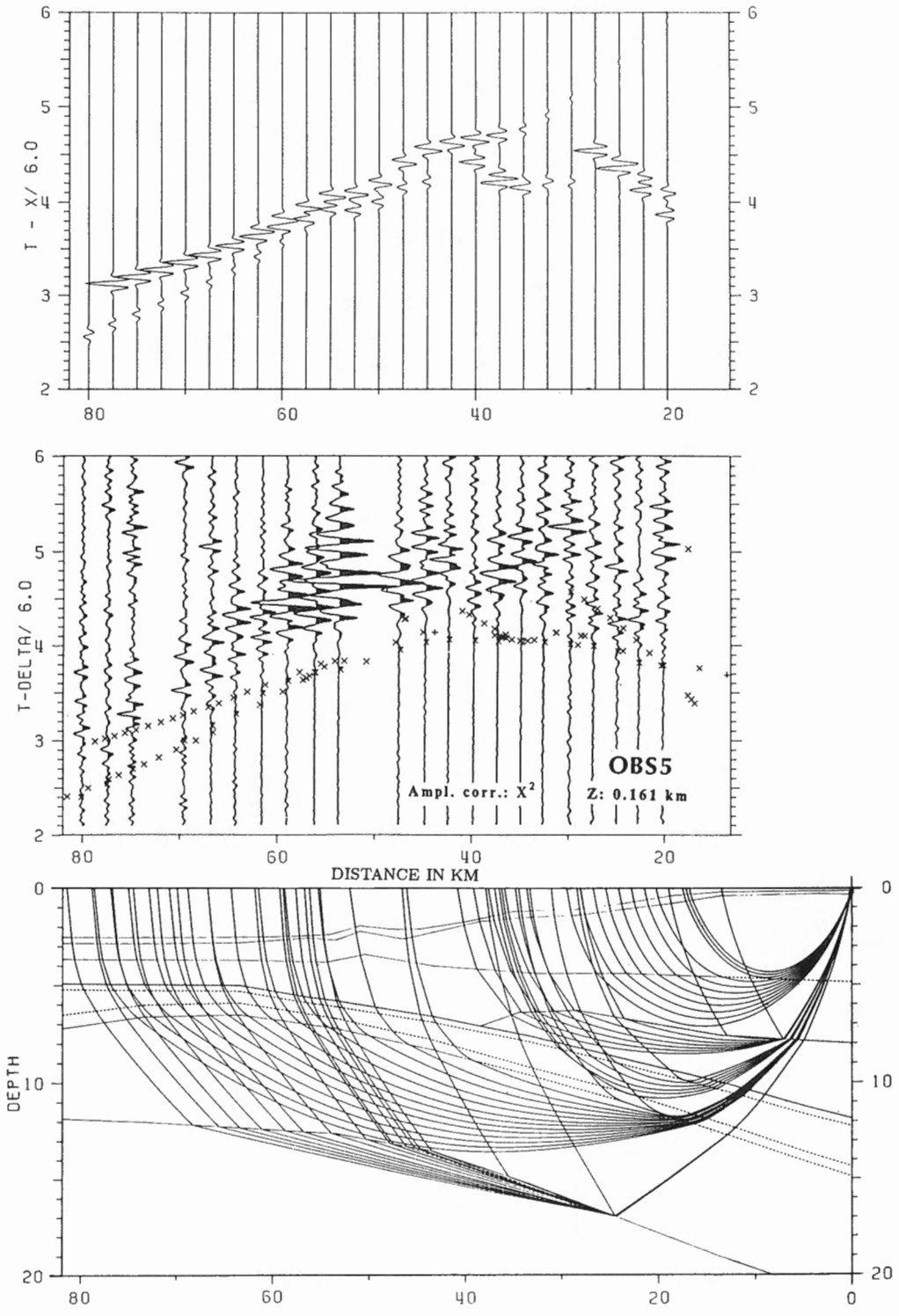

Figure 3. Record section, ray-tracing model, and synthetic seismograms for OBS5.

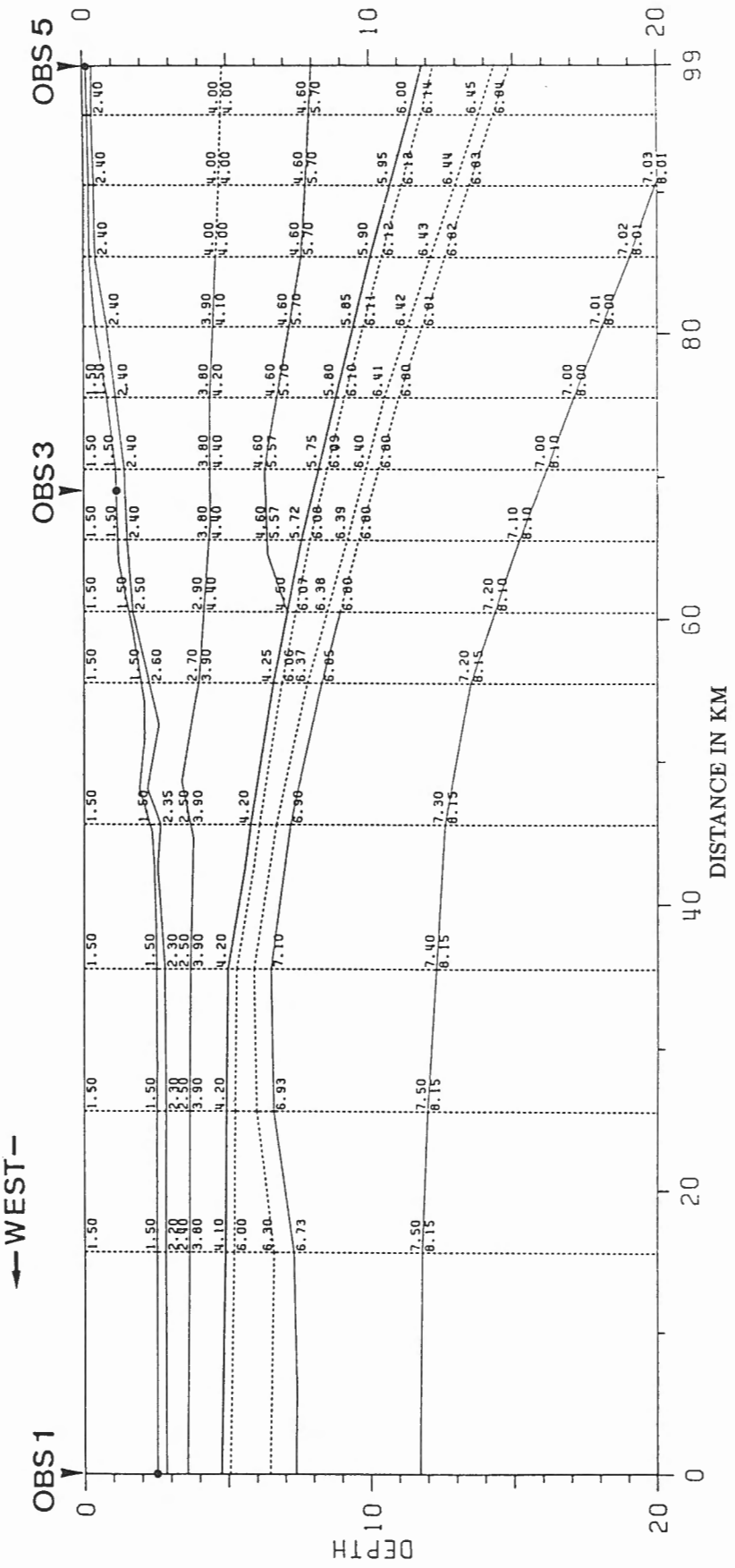

Figure 4. Crustal cross-section with P-wave velocities between OBS1 and OBS5.

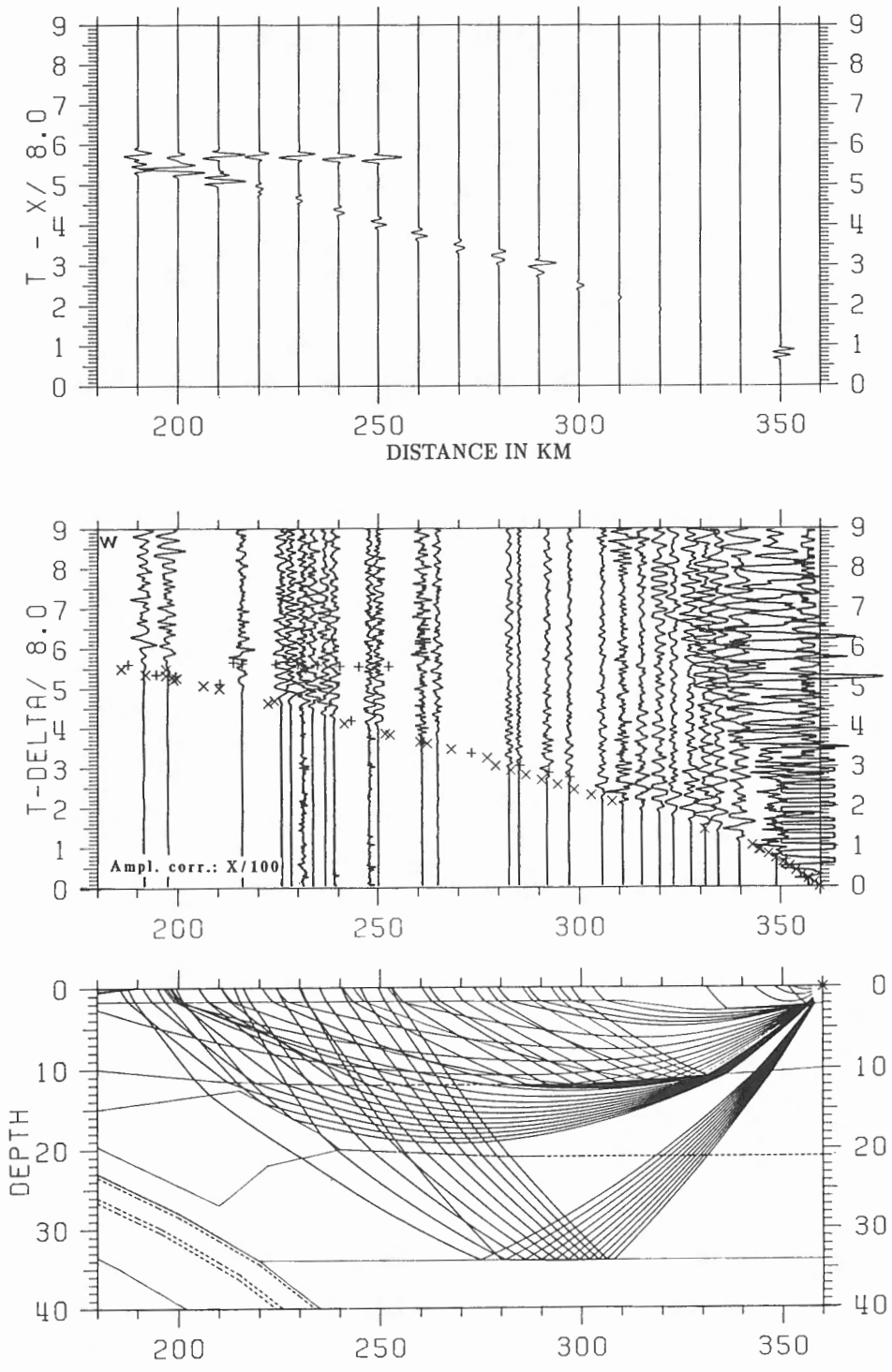

Figure 5. Seismogram section recorded on land from shot J1 with ray-tracing model and synthetic seismograms. Distances are measured from shotpoint P19.

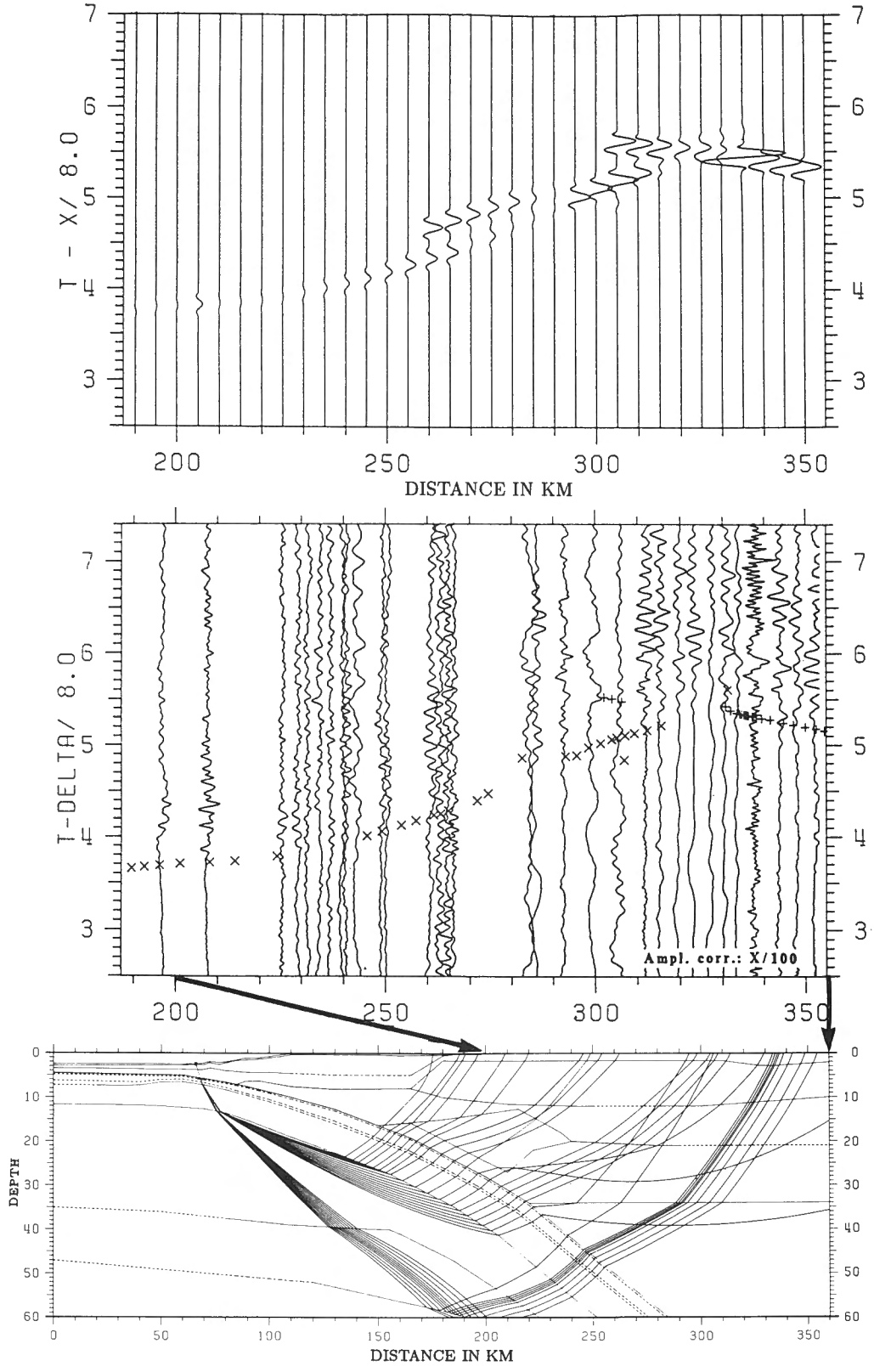

Figure 6. Seismogram section recorded on land from shotpoint P8 with ray-tracing model A and synthetic seismograms.

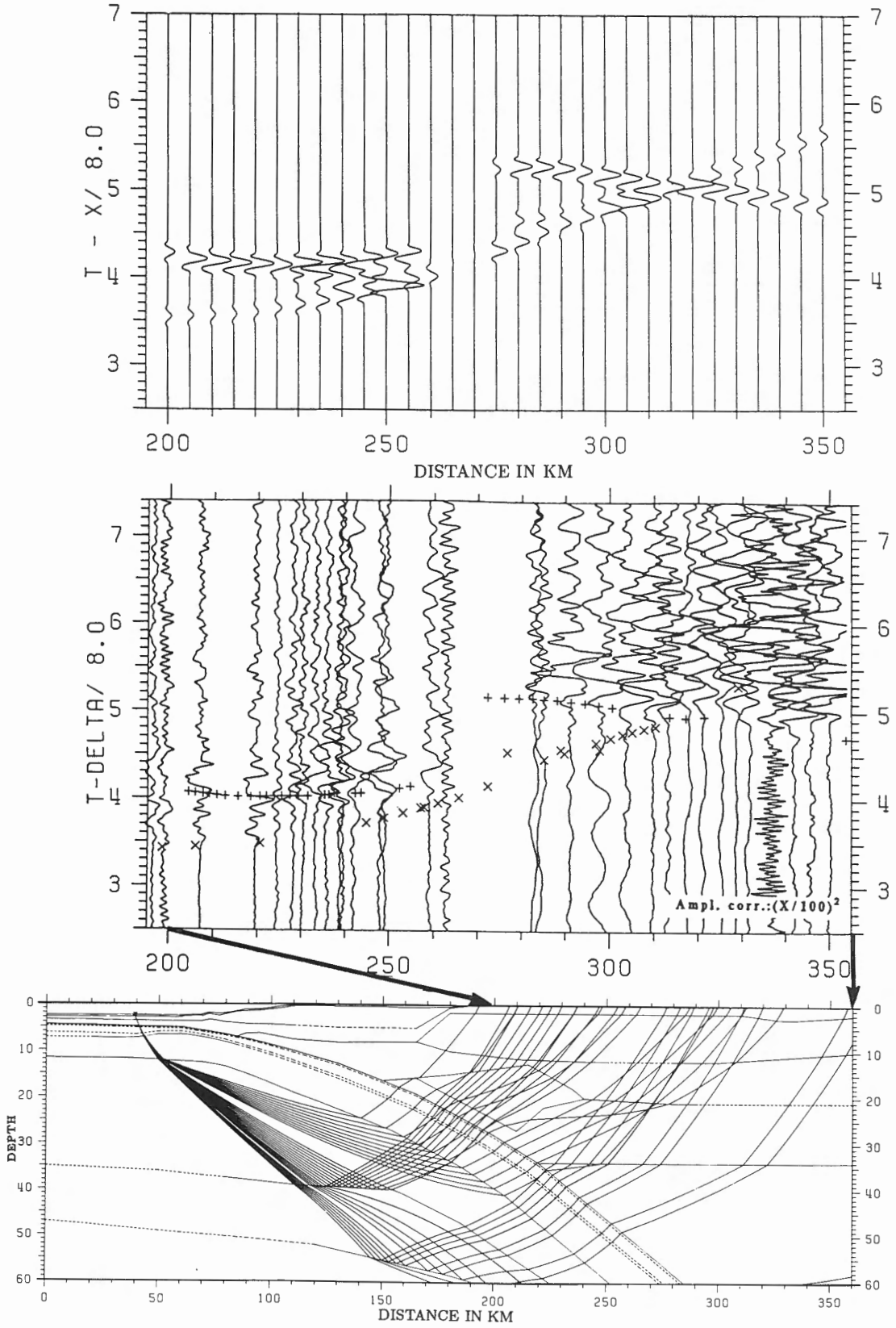

Figure 7. Seismogram section recorded on land from shotpoint P13 with ray-tracing model A and synthetic seismograms.

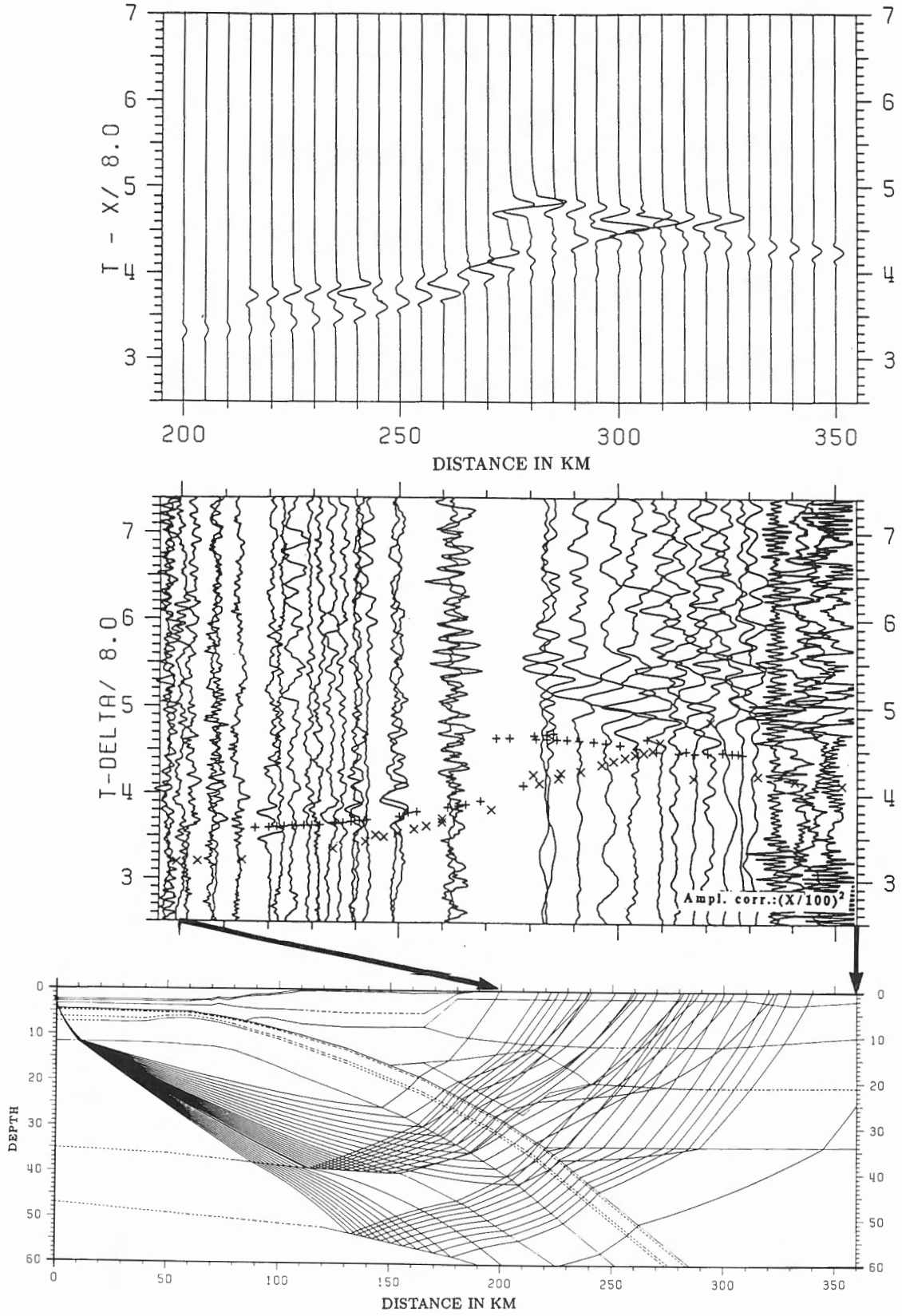

Figure 8. Seismogram section recorded on land from shotpoint P19 with ray-tracing model A and synthetic seismograms.

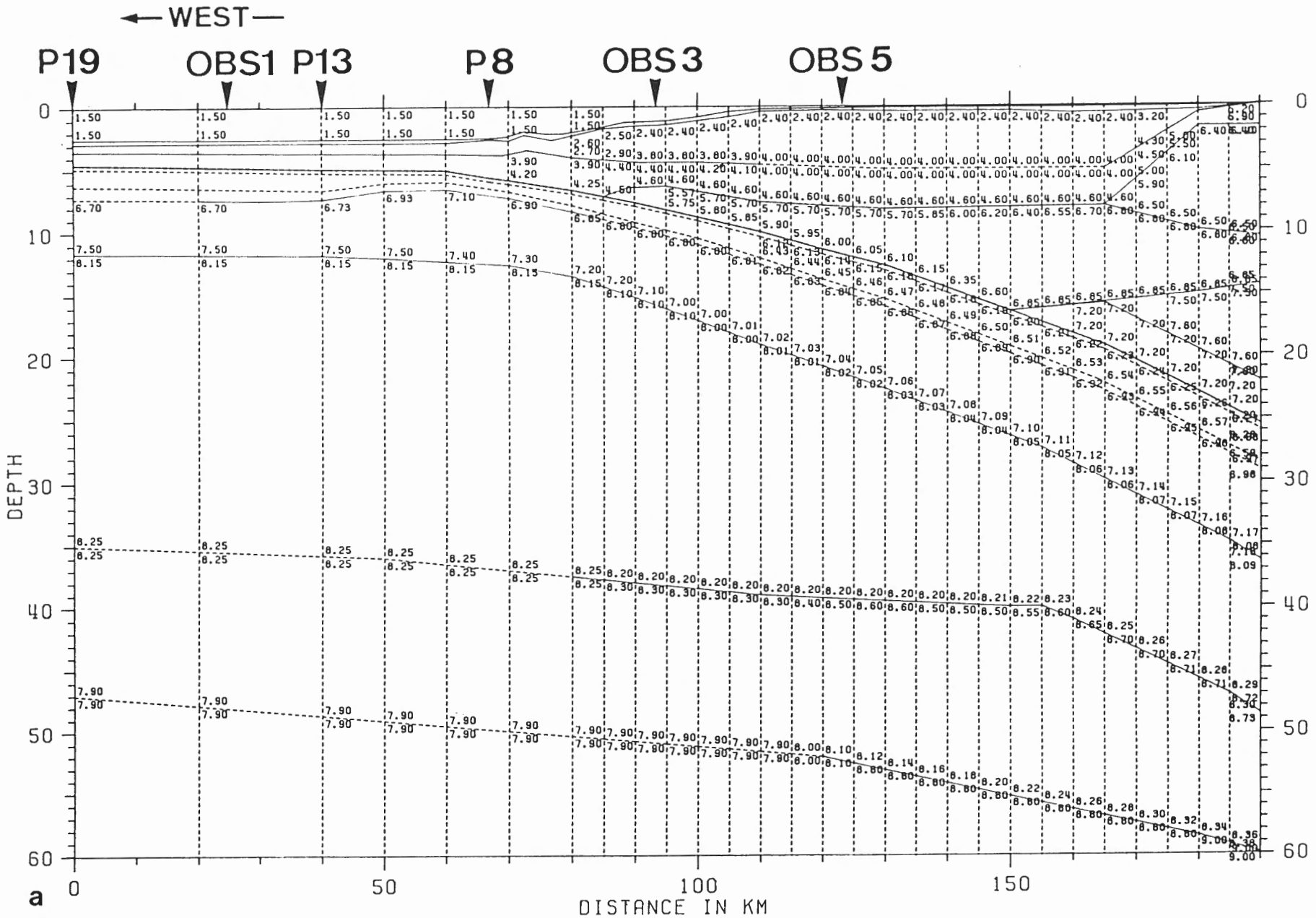

Figure 9a. Lithospheric cross-section of model A with P-wave velocities between shotpoints P19 and J1 with 20 km overlap betwen (a) and (b).

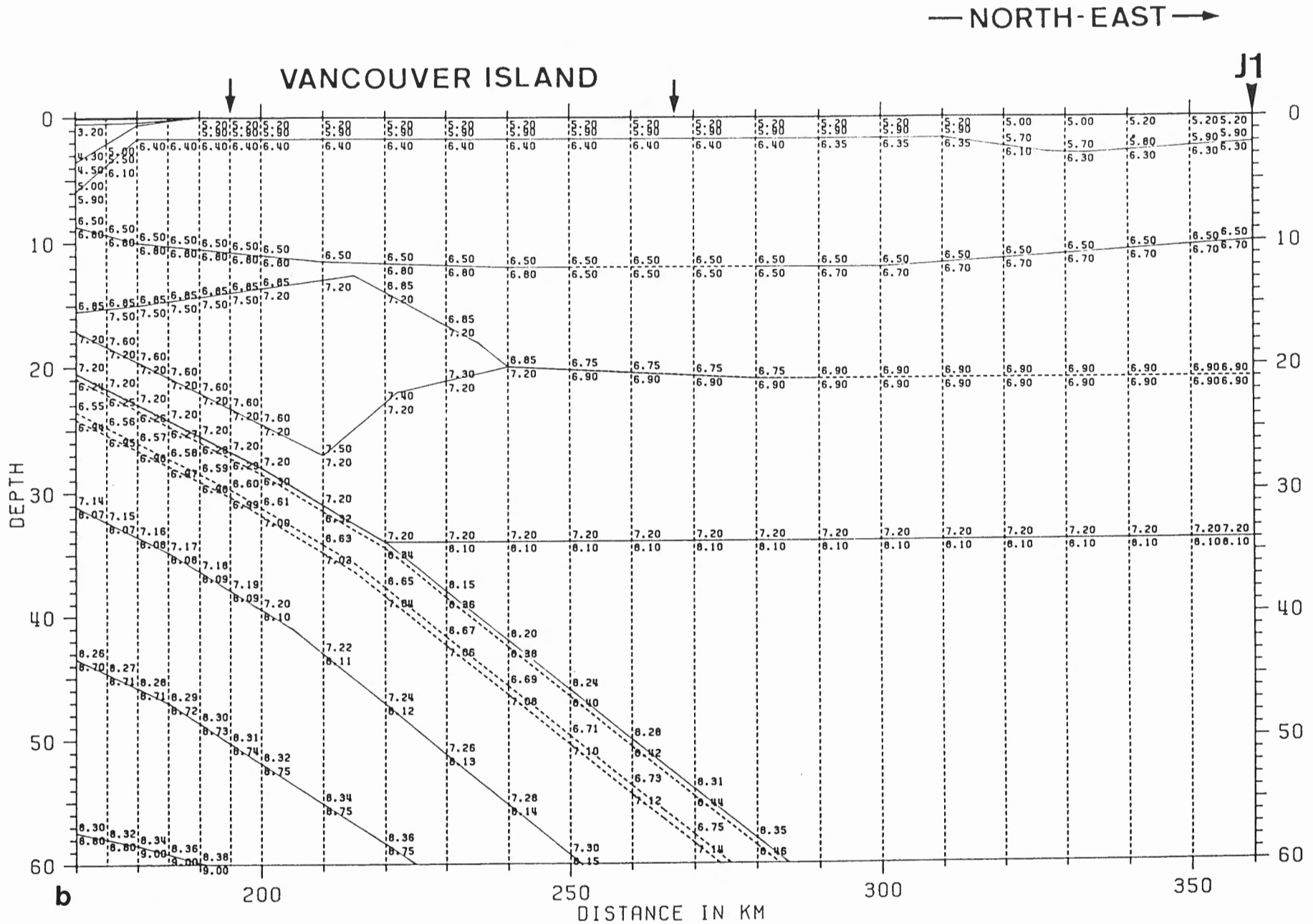

Figure 9. Continued

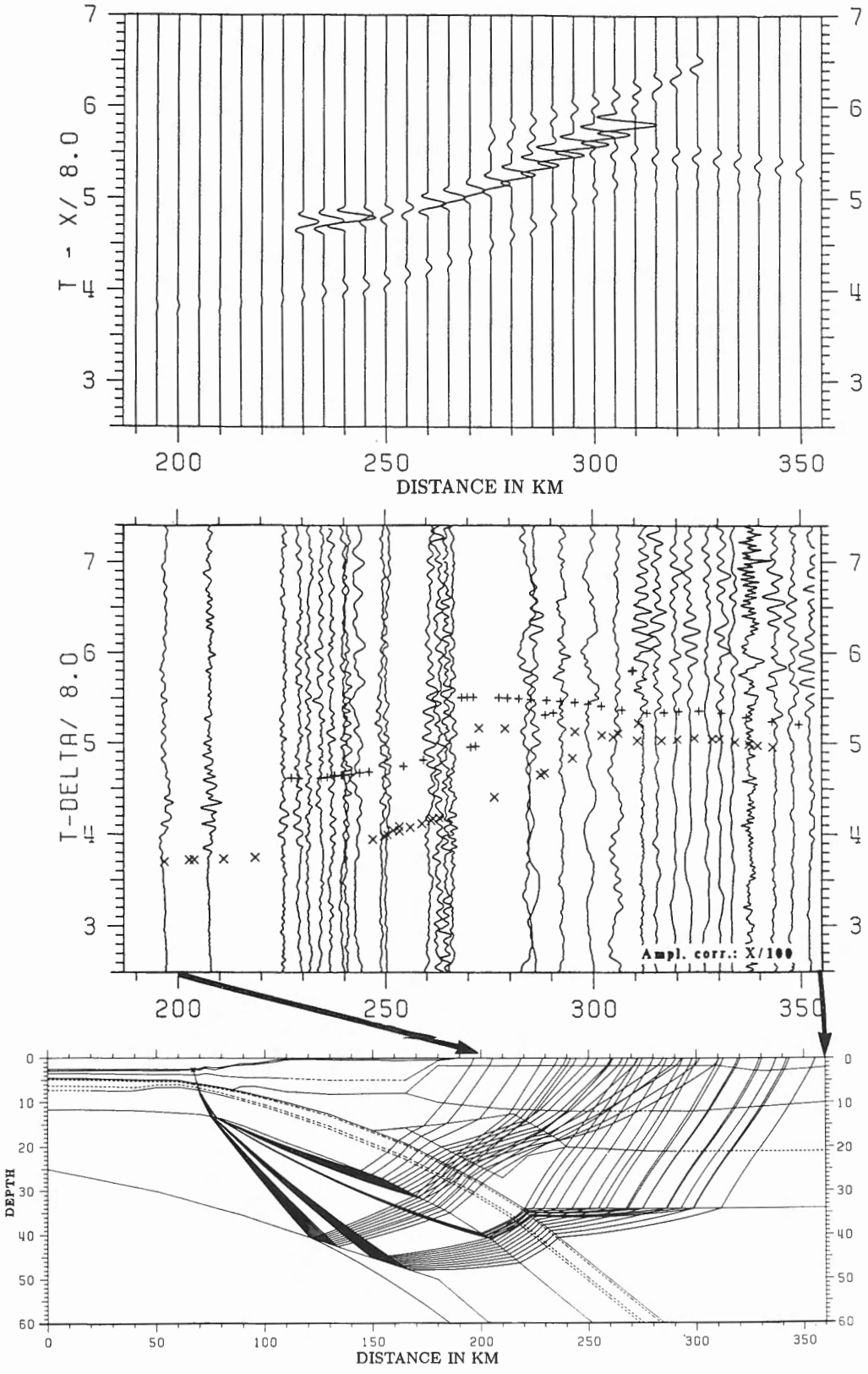

Figure 10. Seismogram section recorded on land from shotpoint P8 with ray-tracing model B and synthetic seismograms.

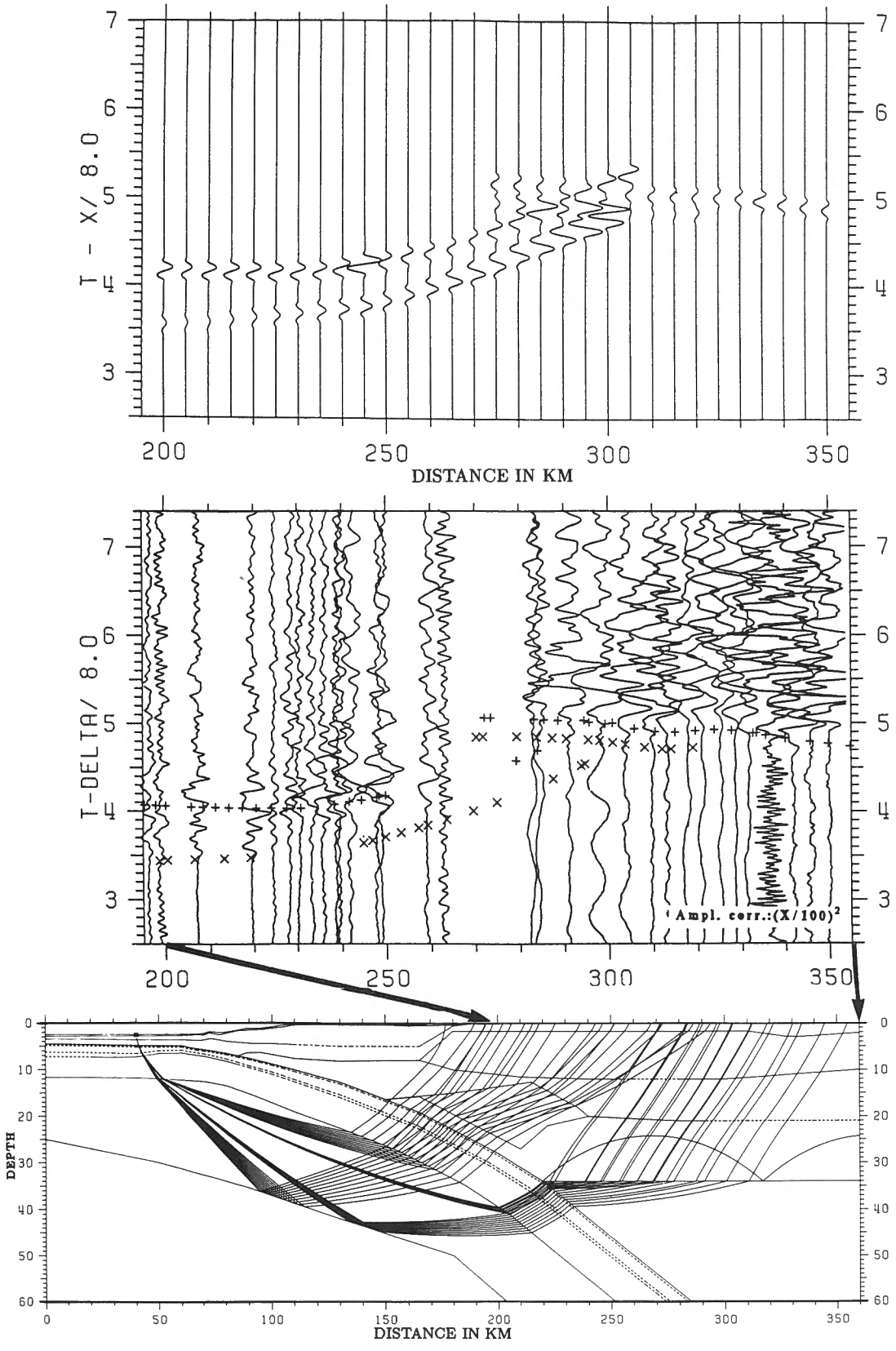

Figure 11. Seismogram section recorded on land from shotpoint P13 with ray-tracing model B and synthetic seismograms.

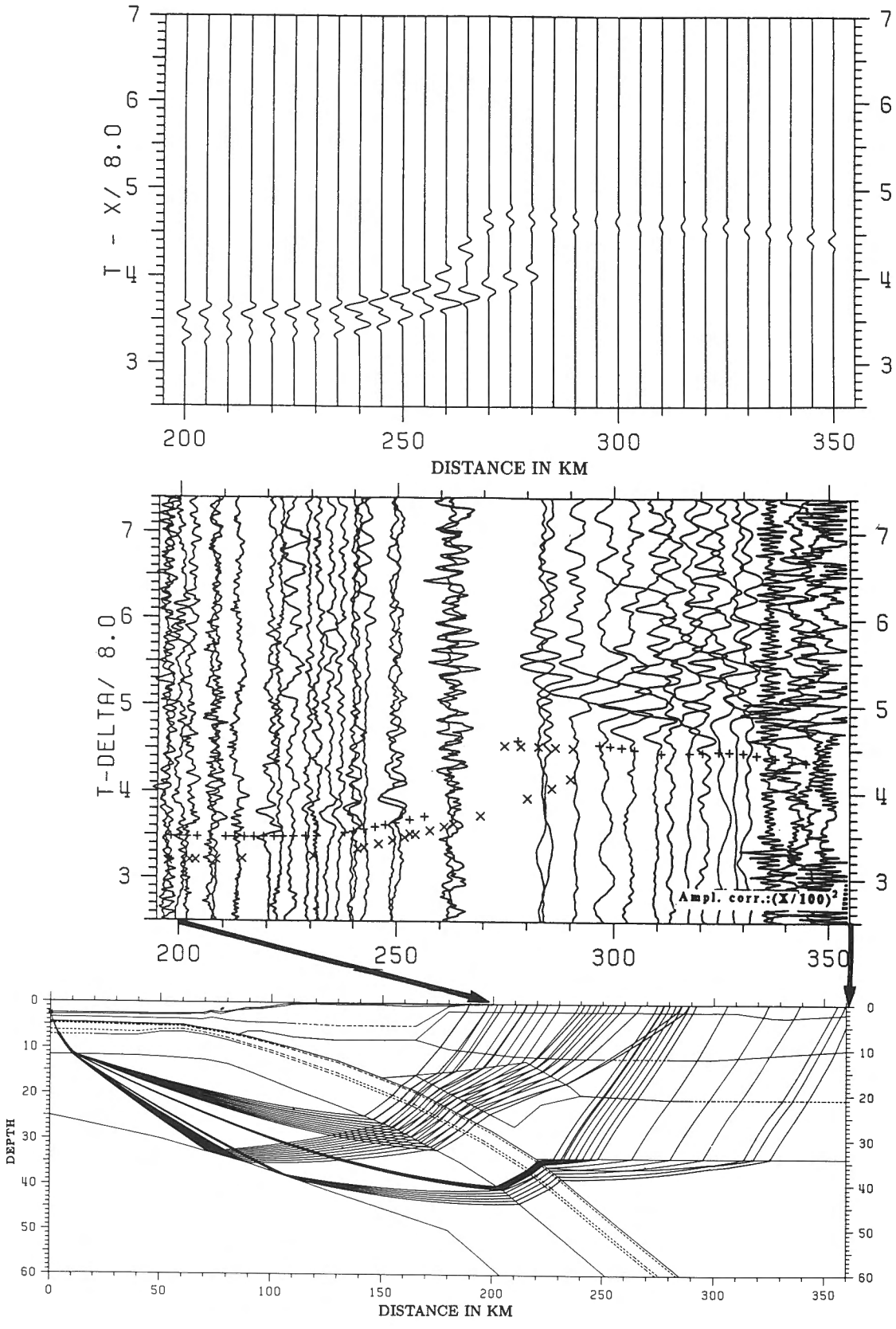

Figure 12. Seismogram section recorded on land from shotpoint P19 with ray-tracing model B and synthetic seismograms.

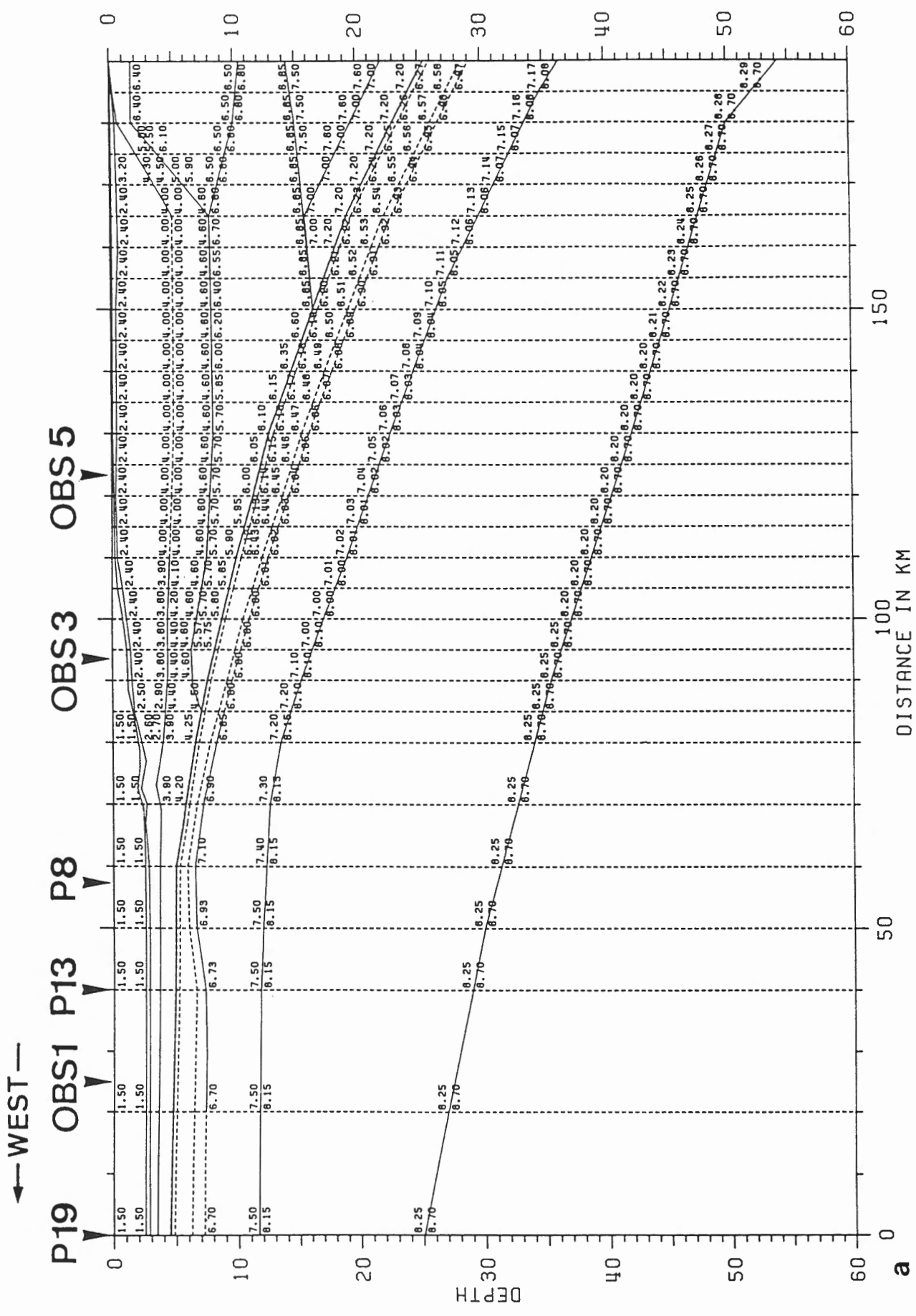

Figure 13. Lithospheric cross section of model B with P-wave velocities between shotpoints P19 and J1 with 20 km overlap between (a) and (b).

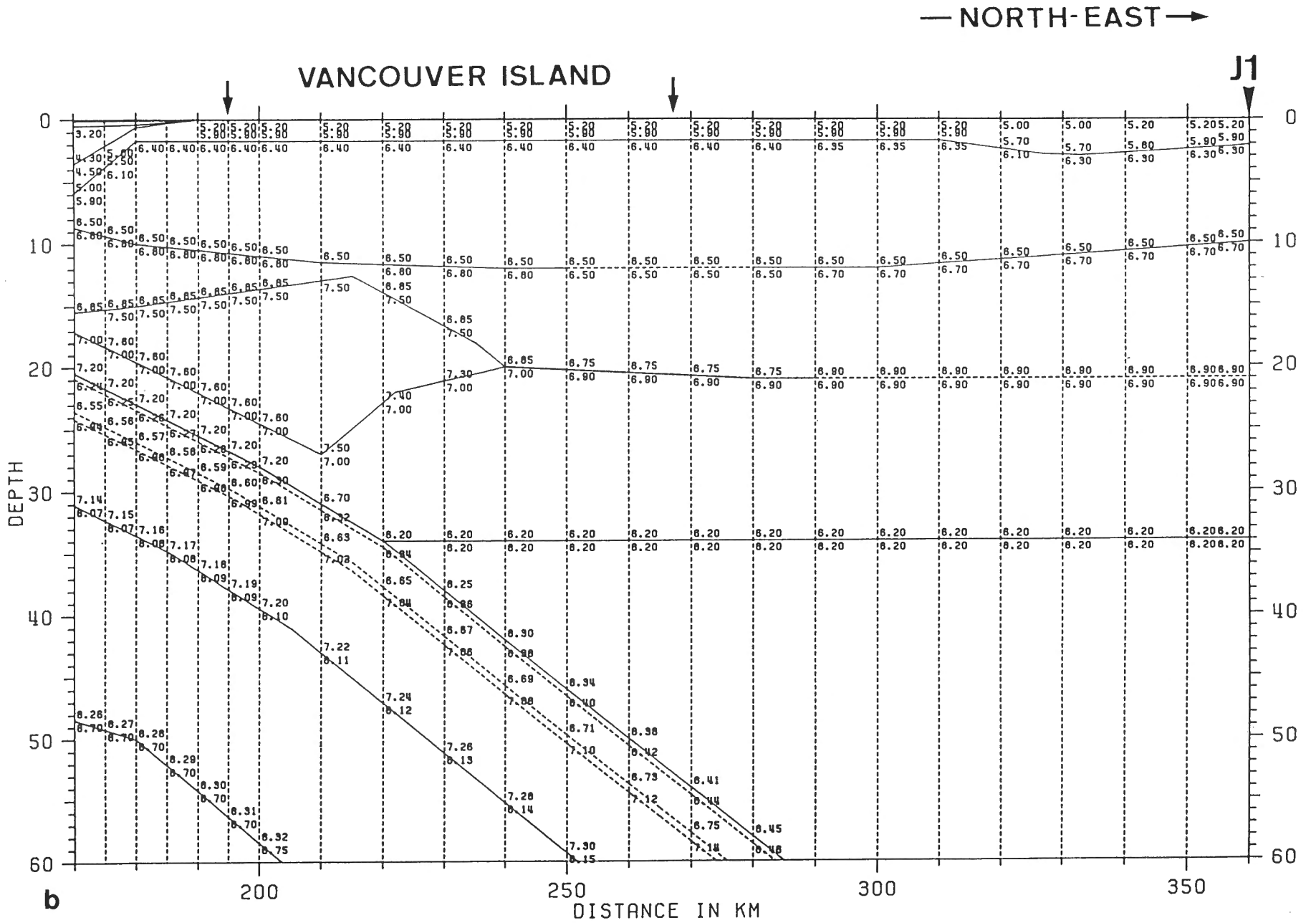
— NORTH-EAST →
VANCOUVER ISLAND
J1
DEPTH
DISTANCE IN KM
0
10
20
30
40
50
60
200
250
300
350
b

As an alternative to model A (Fig. 9), we have also tried to interpret the data with a second model, B (Fig. 10 to 13), which is similar to the one presented by Spence et al. (1985) with a simple lithosphere-asthenosphere boundary. Although the calculated travel times are almost the same, the synthetic amplitudes for the phases from the lithosphere-asthenosphere boundary are significantly smaller for model B than those observed, especially at larger distances. For computational reasons the synthetic seismograms were calculated with a positive velocity contrast of the same amount (Fig. 13) as the negative velocity contrast proposed by Spence et al. (1985) at this boundary. The negative velocity contrast in the Spence et al. (1985) model would produce even smaller amplitudes.

CONCLUSIONS

Our model A may indicate that the lithosphere-asthenosphere transition is not a single interface but occurs in a more complicated way. Only a long profile along strike of the subduction zone can clarify its structure. The transition from lithosphere to asthenosphere occurs in model A in two steps. Although this may still be too schematic, the transition proposed in model B, with only one sharp boundary, is even more simplified and can probably be dismissed on the basis of the amplitude study.

ACKNOWLEDGMENT

Contribution No. 579, Institute of Geophysics, ETH, Zürich

REFERENCES

Červený, V., Molotkov, I.A., and Pšencík, I.
1977 : Ray Method in Seismology ; Charles University Press, Prague, 214 p.

Green, A.G., Clowes, R.M., and Ellis, R.M.
1990 : Crustal studies across Vancouver Island and adjacent offshore margin ; *in* Studies of Laterally Heterogeneous Structures Using Seismic Refraction and Reflection Data, ed. A.G. Green ; Geological Survey of Canada, Paper 89-13, p. 3-25.

Hill, D.P., Kissling, E., Luetgert, J.H., and Kradolfer, U.
1985 : Constraints on the upper crustal structure of the Long Valley-Mono Craters Volcanic Complex, eastern California, from seismic refrac-tion measurements ; Journal of Geophysical Research, v. 90, p. 11135-11150.

Sierro, N.
1988 : Regionale Struktur der Erdkruste in der Nordschweiz ; Ph.D. thesis, Swiss Federal Institute of Technology, Zürich, 250 p.

Spence, G.P., Clowes, R.M., and Ellis, R.M.
1985 : Seismic structure across the active subduction zone of western Canada ; Journal of Geophysical Research, v. 90, p. 6754-6772.

Waldron, D.A.
1982 : Structural characteristics of a subducting oceanic plate ; M.Sc. thesis, University of British Columbia, Vancouver, 121 p.

Migration and amplitude analysis of deep seismic reflection data: processing results of CCSS data sets II and III

Bernd Milkereit[1], Carl Spencer[1] and Louis J. Mayrand[1]

Milkereit, B., Spencer, C. and Mayrand. L.J., Migration and amplitude analysis of deep seismic reflection data: processing results of CCSS data sets II and III; in Studies of Laterally Heterogeneous Structures Using Seismic Refraction and Reflection Data, ed. A.G. Green; Geological Survey of Canada, Paper 89-13, p. 151-164, 1990.

Abstract

New migration and amplitude analysis schemes are applied to multichannel seismic reflection data recorded across Vancouver Island. Based on an integrated interpretation of migrated seismic sections with information from quality control and amplitude decay studies it is concluded that many mid-crustal amplitude anomalies (''bright spots'') along LITHOPROBE's Vancouver Island line 1 are caused by local inhomogeneities.

Résumé

De nouveaux algorithmes de migration et d'analyse d'amplitude sont utilisés pour le traitement des données de sismique réflexion multicanale enregistrées dans l'île de Vancouver. L'interprétation intégrée des coupes sismiques migrées, des études de contrôle de qualité et de dégénérescence des amplitudes permettent aux auteurs de conclure que plusieurs anomalies d'amplitude (''points brillants'') au niveau de la croûte moyenne le long de la Ligne 1 dans l'île de Vancouver sont dues à des perturbations locales des propriétés acoustiques.

[1] Continental Geoscience Division, Geological Survey of Canada, Ottawa, Ontario, K1A 0Y3.

MOTIVATION

Early structural interpretations of Vancouver Island seismic reflection data (Yorath et al., 1985; Green et al., 1986; Clowes et al., 1987) were based on unmigrated line drawings taken from amplitude balanced sections. Reprocessing of the data using near-surface velocity analyses (Mayrand et al., 1987), pre-and poststack migration (Milkereit, 1987a; Green et al., 1987), and true amplitude processing (Mayrand and Milkereit, 1988) helped to resolve some of the conflicts between the interpretation of the surface geology and interpretations of the seismic reflection data. Migration and true amplitude processing results also revealed structural complexity and lateral variations in reflection strength.

Here we use a depth migration of LITHOPROBE seismic reflection line 1 data (CCSS data set II) to identify local amplitude anomalies. Then, as part of a study to determine the feasibility of applying true amplitude processing to the data, we employ a quality control scheme to assess noise characteristics and reject noisy traces within shot gathers. The results are used to perform amplitude decay studies on selected shot gathers and identify local amplitude anomalies (''bright spots''). Finally, a new processing sequence is applied to Vancouver Island line 1 data to produce a new stacked section. Our results indicate that many of the prominent reflections from upper and midcrustal depths along line 1 can be interpreted as strong diffracted events caused by local inhomogenities.

MIGRATION RESULTS

Migration is an essential step in the use of seismic data to map deep structures. The migration of deep reflection data has to deal with low signal-to-noise ratios, steeply dipping events, spurious reflections, and large scale diffraction patterns. In stacked sections continuous dipping reflectors and diffraction patterns are always defocussed so their apparent lengths are frequently overestimated. As shown by Milkereit (1987a), focussing of seismic energy is important in deep crustal reflection profiling because it may provide hints of large impedance contrasts in the crust. Focussing becomes important where apparent dips in stacked sections exceed 20°. Gently and steeply dipping reflections are well represented in the stacked seismic section of Vancouver Island line 1 (Fig. 14 *in* Green et al., 1990a; this figure is contained in the pocket at the back of this volume) and therefore the structural interpretation should be based on migrated data. A description of CCSS workshop topic II is given in Green et al. (1990b).

Migration results are affected by properties of the data such as spatial sampling, end effects, frequency content, phase variations (static errors), and by restrictions in the migration algorithm such as dip limitations, approximations involved in allowing for vertical and horizontal velocity variations, and the finite width of migration apertures. The results of applying conventional frequency-wavenumber (f-k) migration (Stolt, 1978) to the data are shown in Figure 15 of Green et al. (1990a). Reflected energy is concentrated in two bands of dipping reflections (labelled C and E) and in a region to the southwest of the Beaufort Range Fault Zone at 2-4 s travel time. Most of these shallow and midcrustal events appear to be small-scale diffraction patterns in the unmigrated section. Migration noise (smiles in Fig. 15 of Green et al., 1989a) may be due to lateral variations in reflector quality and variable noise levels.

Depth migration in combination with multichannel slowness filtering (SWDS: slowness weighted diffraction stack migration) improves the signal-to-noise ratio of seismic sections compared to conventional migration schemes (Milkereit, 1987a). Diffraction curves based upon a specified velocity model determine those slowness components (Milkereit, 1987b) in the distance-time (x,t) domain that originate at a subsurface point (x,z). Figure 1 shows the trace envelope or ''reflection strength'' (Taner and Sheriff, 1977) of data set II calculated using SWDS migration on amplitude balanced data. A constant gradient velocity model with 6.0 km/s at the top and 7.0 km/s at 30 km depth was used. Much of the uncorrelated background noise has been removed by the SWDS algorithm. Compared to the f-k migration shown in Figure 15 of Green et al. (1990a), the SWDS migration shows significantly less migration noise (smiles). Another important result concerns the focussing of diffracted energy. In the migrated sections the amplitudes of the C and E reflectors are locally about 20 dB above background levels. In addition, the shallow reflections under the Beaufort Range Faults at 5-10 km depth (labelled BS2 in Fig. 1) and between the C and E reflections at 14 km depth (labelled BS1) show strong amplitude anomalies. The width of the two amplitude anomalies (''bright spots'') identified in the depth migrated section does not exceed 5 km. Further analyses of these features will be based on true amplitude data.

AMPLITUDE ANALYSIS OF SHOT GATHERS

True amplitude processing of reflection seismic data is now well established in hydrocarbon exploration and is increasingly used to support the interpretation of deep crustal seismic reflections (de Voogd et al., 1986). The study of lateral variations in amplitude decay can be used to estimate signal penetration and to explain the interpretation of non-reflective zones (Mayer and Brown, 1986). Previous applications of true amplitude processing to shorter (20-30 km) Vancouver Island reflection profiles (lines 2 and 4) revealed strong mid-crustal amplitude anomalies and confirmed the overall high reflection strength of the E-reflector (Mayrand and Milkereit, 1988).

True amplitude processing requires continuous quality control and efficient trace editing. The size of crustal seismic reflection data sets and the large dynamic range of amplitudes are reasons for seeking an alternative to conventional manual editing of traces. Here we discuss the results of applying an automated quality control scheme (Mayrand and Milkereit, 1988) to the shot gathers of Vancouver Island line 1, CCSS workshop topic III (*see* Green et al., 1990b for details). The quality control algorithm is based on signal and noise power estimates for each seismic trace. Graphic displays of these estimates help to identify local source and receiver coupling problems and variable noise conditions, and, ultimately, to remove noisy traces from the processing sequence.

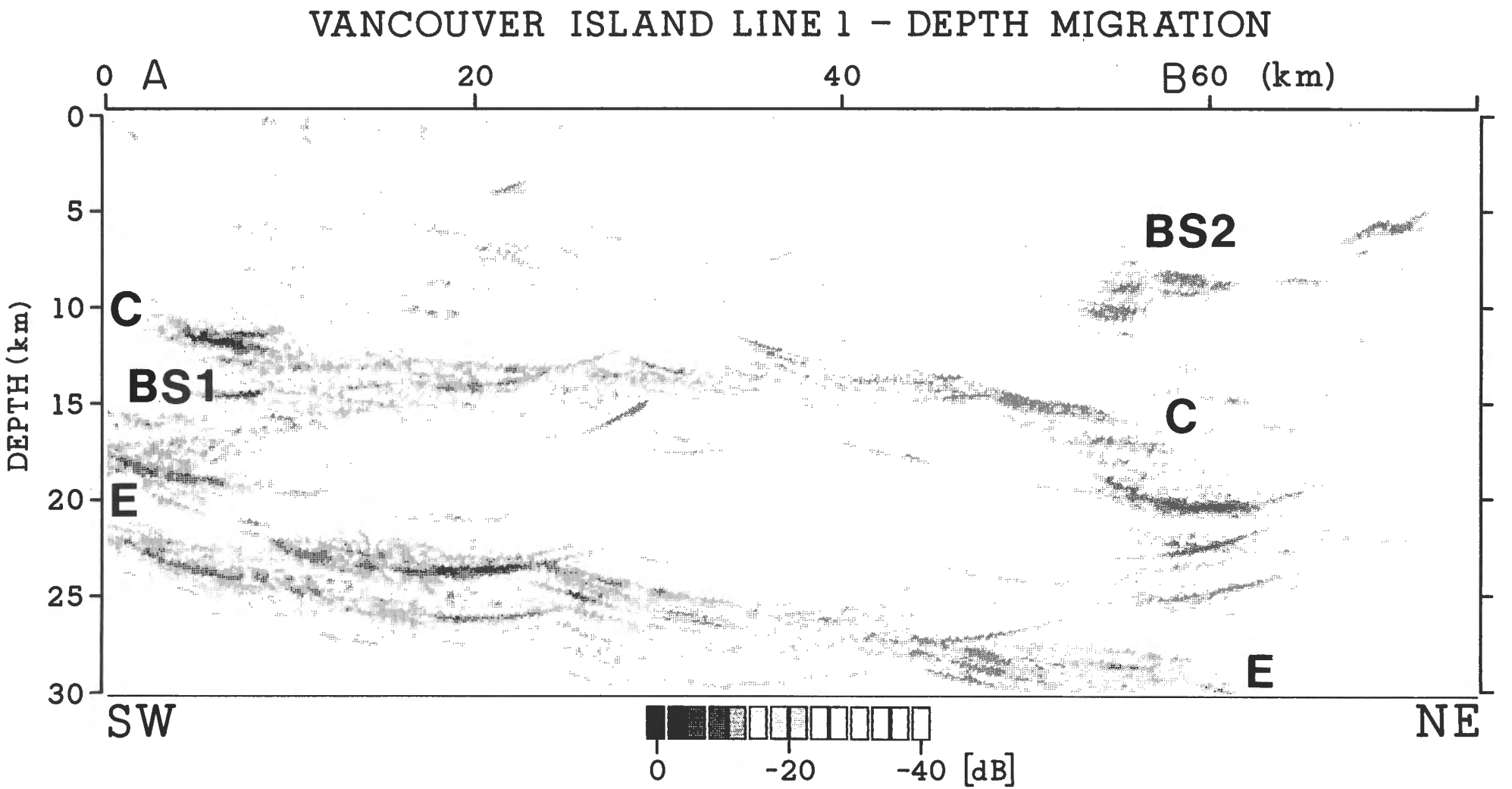

Figure 1. Depth migration of CCSS data set II. The display of apparent "reflection strength" (trace envelope) indicates focusing of energy at the C and E reflector levels and highlights isolated amplitude anomalies, labeled BS1 and BS2.

Quality Control of Deep Crustal Data

The algorithm used for the trace editing was first presented by Mayrand and Milkereit (1988). Noise is assumed to be statistically independent from trace to trace, with zero mean and a variance assumed constant with time for each trace. Such a model is applicable to data sets for which a noise rejection algorithm has taken care of time-dependent noise bursts during acquisition. The data from the Vancouver Island surveys satisfy these requirements since recording equipment with in-field noise rejection capabilities and vertical sweep summation was employed (Clowes et al., 1987). Scans of appropriate time-offset windows were used to give estimates of signal amplitude and noise variance for each seismic trace in order to indentify those traces with little or no signal and those traces with unacceptable noise levels. Two strategies were used:

1. Abnormally low amplitudes of P-wave first arrivals were considered to be reliable indicators of weak or absent reflections at later recording times. Shot gathers were scanned trace-sequentially for their maximum amplitude within the P-wave window. Results of the scans are displayed in Figure 2a as a surface stacking chart for 138 shots and 280 surface stations of CCSS data set III. Maximum amplitudes within the P-wave window for all traces recorded at the same field station are shown along a vertical line on the chart, whereas those for a shot gather are shown along a horizontal line. The amplitude information in the surface stacking chart can be considered as a 138 x 280 pixel digital image I(x,y). A 2-dimensional median filter (Huang et al., 1979) was applied to I(x,y) to give the spatially smoothed image I^F (x,y) in Figure 2b. The approximate position of the vibrators within the 120-geophone station array is indicated by the presence of a three station gap between the sources and the nearest receivers for vibration points (VP) greater than 60. For VPs less than 60, there was no gap and every geophone group was a VP. The scan shows a physically reasonable offset-dependent decay of amplitudes within each shot gather. It may be described approximately by the relation

   $$A(x) \approx A_o\, x^n \quad (-.5 > n > -2.0).$$

   Only small-scale spatial variations in amplitude are observed in these data.

2. Noise power estimates for each trace were used to analyze noise sources and recording conditions. It was assumed that trace amplitudes at late recording times (14 to 16 s travel-time) represented background noise with very little signal and could thus be used to estimate the noise power of a trace. The surface stacking chart of noise power estimates (Fig. 3a) and the median filtered version (Fig. 3b) show that for shots 1 to 60 all traces recorded between stations 1 and 60 were abnormally noisy. Another interesting feature observed in Figures 3a and b is the long wavelength variation in recording conditions during the course of the survey. In particular, note how the overall lower noise levels for shots 60 to 100 correlate with night time operations.

The information about local noise conditions presented in Figure 3 was used as input to the automatic trace editing scheme. The local residual I^R (x,y) is defined as the original image (Fig. 3a) less the median filtered image I^F (x,y) (Fig. 3b):

$$I^R(x,y) = I(x,y) - I^F(x,y).$$

Only local amplitude anomalies remain in I^R. Traces (pixels) with amplitudes greater than a specified threshold can be identified and excluded from further processing. Filled pixels on the residual surface stacking chart (Fig. 4) are trace "kills" that were picked by automatic scanning and median filtering the data. As in conventional trace editing, the display of positive residual noise power estimates in Figure 4 can be used to isolate noisy shots and stations. Some noisy stations (labelled 1 and 2) and noisy shots (labelled 3 and 4) are highlighted in Figure 4.

Determination of lithological or petrophysical parameters from reflection data requires reliable amplitude information. This information can be used to model impedance contrasts, or to identify amplitude anomalies such as non-reflective zones and bright spots that may indicate the presence of physical anomalies such as fluid phases and magmatic lamellae with sequences of low and high velocities. This quality control procedure enabled us to identify noisy traces, receivers and shots for the line. However, it also showed that the considerable variations in receiver and source conditions along this line make it impossible to apply true amplitude processing to these data in a similar fashion to that applied to lines 2 and 4 by Mayrand and Milkereit (1988).

Amplitude Decay Analysis

The quality control algorithm (Fig. 2, 3 and 4) identified shot points 70, 71, and 72 (VPs 1355 — 1359) of data set III as having good signal to noise ratios. In order to interpret the observed event BS1 shown in Figure 1, these shot gathers were subjected to a more detailed amplitude decay analysis. Since these gathers show relatively little noise, amplitude balancing was unnecessary and therefore both vertical and lateral amplitude variations were preserved. No corrections for spherical divergence or attenuation were applied. The display (Fig. 5) of the trace envelope shows amplitude anomalies associated with the C and E reflectors and highlights local bright spots. It is important to note that problems associated with local source and receiver coupling, or superimposed noise cannot be responsible for the amplitude anomaly (labelled BS1 in Fig. 5). The true amplitude gathers also confirm the limited width of the amplitude anomaly as indicated by the depth migrated data shown in Figure 1.

Figure 6 shows the mean reflection strength of the selected shot gathers obtained by stacking trace envelopes. The amplitude decay curve confirms the high reflection strength associated with the C and E reflectors and the localized bright spot (BS1) at location A. The reflection strength of each of these events is 5-10 dB above background noise levels. For comparison, Figure 7 shows three selected shot gathers over the second bright spot under

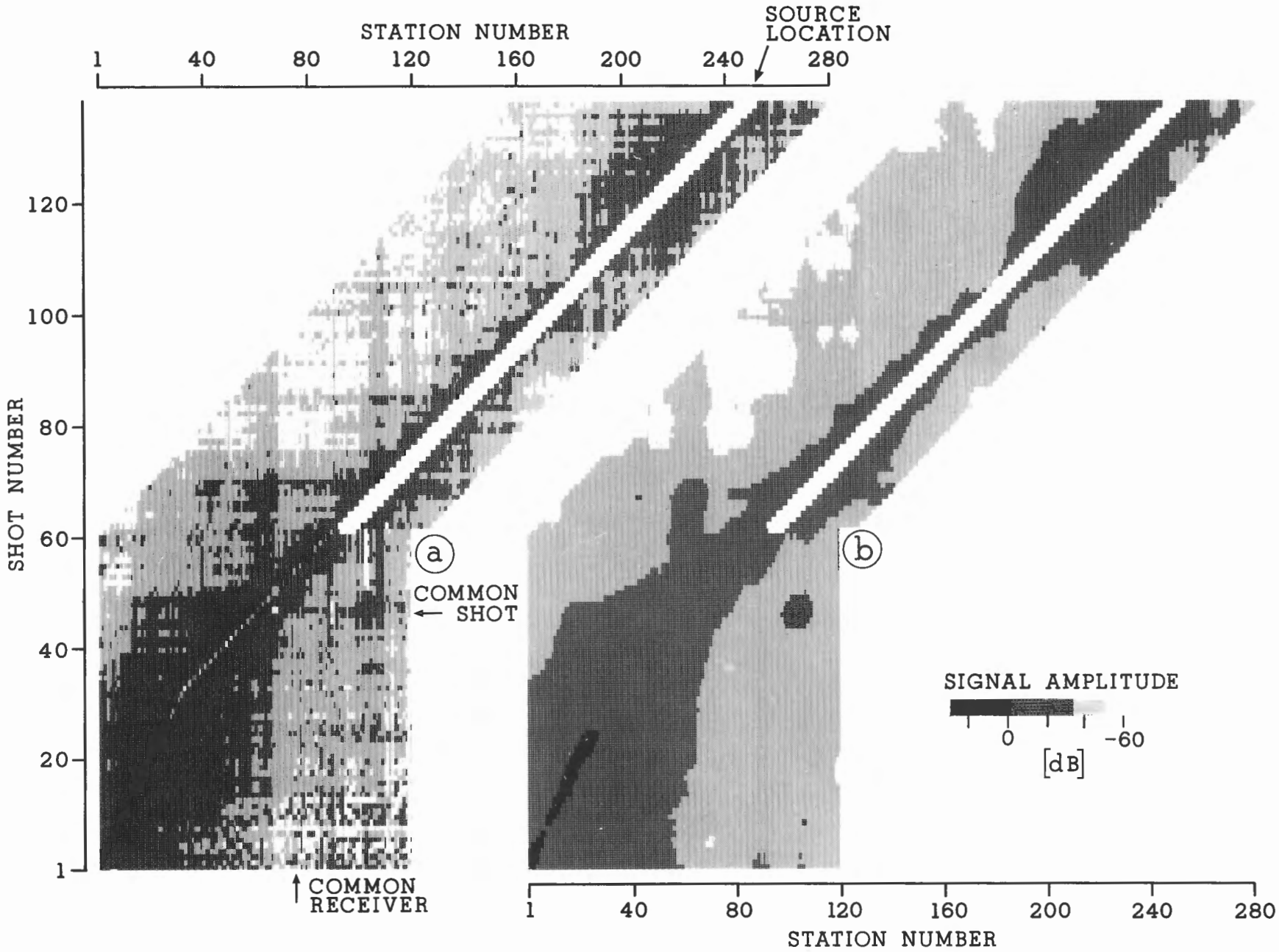

Figure 2. Surface stacking chart of CCSS data set III. (a) Maximum amplitude within the signal window. (b) Median filtered stacking chart of (a). The amplitude scale is normalized with respect to the overall maximum amplitude.

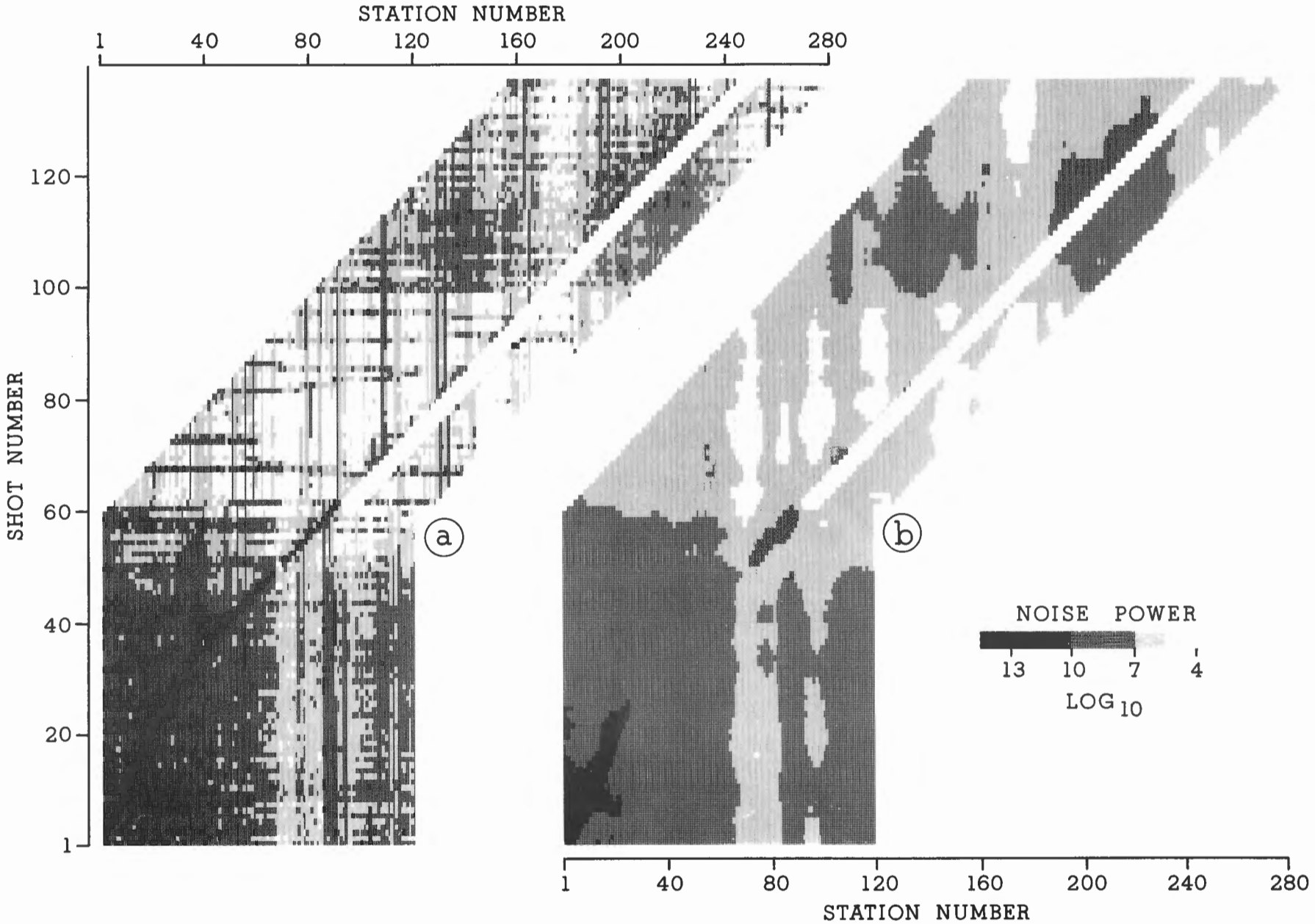

Figure 3. Surface stacking chart of CCSS data set III. (a) Noise power estimate of traces between 14 and 16 s two-way travel time. (b) Median filtered stacking chart of (a).

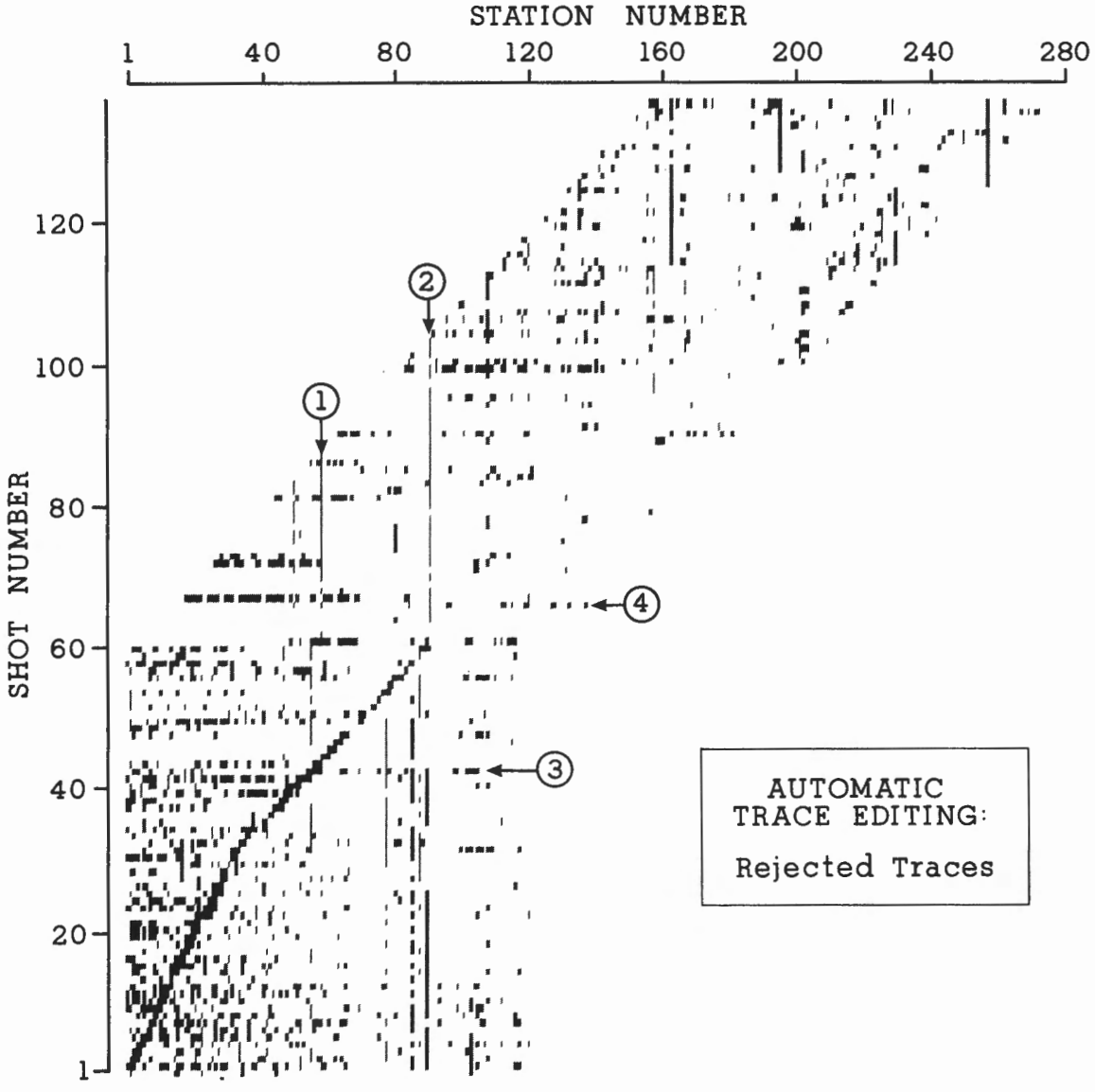

Figure 4. Residual surface stacking chart of CCSS data set III used for trace editing. Shown are traces with anomalous noise power estimates (*see* Fig. 3). Labels 1 and 2 indicate noisy stations, 3 and 4 indicate bad shots.

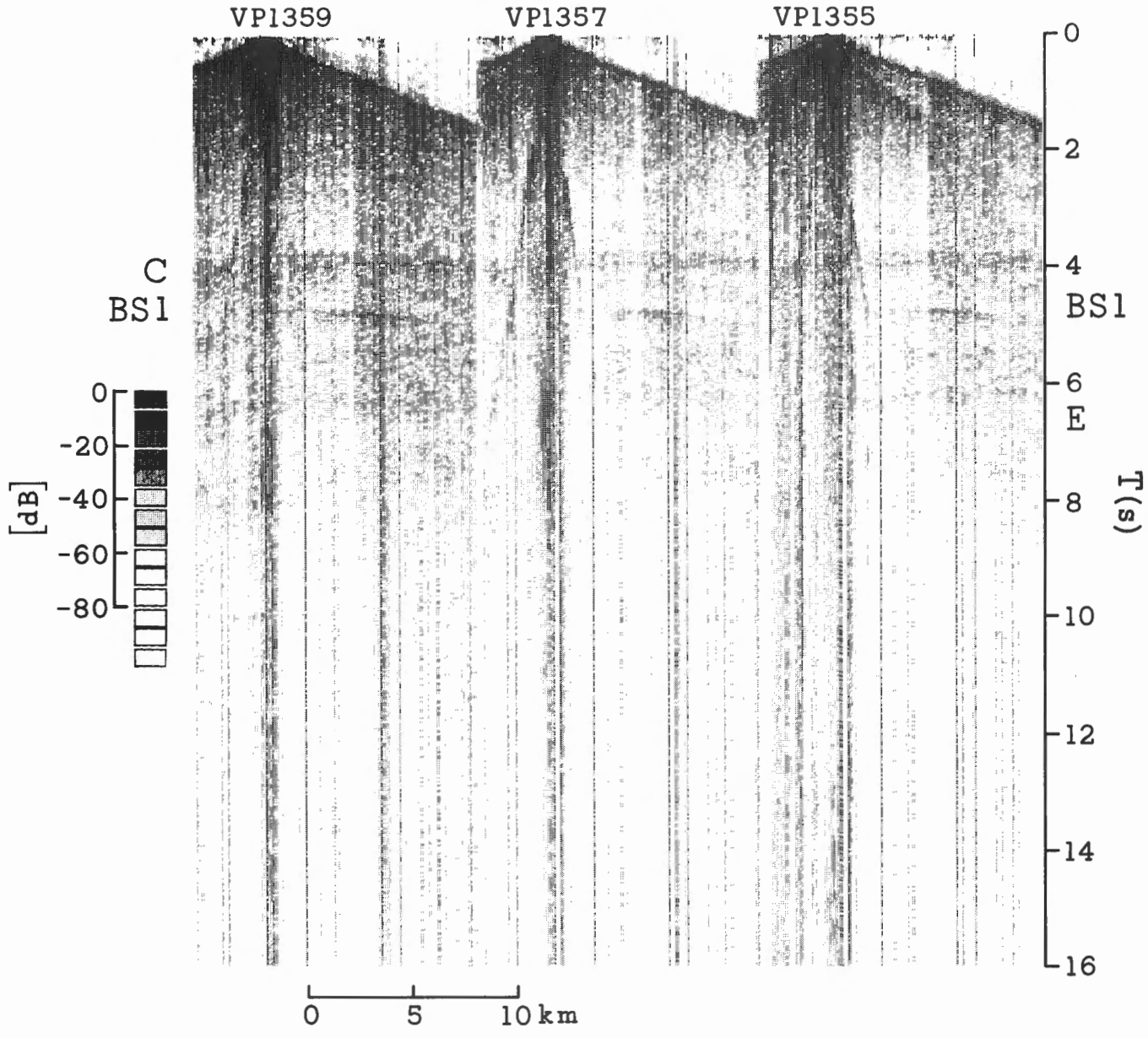

Figure 5. True amplitude display of shot gathers from CCSS data set III, (location A in Fig. 1). Amplitude anomalies are labelled C, BS1 and E ; no time dependent gain applied (VP's 1355-1359 correspond to shot numbers 70-72 in Fig. 2-4). BS1 is the amplitude anomaly at location A in Figure 1.

investigation (labelled BS2 in Fig. 1). The recording conditions for these shots were much noisier than those at location A. Despite these unfavourable conditions the shallow amplitude anomaly (BS2 in Fig. 7) is clearly defined.

Events with similar variations in reflection strength have been observed on the COCORP Death Valley profiles where the bright spots have been interpreted as evidence for a midcrustal magma body (de Voogd et al., 1986), and on the southern Vancouver Island profiles where midcrustal bright spots have been correlated with diffractors caused by local crustal inhomogenities (Mayrand and Milkereit, 1988).

REPROCESSING RESULTS OF DATA SET III

The reprocessing sequence used for this study differs from the sequence described by Clowes et al. (1987) in that revised crooked line processing, spectral balancing and depth migration were applied to the first 8 s of data. In contrast to the exercise distributed to the workshop, the **total** length of line 1 was reprocessed as follows:

1. A new smooth reconstruction line was defined and all data regathered. This resulted in a line approximately 10 km shorter than the original, and a section with much reduced fold at small travel times.

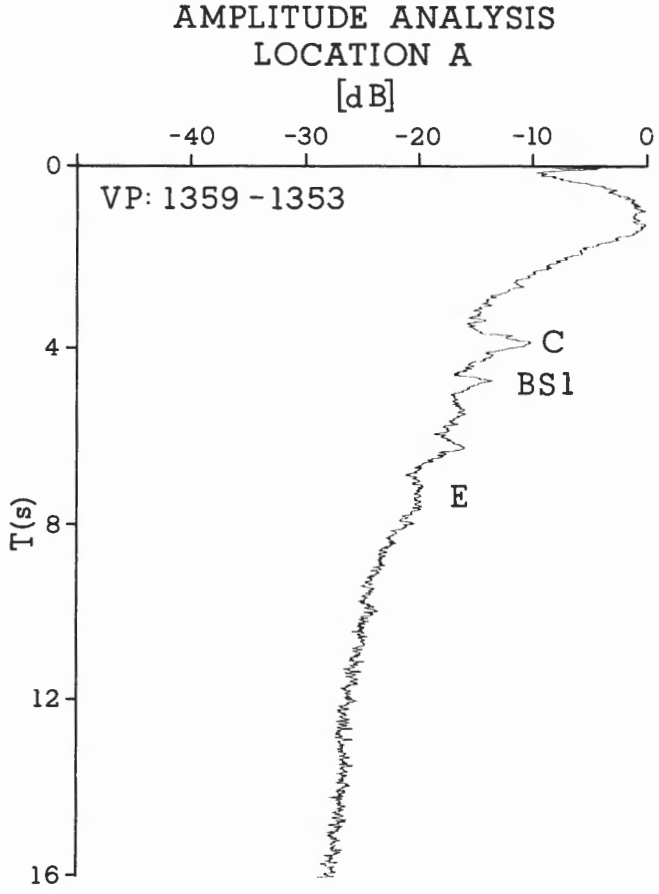

Figure 6. Amplitude decay analysis for location A. The strengths of reflections C, BS and E are well above background level.

2. As outlined in the previous quality control section, true amplitude processing is not feasible for data set III. In order to minimize the influence of noise we applied "spectral balancing" to the data. In this process the frequency content of each seismic trace was equalized over the frequency range 10 to 35 Hz. Before stack, a 0.5 s AGC was applied to account for variable signal to noise conditions; no AGC after stack was applied. Examples of the results of the spectral balancing and AGC are shown in Figure 8. The stacked section can be regarded as a pseudo-true amplitude section, indicating relative variations in reflection strength and coherency. True reflection strengths cannot be recovered from these data. The trace envelope of the reprocessed data is shown in Figure 9. Amplitudes associated with the C reflector (at 4 to 6 s) are approximately 20 dB above background levels. Compared to the original section (Fig. 14 in Green et al., 1990b) the C reflections show improved continuity between 20 and 40 km. The shape of many C reflections and, even more pronounced, of the bright spots at location B, is convex upwards, indicating possible diffracted energy.
3. The high level of diffracted energy is confirmed in the depth migrated image derived from the reprocessed data. A constant gradient velocity model with 6 km/s at the top and 6.5 km/s at 18 km depth was used for the SWDS depth migration (Milkereit, 1987a). Figure 10 shows the trace envelope of the uppermost 18 km of migrated data in the vicinity of the amplitude anomaly BS2. All convex upwards reflections seen in Figure 9 have been focused at a depth of 5 to 10 km.

SUMMARY AND CONCLUSIONS

1. We have presented the results of an automated quality control scheme based on scans of deep crustal data. Amplitude information has been used to identify locally anomalous coupling of sources and geophones, and to estimate the variation of ambient noise levels during the course of the seismic survey. Automatic trace scanning is a computationally inexpensive processing step that can be integrated efficiently into any conventional seismic processing package.
2. Based on the migrated sections and the analysis of common shot gathers, anomalous reflection amplitudes have been confirmed. Interpretation of small-scale midcrustal amplitude anomalies is in good agreement with migration results, indicating local inhomogeneities. There are several possible explanations for the observed strong amplitudes and their lateral variations:
   a. Local changes in composition (low velocity sedimentary rock or high velocity mafic or ultramafic material embedded in material with average crustal velocities).
   b. Constructive thin layer interference or focussing due to complex structures;
   c. Extreme local variations in impedance contrast due to trapped fluids or magma bodies (with zero S-wave velocity).

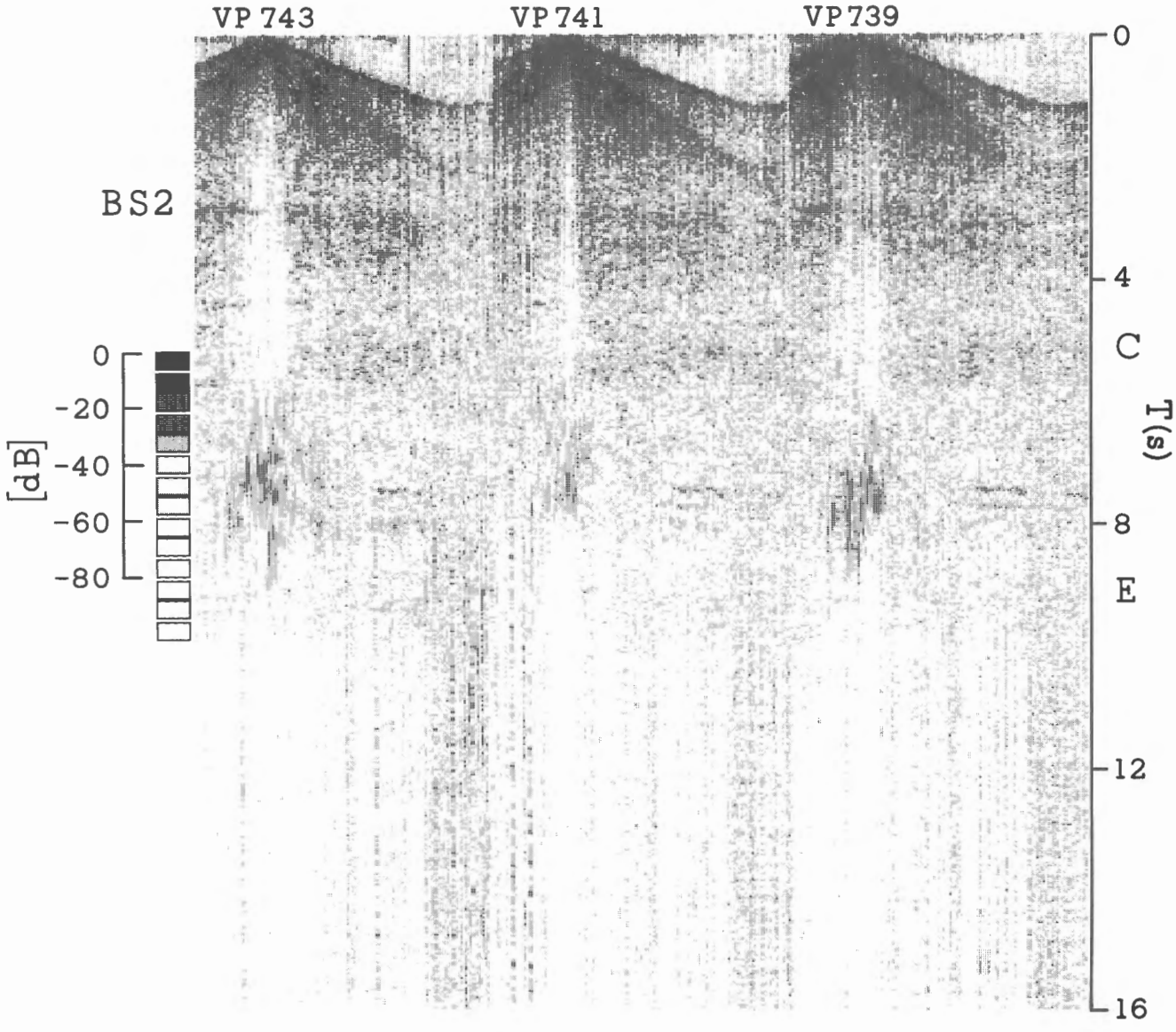

Figure 7. True amplitude display of shot gathers above amplitude anomaly BS2, location B in Figure 1. The shallow amplitude anomaly (BS2) at 3 s is well defined despite the overall high noise level and correlation noise at short source-receiver offsets.

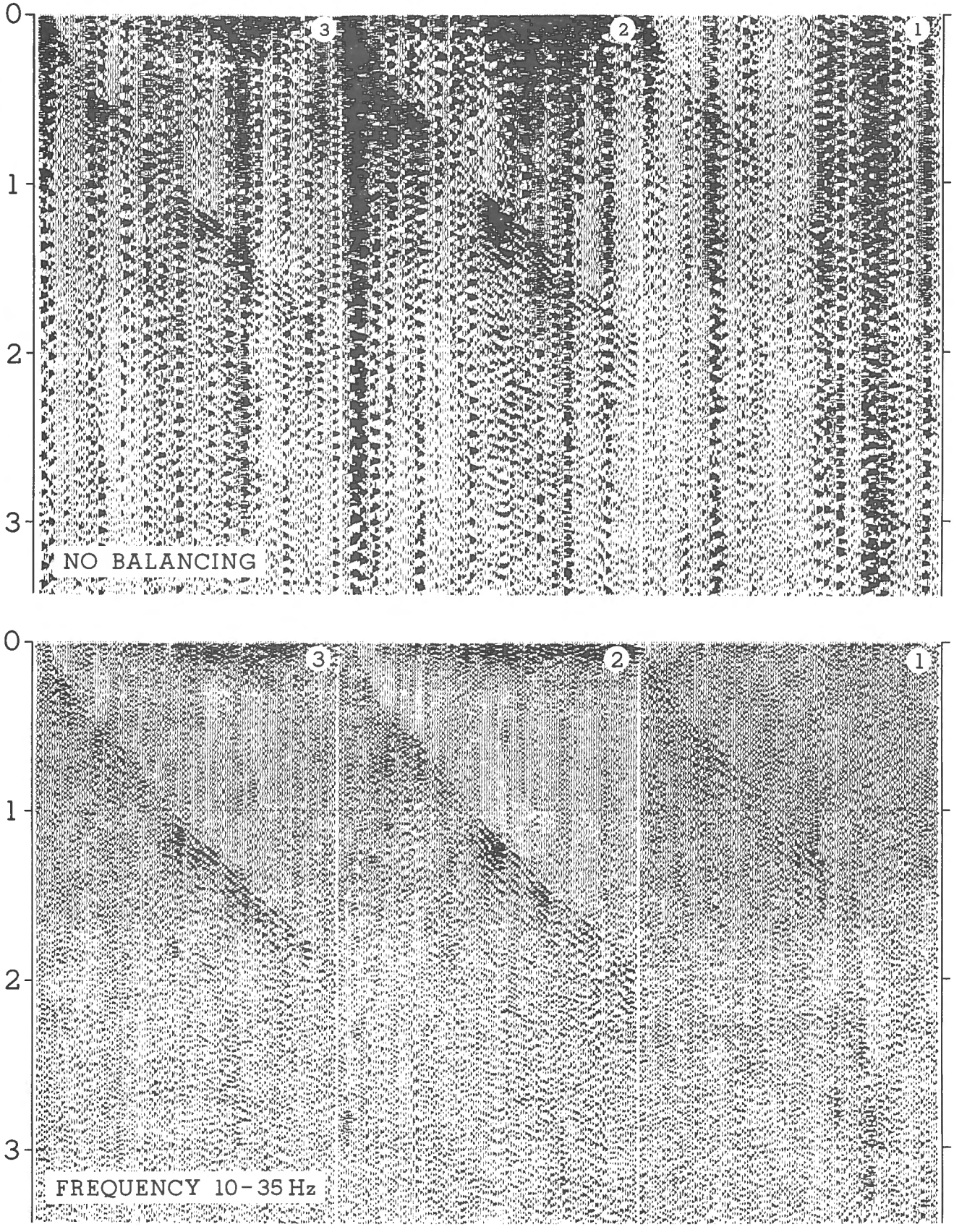

Figure 8. Reprocessing of CCSS data set III : spectral balancing. The noisy input data is shown at the top, the spectral balancing result is shown at the bottom.

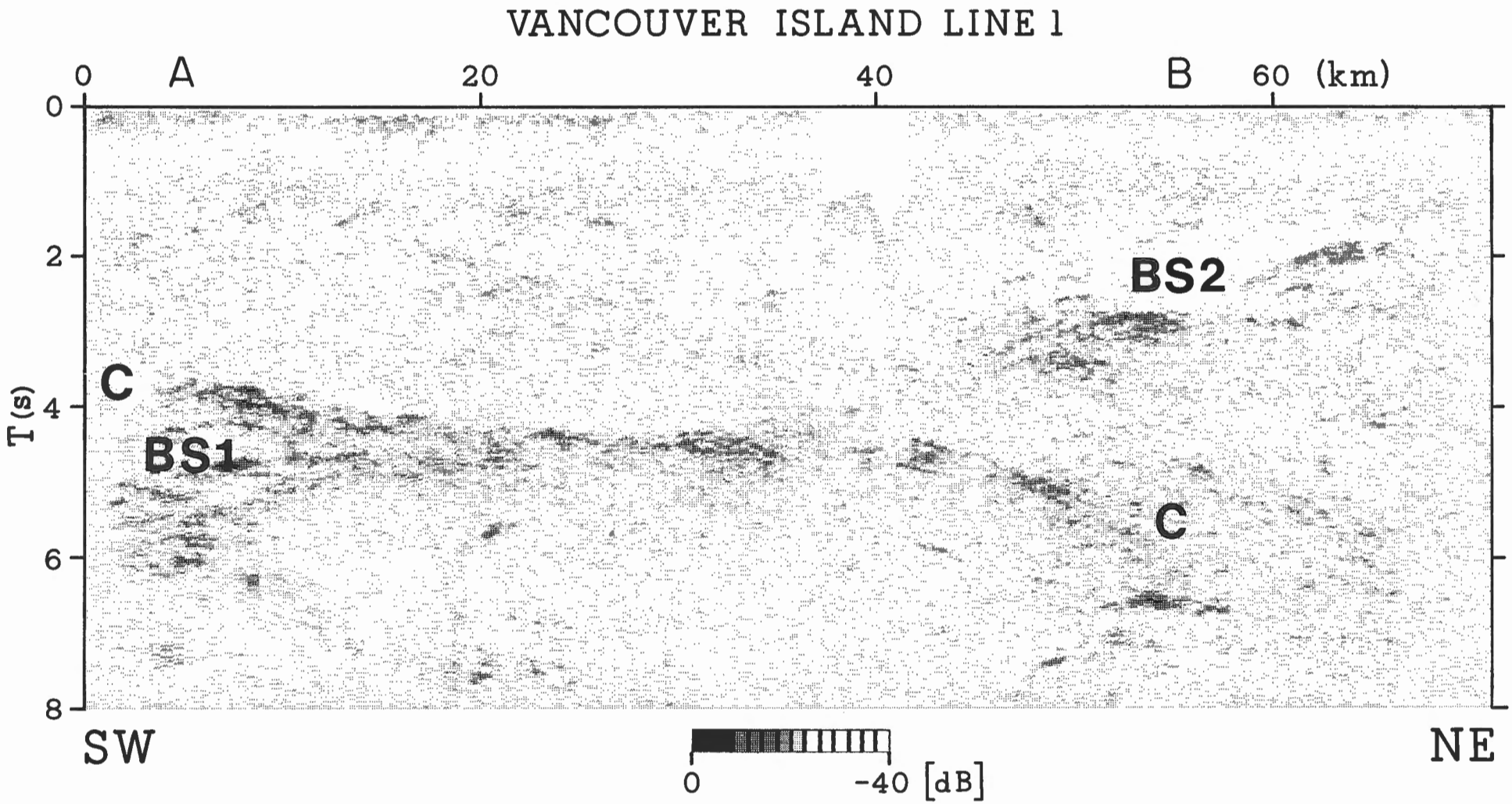

Figure 9. Reprocessing of Vancouver Island seismic reflection line 1 (revised crooked line processing, spectral balancing). Amplitude anomalies associated with the C reflector and the "bright spots" at A and B are highlighted in this trace envelope display.

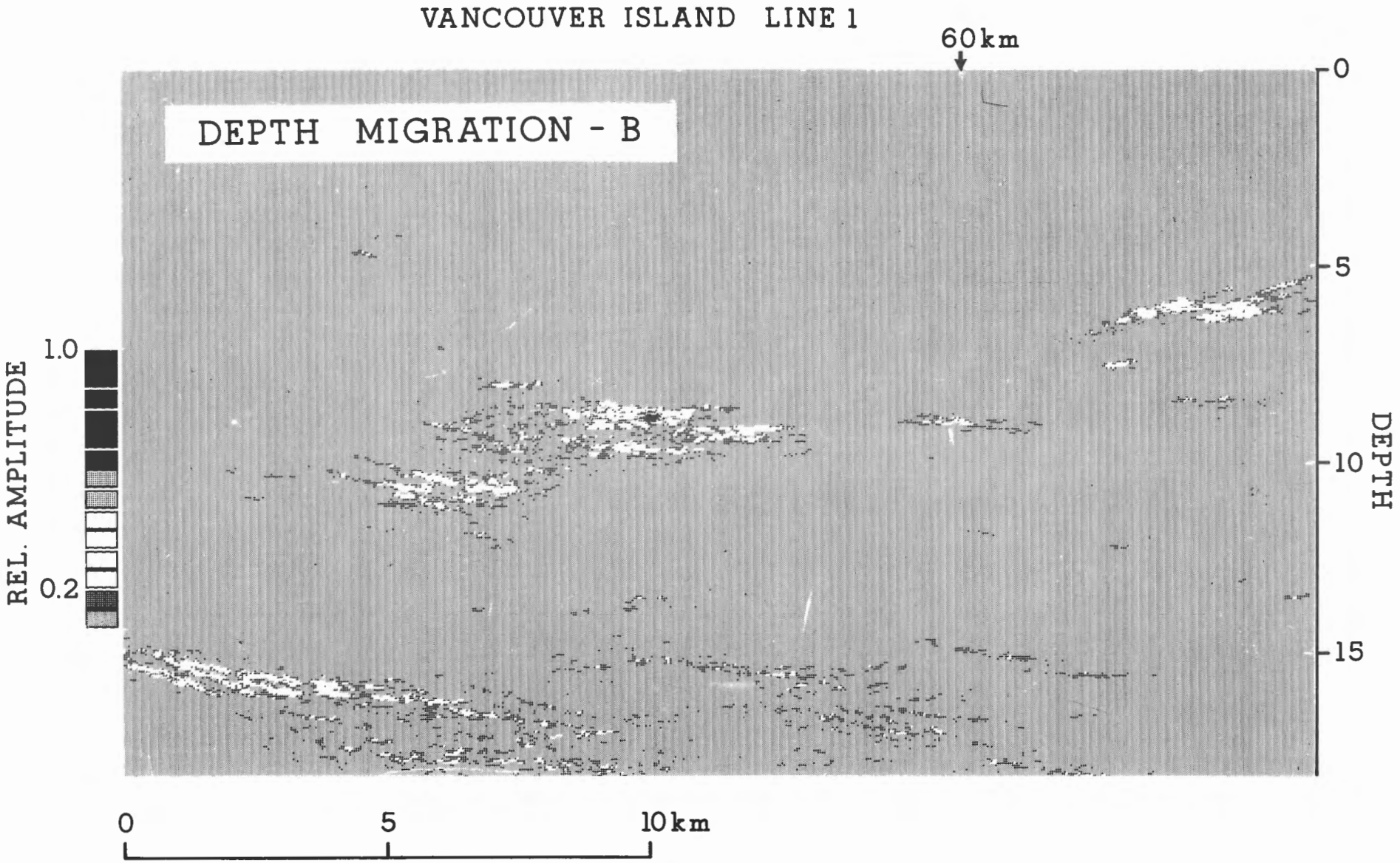

Figure 10. Depth migration of Vancouver Island seismic reflection line 1 data (location B, *see* Fig. 9). Convex reflections seen in Figure 9 have been focused and are well above background noise level.

3. The small-scale shallow amplitude anomalies ("bright spots") beneath the Beaufort Range fault zones (Fig. 7, 9 and 10) may be explained by variations in composition. Limestone associated with the Buttle Lake Formation (Yorath et al., 1985) is a likely candidate for high impedance contrasts there. It is worth emphasizing that the small-scale features described above may not be seen by low frequency refraction experiments.

4. True amplitude analyses have confirmed the existence of local high amplitudes associated with the C reflections and deeper bright spots, indicating a complex subsurface structure where mostly horizontal reflections (C and E) overprint many small-scale inhomogenities of yet unknown composition or structure.

ACKNOWLEDGMENT

Reviews by R.M. Clowes and F. Cook are appreciated.

REFERENCES

Clowes, R.M., Brandon, M.T., Green, A.G., Yorath, C.J., Sutherland Brown, A., Kanasewich, E.R., and Spencer C.
1987 : LITHOPROBE — southern Vancouver Island : Cenozoic subduction complex imaged by deep seismic reflections ; Canadian Journal of Earth Sciences, v. 24, p. 31-51.

de Voogd, B., Serpa, L., Brown, L., Hauser, E., Kaufman, S., Oliver, J., Troxel, B.W., Willemin, J., and Wright, L.A.
1986 : Death Valley bright spot : a midcrustal magma body in the southern Great Basin, California ? ; Geology, v. 14, p. 64-67.

Green, A.G., Clowes, R.M., Yorth, C.J., Spencer, C., Kanasewich, E.R., Brandon, M.T., and Sutherland Brown, A.
1986 : Seismic reflection imaging of the subducting Juan de Fuca plate ; Nature, v. 319, p. 210-213.

Green, A.G., Milkereit, B., Mayrand, L., Spencer, C., Kurtz, R.D., and Clowes, R.M.
1987 : Lithoprobe seismic reflection profiling across Vancouver Island ; Royal Astronomical Society, Geophysical Journal, v. 89, p. 85-90.

Green, A.G., Clowes, R.M., and Ellis, R.M.
1990a : Crustal studies across Vancouver Island and adjacent offshore margin ; *in* Studies of Laterally Heterogeneous Structures Using Seismic Refraction and Reflection Data, ed. A.G. Green ; Geological Survey of Canada, Paper 89-13, p. 3-25.

Green, A.G., Spencer, C., Milkereit, B., Clowes, R.M., and Ellis, R.M.
1990b : Guidelines for workshop topics I to IV ; *in* Studies of Laterally Heterogeneous Structures Using Seismic Refraction and Reflection Data, A.G. Green ; Geological Survey of Canada, Paper 89-13, p. 27-30.

Huang, T.S., Yang, G.J., and Tang, G.Y.
1979 : A fast two-dimensional median filtering algorithm ; Institute of Electrical and Electronics Engineers, Transactions, ASSP-27, p. 13-18.

Mayer, J.R. and Brown, L.D.
1986 : Signal penetration in the COCORP Basin and Range — Colorado Plateau survey ; Geophysics, v. 51, p. 1050-1055.

Mayrand, L.J., Green, A.G., and Milkereit, B.
1987 : A quantitative approach to bedrock velocity resolution and precision — the Lithoprobe Vancouver Island Experiment ; Journal of Geophysical Research, v. 92, p. 4837-4845.

Mayrand, L.J. and Milkereit, B.
1988 : Automated editing and true amplitude stacking of seismic data ; Canadian Journal of Earth Sciences, v. 25, p. 1811-1823.

Milkereit, B.
1987a : Migration of noisy crustal seismic data ; Journal of Geophysical Research, v. 92, p. 7916-7930.
1987b : Decomposition and inversion of seismic data — an instantaneous slowness approach ; Geophysical Prospecting, v. 35, p. 875-894.

Stolt, R.H.
1978 : Migration by Fourier Transform ; Geophysics, v. 43, p. 23-48.

Taner, M.T. and Sheriff, R.E.
1977 : Application of amplitude, frequency and other attributes of stratigraphic and hydrocarbon determination ; *in* Seismic Stratigraphy, ed. C.E. Payton ; American Association of Petroleum Geologists, Memoir 26, p. 310-327.

Yorath, C.J., Green, A.G., Clowes R.M., Sutherland Brown, A., Brandon, M.T., Kanasewich, E.R., Hyndman, R.D., and Spencer, C.
1985 : LITHOPROBE southern Vancouver Island : seismic reflection sees through Wangelia to the Juan de Fuca plate ; Geology, v. 13, p. 759-762.

Reprocessing of seismic reflection data recorded on Vancouver Island, BC: CCSS data set III

P. Valasek [1], P. Finckh [1] and M. Demartin [1]

Valasek, P., Finckh, P., and Demartin, M., Reprocessing of seismic reflection data recorded on Vancouver Island, BC: CCSS data set III; in Studies of Laterally Heterogeneous Structures Using Seismic Refraction and Reflection Data, ed. A.G. Green; Geological Survey of Canada, Paper 89-13, p. 165-174, 1990.

Abstract

A portion of the seismic reflection data from Vancouver Island (CCSS data set III) was reprocessed with emphasis on pre-stack signal to noise enhancement. This was achieved by concentrating the processing on pre-stack velocity filtering followed by deconvolution. The removal of linear noise, including ground roll and source-generated shear waves, enabled clearer definition of shallow reflections and uncovered some new events. Deconvolution effectively balanced the frequency content of the data and contributed to greater resolution of mid-crustal reflectivity and enhancement of a deep 10 s event. This processing technique has some potential drawbacks. In particular, velocity filtering can introduce artifacts, noise can be smeared into apparent "reflections", and steeply dipping reflections can be degraded.

Résumé

Une portion de la ligne sismique réflexion à travers l'île de Vancouver (jeu de données III de la CCSS) a été retraité en mettant l'accent sur l'amélioration de la relation signal/bruit avant la sommation au point miroir. Pour ce faire, les efforts ont été concentrés sur le filtrage des vitesses avant sommation suivi par une déconvolution. L'élimination du bruit linéaire, incluant les ondes de surface et les ondes transversales générées à la source, a permis une définition plus claire des réflexions à faible profondeur et a dévoilé des éléments nouveaux. La déconvolution équilibre efficacement le spectre de fréquences et contribue à une meilleure résolution des réflexions dans l'écorce moyenne ainsi qu'à une amélioration de l'évènement à 10 s. D'autre part, cette technique a quelques désavantages. Particulièrement le filtrage de vitesse peut introduire des évènements artificiels, du bruit peut être étalé en "réflexions" apparentes et des réflexions à fort pendage sont détériorées.

[1] Institute of Geophysics, ETH Hönggerberg, 8093 Zürich, Switzerland.
[2] Istituto per la Geofisica della Litosfera, via Bassini 15, 20133 Milano, Italy.

INTRODUCTION

As a contribution to the CCSS workshop, a seismic reflection data set was reprocessed in an attempt to enhance reflection character and to compare various advanced processing techniques. The data consisted of 20 km of Vibroseis reflection data from the southwest segment of LITHOPROBE line 1 across Vancouver Island (Fig. 2 *in* Green et al., 1990). This segment represents about 1/4 of the total length of line 1 and lies entirely over Paleozoic rocks of Vancouver Island (Fig. 1 *in* Green et al., 1990). The data distributed by the CCSS organizing committee were already demultiplexed, cross-correlated and had instrument-gain recovery applied. A summary of the acquisition parameters is given in Table 1 of Green et al., (1990).

Reprocessing of the data was carried out by the recently established seismic reflection group at the Institute of Geophysics ETH, Zürich. A VAX 11/780 was used as a host computer running the Phoenix hardware/software configuration from Seismograph Service Corporation, Tulsa, Oklahoma. Reprocessing of the Vancouver Island data concentrated on pre-stack signal to noise (S/N) enhancement through frequency-wave number velocity filtering (F-K) and deconvolution. Velocity filtering is not a standard step in the processing of land data. However, in certain cases, strong coherent noise, such as ground roll, contaminates near-surface data. Removal of this noise by velocity filtering can lead to better resolution of shallow events.

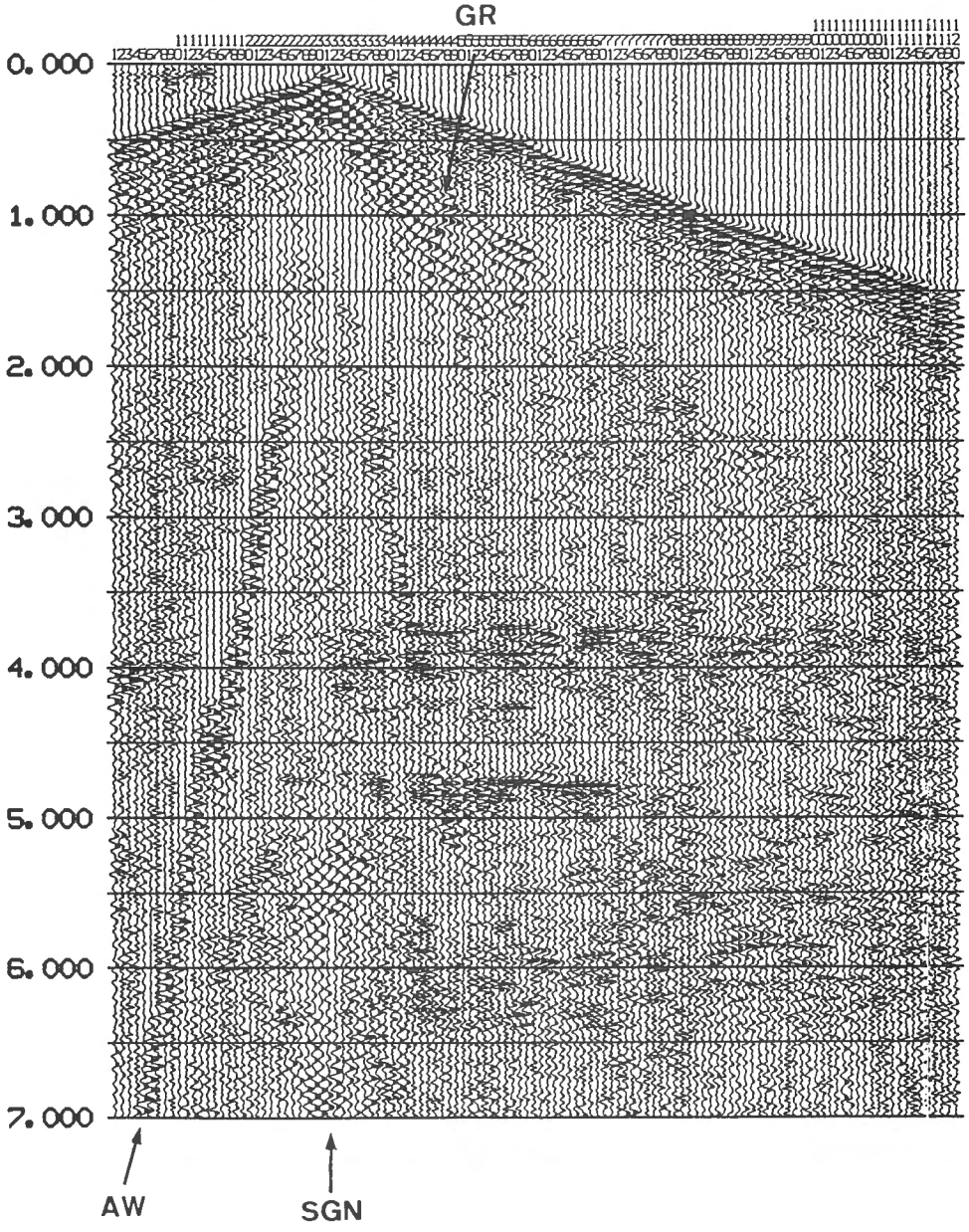

Figure 1. Vibroseis field gather with only AGC applied. Ground roll (GR), air waves (AW) and source generated noise (SGN) contaminate the data above the strong reflectivity beginning at 3.5 s.

Table 1. Processing Parameters

Demultiplex with gain recovery (sample interval 4 ms) *	
Vibroseis correlation *	
True amplitude recovery *	
Crooked line geometry	
Trace editing	
Automatic gain control (AGC):	500 ms window
High-pass frequency filter	> 8 Hz
F-K filtering	Lozenge-shaped to remove coherent noise
AGC removal	500 ms window
Predictive deconvolution	
Minimum lag	2nd zero crossing of autocorrelation function
Maximum lag	240 ms
Percentage of white noise	3 %
Elevation statics	
Datum	mean sea level
Correction velocity	5000 m/s
CDP sort	
Mute	
Normal move out corrections	
CDP Stack	
Residual Statics (surface consistent)	
Correlation windows	3.5 — 4.5 s
Frequency filter	12 — 40 Hz
AGC	2000 ms Window

* performed by processing contractor

DATA DESCRIPTION

The stacked section supplied for this workshop gives a good indication of the overall character of the reflections (Fig. 14 *in* Green et al., 1990; this figure is contained in the pocket at the back of this volume). The original processing applied to this section is summarized in Table 2 of Green et al. (1990). The upper 3.5 s of the section is relatively transparent with only a few short horizontal events and a northeast-dipping event interpreted as the Tofino fault (Clowes et al., 1987 a, b; Green et al., 1987, 1990). Deeper in the section, between 3.5 and 8.5 s, the data are dominated by strong reflectivity bounded by reflections C and E. These events form continuous multicyclic packages that vary from horizontal to strongly arcuate. Below this region the data quality is again largely devoid of coherent events with the exception of the short curved reflection near 10 s, possibly originating from the subducting slab (Clowes et al., 1987a,b).

The signal and noise characteristics of the data were further assessed on the unstacked Vibroseis shot gathers. Figure 1 shows a representative gather contributing to the central portion of the stacked data. Strong reflected energy can be identified beginning below 3.5 s. Above this region, ground roll, shear waves and air waves contaminate the record, masking the shallower events. Low frequency energy stemming from near the Vibroseis source between

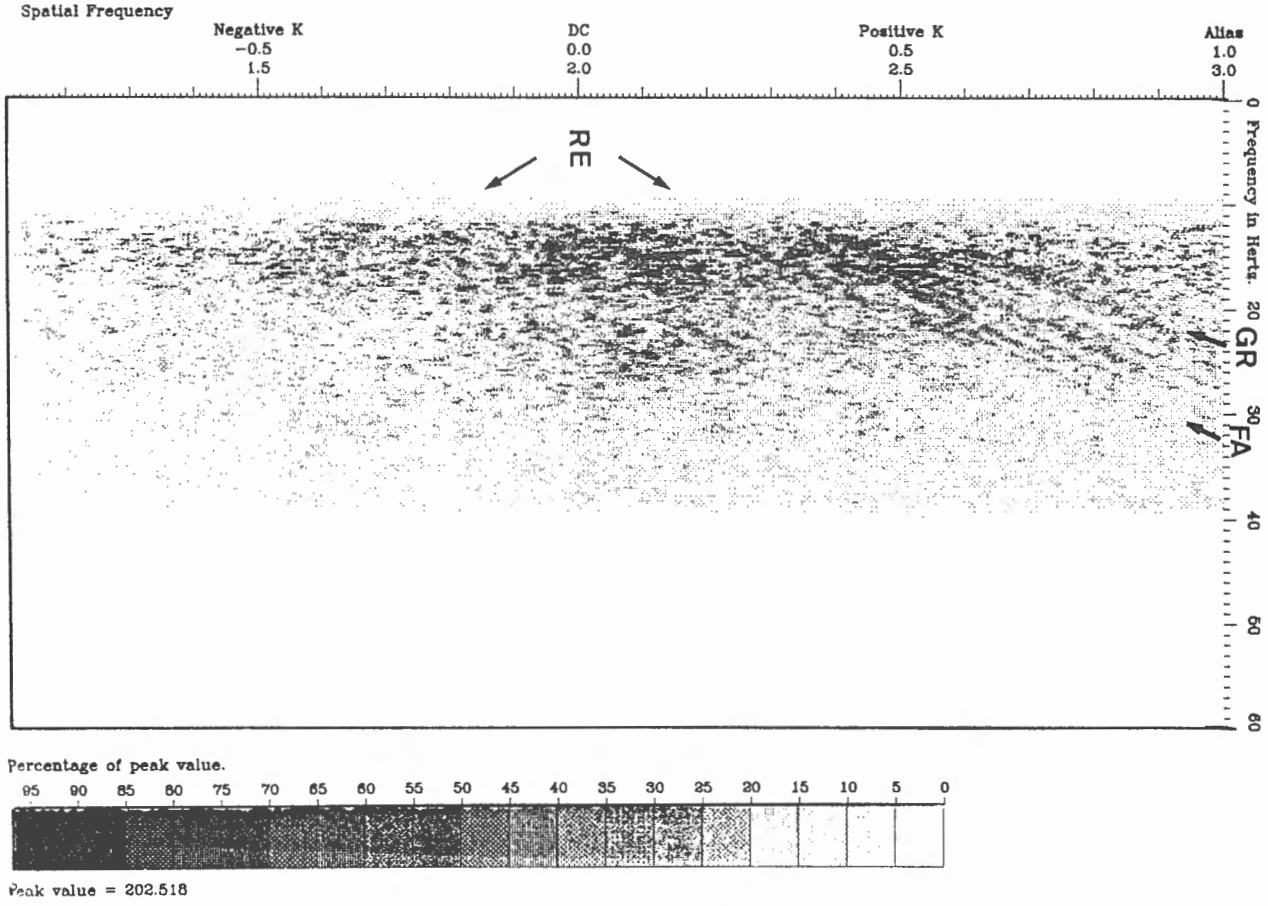

Figure 2. F-K plot of the gather in Figure 1. Note the separation of the ground roll (GR) and first arrivals (FA) from the reflected energy (RE).

5 and 7 s, identified as source generated noise (SNG) on Figure 1, degrades the deeper reflections. Spectral analysis of selected windows shows an unbalanced spectrum with low frequencies dominating the shallow levels of data where noise is most severe.

DATA PROCESSING

We took the approach of velocity filtering followed by predictive deconvolution as a means to enhance the S/N. Removing the coherent noise with velocity filtering should improve the subsequent application of predictive deconvolution by providing more signal-dominated windows for the design of the deconvolution filters. The entire reprocessing flow is outlined in Table 1.

As an initial step True Amplitude Recovery (TAR) was carried out. The gain function $V(z).t.e^{at}$ was used to correct for energy losses due to spherical divergence and anelastic absorption. The parameters for the function were determined by first applying spherical divergence corrections based on velocities from refraction modeling (Egger and Ansonge, 1990) and then statistically matching the trace-amplitude decay with an exponential factor.

Velocity filtering

To suppress coherent noise, which dominated the upper 3.5 s of the data, velocity filtering was applied to the Vibroseis gathers. Transformation of the data in the F-K domain enables coherent noise to be isolated from the primary signal. This provides an efficient means of attenuating the noise by zeroing out its representation in the F-K domain prior to inverse transformation.

Figure 2 shows the shot gather of Figure 1 transformed to the F-K domain. The coherent noise and primary signal are mapped into the separate regions indicated. Care was taken in designing a filter that removed the noise while minimizing unwanted effects. Velocity filtering can introduce artifacts in the data such as ringing from sharp filter edges and smearing of high-amplitude noise bursts or discontinuities in the data. To suppress these effects, a tapered lozenge-shaped F-K filter was designed (Fig. 3). In addition, a high-pass frequency filter and automatic gain control were applied prior to F-K transformation. These steps prevented high amplitude areas, such as ground roll, from swamping weaker amplitudes with their F-K filter responses (March and Bailey, 1983). The gain function was removed following inverse transformation back to the time domain.

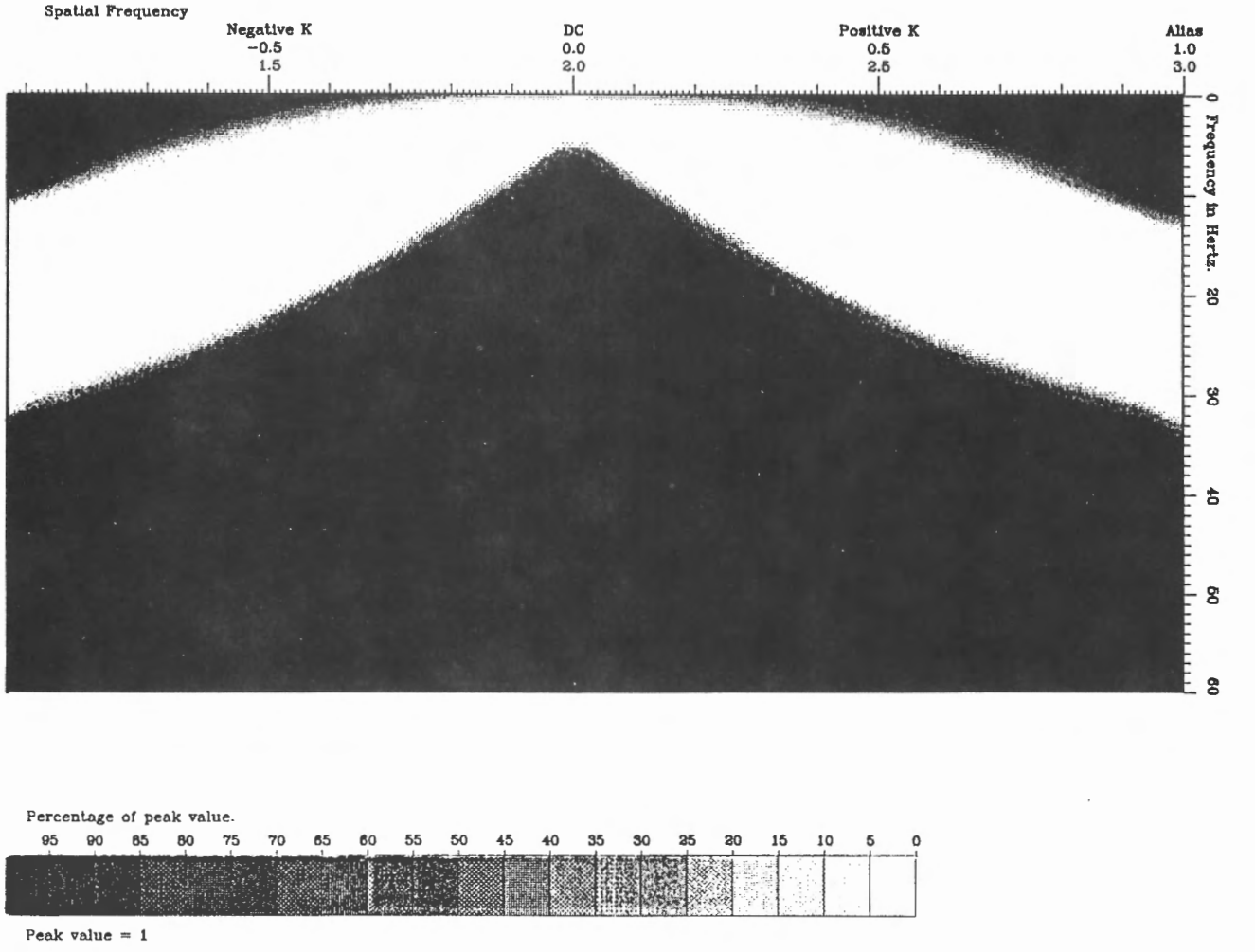

Figure 3. Plot of F-K filter function designed on the basis of Figure 2. The white region will be eliminated prior to transformation leaving only the black area to contribute to the filtered section. The symmetry of the filter is necessary to account for the split spread configuration.

The effect of F-K filtering is shown in Figure 4, which demonstrates the elimination of most of the coherent noise and the improved S/N at all levels. Reflections between 1.5 and 3.0 s, which can now be identified clearly, will have a better chance to stack as coherent events.

Deconvolution

Predictive deconvolution following F-K filtering was applied as a means to improve resolution by reducing random noise and suppressing short period multiples. Figure 5a shows the autocorrelogram of the shot gather in Figure 4 revealing the presence of short period multiples, which were most likely developed from near-surface reverberations. Windows with a high resolution of the primary signal could be chosen to effectively design the deconvolution filters because much of the noise was suppressed by the velocity filtering. Three time windows per trace were selected to account for the time variance of the signal. After deconvolution, the reverberatory nature of the autocorrelation function was suppressed (Fig. 5b) and a more balanced spectrum was produced resulting in improved S/N of the data (Fig. 6).

DISCUSSION

The final processing steps involved sorting the data into crooked-line bins, performing a velocity analysis, and computing residual static corrections (Table 1). The unmigrated, stacked section is shown in Figure 7 with only TAR applied and in Figure 8 with post-stack AGC. Different aspects of the data are emphasized in the two displays. The advantage of velocity filtering can be seen in Figure 8 with improved reflectivity at shallow levels. In particular, a subhorizontal event can be identified trending across most of the section at 2.0 s. In addition, a new reflection can

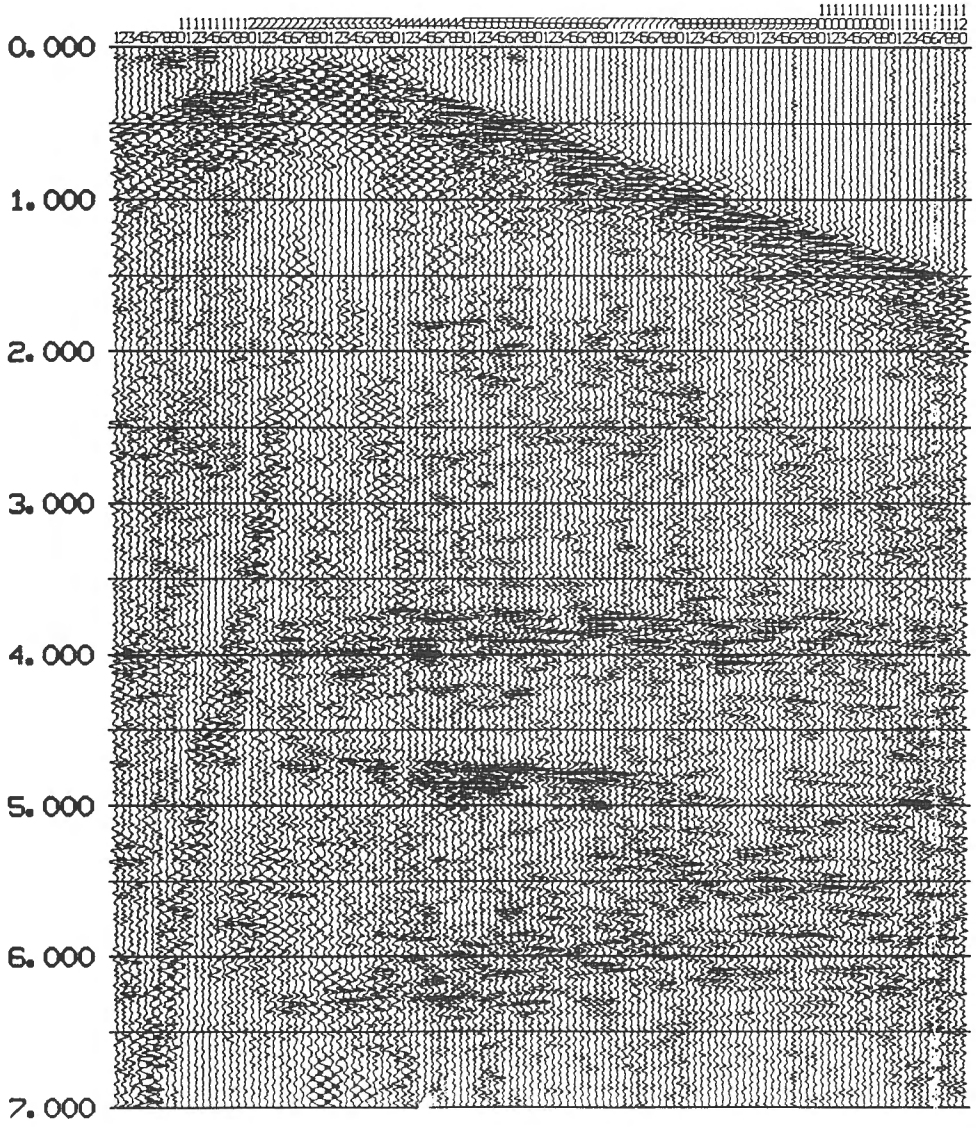

Figure 4. Field gather from Figure 1 after F-K filtering. Most of the ground roll has been removed and reflections at all times have been enhanced, particularly in the shallow region between 1.5 and 3.0 s.

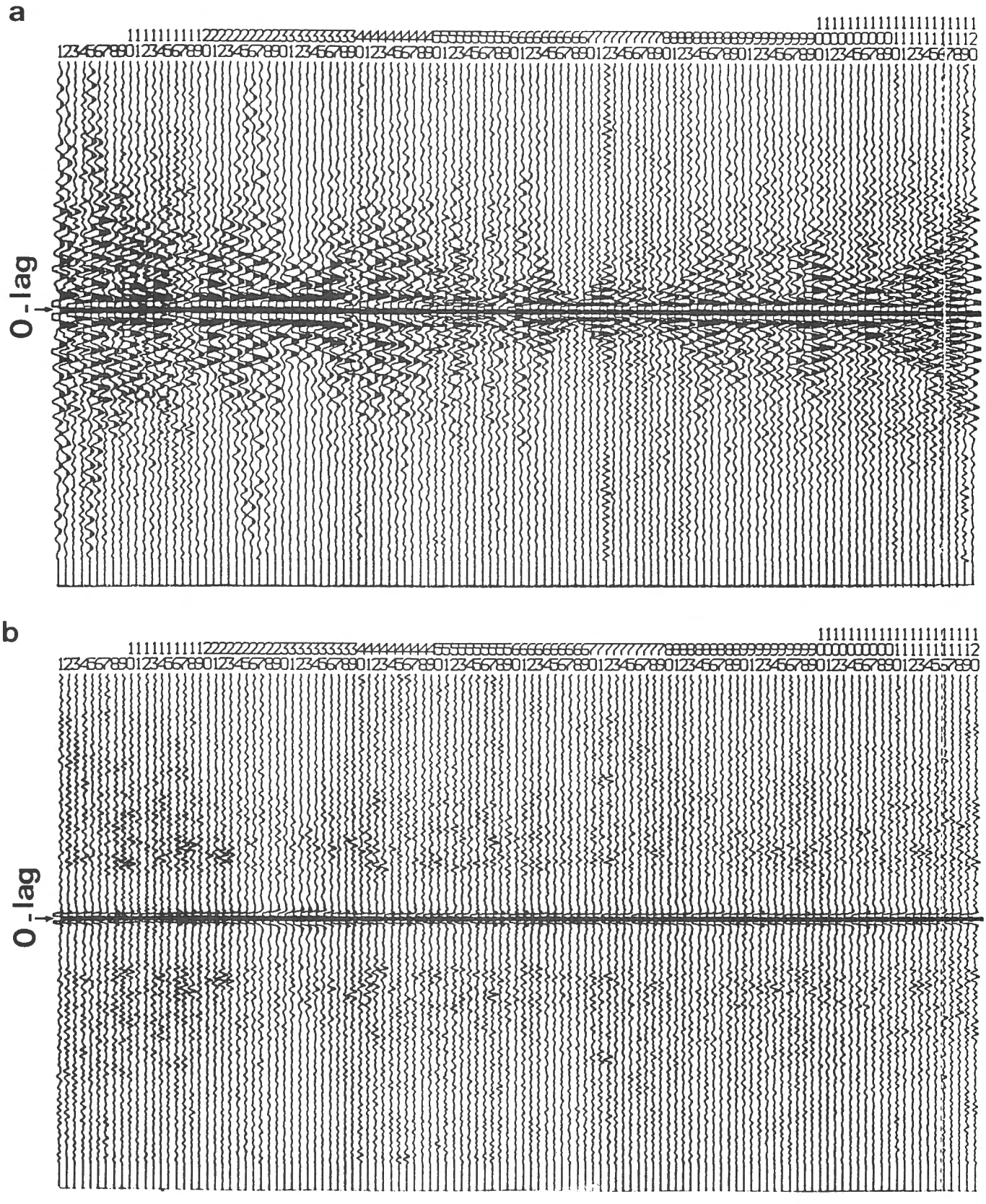

Figure 5. (a) Autocorrelogram of the field gather of Figure 4 before predictive deconvolution. (b) Autocorrelogram after predictive deconvolution showing effective suppression of the ringing nature of the autocorrelogram.

be seen at the surface near CDP 75 dipping northeast down to 2.0 s on the right-hand edge of the section. Note the degradation of the Tofino fault reflection, which is faintly seen dipping more steeply to the northeast from 0.5 s on the left of the section to 3.4 s on the right. This degradation may be the result of the velocity filtering "eliminating" steeply dipping events. Other negative effects of velocity filtering are possible artifacts or smeared noise seen as short discontinuous events in some areas.

Deeper in the section the mid-crustal reflectivity bounded by events C and E is better resolved (Fig. 7). Also, the deeper event at 10 s can be traced more confidently across the section. In general, the combination of velocity filtering with deconvolution has resulted in improved S/N at all levels.

ACKNOWLEDGMENTS

This is Contribution Nr. 595 of the Institute of Geophysics, ETH Zürich.

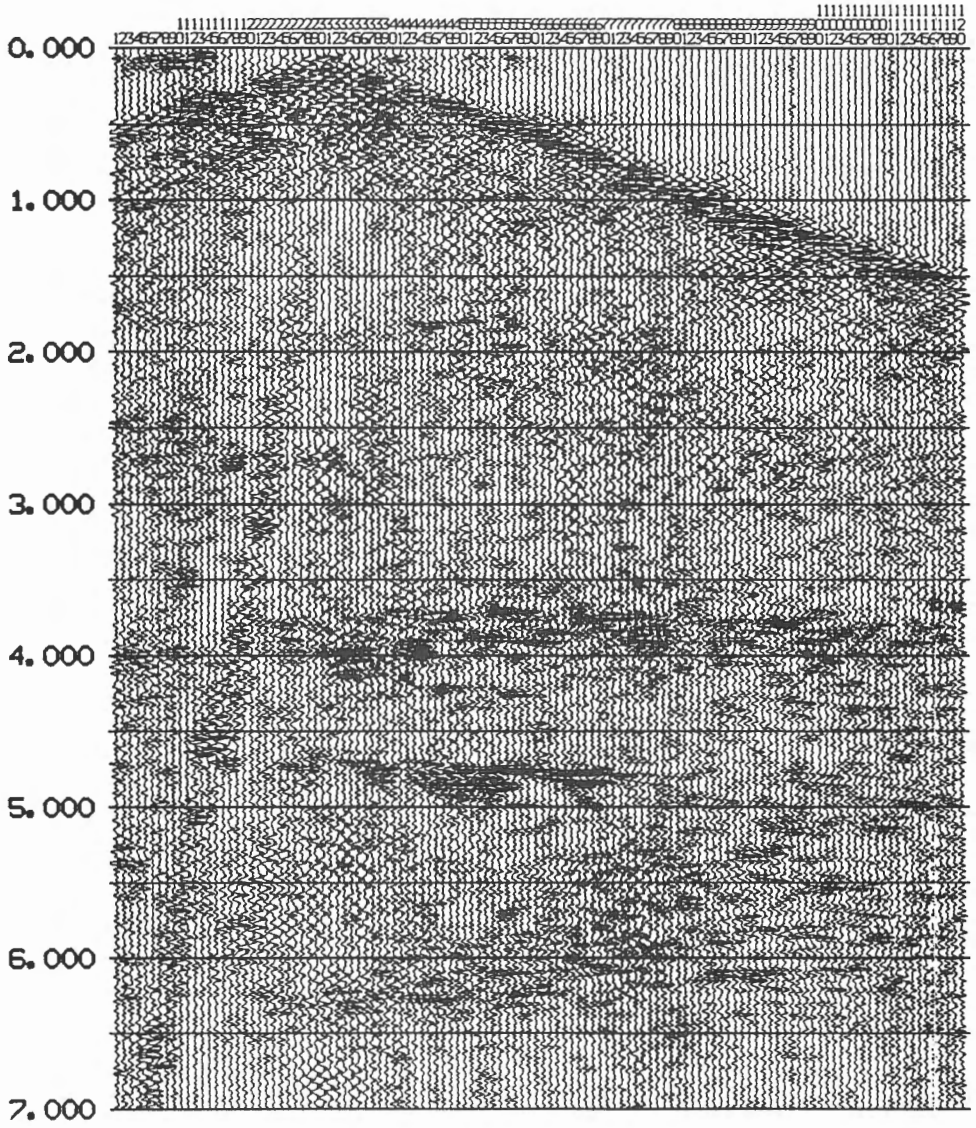

Figure 6. Field gather of Figure 1 after F-K filtering and predictive deconvolution. The reflected wavelets have been sharpened and the signal to noise increased.

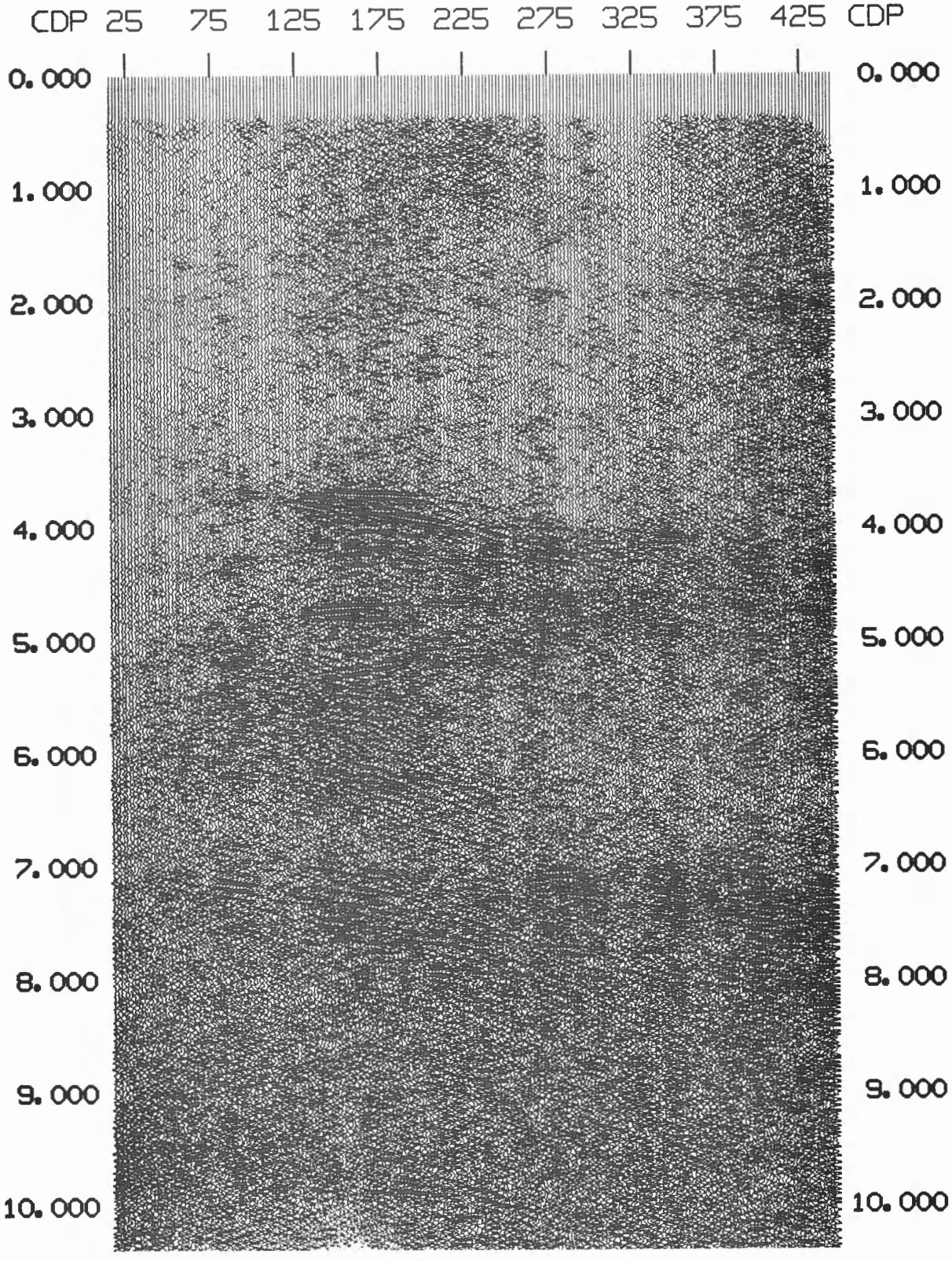

Figure 7. Stacked section with pre-stack processing applied as described in the text, displayed with only "True Amplitude Recovery" (TAR) applied. Note (1) the more detailed structures in the shallow part of the section, (2) the improved reflectivity between 3 and 8 s and the associated increased lateral continuity, and (3) the more continuous deep event at 10 s.

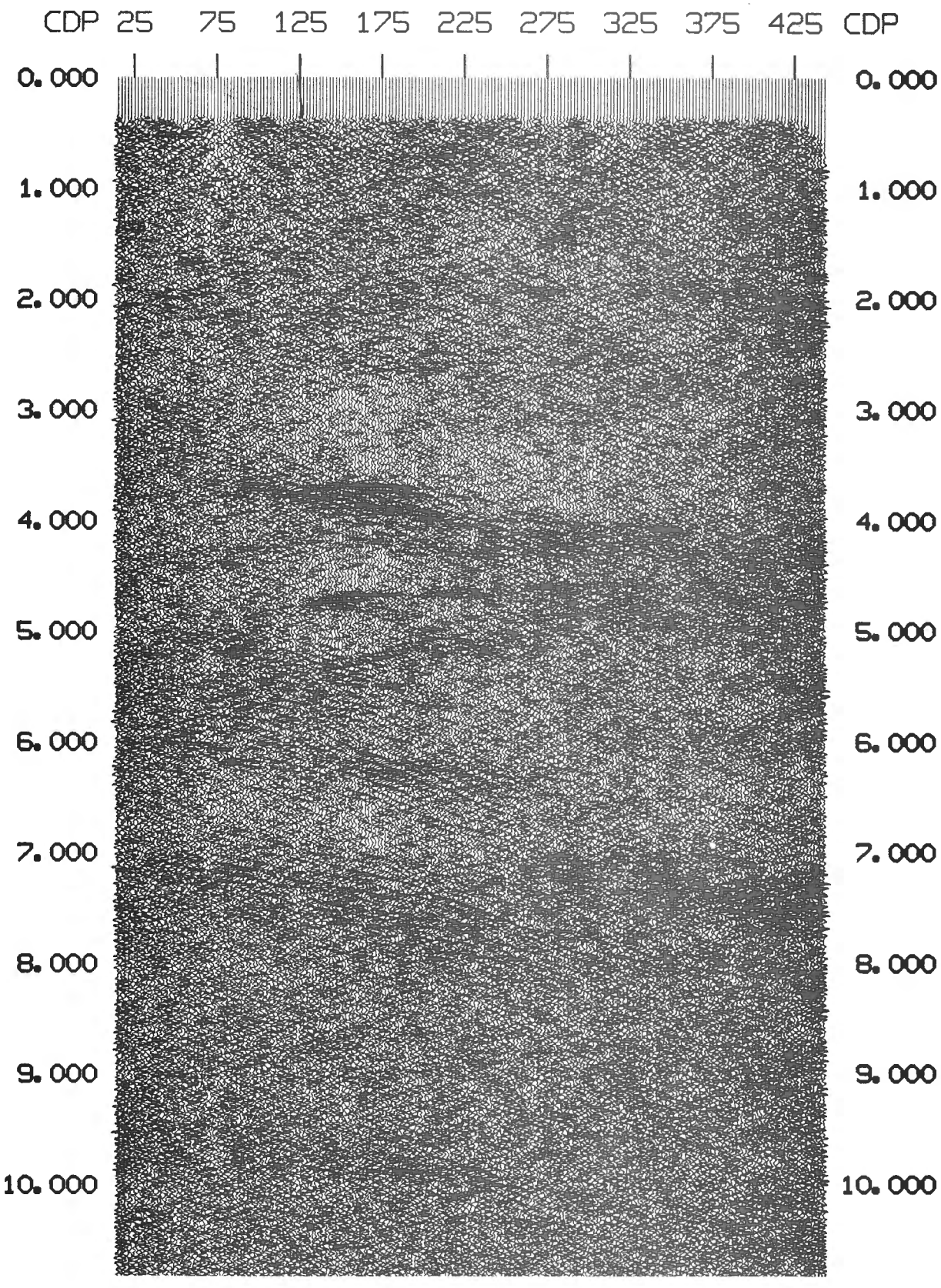

Figure 8. Stacked section with pre-stack processing applied as described in the text, displayed with post-stack AGC. The improved details of the near surface can be more clearly seen in this figure.

REFERENCES

Clowes, R.M., Brandon, M.T., Green, A.G., Yorath, C.J., Sutherland Brown, A., Kanasewich, E.R., and Spencer, C.
1987a : LITHOPROBE — Southern Vancouver Island Cenozoic subduction complex imaged by deep seismic reflections ; Canadian Journal of Earth Sciences, v. 24, p. 31-51.

Clowes, R.M., Yorath, C.J., and Hyndman, R,D.
1987b : Reflection mapping across the convergent margin of western Canada ; Royal Astronomical Society, Geophysical Journal, v. 89, p. 79-84.

Egger, A. and Ansorge, J.
1990 : Interpretation of seismic refraction data — CCSS data set 1 ; *in* Studies of Laterally Heterogeneous Structures Using Seismic Refraction and Reflection Data, ed. A.G. Green ; Geological Survey of Canada, Paper 89-13, p. 133-150.

Green, A.G., Milkereit, B., Mayrand, L., Spencer, C., Kurtz, R.D., and Clowes, R.M.
1987 : Lithoprobe seismic reflection profiling across Vancouver Island ; Royal Astronomical Society, Geophysical Journal, v. 89, p. 85-90.

Green, A.G., Clowes, R.M., and Ellis, R.M.
1990 : Crustal Studies across Vancouver Island and adjacent offshore margin ; *in* Studies of Laterally Heterogeneous Structures Using Seismic Refraction and Reflection Data, ed. A.G. Green ; Geological Survey of Canada, Paper 89-13, p. 3-25.

March, D. W. and Bailey, A. D.
1983 : A review of the two-dimensional transform and its use in seismic data processing ; First Break, v. 1(1), p. 9-21.

Reprocessing Vancouver Island LITHOPROBE data

R. Hawthorne [1]

Hawthorne, R., Reprocessing Vancouver Island LITHOPROBE data ; in Studies of Laterally Heterogeneous Structures Using Seismic Refraction and Reflection Data, ed. A.G. Green ; Geological Survey of Canada, Paper 89-13, p. 175-190, 1990.

Abstract

In spring 1987 Western Geophysical undertook the reprocessing of a small section of LITHOPROBE deep seismic reflection line 84-01, which was collected in 1984 across Vancouver Island. A variety of processing schemes were tested on the data. Using different combinations of modern processing algorithms a number of seismic sections were generated. Techniques such as dip move out (DMO) and radial predictive filtering (RPF) resulted in a substantial increase in signal to noise ratio and continuity of reflections throughout both the shallow and deeper parts of the reprocessed sections.

Résumé

Au cours du printemps de 1987, la Western Geophysical a entrepris le retraitement d'une petite partie du profil (84-01) de sismique réflexion profonde de LITHOPROBE réalisé en 1984 à travers l'île de Vancouver. Diverses méthodes de traitement ont été mises à l'essai et différentes combinaisons d'algorithmes de traitement ont été utilisées pour produire un certain nombre de coupes sismiques. Certaines techniques, comme le delta-t dû au pendage (DMO) et le filtrage prédictif radial (RPF), se sont traduites par une augmentation importante du rapport signal à bruit et une continuité de réflexion à travers les parties supérieures et profondes des coupes retraitées.

[1] Western Geophysical, 2612-37 Avenue N.E., Calgary, Alberta, T2H 1X6

INTRODUCTION

As a contribution to the Commission on Controlled Source Seismology (CCSS) workshop in Whistler, British Columbia, Western Geophysical of Canada reprocessed the southeast portion of LITHOPROBE seismic reflection line 1 from Vancouver Island. The original "raw" data and the commercially processed stacked sections were distributed to workshop participants on computer tapes in SEGY format.

REPROCESSING

Reformatting

The data were converted to an internal Western Geophysical format and processing was conducted using a 4 ms sample rate and a 16 s record length. X-Y co-ordinates and elevations of the receivers and vibration points were incorporated in the headers for subsequent crooked profile processing.

Noise — reduction by deconvolution

Upon reviewing the raw data it was evident that the most significant problems with the data concerned a variety of noise components that included multiple refractions, ground roll, air waves, out-of-plane noise bursts and numerous diffractions. Previous processing had employed a long-window AGC to handle the random noise. This approach, which normalizes the energy to give low amplitude reflections and random noise similar weight in the stack, was attempted with some success, but the principal problems associated with the varying frequency content of the different noise elements were not resolved. Where dominant, the high amplitude noise would overwhelm the deconvolution operator and if applied to the whole trace would result in major distortions. A superior approach involves applying multi-window (multi-gate) deconvolution in anticipation that the noise trains would fall within just one of the windows ; a four-window deconvolution was used in this study. Such processing may result in deterioration of the data in one of the windows, but it would not affect the entire trace.

Noise trains varied on each trace, and all traces seemed to have one or more components of noise. Clearly, editing individual noise trains and noise bursts would be a long and tedious task. Obvious bad stations were killed, but the majority of noise bursts were handled by the multi-window deconvolution. After several tests, a 180 ms operator with a prediction distance of 24 ms and pre-whitening of .1 % was found to be appropriate.

Initial brute stack

Figure 1 shows our initial brute stack with the final velocity function applied. The data are quite noisy at this stage of processing. This section was computed without crooked profile processing ; it was stacked in a conventional straight-line fashion using straight ray distances for normal moveout (NMO) corrections.

Crooked profile plot

The crooked profile plot of Figure 2 shows the shot and receiver locations on the bottom, midpoint positions of the traces in the middle, and the final crooked profile bins and common depth point (CDP) tracking along the top. The CDPs are scattered, especially those with long offsets. Several tests on the optimum bin width were conducted. We found that higher fold was more important for signal to noise enhancement than restricting the areal extent of the common midpoints. Therefore, all offsets were incorporated in the subsequent processing.

Crooked profile brute stack

After accounting for the crooked character of the profile and applying the same final velocities, the section in Figure 3 was derived. Except for a reduction in length of the section, it looks similar to the brute stack of Figure 2. Some reflections and diffractions appear smoother after crooked profile processing, perhaps compensating for some cross-and in-line dip effects.

Automatic static corrections and constant velocity stacks

An automatic statics program was run on the data using a relatively large window between 3.0 and 9.0 s and a maximum shift of plus or minus (+/-) 24 ms per trace. The 3.0-9.0 s window encompassed the highest energy in the data and the 24 ms maximum shift was based on a cursory study of first breaks, in which it was concluded that elevation changes were the dominant effect and that "weathering" corrections were likely to be comparatively minor. After computing and applying the automatic static corrections, the reflection quality throughout the section improved greatly, both in signal to noise ratio and continuity (Fig. 4). The improvement was especially noticeable in the 3.0 to 9.0 s window.

A number of constant velocity stacks were computed for the portion of line provided to CCSS workshop participants. As expected from the high refraction velocities observed on the raw records, stacking was not very sensitive to velocity changes below about 2.0 s ; a wide range of velocities resulted in stacks of similar quality. Based on velocity picks of short reflection bands it was concluded that velocities in the shallow section were fairly constant along the line, so a single velocity function was used for the entire CCSS section.

Trim static section

Trim statics were computed for three correlation windows : 1.0-4.4 s, 4.4-6.6 s and 6.6-9.0 s. A two trace model with maximum shift of +/- 12 ms was employed. These static corrections were not surface consistent ; they were designed to optimize the stack response within each common midpoint. Figure 5 shows the marginal improvements in signal to noise ratio that resulted from this process.

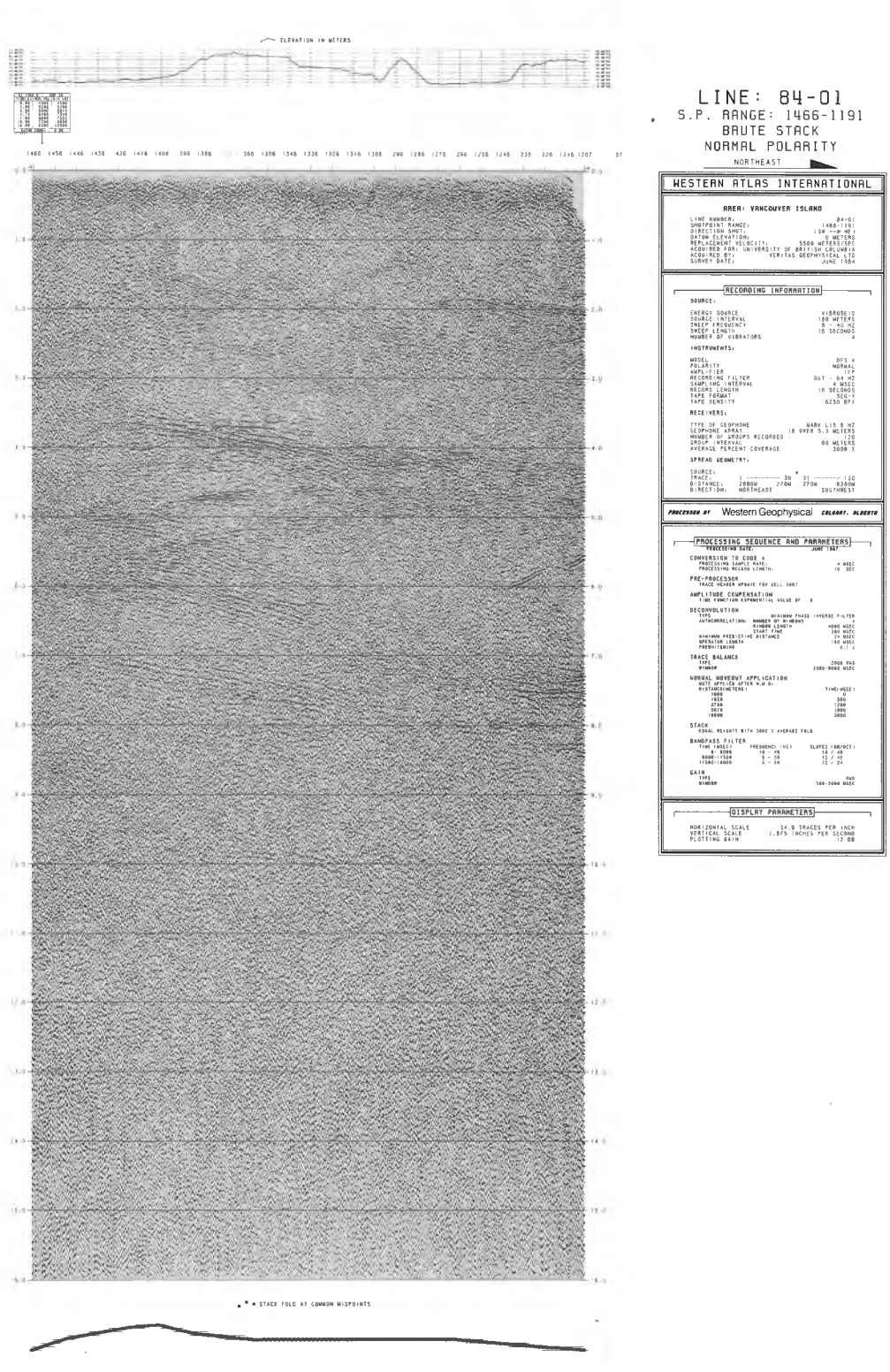

Figure 1. Initial brute stack without crooked profile processing. The final velocity function was used for normal moveout corrections.

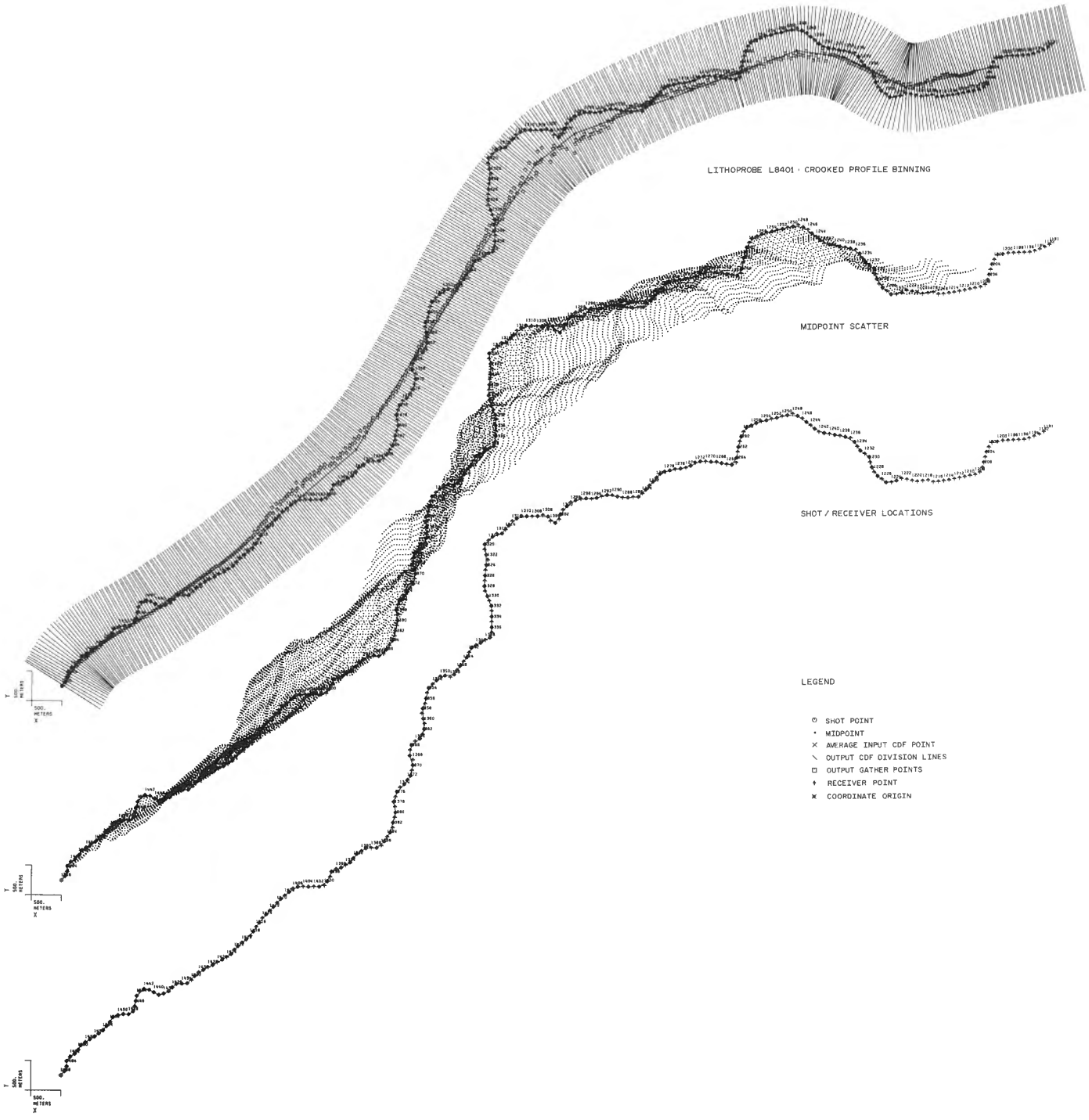

Figure 2. Shot-receiver geometry (bottom), midpoints of each shot-receiver pair (middle), and crooked profile bins (upper).

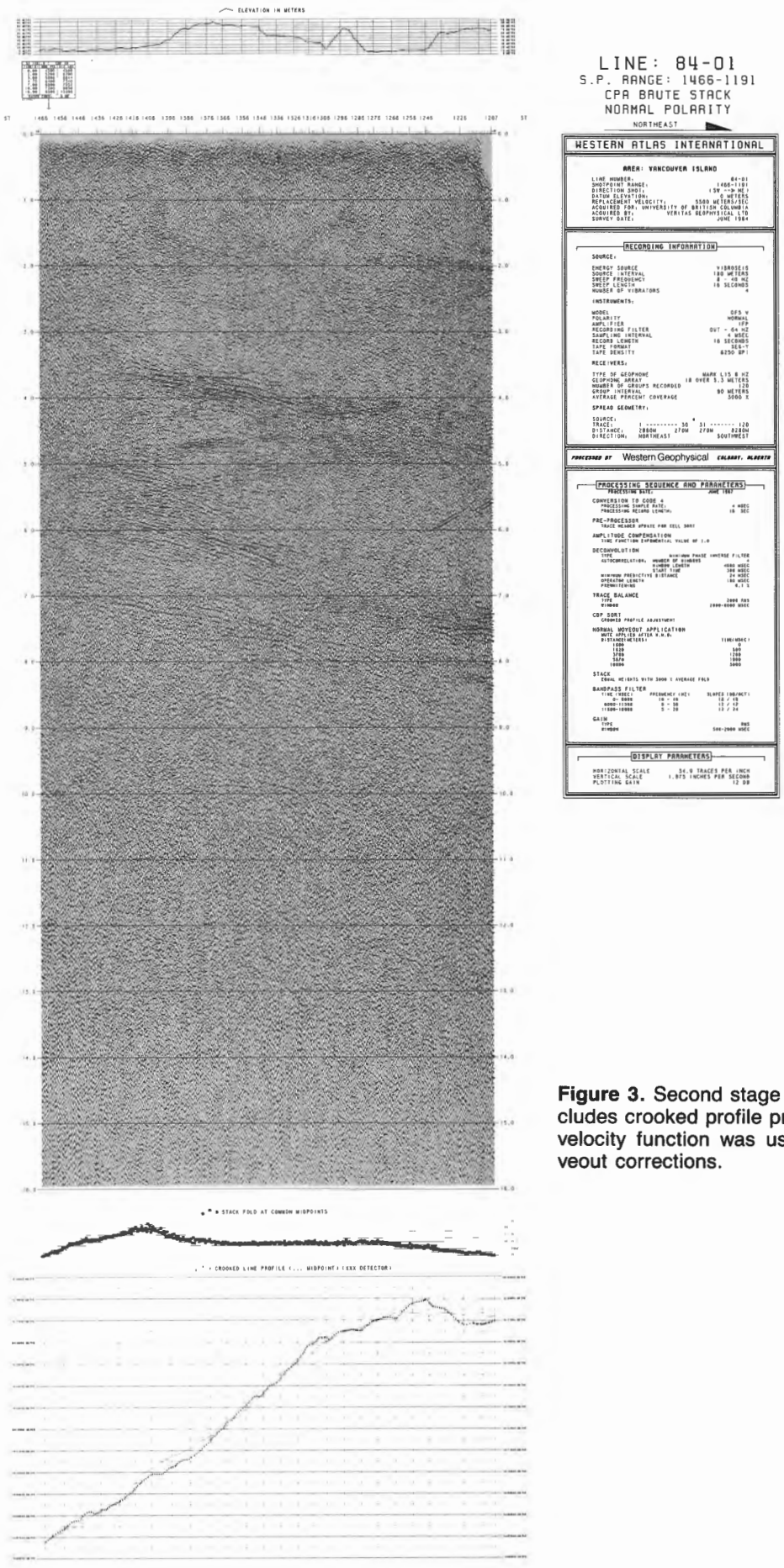

Figure 3. Second stage brute stack that includes crooked profile processing. The final velocity function was used for normal moveout corrections.

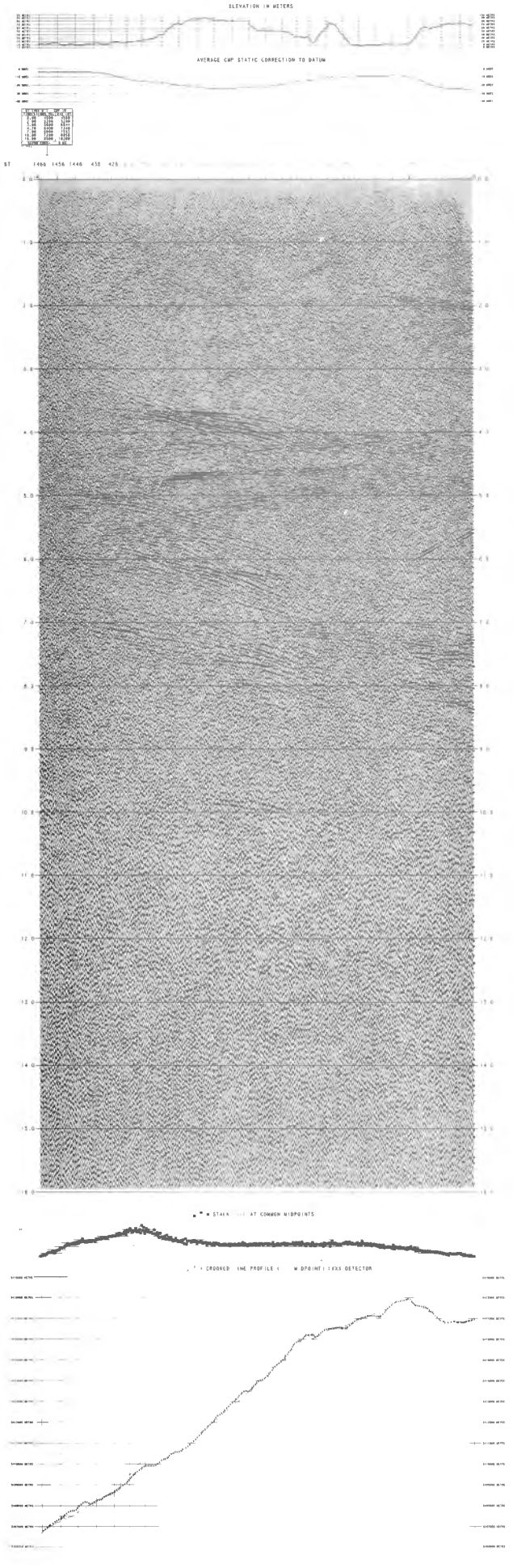

Figure 4. Seismic section after application of the automatic statics routine (*see* text for details).

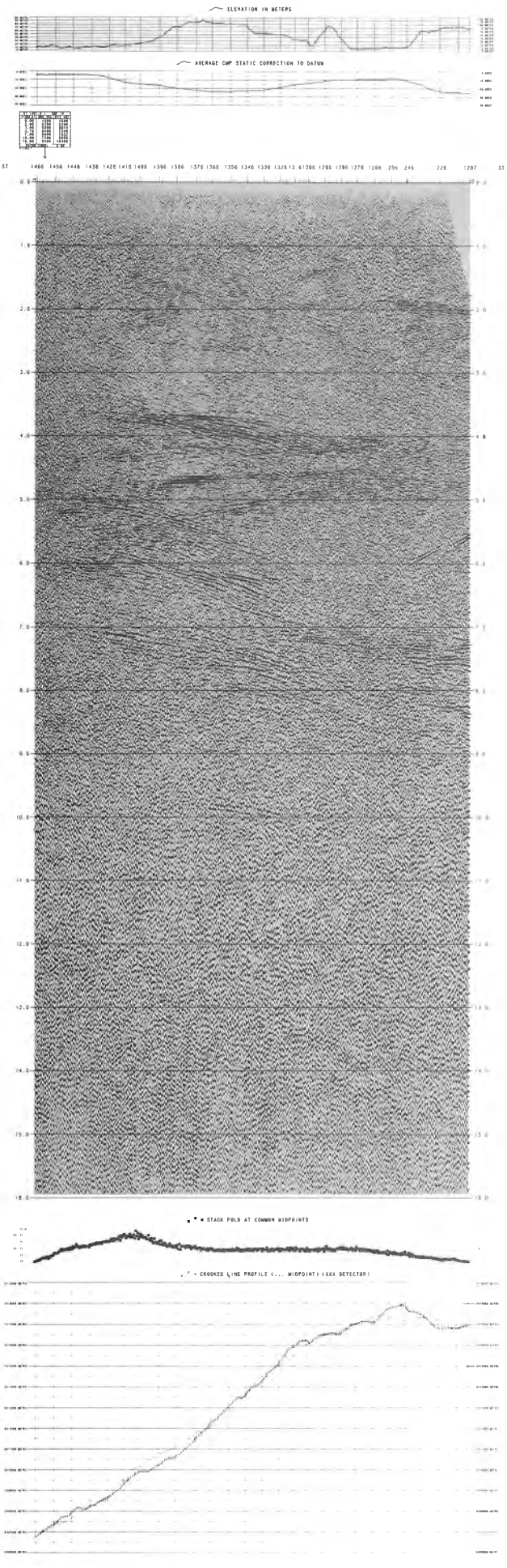

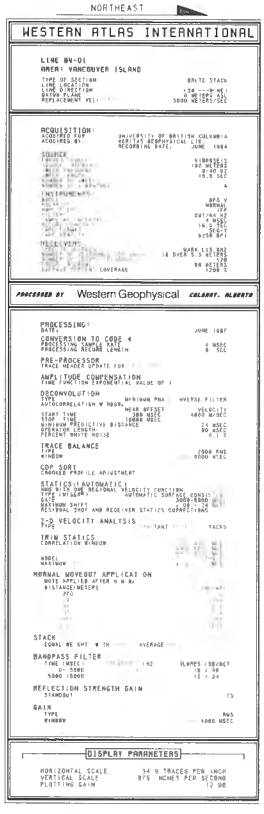

Figure 5. As for Figure 4, but after application of the trim statics routine (*see* text for details).

Dip moveout section

Dip moveout (DMO) performs two functions in a data set of this type. It compensates for "errors" in stacking velocity caused by the dip of events, and it reduces the dip-dependent smear of CDPs by placing reflections at their correct common reflection point positions. An additional benefit derived from this process is that it leads to superior reduction of surface-oriented noise (Rayleigh and Love waves — ground roll) during stacking (this phenomenon is described by Ken Larner in an internal Western Geophysical paper "Suppression of backscattered noise by partial prestack migration"); surface wave velocities are quite different from the stacking velocities throughout the section. A comparison between the DMO section in Figure 6 and the section in Figure 5 demonstrates that the signal to noise ratio and overall coherency have been greatly improved. It is not certain which aspect of DMO was primarily responsible for the improvements. However, based on the high stacking velocities, we suggest that the attenuation of surface wave noise was an important element of DMO. Because of the wide variation of dips in the data, the same results could not have been achieved through F-K filtering.

Radial predictive filtered section

The DMO stack was passed through Western Geophysical's radial predictive filter program (RPF), which is designed to enhance coherency and eliminate noise outside a specified range of dips. Filter parameters were chosen to pass events that had dips within +/- 8 ms per trace and attenuate events outside that range. The data were crosscorrelated in increments of +/- 1 ms per trace to determine the optimum coherency for each event. The RPF program computes a model trace by assigning the highest correlation estimate to each sample of each trace. These model traces have a synthetic appearance, much like the line drawings used in previous LITHOPROBE interpretations. To present a visually more pleasing image, we have added a portion of the original data back to the model section. In Figure 7, 40 % of the unfiltered section was added back. RPF has resulted in a section with improved signal to noise ratio, clarifying many shallow events.

Original processed section

The original processed section is shown in Figure 8. It represents the "final product" of another commercial processing company. In comparing Figure 8 to Figures 5 to 7 it is apparent that we have (a) improved the overall signal to noise ratio, and (2) extracted new information from the shallow and middle parts of the section. Multi-window deconvolution and DMO were the two most important new processes applied to the data. These results are consistent with our experiences in processing data from the Arctic, North Africa and South America; in most of these examples the signal to noise ratio was noticeably improved by using a combination of multi-window deconvolution and DMO. Historically, data collected off the east coast of Canada were F-K filtered twice, once in the shot domain and once in the receiver domain to suppress near-surface scattered noise. However, we have found that DMO is more effective than F-K filtering at suppressing background noise. Furthermore, DMO does not result in the "wormy" looking sections that are typical of F-K filtering, and instead of degrading the dipping structures it actually enhances them.

Dual Polarity section

The section in Figure 7 is replotted in Figure 9 using a display-enhancement technique that we refer to as dual polarity. This display is achieved by plotting all peaks and troughs as peaks and plotting only every third sample. Random noise, which should have approximately equal positive and negative components, appears with relatively uniform amplitude and on the dual polarity display tends to be less obvious compared to the signal. This display is useful for observing faults, which appear in association with shadowed zones. We have used this technique for displaying data from the Alberta foothills, and it is now widely accepted in Europe for displaying data collected across highly structured plays in the North Sea. We find that people like it better the longer they look at it.

Migrated section — normal and dual polarity displays

The migrated section in Figure 10 is included with a disclaimer. We are not convinced that we have the appropriate velocities to migrate this section properly, and we note that the migration aperture for a large portion of the data (3.0 s and below) is wider than the length of the section, so events cannot be moved to their correct positions. Taking these factors into account, migration appears to have collapsed diffractions and clarified a few of the faults in the 4.0 — 8.0 s range on the left side of the section. Some reflections along the right side of the section near 1.0 s and 2.0 s have also been better defined. The shallow events are further enhanced in the dual polarity display of Figure 11. Because of the limited aperture of the data, the "wormy" image below 8.0 s is not reliable.

Comments on the proposed Moho event

As stated during the workshop, I am going to use the processors prerogative of pointing out a problem with a portion of the data and then leave it to others to judge its significance. A reflection at approximately 10 s centred near shotpoint 1346 was identified as the Moho in one figure of the workshop material; it was marked with a question mark. We have performed what we refer to as mute tests, which involve stacking the data with progressively increasing maximum offset ranges. Figure 12 shows portions of these distant dependent stacks centred near the "Moho" event; the maximum offset range in metres is indicated along the top of each section. At offsets up to 900 m the data are noisy, due mainly to the low fold. As the offsets are increased to 1800 m the quality improves and then stays relatively constant to 2700 m. As traces with greater than 2700 m offset are added into the stack, the "Moho" event deteriorates significantly. The deterioration is unlikely to be caused by application of incorrect

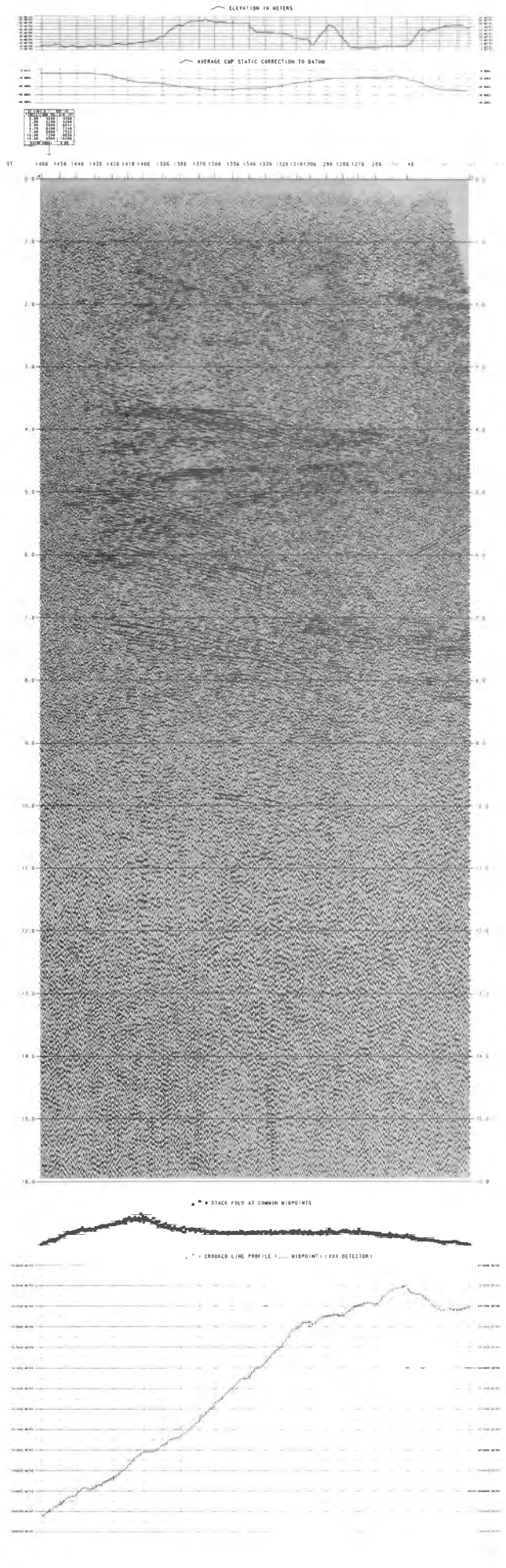

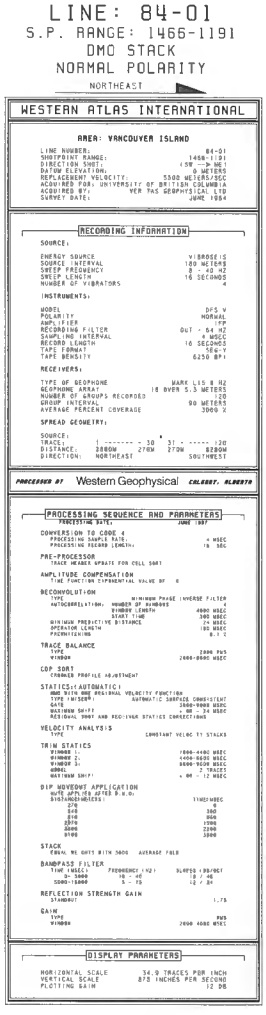

Figure 6. As for Figure 5, but after application of dip moveout (DMO ; *see* text for details).

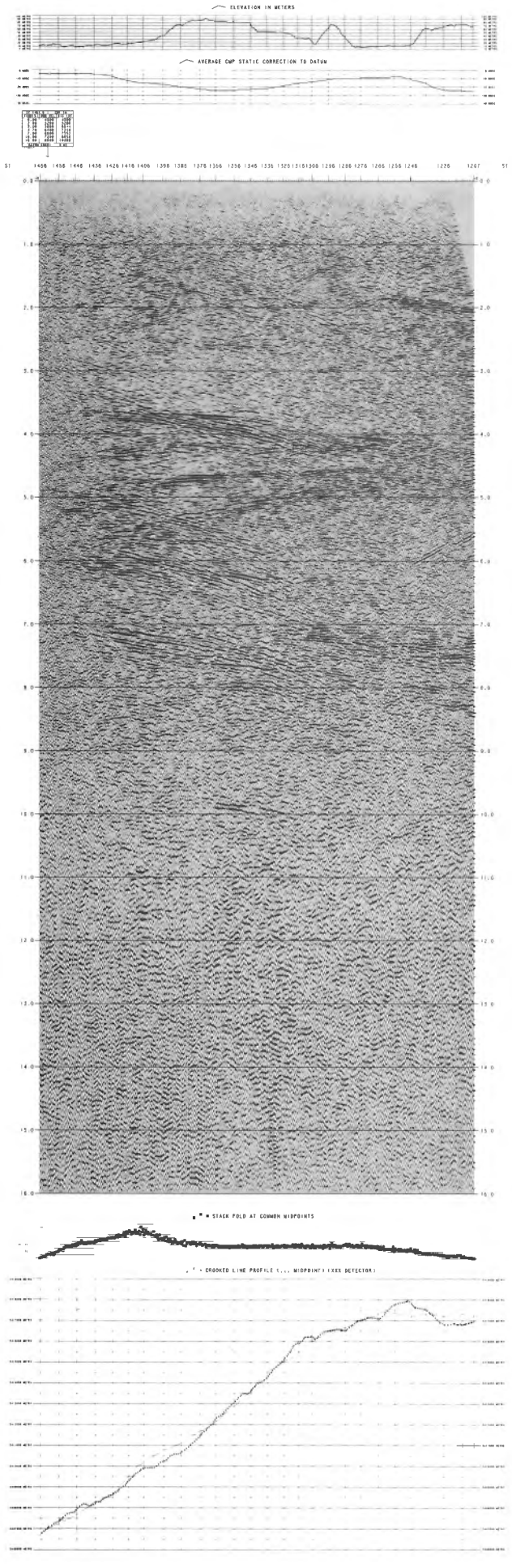

LINE: 84-01
S.P. RANGE: 1466-1191
DMO/RPF STACK
NORMAL POLARITY
NORTHEAST

WESTERN ATLAS INTERNATIONAL

AREA: VANCOUVER ISLAND

LINE NUMBER:	84-01
SHOTPOINT RANGE:	1466-1191
DIRECTION SHOT:	SW --> NE
DATUM ELEVATION:	0 METERS
REPLACEMENT VELOCITY:	2500 METERS/SEC
ACQUIRED FOR:	UNIVERSITY OF BRITISH COLUMBIA
ACQUIRED BY:	VERITAS GEOPHYSICAL LTD
SURVEY DATE:	JUNE 1984

RECORDING INFORMATION

SOURCE:

ENERGY SOURCE	VIBROSEIS
SOURCE INTERVAL	100 METERS
SWEEP FREQUENCY	8 - 40 HZ
SWEEP LENGTH	16 SECONDS
NUMBER OF VIBRATORS	4

INSTRUMENTS:

MODEL	DFS V
POLARITY	NORMAL
AMPLIFIER	IFP
RECORDING FILTER	OUT - 64 HZ
SAMPLING INTERVAL	4 MSEC
RECORD LENGTH	15 SECONDS
TAPE FORMAT	SEG-Y
TAPE DENSITY	6250 BPI

RECEIVERS:

TYPE OF GEOPHONE	MARK L15 8 HZ
GEOPHONE ARRAY	18 OVER 5.1 METERS
NUMBER OF GROUPS RECORDED	120
GROUP INTERVAL	90 METERS
AVERAGE PERCENT COVERAGE	3080 %

SPREAD GEOMETRY:

SOURCE:

TRACE:	1 ---------- 30	31 ------- 120		
DISTANCE:	2860M	270M	8280M	
DIRECTION:	NORTHEAST		SOUTHWEST	

PROCESSED BY: Western Geophysical CALGARY, ALBERTA

PROCESSING SEQUENCE AND PARAMETERS

PROCESSING DATE: JUNE 1987

CONVERSION TO CODE 4
PROCESSING SAMPLE RATE: 4 MSEC
PROCESSING RECORD LENGTH: 16 SEC

PRE-PROCESSOR
TRACE HEADER MPRATE FOR CELL SORT

AMPLITUDE COMPENSATION
TIME FUNCTION EXPONENTIAL VALUE OF 1.8

DECONVOLUTION

TYPE	MINIMUM PHASE INVERSE FILTER
*ANTICIPATED(AT) 88: NUMBER OF WINDOWS	4
WINDOW LENGTH	4000 MSEC
START TIME	300 MSEC
MINIMUM PREDICTIVE DISTANCE	24 MSEC
OPERATOR LENGTH	168 MSEC
PREWHITENING	0.1 %

TRACE BALANCE

TYPE	2000 RMS
WINDOW	2040-3080 MSEC

CDP SORT
CROOKED PROFILE ADJUSTMENT

STATICS(AUTOMATIC)
NMO WITH NMO RESIDUAL VELOCITY FUNCTION
DATUM (ATSUMP): AUTOMATIC SURFACE CONSISTENT
GATE 3600-3096 MSEC
MAXIMUM SHIFT ± 88 - 24 MSEC
RESIDUAL SHOT AND RECEIVER STATICS CORRECTIONS

VELOCITY ANALYSIS
TYPE CONSTANT VELOCITY STACKS

TRIM STATICS

WINDOW 1:	1000-4000 MSEC
WINDOW 2:	4400-6600 MSEC
WINDOW 3:	6600-9000 MSEC
GATES	7 TRACES
MAXIMUM SHIFT	± 88 - 12 MSEC

DIP MOVEOUT APPLICATION
MUTE APPLIED AFTER D.M.O.
DISTANCE(METERS):

2760	0
5520	200
8280	600
2070	1000
3680	2200
8100	3000

STACK
EQUAL WEIGHTS WITH 3000 AVERAGE FOLD

BANDPASS FILTER

TIME (MSEC):	FREQUENCY (HZ):	SLOPES (DB/OCT):
0- 5000	10 - 40	18 / 48
5000-10000	5 - 15	12 / 24

REFLECTION STRENGTH GAIN
EXPONENT 1.73

GAIN

TYPE	RMS
WINDOW	2000-4000 MSEC

RADIAL PREDICTIVE FILTER
DIP LIMIT +/- 8 MS/TRACE
ADD-BACK ERC OF UNFILTERED DATA

DISPLAY PARAMETERS

HORIZONTAL SCALE	34.9 TRACES PER INCH
VERTICAL SCALE	1.875 INCHES PER SECOND
PLOTTING GAIN	12 DB

Figure 7. As for Figure 6, but after application of the radial predictive filter (RPF ; *see* text for details).

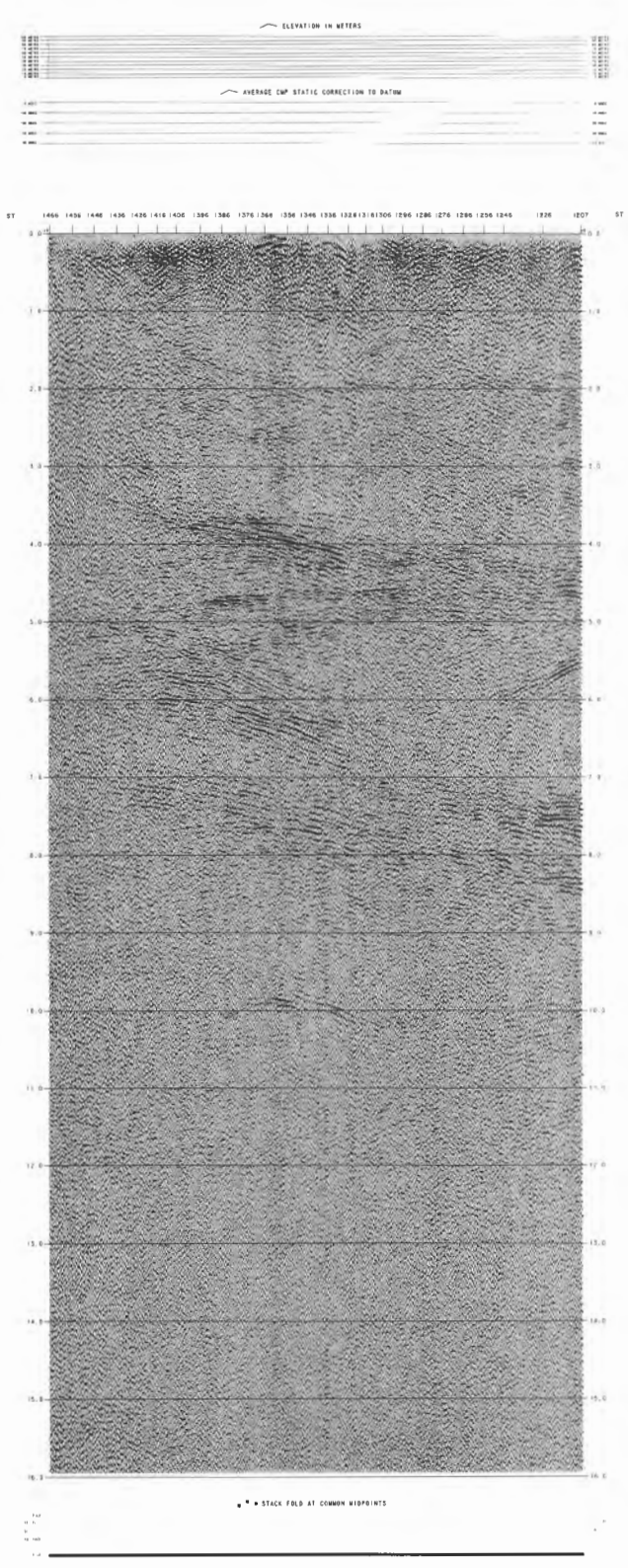

Figure 8. The original processed section provided by the CCSS workshop organisors.

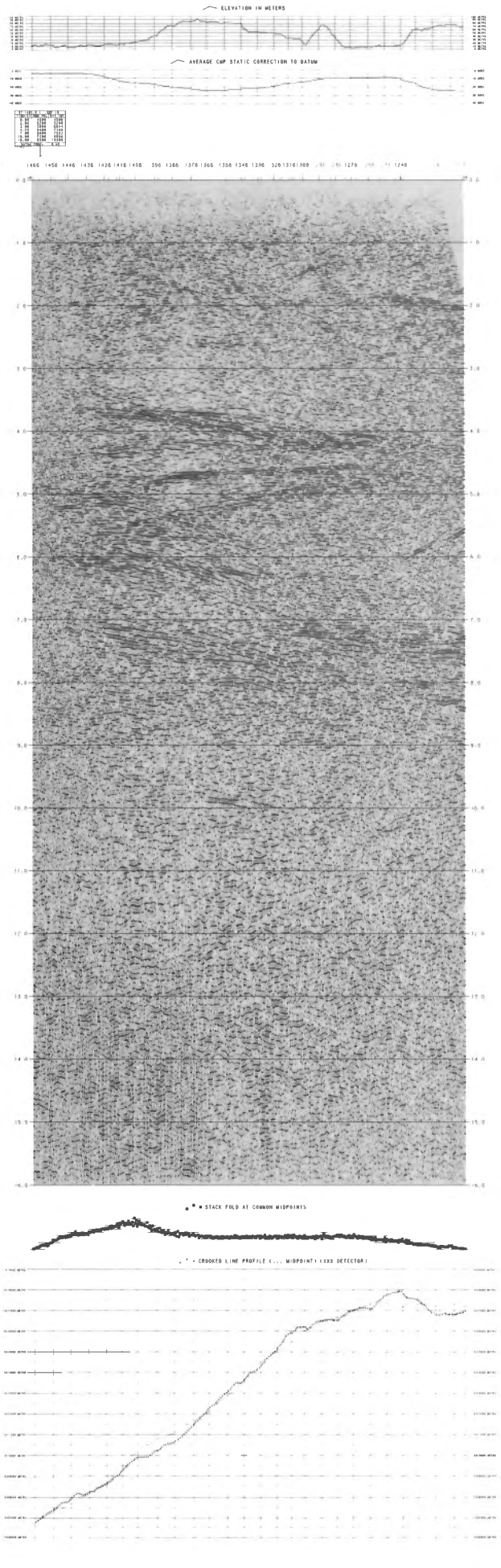

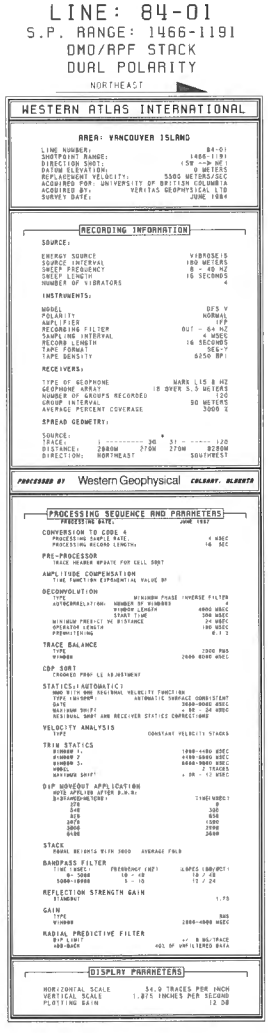

Figure 9. As for Figure 7, but with dual polarity display (*see* text for details).

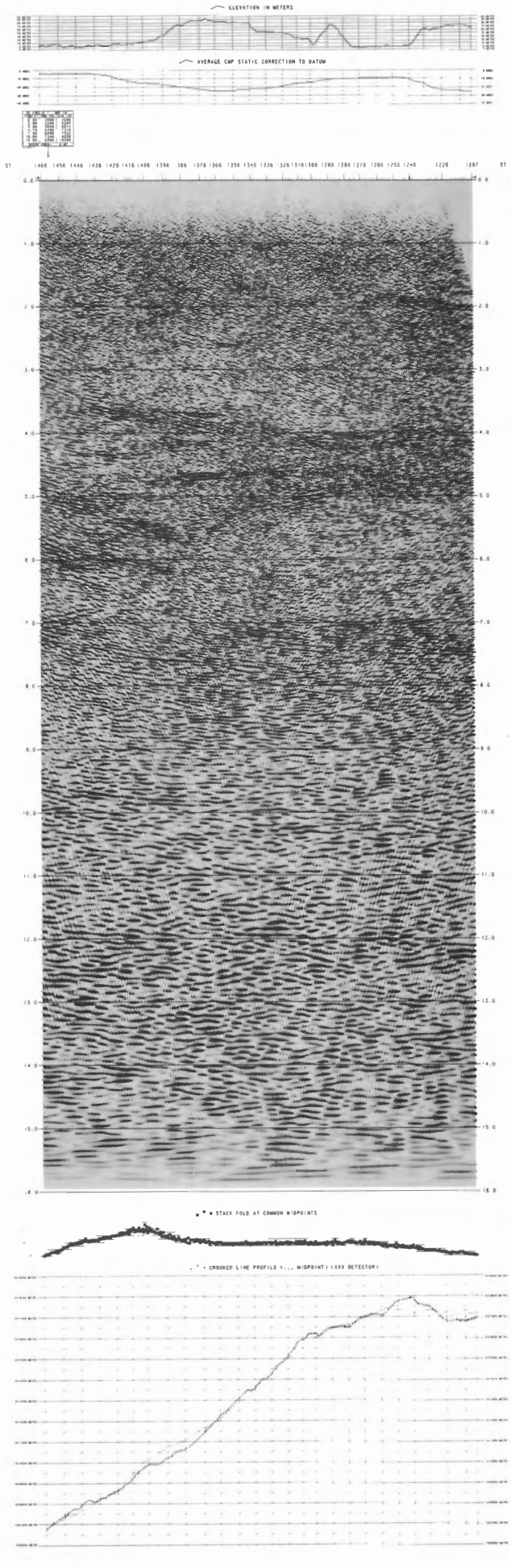

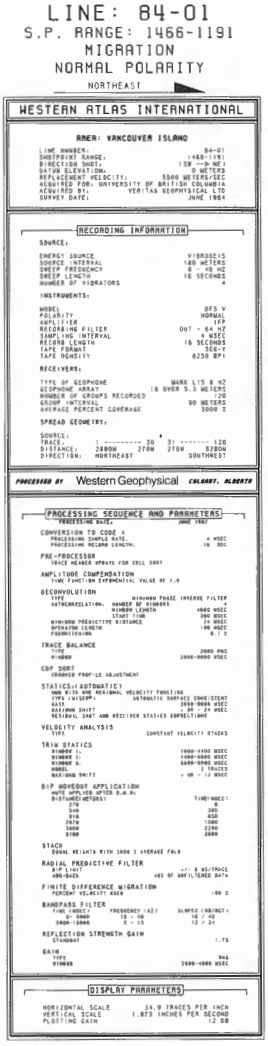

Figure 10. As for Figure 7, but after migration (*see* text for details and disclaimer).

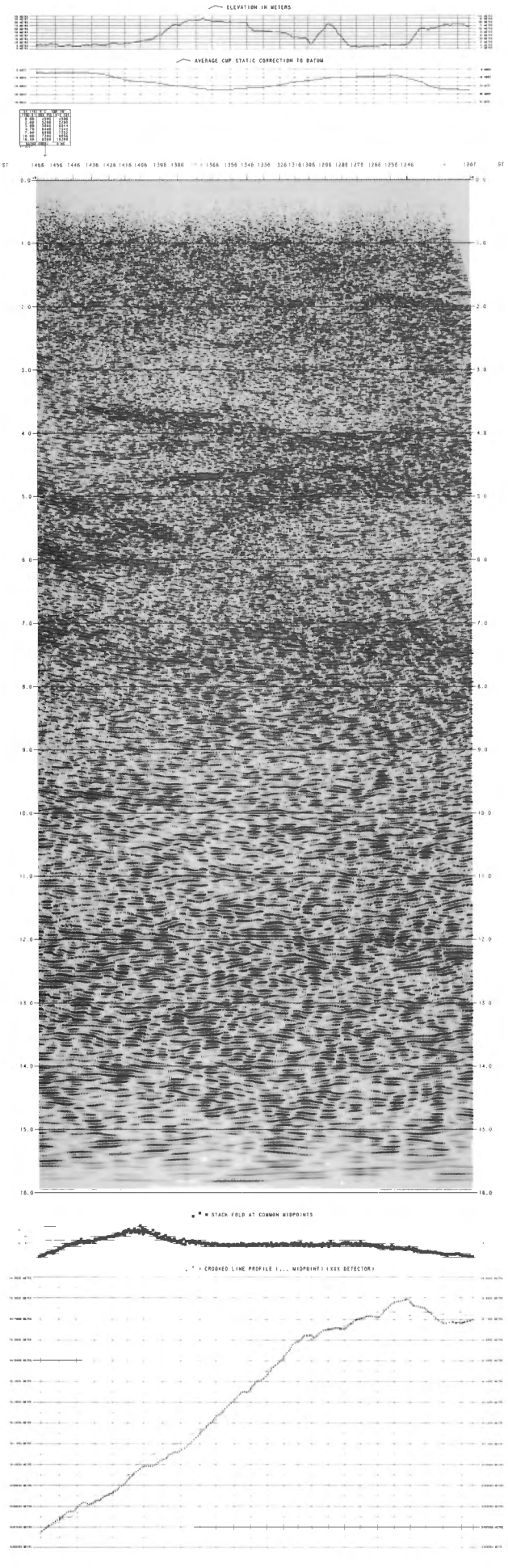

Figure 11. As for Figure 10, but with dual polarity display.

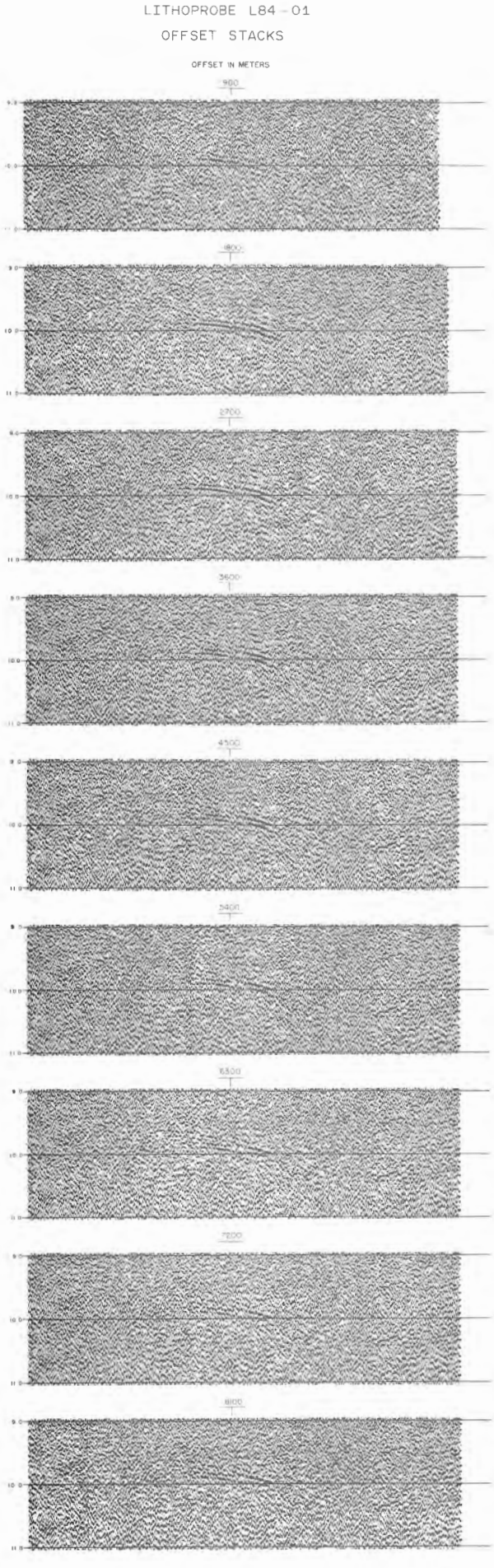

Figure 12. Stacks computed for different maximum offsets (traces from 0 to 900 m are included in the 900 m stack, traces from 0 to 1800 m are included in the 1800 m stack etc.) near the proposed "Moho" event.

stacking velocities — there is very little moveout at Moho depths. If this event was a genuine deep reflection its image should improve with increasing offset. As this does not happen, I suggest that the proposed "Moho" event is instead due to side scatter.

CONCLUSIONS

The CCSS seismic reflection data obtained from southeast Vancouver Island were improved by the reprocessing we have performed; multi-window deconvolution and DMO were particulary effective. There is sufficient improvement in the shallow section to warrant a re-interpretation of the data. Noise trains and noise bursts associated with diffractions, point scatterers and cultural noise will always be a problem with these type of data. The noise could be attenuated more effectively by multichannel processing if the data were recorded with a larger number of channels (240 or 480), allowing smaller group intervals, higher fold, longer offsets, and/or combinations thereof with a relatively small increase in cost.

Reflection seismic data from Vancouver Island processed using Geovecteur[1] software package on a Cray supercomputer (CCSS topic III)

L. Levato[2], D. Alioth[2], R. Olivier[2] and J.-J. Wagner[2]

Levato, L., Alioth, D., Olivier, R. and Wagner, J.-J., Reflection seismic data from Vancouver Island processed using Geovecteur software package on a Cray supercomputer (CCSS topic III) ; in Studies of Laterally Heterogeneous Structures Using Seismic Refraction and Reflection Data, ed. A.G. Green ; Geological Survey of Canada, Paper 89-13, p. 191-205, 1990.

Abstract

The southwestern portion of LITHOPROBE reflection line 1 from Vancouver Island (CCSS data set III) has been reprocessed using GEOVECTEUR software running on the CRAY-1S/2300 of the Computer Centre of l'Ecole Polytechnique Fédérale de Lausanne. The most effective steps in improving the seismic section were : zero-phase deconvolution, surface consistent residual static corrections and dip moveout (DMO). Zero-phase deconvolution attenuated the ground-roll, residual static corrections significantly improved the section, and dip moveout made an important contribution in determining the velocity functions for stack and migration. The final stack shows improved continuity of reflections and brings out intersecting events at about 5.7 s. The post-stack migration after DMO successfully uncrossed these events and improved the seismic image.

Résumé

La partie sud-ouest de la ligne de sismique réflexion 1 du projet LITHOPROBE dans l'île de Vancouver (jeu de données III de la CSSC) a été retraitée à l'aide du logiciel GEOVECTEUR installé sur le CRAY-1S/2300 du Centre de Calcul de l'Ecole Polytechnique Fédérale de Lausanne. Des améliorations notables ont été apportées par : la déconvolution "phase nulle", les corrections statiques résiduelles (surface consistante) et la migration partielle avant sommation (dip moveout — DMO). La déconvolution "phase nulle" a attenué considérablement le bruit des ondes de surface, les corrections statiques résiduelles ont amélioré le profil de façon remarquable et le DMO a été déterminant dans le choix d'une loi de vitesse appropriée pour la sommation et la migration après sommation. Le profil sismique final montre une meilleure continuité de tous les réflecteurs et met en évidence deux événements qui s'intersectent aux environs de 5.7 s. La migration après sommation et après DMO a décroisé ces événements et a amélioré l'image sismique.

[1] Trademark of Compagnie Générale de Géophysique.

[2] Groupe Romand d'Analyse Numérique de Sismique Réflexion (GRANSIR PNR20), Institut de Géophysique, Université de Lausanne, Château de Bassenges, CH 1024 ECUBLENS, Switzerland.

INTRODUCTION

Switzerland, like several other countries, has developed a program to study deep geological structures. As part of this program, PNR20, three deep reflection profiles have been collected in the Swiss Alps and two seismic reflection data processing centres have been established (Schweizerische Arbeitsgruppe für Reflexionsseismik, 1988). Our group, GRANSIR at the University of Lausanne, has access to facilities of the computer centre of l'Ecole Polytechnique Fédérale de Lausanne (EPFL). Specifically, the processing is performed on a CRAY-1S/2300 supercomputer (Fig. 1) using Compagnie Générale de Géophysique (CGG) Geovecteur software (Compagnie Générale de Géophysique, 1986).

The aim of CCSS topic III was to produce an enhanced image of the southwest portion of onshore LITHOPROBE seismic reflection line 1. The field parameters for the survey and the material used are described in Green et al. (1990a, b). The crooked line processing of data set III yielded 444 common depth point (CDP) bins spaced at 45 m intervals.

PHASE 1 : PRE-STACK PROCESSING AND TESTS

Figure 2 summarizes the main steps of the processing performed in this study. After converting the data from SEGY to Geovecteur format, we selected an appropriate CDP line geometry. First, the geometry of the field spread was used to compute the CDP distribution for the various pairs of source and receiver locations corresponding to the 120 traces recorded from each vibrator point (VP). Since the seismic line was not straight, the result was a "swath" of CDP points. In a second pass, the region covered by the CDP "swath" was divided into numerous small sections, or bins, and each trace was assigned to one of these bins (Fig. 3). To work in 2-D it was necessary to project the "swath" on to an average CDP line chosen on the basis of the CDP distribution. Usually an average line is chosen to pass through the CDP concentration in such a way as to minimize deviations from a general average direction and to avoid any sudden direction changes. In processing the Vancouver Island data we chose the smooth line shown in Figure 4.

After spherical divergence compensation, two different deconvolution "modules" were tested on several common source records : a spiking deconvolution, and a zero-phase deconvolution between 8 and 40 Hz (the source sweep) in which the traces were fed through several overlapping band-pass filters and then equalized in a sliding window of fixed length. Zero-phase deconvolution more effectively attenuated the slowly propagating low frequency noise (Fig. 5), and thus was chosen for subsequent processing.

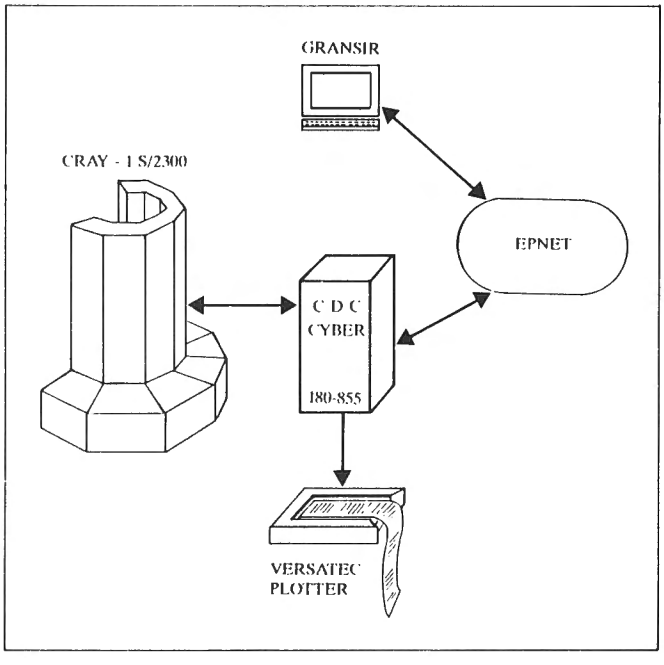

Figure 1. Gransir seismic processing resources.

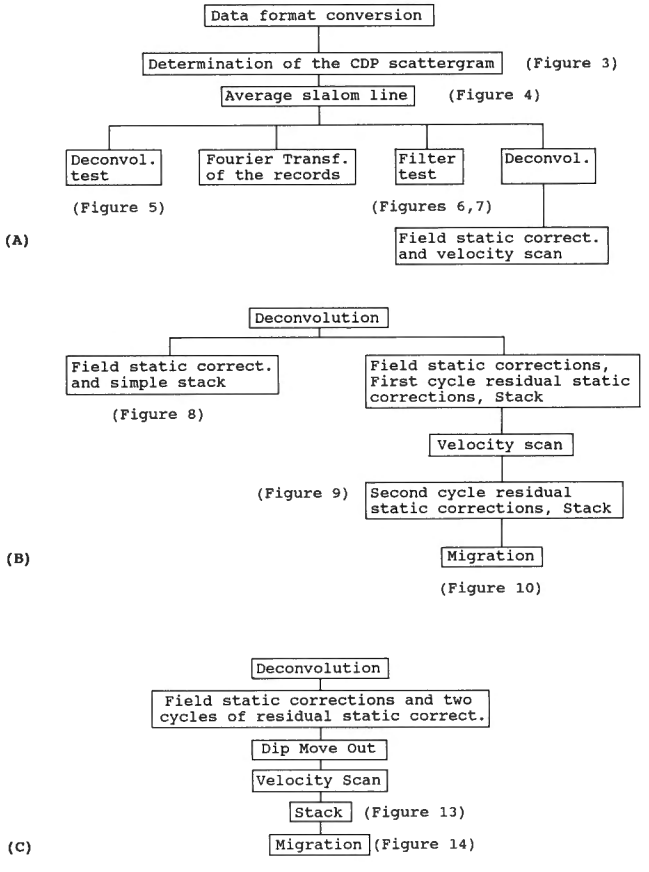

Figure 2. Processing sequence for : A) pre-stack processing ; B) stack and migration ; C) stack and migration after dip move out.

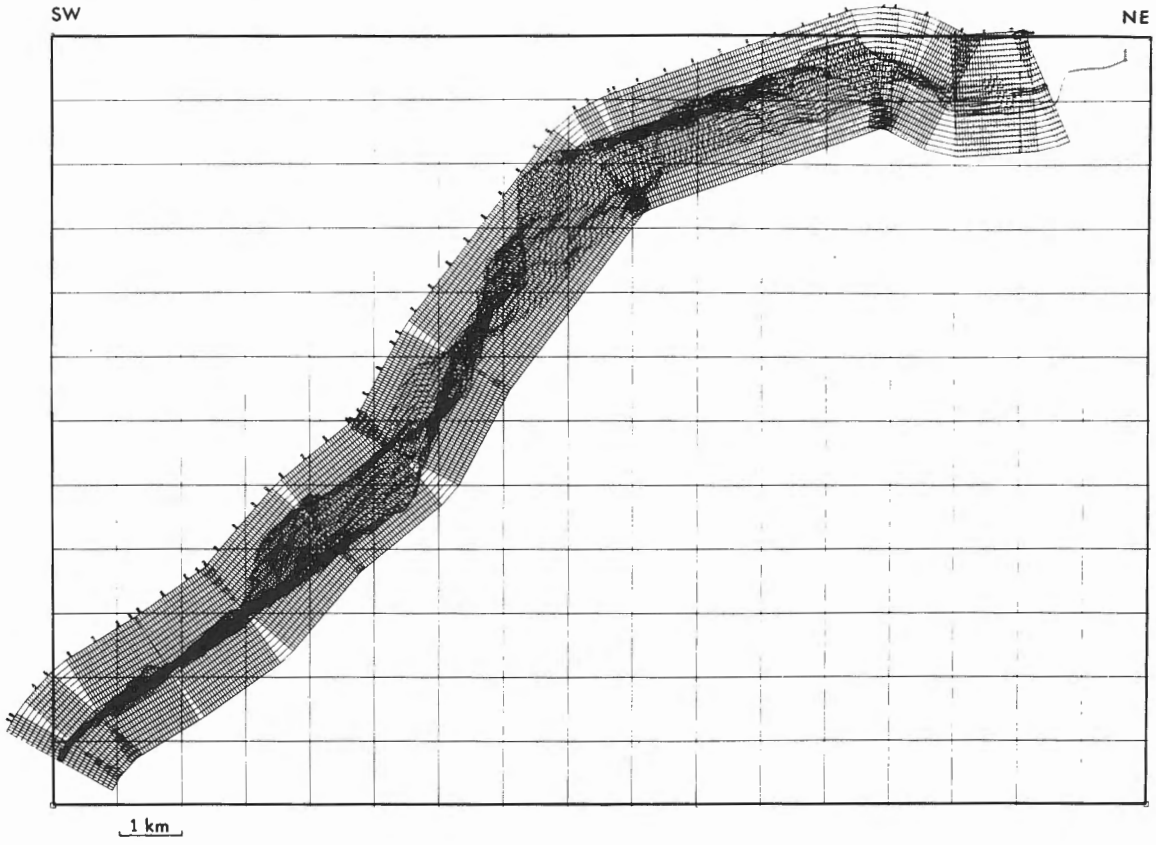

Figure 3. CDP swath and associated bins. The length and width of each bin are 90 m and 45 m respectively.

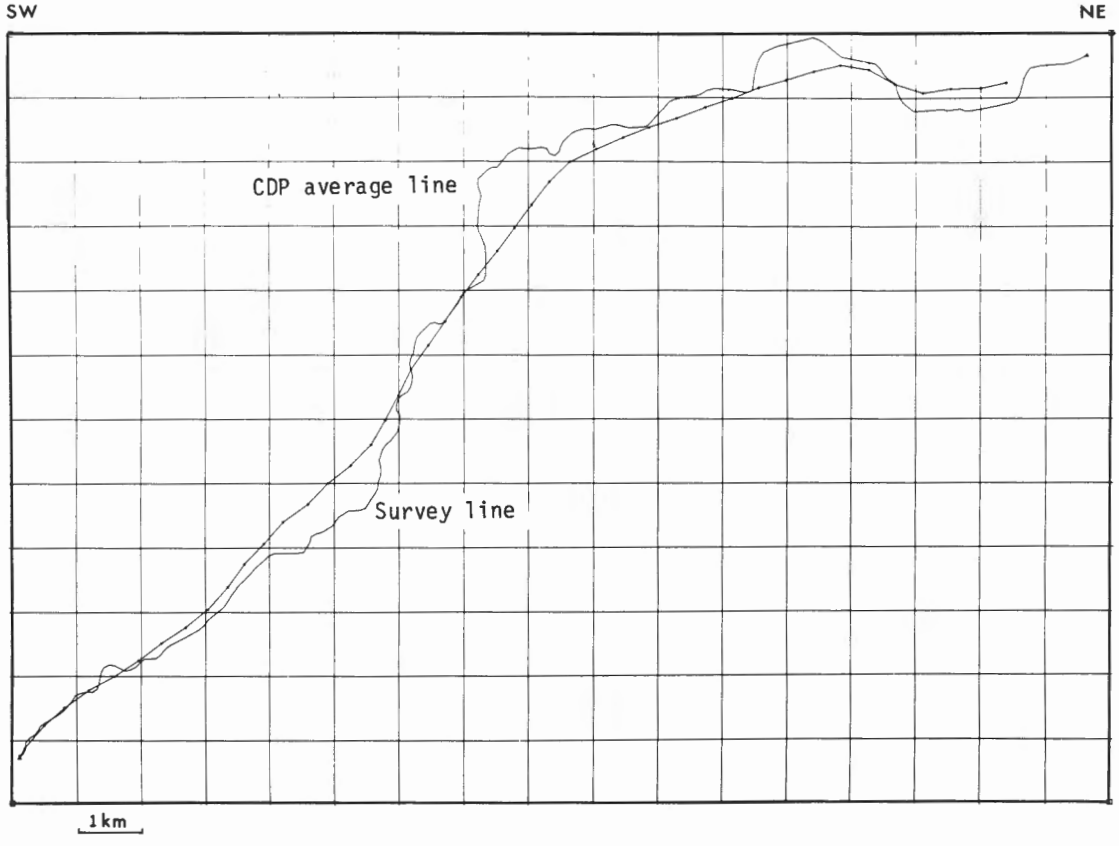

Figure 4. Survey line (light) and selected CDP average line.

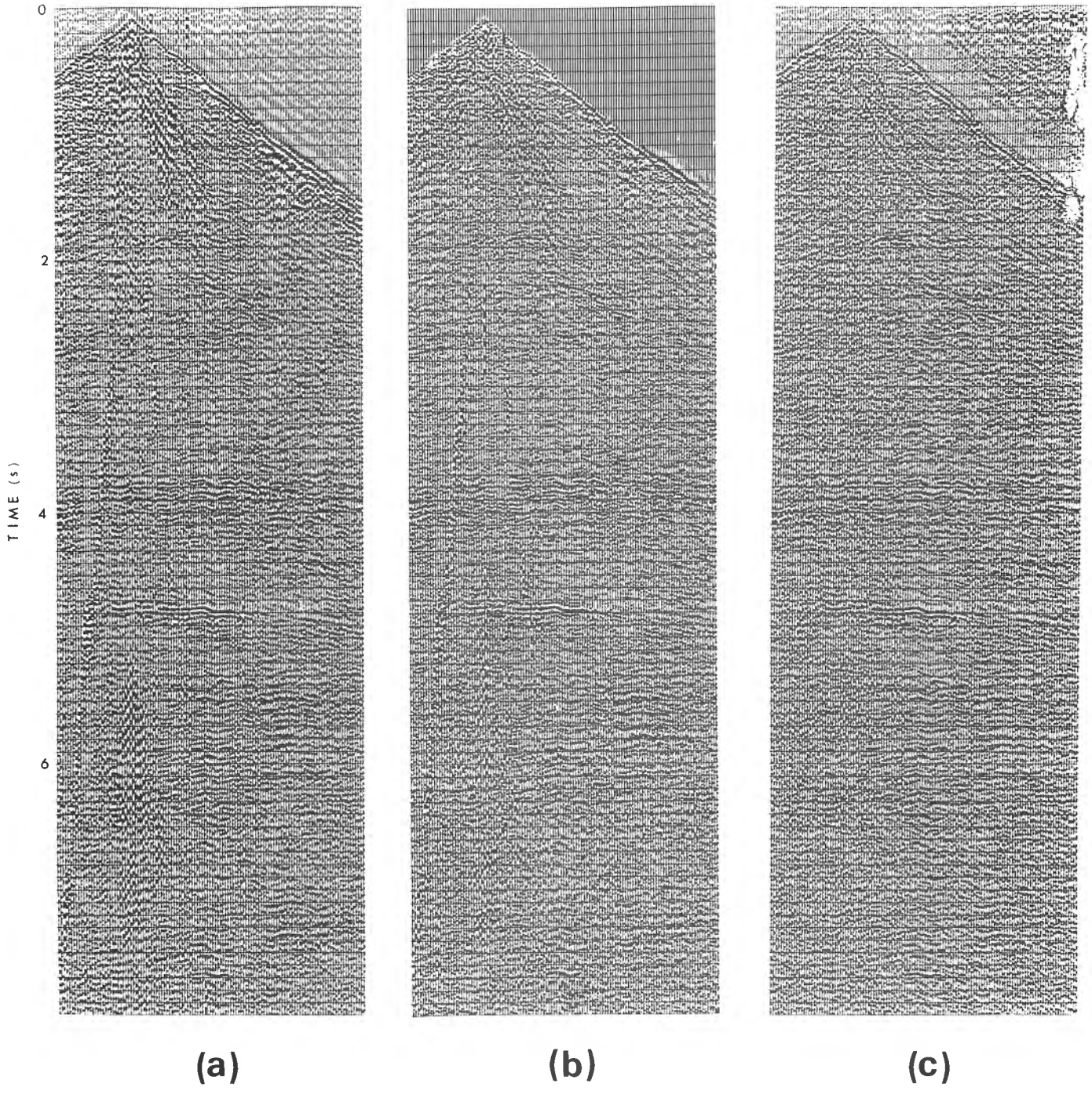

Figure 5. Deconvolution tests: a) VP gather 65 with no processing; b) spiking deconvolution; c) zero-phase deconvolution.

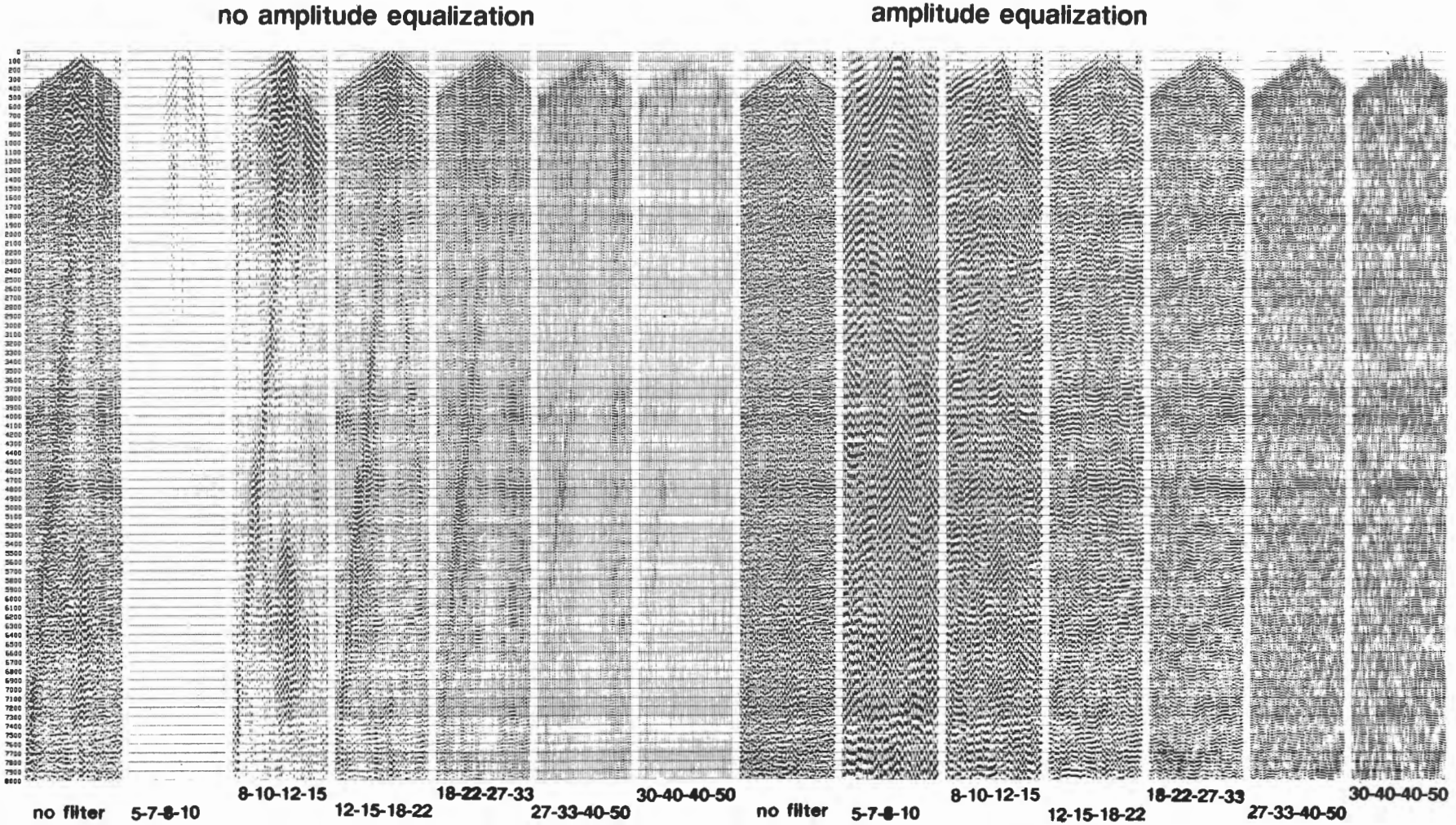

Figure 6. Band-pass filter tests applied to 0-8 s of VP. The figures under each column are: cut-on, roll-on, roll-off, cut-off frequencies of each band pass filter.

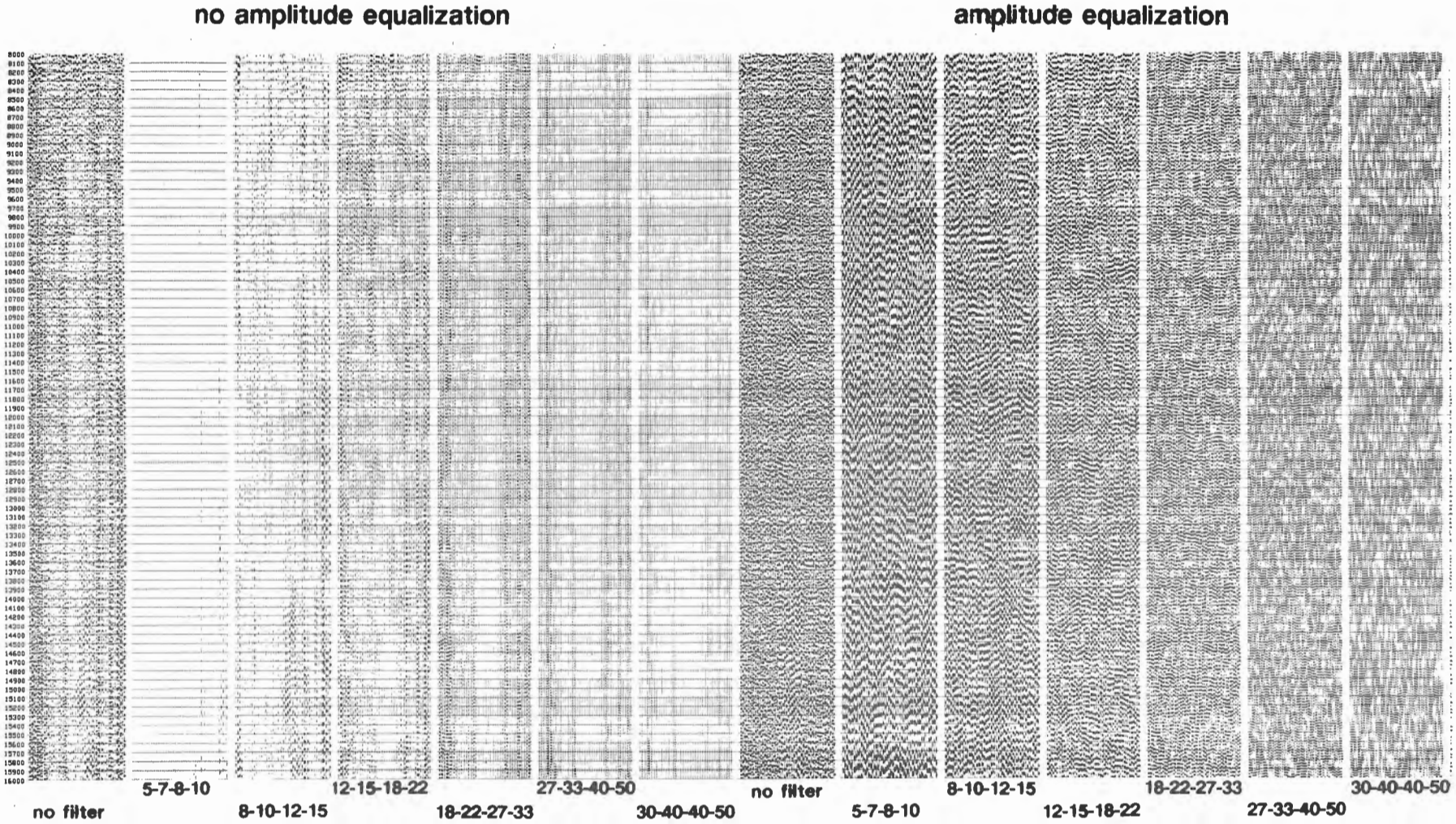

Figure 7. Band-pass filter tests applied to 9-16 s of VP 65. The figures under each column are : cut-on, roll-on, roll-off, cut-off frequencies of each band pass filter.

An analysis of the frequency content of recorded signals was performed to determine the appropriate frequency bands for deconvolution. This analysis was carried out for the common source gather VP 65, which contained strong events. The 120 traces were filtered with six overlapping symmetric band-pass filters covering the range 5-50 Hz (Fig. 6 and 7). There was strong coherent noise up to 12 Hz in the upper 8 s, which was not present between 8 and 16 s. Therefore in the window 0-8 s we deconvolved in the range 10-40 Hz and in the 8-16 s window the whole bandwidth (8-40 Hz) was retained for deconvolution.

PHASE 2 : STACK AND MIGRATION

To determine the most suitable stacking velocities, we computed constant velocity stacks for three different time windows (1.5-4.5 s, 4.0-7.0 s, and 7.0-10.0 s). The velocities scanned were 2.5, 3.0, 3.5, 5.0, 6.0, 8.0, and 9.0 km/s. Because of the high velocities and the relatively short spread length, discrimination of stacking velocities was found to be low. Therefore, we used the refraction velocity model of Spence et al. (1985), and selected six velocity-time points for the stack (Table 1 (a)).

Figure 8 shows the LITHOPOBE line 1 section stacked with the refraction-based velocities. Elevation static corrections, using a constant near-surface velocity of 5.8 km/s was applied.

A major improvement in the quality of the stacked section was obtained after computing surface consistent, automatic residual static corrections (Garotta and Paturet, 1978). After resampling the data to 8 ms, two sets of residual static corrections were computed in two passes with the Geovecteur SATAN statics "module". The velocity scan was repeated following the first pass of residual static corrections, but there were no significant differences in velocity picks. The stacked section in Figure 9 was obtained after applying the elevation static corrections and two passes of residual static corrections. This new section is noticeably superior to that of Figure 8 ; reflections are stronger and more continuous at all depths.

Attempts to migrate the stacked section of Figure 9 did not yield satisfactory results. Two different methods were used : finite difference wave equation and frequency-wavenumber (FK) migration. Two different velocity distributions were used for the finite difference migration : the stacking velocities and the stacking velocities reduced by 10 % (Fig. 10). For FK migration we used five constant velocities : 4.1 km/s, 4.55 km/s, 5.0 km/s, 5.45 km/s and 5.9 km/s.

Table 1. a) Stacking velocities before DMO ; b) Stacking velocities after DMO ; c) Migration velocities after DMO.

(a)		(b)		(c)	
Time (s)	Velocity (km/s)	Time (s)	Velocity (km/s)	Time (s)	Velocity (km/s)
0.1	2.5	0.35	3.0	0.1	1.5
0.1	3.5	1.0	3.5	1.5	2.5
1.5	5.0	1.8	5.0	4.0	4.0
4.0	6.0	4.0	6.5	5.0	4.7
6.0	7.0	7.0	7.0	6.0	5.1
7.5	7.5		8.2		6.0
	8.2				

PHASE 3 : DIP MOVEOUT, STACK, AND MIGRATION

Dip moveout (DMO) is a procedure for stacking both dipping and horizontal reflectors with their correct stacking velocities. For a dipping reflector the moveout is composed of two terms, one associated with the zero-dip normal moveout and the second related to reflector dip. These two corrections can be applied separately. To correct for the effect of dip, it is necessary to recognize the dip itself. The DMO corrections cannot be applied to CDP gathered traces but are applied instead to common offset gathers. To reduce the number of traces to be DMO processed, we applied DMO to partial stacks computed from six different groups of offsets : 0-1380 m, 1380-2760 m, 2760-4140 m, 4140-5520 m, 5520-6900 m, and 6900-8280 m. The DMO-corrected partial stacks were then added together. The total moveout correction procedure was : 1) partial NMO, 2) DMO, 3) residual NMO.

The partial NMO corrections were small because of the limited range of offsets in each partial stack (1380 m). We used the velocity function (a) of Table 1 for both partial NMO and DMO corrections.

Velocity scans after DMO led to the velocity function (b) in Table 1 for the residual NMO corrections. Due to the greater range of offsets involved in this step (8280 m), the residual corrections were larger than the partial ones, thus velocity function (b) had more weight than velocity function (a).

Examples of DMO corrected partial stacks for 0-1380 m and 4140-5520 m are shown in Figures 11 and 12. The total stack after DMO is shown in Figure 13.

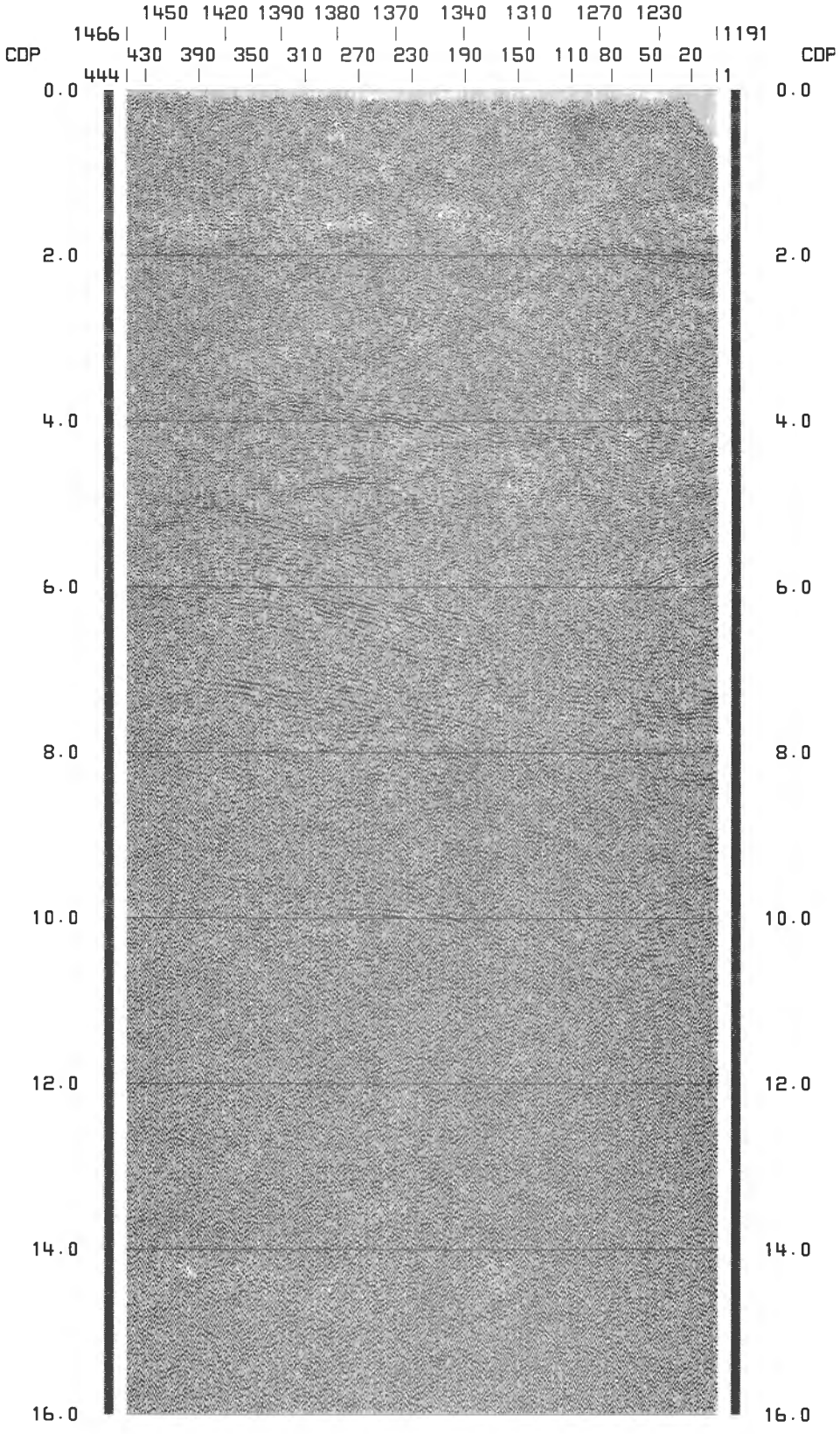

Figure 8. Stacked section of the south-western part of reflection line 1. Elevation statics only have been applied. Velocity function shown in Table 1 (a). Unless otherwise specified, for this and subsequent figures the numbers on the horizontal axis are geophone positions and CDP's. The vertical axis is two-way time in seconds. The section is displayed from SW (left) to NE (right).

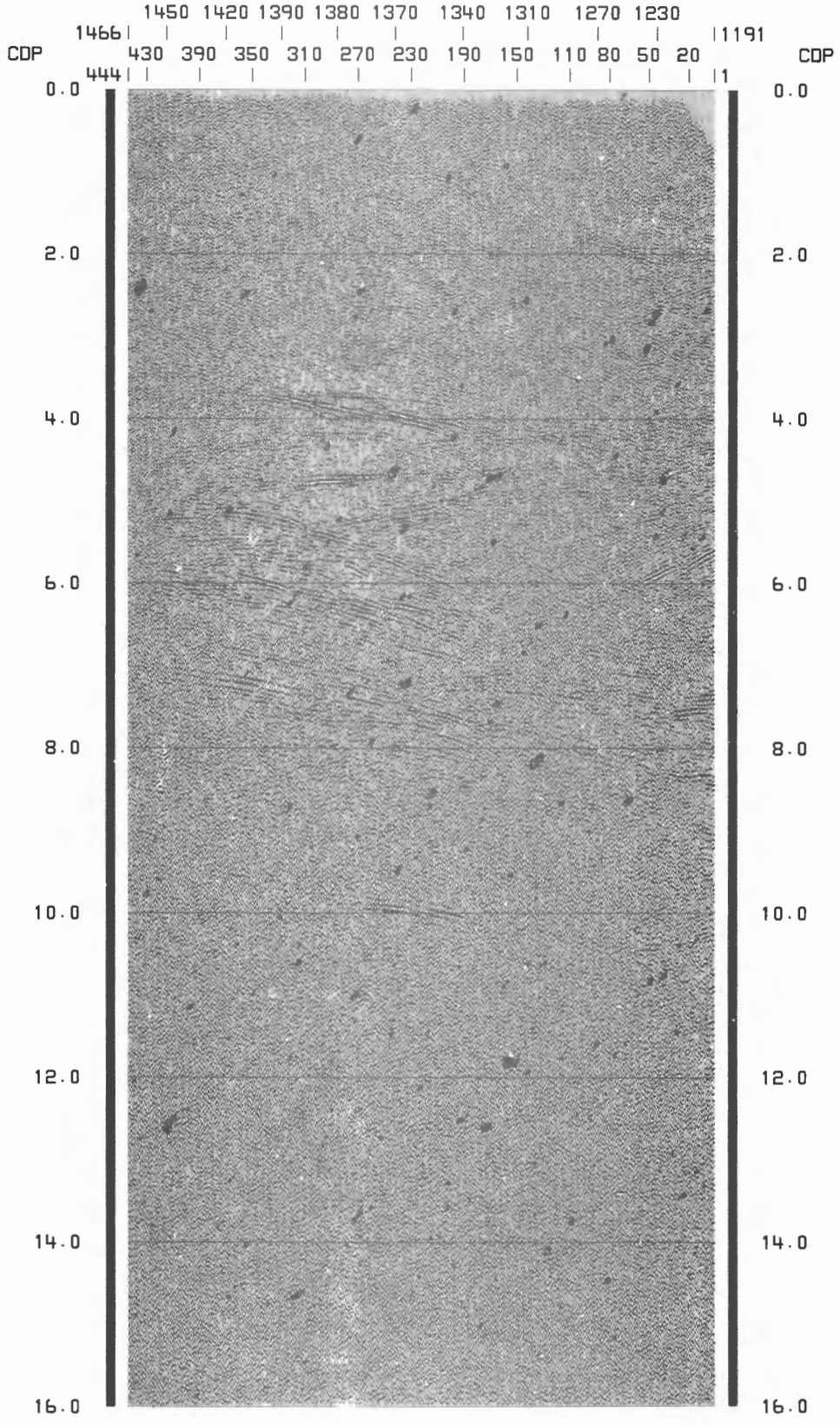

Figure 9. Stacked section after the application of two passes of surface consistent automatic residual static corrections.

Based on constant velocity FK migration tests after DMO, a velocity function for the finite difference wave equation migration was selected (Table 1 (c)). The first 8 s of the migrated section are shown in Figure 14. Table 2 shows the processing steps performed to produce Figure 14 and Table 3 shows the associated CRAY CPU time.

DISCUSSION

Zero-phase deconvolution provided superior rejection of slowly propagating low-frequency noise compared to spiking deconvolution. Selection of the frequency range 10-40 Hz for deconvolution in the upper 8 s was based on the results of a frequency analysis that showed strong coherent noise up to 12 Hz between 0 and 8 s. This noise was not present between 8 and 16 s.

The most obvious improvement in the stacked section was achieved after application of surface consistent residual static corrections (compare Fig. 9 and 8). Most of the key horizons are more continuous, in particular the horizons C=D1, D2, and E1 (Green et al., 1989b). Moreover, intersecting events at about 5.7 s, below horizon D, become evident. These features suggest that migration may improve the section. The failure of the initial post-stack migration to produce a satisfactory image was probably due to the difficulty in picking appropriate velocities for both dipping and flat events. DMO before stack was thus explored. It did not significantly improve the quality of the seismic section (compare Fig. 13 to Fig. 9), although there is a slight enhancement of three events: at 2.7 s between CDPs 230 and 270, a second one at about 4.2 s, and a very weak one between 9 and 10 s. Perhaps more improve-

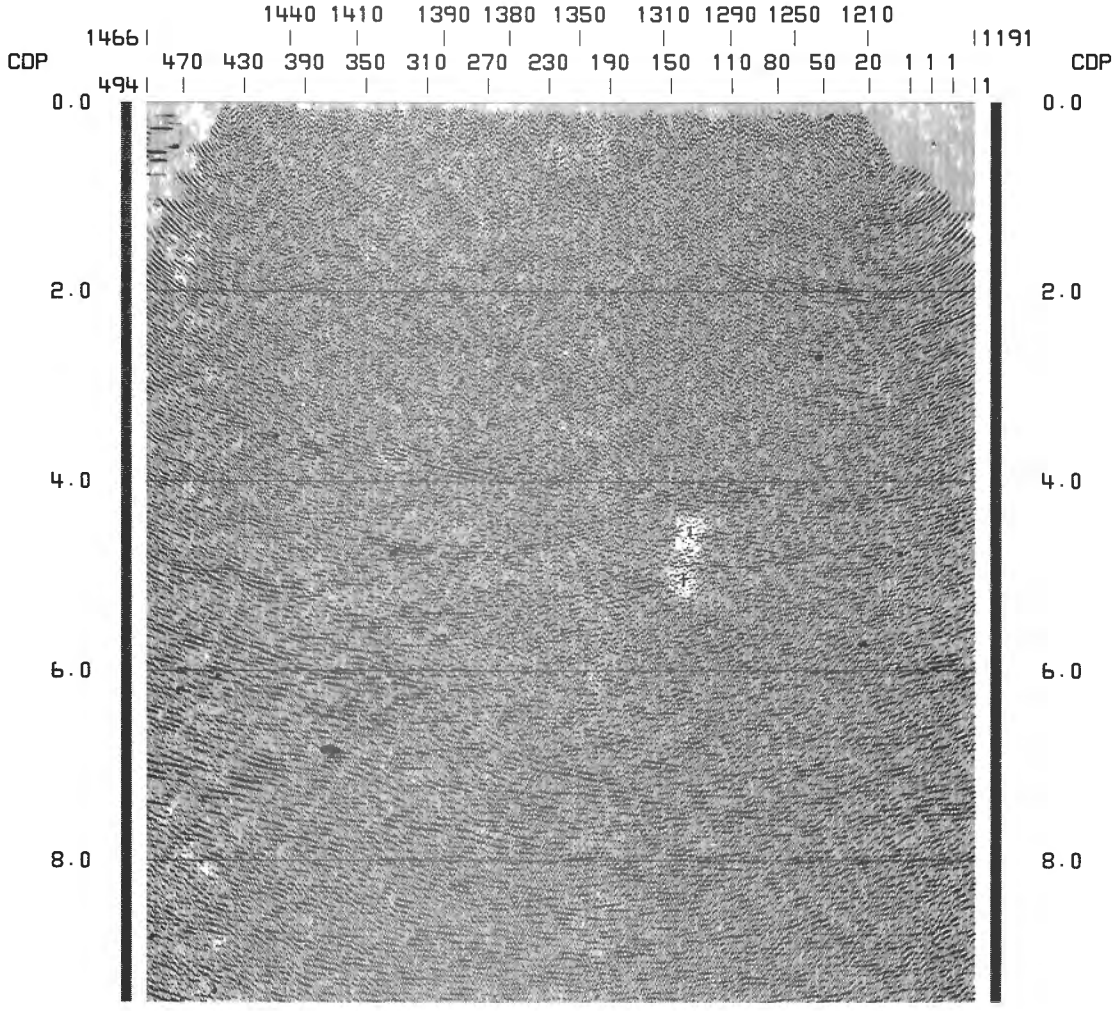

Figure 10. Migrated stacked section before DMO. The migration velocities are the velocities in Table 1 (a) reduced by 10 %.

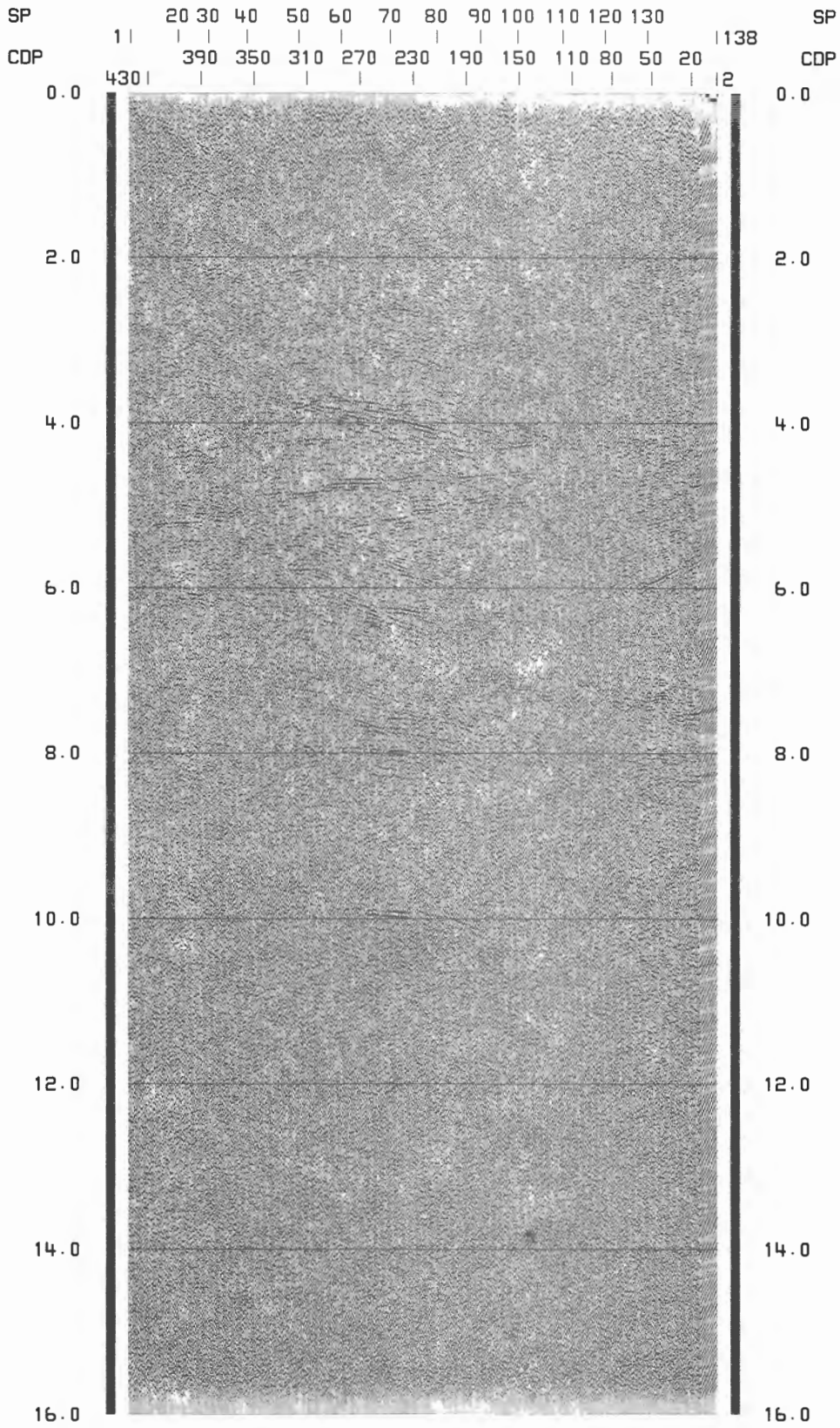

Figure 11. DMO Partial stack for offsets between 0 m and 1380 m. Horizontal axis shows VP's and CDP's.

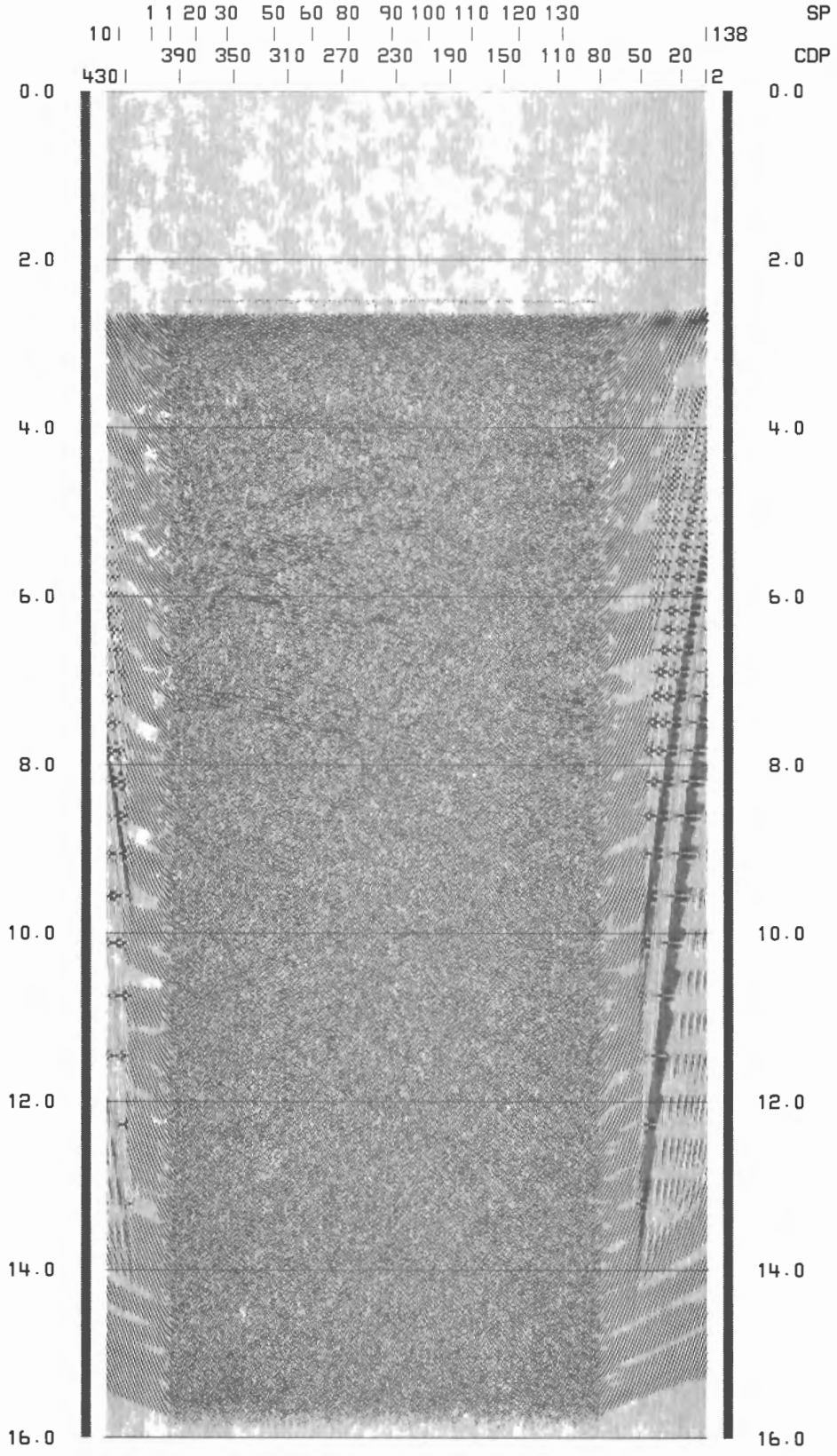

Figure 12. DMO corrected partial stack for offsets between 4140 m and 5520 m. Horizontal axis shows VP's and CDP's.

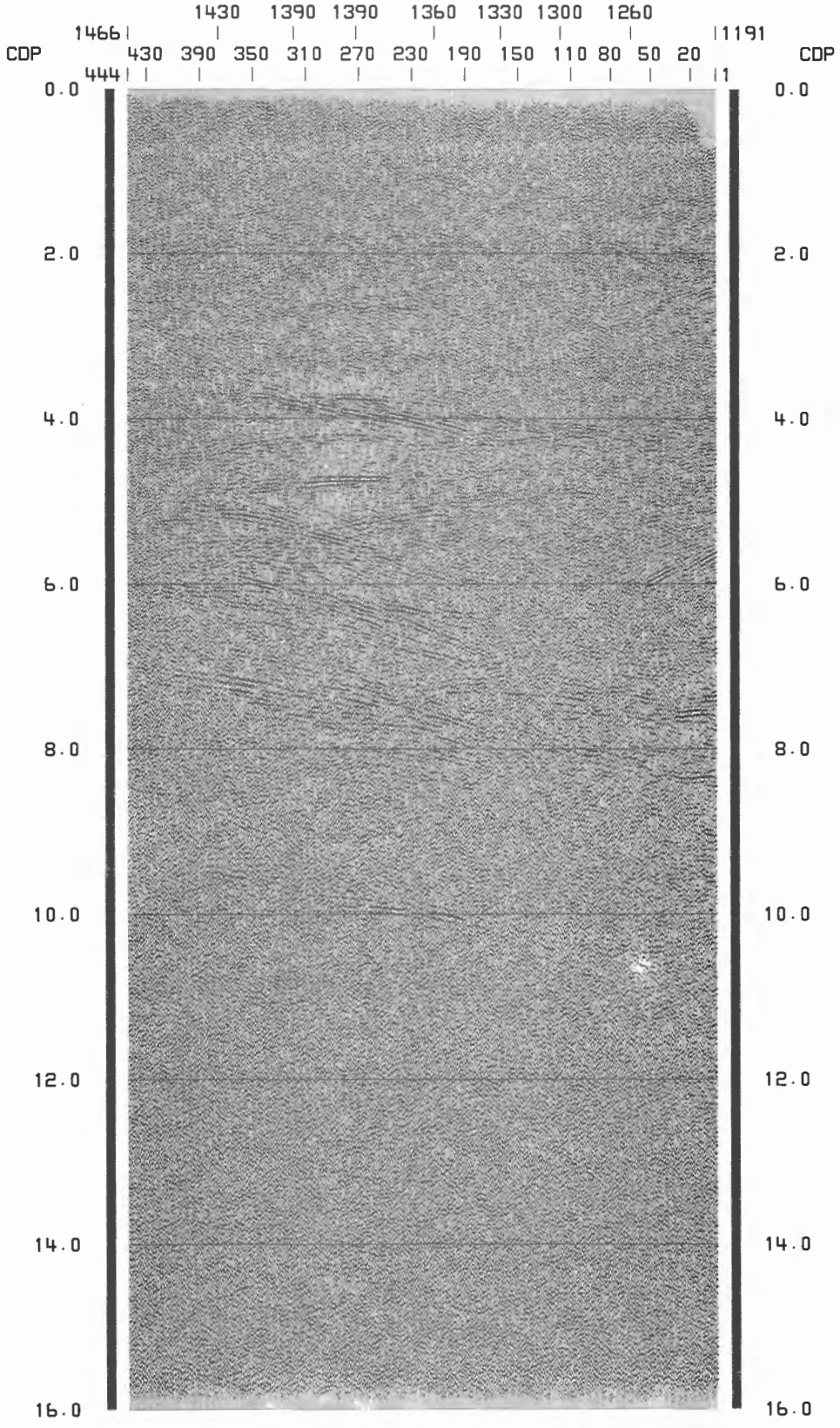

Figure 13. Stacked section after DMO.

Table 2. Processing steps used for the migrated stacked section of Figure 14. The post-stack filter and equalizations outlined below were applied to all stacked sections. Demultiplex and correlation were included in the original data set.

SPHERICAL DIVERGENCY COMPENSATION
CROOKED LINE GEOMETRY
FIRST BREAK MUTE (x3600t920 ; x9130t1820)
NMO
ZERO PHASE FILTER (0-8s 10-40 Hz ; 8-16s 8-40 Hz)
RESAMPLING AT 8 ms
FIELD STATIC CORRECTIONS
RESIDUAL STATIC CORRECTIONS (two cycles)
DIP MOVEOUT
STACK (t350v3000 ; t1000v3500 ; t1800v5000 ; t4000v6500 ; t7000v7000 ; vf8200)
BANDPASS FILTER (0-5s 10 16 30 40 Hz ; 7-16s 6 12 20 30 Hz)
TRACE TO TRACE EQUALIZATION (3500-10500 ms)
REGIONAL EQUALIZATION
AUTOMATIC GAIN CONTROL (window 600 ms)
RESAMPLING AT 4 ms

Table 3. Some statistics related to CRAY CPU TIME used in the processing

CDP distribution	13 s
Average slalom line	66 s
Velocity analysis	559 s, 565 s, 600 s
Deconvolution	21 s
Simple stack	42 s
Residual static corrections	73 s, 83 s
Finite difference wave equation migration	191 s
Dip moveout	188 s

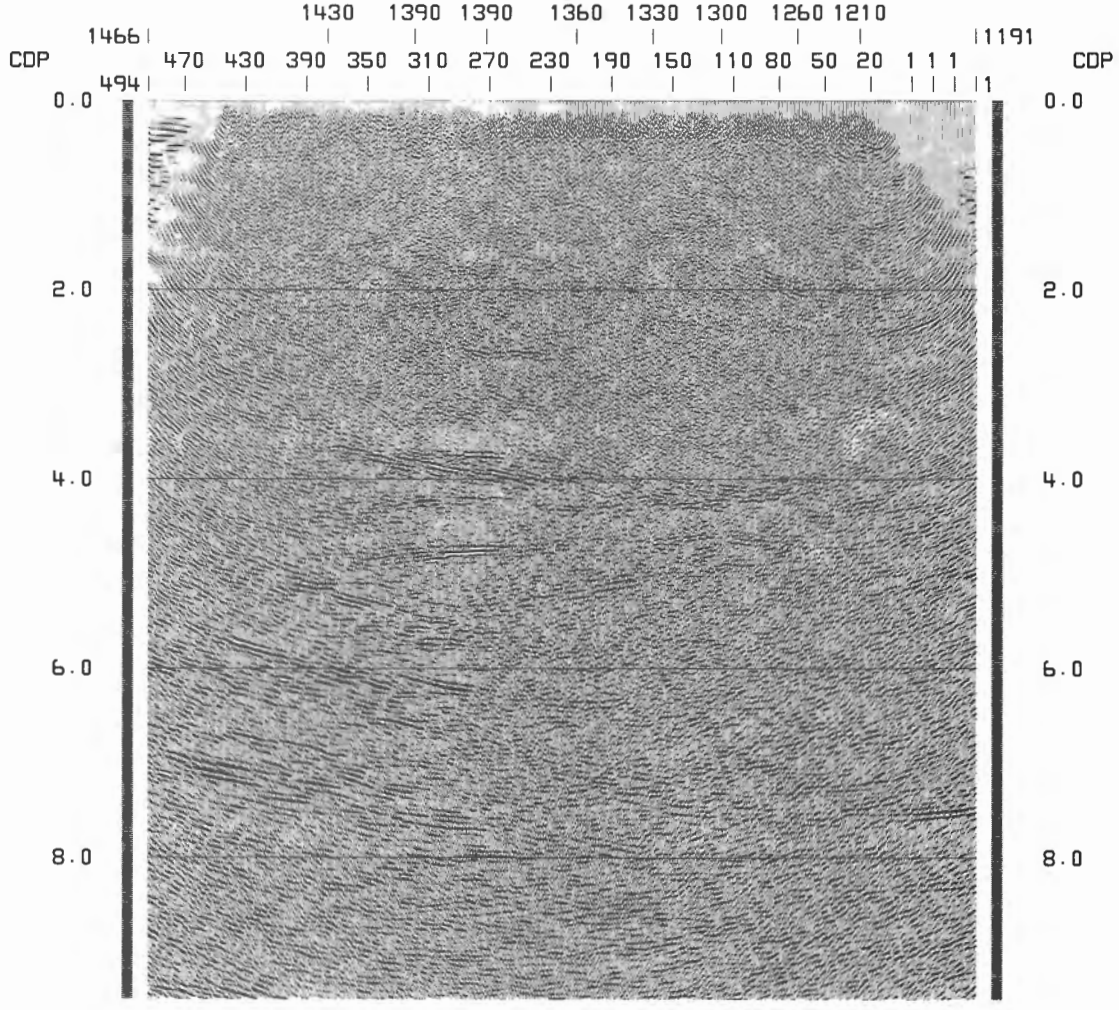

Figure 14. Migrated stacked section after DMO.

ment could have been obtained by considering a larger number of partial stacks in the DMO processing (i.e. twelve instead of six). Post-DMO FK migration tests were useful for determining a velocity function (Table 1, (c)) for the finite-difference migration (Fig. 14). Note how the intersecting events at 5.7 s have been successfully uncrossed and the events at 2.7 s and 4.2 s strengthened (compare Fig. 14, 10 and 9).

An event F at 10 s (Green et al., 1990b) is of special interest. This event is overstretched by migration if the velocity is greater than 4.1 km/s, which is lower than the migration velocities required to improve the continuity of reflections in the upper part of the section (e.g. 4.1 km/s at 4 s to 5.0 km/s at 8 s). Moreover, the partially stacked sections after DMO corrections show that event F disappears at large offsets (e.g. >4140 m) (compare Fig. 11 and 12).

A comparison of our final stacked and migrated sections (Fig. 13 and 14) to the section distributed to the CCSS participants (Fig. 14 in Green et al., 1990b; this figure is contained in the pocket at the back of this volume) demonstrates the improvements achieved by our reprocessing.

ACKNOWLEDGMENTS

GRANSIR is financed by the Swiss National Research Project no. 20 (PFN20/PNR20) of the Swiss National Foundation of Scientific Research. Our thanks are due to Martin Ouwehand of our research group for his help with operating system interfacing, as well as the staff of the Computer Centre of EPFL for their technical assistance. We thank Martine Da Silva and Sam Narayan of CGG for introducing us to the use of Geovecteur and for their positive suggestions. Larry Brown (Cornell University) kindly read and commented on a draft version of this paper. We thank Frederick Cook, Alan Green and Carl Spencer for their constructive criticism.

REFERENCES

Garotta, R. and Paturet, D.
1978 : Seismic Processing SATAN I, Calculation of high frequency static corrections ; Compagnie Générale de Géophysique Technical Series No. 508.78.05, p. 1-12.

Compagnie Générale de Géophysique
1986 : Geovecteur Seismic software package on Cray supercomputers ; Compagnie Générale de Géophysique Technical Series No. 543.86.04, p. 1-8.

Green A.G., Spencer C., Milkereit, B., Clowes, R.M., and Ellis, R.M.
1990a Guidelines for workshop topic I to IV ; *in* Studies of Laterally Heterogeneous Structures Using Seismic Refraction and Reflection Data, ed. A.G. Green ; Geological Survey of Canada, Paper 89-13, p. 3-25.

Green, A.G., Clowes, R.M., and Ellis, R.M.
1990b : Crustal studies across Vancouver Island and adjacent offshoremargin ; *in* Studies of Laterally Heterogeneous Structures Using Seismic Refraction and Reflection Data, ed. A.G. Green ; Geological Survey of Canada, Paper 89-13, p. 3-25.

Spence, G.D.,Clowes, R.M., and Ellis, R.M.
1985 : Seismic structure across the active subduction zone of western Canada ; Journal of Geophysical Research, v. 90, p. 6754-6772.

Schweizerische Arbeitsgruppe für Reflexionsseismik,
1988 : Vorläufige Ergebnisse der Alpentraversen des NFP-20 "Geologische Tiefenstruktur der Schweiz" ; Bulletin. Ver. Schweiz. Petroleum-Geology, u.-Ing., v. 54, p. 1-30.

A research note on the interpretation of seismic reflection line 1 across Vancouver Island: CCSS data set III

X. Berastegui[1] and E. Banda[2]

Berastegui, X. and Banda, E., A research note on the interpretation of seismic reflection line 1 across Vancouver Island: CCSS data set III; in Studies of Laterally Heterogeneous Structures Using Seismic Refraction and Reflection Data, ed. A.G. Green; Geological Survey of Canada, Paper 89-13, p. 207-212, 1990.

Abstract

An interpretation of LITHOPROBE seismic reflection data collected across Vancouver Island has been attempted using a combination of visual identification of seismic events (line drawing), and seismic facies and seismic fabric concepts. Four seismic facies have been identified. These together with the line drawing have allowed us to define seismic fabrics that are interpreted as different geological units. A depth conversion has been performed using published seismic refraction velocity values. Our geological interpretation includes some features that contrast with previously published interpretations.

Résumé

Une interprétation des données de sismique-réflexion de LITHOPROBE recueillies à travers l'île de Vancouver a été proposée. Elle est le résultat d'une combinaison de l'identification visuelle d'événements sismiques (tracé simplifié) et de concepts de faciès et de fabriques sismiques. Quatre faciès sismiques ont été déterminés. Ces faciès combinés au tracé simplifié du profil ont permis de définir des fabriques sismiques considérées comme des unités géologiques différentes. Une conversion de profondeur a été réalisée en recourant aux valeurs de vitesse publiées de sismique réfraction. La présente interprétation géologique comprend des éléments différentes de ceux contenus dans les interprétations déjà publiées.

[1] Servei Geologic de Catalunya, D.P.T. i O.P., Diputacio 92, 08015 Barcelona, Spain.
[2] Institut de Geologia Jaume Almera, CSIC, Marti i Franques s/n, 08028 Barcelona, Spain.

INTRODUCTION

An interpretation of LITHOPROBE seismic section 1 recorded across Vancouver Island (Yorath et al., 1985) was attempted for several reasons : a) it appeared an ideal data set on which to apply the seismic fabric concept as advanced by Allmendinger et al. (1987) ; b) available refraction data provided significant information for converting reflection travel times to depths ; and c) the results were to be compared with those obtained by a number of other research groups.

We have used the onshore seismic reflection data set (Yorath et al., 1985), and velocity depth functions obtained from seismic refraction data. The offshore seismic section was not used because only the migrated section was supplied ; this marine section was heavily contaminated by "smiles", preventing us from accurately interpreting the deep events.

In applying the seismic fabric concept we have obtained an interpretation that is, in some respects, at variance with published results. A geological interpretation of the seismic results has also been attempted.

INTERPRETATION METHOD

Seismic interpretation was carried out using the following procedures :

1. Line drawing construction.

As expected, the results of interpreting the seismic section in terms of a line drawing (Fig. 1) do not differ substantially from those published by Yorath et al. (1985).

2. Identification of seismic facies.

In this step the concept of seismic facies was applied. The parameters used for the visual identification of facies were frequency, continuity and amplitude of the reflectors. Four seismic facies were identified according to the characteristics outlined in Table 1 and shown in Figure 2.

Figure 3 displays the identified seismic facies along the whole profile superimposed on the line drawing.

3. Integration of the line drawing and seismic facies interpretation.

This step was performed using the concept of seismic fabric introduced by Allmendinger et al. (1987). Seismic fabric is defined here as the sum of structural features and seismic facies in much the same way as rock fabric is defined as the sum of structural and textural features. Applying this concept to seismic reflection data implies that different experimental design and data processing would affect the seismic section in such a way that fabrics would be equally identifiable.

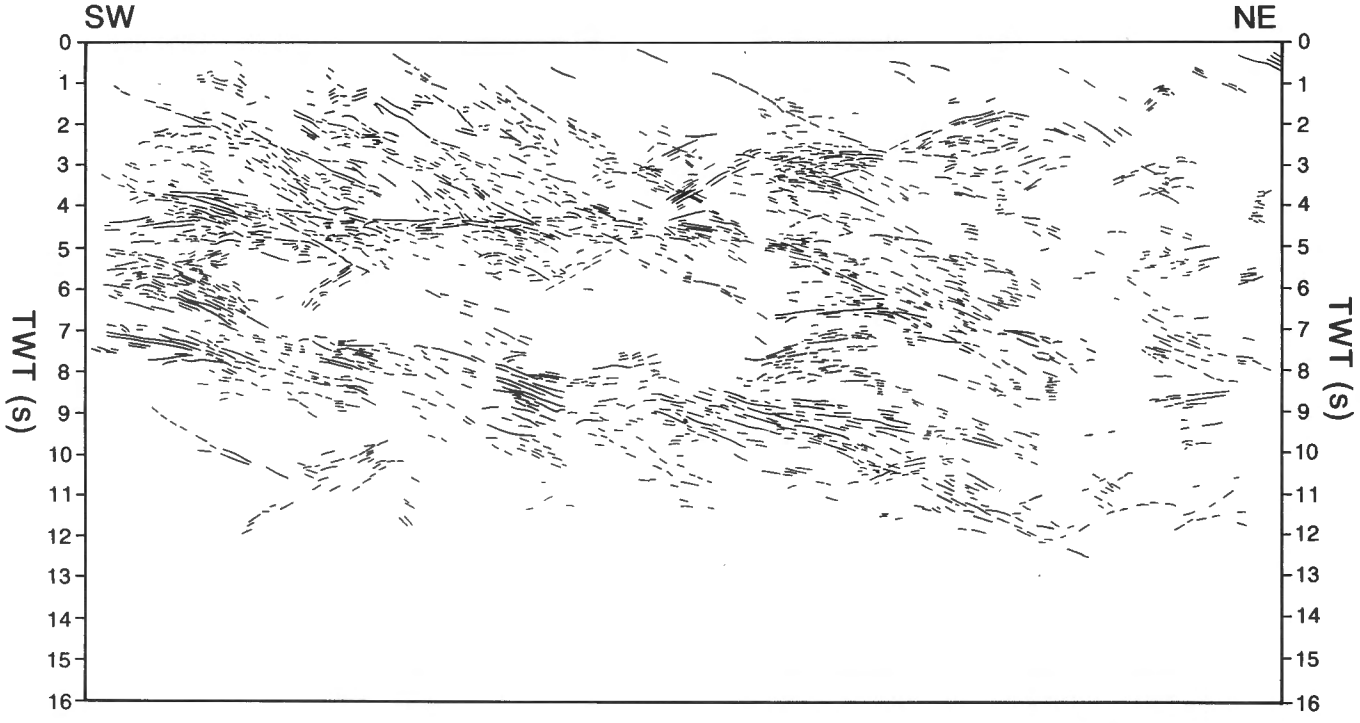

Figure 1. Line drawing derived from LITHOPROBE seismic reflection data collected across Vancouver Island.

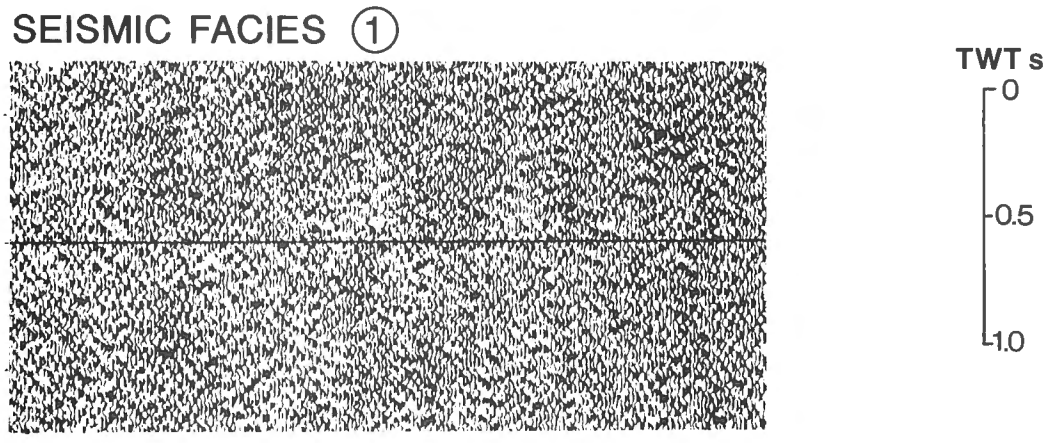

Figure 2. Seismic facies identified according to the following definitions : 1) reflection-free ; 2) weak amplitude, low frequency and moderate continuity ; 3) strong amplitude, high frequency and good continuity ; 4) strong amplitude, low frequency and good to moderate continuity.

Table 1

Seismic facies	Characteristics
1.	Reflection free.
2.	Reflections of weak amplitude, low frequency and moderate continuity.
3.	Reflections of strong amplitude, high frequency and good continuity.
4.	Reflections of strong amplitude, low frequency and good to moderate continuity.

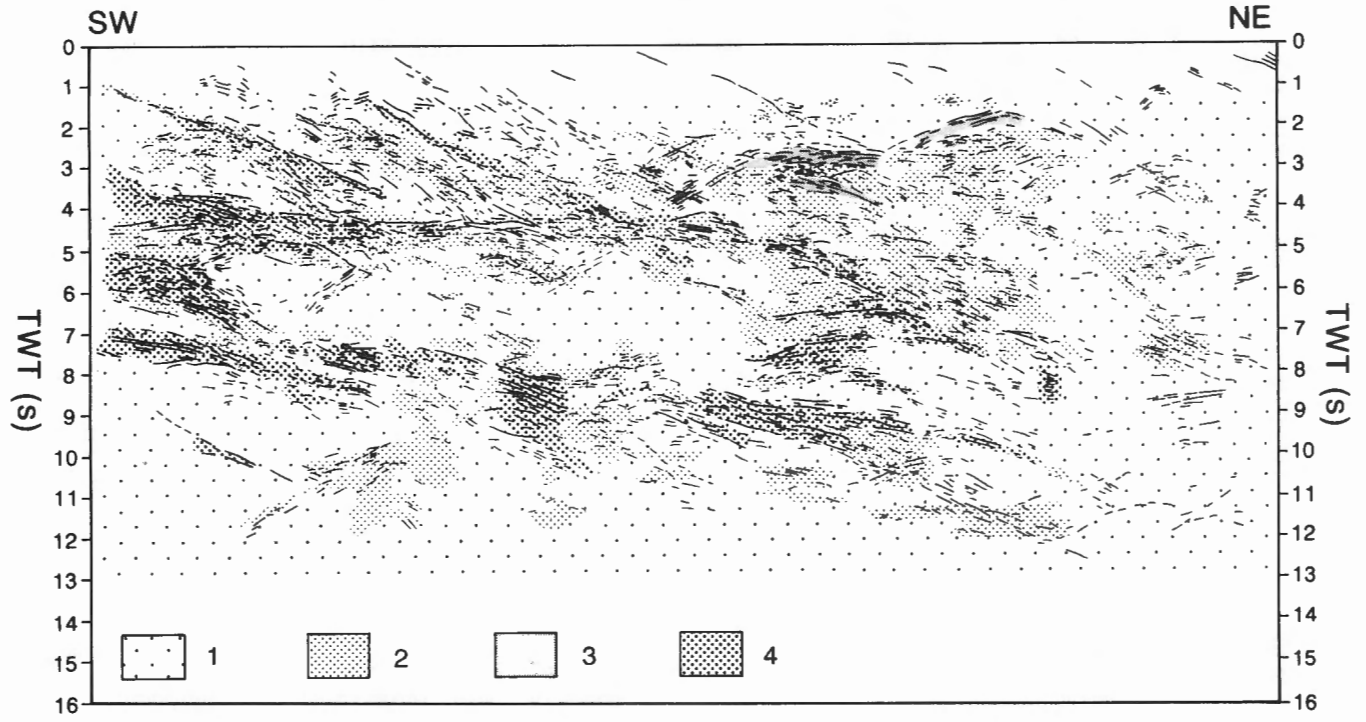

Figure 3. Superposition of seismic facies 1-4 (*see* Fig. 2) and the main features of the line drawing.

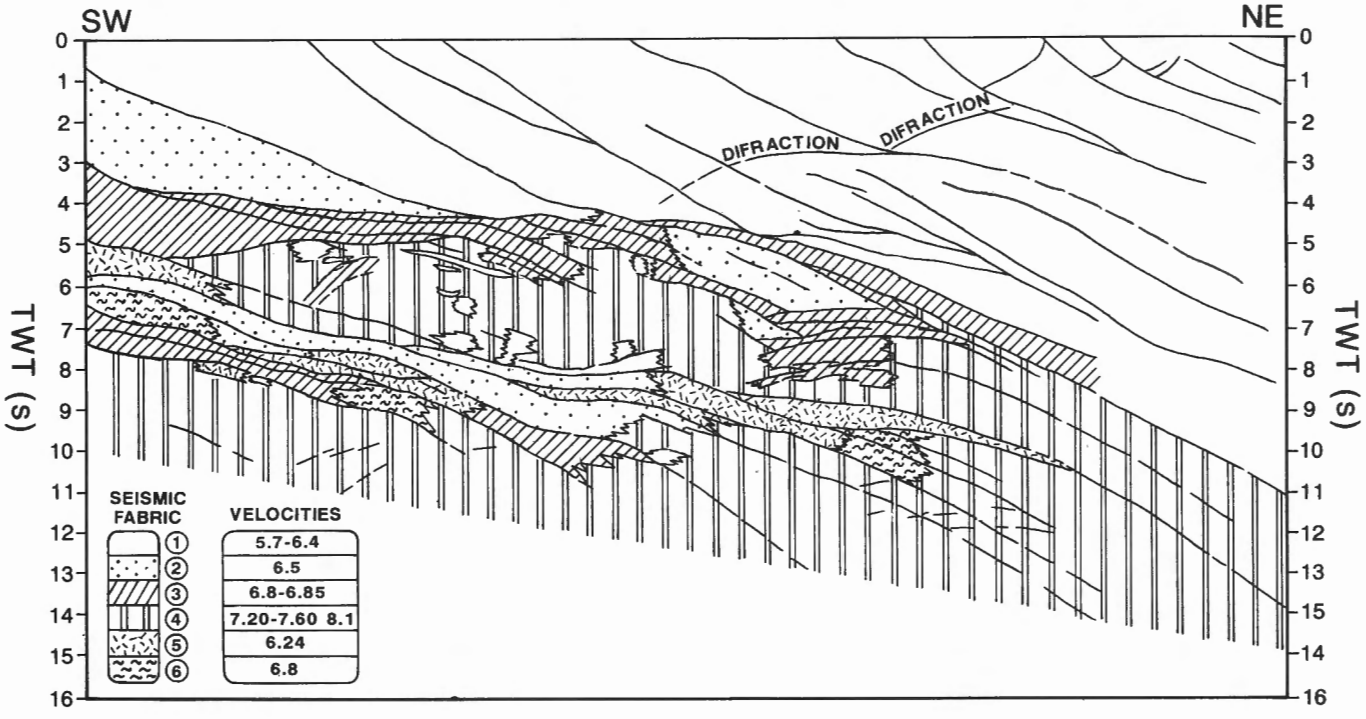

Figure 4. Seismic fabrics identified after a joint interpretation of the line drawing and the seismic facies (for seismic fabric description see text). Velocities are P-wave velocities obtained from a refraction survey (after Egger and Ansorge, 1990, and Drew and Clowes, 1990).

Table 2

Seismic fabric	Characteristics
1.	Dominated by facies 2 and facies 1. Facies 4 is only present along thrust faults.
2.	Dominated by seismic facies 1 with inclusions of facies 2. Based on the work of Shouldice (1971) and Yorath (1980) this fabric is identified and attributed to a volcanic complex.
3.	Dominated by seismic facies 4 with a considerable amount of facies 2.
4.	Essentially corresponds to seismic facies 1.
5.	Dominated by facies 4. Facies 1 is also present.
6.	Dominated by facies 1 and/or facies 2.

In the LITHOPROBE Vancouver Island example the fabric identification was carried out by superposing the line drawing (Fig. 1) on the seismic facies interpretation (Fig. 3). The grouping of seismic facies is complemented by the grouping of reflections according to their geometric pattern. This procedure defines units that correspond to the seismic fabrics outlined in Table 2 and shown in Figure 4.

The boundaries between seismic fabrics may have tectonic significance. In this example, our seismic fabric interpretation goes beyond that of Allmendinger at al. (1987) because more details are taken into account. For the sake of clarity the results shown in Figure 4 do not include contacts between seismic facies within any of the seismic fabric groups.

4. Travel time conversion into depth.

The time-interpreted section derived from steps 1-3 was converted to depth using essentially the seismic refraction-derived velocities of Egger and Ansorge (1990). Other interpretations, such as that of Drew and Clowes (1990),

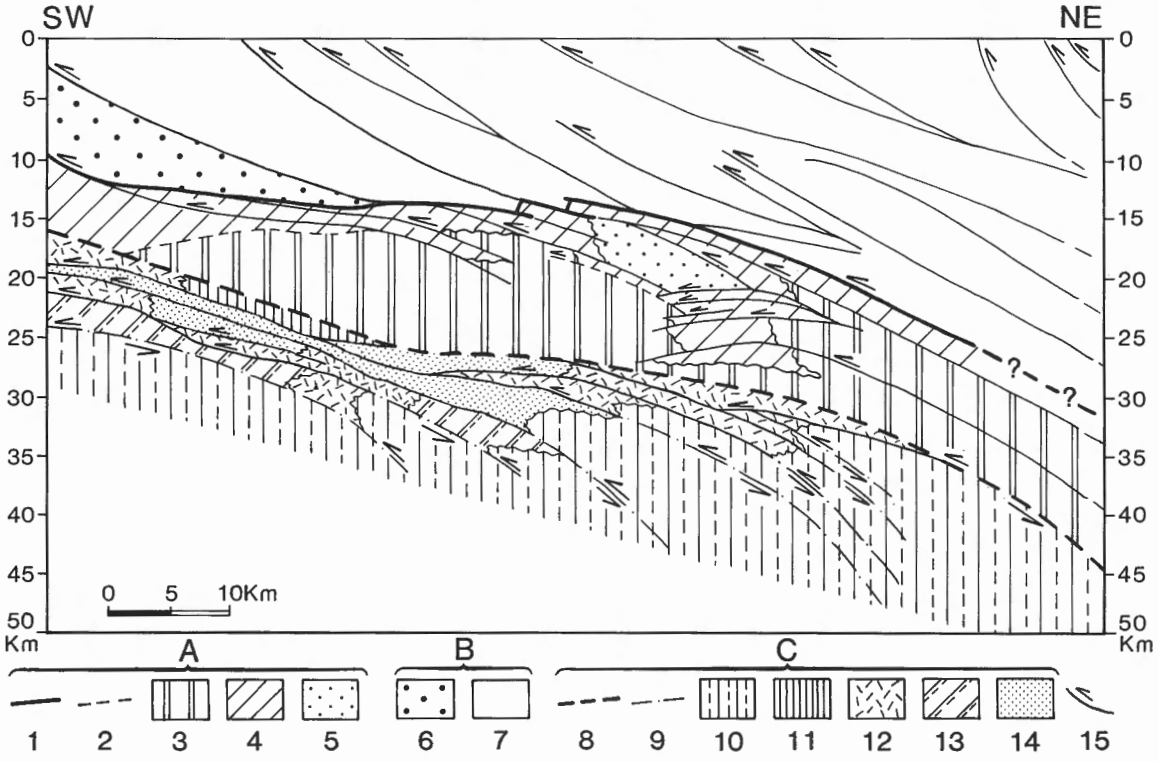

Figure 5. A : Ancient subduction complex (Eocene and older) with : 1 — top of the ancient subduction complex, 2 — ancient upper-lower crust boundaries, 3 — lower oceanic crust, 4— upper oceanic crust and 5 — volcanics. B : Ancient accretionary complex (Paleozoic-early Eocene) with : 6 — seamount complex (Metchosin volcanics)-early Eocene, 7 — undifferentiated metavolcanic, metasedimentary and igneous rocks (Wrangelia) and late Carboniferous Nanaimo sediments. C : Modern subduction complex (upper Eocene to present) with : 8 — top of the modern subduction complex (top of the Juan de Fuca Plate), 9 — upper-lower crust boundaries, 10 — lower oceanic crust, 11 — fragments of ancient lower oceanic crust, 12 — metasediments (and volcanics), 13 — upper oceanic crust, 14 — volcanics, and 15 — thrust faults.

were also taken into account. Because our seismic fabrics did not coincide with the velocity layers/ blocks obtained from refraction work, assigning velocities to the fabrics was somewhat subjective ; average velocities had to be used in some cases.

An additional problem was found at the northeast end of the profile, where horizontal discontinuities in the proposed refraction models were not represented in the reflection data. Migration of the seismic reflection data will relocate and steepen dipping reflectors. Therefore, no horizontal reflectors can be interpreted at the northeast end of the profile (Fig. 1).

DISCUSSION

In applying the procedures described above, we have focused on the data below 2 s travel time because of our unfamiliarity with the surface geology and the noisy character of the data above 2 s. However, the results of Shouldice (1971) and Yorath (1980) in identifying the basic volcanic complex under the Tofino fault have been used to assign seismic facies to that complex.

The interpretation technique used in this note seems to offer some new results (Fig. 5) with regard to the boundaries and internal structure of the three main structural units defined by Yorath et al. (1985) : an ancient subduction complex (Eocene and older), an accretionary complex (Paleozoic — early Eocene) and a modern subduction complex (Eocene to present). The gross features are in accord with previous interpretations, but some important details are at variance with published results (Fig. 5). For example, we interpret the top of the Juan de Fuca plate at a much shallower depth (15 km at the southwest end of the profile) than other interpretations (Yorath et al., 1985 ; Clowes et al., 1987 ; Fig. 15 of Green et al., 1990). Unfortunately, the offshore migrated reflection profile (line 85-01) made available to us does not help in defining this boundary.

From the crude geological interpretation given in Figure 5 it may be suggested that the two subduction zones (ancient and present) correspond to an island arc-continent collision followed by an ocean-continent collision. This interpretation would explain the anomalous thickness, close to 10 km, of the ancient oceanic crust as interpreted here (Fig. 5). Such an interpretation has, of course, to be contrasted with other interpretations, and, especially, with results from other geophysical and geological techniques.

REFERENCES

Allmendinger, R.W., Hauge, J.A., Hauser, E.C., Potter, C.J., Klemperer, S.L., Nelson, K.D., Kneupfer, P., and Oliver, J.
1987 : Overview of the COCORP 40°N Transect, Western U.S.A. : The fabric of an orogenic belt ; Geological Society of America, Bulletin, v. 98, p. 308-319.

Clowes, R.M., Yorath, C.J., and Hyndman, R.D.
1987 : Reflection mapping across the convergent margin of western Canada ; Royal Astronomical Society, Geophysical Journal, v. 89, p. 79-84.

Drew, J.J. and Clowes, R.M.
1990 : A reinterpretation of the seismic structure across the active subduction zone of western Canada ; *in* Studies of Laterally Heterogeneous Structures Using Seismic Refraction and Reflection Data, ed. A.G. Green ; Geological Survey of Canada, Paper 89-13, p. 115-132.

Egger, A. and Ansorge, J.
1990 : Interpretation of seismic refraction data, CCSS data set I : Vancouver Island — continental margin ; *in* Studies of Laterally Heterogeneous Structures Using Seismic Refraction and Reflection Data, ed. A.G. Green ; Geological Survey of Canada, Paper 89-13, p. 133-150.

Green, A.G., Clowes, R.M., and Ellis, R.M.
1990 : Crustal studies across Vancouver Island and adjacent offshore margin ; *in* Studies of Laterally Heterogeneous Structures Using Seismic Refraction and Reflection Data, ed. A.G. Green ; Geological Survey of Canada, Paper 89-13, p. 3-25.

Shouldice, D.H.
1971 : Geology of the western Canadian continental shelf ; Bulletin of Canadian Petroleum Geologists, v. 13, p. 239-249.

Yorath, C.J.
1980 : The Apollo structure in Tofino Basin, Canadian-Pacific continental margin ; Canadian Journal of Earth Sciences, v. 17, p. 758-775.

Yorath, C.J., Green, A.G., Clowes, R.M., Sutherland Brown, A., Brandon, M.T., Kanasewich, E.R., Hyndman, R.D., and Spencer, C.
1985 : LITHOPROBE, Southern Vancouver Island : Seismic reflection sees through Wrangelia to the Juan de Fuca Plate ; Geology, v. 13, p. 759-762.

Complex response to a "simple" crustal model: Implications for deep crustal reflection interpretation

Roy A. Johnson[1]

Johnson, R.A., Complex response to a "simple" crustal model: Implications for deep crustal reflection interpretation; in Studies of Laterally Heterogeneous Structures Using Seismic Refraction and Reflection Data, ed. A.G. Green; Geologial Survey of Canada, Paper 89-13, p. 213-217, 1990.

Abstract

One topic of the Commission on Controlled Source Seismology (CCSS) workshop at Whistler, British Columbia, concerned the interpretation of a synthetic seismic reflection section based on a generalized model of actively extending terranes. The upper to middle parts of the model contained sedimentary basins, granitic plutons and zones of partial melt or magma. Underlying these structures were a crustal duplex, a lense-shaped mafic complex and an abrupt crust-mantle transition. Cutting through the crust from near the surface to the mantle was an anastomosing shear zone similar to the type proposed by Wernicke. Lateral velocity variations associated with structures at different crustal levels caused significant distortion of deeper reflections through focusing, defocusing and, most importantly, travel time delays. Lack of continuous reflections from the shear zone suggests that, although such through-going structures seem unlikely, interpreters of deep crustal seismic reflection data might fail to detect their presence.

Résumé

L'atelier de la Commission sur la sismologie à source contrôlée (CSSC) tenu à Whistler (Colombie-Britannique) a porté, entre autres, sur l'interprétation d'une coupe de sismique réflexion synthétique fondée sur un modèle généralisé de terrains en distension. Les parties supérieure à intermédiaire du modèle contiennent des bassins sédimentaires, des plutons granitiques et des zones de roches en fusion partielle ou de magmas. Ces structures reposent sur un duplex crustal formé d'un complexe mafique lenticulaire et d'une transition croûte-manteau abrupte. Une zone de cisaillement anastomosée, semblable à celle proposée par Wernicke, recoupe la croûte de la quasi surface jusqu'au manteau. Des variations de vitesse latérales, associées à des structures se trouvant à différents niveaux de la croûte, ont causé une distorsion importante des réflexions profondes par suite de focalisations, de défocalisations et, plus encore, de retards dans les temps de parcours. L'absence de réflexions continues dans la zone de cisaillement indique que, malgré la présence improbable de structures de recoupement, celles-ci peuvent ne pas être décelées dans les données de sismique réflexion de la croûte profonde.

[1] Department of Geosciences, University of Arizona, Tucson, Arizona, 85721, U.S.A.

INTRODUCTION

Interpretation of deep seismic reflection data is dependent on the quality of the reflection image that can be obtained. Distortion of the image caused by lateral velocity variations associated with even fairly simple structure can make interpretation of crustal structure very difficult, especially in the presence of significant noise. Furthermore, inappropriate or inadequate data processing can compound the problem. Synthetic seismic reflection data generated from known models provides an opportunity to evaluate the difficulties involved in deep crustal reflection interpretation. Such a synthetic seismic reflection section (data set V) was prepared as an exercise for the Commission on Controlled Source Seismology (CCSS) workshop at Whistler, British Columbia, 1987.

The generalized two-dimensional crustal model (Fig. 1) used to generate the synthetic seismic reflection section for CCSS data set V (Fig. 2) included structures found or suspected in many areas of the world, particularly in actively extending areas. This model, which evolved from discussions between Scott Smithson (University of Wyoming) and Walter Mooney (U.S.A. Geological Survey), bears some resemblance to the Basin and Range Province of the western U.S. One of the principal goals of the modeling exercise was to demonstrate the complexity of reflection sections recorded over relatively simple crustal structures. It is important to note that data set V was obtained using simplified assumptions about wave propagation.

Close approximations to the true model could be deduced through careful (time-comsuming) interpretation, but not all parameters could be recovered unambiguously. Velocity was not provided, because it is not generally available for the middle and deep crust in actual reflection interpretations ; although stacking velocities are useful for shallow seismic sections, they lack sensitivity for deeper reflectors, particularly where reflector continuity is limited and source-receiver offsets are relatively short. In most instances, stacking velocities for the deep crust are no better than the interpreter's "best guess".

MODELING

The synthetic seismic reflection data were generated using Sierra Geophysics Inc. seismic reflection modeling software on the University of Wyoming Program for Crustal Studies VAX 11/780. Plots of the model and synthetic seismograms were generated on the University of Wyoming VAX 11/780 and on the University of Arizona Reflection Seismology CONVEX C-120.

The model (Fig. 1) is reduced to an arbitrary flat datum so that mountain-peak and valley-floor topography does not affect travel times. Thus, zero time in the synthetic data is equivalent to a datum of static-corrected data.

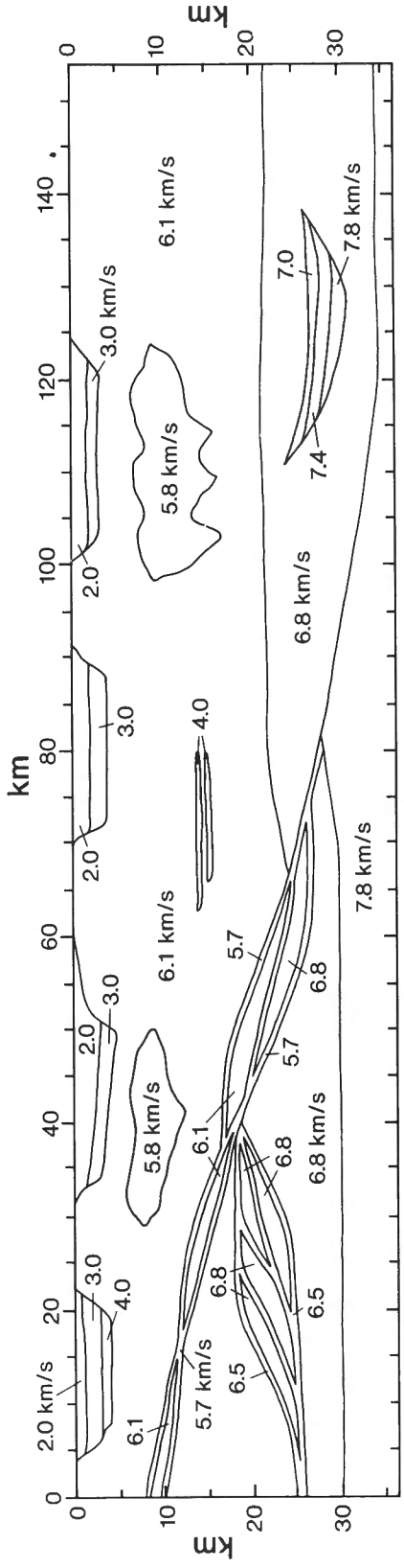

Figure 1. Generalized two-dimensional velocity model used to generate the synthetic seismic section for CCSS data set V. Velocities are in km/s. The model is similar to that proposed for many actively extending terranes, especially the Basin and Range Province of the western U.S.A.

Velocities in the model range from 2.0 km/s for shallow sediments to 7.8 km/s for the upper mantle and one layer of a lower crustal layered mafic complex. Four fault-bounded sedimentary basins at the surface are juxtaposed against crystalline rocks. Except for one, these basins are flat-bottomed and roughly symmetric, which is in contrast to the dominantly fault-bounded half-grabens of the Basin and Range Province. The upper crust, which was assigned a velocity of 6.1 km/s, contains two irregularly shaped granitic bodies (V = 5.8 km/s) and two closely spaced subhorizontal zones of partial melt or magma (V = 4.0 km/s).

Cutting through the crust and extending to the Moho is an anastomosing shear zone (mylonite) along which major simple-shear extension of the lithosphere might have occured (Wernicke, 1985). Our initial thought was that such a through-going zone of crustal shear would be relatively easy to detect. As discussed later, this was not the case.

Intersected and truncated by this shear zone is a stylized crustal duplex (v = 6.5 km/s) that may have accommodated crustal thickening during pre-extensional orogenesis, such as occurred in much of the Basin and Range Province. Individual branches of this duplex zone may also be mylonitic.The roof thrust of the duplex arbitrarily forms the boundary between the upper and lower crust (Conrad discontinuity). Farther to the right in the model, the Conrad discontinuity is characterized as an irregular surface between about 20 and 25 km depth, although it is not universally identified on refraction or reflection records and thus its nature is not well contrained.

A lens-shaped layered mafic complex is the lowest feature in the crustal model (V = 7.0, 7.4 and 7.8 km/s). This complex overlies the crust-mantle boundary, which was modeled as a step in velocity from 6.8 to 7.8 km/s. The Moho has been cut by the through-going crustal shear zone in the center of the model, and crustal thickness decreases by about 4 km from right to left.

Three dimensional effects and diffractions were to be added to the model, but it was felt that even without these elements of reality, the synthetic data were sufficiently complex ! Important model parameters are given in Table 1. Velocities and densities (not shown in Fig. 1) assigned to each body were used for computing reflection coefficients at boundaries and spherical divergence. Because automatic gain control (AGC) was applied to the synthetic data, variations in the reflection coefficients due to changes in velocity and density had little effect. For this reason, and because many events were not visible without some further adjustment, the data were processed with reflection coefficients set to unity. AGC has the effect of compensating for spherical divergence, so, as for many "final stack" seismic sections to which AGC has been applied, reflection amplitudes in Figures 2 and 3 appear fairly constant with increasing time.

Table 1. Model parameters for CCSS data set V

Parameter	Value
Type of modeling	Sierra Geophysics Inc., 2-D normal-incidence ray trace, no diffractions.
Wavelet	20 Hz Ricker, duration 496 ms.
Sample rate	8 ms.
Number of traces	771.
Station spacing = trace spacing	200 m.
Total simulated line length	154 km.
Vertical axis labeled in seconds	
Horizontal axis labeled by station	

Finally, nonrepeating gaussian noise was added to the data to simulate realistic signal-to-noise ratios (S/N). The noise was bandlimited using a 8-12-28-35 Hz trapezoidal window ; noise with frequencies less than 8 Hz or more than 35 Hz was excluded, and noise with frequencies between 12 and 28 Hz was passed unattenuated. Average noise level was chosen so that signal to average noise amplitude was about 2.

DISCUSSION OF SYNTHETIC RESULTS

Complex as this synthetic data set appears (Fig. 2), it is far simpler than most observed crustal reflection data sets ; true reflections are rarely coherent for more than a few kilometres due to noise, changes in surface coupling, travel-path distortions, and variations in lithology and structure. As for real data, steeply dipping events (e.g. basin margins) are not easily recognized. Comparison of data set V (Fig. 2) to the noise-free data (Fig. 3) suggests that steeply dipping events are more difficult to observe in the presence of high noise levels, especially where spatial aliasing may be a problem.

Upper crustal velocity variations distort reflection images. Low-velocity sediment-filled basins cause pull-down of all deeper horizons, and since the velocity contrast from basin to range is high, pull-down beneath basins dominates the effects of deeper velocity changes. Thus, interpretation of upper to middle crustal intrusive bodies and magma lenses in the synthetic data is complicated by major time offsets that could be interpreted erroneously as fault truncations. The Moho exhibits variations in travel time by more than 1 s due to the overlying basins, and in some areas, apparent dip of the Moho is introduced. Moho reflections in observed Basin and Range reflection data are offset by up to 1 s in a similar manner. Velocity pull-down also makes recognition of the crustal duplex and the through-going anastomosing shear zone difficult.

Although the effect is generally well known, basin reflections are distorted in time with respect to their true dimensions ; "synformal" basins appear narrower with depth and seem to be much deeper. Low sedimentary velocities also help create the situation that significantly different crustal levels are juxtaposed in the time section, perhaps adding to the impression of large structural offsets.

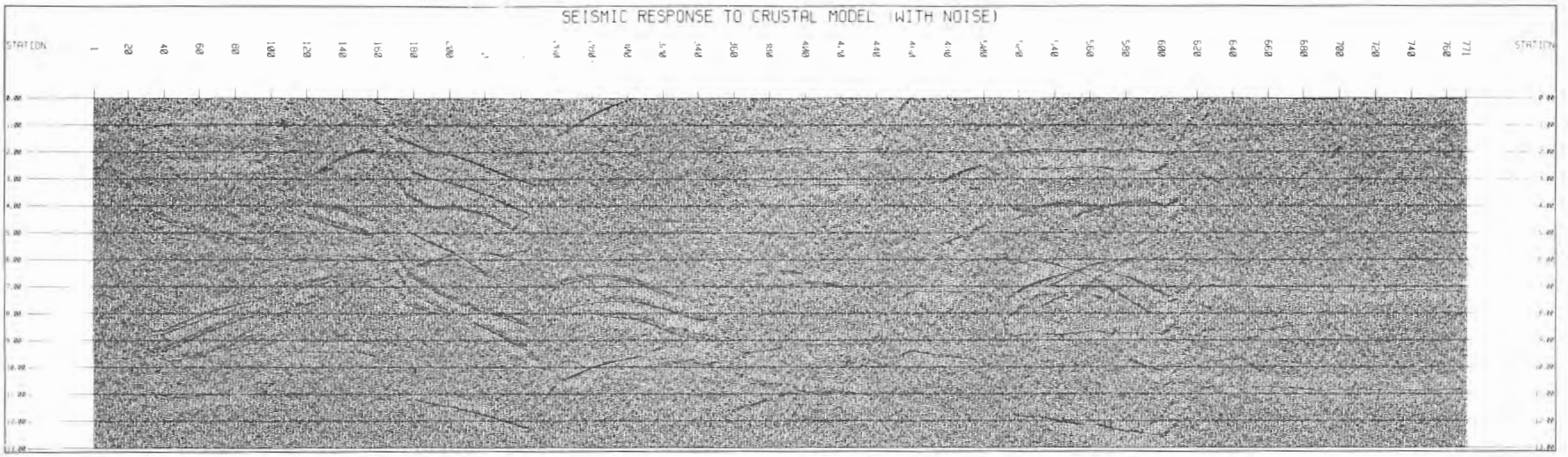

Figure 2. CCSS data set V : synthetic seismic reflection section with noise. The signal to average noise level is approximatly 2.

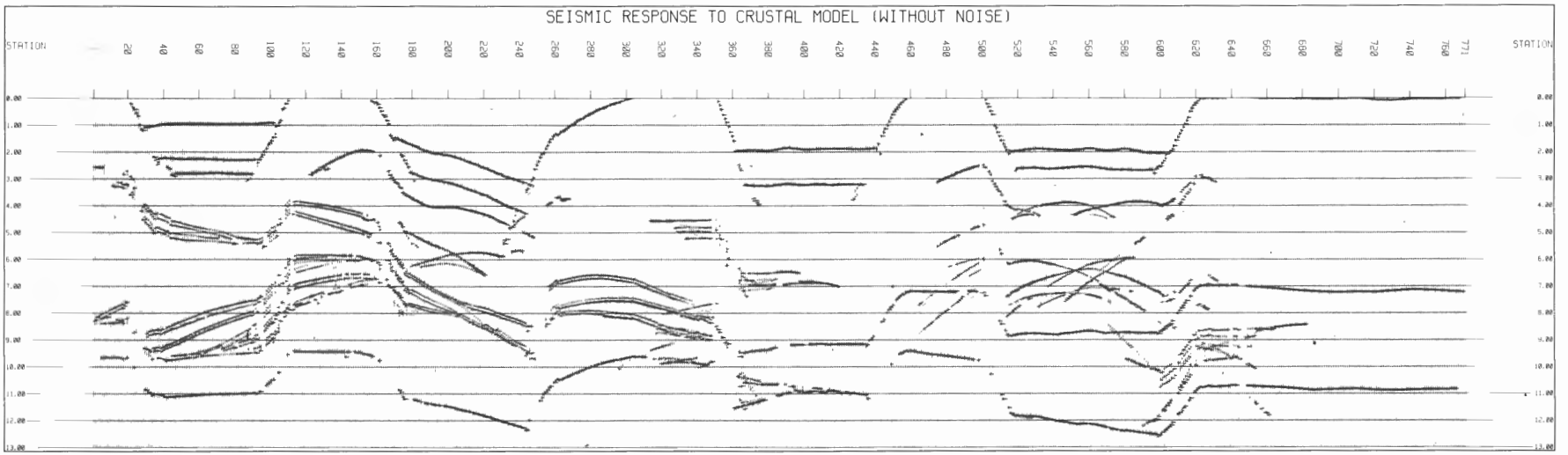

Figure 3. Synthetic seismic reflection data set as for Figure 2, but without noise.

Automatic gain control reduces amplitude variations in this data set particularly, and in real data sets generally. Unambiguous interpretations of magma bodies or zones of partial melt, where velocity contrasts may be high and reflection amplitudes strong, are not possible on the basis of stacked seismic reflection sections to which AGC has been applied. Such interpretations, and for that matter any interpretations that are based on amplitude, need to consider the unprocessed field records.

A primary objective in developing the model in Figure 1 was to investigate the nature of reflections from a crustal simple-shear zone of the type proposed by Wernicke (1985). Initial expectations were that such a zone, probably composed of mylonites perhaps with anastomosing geometries, could be traced readily into the deep part of the synthetic section. Lack of compelling evidence for such crustal-scale detachments in seismic reflection data collected in the Basin and Range Province has been used as evidence against their existence as first order features. However, results of this modeling exercise suggest that reflections from fairly simple crustal-scale detachments could be difficult to recognize due to the effects of complex velocity variations in the upper crust. Detachments that begin at the surface and continue to the Moho (and that offset the Moho) are controversial because they are difficult to support rheologically in the high heat flow environment of the Basin and Range Province. Nevertheless, dismissal of this concept based solely on their apparent absence in seismic reflection data now seems less clear-cut.

ACKNOWLEDGMENTS

This work was supported in part by National Science Foundation grants EAR-8306542 and EAR-8804667. Support was also received from a Shell Faculty Career Initiation Award. I am grateful to A.G. Green who materially contributed to preparation of the abstract.

REFERENCE

Wernicke, B.
1985 : Uniform-sense normal simple shear of the continental lithosphere ; Canadian Journal of Earth Sciences, v. 22, p. 108-125.

Modeling of synthetic seismic reflection data: CCSS workshop 1987 — data set V

M.R. Warner[1]

Warner, M.R., Modeling of synthetic seismic reflection data: CCSS workshop 1987 — data set V; in Studies of Laterally Heterogeneous Structures Using Seismic Refraction and Reflection data, ed. A.G. Green; Geological Survey of Canada, Paper 89-13, p. 219-224, 1990.

Abstract

CCSS workshop 1987 data set V consisted of an unmigrated normal incidence, two dimensional, synthetic seismic section. The aim of the workshop was to recover the original model from which the synthetic section was generated. Velocity information was obtained from pull down on deep reflections, from polarity reversals, and directly from the results of migration. An initial line drawing of the original data was migrated to give a starting model. This model was progressively refined by generating synthetics for comparison with the original section. The final model thus produced matches closely with both the geometry and velocity structure of the original model.

Résumé

Le jeu de données V de l'atelier de la CSSC consistait en un profil sismique synthétique, non migré, à incidence normale et bidimensionnel. Le but de cet exercice était de retrouver le modèle original qui avait servi de base à l'élaboration du profil synthétique. De l'information de vitesse a été obtenue à partir de la dépression des réflexions profondes, des renversements de polarité ainsi que directement à partir des résultats de la migration. Le modèle de départ a été constitué à partir de la migration d'une représentation simplifiée des données. Ce modèle a été progressivement raffiné au travers de sections synthétiques que l'on a comparées au modèle original. Le modèle finale ainsi produit donne une bonne représentation à la fois de la géométrie et de la structure de vitesse.

[1] BIRPS, Bullard Labs., Madingley Road, Cambridge, CB3 0EZ, England (now at Department of Geology, Imperial College, Prince Consort Road, London, SW7 2BP, England).

INTRODUCTION

The interpretation of unmigrated seismic reflection data in general involves three stages: construction of a velocity model, migration of the data to determine detailed reflector geometry, and finally, geological interpretation of the results. In practice, this is often an iterative process since the results of stages two and three are used to modify the model used in stage one. For CCSS data set V no velocity information, other than that implicit in the zero offset reflection section, was available (Johnson, 1990). Obtaining an accurate velocity model was therefore a major part of the interpretation.

Before starting accurate computer migration and modeling of the data set, I made an initial interpretation, removing by hand velocity pull down and migration effects. To my surprise, this initial interpretation was rather similar to the final picture produced by accurate modeling. It was clear that computer modeling was necessary to refine the details of the structure but that manual interpretation was perfectly adequate to obtain the gross characteristics.

VELOCITY DETERMINATION

For real data sets there are usually several primary sources of velocity information, including stacking velocities, diffraction migration velocities, regional refraction information, first break velocities, well logs and regional geological information. For the synthetic data provided, none of this information was available. The section does, however, contain some velocity information. In particular, the basins produce velocity pull down on the deeper reflections, some events show polarity reversals indicating underlying low velocity zones, reflection amplitudes vary (notwithstanding the automatic gain control applied), and the antiformal diffraction-like events and bowties must migrate to give realistic surfaces. I assumed that the velocity model contained no significant velocity gradients and no hidden velocity discontinuities (i.e., all velocity changes produced reflections), and I used "conventional" values for those parts of the model left undetermined.

Figure 1 shows the velocity values obtained in this way. A comparison with those actually used to produce the original synthetic section shows that there are few significant differences in the main regions of the model. The sedimentary velocities are rather too low and the velocities within the two layered sequences are poorly determined.

Implicit in my use of velocity pull down to determine velocities is the assumption that the basins are not isostatically compensated by topography on the Moho or other deep interface, and that the basin bounding faults are not vertical features penetrating and offsetting the whole section. Both assumptions can be seen to be correct since the pull down is the same for both horizontal and dipping, and shallow and deep reflections.

MIGRATION AND MODELING

Figure 2 shows my initial line drawing of the section; it contains all the significant coherent events I could see. Since the synthetic section contained no coherent noise of any kind, all these events must represent primary reflections. Figure 3 shows the results of migrating this line drawing using an initial velocity model similar to that

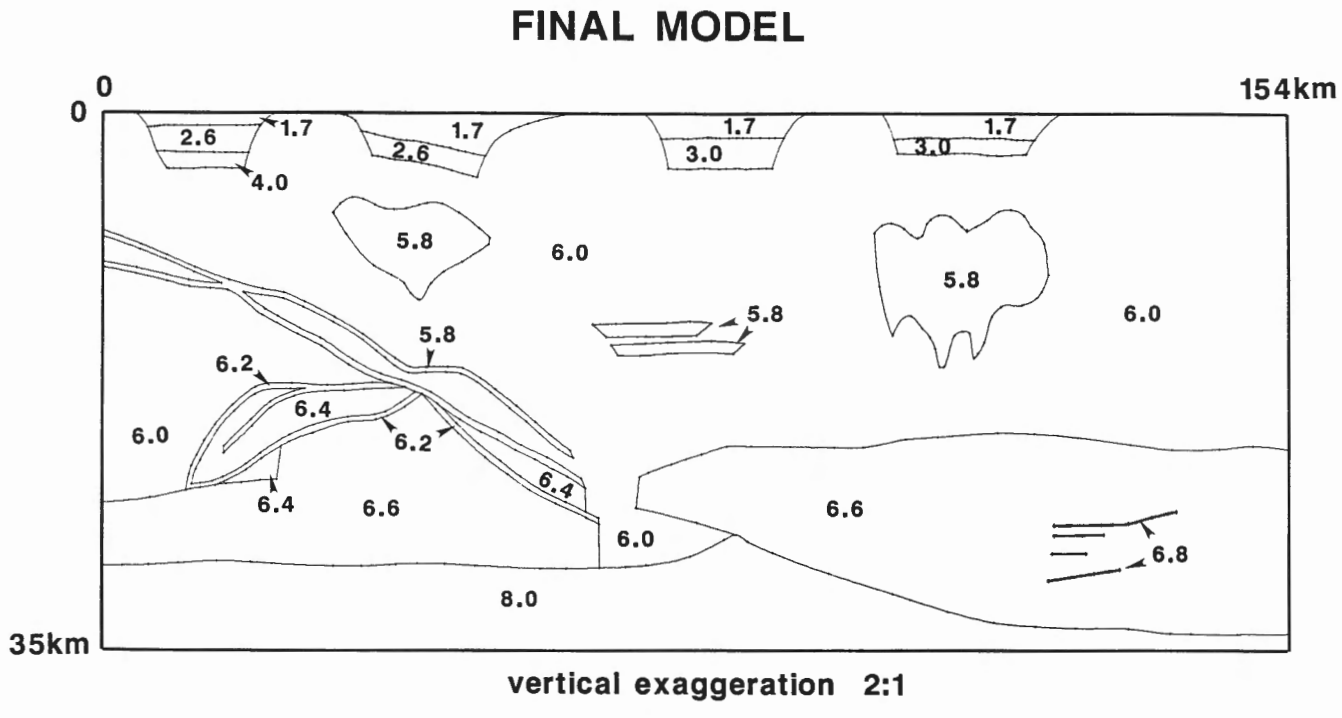

Figure 1. Final velocity model deduced from CCSS data set V. P-wave velocities are given in km/s. Vertical Exaggeration is 2 : 1.

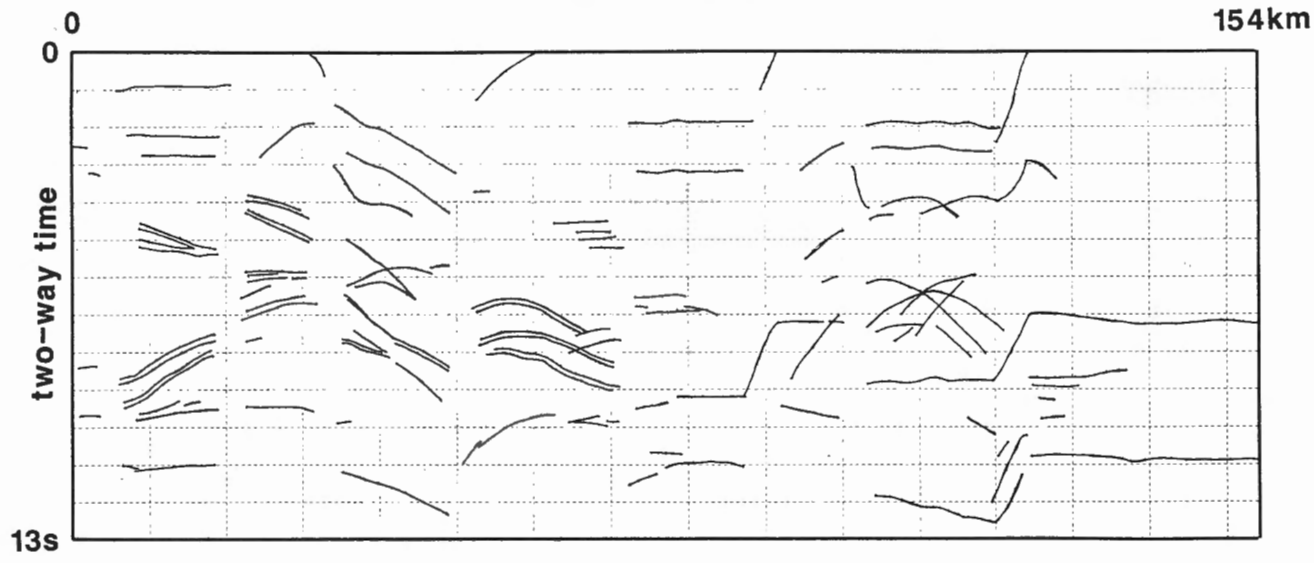

Figure 2. Initial line drawing showing all coherent events that could be identified on the synthetic seismic section of CCSS data set V. Vertical exaggeration is 2 : 1.

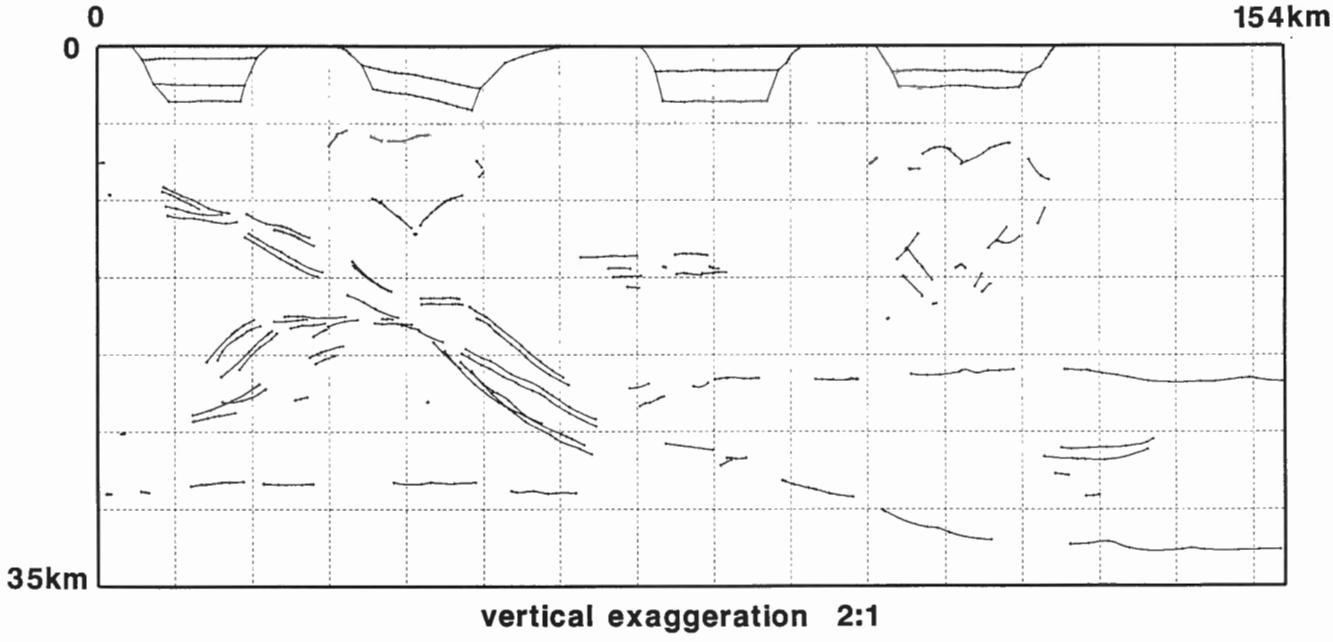

Figure 3. Migrated depth section obtained from the line drawing shown in Figure 2. Vertical exaggeration is 2 : 1.

shown in Figure 1. Not every event could be migrated since the velocity model had errors. This migrated section was then used as the basis for a starting model, shown in Figure 4, which was used to generate an initial synthetic section. The model was successively refined by comparing the synthetics with the original data and changing both the velocity model and reflector geometry. The final model shown in Figure 1 was obtained after about six iterations.

Figures 5a and 5b show a comparison between the original synthetic data and the synthetic data generated from my final model. With few exceptions, events on both match to about 50 ms. I had difficulty matching amplitudes consistently between the two sections, however, as I was unable to recreate the same noise and automatic gain control (AGC) characteristics.

INTERPRETATION AND COMPARISON WITH THE ORIGINAL CRUSTAL MODEL

An unbiased interpretation of my final model is no longer possible, as I have now seen the original model from which the data were prepared. The passage below is a direct quote from my abstract, which was written before the original model was revealed at the workshop:

"The interpreted section shows four sedimentary basins. These basins do not appear to link into deeper events within the section. The crystalline crust contains two pluton-like low velocity zones in which the velocities cannot be dramatically different from those in the basement. A major feature of the section is a series of thin, low-velocity channels cutting the mid-crust (one of these is locally a high velocity channel). These presumably represent faults or shear zones. I have not yet successfully modeled the interaction of these shear zones with the lower crust, although at least one appears to decouple into and offset the Moho. The top of the lower crust (the Conrad?) is well developed in the east and appears to be associated with the lowermost shear zone in the west. Two areas of horizontal layering have not been modeled in detail and probably represent layered igneous intrusions."

It is clear from this passage, and from Figures 1 and 6 that the derived model is surprisingly similar to the original crustal model. The only significant differences are in the interaction of the shear zones with the lower crust and Moho, and the details of the two layered sequences. The former in particular was difficult to model convincingly, presumably because shallow errors in the model accumulate as one moves down the section.

Having seen the "answer" it is now clear that the first two or three iterations made significant improvements to the model, but the later iterations did not, despite improving the fit between the data and the synthetics. Some fine details of the two models do not match, for example, detailed fault geometries in the basins and the detailed shape of the plutons, despite the close similarity of the two sets of seismograms.

DISCUSSION

An exercise that involves inverting synthetic data is always somewhat artificial and this was no exception. The original synthetic section was produced using geometric ray theory rather than wave theory, which means that there were no diffractions and that fine details of the model were disproportionately important. The section contained no source generated or coherent noise and all the reflections were

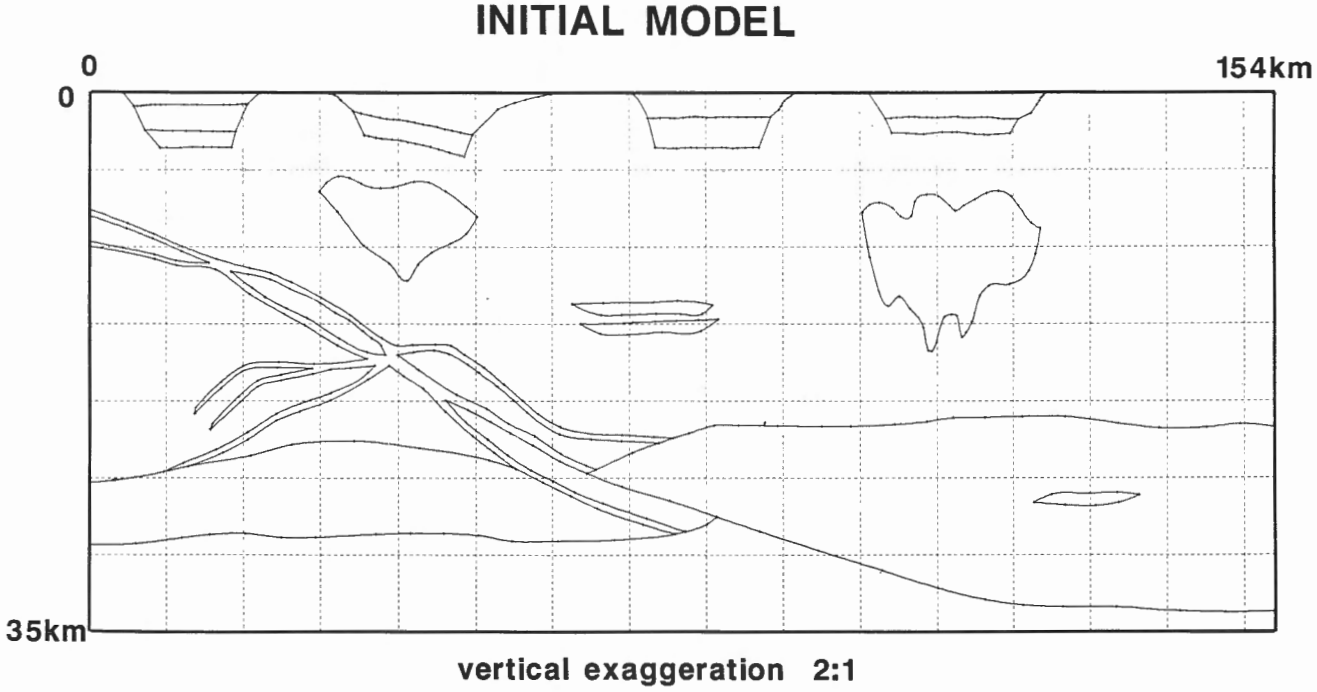

Figure 4. Initial velocity model based on information extracted from Figures 2 and 3. The velocities are broadly similar to those in Figure 1. Vertical exaggeration is 2:1.

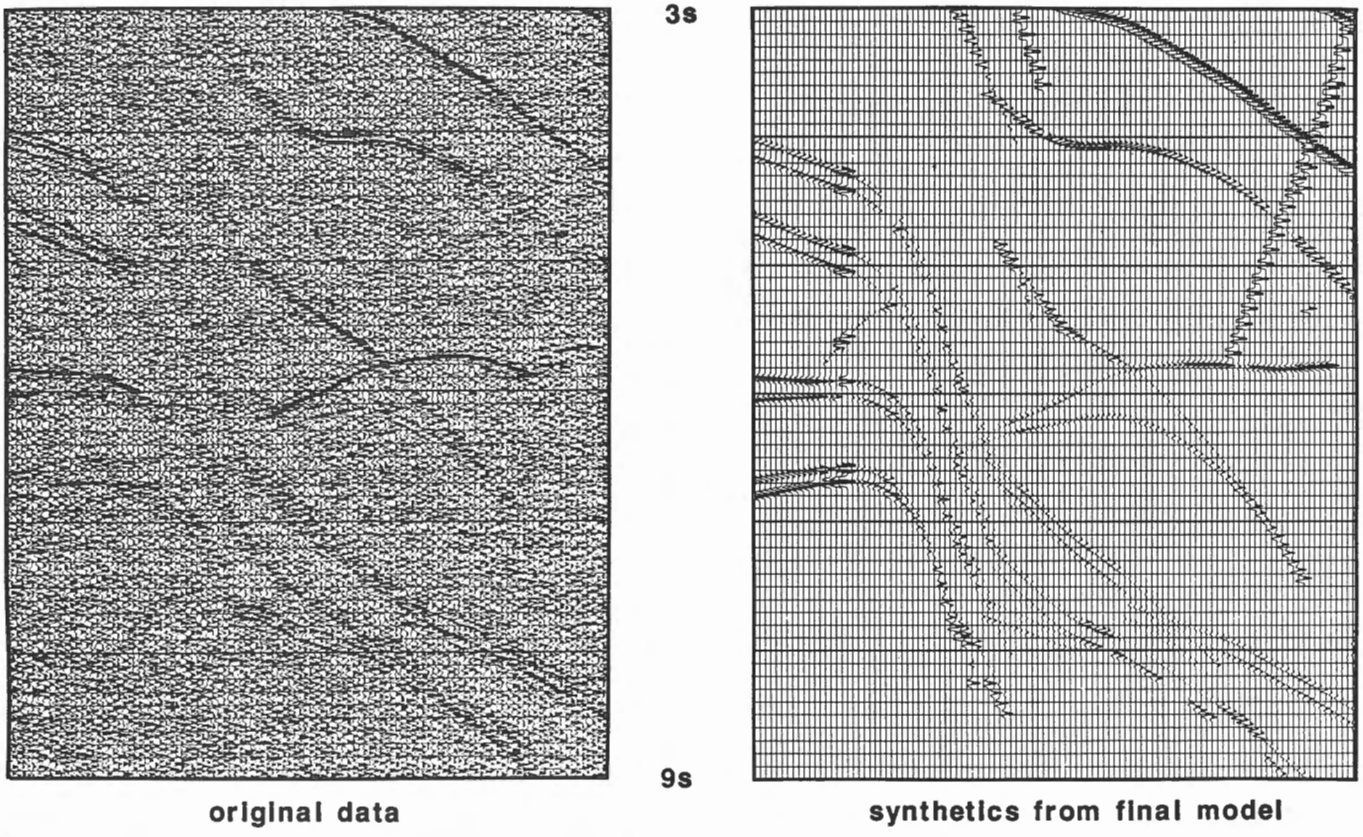

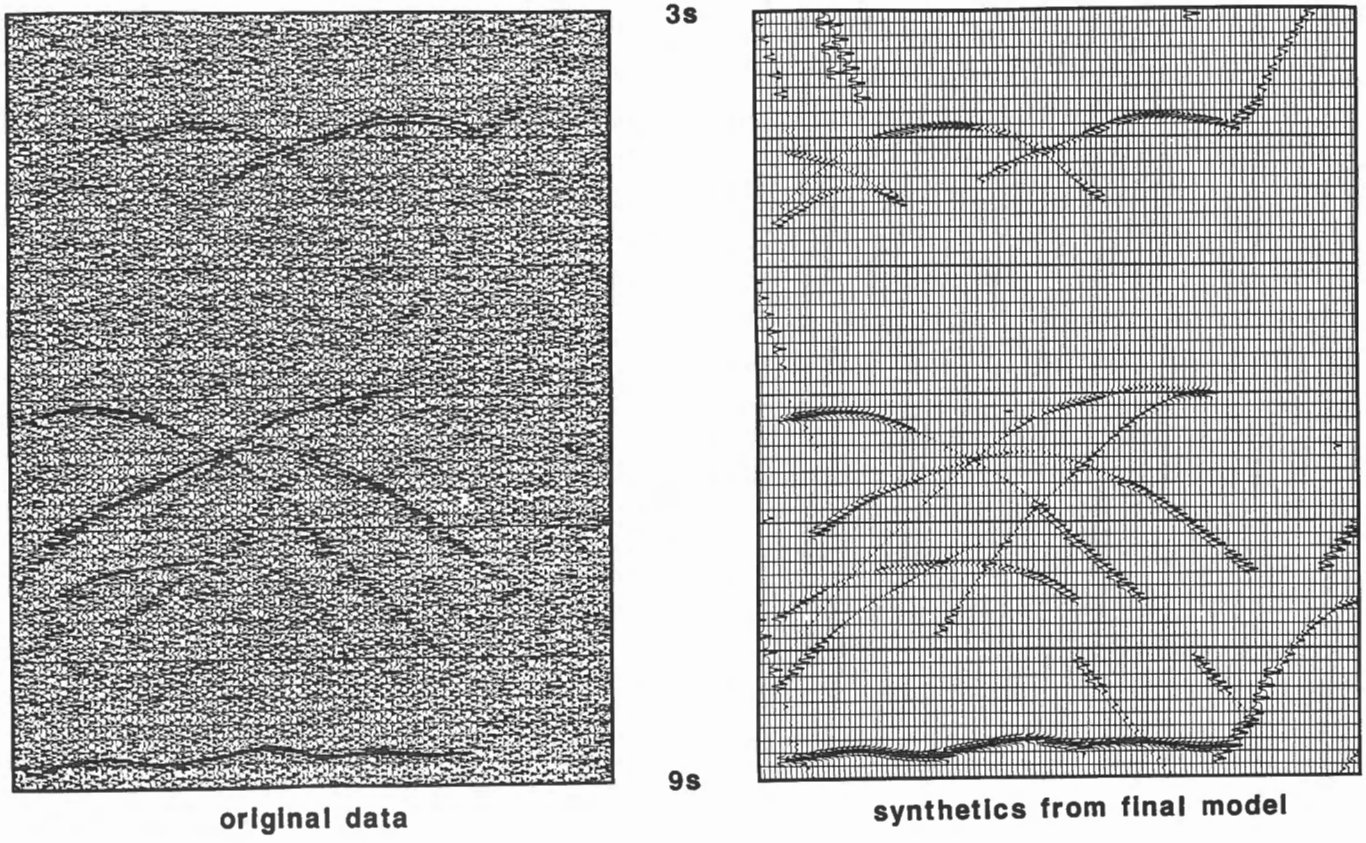

Figure 5 (a and b). Comparison of portions of the original synthetic seismic section with portions of the synthetic section generated from the final model in Figure 1.

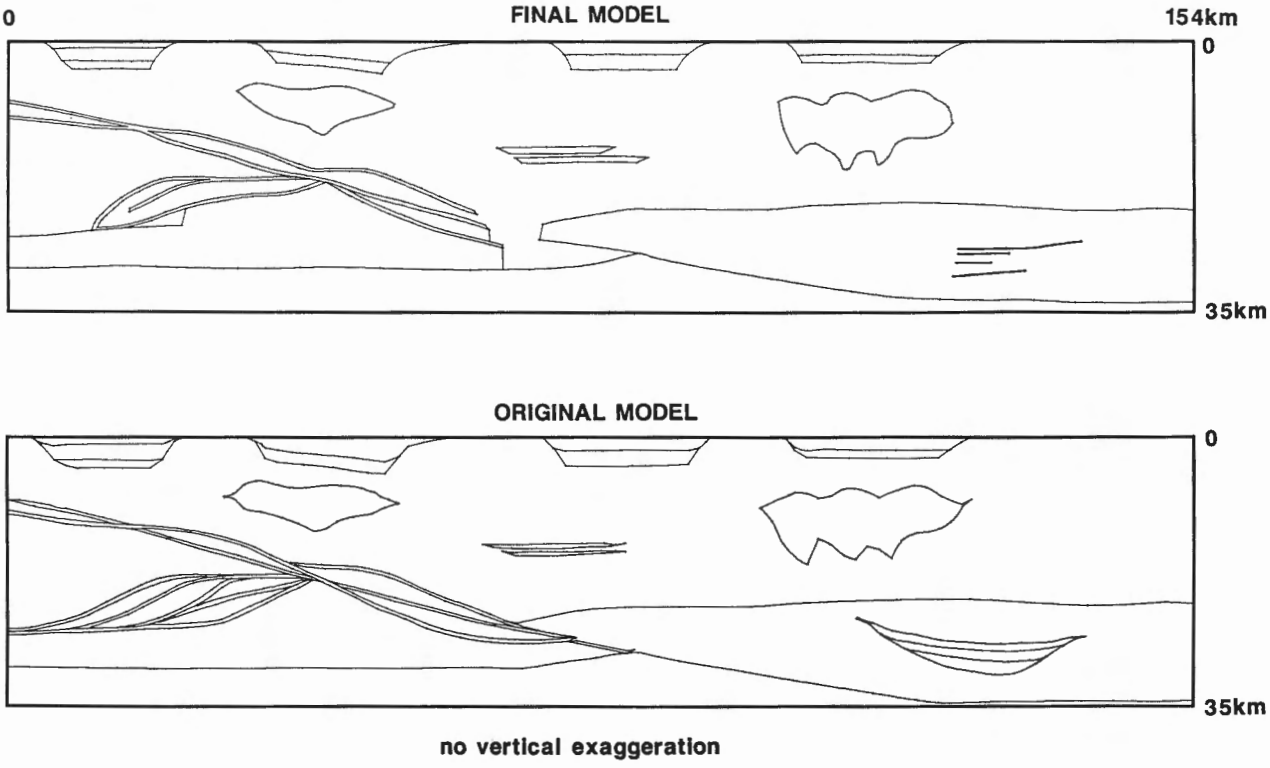

Figure 6. Comparison of the original model used to generate the synthetic seismic section of CCSS data set V with the final model produced in this study. No vertical exaggeration.

from within the plane of the section. In addition there is the inevitable problem that the interpreter tries to guess the reasoning behind parts of the model rather than tackle the data without preconceptions.

To a large extent, I found the problems I was trying to solve and the methods I was using during this exercise were not really those I apply to real data. The major problem with this data set was determining the velocity structure and removing its somewhat unrealistic distorting effects. With real data the problems are more usually to do with following events through non-stationary and coherent noise, trying to interpret three dimensional geology from a few two dimensional lines, and attempting to make geological sense of the result. Notwithstanding these problems, I found this a useful and instructive exercise and was agreeably surprised at the closeness of fit between the two models.

ACKNOWLEDGMENTS

The interactive modeling was performed on the Bullard Lab's VAX 11-750 using the Advanced Interactive Modeling System (AIMS) courtesy of Geoquest International Inc. I should like to thank Roy Johnson, Scott Smithson and Walter Mooney for preparing an interesting and challenging exercise.

REFERENCE

Johnson, R.A.
1990 : Complex response to a "simple" crustal model : Implications for deep crustal reflection interpretation ; *in* Studies of Laterally Heterogeneous Structures Using Seismic Refraction and Reflection Data, ed. A.G. Green ; Geological Survey of Canada, Paper 89-13, p. 213-217.